DOCTOR OF PHILOSOPHY

A qualitative and quantitative analysis of the developing human lumbar vertebral column

Goodchild, Samantha

Award date:
2019

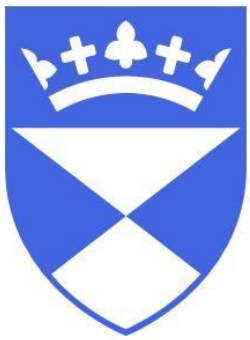

University of Dundee

A Qualitative and Quantitative Analysis of the Developing Human Lumbar Vertebral Column

Samantha Louise Goodchild

PhD in Anatomy and Forensic Anthropology

Supervisors:

Professor Dame Sue Black

Dr Craig Cunningham

Centre for Anatomy and Human Identification

School of Science and Engineering

University of Dundee

November 2019

Contents

List of Appendices

All appendices associated with this thesis can be found on a disc which is supplied with physical copies of this thesis.

Glossary of Terms

Accrual	Accumulation
Adolescence	The period of growth and development after puberty
Adult	An individual that has reached sexual maturity
Anlage	Rudimentary base/ template
Anterior	Towards the front
Apoptosis	Programmed cell death
Appendicular	(Skeleton) the bones of the girdles and upper and lower limbs
Axial	(Skeleton) bones of the cranium, thorax, vertebral column On an axis
Biomechanics	The study of internal and external forces on the skeletal system
Binarisation	Conversion of different grey levels to black and white
Childhood	The period of life after infancy but before puberty
Compression	To press together or condense
Concentric	A circular structure originating or surrounding a central point
Degeneration	Deterioration/ loss of functionality
Fetal	The period of growth from the 2nd month gestation to birth
Gait	Movement relating to standing or walking
Hemi	Half
Hierarchical	A ranked system
Infancy	Period of growth after birth but before childhood
Inferior	Towards the bottom/ lower
Lateral	Away from the midline
Load	The weight placed upon a structure
Longitudinal	Lengthwise
Medial	Closer to the midline
Morphology	The form/ structure of something, for example a bone
Ossification	The process by which bone is formed
Osteogenesis	The formation of bone
Perinatal	Around the time of birth
Posterior	Towards the back

Postnatal	After birth
Prenatal	Before birth
Proximal	Closer to the point of origin
Qualitative	To describe something using its qualities, for example its size, shape or appearance
Quantitative	To describe something using measurements/ numerical values
Sagittal	An anatomical plane that separates the body into left and right
Seriation	To arrange in an order or a series
Strain	The deformity of a material under stress
Stress	The amount of force placed on a material per unit area
Superior	Towards the top
Tension	To pull apart/ stretch
Transverse	An anatomical plane that is at a 90° angle

List of Abbreviations

ALL	Anterior longitudinal ligament
ANOVA	Analysis of Variance
BFA	Bone functional adaptation
BMD	Bone mineral density
BV/TV	Bone volume fraction
C	Central
DA	Degree of anisotropy
FEA	Finite element analysis
FEM	Finite element modelling
FOV	Field of View
I	Inferior
iu	*In utero*
IV	Intervertebral
KVP	Machine power
L1	1st lumbar vertebra
L2	2nd lumbar vertebra
L3	3rd lumbar vertebra
L4	4th lumbar vertebra
L5	5th lumbar vertebra
MCP	Multiple pairwise comparison
OPG	Osteoprogeterin
PLL	Posterior longitudinal ligament
PTH	Parathyroid hormone
ROI	Region of interest
S	Superior
SEM	Scanning electron microscope
SMI	Structural model index
Tb.N	Trabecular number
Tb.Sp	Trabecular separation
Tb.Th	Trabecular thickness
VOI	Volume of interest
µCT	Micro-CT

List of Figures

List of Tables

Acknowledgements

I would like to thank my supervisors, Professor Dame Sue Black and Dr Craig Cunningham, for their tireless support throughout this project. Thank you both for your many suggestions and insights, and for your enthusiasm. Without your support and guidance, particularly in the final stages of this journey, this thesis would not have happened. Thank you both for your patience and for believing in me, particularly at times I did not believe in myself.

I would also like to thank Miss Laura Daly and Dr Laszlo Csetenyi, of the University of Dundee, for the access and technical support regarding the imaging equipment used in this project, along with their constant support when things started going wrong, which was quite often!

I would like to express my gratitude to the University of Dundee for accepting me on the Greenhouse Studentship and funding this research, without which this project would not have been possible.

I would like to express my love and thanks to my family for their support throughout my entire time at University. In particular, I would like to thank my Mum and Dad, my sister Christie and my Auntie Susie. Without you all supporting and believing in me this never would have been possible. I apologise for all the tears and the tantrums along the way. I hope I have made you proud.

Thank you to my friends and colleagues at both the University of Dundee and UCLan, the former for being there from the beginning, and the latter for being there at the end.

Finally, I would like to thank all of my friends from Dundee University Karate Club, Goju Ryu Karate Dundee, FFD Crossfit and Reebok Crossfit Spectrum. Without you guys I would have spent the time during my PhD considerably more stressed, and probably a lot fatter!

Declaration

The candidate, Samantha Goodchild, is the author of this thesis. Unless otherwise stated, all references cited have been consulted by the candidate. The work, of which the thesis is a record, has been completed by the candidate. No portion of the work referred to in this thesis has been submitted in support of an application for another degree or qualification at this or any other university, or other institute of learning.

Samantha Goodchild

Copyright

Statement

We certify that Samantha Goodchild has spent four years of research under our supervision. Samantha has fulfilled the conditions of Ordinance 39 and is qualified to submit the accompanying thesis in application for the degree of Doctor of Philosophy.

_____

Professor Dame Sue Black

_____

Dr Craig Cunningham

Summary

The human adult lumbar vertebral column plays an important role in load-bearing and weight-transmission between the trunk and the lower limb, while its other functions include acting as a site for haematopoiesis, an area of attachment for soft tissue structures and protection of the spinal cord. While there is a rich source of research focusing on the internal trabecular architecture of the adult lumbar vertebrae, the ontogenetic development of this region is less well understood. This project aimed to both qualitatively and quantitatively assess the developing internal trabecular architecture of the lumbar vertebral centra and to document architectural changes throughout the maturation process.

The project aimed to meet three specific objectives. Objective a). aimed assess regional variation in the trabecular architecture of the developing lumbar centra, for example how does the central region of the centrum differ from the peripheral region and are there any differences present between the superior and inferior, or anterior and posterior regions. Objective b). aimed to assess developmental changes in trabecular architecture within the lumbar centra, focusing on quantifying the differences in trabecular architecture between the fetal period, perinatal period, infancy and early childhood. Finally, objective c). aimed to assess vertebral level specific changes in trabecular architecture during development by identifying whether there are any differences in trabecular architecture between the lumbar levels L1, L3 and L5. The imaging modalities of radiography and micro-computed tomography were utilised to achieve these objectives.

Qualitative and quantitative analysis of the developing fetal and perinatal lumbar vertebral centrum identified significant differences in trabecular architecture between central and peripheral regions of the developing centrum. In the fetal and perinatal periods both regions displayed a structure predominantly driven by ossification with trabeculae in close proximity to the primary centre of ossification thicker and more mature than in peripheral regions, which displayed a radial pattern of thin trabeculae extending outwards from the ossification centre. The presence of vasculature greatly influenced the internal architecture of the centrum from the fetal period into childhood, with a lower number of thicker, more

plate-like trabeculae within the central region, forming a structure similar to that of the adult prior to the onset of load-bearing beyond *in utero* movements.

This study has identified that the lumbar vertebral centra undergo three significant phases of development. The first phase is characterised by increased radiographic intensity and increased bone volume fraction driven by an increase in trabecular number. It is highly likely that this early period of bone mineral accrual acts as a preparatory mechanism to create a reservoir of minerals to facilitate re-organisation in the early postnatal period. The second phase is defined by significant loss of bone, in particular trabecular number and bone volume fraction, as well as increased remodelling of the trabecular struts into more rod-like structures.

The final phase represents the period by which the internal trabecular architecture of the lumbar centrum is remodelled, likely in response to increased biomechanical demand. The attainment of developmental milestones, in particular sitting and standing unaided, which occur between around 6 months to 1.5 years of age, are considered of particular importance as these movements act to increase the compressive load placed upon the vertebral column leading to remodelling of the trabecular architecture into a mechanically optimal structure.

From the perinatal period onwards, the fifth lumbar vertebral centrum consistently displayed a trabecular architecture linked to increased mechanical strength compared to the first and third lumbar levels. The likely reason for this is due to the increased load placed upon it as the most inferior lumbar vertebra. Furthermore, the positioning of the pelvis and the load transfer between L5 and S1 also likely contributes to this differing architecture. There was no evidence that the earlier appearance of the upper lumbar vertebral centra led to any differences in trabecular architecture, or that the developing lumbar lordosis prompted any changes in trabecular architecture between vertebral levels.

1 Introduction

1.1 Introduction and Rationale

Following the introduction of 'The Law of Transformation' (Wolff, 1870, 1892; Lanyon, 1974) and its later revisions, the 'mechanostat' theory (Frost, 1996, 2004) and Bone Function Adaptation (BFA) (Ruff *et al.*, 2006), researchers have become increasingly interested in the relationship between bone structure and its biomechanical competence (Lanyon, 1974; Goldstein, 1987; Frost, 1996; Huiskes, 2000; Sommerfeldt and Rubin, 2001; Frost, 2004; Pearson and Lieberman, 2004; Chen *et al.*, 2010). The study of trabecular architecture within load-bearing skeletal elements gives an understanding of its biomechanical capabilities, as well as the factors that influence bone modelling and remodelling. The reaction of bone to load-bearing has continued to inspire a plethora of studies focusing on adult trabecular structure at areas of significant biomechanical importance (Smit, 1997; Hildebrand *et al*., 1999; Fields *et al*., 2009; Hammer, 2010; Boyle and Kim, 2011; Parkinson and Fazzalari. 2013).

Historically, the assessment of the internal trabecular architecture within bone has been a destructive process, with histological methods the only way of assessing bone microstructure (Sato, 1967; Amstutz and Sissons, 1969; Whitehouse *et al*., 1971). However, with recent technological advancements, it is now possible to both visualise and quantify internal bone architecture without causing destruction to the sample, which is of particular importance when considering the irreplaceable nature of juvenile skeletal material. The study of trabecular architecture is an important area of multidisciplinary research with anatomical, forensic and clinical applications (Cunningham, 2009; Maclean, 2017).

Recent literature assessing trabecular architecture has focused on skeletal areas of biomechanical importance, such as the long bones (Ryan and Krovitz, 2006; Skedros and Baucom, 2007; Jang and Kim, 2008, 2010a; Boyle and Kim, 2011), the pelvic complex (Dalstra and Huiskes, 1995; Martinon-Torres, 2003; Cunningham and Black, 2009a) and the vertebral column (Sato, 1967; Amstutz and Sissons, 1969; Whitehouse *et al*., 1971; Kneissel *et al*., 1997; Banse *et al*., 2001; Thomsen *et al*., 2002a; b; c; d; Gong *et al*., 2005; Jang and Kim, 2010b; Thomsen *et al*., 2013). However, there is limited research focusing on the

developing trabecular architecture of other load-bearing structures, notably the lumbar vertebral column. Other work on load-bearing elements of the skeleton has focused predominantly on the appendicular skeleton (Salle *et al.*, 2002; Ryan and Krovitz, 2006; Gosman and Ketcham, 2009; Cunningham and Black, 2009a; 2010; Abel and Macho, 2011; Maclean, 2017).

The lumbar vertebral column plays an important role in load bearing. Gross morphology and trabecular bone architecture has been shown to reflect this function and is organised to facilitate optimal load transfer (Briggs *et al*., 2004). There has been a wide base of research focusing on the internal architecture of the lumbar vertebral column in the adult, focusing on adult vertebral biomechanical strength, along with age-related degeneration and osteoporosis (Haidekker *et al*., 1999; Thomsen *et al*., 2002a; Agarwal *et al*., 2004; Buckley *et al*., 2007; Thomsen *et al*., 2013). The study of adult vertebral bone has identified a characteristic internal architecture of thick, well-spaced, vertically oriented trabeculae observed in the central portion of the vertebral body, reinforced by dense horizontally oriented trabeculae at the superior and inferior aspects (Amstutz and Sissons, 1969; Whitehouse *et al*., 1971; Kneissel *et al*., 1997; Thomsen *et al*., 2002d; Briggs *et al*., 2004). This trabecular architecture is optimal considering the primary load placed upon the vertebral column in sitting and standing is axial compression. The vertically oriented trabeculae within the central region follow the trajectory of these compressive forces, while the superior and inferior regions reinforce the central region and act to convert other loads such as shear and torsion into compressive load (Smit *et al*., 1997; Ferguson and Steffen, 2003; Briggs *et al*., 2004).

While a limited number of studies researching the development of the vertebral trabecular architecture exist, there is a focus on fetal and perinatal development (Kneissel *et al*., 1997; Nuzzo *et al*., 2003; Acquaah *et al.*, 2015). Findings suggest that the fetal trabecular structure does not mirror that of the adult and is instead influenced by the pattern of ossification within the vertebral centra, with more dense trabeculae located centrally and less mature bone located peripherally (Roschger *et al*., 2001; Nuzzo *et al*., 2003; Acquaah *et al*., 2015). Furthermore, loss of trabeculae has been shown to be characteristic of infancy, followed by selective thinning and thickening of trabeculae in relation to mechanical loading, presumably commencing the development of the

characteristic adult structure (Acquaah *et al*., 2015). These findings are similar to studies on juvenile long bones, which state that the adult trabecular structure develops only when the bone commences its load-bearing function (Salle *et al*., 2002; Ryan and Krovitz, 2006; Gosman and Ketcham, 2009; Hammer, 2010). However, the research on the pelvic girdle has contradicted these findings with studies reporting a trabecular structure that mirrors that of the adult, which then becomes reinforced following weight-bearing, implying that genetics, along with other factors such as the presence of vasculature and the pattern of ossification, *in utero* limb movements, nutritional availability and hormone levels, may play a role in the development of trabecular architecture (Cunningham and Black, 2009a; 2009b; 2010; Maclean, 2017).

Although there is some limited research into the development of fetal and infant lumbar vertebral microarchitecture, the age ranges this data considers does not incorporate all developmental milestones associated with load-bearing that occur prior to adulthood. Motor milestones such as sitting unaided, standing, independent walking, running and the development of a mature gait may all play an important role in the attainment of the adult trabecular architecture observed. While sitting unaided occurs between around 4-10 months and walking independently occurs between around 10 to 16 months of age (Keen, 1993; Garrett *et al., 2002;* WMGRSG, 2006; Sheldrick and Perrin, 2013; Hadders-Algra, 2018), a mature, adult gait is not achieved by an individual until between 5 to 9 years of age, suggesting that trabecular architecture most likely continues to undergo development in this region until maturity (Keen, 1993; Chester *et al*., 2006; Hadders-Algra, 2018).

An understanding of the developing trabecular architecture of the lumbar vertebral column is vital in understanding the potential genetic, epigenetic and external factors that lead to the attainment of the optimal trabecular arrangement observed in the adult. By understanding the normal pattern of bone development within the lumbar vertebral column, abnormal patterns can be more easily identified. Numerous studies have implied the importance of the early developmental period on adult vertebral bone architecture (Bachrach, 2001; Cooper *et al*., 2005; Goldberg, 2006; Ay *et al*., 2011; Acquaah *et al.*, 2015). The prevalence of osteoporosis is increasing, and the vertebral body is a predominant site for osteoporotic fracture in older individuals (Banse *et al*., 2001; Adams and

Dolan, 2005; Prakash *et al*., 2007; Parkinson *et al*., 2012). An understanding of early vertebral bone development may shed light on the potential mechanisms leading to poor bone health in the adult and the subsequent osteoporotic compressive fractures often observed as a result.

Furthermore, as trabecular structure is closely related to function, and different skeletal areas perform different functions, the characteristic architecture of the developing lumbar vertebrae may differ with other areas within the juvenile skeleton to make it possible to separate developing lumbar vertebrae from other skeletal and non-skeletal elements in the assessment of damaged fetal remains in a forensic setting.

1.2 Aims and Objectives

The overarching aim of this project was to document both qualitatively and quantitatively the trabecular architecture of the developing lumbar vertebrae and to understand the changes that occur in bone morphology in relation to the changing functions of the vertebral column with age. This was approached in two stages. The first, preliminary stage of the project utilised radiography to identify 'trends' in the patterns of radiographic intensity seen within developing lumbar vertebrae from the ages of 28 weeks *in utero* through to late adolescence to understand general development within the lumbar vertebral column as a whole. The second, quantitative stage of the project used µ-computed tomography to assess the developing trabecular architecture within the centra of the first, third and fifth lumbar vertebrae in individuals between the ages of 28 weeks *in utero* to around 8 years of age. This was undertaken to describe the trabecular structure at different ages and understand how the trabecular structure develops in relation to developmental milestones.

The specific objectives of the project were:

1. To qualitatively and quantitatively document the trabecular architecture in the 1st, 3rd and 5th lumbar vertebrae throughout development.

2. To identify any changes in lumbar vertebral trabeculae architecture throughout development.

3. To identify whether there are any significant differences in trabecular architecture between L1, L3 and L5 throughout development.

2 The Structure and Function of Bone

2.1 Bone Structure

2.1.1 *Bone microstructure*

At the microstructural level, bone tissue is a hierarchical structure consisting of an organic extracellular matrix (~22-25%), water (~5-8%) and inorganic mineral (~70%) (Sommerfeldt and Rubin, 2001; Wang and Puram, 2004; Tzaphlidou, 2005). The quality of these constituents, along with their organisation, are important factors in the mechanical strength of bone tissue (Currey, 2003a; Viguet-Carrin *et al.,* 2006).

The organic extracellular matrix of bone primarily consists of Type I collagen fibrils, along with cellular material and numerous proteins that have both signalling and mineralisation initiation functions (Sommerfeldt and Rubin, 2001; Tzaphlidou, 2005). Collagen is formed from proteins and is important in maintaining the structural integrity of bone (Tzaphlidou, 2005; Viguet-Carrin *et al.*, 2006) and has been linked to bone toughness (its ability to absorb energy) (Currey, 2003a; Viguet-Carrin *et al.*, 2006). Collagen is hierarchical in its structure: molecularly, it is formed from three chains of proteins organised in a triple-helix formation. The resulting collagen fibrils are organised in concentric weaves. Finally, the resulting collagen fibres form a calcified collagen-mineral network (Wang and Puram, 2004). The orientation of collagen fibres has been closely linked to the ability of collagen to absorb energy, for example, it has been found that longitudinal fibres are more common in bone regions supporting tensile loads, while transverse fibres are more abundant in regions under more compressive loading (Viguet-Carrin *et al.*, 2006). Collagen disorders can lead to abnormal collagen structure, which affects bone mineral density and leads to thinner bony struts within trabecular architecture (Tzaphlidou, 2005). Changes in collagen structure may alter the deposition and amount of mineral within bone, due to the complex nature of their relationship (Viguet-Carrin *et al.*, 2006). Osteogenesis imperfecta is a collagen disorder characterised by bone brittleness. It is thought that this brittleness is the result of disorganisation and loss of crosslinks between collagen fibrils (Currey, 2003a; Tzaphlidou, 2005). Calcium hydroxyapatite crystals comprise the inorganic mineral component of bone, acting as a readily available store of calcium and phosphate ions. Calcium hydroxyapatite crystals are plate shaped and their morphology and deposition

are influenced by collagen orientation. Due to the process of bone remodelling, the mineral component of bone does not display the same organised, uniform structure seen in its organic counterpart (Roschger *et al.*, 2012). It is thought that the stiffness of bone is related to the quality of the mineral component (Wang and Puram, 2004).

2.1.2 *Bone macrostructure*

At the macrostructural level, bone tissue can be present in several different forms. These include: 1. Woven bone, 2. Lamellar bone, the mature bone type found in adult humans, and 3. Plexiform bone, which is characteristic of animals undergoing a rapid increase in bodyweight early in life (Currey, 2003b) (Figure 2.1).

Woven bone is both irregular and disorganised in its pattern of collagen, which is deposited in a rapid, unsystematic arrangement in an area of immediate need, for example at the site of growing bone or a fracture. Woven bone is almost always a precursor to lamellar bone (Kerr, 2010).

Lamellar bone forms the two structural components that together create the gross macrostructure of bone tissue. Cortical, or compact, bone forms an outer, dense, protective layer, while trabecular, or cancellous, bone is comprised of bony spicules within the marrow cavity, contributing to mechanical support and is found in load and weight-bearing areas of the skeleton (Hadjidakis and Androulakis, 2006). The human adult skeleton is formed of around 80% cortical bone and 20% trabecular bone; however, different skeletal elements have different ratios of cortical and trabecular bone. For example, vertebral bone comprises around only 25% cortical bone compared to 75% trabecular bone (Clarke, 2008).

A layer of vascularised connective tissue, called the periosteum, surrounds the external surface of bone. The periosteum is important in bone growth and repair and plays a significant role in the vascularisation of bone (Dwek, 2010; Burr and Guillot, 2012). Along with the endosteum, which is the connective tissue on the internal aspect of bone, the periosteum contains cells known as bone-lining cells, or osteoprogenitor cells, which play an important role in bone remodelling (Dwek, 2010; Kerr, 2010).

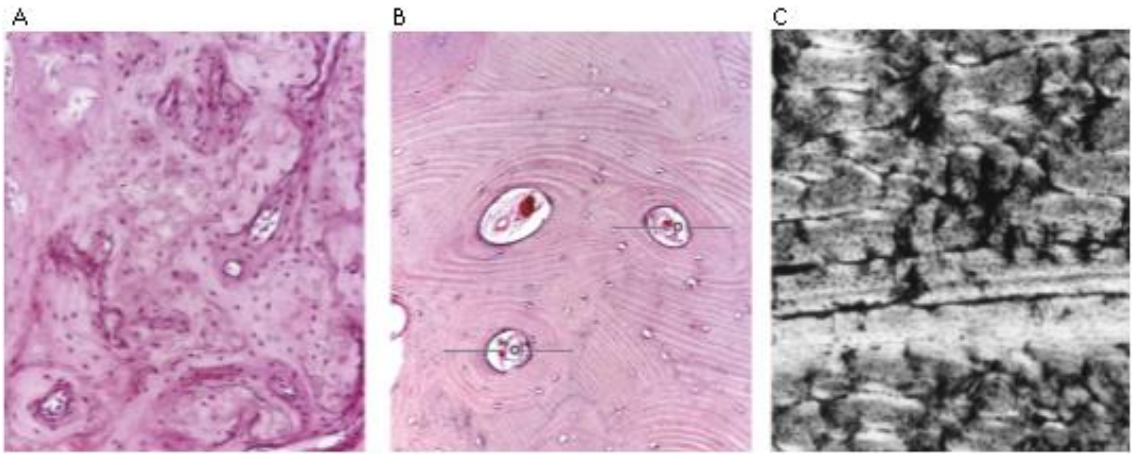

Figure 2.1: Bone in its three macrostructural forms. A. Immature (woven) bone (Pawlina and Ross, 2019). B. Mature (lamellar) bone, where O is osteon (Pawlina and Ross, 2019). C. Plexiform bone (Cuijpers, 2006).

2.1.2.1 Cortical Bone

Cortical bone is the outer, dense layer of bone found at sites such as the bone shaft and the surfaces of flat and irregular bones. It occurs in units comprising layers of mineralised collagen fibrils tightly stacked together and differing in their orientation to each other (Weiner *et al.*, 1999; Ji and Gao, 2004). Its structural unit is the osteon, also known collectively as Haversian systems, which are concentric structures surrounding a central capillary (Figure 2.2) (Sommerfeldt and Rubin, 2001; Clarke, 2008; Dion and Ste-Marie, 2012). Transverse channels carrying vasculature also exist between osteons, which are known as Volkmann's canals (Fonseca, 2012). Primary osteons are created through the modelling of areas of woven bone. Secondary and tertiary osteons are created in the remodelling process, where areas of the primary osteon are resorbed, and new osteons are produced, overlaying the original structure (Kerr, 2010).

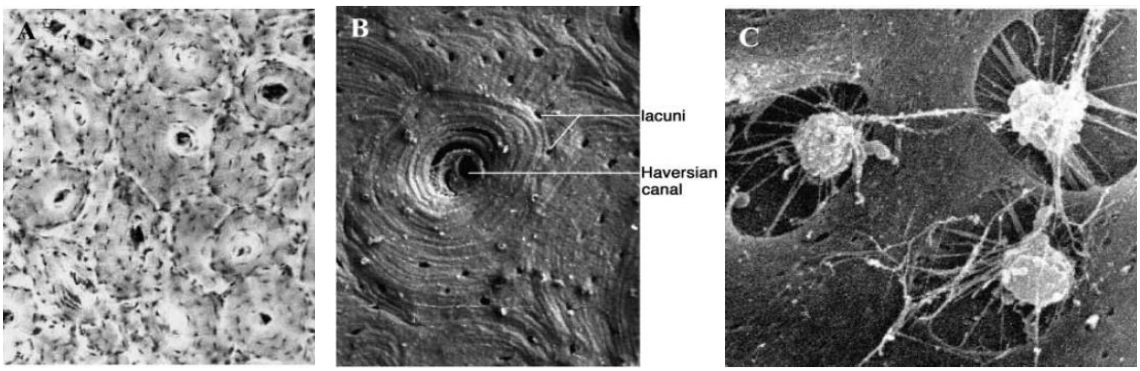

Figure 2.2: A. light microscope image of osteons. B. scanning electron microscope (SEM) image of a single osteon. C. Higher resolution SEM image of osteocytes sitting within lacunae (Sommerfeldt and Rubin, 2001).

2.1.2.2 Trabecular bone

Trabecular bone is mainly comprised of plate and rod-like trabecular struts dispersed within bone marrow which interconnect to form an anisotropic, or unorganised, structure that plays a critical role in the mechanical capabilities of trabecular bone (Clarke, 2008). Plate-like trabeculae have been linked directly to mechanical integrity within trabecular structures (Wang *et al.*, 2015). Trabecular bone turnover is significantly higher than that of cortical bone, in part due to its importance in mechanical strength, but also due to its importance in mineral metabolism (Clarke, 2008). At the microstructural level, the collagen within trabecular bone has been observed to be compactly woven in structure with densely packed mineral plates (Tzaphlidou, 2005). Like cortical bone, trabecular bone is a form of lamellar bone. It is also formed of Haversian systems, however, is not formed of true osteons like cortical bone. Instead, hemiosteons are the structural unit of trabecular bone. This is due to the partial resorption of osteons in modelling and remodelling of trabecular struts (van Oers *et al*., 2008; Dion and Ste-Marie, 2012).

2.2 Bone modelling and remodelling

2.2.1 *The Basic Multicellular Unit*

At the cellular level, bone is comprised of specialised cells that form a unit responsible for the maintenance of bone. These are osteoblasts, osteoclasts and osteocytes and together they form the basic multicellular unit (BMU) (Sommerfeldt and Rubin, 2001; Hadjidakis and Androulakis, 2006; Van Oers *et al.*, 2008).

Osteoclasts are involved in the resorption of bone tissue at resorption sites, called Howship's lacunae, through the secretion of lytic enzymes (Sommerfeldt and Rubin, 2001) and are derived from haemopoietic stem cells (Sommerfeldt and Rubin, 2001; Harada and Rodan, 2003). Osteoclasts are highly specified cells that are well equipped to undertake their function. They are multinucleated cells with an apical membrane that allows a tight connection with the calcified matrix (Sommerfeldt and Rubin, 2001).

Osteoblasts are involved in the formation of bone through the secretion of extracellular matrix and are mesenchymal in origin, helping to regulate the mineralisation of bone. They are cuboidal in shape and are located anchored to

extracellular matrix at the bone surface. Osteoblasts are the mature form of osteoprogenitor cells (Sommerfeldt and Rubin, 2001).

Osteocytes are the most common type of bone cell and live longer than osteoblasts and osteoclasts. Osteocytes are formed through the differentiation of mature osteoblasts that have become trapped and eventually imbedded within the extracellular matrix. This differentiation process is characterised by the formation of dendritic processes. Osteocytes sit in hollow spaces called lacunae (Figure 2.2C) and are connected to one another via cell processes within narrow canaliculi. This communication between cells allows the passage of nutrients, as well as biochemical signals which are important in the maintenance of bone (Bonewald, 2007). Osteocytes also have connections to bone lining cells and osteoblasts out with the extracellular matrix (Sommerfeldt and Rubin, 2001; Prideaux and Bonewald, 2012). Young osteocytes retain the structural characteristics of the osteoblast but have a reduced cell volume and are less capable of protein synthesis. However, as osteocytes age and become embedded deeper into the calcified extracellular matrix, their cell volume decreases further, and glycogen begins to accumulate within the cytoplasm of the cell (Hadjidakis and Androulakis, 2006). Osteocytes do undergo apoptosis (cell death), and this process has been related to the determination of the strength of a bone tissue. In cases of increased osteocyte apoptosis, bone fragility has also been found to increase, implying that osteocytes are important in the maintenance of bone strength (Aguirre *et al.*, 2006).

2.2.2 *Bone modelling*

Bone modelling is the process by which bone adapts its morphology in response to physiological or mechanical influences (Roberts *et al*., 2004; Clarke, 2008; Brandi, 2009), is important in skeletal growth and is characterised by bone resorption and formation. Bone modelling is an uncoupled process, with bone resorption and bone formation independent from one another and controlled by a variety of factors, most importantly: functional loading of skeletal elements (Roberts *et al.*, 2004).

2.2.3 *Bone remodelling*

2.2.3.1 The importance of bone remodelling

Unlike bone modelling, bone remodelling is a selective process that begins before birth, and continues until death, characterised by bone turnover (Roberts *et al.*, 2004; Clarke, 2008; Brandi, 2009), strengthening bone structure and allowing it to continue to undertake its function effectively. As bone is subjected to constant stresses through everyday life, microfractures occur that affect the integrity of the structure. Remodelling occurs at these sites to regain structural integrity (Hadjidakis and Androulakis, 2006) and also on a larger scale at areas of bone fracture. However, it is important to note that stress and mechanical loads are not the only factors affecting the remodelling of bone, changes in nutritional status and metabolic requirements also affect the bone remodelling response (Sommerfeldt and Rubin, 2001; Pearson and Lieberman, 2004). Bone remodelling is dynamic and requires coordination of cells comprising the BMU to maintain homeostasis within bone (Marie, 2012). Remodelling occurs through a cycle consisting of four phases: Activation, resorption, reversal and formation (Raisz, 1999; Hadjidakis and Androulakis, 2006; Seeman and Delmas, 2006; Clarke, 2008; Fonseca, 2012; Marie, 2012) (Figure 2.3).

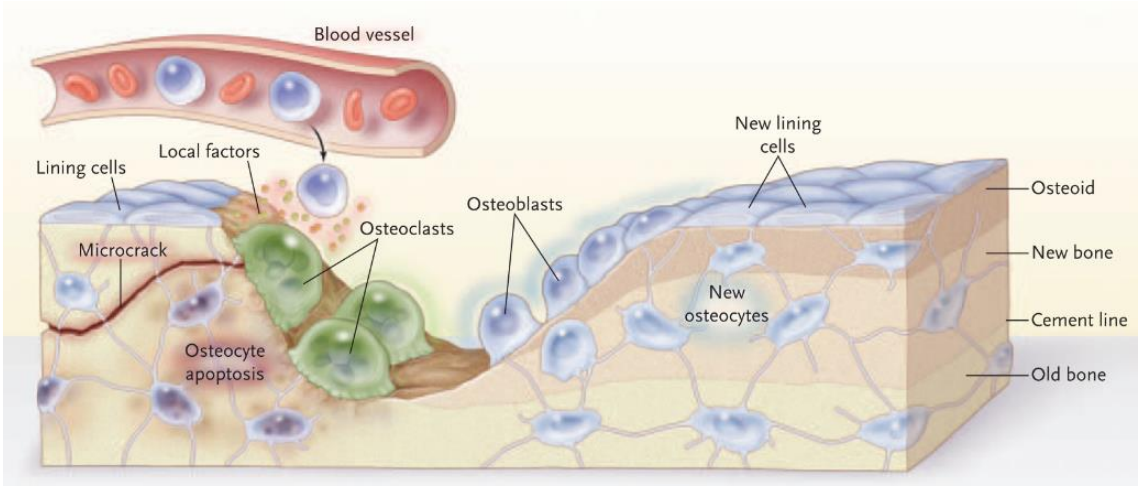

Figure 2.3: A visual representation of the phases of bone remodelling (Seeman and Delmas, 2006).

2.2.3.2 Activation

Bone remodelling is initiated through the recruitment of osteoclast precursors from the blood to the site undergoing remodelling, or the initiation of the differentiation of osteoprogenitor cells within the periosteum (Clarke, 2008). These precursor cells will differentiate into osteoclasts (known as osteoclastogenesis) to resorb bone. For osteoclast precursors to differentiate into osteoclasts successfully, RANKL, a transmembrane ligand on osteoblasts, must bind to RANK, a receptor found on preosteoclasts. Osteoprogeterin (OPG), a protein decoy, can also bind to RANKL, blocking its association with RANK and hence inhibiting osteoclast precursor differentiation (Figure 2.4) (Aubin and Bonnelye, 2000; Hofbauer *et al.*, 2000; Hadjidakis and Androulakis, 2006).

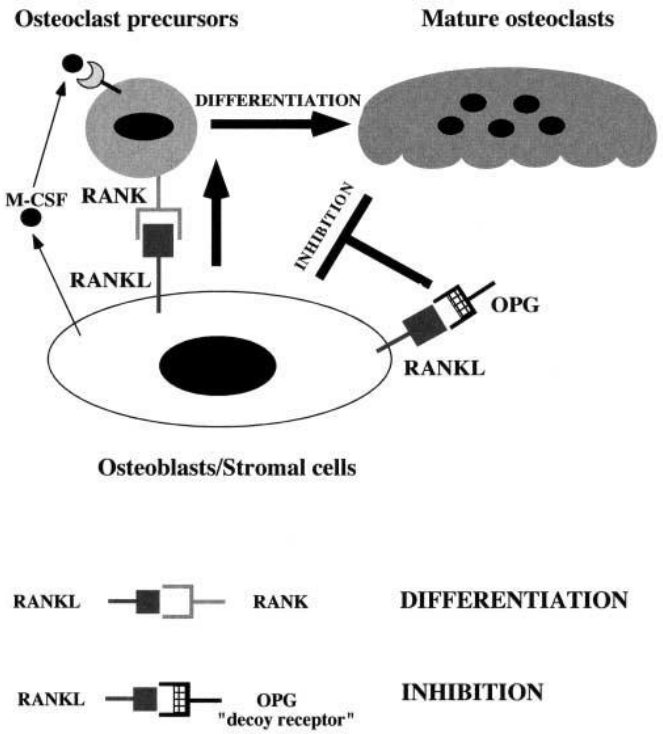

Figure 2.4: Schematic of the interaction between osteoblasts and osteoclasts (Aubin and Bonneyle, 2000).

2.2.3.3 Resorption

The resorption phase is initiated by movement of activated osteoclasts to the area of remodelling. Osteoclasts attach themselves to the bone surface and commence resorption via acidification and proteolysis of the bone matrix and hydroxyapatite crystals (Hadjidakis and Androulakis, 2006, Soysa and Alles, 2016). It has been observed that in cortical bone, osteoclasts dig tunnels through

solid bone, while in trabecular bone, they dig trenches out of the trabeculae undergoing remodelling (van Oers *et al.*, 2008).

2.2.3.4 Reversal

Unlike in bone modelling, bone resorption and formation are tightly coupled (Martin and Sims, 2005; Maes and Kronenberg, 2016). In the reversal phase, resorption transitions to formation. Initiation of the reversal phase occurs with osteoclasts releasing osteogenic signals. Cavities left over from the resorption phase contain multiple mononuclear cell types, such as released osteocytes and preosteoblast cells. Mononuclear cells known as reversal cells are also present within these cavities (Andersen *et al.*, 2013). It is thought that these reversal cells play an important role in the modification of eroded matrix left by osteoclasts during the resorption phase of bone remodelling, which is important in the recruitment of preosteoblasts to the area (Delaisse, 2014).

2.2.3.5 Formation

The final phase is formation of new bone through osteoblastic activity, which can continue for around 4 to 6 months (Hadjidakis and Androulakis, 2006; Clarke, 2008). Initially, osteoblasts deposit collagen rapidly at the site of bone resorption, which is then mineralised. During this process, osteoblasts become embedded within the mineralising extracellular matrix and the transition from osteoblast to osteocyte occurs (Schaffler *et al.*, 2014). The final product of formation is a new osteon (in cortical bone) or hemiosteon (in trabecular bone) (van Oers *et al.*, 2008).

2.2.3.6 Regulation of bone remodelling

During the activation phase, the OPG/ RANKL/RANK pathway is closely regulated by several factors (Hadjidakis and Androulakis, 2006). For example, decreased calcium levels leads to an elevation in parathyroid hormone (PTH) levels. Increased levels of PTH leads to the increased the production of a ligand associated with OPG. This ligand binds to OPG so that RANKL cannot. In this case, RANKL is free to bind to RANK and stimulate bone resorption. Furthermore, high levels of PTH also inhibits the secretion of OPG, lead to the increased likelihood of RANK-RANKL association and hence osteoclast activation. In this way, PTH releases calcium and phosphates into the bloodstream (Sommerfeldt and Rubin, 2001; Carter and Schipani, 2006). Conversely, the introduction of

higher oestrogen levels increases OPG production, inhibiting osteoclast activation. There are several other proteins and cytokines that affect this regulatory mechanism (Manolagas, 2000; Pearson and Lieberman, 2004), some of which can be seen in Table 2.1.

Table 2.1: Effects of different proteins and cytokines on RANKL and OPG production. An increase in RANKL/ decrease in OPG leads to osteoclast activation, while a decrease in RANKL/ increase in OPG leads to osteoclast inhibition (Hadjidakis and Androulakis, 2006).

	RANKL	OPG
Transforming growth factor-β[58]	–	↑
Parathyroid hormone[59]	↑	↓
1,25$(OH)_2$ vitamin D_3[60]	↑	–
Glucocorticoids[61]	↑	↓
Estrogen[62]	–	↑
Basic fibroblast growth factor 2[63]	↑	↓
Prostaglandin E_2[64]	↓	↑

Calcitonin, a hormone produced in the thyroid, has been implicated in the regulation of bone remodelling and maintenance of homeostasis. Calcitonin acts on bone to inhibit osteoclastic bone resorption. Calcitonin binds to a receptor (CTR) located on osteoclasts that impairs the enzyme activity of the cell, reducing bone resorption. Calcitonin has also been implicated in bone formation, with studies identifying that increased levels may have an inhibitory effect, although the mechanism by which this occurs is not well understood (Davey and Findlay, 2013).

Vitamin D is involved in the maintenance of calcium homeostasis and hence, bone mineralisation resorption (Goldberg, 2006; Eisman and Bouillon, 2014). Vitamin D achieves this by stimulating osteoclastogenesis through the RANKL/OPG pathway, increasing RANKL production and leading to osteoclast activation (Baldock, 2006; Hadjidakis and Androulakis, 2006). In cases of decreased levels of serum vitamin D, a decrease in intestinal calcium absorption can be observed, which in turn leads to an increase in PTH levels. As PTH is involved in the activation of osteoblasts and the maturation of osteoclasts, this leads to bone resorption (Holick, 2007). Furthermore, vitamin D deficiency causes muscle weakness and could have a knock-on effect for mechanical stimulation required in the regulation of bone homeostasis (Holick, 2007).

Osteocytes also secrete regulatory factors that help to control bone remodelling (Heino *et al*., 2002). The secretion of TGF-β by osteocytes inhibits

bone resorption. This is modulated by oestrogen and hence osteocytes and oestrogen have an active inhibitory role in the regulation of bone resorption (Heino et al., 2002).

2.3 The development of bone

Skeletal morphogenesis is a ‘highly coordinated, sequential’ process involving the migration, aggregation and condensation of cells followed by organogenesis (Dirckx *et al.*, 2013). The formation of bone can occur via two processes: intramembranous ossification and endochondral ossification (Provot *et al.*, 2012; Maes, 2013; Cunningham *et al.*, 2016; Shahi *et al.*, 2017).

2.3.1 *Intramembranous ossification*

Intramembranous ossification is the formation of dense cortical or diploic bone within the skeleton. Two types of intramembranous ossification exist: dermal and perichondral (Cunningham *et al.*, 2016). Dermal intramembranous ossification describes the process of bone formation from neural crest cells and leads to the development of diploic bone, which forms the majority of the bones of the cranium. The second type of intramembranous ossification, perichondral, forms the cortical shell of bones of the axial and appendicular skeleton. Both types of intramembranous ossification commence with mesenchymal condensations at areas of future bone. Condensations differentiate directly into osteoblasts that deposit bone matrix which is subsequently calcified, burying osteoblasts and initiating their formation into osteocytes (Blair *et al*., 2002; Mackie *et al*., 2008; Maes, 2013; Cunningham *et al.*, 2016).

2.3.2 *Endochondral ossification*

Endochondral ossification begins with mesenchymal progenitor cells forming condensations at sites of bone formation. However, instead of directly differentiating into osteoblasts, these mesenchymal cells differentiate into chondrocytes that deposit an extracellular matrix rich in type 2 collagen and proteoglycans (Blair *et al.*, 2002). A cartilaginous anlage of the developing bone is formed and enlarges through chondrocyte proliferation and extracellular matrix production.

Perichondral ossification, a form of intramembranous ossification, commences through the formation of a bone collar within the perichondrium, a

connective tissue structure surrounding the cartilaginous anlage (Dirckx *et al.*, 2013). Chondrocytes at the centre of the anlage stop proliferating and mature to become hypertrophic. Hypertrophic chondrocytes direct cells within the perichondrium to differentiate into osteoblasts and commence the secretion of extracellular matrix and type 1 collagen. Osteoblasts differentiate directly from perichondral mesenchyme, the initial step in cortical bone formation (Colnot *et al.*, 2004). The formation of the periosteal shell initially prevents nutrient diffusion into the cartilaginous anlage, a process that initiates endochondral ossification. Once endochondral ossification is initiated, hypertrophic chondrocytes produce vascular endothelial growth factor (VEGF) which stimulates angiogenesis, the formation of blood vessels, from the perichondrium into the cartilaginous anlage. Vascularisation of the cartilaginous anlage is a vital step in endochondral ossification as developing vasculature introduces cells such as osteoprogenitor cells, osteoblasts, osteoclasts and haematopoietic cells to the area (Alini *et al.*, 1996; Olsen *et al.*, 2000; Petersen *et al*., 2002; Colnot *et al.*, 2004; Maes, 2013; Jiang *et al.*, 2017). The initial area of osteogenesis is known as the primary ossification centre, and the main artery supplying the primary centre is known as the dominant nutrient artery (Trueta, 1963). Arterial invasion occurs at multiple sites alongside the dominant nutrient artery and brings with it the cells associated with bone formation. These cells begin to lay down bone which extends out from the primary ossification centre. The chondrocytes within the peripheral areas of the cartilaginous anlage begin to proliferate to continue the ossification process. As ossification continues, a multi-layered structure known as the growth plate forms and comprises four zones: the resting zone, the proliferative zone, the transformation zone and the zone of ossification (Figure 2.5) (Burdan *et al.*, 2009; Cunningham *et al.*, 2016). In the resting zone, chondrocytes are unorganised and scattered. The functions of the resting zone are thought to include containment of stem-cells that give rise to cells within the proliferating zone, directing the alignment of cells within the proliferating and hypertrophic zones, and inhibiting terminal differentiation of nearly all chondrocytes in the proliferative zone and hence aid in the formation of the distinctive proliferative and hypertrophic zones found at the growth plate (Abad *et al.*, 2002). In the proliferating zone, chondrocytes flatten out, forming longitudinal columns of rapidly proliferating cells (Burdan *et al.*, 2009). The transformation zone is separated into the hypertrophic zone and degeneration zone (Burdan *et al.*, 2009). In the hypertrophic zone,

chondrocytes mature into hypertrophic chondrocytes, stop dividing and become enlarged. In the degeneration zone, chondrocyte apoptosis occurs, and ossification is initiated by vascularisation and bone cell invasion (Abad *et al.*, 2002). It is also thought that in some cases, chondrocytes differentiate into osteoprogenitor cells rather than undergo apoptosis, and contribute to the formation of new bone tissue, which occurs in the zone of ossification (Hall, 2015). As with intramembranous ossification, once new bone has been laid down, it is then subject to bone modelling and remodelling to achieve its adult morphology.

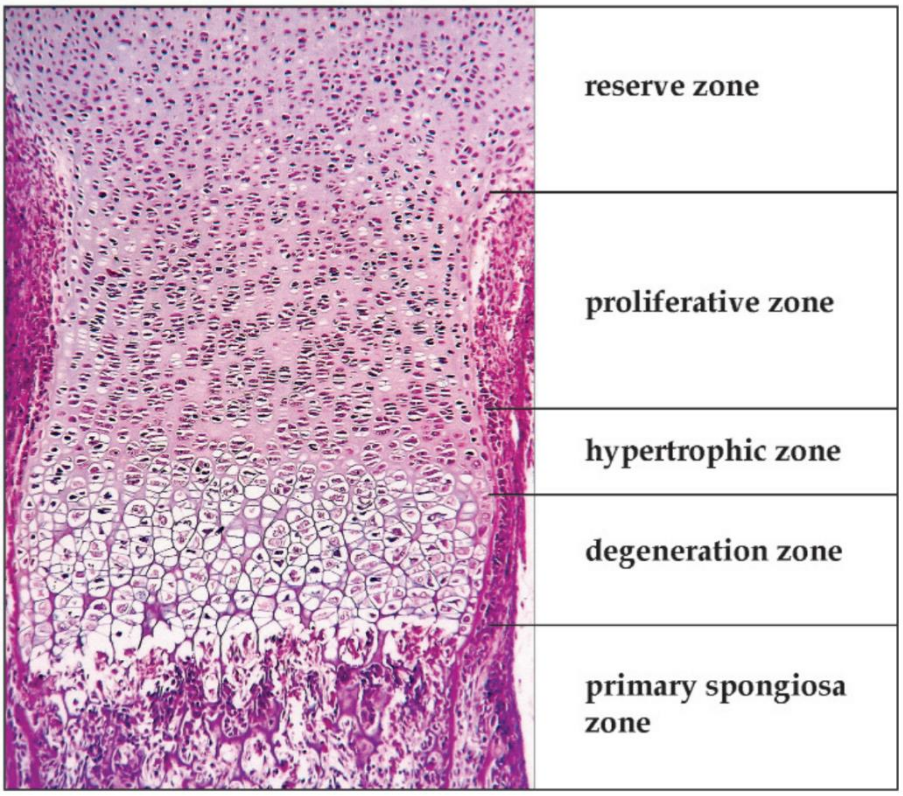

Figure 2.5: A longitudinal histological section of the proximal femoral epiphysis displaying the distinct layers of the growth plate. The reserve, or resting zone, the proliferative zone, the transformation zone (formed of the hypertrophic and degenerative zones) and the ossification zone (primary spongiosa zone) (Burdan et al., 2009).

Eventually, the remaining chondrocytes are restricted to the growth plate ends of diaphysis (the shaft of the long bone), an area known as the growth plate, and drive the process of bone growth through bone lengthening (Byers *et al.*, 2000; Abad *et al.*, 2002). Figure 2.6 presents an overview of the stages of bone lengthening in endochondral ossification.

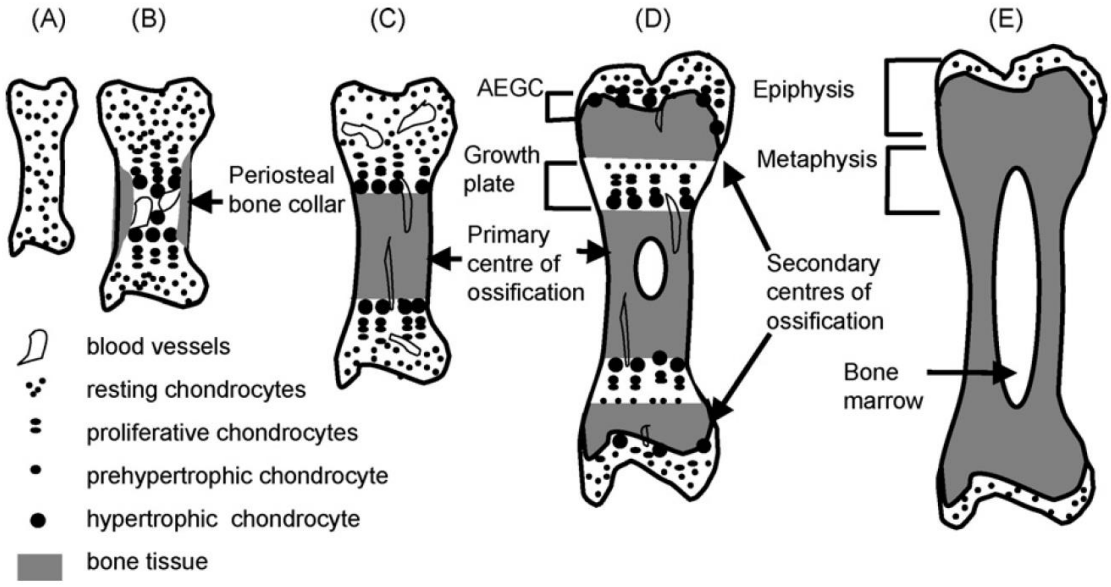

Figure 2.6: A schematic displaying the stages of endochondral formation. At A, the developing bone is present as a cartilaginous anlage. At B, perichondral intramembranous ossification forms a bone collar around the cartilaginous anlage and vascularisation of the anlage occurs. At C, the primary centre of ossification and the growth plate is formed. At D, the secondary centres of ossification have formed and are separated from the primary centre of ossification by the growth plate. At E, the adult structure is displayed (Mackie et al., 2008).

2.3.3 *Postnatal development of bone*

After the initial period of ossification in the fetal period, skeletal growth occurs in two forms: changes in bone size and changes in bone shape (Land and Schoenau, 2008; Acquaah *et al*., 2015). Together, these are termed allometric growth (Gayon, 2000). Allometric growth is achieved through the longitudinal and radial growth of bone (Clarke, 2008). These changes in size and shape occur through the process of bone deposition. Longitudinal growth occurs at the growth plate while radial growth is bought about through periosteal bone apposition occurring at the perichondrium, leading to changes in width (Prentice, 2001).

The growing bone can be separated into sections: the diaphysis, the growth plate and the epiphysis. The diaphysis is the shaft of the bone and includes the primary centre of ossification, the growth plate is the driving force of bone lengthening and is formed of its own layers of proliferating and hypertrophic chondrocytes. The epiphysis is a secondary centre of ossification within the cartilaginous anlage that has its own growth plate and follows the same bone lengthening process as the diaphysis (Mackie *et al*., 2008; Cunningham *et al.*, 2016). The growth plates of both the epiphysis and diaphysis expand towards each other throughout postnatal development and eventually form a single bipolar growth plate. The marrow spaces of the diaphysis and epiphysis are

sealed, and the union of the diaphysis and epiphysis can be detected by an epiphyseal line. Fusion of the epiphysis and diaphysis signals the end of longitudinal growth for the skeletal element in question (Cunningham *et al*., 2016).

The allometric growth seen in the postnatal period is a result of the bone modelling and remodelling that occur in these periods, which are in relation to a number of factors, including, but not limited to: mechanical stimulation, genetics, nutrition and hormonal influences (LeVeau and Bernhardt, 1984).

Infancy, childhood and adolescence have all been identified as important periods for bone growth and development. In particular, infancy and early adolescence have been identified as periods of more rapid growth. Infancy, which encompasses the first three years of life, is characterised by a period of more rapid growth (del Rio *et al*., 1994). Increases in the size and shape of maturing skeletal elements is paired with an increase in bone mineral density (BMD), an indication of the mass of mineralised bone present within a skeletal element (Ay *et al*., 2011). Puberty has also been identified as a period of increased growth, with a significant increase in BMD occurring during this period (del Rio *et al*., 1994). Postnatal growth in infancy, childhood and adolescence have all been found to determine peak skeletal bone mass, with the BMD of lumbar vertebrae observed to peak in the 2nd decade of life (Kneissel *et al*., 1997). A number of factors have been found to affect peak bone mass in childhood and adulthood (Javaid and Cooper, 2002), which can be viewed in figure 2.7. In particular, hereditary (genetic) factors, exercise and mechanical stimulation, and nutritional intake play a role in determining peak bone mass in early life. In later life, while hereditary factors do continue to play a role, this is through the effects caused in early life. However, mechanical stimulation and nutritional availability continue to play a role in the maintenance of peak bone mass in later life, while structural errors such as fractures are also introduced. Furthermore, the environment consistently affects the potential peak bone mass an individual can attain throughout life and comprise factors such as smoking and alcohol consumption.

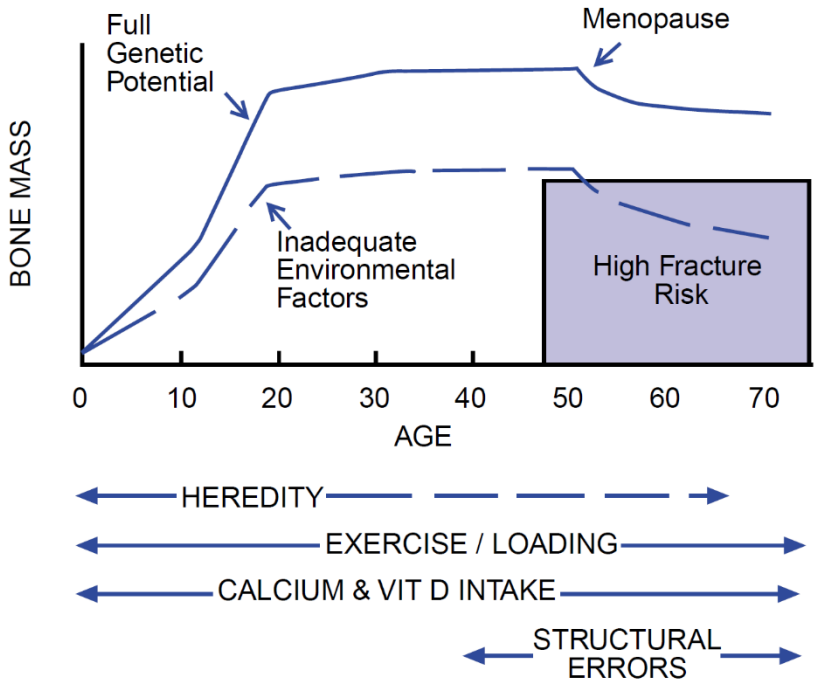

Figure 2.7: Schematic representing the factors that affect peak bone mass with age (Javaid and Cooper, 2002).

2.3.4 *Factors affecting bone development*

2.3.4.1 Genetic Factors

Genetic programming plays an important role in early bone formation and development, while in later life, environmental factors become more important determinants (Cooper *et al*., 1997).

Each step of the process for endochondral ossification is under the close control of genetic factors. An understanding of the genetic control of ossification can be gleaned from gene mutations. The study of gene mutations and the associated abnormalities observed in terms of bone development can give insight into the role particular genes play (Mundlos and Olsen, 1997; Olsen *et al.*, 2000; Karsenty, 2001; Mackie *et al*., 2008; Nishimura *et al.*, 2012; Shahi *et al.*, 2017).

Mechanisms underlying early condensation, segmentation, differentiation and patterning define the precise arrangement of body axes (Dirckx *et al.*, 2013). Initial patterning of the axial skeleton, and control of the initial mesenchymal condensations in areas of future bones is under the control of multiple genes and transcription factors including HOX and PAX genes and members of the transforming growth factor-β (TGF-β) family such as bone morphogenetic

proteins (BMPs) (Mundlos and Olsen, 1997; Olsen *et al.*, 2000; Blair *et al.*, 2002; Mackie *et al.*, 2008; Shahi *et al.*, 2017; Sorrell *et al.*, 2018).

The factors acting on chondrocytes can be separated into three groups: systemic factors such as growth hormone (GH) and thyroid hormone (in the form of triiodothryronine, T3); secreted factors like insulin-like growth factors (IGFs), the Wnt protein family, BMPs, Indian hedgehog (Ihh) and fibroblast growth factors (FGFs); and finally, transcription factors such as SOX9 and Runx2. An overview of these factors and their roles can be seen in Figure 2.8 (Mackie *et al.*, 2008).

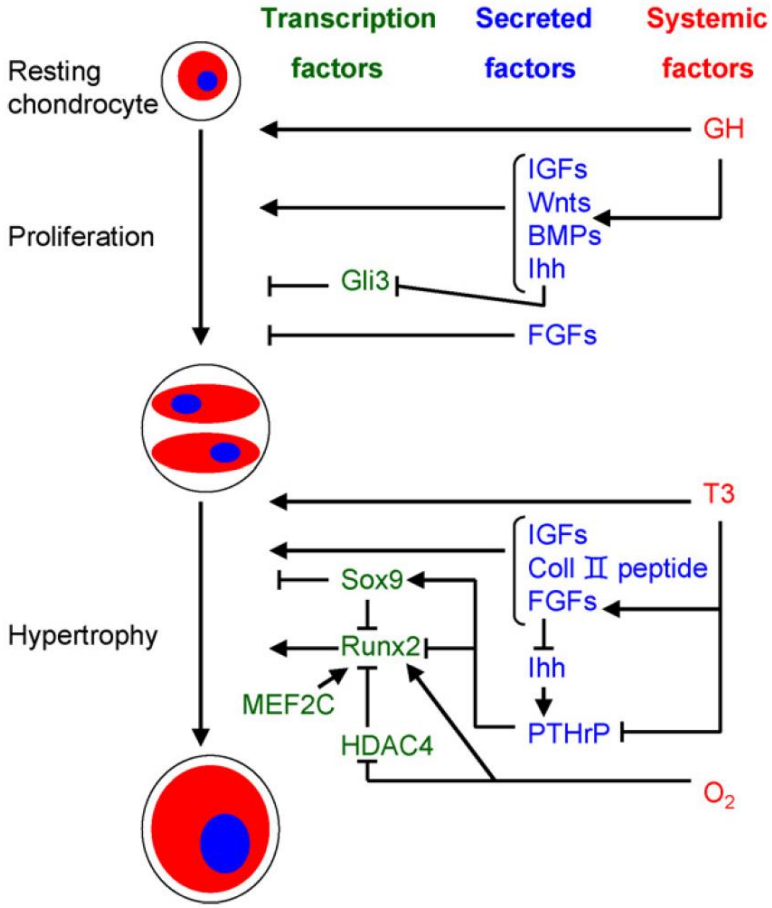

Figure 2.8: Schematic displaying the factors regulating the proliferation and hypertrophy of chondrocytes in the growth plate (Mackie et al., 2008).

It has been concluded that around 60-80% bone mass is heritable, with heredity likely to be polygenic (Prentice, 2001). Some of the many genes implicated in bone mineral accrual and attainment of peak bone mass include receptors for vitamin D, oestrogen, calcitonin and parathyroid hormone (McDevitt and Ahmed, 2014).

2.3.4.2 Nutritional and hormonal factors

Skeletal growth and mineralisation is dependent on nutritional and hormonal factors during gestation, infancy, childhood and adolescence (del Rio *et al.,* 1994).

Peak bone mass and later fracture risk is influenced by nutritional exposures *in utero*, in infancy and during childhood and adolescence. Key nutrients that play a role include calcium, vitamin D, vitamin K, phosphorus, potassium, magnesium, protein and sodium (Specker, 2004; Goldberg, 2006). Calcium has been identified as particularly important in bone development and growth (Agarwal *et al*., 2004; Bachrach, 2001; Greer and Krebs, 2006; Holick, 2007).

Vitamin D has also been identified as important for skeletal development. Sources of vitamin D include exposure to sunlight, and from diet and the production of its active form is closely regulated by levels of calcium, PTH and phosphorus (Holick, 2007). Deficiencies in vitamin D during development and growth leads to rickets, retarded growth and skeletal deformation. Fracture risk may increase in later life. In adulthood, a deficiency leads to osteomalacia, along with increased likelihood of osteopenia and osteoporosis, muscle weakness and fracture risk (Cooper *et al.*, 2005; Holick, 2007). Deficiencies in vitamin D in early life are thought to prevent the maximal mineralisation of bone tissue, and increased deficiency stimulates the parathyroid glands, leading to hyperthyroidism (Holick, 2007). Vitamin D is also involved in the mechanism for angiogenesis and regulation of hypertrophy in chondrocytes. Lack of vitamin D leads to elongated areas of hypertrophic chondrocytes within the growth plate, indicating a lack of angiogenesis (Alini *et al.*, 1996).

Endocrine function has been identified as important in bone development, growth and bone mineral accrual. Prior to puberty, growth hormone plays a significant role in bone development, with deficiencies in growth hormone leading to reduced bone mineral accrual, reduced bone growth and delayed maturation (Bachrach, 2001). At puberty, the introduction of sex steroids, such as oestrogen, at higher concentrations also has a significant effect on bone development, particularly in terms of bone mineral density in the spine, and deficiencies can

lead to a delay in epiphyseal closure in long bones (Bachrach, 2001; del Rio *et al.,* 1994).

The hypothalamic-pituitary-thyroid (HPT) axis plays an important external regulatory role in bone development. In children, hypothyroidism can lead to arrested growth and a delay in bone maturation, while the reverse can cause accelerated growth characterised by short stature and potentially craniosynostosis due to premature closure of growth plates. In adults, hypothyroidism leads to a reduced bone turn over, indicating issues with bone resorption, while hyperthyroidism indicates the opposite (Waung *et al.*, 2012). Thyrotropin-releasing hormone (TRH) is produced by the hypothalamus and stimulates the release of thyroid stimulating hormone (TSH) from the pituitary gland. TSH acts on both the thyroid gland (producing the hormones T3 and T4) and bone tissue. Together, TSH, T3 and T4 all act on a number of tissues, including bone, the gonads and the HPT axis to stimulate the production of hormones important in the regulation of bone, for example oestrogen and growth hormone (Bassett and Williams, 2008).

2.3.4.3 Mechanical Stimuli

The effects of mechanical stimuli on bone maintenance and the mechanisms by which this occurs is discussed in Section 2.4. However, mechanical stimulation has also been implicated in the initiation of osteogenesis (LeVeau and Bernhardt, 1984; Nowlan, 2015; Shea *et al.*, 2015; Verbruggen *et al.*, 2016). Mechanical stimulation in the fetal period is in the form of *in utero* limb movements (Verbruggen *et al.*, 2016) which occur from around 7 weeks gestation and comprise twitching, stretching, whole body movements, isolated limb movements, head and neck movements, and movements of the jaw (Nowlan, 2015). Independent limb movements occur from around the 9th week *in utero* and coincide with the initiation of osteogenesis within the limbs. Any reduction in fetal movements can affect skeletal development, for example in FADS (Fetal Akinesia Deformation Sequence) where a lack of fetal movements leads to thin, hypomineralised bones prone to fracture and spinal abnormalities such as scoliosis (Nowlan, 2015; Shea *et al.*, 2015).

One mechanism by which mechanical stimuli is thought to affect osteogenesis is through the stimulation of hypertrophic chondrocytes. In animal

models with reduced musculature during development, the hypertrophic zone within the growth plate was observed to decrease in size compared to models with normal musculature (Nowlan *et al.*, 2010). Nowlan *et al.* (2012) discovered four genes involved in endochondral ossification to be mechanosensitive: ColX, FGFr3, Ihh and Runx2, all of which are involved in the regulation of chondrocyte hypertrophy (Mackie *et al.*, 2008; Shea *et al.*, 2015). The Wnt signalling pathway, which is involved in embryonic patterning, chondrocyte hypertrophy and osteoblastogenesis, has also been studied and relies on mechanotransduction in its regulation of other signalling factors (Shea *et al.*, 2015). It is also thought that mechanical load stimulates hypertrophic chondrocytes to produce VEGF, stimulating angiogenesis and subsequently endochondral ossification in normal development (Jiang *et al.*, 2017). Decreased fetal movements lead to a decrease in the number of hypertrophic chondrocytes, and no method of stimulation to produce VEGF and initiate osteogenesis.

2.4 Bone adaptation

2.4.1 *The law of transformation*

It is well accepted that form follows function, indicating that the function of a biological material largely determines its form. Bone is no exception and multiple theories exist to explain the mechanical and regulatory processes through which bone tissue succeeds in its many roles. These include Wolff's Law (Lanyon, 1974), the 'mechanostat' theory (Frost, 1996), and bone functional adaptation (BFA) (Ruff *et al.*, 2006).

The introduction of 'The Law of Transformation', simply known as Wolff's Law, in 1892 has led to increased understanding of bone biomechanics. It stated that the structure of bone is closely related to its function, with internal bone trajectories found to adapt over time to mirror the pattern of external mechanical stimuli (Lanyon, 1974; Frost, 2004). While the fundamental framework of Wolff's Law was accurate, the theory was based upon rigid mathematical equations that governed the development of trabecular architecture in weight bearing bones, termed 'Trajectorial theory' (Lanyon, 1974; Ruff *et al.*, 2006). These mathematical equations were based on a number of incorrect assumptions including acceptance that the applied load was static and that bone was a solid, isotropic structure when in reality, applied loads are dynamic and bone is neither solid, nor isotropic. Ruff *et al.* (2006) proposed that the general concept of Wolff's Law

should not be overlooked due to these incorrect assumptions and instead should be considered as ‘Bone Functional Adaptation’ (BFA). Figure 2.9 identifies the key concepts of BFA. Put simply, increased stress leads to the deposition of new bone for structural enhancement, while areas that are under a decreased amount of stress undergo bone resorption.

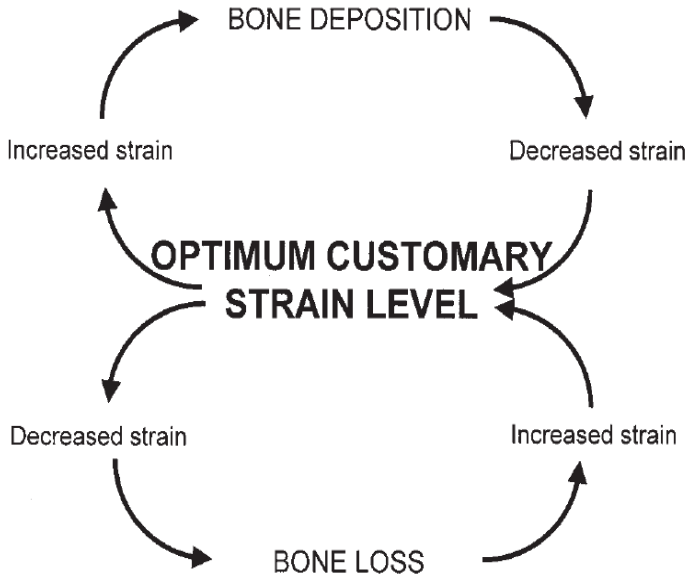

Figure 2.9: A flow chart of the basic concepts surrounding BFA (Ruff et al., 2006).

2.4.2 *Mechanotransduction*

Mechanotransduction is the ‘process by which mechanical energy is converted into electrical and/or biochemical signals (Burger and Klein-Nulend, 1999). In 1881, Roux suggested that local cells regulated the formation and functional adaptation of trabecular architecture (Huiskes, 2000). However, only more recently has this theory been better understood. Similar to Roux’s paradigm, Frost (1996) published the ‘mechanostat’ theory, a homeostatic regulatory mechanism for the adaptation of bone. A negative feedback loop was proposed, with a decrease in strain magnitude leading to bone resorption, and an increase of bone formation. While it was accepted that mechanical stress acted as the stimulus, with osteoblasts and osteoclasts as the effector cells, the sensory mechanism was not well understood (Hughes and Petit, 2010).

It has now been postulated that, at the cellular level, it is the mechanosensory function of osteocytes that leads to bone remodelling (Ajubi *et al*., 1999; Burger and Klein-Nulend, 1999; Aguirre *et al*., 2006; Bonewald, 2007;

Van Oers *et al.*, 2008). As mentioned previously, osteocyte apoptosis is regulated by changes in mechanical loading. It is thought that the fluid-flow model prevents osteocyte apoptosis, and hence, reduced mechanical stimulation leads to osteocyte apoptosis (Aguirre *et al.*, 2006). Osteocytes are surrounded by interstitial fluid-filled lacunae and are connected to one another through dendritic processes (Sommerfeldt and Rubin, 2001; Bonewald, 2007; Burra *et al*., 2010; Prideaux and Bonewald, 2012). Fluid flow explains that, upon the application of mechanical loading, a fluid pressure gradient is formed, and interstitial fluid will move from areas of compression to areas of tension within the lacuna-canalicular network connecting osteocytes and bone lining cells. This interstitial fluid movement is sensed by osteocytes and the mechanical signal is converted into a biochemical signal that stimulates osteoblast movement to the site. If mechanical loading drops below a threshold, osteocyte apoptosis occurs (Ajubi *et al*., 1999; Hughes and Petit, 2010; Qin and Hu, 2014). A number of signal transduction pathways have been hypothesised for the fluid-flow mechanism. One such hypothesis has studied the role of prostaglandins in mechanobiochemical signalling. Prostaglandins were observed to be secreted by osteocytes under fluid-flow and acted as a signalling molecule for the recruitment of preosteoblasts, initiating bone formation (Ajubi *et al.*, 1999; Tian *et al.*, 2008; Burra *et al.*, 2010). Furthermore, in experimental studies, unloading of loaded skeletal elements has been linked to an increase in osteocyte apoptosis through the production of nitric oxide (NO) and increased expression of NO synthases (NOS) (Basso and Heersche, 2006; Vezeridis *et al.*, 2006).

3 Adult Anatomy of the Lumbar Vertebral Column

3.1 Functions of the vertebral column

The skeletal component of the vertebral column consists of 7 cervical, 12 thoracic, 5 lumbar, 5 sacral and between 4 and 8 coccygeal vertebrae (White *et al.*, 2012). The vertebral column as a whole acts to perform numerous functions, most importantly: 1) It facilitates locomotion; 2) It both permits and limits movements such as flexion, extension and rotation along its vertical axis; 3) It is an important site for the attachment of soft tissue; 4) It is a load-bearing structure involved in the transference of weight from the upper body through the pelvic complex and into the lower limbs; 5) It is a site for haematopoiesis; 6) Finally, a significant role of the vertebral column is the protection of the spinal cord and meninges (Palastanga *et al.*, 2002; Moore *et al.*, 2019).

3.2 Osteology of the lumbar vertebral column

While all vertebrae share a basic structure, each region has specific characteristics due to localised regional requirements (Cunningham *et al*., 2016). The basic structure of a human vertebra includes an anterior vertebral body and a posterior neural arch, which together create a vertebral foramen through which neurovascular structures travel (Figure 3.1).

Lumbar vertebrae can be easily distinguished from cervical, thoracic and sacral vertebrae in the adult. The characteristic kidney-shaped bodies of the lumbar vertebrae are the largest of the vertebral column (Ebraheim *et al.*, 2004). The vertebral bodies increase in size from superior to inferior until the level of L5/S1 where they begin to decrease in size (Pal and Routal, 1987; Prakash *et al*., 2007). This shape and size leads to increased surface area to withstand heightened loads, with the fifth lumbar vertebra presenting the largest endplate surface area to accommodate not only increased compression, but also torsion (Boszczyk *et al*., 2001). The shape of the vertebral foramen is also characteristic, with the lumbar region presenting a relatively small and almost triangular shaped foramen (Figure 3.1), due to the spinal cord having ended around the level of L1/L2 and only the cauda equina continuing after this point (Ebraheim *et al*., 2004).

The neural arch of each lumbar vertebra has seven processes extending from it. Four articular processes are present, each with an articular facet. The inferior articular facets of one vertebra will articulate with the superior facets of the vertebra directly inferior to it. In the lumbar region, the superior articular facets face posteromedially while the inferior facets face anterolaterally (Figure 3.1). This orientation is characteristic to this region and is important in maintaining the stability of the articulation between the two facets during load bearing (Ebraheim *et al*., 2004). Unlike other regions of the column, mammillary processes can be found extending from the posterolateral aspect of the superior articular processes in the lumbar region. The mammillary processes are a site of attachment for intrinsic lumbar musculature (Moore *et al.*, 2019). Each vertebra also has two transverse processes extending laterally from the vertebral arch (Figure 3.1). In the lumbar region, these act as areas of attachment for musculature and ligaments and are relatively small and thin compared to other vertebral regions. The transverse processes of lumbar vertebrae may also present an accessory process which, if present, can be found dorsally. Posteriorly, a single process extends from the vertebral arch, the spinous process. In the lumbar region, these are characterised by their size and shape, large and rectangular, and their vertical orientation (Figure 3.1) (Ebraheim *et al*., 2004).

Bilateral regions of bone connect the neural arch to the vertebral body and are called pedicles (Figure 3.1). Their width increases from the first to fifth lumbar vertebra (Ebraheim *et al*., 2004), likely in response to increased load. Differences have been found in both the horizontal and vertical diameters of the pedicles between males and females (Amonoo-Kuofi, 1995) and they have also been identified as important structures in the transmission of load through the vertebral body (Pal and Routal, 1987). The superior intervertebral notch is a small depression on the superior aspect of each pedicle. An inferior notch is also present which is much larger than its superior counterpart. In articulation, these notches form an intervertebral foramen, which primarily facilitate passage of spinal nerves at their associated vertebral level. Posterior to the transverse processes, and connecting them to the spinous process, are the laminae (Figure 3.1). These are relatively thick compared to other regions of the vertebral column and are more vertically oriented, with a roughened surface for ligamentous attachment (Ebraheim *et al*., 2004).

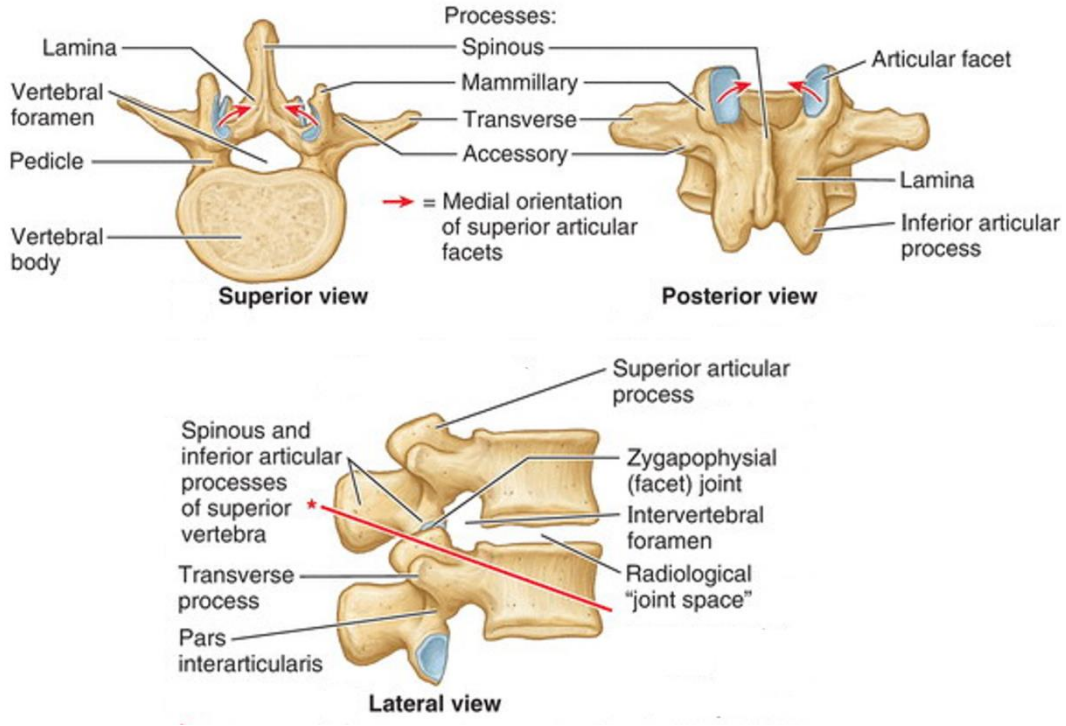

Figure 3.1: The osseous features of a typical lumbar vertebra: Superior, posterior and lateral views (Moore et al., 2019).

On the superior and inferior aspects of each vertebral body sit the vertebral endplates. Each endplate consists of a thicker outer cartilaginous ring and a thinner bony centre. The endplates are thought to aid in the compressive capabilities of the vertebral body (Hou *et al*., 2013).

3.3 Joints of the lumbar vertebral column

Two joint types are present in the lumbar region of the vertebral column. Intervertebral discs are associated with the vertebral bodies of the lumbar vertebrae, while facet joints are associated with the neural arches.

Intervertebral discs are secondary cartilaginous structures consisting of an inner part, the nucleus pulposus, and an outer part of concentric fibrocartilage, the annulus fibrosus (Figure 3.2) (Ebraheim *et al.*, 2004). The annulus fibrosus distributes pressure equally over the disc (Jang and Kim, 2010a), attaching to the epiphyseal rims of the inferior aspect of the superior vertebra, and the superior aspect of the inferior vertebra, with fibres running obliquely to restrict rotation between each vertebra.

Meanwhile, the inner nucleus pulposus is an avascular, gelatinous-like substance that compresses when loaded and hence acts as a shock absorber (Been *et al*., 2010; Jang and Kim, 2010a; Gocmen-Mas *et al*., 2010). Intervertebral discs are thickest within the lumbar region, due to their role in shock absorption, and the transference of load to the lower lumbar vertebral bodies (Been *et al*., 2010; Jang and Kim, 2010a). The mobility of the vertebral column is in part a result of the degree of elasticity and compression of the intervertebral discs (Moore *et al.,* 2019). With increasing age, the intervertebral discs are known to degenerate and lose their absorptive and elastic properties (Jang and Kim, 2010a). The articulation between the intervertebral disc and vertebral bodies of the fifth lumbar and first sacral vertebrae is known as the lumbosacral joint/ junction. The lumbosacral angle is larger than those between lumbar vertebrae due to the angular position of the sacrum, and it is approximately 140° (Palastanga *et al*., 2002).

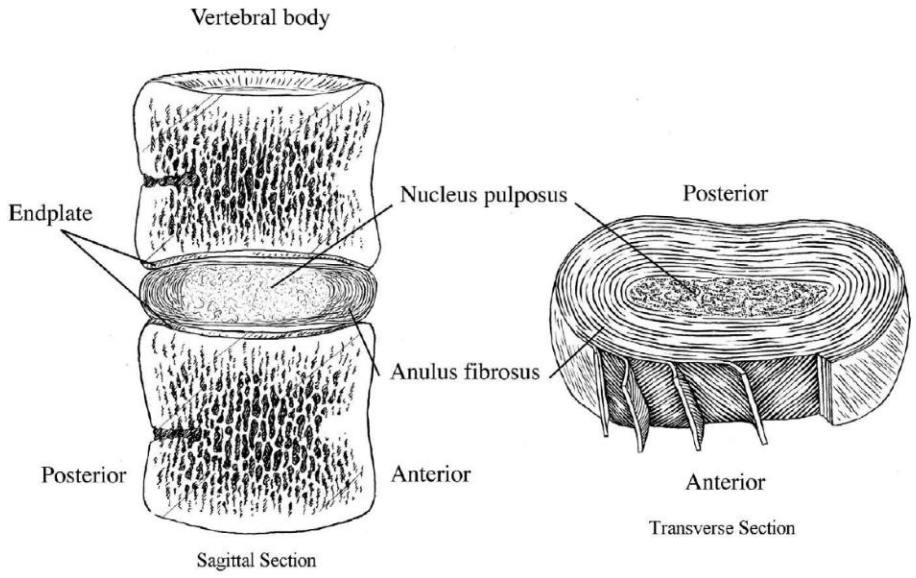

Figure 3.2: Sagittal and transverse sections of an intervertebral disc (Ebraheim et al., 2004).

3.4 Curvatures of the vertebral column

The adult vertebral column is formed of four curvatures. The primary curvatures of the thoracic and sacral regions are concave anteriorly and are known as kyphoses, the secondary curvatures of the cervical and lumbar regions, which develop postnatally, are convex anteriorly (Palastanga *et al*., 2002).

These curvatures are caused predominantly by changes in shape of the intervertebral discs and some contribution from the vertebral bodies, with 90% of the lumbar lordosis due to posterior wedging in the IV discs and 10% due to posterior wedging of the vertebral bodies (Been *et al*., 2010; Sparrey *et al*., 2014). However, age-related changes in the lumbar lordosis are much more likely to be due to lumbar vertebral degeneration rather than IV disc morphology (Sparrey *et al.,* 2014).

The lumbar lordosis is unique to humans and is particularly important in allowing the vertebral column to maintain an upright posture and transfer weight from the upper body through the trunk to the lower limbs (Sparrey *et al*., 2014). The lumbar lordosis in an adult human can range from 30°-80° (Been *et al*., 2010), averaging at around 41° (Adams and Hutton, 1980).

3.5 Movements of the vertebral column

The vertebral column facilitates a range of movements based around a central axis. Movement is complex and depends on musculature as well as osseous structures, ligaments and joints (Colloca and Hinrichs, 2005). The movement of the vertebral column is particularly dependent upon the flexibility of the intervertebral discs (Palastanga *et al*., 2002). Movements include flexion and extension, lateral flexion and extension, and rotation.

The central axis runs vertically from the base of the skull to a point just anterior to the sacrum, known as the ‘centre of gravity of the body’. Due to the curvature of the vertebral column, the line of gravity travels through the centre of each cervical vertebral body, runs anterior to the thoracic vertebral bodies, and directly posterior to the lumbar vertebral bodies, while remaining anterior to the lumbar neural arches. It also passes through the bodies of the second and twelfth thoracic vertebrae, the fifth lumbar vertebra and the sacral promontory before reaching the centre of gravity anterior to the first sacral vertebra (Figure 3.3). This axis does not stay constant, and changes to accommodate movement and bipedalism (Palastanga *et al*., 2002). Pal and Routal (1987) hypothesised that the cervical, thoracic and lumbar regions of the vertebral column bear weight through two separate columns. The anterior column is formed by the vertebral bodies, while the posterior column is formed by the articulating laminae. In the lumbar region, the anterior column bears the majority of load passing through the lumbar

region until the level of the fourth lumbar vertebra, where weight is transferred predominantly to the posterior column.

Movements of the vertebral column as a whole are generated through the accumulation of movements between adjacent vertebrae (Moore *et al*., 2019). Flexion of the vertebral column is the forward bending motion of the column about a transverse axis while extension is the opposing movement (Figure 3.9). This pair of movements occur mainly in the cervical and lumbar regions (Palastanga *et al*., 2002; Moore *et al*., 2019). Lateral flexion, also known as ‘side bending’ is the lateral movement of the vertebral column about an anteroposterior axis (Figure 3.4) (Palastanga *et al*., 2002). Lateral extension is the compensatory movement, returning the vertebral column to its upright anatomical position (Figure 3.4). These movements are also found to occur more in the cervical and lumbar regions (Moore *et al*., 2019). Rotation, or torsion, is the twisting movement of the column about a vertical axis (Figure 3.4), which occurs primarily in the thoracic region (Palastanga *et al*., 2002; Moore *et al*., 2019).

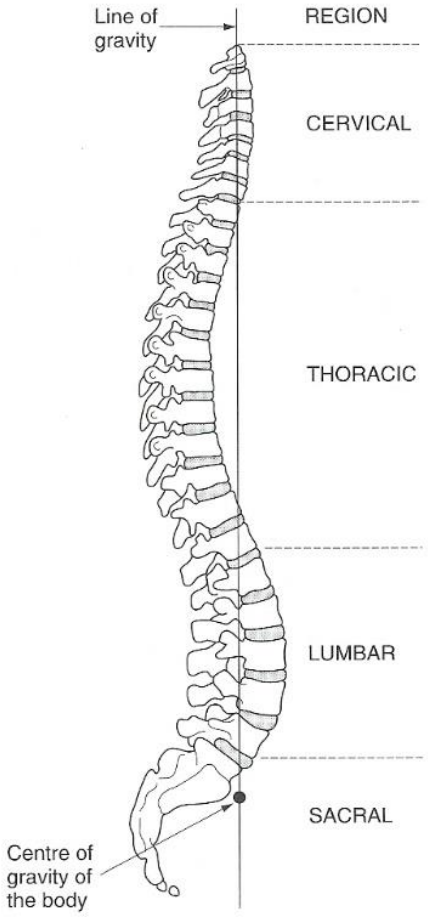

Figure 3.3: An illustration of the line and centre of gravity and their association with the adult vertebral column (Palastanga et al., 2002).

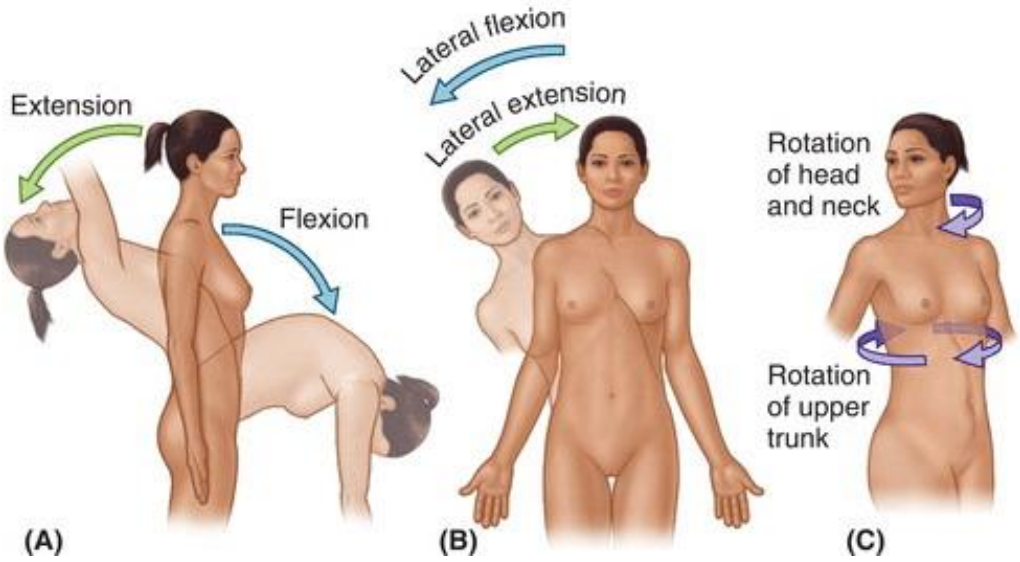

Figure 3.4: Movements of the vertebral column. A) Flexion and extension. B) Lateral flexion and extension. C) Rotation (Moore et al., 2019).

In the lumbar region, the intervertebral discs that help to produce these movements are thicker, restricting movement somewhat, and increasing stability of the column. In particular, the lumbosacral junction is restricted to flexion and extension, allowing only marginal lateral flexion and no rotation. This is, in part, due to the orientation of the facet joints between L5 and S1, along with more extensive soft tissue in this region for further stabilisation of the joint. A small degree of rotation occurs between the lumbar vertebrae, although this is once again restricted by the bony articular facet joints. Similar to the lumbosacral junction, the least restricted movement of the lumbar vertebral column is flexion, followed by extension and lateral flexion (Palastanga *et al*., 2002).

3.6 Musculature of the lumbar vertebral column

The musculature associated with the lumbar region of the vertebral column include the extrinsic and intrinsic muscles of the back and posterior abdominal wall muscles.

The extrinsic group of back musculature consists of a superficial layer involved in the movement of the upper limb and an intermediate layer of accessory respiratory muscles, of which one muscle in each group is associated with the lumbar vertebrae: latissimus dorsi and serratus posterior inferior. The intrinsic muscles of the back act to control the movements of the vertebral column and maintain posture. Only muscles of the erector spinae (Figure 3.5), transversospinales and segmental muscles (Figure 3.6) are associated with the

lumbar vertebrae, more specifically, iliocostalis lumborum (erector spinae), multifidus and rotatores lumborum (transversospinales) and the lumbar intertransversarii and lumbar interspinales muscles (segmental muscle group) (Table 3.1) (Drake *et al*., 2010; Moore *et al*., 2019).

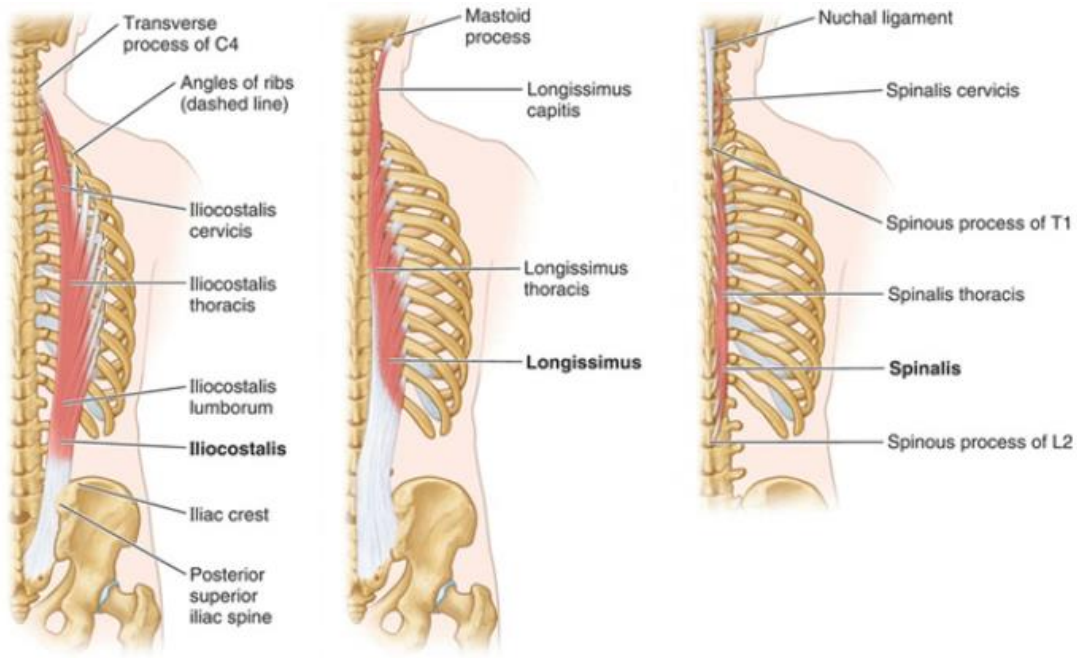

Figure 3.5: An illustration of the three columns of the erector spinae muscle group and their subsections (Moore et al., 2019).

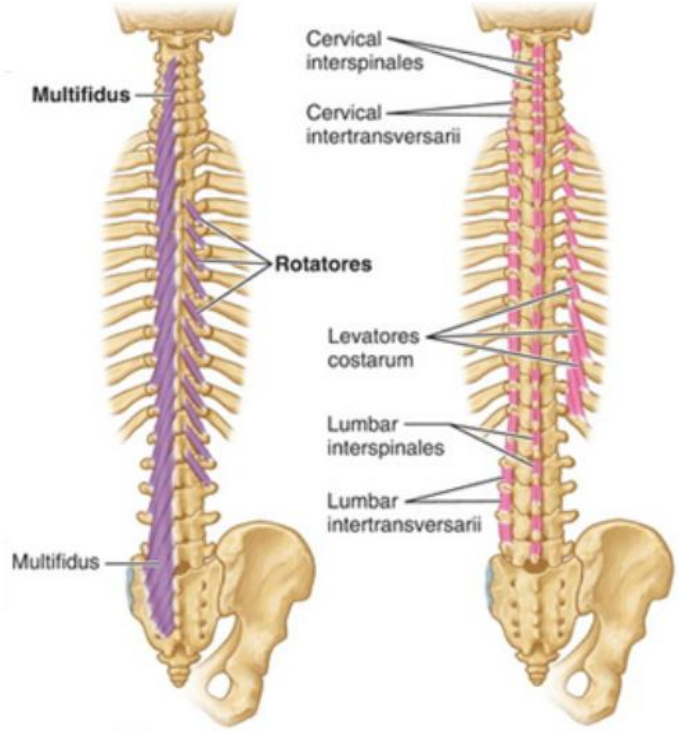

Figure 3.6: Illustration of the transversospinales and segmental muscles (Moore et al., 2019).

Table 3.1: Table summarising the layers of musculature with origins and insertions in the lumbar region. The table also describes the innervation and actions of these muscles (Drake et al., 2010 and Moore et al., 2019).

Layer	Muscle	Origin	Insertion	Innervation	Action
Superficial Extrinsic	Latissimus Dorsi	Spinous processes of T7 to L5 and sacrum, the iliac crest and the 10th to 12th ribs	Floor of the intertubercular sulcus of the humerus	Thoracodorsal nerve	Extension, adduction and medial rotation of the humerus
Intermediate Extrinsic	Serratus Posterior Inferior	Spinous processes of T11 to L3 and the associated supraspinous ligaments	Lower borders of the 9th to 12th ribs (lateral to the angle of the rib)	Anterior rami of the 9th to 12th thoracic nerves	Depression of ribs 9-12
Intrinsic (Erector Spinae)	Iliocostalis lumborum	The sacrum, spinous processes of T11 - L5, the supraspinous ligaments and the iliac crest	Angles of the lower 6/7 ribs	Segmental branches of the posterior rami of spinal nerves	Extension and rotation of the vertebral column
Intrinsic (Transversospinales)	Multifidus	The sacrum, the posterior superior iliac spine, the mammillary processes of L1-5, the transverse processes of T1-12 and the articular processes of C3-7	the base of the spinous processes of all vertebrae from C2 to L5 (individual fibres running supero-medially and spanning between 2 to 4 vertebrae		(Stabilisation of individual vertebrae during movement)
	Rotatores Lumborum	Mamillary processes of L1-5	Spinous process of L1-5 (individual fibres travel superomedially and insert into adjacent vertebrae or span two vertebrae		(Also aid in stabilisation)
Intrinsic (Segmental)	Lumbar Intertransversarri	Run between the transverse processes of adjacent vertebrae			Stabilisation of individual vertebrae during movement of the vertebrae column as a whole
	Lumbar interspinales	Run between the spinous processes of adjacent vertebrae			

It is important to note that other observations have been made in the study of the erector spinae muscle group. Bogduk (1980) observed medial (longissimus thoracis) and lateral (iliocostalis lumborum) divisions of erector spinae in the lumbar region that originated from the iliac crest and an intermuscular aponeurosis, with fibres running superomedially to attach to the accessory and transverse processes of the lumbar vertebrae respectively. However, this finding that iliocostalis lumborum has attachments to the lumbar vertebrae has been argued, with similar studies finding no such insertion (Bustami, 1986). Multifidus fibres primarily act to stabilise individual vertebrae during movement (Moore *et al*., 2019), in particular the deep fibres, while more superficial fibres aid erector spinae in producing extension and rotation movements (MacDonald *et al*., 2006). Psoas major, a muscle of the posterior abdominal wall, has also been observed to attach to the transverse processes of the lumbar vertebrae, as well as the lateral bodies of the 12th thoracic to the fifth lumbar vertebrae and associated intervertebral discs (Stokes and Gardner-Morse, 1999; Jemmett *et al*., 2004; Moore *et al*., 2019).

3.7 Ligaments of the lumbar vertebral column

Ligaments act to support the vertebral column by creating strong bonds between bony features and limiting excessive movements that may cause damage (Drake *et al*., 2010). There are ligaments associated with the bodies of each vertebra, as well as those associated with the neural arch, and finally, a small number that connect vertebrae to adjacent structures.

Two ligaments are associated with the lumbar vertebral bodies. These are the anterior and posterior longitudinal ligaments (Ebraheim *et al*., 2004; Drake *et al*., 2010; Moore *et al*., 2019). A number of ligaments are associated with the neural arches (Palastanga *et al*., 2002; Ahn *et al*., 2014; Moore *et al*., 2019). These include the ligamentum flava, supraspinous ligaments, interspinous ligaments and intertransverse ligaments. Finally, two ligaments act to attach the lumbar vertebral column to other areas: the iliolumbar ligament and the lumbosacral ligament (Nathan *et al*., 1982; Moore *et al*., 2019). The attachment sites and functions of these ligaments can be found in Table 3.2 (Figure 3.7).

Table 3.2: Table summarising the ligaments of the lumbar vertebral column, their attachments, and their functions (Nathan et al., 1982; Palastanga et al., 2002; Ebraheim et al., 2004; Drake et al., 2010; Ahn et al., 2014; Moore et al., 2019).

Ligament	Attachments	Function
Anterior longitudinal ligament (ALL)	Broad fibrous band attaching to the anterolateral aspect of each vertebral body and associated IV discs Originals from the pelvic surface and runs the entire length of the column, terminating at the area of the occipital bone anterior to the foramen magnum and the anterior tubercle of C1	Limits extension of the vertebral column
Posterior longitudinal ligament (PLL)	Thinner fibrous band that (weaker then ALL), attaching to the posterior aspect of each vertebral body and associated IV discs Runs from the posterior body of the C2 to the sacrum	Stabilises the vertebral column in flexion Aids in prevention of posterior herniation of the nucleus pulposus of the IV disc Fixes fatty deposits and vasculature in place between the ligament and the vertebral body
Ligamentum flavum	Passes bilaterally between the laminae of adjacent vertebrae	Acts to resist separation of the laminae in flexion Assist in extension
Supraspinous ligaments	Cord-like extension of the nuchal ligament, attaching to the tips of the spinous processes from C7 to the sacrum	Resists flexion Site of muscle attachment (serratus posterior inferior, iliocostalis lumborum) Stabilises vertebral column
Interspinous ligaments	Between adjacent spinous processes, from root to apex Membranous and weaker than supraspinous ligaments	Resists separation of spinous processes
Intertransverse ligaments	Between adjacent transverse processes. Also membranous and weaker than supraspinous ligaments	Resists separation of transverse processes
Iliolumbar ligament	Originates from L5, fibres radiate out towards anterior aspect of each ilium	Stabilises lumbosacral joint
Lumbosacral ligament	Passes from L5 to the ala of the sacrum	Stabilises lumbosacral joint

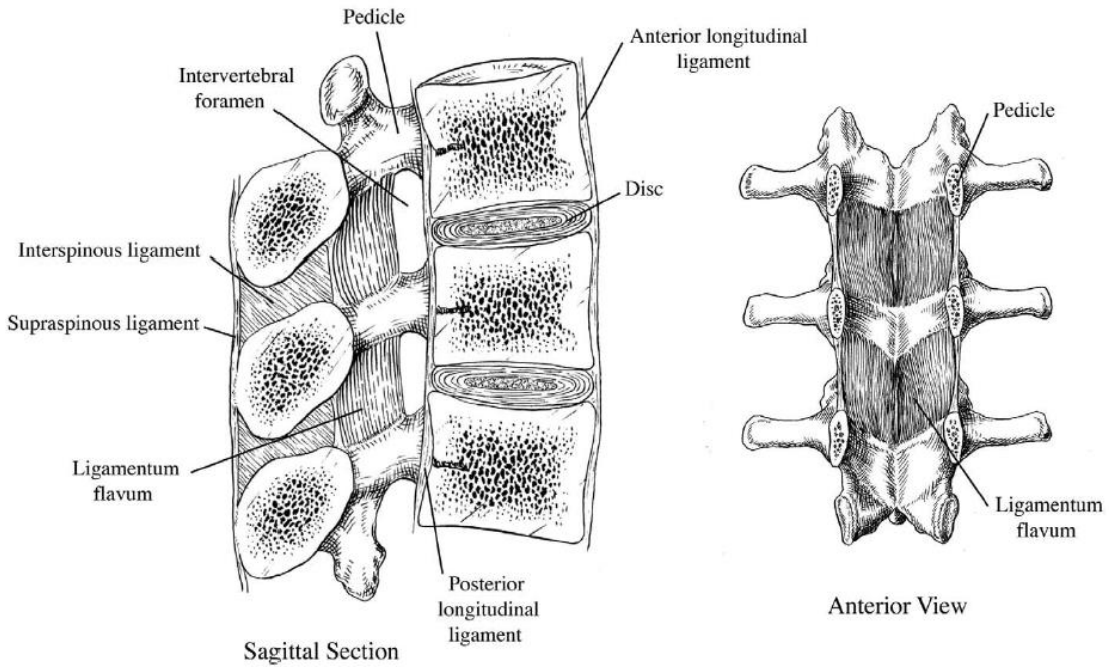

Figure 3.7: Sagittal section and anterior view (with vertebral bodies removed) of the lumbar vertebral column showing the associated ligaments (Ebraheim et al., 2004).

3.8 Neurovascular supply of the lumbar vertebral column

Perhaps one of the most important functions of the vertebral column as a whole is the protection of the spinal cord. The spinal cord is a neural structure extending from the brain stem down to L1/L2. The distal end of the spinal cord, the conus medullaris, is a cone shaped structure that gives rise to nerve roots collectively known as the cauda equina (Ebraheim *et al*., 2004). There is an enlargement of the spinal cord in the lower thoracic/ upper lumbar region due to the lumbosacral plexus, the associated increased mass of nerve fibres travelling to and from the pelvis and lower limbs. Due to the close proximity of the spinal cord to the vertebral column, there are a number of neural structures that are spatially associated with the vertebrae. The spinal cord gives rise to spinal nerves that exit the vertebral column at their associated spinal level. In the lumbar region, the spinal nerves exit below the pedicles of the associated vertebra (Ebraheim *et al.*, 2004). Facet joints are innervated by articular branches of medial branches originating from the posterior rami of spinal nerves, while meningeal branches, also known as sinuvertebral nerves (Adams and Dolan, 2005) supply the

vertebral column, including the periosteum, annulus fibrosus of the intervertebral disc, and ligamentous structures (Moore *et al*., 2019).

The morphology of the lumbar vertebra is heavily influenced by its vascular supply. Multiple vascular foramina of varying size are present on both the anterolateral and posterior surfaces of the vertebral body. Generally, the arterial supply to the vertebral column consists of branches from the abdominal aorta that form a number of arterial anastomoses supplying the vertebral body, arch and spinal cord (Crock, 1996). Supplying the external aspect of the lumbar vertebrae are a number of extra-osseous arteries, while the internal structure is supplied by intra-osseous arteries.

In the lumbar region, segmental arteries arising from the aorta give rise to multiple branches that supply the entirety of the lumbar region. Four pairs of lumbar arteries originate directly from the abdominal aorta. The fifth lumbar vertebra is supplied by the iliolumbar arteries, which arise from the posterior division of the internal iliac arteries. In some cases, rather than being supplied by iliolumbar arteries, the fifth lumbar vertebra is supplied by a fifth pair of lumbar arteries, which originate from the median sacral artery and replace the iliolumbar arteries (Ratcliffe, 1980; Ebraheim *et al*., 2004). These branches will eventually anastomose with, and contribute to, the anterior and posterior spinal arteries that supply the spinal cord (Palastanga *et al*., 2002).

The segmental arteries course around the anterior and lateral aspects of each vertebral body, towards the intervertebral foramina (Figure 3.8) (Ratcliffe, 1980; Crock, 1996), giving branches into and around the vertebral bodies. Periosteal branches (Figure 3.9) supply the periosteum surrounding the vertebrae, while equatorial branches pierce the periosteum and supply peripheral areas within the vertebral body (Moore *et al*., 2019). The main stem of each lumbar artery then continues posteriorly to give further branches which course through their associated intervertebral foramen to supply the spinal cord (Ratcliffe, 1980). The first branches lie on the posterior aspect of the vertebral body and bifurcate into superior and inferior branches, forming an arcade in the floor of the spinal canal. These superior and inferior branches anastomose with their counterparts above and below, meaning the vertebral column receives dual supply from two vertebral levels (Prakash *et al*., 2007). This arterial arcade gives rise to branches that pierce the superior and inferior end plates to become

metaphyseal branches. In the centre, radially directed branches become the nutrient arteries (Figure 3.9), supplying the internal aspect of the vertebral body. Another set of branches lie on the periosteum at the roof of the spinal canal, forming an arcade. Branches from here penetrate the pedicles, the anterior surface of the lamina and the base of the spinous process of the associated vertebra. Other branches give rise to the anterior and posterior radicular arteries (Figure 3.8) supplying the cauda equina and conus medullaris of the spinal cord (Crock, 1996).

The blood supply to the internal aspect of the vertebral body has been found to be highly organised, with different zones supplied by different arterial branches. The most central part of the vertebral body is supplied by anastomosing nutrient arteries, the largest in diameter of the inter-osseous arterial supply (Ratcliffe, 1980). The central periphery is supplied by equatorial branches, while superiorly and inferiorly, these branches are called metaphyseal arteries (Ratcliffe, 1980; Palastanga *et al*., 2002). In the adult some arterial anastomoses are closed off and become end arteries that supply a specific area of the vertebral body. This occurs more frequently within the central area supplied by nutrient arteries, meaning that with increasing age, blood supply to the centre of each vertebral body decreases (Ratcliffe, 1981; 1982).

It is important to consider that the lumbar vertebral column also acts as a site of haematopoiesis (Drake *et al*., 2010). For this reason, there must also be extensive venous drainage to accommodate this function. Within the vertebral body, two venous plexuses are formed by spinal veins. These are the external and internal venous plexuses (Ebraheim *et al*., 2004). The external venous plexus has both anterior and posterior branches, with the anterior branches sitting anterior to the vertebral body, and the posterior branches sitting posterior to the spinous process. These external venous plexuses are connected by the internal venous plexus located within the intervertebral foramen. The internal venous plexus also has anterior and posterior branches. The posterior internal venous plexus sits within the intervertebral foramen, giving branches between the spinous processes that communicate with the posterior external venous plexus. The posterior internal venous plexus also gives an anterior branch into each vertebral body, known as the basivertebral vein. This gives branches that form the anterior internal vertebral plexus within the vertebral body and acts as a

communication between the plexus and the anterior external venous plexus (Figure 3.9) (Moore *et al*., 2019).

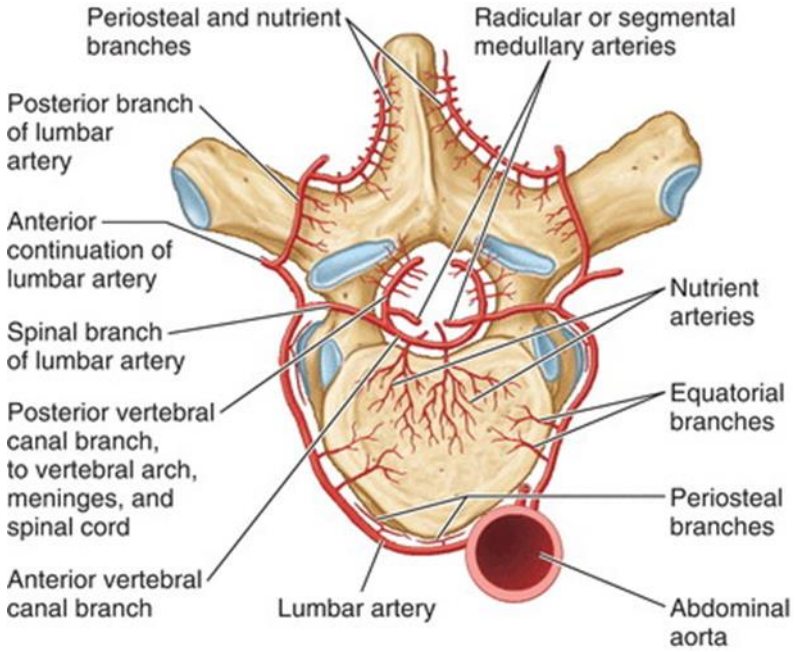

Figure 3.8: An illustration of the arterial supply of a lumbar vertebra (Moore et al., 2019).

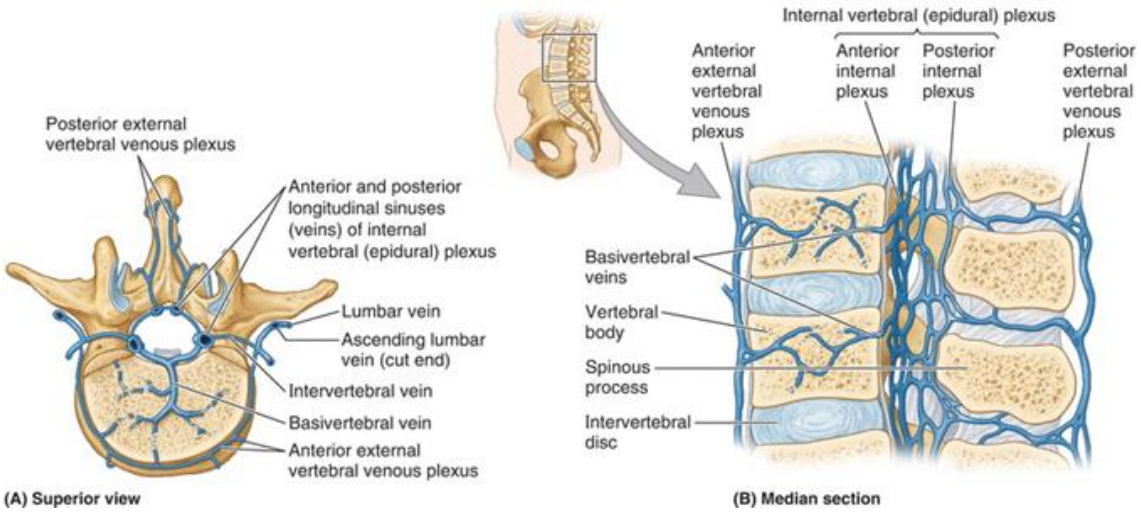

Figure 3.9: Illustration of the venous drainage of the lumbar vertebral column (Moore et al., 2019).

3.9 Functional anatomy of the lumbar vertebral column

3.9.1 *Forces acting on the lumbar vertebrae*

Due to the vertebral column's vital role in movement along with transmission of body weight from the trunk to the pelvic complex, it is appropriately designed to accommodate axial loading (Briggs *et al*., 2004). Compressive forces, a result of axial loading, are the largest forces that act upon the lumbar vertebral column. The position and activity of the body greatly affects the load that passes through the lumbar vertebral column (Briggs *et al.*, 2004). During erect standing, the human vertebral column is under direct compression (Ferguson and Steffen, 2003) and this force can increase with movement, for example from sitting to standing and from standing to flexion (Briggs *et al.*, 2004). The anatomy of the lumbar region is optimised to withstand this, and the vertebral bodies, intervertebral discs, lumbar lordosis and musculature all play a role in this (Davis, 1959; Adams and Hutton, 1980; Vaz *et al.*, 2002; Daggfeldt and Thorstensson, 2003; Briggs *et* al, 2004; Adams and Dolan, 2005; Barrey *et al.*, 2013).

The lumbar vertebral column is also subject to loads beyond axial compression. Finite element analysis (FEA) can be utilised to apply different loads to computerised models of the lumbar vertebral column to understand how these loads are transferred through the vertebral body (Smit, 1996; Smit *et al*., 1997; Daggfeldt and Thorstensson, 2003; Gong *et al*., 2007; Cristofolini *et al.*, 2013). Smit (1996) applied seven loads (lateral shear force, anterior shear force, axial compression, flexion, extension, side bending and axial torsion) to a computerised vertebral model and found that axial compression was the principle vertebral stress, and rather than respond to shear and torsional forces directly, these loads were transformed into compressive and tensile forces (Smit *et al*., 1997). For example, in the case of axial torsion, horizontal compression acted on the posterior aspect of the vertebral body in close association with the pedicle. This indicates that in axial torsion, the facet joints translate this force, a finding that had previously been proposed by Adams and Hutton (1980). The facet joints are involved in force resistance and stability of the lumbar vertebral column and are responsible for resisting shear and torsion, as well as some compressive strength during spinal extension (Boszczyk *et al*., 2001; Adams and Dolan, 2005).

The lumbar vertebral end plates play a significant role in the ability for the lumbar vertebral bodies to withstand compressive forces through axial loading (Ferguson and Steffen, 2003; Hou *et al.*, 2013). Figure 3.10 displays the mechanical properties of the end plate in a lumbar vertebra. Endplate strength has been found to be greatest posterolaterally, at the region of the pedicles, while central areas display lower mechanical strength (Ferguson and Steffen, 2003). Meanwhile, the IV discs play an important role in the even dissipation of compressive loads over the vertebral bodies. Normally, the vertebral body and pedicle is the area of the vertebra under the most axial loading and hence the majority of compressive forces travel through this region. However, in individuals with degenerated IV discs, compressive loads cannot be dissipated evenly over the vertebral body and the pedicles and neural arch become more axially loaded (Figure 3.11) (Adams and Dolan, 2005).

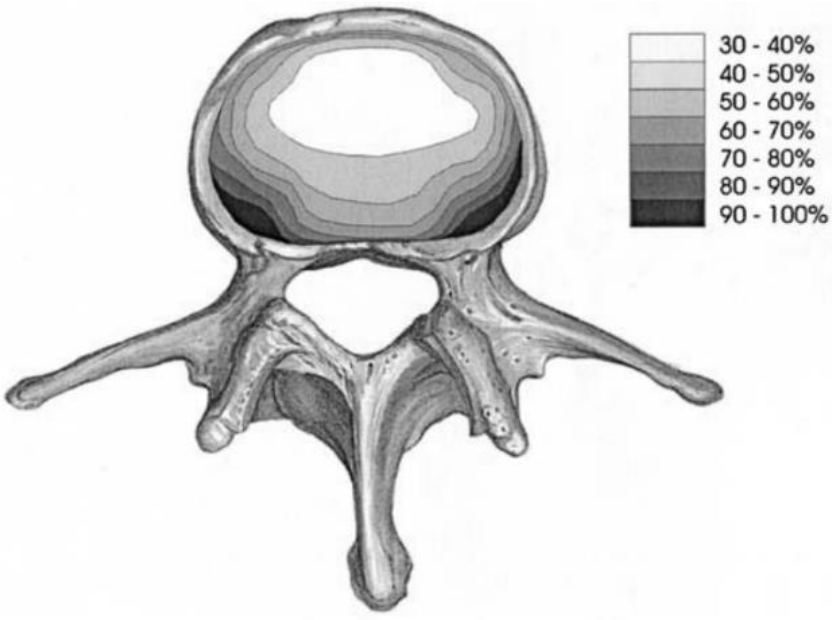

Figure 3.10: Percentage values for mechanical strength at different areas of the lumbar vertebral end plate (Ferguson and Steffen, 2003).

…

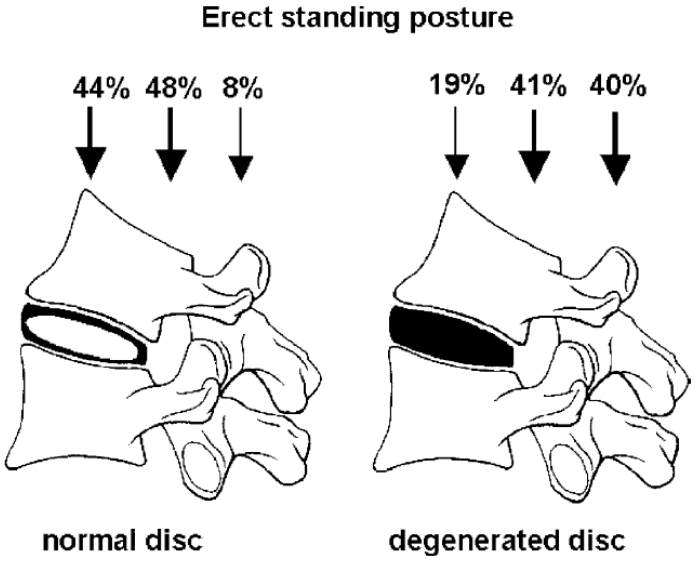

Figure 3.11: The percentages of compressive loading acting upon the lumbar vertebral bodies in individuals with normal IV disc anatomy and individuals with degenerative IV discs (Adams and Dolan, 2005).

Finite element analysis can also indicate how the musculature that surrounds the lumbar vertebral column acts upon the skeletal structures. The muscles (and muscle groups) surrounding, originating from and attaching to the lumbar region all act to produce movement in the region as well as support the column as it undergoes specific movements or is placed under particular stresses (Daggfeldt and Thorstensson, 2003).

Finite element modelling (FEM) has distinguished that placing the lumbar vertebral column in flexion translates to axial compression placed on the lumbar vertebral bodies, specifically at the posterior aspect, as well as producing anterior shear forces which are translated into compression at the pedicles. Flexion of the lumbar spine is not produced by musculature within the back but is instead characterised by their relaxation (Colloca and Hinrichs, 2005). Biomechanically, the extensor muscle groups associated with the lumbar vertebral column, such as the erector spinae, have short levers. During flexion of the spine and the relaxation of this muscle group, these muscular levers lengthen, applying a tensile force to the lumbar vertebral bodies (Daggfeldt and Thorstensson, 2003; Briggs *et al*., 2004). Meanwhile, when the extensor muscles of the back contract to produce extension of the lumbar vertebral column, the forces produced are translated into axial compression in the central region of the vertebral body (Smit

et al., 1997). Another load placed upon the lumbar vertebral column is axial torsion, or shear force, which is translated into compressive force by the pedicles. Axial torsion/ shear forces are produced through rotational movements commonly created during the normal human bipedal gait cycle and are produced by muscles of the posterior abdominal wall (Smit *et al*., 1997; Boszczyk *et al.*, 2002). Changes in the lumbar lordosis can affect the force output by musculature. If the lumbar lordosis becomes more kyphotic in nature, intramuscular pressure is found to increase, which in turn leads to increased muscular tension and increased force placed upon bony attachment sites within the lumbar vertebral column (Briggs *et al.*, 2004).

While finite element analysis enables researchers to study how trabecular architecture is affected by the loads placed upon it, along with how these loads are produced, it does have a number of limitations. Firstly, in studies that consider the effects of muscular force on bone, many models are simplified. For example, multiple muscles are considered as a single muscular mass. This leads to a simplification of the forces placed upon the bones within the model as while muscle compartments generally act together to produce the same movement, each muscle within a muscle group often has a secondary function that may place different forces onto the skeletal element in which it attaches (Daggfeldt and Thorstensson, 2003). Secondly, finite element modelling of the skeletal aspect of the model within FEA studies can also be simplified or inaccurate. For some studies, the model is based on a bone sample, or bone cube. These smaller sections of bone may not act in the same way as the whole bone, or a collection of bones in the case of the lumbar vertebrae. It has already been found that the end plates play a significant role in distribution of force, and the cortical shell is also involved. A lack of these structures within a model would lead to more inaccurate force distribution over the cube of trabecular bone. In studies where the whole bone has been modelled, while more accurate results can be gleaned, limitations still exist. For example, Smit (1996) created a finite element model of a stack of lumbar vertebrae, however, all vertebrae within the stack were based on L4. As there has been inconclusive research on whether trabecular architecture differs between lumbar vertebral levels, the accuracy of this model is questionable. That being said, as our knowledge of trabecular architecture within the lumbar vertebral column improves and technology continues to

advance, improvements in finite element models can be made and though each model created has its inaccuracies, their analysis continues to improve understanding.

3.9.2 *The trabecular architecture of the lumbar vertebrae*

3.9.2.1 Regional changes in trabecular architecture

Lumbar vertebral bodies show a complex and variable internal pattern consisting mainly of horizontally and vertically aligned trabeculae, with the central region differing in architecture to the superior and inferior regions (Figure 3.12). The central region displays a lower number of thick and well-spaced trabeculae, while the endplates display a larger number of thinner, less separated trabeculae (Amstutz and Sissons, 1969; Whitehouse *et al.*, 1971; Kneissel *et al*., 1997; Thomsen *et al*., 2002a). While the trabeculae within the central region are predominantly vertical, horizontal trabeculae are also present, with both orientations thicker in the central compared to endplate regions (Thomsen *et al*., 2002a). The superior and inferior areas appear denser than the central area, due to horizontally oriented trabeculae in a closer arrangement.

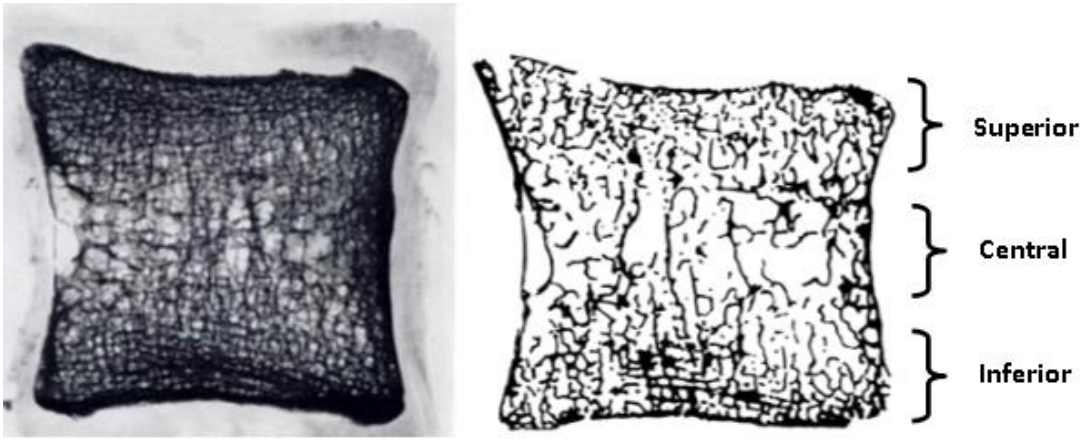

Figure 3.12: Left: Radiograph of a slice of lumbar vertebral body. Right: Outline drawing of a histological section with the central, superior and inferior regions labelled (Adapted from Amstutz and Sissons, 1969).

The central region displays predominantly vertically oriented trabeculae arranged in relation to the compressive forces placed upon it (Amstutz and Sissons, 1969; Whitehouse *et al.*, 1971; Kneissel *et al*., 1997; Thomsen *et al.*, 2002a). While fewer trabeculae are present in this region, likely due to lack of

occupiable free space between vascular structures and bone marrow, the trabeculae within the region are reinforced both by horizontal struts and a thicker, predominantly plate-like structure (Thomsen *et al*., 2002a). These parameters have been linked to bone strength (Ding *et al*., 2002; Liu *et al*., 2008; Nazarian *et al*., 2008). This is not the only example of trabecular architecture following the trajectory of load bearing and has been observed in early communications (von Meyer, 1867; Wolff, 1892). The trabecular architecture of load bearing bones such as the femur is also arranged in response to stress distribution placed upon them (Jang and Kim, 2008; Hammer, 2015).

The lumbar vertebral end plates play a significant role in the ability of the lumbar vertebral bodies to withstand compressive forces through axial loading (Ferguson and Steffen, 2003; Hou *et al.*, 2013). Vertebral compressive strength tests have revealed that the endplates are important in withstanding compressive forces (Grant *et al*., 2001). This was corroborated by removal of the vertebral endplates, particularly in peripheral areas, leading to a decrease in compressive vertebral strength (Hou *et al*., 2013). The inferior end plate has been found to be more mechanically strong than its superior counterpart (Grant *et al*., 2001) with the inferior end plate found to contain a higher number of trabeculae and hence a denser structure than the superior region (Banse *et al*., 2001; Gong *et al*., 2005).

The trabecular architecture of the posterior aspect of the lumbar vertebral body has been observed to be denser, with a higher number of closely associated trabeculae, than the anterior and central regions (Chen *et al*., 2008), in particular the superior half of the posterior region, attributed to its association with the pedicles (Banse *et al*., 2001). As endplate strength has been found to be greatest posterolaterally, at the region of the pedicles, this trabecular architecture is unsurprising (Ferguson and Steffen, 2003).

Another important discovery was that bone volume fraction and trabecular number are lower in lower lumbar vertebrae such as L4 compared to upper lumbar vertebrae, while trabecular separation is higher, indicating a less dense and more separated trabecular structure in the lower regions (Banse *et al*., 2001). The number of horizontal trabeculae has also been found to decrease between L1 and L5 (Buck *et al*., 2002).

3.9.2.2 Age and sex related changes in trabecular architecture

The prevalence of osteoporosis among aging individuals is increasing, and its recognition as a developing health problem is increasing (Briggs *et al*., 2004; Bauer and Link, 2009; Parkinson *et al*., 2012; Giambini *et al*., 2014; Maquer *et al*., 2015). Osteoporosis is a reduction in the amount of bone tissue of an individual, leading to a weaker, damaged trabecular structure and increased fracture risk (Agarwal *et al*., 2004; Briggs *et al*., 2004). By understanding the changes that occur in aging and the characteristics of osteoporotic bone, diagnosis and treatment can be more efficient (Guo and Kim, 2002). Hence, a plethora of studies have used histomorphometric parameters to compare quantitatively healthy, aging and osteoporotic bone specimens.

When inspected visually, the trabecular architecture of vertebrae from younger individuals differs significantly from older specimens. While a clear difference between the central region and the endplate region is easily identifiable in younger specimens, this difference is less obvious in older individuals (Figure 3.13) (Kneissel *et al*., 1997; Thomsen *et al*., 2002a). When assessed quantitatively, bone volume fraction and trabecular number decrease with age, while trabecular separation increases (Kneissel *et al*., 1997; Thomsen *et al*., 2000, 2002a; b; Jang and Kim, 2010). Connectivity has also been shown to decrease, most likely due to the loss in number of trabeculae (Kneissel *et al*., 1997; Thomsen *et al*., 2000; Guo and Kim, 2002; Thomsen *et al*., 2002b; Chen *et al*., 2008). Assessment of the structural model index has shown a shift from plate-like trabeculae in younger individuals to more rod-like trabeculae in older individuals. Plates are considered to be stronger and more efficient in weight-bearing than rods, which may explain the decrease in strength of vertebrae and increase of fracture risk with age (Kneissel *et al.*, 1997; Roschger *et al.*, 2001; Chen *et al*., 2008; Thomsen *et al.,* 2013).

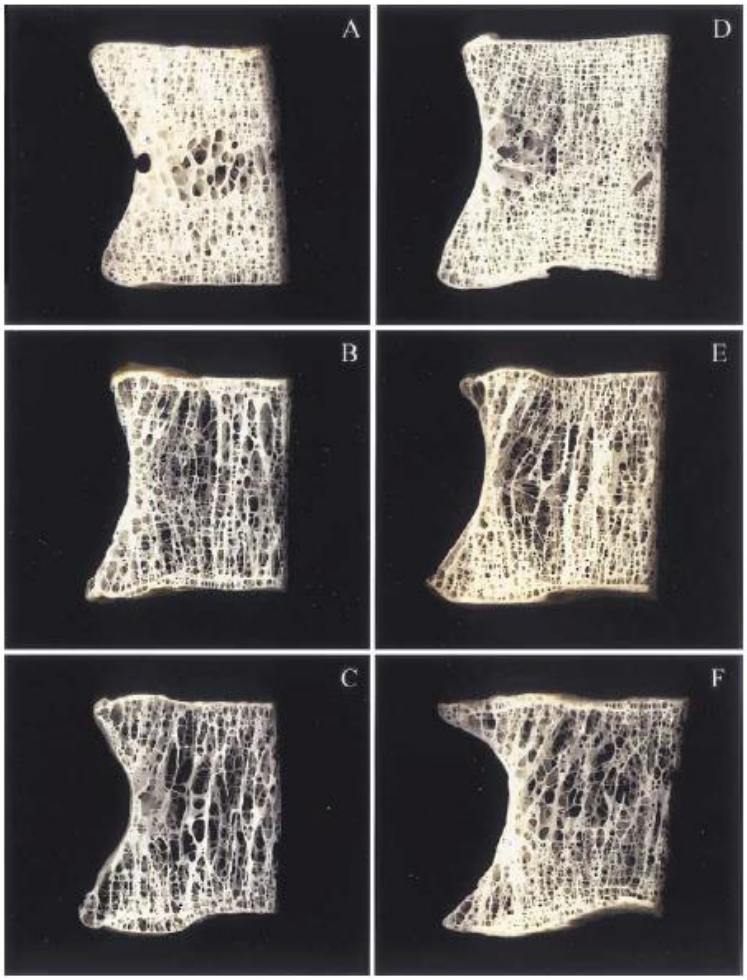

Figure 3.13: Photographs A, B and C show female individuals at the ages of 37, 72 and 81 years respectively, while D, E and F are male specimens of ages 24, 74 and 80 years respectively (Thomsen et al., 2002a).

The literature shows an inconsistency of findings in this area. This could be due to the population tested, for example, Kneissel *et al*. (1997) studied a Nubian population dating back to between the 6th and 10th century AD and noticed that degeneration occurred more rapidly than in studies of modern populations. Furthermore, the majority of aging studies are cross-sectional, meaning that they do not test the pattern of aging within a single individual, but compare individuals of different ages. Finally, the varying sizes of regions of interest tested between studies may also cause inconsistencies (Thomsen *et al*., 2000). Trabecular thickness has been found to both decrease with age (Kneissel *et al*., 1997; Thomsen *et al*., 2000; 2002a) and to be independent of age (Agarwal *et al*., 2004; Gong *et al.,* 2005). These findings are of particular importance as current treatments for osteoporosis include parathyroid hormone (PTH) which acts to increase trabecular thickness (Guo and Kim, 2002). However, in computer

simulations, it has been found that a decrease in the number of trabeculae is more detrimental than a decrease in thickness (Guo and Kim, 2002). Some have assumed that a loss in trabecular number must lead to a compensatory mechanism, most likely an increase in the thickness of remaining trabeculae. However, Thomsen *et al*. (2002b) could not verify this and stated that the reason trabecular thickness is not affected significantly may be because only the thinnest trabeculae are lost. Moreover, increasing trabecular thickness may not be the only compensatory mechanism, an increase in cross-sectional area would also increase vertebral strength and stability.

Age related changes have been found to be region-dependent. Differences have been found in the degeneration of horizontal and vertical trabeculae. In younger individuals, the ratio of vertical to horizontal trabeculae is 2:1, while in older individuals, this increases to 5:2, and while overall, more vertical trabeculae are lost over time, the relative loss for horizontal trabeculae is larger (Thomsen *et al*., 2002b) likely due to the decreased thickness of horizontal trabeculae when compared to vertically oriented struts. In the comparison of the central and endplate regions of the vertebral body, bone volume fraction and trabecular number have been found to decrease more at the endplates (Thomsen *et al*., 2002a). Additionally, these two parameters also decrease more in peripheral areas, in particular at the anterior region of the vertebral body (Gong *et al*., 2005). While overall, Gong *et al*. (2005) found trabecular thickness remained constant with aging, the central region showed a decrease in trabecular thickness while trabeculae in the anterior and posterior regions increased. Given these findings, it is appropriate to conclude that changes in vertebral structure are both age and region dependent (Thomsen *et al*., 2002a; b).

Another contradictory finding in the literature is whether there are differences between the sexes. While some have discovered none (Thomsen *et al*., 2002b), Kneissel *et al*. (1997) found that females presented a less dense, less connected trabecular structure compared to males. This was corroborated by Banse *et al*. (2001) who also identified that females had more rod-like trabeculae and higher trabeculae separation. It has also been argued that sex differences occur with aging. Some have found that female individuals display quicker degeneration (Thomsen *et al*., 2013) while others have found that the connectivity of the male structure decreases more compared to females (Agarwal *et al*., 2004).

Finally, a number of studies have found no link between sex and aging (Thomsen *et al*., 2002a; b). These contradictions may be due to overall sample size, or an uneven distribution between male and female specimens within the sample (Agarwal *et al*., 2004).

4 The Development of the Lumbar Vertebral Column

4.1 Early embryological development

4.1.1 *Gastrulation and notochord development*

Gastrulation is the formation of the trilaminar embryonic disc. Three distinct germ layers, the ectoderm, mesoderm and endoderm, are formed from the epiblast. This process occurs in the third week of gestation (Kaplan *et al.*, 2005; Sadler, 2019).

Formation of the notochord begins with prenotochordal cells invaginating the primitive node and migrating in a cranial direction towards the prechordal plate. As the three germ layers develop and the hypoblast is gradually replaced with the endodermal cell layer, these prenotochordal cells separate from the endoderm and form a solid cord like structure, the definitive notochord. This will develop into the axial skeleton. The cranial end of the notochord begins its development first, while the caudal region develops later (Kaplan *et al*., 2005; Sadler, 2019) The notochord will later regress in the region of the lumbar centra, however it plays an important role in both the segmentation of the vertebral column and the development of the intervertebral discs before commonly regressing after birth (Carlier, 1890; Musgrove, 1891; Fleming *et al*., 2001; Fleming *et al.*, 2004; Forero *et al.*, 2018).

4.1.2 *Neurulation*

Neurulation is the formation of the neural tube, the future brain and spinal cord (Detrait *et al*., 2005; Bassuk and Kibar, 2009). Primary neurulation is the formation of the neural tube from the neural plate. The presence of both the notochord and prechordal mesoderm induces the formation of the neural plate by thickening the ectoderm in close proximity. The cells of the plate become known as the neuroectoderm. At the end of the third week, and hence the start of the embryonic period, the lateral edges of the neural plate begin to elevate to become neural folds and consequently, a neural groove between them. These folds begin to migrate towards each other, eventually meeting and fusing in the midline. This fusion occurs in the cervical region around the 5th somite (Detrait *et al.*, 2005). Failure of fusion leads to neural tube defects such as ancephaly and spina bifida and is thought to be under genetic and environmental control (Northrup and Volcik, 2000; Gelineau-van Waes and Finnell, 2001; Detrait *et al*., 2005; Bassuk

and Kibar, 2009; Petronic *et al.*, 2011). A number of theories exist in relation to the fusion of the neural tube. One theory states that fusion occurs first in the cervical region, and continues bidirectionally, with the cranial neuropore closing first, while a second theory proposes that closure of the neural tube occurs simultaneously in multiple areas of the tube (Northrup and Volcik, 2000). Ultimately, the cranial neuropore is the first to close, occurring at around day 25, when 18-20 somites have formed. Subsequently, the caudal neuropore closes around day 28, at the 25-somite stage. This event marks the completion of primary neurulation, with the developing central nervous system represented by a closed tube, narrow at the caudal end denoting the future spinal cord, and broader in the cephalic region with characteristic dilations called brain vesicles. Secondary neurulation consists of a secondary neural tube arising from the tail bud of the primitive streak at the caudal end of the embryo. Cells proliferate, undergo condensation and finally cavitation and fusion with the neural tube formed by primary neurulation (Bassuk and Kibar, 2009).

During the folding of the neural tube, a number of cells at the lateral border and crest separate from their counterparts. These are known as neural crest cells. These cells undergo a transition from epithelial type cells to mesenchyme, which is a loosely organised embryonic connective tissue. The neural crest cells migrate along two different pathways. The first is a dorsal pathway where cells enter the ectoderm through small perforations in the basal lamina. These cells become melanocytes within the skin and hair follicles. The second pathway is in a ventral direction and travels through the anterior half of each somite, developing into cells of the nervous system such as Schwann's cells. The craniofacial skeleton is also formed from neural crest cells (Bassuk and Kibar, 2009; Cunningham *et al.*, 2016; Sadler, 2019)

The ectodermal germ layer is a precursor for a number of tissues including the central and peripheral nervous systems, sensory epithelium of the of the ear, nose and eyes, the epidermis as well as glands such as subcutaneous, mammary and pituitary (Sadler, 2019).

The mesodermal layer begins as a thin sheet of loose woven tissue flanking the notochord in the midline (Kaplan *et al.*, 2005). Cells closest to the midline proliferate to form the paraxial mesoderm. More lateral to this, the remaining mesoderm is known as the lateral plate. The lateral plate is divided into

two layers by the establishment of intercellular cavities. The layer continuous with the mesoderm covering the amnion is known as the lateral plate, or somatic, mesoderm. The second layer, continuous with the mesoderm enveloping the secondary yolk sac is known as the visceral, or splanchnic, mesoderm. Finally, intermediate mesoderm connects the lateral plate and paraxial mesoderm. The intermediate mesoderm differentiates into urogenital structures. The lateral plate mesoderm differentiates into parietal/somatic and visceral/splanchnic layers. The parietal mesoderm pairs with the ectoderm to form the lateral body wall folds, going on to form the dermis of the skin in the body wall and limbs, as well as bony and cartilaginous limb tissue (Sadler, 2019).

4.1.3 *Segmentation and resegmentation*

The paraxial mesoderm becomes a segmented, organised structure within the third week of gestation. Each segment is known as a somitomere, and their formation is known as somitogenesis (Sadler, 2019). Appearance of somitomeres occurs first in the cephalic region of the embryo, proceeding in a cephalocaudal manner. In the regions of the developing cranium, somitomeres develop into neuromeres. Out with this region, the somitomeres develop into somites, a process beginning in the occipital region and continuing craniocaudally until the end of the fifth week of gestation. At this point of development, there are approximately 42-44 pairs of somites (Kaplan *et al.*, 2005). These include 4 occipital, 8 cervical, 12 thoracic, 5 lumbar, 5 sacral and 8-10 coccygeal pairs. This initial separation of the paraxial mesoderm into somites is known as segmentation. This segmentation is under the control of a number of signalling pathways (Jacobson and Sater, 1988; Müller and O'Rahilly, 1994; Pourquie, 2001; Gibb *et al*., 2010; Pourquie, 2011; Forero *et al.*, 2018). Loss of somites occurs in the occipital and coccygeal region. At this point, all cells have undergone epithelialisation. Cells at the dorsomedial and lateroventral edges of the somite form the myotome, while the cells in between these form the dermatome (Kaplan *et al.*, 2005). Cells in the ventral and medial walls migrate to surround the neural tube and notochord, transition to mesenchymal cells and form the sclerotome (Fleming *et al.*, 2001). Collectively, the sclerotomes form the bony and cartilaginous tissue, the myotomes form the segmental muscle groups and the dermatomes form the dermis of the back (Sadler, 2019).

The sclerotome undergoes cavitation, with diffuse core cells forming within the cavity. This causes the sclerotome to rupture medially. Core cells and cells from the ventromedial wall of the sclerotome migrate towards the anterior notochord and the posterior neural tube, thought to be induced by signalling from the notochord itself (Fleming *et al.*, 2001). Cells surrounding the notochord are precursors for the vertebral centra, while cells surrounding the neural tube will develop into the neural arches. It is thought that each sclerotome is separated into dense caudal and loosely arranged cranial sections by spinal nerves emerging from the neural tube (Fig. 4.1). At this point, the area between these sections is 'cell-free' (Kaplan *et al.*, 2005) but will eventually develop into the intervertebral disc. The cranial and caudal sections then reform, with the caudal sections of upper sclerotomes fusing with the cranial sections of lower sclerotomes (Wyburn, 1944). It is these newly created resegmented sclerotomes that develop into the vertebral column. The vertebral centra are formed from two sclerotomes as they consist of both dense and loosely arranged cells, while the neural arches form only from the dense caudal part of the sclerotome, which now sits in the upper portion of the resegmented structure (Bagnall *et al.*, 1988; Selleck and Stern, 1991; Aoyama and Asamoto, 2000). Resegmentation offers an explanation as to why cervical vertebrae are formed from 8 somites and why there is an 8th cervical nerve, with named nerves exiting above their associated vertebrae, rather than below, as seen with thoracic, lumbar and sacral nerves. Resegmentation of the cervical somites leads to the first cervical vertebra being formed by the caudal aspect of C1 sclerotome and the cranial aspect of C2, with the C1 spinal nerve separating the C1 sclerotome and henceforth appearing above the C1 vertebra. In the lower cervical region, the C8 somite contributes to both C7 and T1 vertebrae, with the 8th cervical nerve exiting inferior to C7. Therefore, the T1 spinal nerve is inferior to the T1 vertebra (Cunningham *et al.,* 2016).

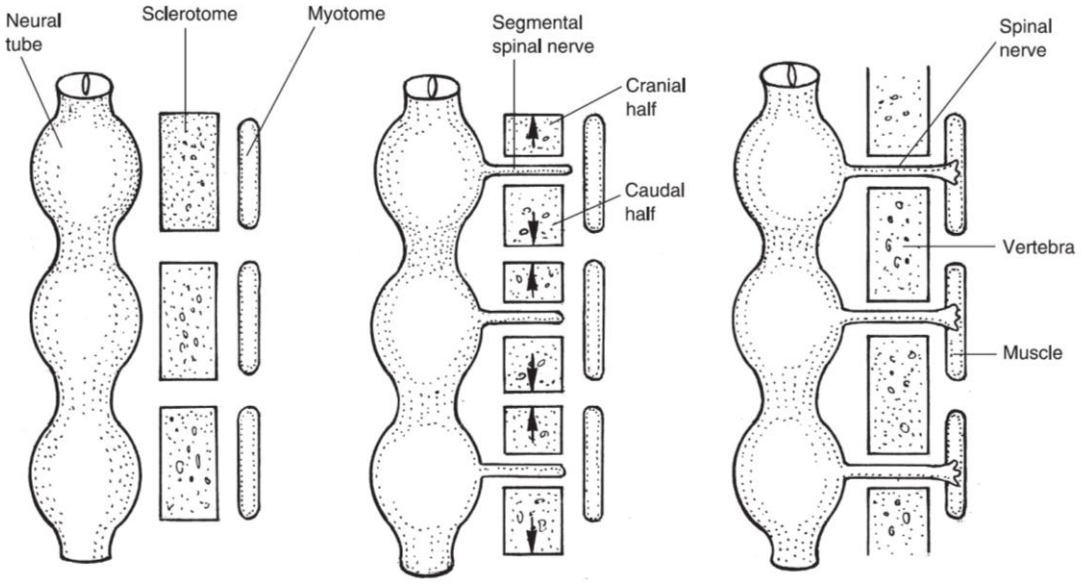

Figure 4.1: Schematic of the resegmentation of the sclerotome into dense caudal and loose cranial parts by spinal nerves before recombining to form the precursors of the vertebrae (Cunningham et al., 2016).

4.2 Chondrification

During the 6th week of gestation, signals from the notochord and neural tube induce chondrification of the sclerotome (Kaplan *et al.*, 2005). Six chondrification centres appear including two lateral centres for each centrum, which quickly fuse to become one (Cunningham *et al.*, 2016). Two centres for the neural arch appear, one for each hemi-arch, appearing in the region of the future lamina and extending to the transverse and articular processes as well as the pedicle. These centres fuse at the spinous process at around the 4th month of gestation. Finally, two centres appear for each costal process (Figure 4.2). In the lumbar region, the costal chondrification centres contribute to the transverse processes (Maat *et al.*, 1996). In the area of the centrum, the notochord regresses. However, in the area of the intervertebral disc, the notochord remains and has a significant role in the development of the intervertebral disc. While uncommon, the persistence of the notochord in the area of the centrum is not unheard of (Musgrove, 1891). The appearance of these chondrification centres is important and failure to appear leads to congenital deformities such as butterfly vertebra (Müller *et al.*, 1986), congenital scoliosis and spina bifida (O'Rahilly *et al.*, 1990; Northrup and Volcik, 2000; Bassuk and Kibar, 2009).

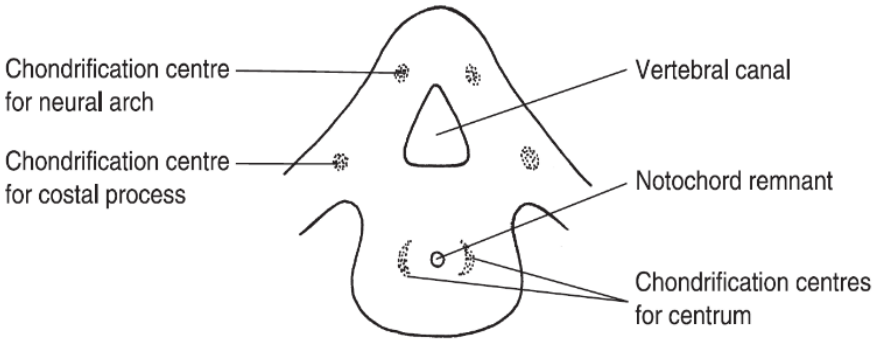

Figure 4.2: The chondrification centres of the developing lumbar vertebrae. Two lateral centres appear for the centrum, two chondrification centres are present for the neural arch in the area of the future lamina, and two costal processes which in the lumbar vertebrae contribute to the transverse processes (Cunningham et al., 2016).

4.3 Ossification

4.3.1 *Primary Centres*

Ossification of the cartilaginous template begins around the 2nd month *in utero*. Typically, each vertebra is formed from at least three primary centres (O'Rahilly *et al.*, 1990; Szpinda *et al.*, 2013a; b; c). The vertebrae tend to follow a typical pattern of ossification. The centrum has been observed to arise from either one or two centres. In cases where the centrum is derived from two centres, these are anterior and posterior, and are connected by a bony bridge housing vasculature (Fazekas and Kósa, 1978). Initiation of ossification of the centra occurs dorsally to the notochord and is endochondral in nature (Maat *et al.*, 1996). It has been suggested that ossification occurs within the region of the notochordal remnants and that the notochord releases an angiogenic-inhibiting factor that prevents the penetration of vascular tissue within the region. Therefore, ossification within the centra initially occurs in a ring formation around the notochord until its regression, and ossification of the avascular area occurs with the invasion of vasculature from the surrounding ossification centre (Skawina *et al.*, 1997). Initiation of the ossification of each neural hemi-arch occurs in the perichondrium of the internal aspect of the lamina and therefore undergoes perichondral intramembranous ossification initially (Maat *et al.*, 1996). After the formation of the periosteal bone collar surrounding the neural hemiarch, vascular invasion occurs, and endochondral ossification commences. The neural

hemiarches are distinct in that they display three growth plates: one for the extending pedicle, one for the extending lamina (that will eventually join in the region of the spinous process) and one for the transverse process. Ossification of the neural hemiarches occurs centripetally (Chandraraj and Briggs, 1991).

The first primary centres for the centra appear in the region of the lower thoracic and upper lumbar regions. From here, ossification occurs bidirectionally, with ossification of the fifth lumbar vertebral centrum occurring by the end of the 3rd month in utero and the upper cervical region by the end of the 4th month in utero (Bagnall *et al.*, 1997a). The appearance for the ossification centres of the neural hemi-arches has been debated. Traditionally, it was thought that ossification commenced around the level of the fifth cervical vertebra during the 2nd month of gestation and continued bidirectionally (Figure 4.3, B) (Cunningham *et al.*, 2016). However, Bagnall *et al.* (1977a) used radiographic analysis to construct a developmental pattern of neural hemi arch and centrum ossification and found that ossification commenced in two areas, in the upper thoracic region in the 3nd month of gestation, and then in the lower thoracic region in the 3rd to 4th month of gestation and continued bidirectionally (Figure 4.3, A). No sex-related, or left-right differences, have been found in the appearance of the primary ossification centres (Szpinda *et al.*, 2013a; b; c).

Bagnall *et al.* (1977a) also stated that ossification in the neural hemi-arches was most likely initiated by muscle attachment and fetal movement, which has long been speculated (Bardeen, 1905; LeVeau and Bernhardt, 1984; Nowlan, 2015; Shea *et al.*, 2015; Verbruggen *et al.*, 2016). While this study improved on previous works by increasing the sample size and hence improving the validity of the results found, the methodology was somewhat limiting in that the appearance of ossification centres were identified radiographically, meaning that in cases where centres were considered to have not appeared, this may not have been the case. Histological analysis, while destructive, is more accurate in the earlier identification of ossification centres. Even with this methodological flaw, the results found contradicted earlier studies. No correlation was found between neural hemi arch and centrum appearance, implying that these centres developed independent of each other. Furthermore, no uniformity was found regarding which appeared first, neural hemi arches or centra. In the case of the lumbar vertebral column, the centra complete ossification prior to the neural hemi-

arches. The lack of fixed sequence in the appearance of ossification centres in the vertebral column may be due to a number of factors. Firstly, the inductive mechanisms of ossification may differ. Due to its largely haematopoietic function, and the vital importance of angiogenesis in osteogenesis, the initiation of ossification within the lumbar centra may be due to the timing and presence of vasculature, as well as approximation to the notochord (Wyburn, 1944). Meanwhile, ossification of the neural hemi-arches is likely initiated following signalling from the neural tube, which is in close proximity (Wyburn, 1944). Furthermore, the neural hemiarches are a site of attachment for both extrinsic and intrinsic musculature and may be affected more by fetal movement than the vertebral centra.

Two postnatal fusion events occur within the developing lumbar vertebrae. The fusion of the neural hemiarches to form the neural arch is known as fusion of the posterior arch, while fusion between the neural arch/ neural hemiarches and the centrum is known as neurocentral fusion. As with the appearance of ossification centres for the centrum and neural hemiarches, these two fusion events occur independent of each other and begin at specific vertebral regions. Posterior arch fusion commences prior to neurocentral fusion and begins in the lower thoracic region at around 1 year of age. While posterior arch fusion reaches the cervical vertebrae by the third year of life, it does not reach L5 until around the 5th year. Meanwhile, neurocentral fusion commences in two regions: the lower cervical region at around 3 to 4 years of age, and the lower lumbar region at approximately 2-3 years of age, continuing bidirectionally until reaching the region of the lower thoracic vertebrae at around 5 years of age. Therefore, while it is more common for the upper lumbar vertebrae to undergo posterior arch fusion prior to neurocentral fusion, at the level of the lower lumbar vertebrae, neurocentral fusion is most likely to occur first (Figure 4.3) (Maat *et al.*, 1996; Cunningham *et al.*, 2016).

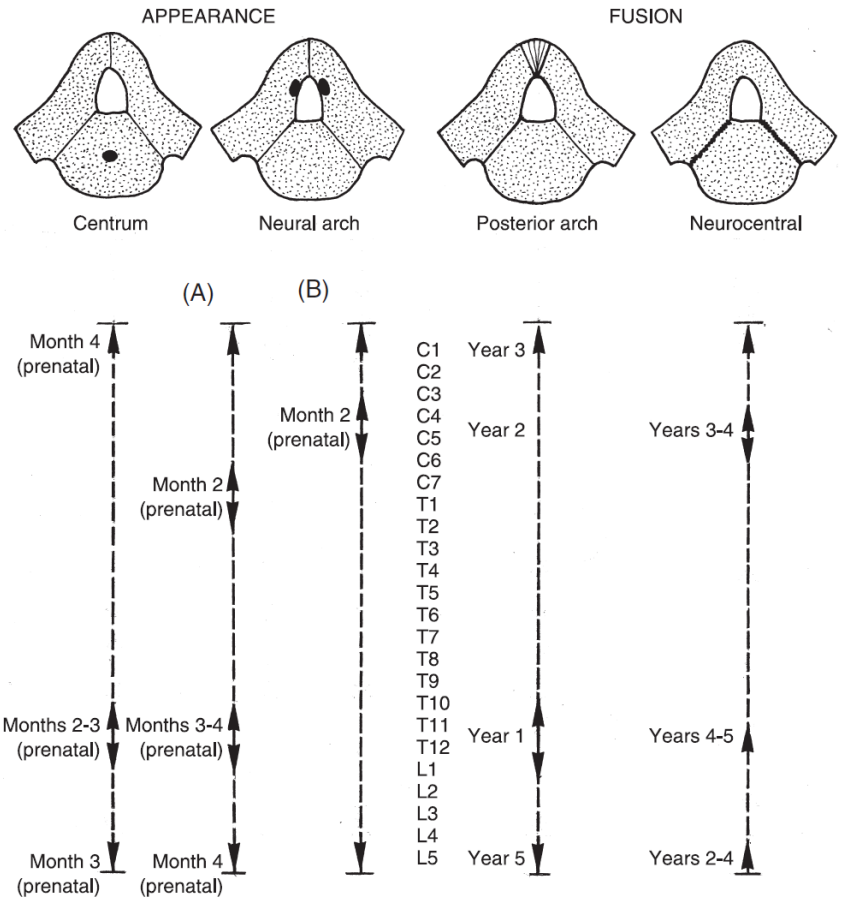

Figure 4.3: Schematic of (left) the appearance of the centrum and neural hemiarches where A: Bagnall et al (1977a) theory of the appearance of the neural hemiarches and B. Traditional theory of appearance of the neural hemiarches; and (right) the fusion of the posterior arch and neurocentral junction (Cunningham et al., 2016)

4.3.2 *Secondary Centres*

Typically, lumbar vertebrae have seven secondary centres of ossification, also known as epiphyses. These include one for the tip of each transverse process, one for the tip of each mamillary process, one of the tip of the spinous process, one superior and one inferior annular ring epiphysis (Figure 4.4). All secondary centres of ossification generally appear at the start of puberty and fuse around the end of puberty (Cardoso and Ríos, 2011; Cunningham *et al.*, 2016).

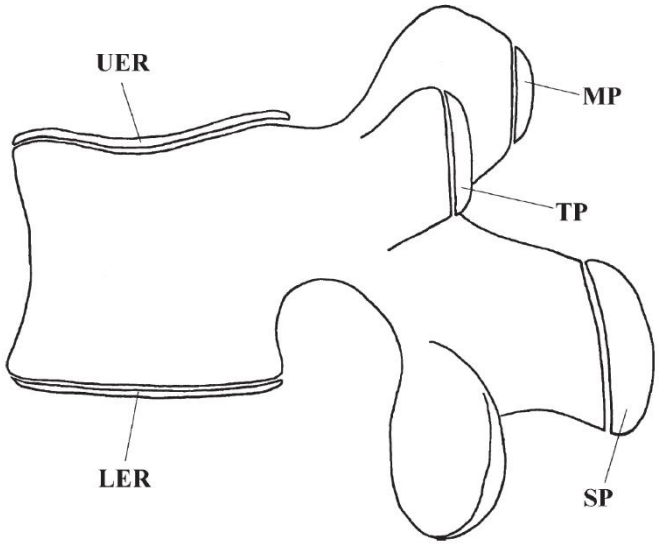

Figure 4.4: Lateral view of a lumbar vertebra and its epiphyses. UER: Upper epiphyseal ring; LER: Lower epiphyseal ring; MP: Mamillary process (paired) TP: Transverse process (paired) and SP: Spinous process (Cardoso and Ríos, 2011).

While all epiphyses generally appear and fuse during puberty, a consistent pattern in relation to fusion has been observed. Generally, the first secondary centres to fuse are the mamillary processes at around 11-19 years of age (Cardoso and Ríos, 2011) although have been observed as appearing as early as 6-8 years of age in relation to musculature (Fazekas and Kósa, 1978). The mamillary processes are followed by the transverse processes and the spinous process (~15-21 years of age) and finally the superior and inferior annular ring epiphyses (~14-23 years of age) (Cardoso and Ríos, 2011). In the cases of the paired mamillary and transverse processes, no differences between the appearance and fusion of the left and right epiphyses has been observed (Cardoso and Ríos, 2011). The fusion of the superior and inferior annular rings has been of some interest in age estimation of unknown skeletal remains (Albert and Maples, 1995; Albert *et al*., 2010; Cardoso and Ríos, 2011). Prior understanding had been that the rings appear around puberty and had fused by the age of 25. In a study of annular ring epiphyseal fusion, Albert and Maples (1995) found no fusion in any individual prior to the age of 14 years in females, and 16 years in males, and fusion had occurred in the sample by 25 years of age. No observations were made on appearance of the secondary epiphyses. No significant differences were found between the fusion of the superior and inferior rings to the lumbar vertebral body. Females were shown to mature slightly earlier

than males (Albert *et al*., 2010) although not all studies have found significant differences between the sexes for fusion times. However, differences were found in the timings of annular ring fusion between levels of the lumbar vertebral column, with L5 annular ring epiphyses generally fusing prior to upper lumbar vertebrae (Cardoso and Ríos, 2011).

4.4 Vascular development

Vascularisation of the cartilaginous anlage is a vital step in ossification (Alini *et al.*, 1996; Olsen *et al*, 2000; Petersen *et al*., 2002; Colnot *et al.*, 2004; Maes, 2013; Jiang *et al.*, 2017). The adult vascular anatomy of the vertebral column has been extensively mapped and studied (Crock and Yoshizawa, 1976; Ratcliffe, 1980; Crock, 1996), however the development of this vasculature has been somewhat neglected.

The development of the arterial anastomoses seen within the adult lumbar vertebrae commences within the fetal period. Three concentric zones of vascular architecture within the fetal centrum have been observed (Skawina *et al.*, 1997; Demed *et al.*, 2013). These consist of a peripheral zone, an intermediate zone and a central zone (Figure 4.5). The intervertebral region has consistently been found to be avascular in the fetus (Guida *et al.*, 1969; Ratcliffe *et al.*, 1981; Skawina *et al.*, 1997; Demed *et al.*, 2013).

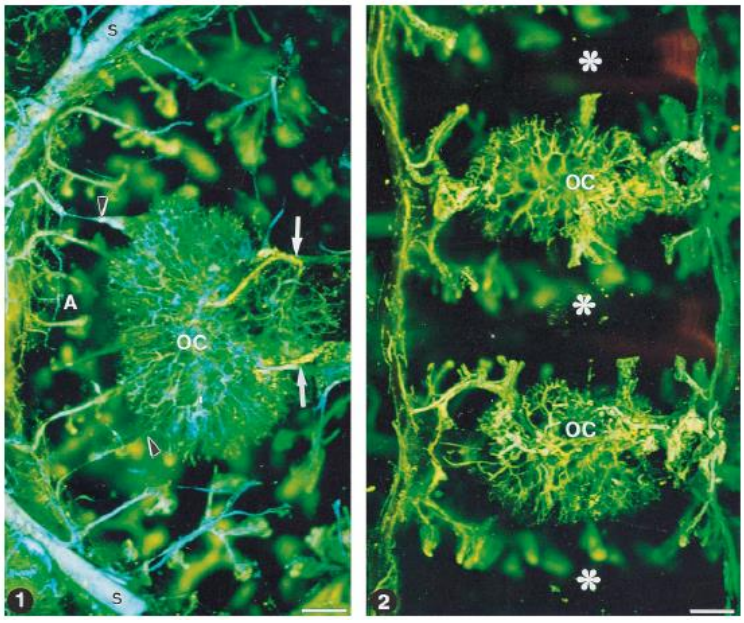

Figure 4.5: Left: Superior view of the vasculature of a vertebral centrum at 21 weeks in utero, where OC is the ossification centre and the white arrows show the posterior nutrient arteries. Right: 2 adjacent vertebral centra in a 23 weeks in utero individual where OC is the ossification centre and the asterisks display the avascular IV regions (Skawina et al., 1997).

The peripheral zone comprises perichondral vessels that form a centripetally directed arcade-like anastomosis (Demed *et al.*, 2013) while the intermediate zone consists of radial vessels (Skawina *et al.*, 1997; Demed *et al.*, 2013). The peripheral and radial zones of vessels are formed from the postcentral and metaphyseal anastomoses of the segmental arteries (Ratcliffe, 1981; Skawina *et al.*, 1997; Demed *et al.*, 2013). The segmental arteries were found to be present and equal in size in both fetal and infant individuals, giving perichondral branches which travelled superiorly and inferior to anastomose with each other. By 6 months of age, two C shaped anastomoses lay upon the anterolateral surfaces of the vertebral centra, the future metaphyseal anastomoses (Ratcliffe, 1981).

The central zone comprises ossification centre vessels (Skawina *et al.*, 1997; Demed *et al.*, 2013). Ratcliffe (1981) identified that at least four arteries supply each vertebral centrum to form the central zone: one to two nutrient arteries arise from the postcentral anastomosis and enter the vertebral centra posteriorly, and multiple from each segmental artery anterolaterally. This has also been observed in other communications (Guida *et al.*, 1969; Skawina *et al.*, 1997; Demed *et al.*, 2013). All of these arteries supply the ossification centre and travel medially. These branches, termed equatorial branches after their direction of travel, do not branch initially, but upon reaching the centre of ossification, give superior and inferior branches towards the IV discs in the fetal individuals, and in older individuals, are radial in all directions (Ratcliffe, 1981). In the second trimester, it has been observed that the area of the notochord is avascular and as a result, the nutrient arteries form a ring-shaped anastomosis around the notochord initially before penetrating the area of the regressing notochord (Skawina *et al.*, 1997).

Throughout the fetal period, and through early childhood, the architecture of the vasculature within the lumbar centra continues to develop. For example, Ratcliffe (1981) identified that the metaphyseal branches observed were relatively simple in the fetus but became more complex in early childhood. Furthermore, the metaphyseal and postcentral anastomoses present within the fetal period branch less than in early childhood. The segmental arteries were found to be present and equal in size in both fetal and infant individuals (Figure 4.6). Skawina *et al.* (1997) and Demed *et al.* (2013) both studied fetal individuals

within the 2nd trimester and found that, while the general architecture of the adult was present, the vessels present grow centripetally from the periphery and centrifugally from the ossification centre to meet and form the extensive anastomosis by infancy. By the age of 7 years, these anastomoses begin to reduce and by the age of 15, the general adult structure has been attained (Ratcliffe, 1982).

The venous drainage of the developing lumbar centra has also been studied (Skawina *et al.*, 1997). Like in the adult, the venous drainage has been found to follow the arterial supply in the juvenile centrum, although in some cases, features observed within the adult such as the subchondral venous network and horizontal veins of the vertebral endplate had yet to develop within the fetus (Skawina *et al.*, 1997). Posterior vessels were observed to be almost exclusively responsible for drainage in the fetus, running alongside the posterior nutrient arteries (Skawina *et al.*, 1997). Sinusoidal vessels were also observed within the developing centrum (Skawina *et al.*, 1997).

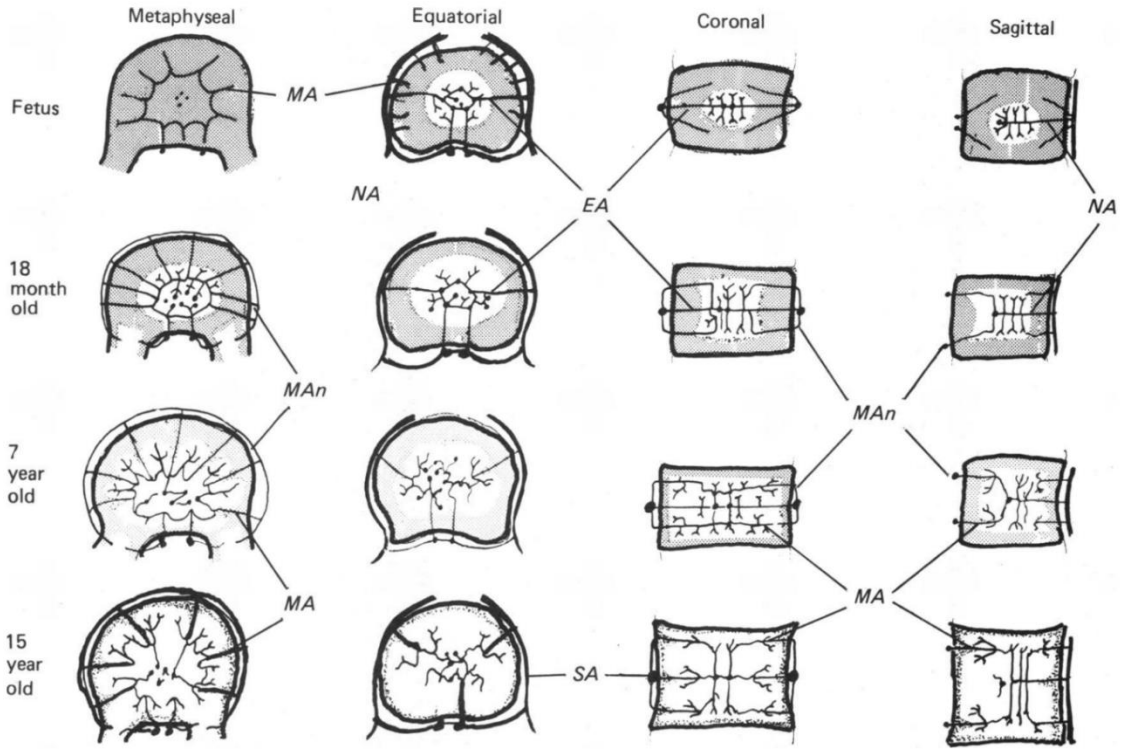

Figure 4.6: Diagrams displaying the development of the vasculature of the vertebral centrum/ body in the fetus, at 18 months old, at 7 years of age and at 15 years of age. MA: Metaphyseal artery; MAn: Metaphyseal anastomosis; NA: Nutrient artery, EA: Equatorial artery and SA: Segmental artery (Ratcliffe, 1981).

4.5 Development of the curvatures of the vertebral column

Throughout development, the vertebral column adopts a characteristic curvature. The primary curvature, also known as a kyphosis, is concave anteriorly (C-shaped) and present in the early stages of development. In the adult, it is only the thoracic and sacro-coccygeal regions that present a kyphosis. The cervical and lumbar regions develop a secondary curvature, a lordosis, which is convex anteriorly.

In the fetal period, the entirety of the spine is kyphotic in nature (C shaped) (Bagnall *et al.*, 1977b; Keen, 1993) however by the age of 5 years, a characteristic lumbar lordosis is present, which continues to develop throughout childhood (Giglio and Volpon, 2007). The lordoses of the spine develop primarily through the altered morphology of the IV discs, which undergo posterior wedging of the to produce the lumbar lordosis (Been *et al*., 2010).

4.5.1 *Mechanical stimulation and curvature development*

It is well accepted that mechanical stimulation is a factor in the initiation of ossification (LeVeau and Bernhardt, 1984; Nowlan, 2015; Shea *et al.*, 2015; Verbruggen *et al.*, 2016), as well as in the postnatal development of the facet joints (O'Rahilly *et al.*, 1990; Boszczyk *et al.*, 2002). Therefore, it is acceptable to assume that mechanical stimuli play a role in the development of the lumbar lordosis.

While it was originally thought that both the cervical and lumbar secondary lordoses developed postnatally, this has been contested. Bagnall *et al.* (1977b) studied the onset of the development of the secondary cervical curvature and found evidence of a lordosis in the cervical region in the fetus. This was attributed to *in utero* movements including movements of the head and neck and the gasp reflex. However, no evidence of a secondary lumbar curvature was found. More recently, Choufani *et al.* (2009) identified the presence of a lumbosacral lordosis within a fetal sample. However, this lordosis was only present at the level of the IV disc between L5 and S1 rather than the length of the lumbar column and it was speculated by the authors that the early lordosis seen was genetically determined. However, if there is evidence of the formation of a cervical lordosis in the fetal period developing in relation to *in utero* reflexive movements, it is certainly possible that the lumbar lordosis also begins to occur in the fetal period,

with i*n utero* movements playing a role in its potential prenatal development. It is accepted that *in utero* movements commence at around week 5/6 of gestation (Lacquaniti *et al.*, 2012; Hadders-Algra, 2018). Early movements comprise movements of the head and neck and side bending of the trunk, followed by reflexive limb movements that act as locomotor precursors (Zelazo *et al*., 1972; Bagnall *et al.,* 1977b; Thelen and Fisher, 1982; Malina, 2004; Lacquaniti *et al.*, 2012; Hadders-Algra, 2018).

While the development of the lumbar lordosis may commence in the fetal period, it is clear that the majority of its development occurs postnatally. Evolutionarily, humans have developed the lumbar lordosis in response to upright posture and locomotion (Sparrey *et al*., 2014) hence it is well established that the attainment of upright posture and other development milestones facilitates the development of the lumbar lordosis (Keen, 1993). There is an array of literature focusing on the development of locomotion and attainment of gross motor developmental milestones and the ages at which these occur (Keen, 1993; Garrett *et al.*, 2002; WMGRSG, 2006; Sheldrick and Perrin, 2013; Hadders-Algra, 2018). Developmental milestones are specific voluntary movements that an infant or child gains the control and coordination of, and their acquisition is used to assess the developmental maturity of the individual in question (Malina, 2004). Of the major motor developmental milestones, independent walking (locomotion) is perhaps the primary milestone of early life, and the developmental milestones that occur prior to that are postural changes vital in allowing the individual to achieve independent walking (Malina, 2004). An overview of average ages of attainment for the major motor developmental milestones can be viewed in Table 4.1 (Keen, 1993; Garret *et al.*, 2002; WMGRSG, 2006; Sheldrick and Perrin, 2013; Hadders-Algra, 2018). As research suggests that the lumbar lordosis has been established by the age of 5 years (Keen, 1993; Giglio and Volpon, 2007) and research also suggests a mature gait is achieved around this point (Chester *et al*., 2006), there is the potential that these early developmental milestones, when attained, play a role in the development of the lumbar lordosis.

Table 4.1: Overview of the attainment of developmental milestones in the literature.

		Keen (1993)	Garrett *et al.* (2002)	WMGRSG (2006)	Sheldrick and Perrin (2013)	Hadders-Algra (2018)
Age of Attainment	**Control of the head**	~4 months	-	~1.5 months	1.5-3.5 months	~2 months
	Rolling	~5 months	-	-	3-8 months	4-7 months
	Sitting independently	~7 months	4-9 months	~6 months	6-11 months	6-7 months
	Sitting up	-	-	-	7-12.5 months	-
	Crawling	~7 months	5-14 months	~7 months	7-13 months	10 months
	Standing with assistance	~11 months	5-12 months	-	-	10 months
	Walking with assistance	~12 months	6-14 months	~9 months	8-15 months	10 months
	Standing independently	~13 months	7-17 months	-	8-18 months	-
	Walking independently	~14 months	8-18 months	-	10-20 months	12-14 months
	Attainment of mature gait	-	-	-	-	7-9 years

The attainment of developmental milestones such as sitting unaided, standing and walking all place increased axial compressive force onto the vertebral column. Wedging of the IV discs account for 90% of the adult lumbar lordosis (Been *et al*., 2010; Sparrey *et al*., 2014) and play a major role in the dissipation of compressive forces placed upon the lumbar vertebral column (Been *et al*., 2010; Jang and Kim, 2010; Gocmen-Mas *et al*, 2010). The addition of axial compression through the attainment of these early developmental milestones are the most likely driving force for the morphological changes seen in the IV discs during lumbar lordosis development.

LeVeau and Bernhardt (1984) proposed a potential mechanism for the development of the lumbar lordosis was due to forces placed upon the lumbar vertebral column through the musculature of the trunk. They stated that, during the fetal period, the developing spine is in a position of flexion which leads to shortening and tightness of the muscles of the trunk, in particular iliopsoas, during

their development. Then, as the infant develops and is able to roll into a prone position and crawl, the shortened muscle cannot lengthen to accommodate such extension and the lumbar lordosis begins to form. Furthermore, weakness of the abdominal muscles also allows for lordotic development in the same fashion. They also identified that abnormal posture led to increased lumbar lordosis which implies musculature does play a role in curvature development.

4.5.2 *Pelvic positioning and the lumbar lordosis*

It has been postulated that the position of the pelvis has an effect on spinal posture and that the development of the posterior pelvic tilt characteristic of erect posture is related to the development of the lumbar lordosis (Poussa *et al*., 2005; Choufani *et al.*, 2009).

The posterior positioning of the pelvis, which is thought to begin development in the fetal period (Choufani *et al.*, 2009) is a strong predictive factor in normal attainment of developmental milestones (Gajewksa *et al.*, 2018). The positioning of the pelvis has long been studied in relation to the evolution of bipedalism and erect posture, with a posterior shift in the sacrum and development of a lumbar lordosis to accommodate bipedalism (Lovejoy, 2005; Whitcome *et al.*, 2007).

Furthermore, sex differences in the angle of the lumbar lordosis have been observed in older children and adolescents (Poussa *et al.*, 2005). As the pelvis is structurally formed to accommodate bipedalism in all individuals, as well as parturition in females, the sexual dimorphism seen within the lumbar vertebral column may be due to the changes in sacral positioning to accommodate the latter function in females (Poussa *et al.*, 2005).

4.6 Trabecular architecture in the juvenile

4.6.1 *General development of trabecular architecture*

Research into the trabecular architecture within the juvenile and its development has increased recently with the advancements in non-invasive imaging techniques (Guldberg *et al.*, 2004). Studies most often focus on skeletal elements of importance in load-bearing and weight transfer, such as the long bones (Salle *et al*., 2002; Ryan and Krovitz, 2006; Goldman *et al.*, 2009; Gosman and Ketcham, 2009; Reissis and Abel, 2012), the pelvic complex (Cunningham and Black, 2009a; b; 2010; Abel and Macho, 2011; Maclean *et al.*, 2014,

Maclean, 2017), and the vertebral column (Kneissel *et al*., 1997; Roschger *et al*., 2001; Nuzzo *et al.*, 2003; Acquaah *et al.*, 2015). Other skeletal areas, such as the scapula (Rissech and Black, 2007; O'Malley, 2013) and the mandibular condyles (Mulder *et al.*, 2007; 2008) have also been considered.

Studies on the long bones have mainly focused on bones of the lower limb: the femur and the tibia. These studies have consistently reached the same conclusions: trabecular architecture is developed in response to mechanical loading during the development of locomotion to reach its final adult morphology (Ryan and Krovitz, 2006; Goldman *et al.*, 2009). Studies of both the proximal femur and proximal tibia have indicated that the fetal trabecular structure is dense and relatively undifferentiated in the fetal period and at birth (Salle *et al*., 2002; Gosman and Ketcham, 2009) and that the changes in internal architecture and external bone shape that occur in order to attain adult morphology do so in response to loading and the development of bipedalism post-birth (Ryan and Krovitz, 2006; Reissis and Abel, 2012).

Research into the pelvic complex has focused on the ilium (Cunningham and Black, 2009a; b; c; 2010; Abel and Macho, 2011), the ischium (Maclean *et al.*, 2014; Maclean, 2017) and the sacrum (Yusof, 2013). Quite unlike research in the long bones, studies into juvenile iliac architecture have observed that trabecular bundles present within the adult were found within the perinate, even though load bearing had not yet occurred (Cunningham and Black, 2009a; b; 2010; Abel and Macho, 2011). This implies that the morphology of the internal trabecular architecture is driven by other factors alongside mechanical stimuli. For example, the pattern of ossification and the associated vascularisation of the skeletal element in early development (Roschger *et al.*, 2001; Nuzzo *et al.*, 2003; Cunningham and Black, 2010).

Three stages of the development of trabecular structure have been described (Acquaah *et al.*, 2015). The first stage, gestational overproduction, comprises an increase in bone volume fraction and bone mineral density. This overproduction is followed by constructive regression, the removal of the excess mineral content and surplus bone laid down in the first stage. Finally, refinement occurs, which involves the sculpting of the remaining trabecular architecture in relation to load-bearing (Acquaah *et al.*, 2015). Even prior to the coining of the term constructive regression, multiple authors had observed decreases in

trabecular number, bone volume fraction and bone mass density in early infancy (Kneissel *et al*., 1997; Roschger *et al*., 2001; Nuzzo *et al.*, 2003; Ryan and Krovitz, 2006; Gosman and Ketcham, 2009; Reissis and Abel, 2012; O'Malley, 2013; Maclean *et al.*, 2014; Maclean, 2017).

Overall, it appears the trabecular architecture in the fetus, while having not yet achieved adult morphology, is in some way predetermined (Cunningham and Black, 2010; Abel and Macho, 2011; Acquaah *et al.*, 2015). After the fetal period, the trabecular architecture undergoes a period of regression in which trabecular number and bone volume fraction decreases, before mechanical loading influences trabecular architecture to adopt its characteristic, functional adult morphology (Acquaah *et al.*, 2015).

4.6.2 *The trabecular architecture of the juvenile vertebral column*

In the fetal period, a characteristic pattern of trabecular architecture in the vertebral centrum has been observed. A central region of thick, plate-like, well spaced radial trabeculae was observed to be surrounded by a peripheral region of immature bone, characterised by a higher number of thinner, more immature trabeculae closer to the growth plate (Figure 4.7a) (Roschger *et al*., 2001; Nuzzo *et al*., 2003). This period was also characterised by gestational overproduction with increased bone volume fraction and increased trabecular number leading to a significantly denser structure than its adult equivalent (Kneissel *et al.*, 1997; Roschger *et al*., 2001; Nuzzo *et al.*, 2003; Acquaah *et al.*, 2015). The architecture within this region has been related to the pattern of ossification within the vertebral centra (Roschger *et al*., 2001; Nuzzo *et al.*, 2003).

Postnatally, the transition from radial trabecular architecture to the characteristic vertical struts, reinforced by horizontal struts at the superior and inferior portions, seen within the adult lumbar vertebral bodies commences (Figure 4.7b) (Kneissel *et al*., 1997; Roschger *et al.*, 2001). Quantitatively, postnatal changes in the trabecular architecture are characterised by a peak in trabecular number in the 1st year of life, and a consistent increase in trabecular thickness until adolescence (Roschger *et al.*, 2001). Constructive regression occurs postnatally and allows for the sculpting of the architecture produced in the fetal period (Acquaah *et al.*, 2015) and remodelling of the trabecular architecture results in more plate-like trabeculae in older individuals (Kneissel *et al.*, 1997).

By the age of around 8 years, the characteristic trabecular architecture observed in the adult has developed with the central portion of the vertebral body displaying thickened, plate-like predominantly vertically oriented trabeculae which the end plates display a higher number of thinner trabecular of both horizontal and vertical orientation (Figure 4.10c) (Roschger *et al.*, 2001) however, studies of bone mineral density within the lumbar spine have reported increases in BMD until adolescence (del Rio *et al.*, 1994; Roschger *et al.*, 2001).

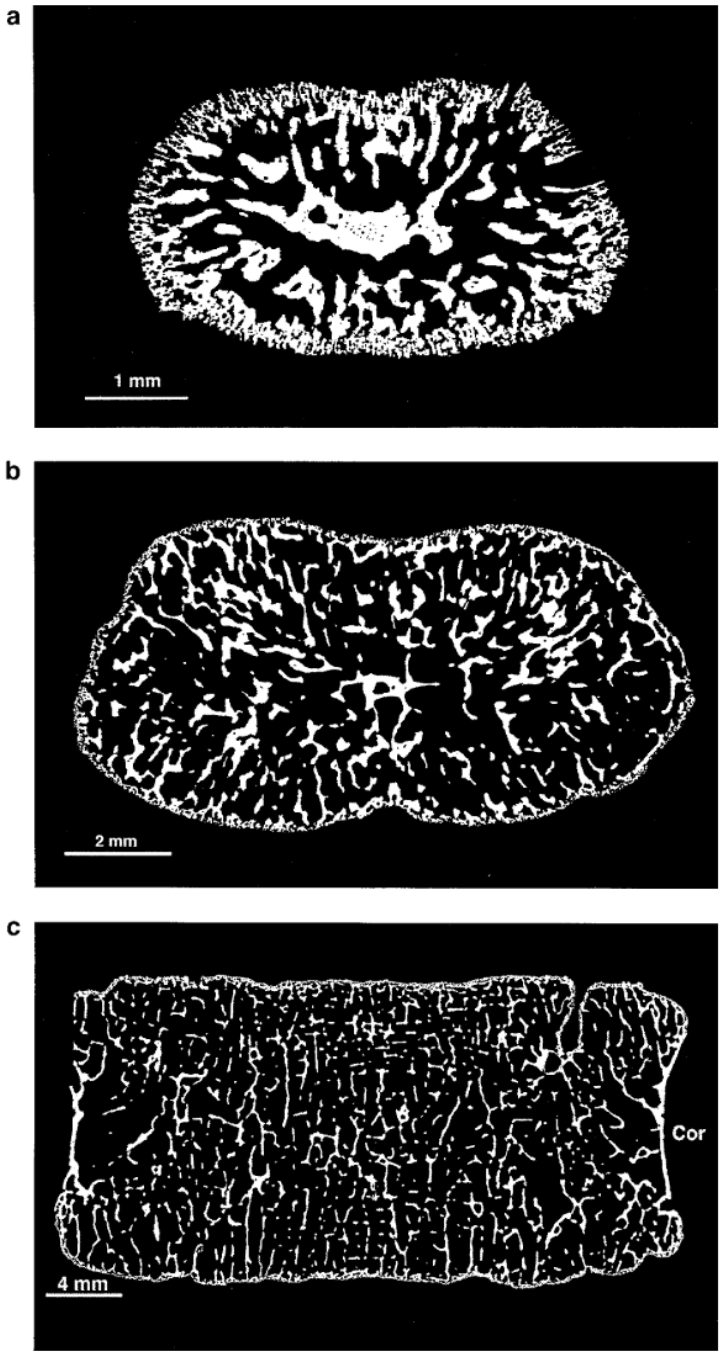

Figure 4.7: Binary backscattered electron images of the frontal sections of L4 vertebral bodies from A. 17 week in utero individual; B. 5 weeks postnatal individual; C. 8 year old individual; where 'cor' is cortical bone (Roschger et al., 2001).

5 A Qualitative Analysis of the Developing Lumbar Vertebral Column

5.1 Aims

This part of the study utilised digital radiography and colour gradient mapping to visualise and identify bone intensity patterns within the developing structure of the human lumbar vertebral column. The aim of this preliminary investigation was to gain an understanding of the potential developmental pattern of the human lumbar vertebral column from a qualitative perspective, thus identifying areas for further quantitative analysis.

5.2 Sample

5.2.1 *The Scheuer Collection*

All lumbar vertebrae utilised were part of the Scheuer collection. The Scheuer collection is an active repository of juvenile remains housed at the Centre for Anatomy and Human identification at the University of Dundee (Cunningham *et al*., 2016; Maclean, 2017).

The collection comprises over 150 partial and complete skeletons of archaeological, historical, anatomical and forensic origins. While a small number of individuals within the collection are of known sex and age at death, the majority of individuals are of estimated age. This is assigned using dentition where possible and, where not possible, metric and morphological skeletal aging techniques.

5.2.2 *Sample collection and exclusion*

Individuals were selected based on several factors. These included the vertebral levels present for the individual in question, the quality of the lumbar centra and hemiarches, and the ages or estimated ages of the individuals.

5.2.2.1 Seriation of lumbar vertebrae

Seriation of the lumbar centra and neural hemiarches was achieved using the methodologies stated in Cunningham *et al.* (2016). Seriation became easier with the increasing age of individuals as events such as neurocentral fusion facilitated more accurate identification of vertebral level. For younger individuals (under ~2 years of age) the skeletal inventory for each individual was utilised if

available and was particularly important in cases of missing vertebral elements. However, when documentation was not available, or the vertebral elements present for an individual did not match the documentation, seriation became more difficult. If any lumbar vertebral centra were not present, it was not possible to accurately identify the vertebral level from which the centrum in question belonged. In cases where there were missing elements, these individuals were excluded from the project.

5.2.2.2 Bone quality and exclusion

Due to differing origins within the collection, the bone quality and state of preservation varied between individuals. Any individual that displayed over 30% damage to cortical bone, damage to trabecular bone or signs of pathology were considered to have low bone quality and were excluded from the sample. One subset of individuals, while presenting high bone quality, were observed to have small holes within the centra for each individual. This was most likely from attempts to seriate the columns by hanging the centra on wire for anatomical presentation, as these individuals were anatomical in origin. For this collection of individuals, it was decided that they would be included in the sample as they represented an age range that was underrepresented within the Scheuer collection. It was concluded that, after radiographic and µCT analysis, their scans would be examined and, should any damage to the trabecular architecture present itself, these individuals would be excluded. Once scanning had taken place and the examination of these scans had occurred, these individuals were included within the final sample for both analyses as no significant damage to the underlying trabecular architecture was observed.

5.2.2.3 Age estimation and selection of age cohorts

Any individuals of unknown age were estimated using the methodologies described by Cunningham *et al.* (2016). Age cohorts were chosen based on the best fit for age ranges estimated. As only three fetal individuals were found to be acceptable for the project, these individuals were placed within their own cohort, even though they can be considered perinates under the definition given by Cunningham *et al.* (2016). For the minority of younger individuals that were of known age, the cut off age for acceptance into the perinatal cohort was 4 weeks of age. While the given definition of perinate only extends to 7 days post-birth, this was extended to include neonatal individuals (up to 28 days post-birth) as

individuals of this age were few in number and it was felt that they did not belong within the older age cohort. Due to the estimated age ranges given for older individuals, the remaining age cohorts were created to reflect this: 4 weeks to 2 years, 3 to 5 years, 6 to 8 years, 9 to 12 years, 13 to 16 years and 17 years + (encompassing individuals labelled ‘late adolescent’). It is important to note that while the fetal and 4 weeks to 2 years of age cohorts were named as such, the fetal cohort comprised individuals ranged between 28 and 32 weeks *in utero* and the youngest individual of the 4 weeks to 2 years of age cohort was 7 weeks of age. These initial age ranges were deemed suitable at the time of data collection. However, during both qualitative and quantitative analysis, these age cohort ranges were adjusted. For more information regarding these adjustments, please refer to sections 5.4.1.5 and 7.2.4. Figure 5.1 displays the seriated lumbar vertebral columns of individuals at different ages.

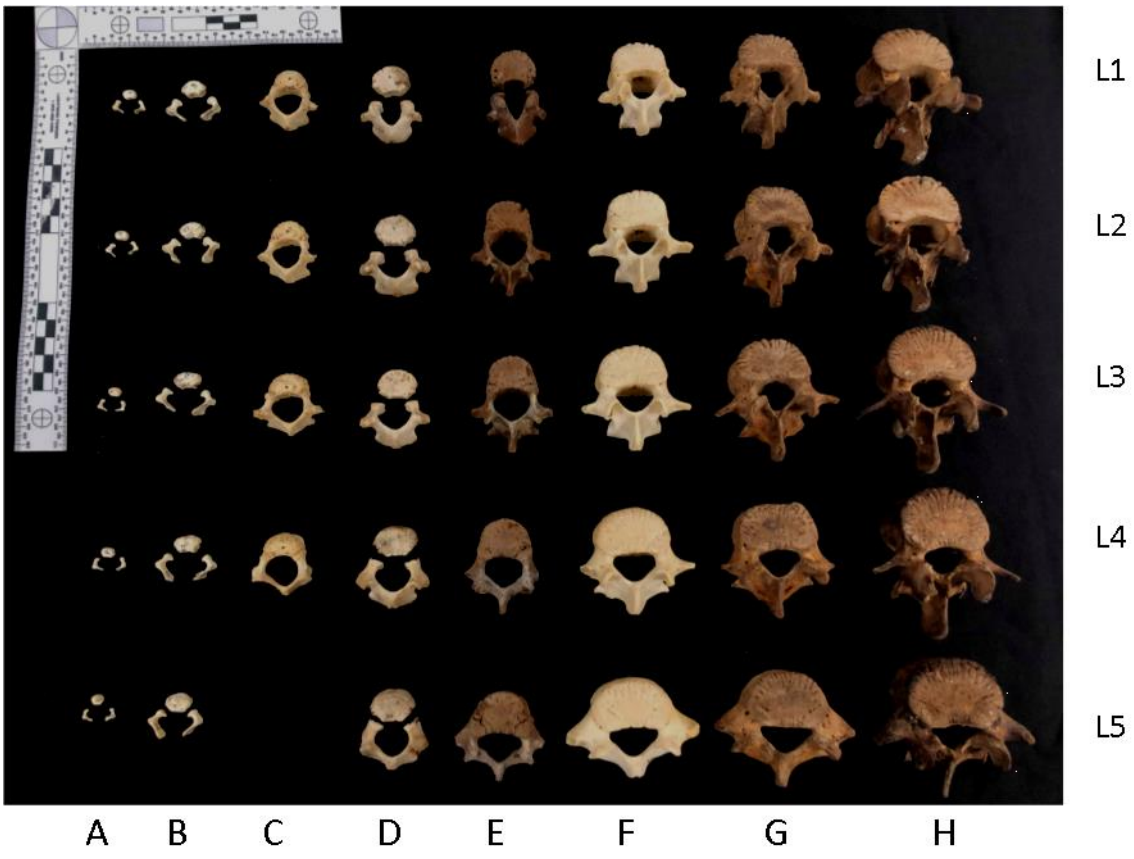

Figure 5.1: Seriated lumbar vertebral columns. A. 28 weeks in utero. B. Perinate. C. 7 months. D. 3 years. E. 6-8 years. F. 9-12 years. G. 14 years. H. 17 years.

5.3 Materials and methodology

5.3.1 *Sample Collection*

A total of 291 lumbar vertebrae from 69 individuals of known and estimated age ranging from 28 weeks *in utero* to late adolescence were chosen for qualitative analysis. The demographic of this sample can be seen in Table 5.1. Further information about this sample can be found in Appendix 5.1.

Table 5.1: Sample demographic for qualitative analysis

Age Cohort	No. Of Individuals	No. of L1	No. of L2	No. of L3	No. of L4jh	No. of L5	Total no. of Vertebrae
Fetal	3	3	3	3	3	2	14
Perinatal	14	14	13	13	13	11	64
4 weeks-2y	14	10	12	11	9	5	47
3-5y	11	10	9	9	10	5	43
6-8y	7	6	6	6	5	7	30
9-12y	6	5	5	5	5	6	26
13-16y	2	2	2	2	2	2	10
17y+	12	12	12	12	11	10	57
Total	69	62	62	61	58	48	291

5.3.2 *Selection of Radiography Parameters*

A Kodak DXS 4000 Pro portable radiography machine was used to scan the chosen sample. A number of parameters were set to produce the required radiographic image: exposure time, binning, machine power (KVP), the addition of an x-ray filter, the F-Stop, the Field of View (FOV), the focal plane and the addition of a reference scan. It was important to identify the optimal parameters to produce optimal image quality prior to scanning of the sample, to achieve the highest resolution images for analysis. For this, a fetal individual was scanned multiple times, with each parameter considered separately to identify the correct option for the scanning of bone. A fetal individual was chosen as these individuals comprise the smallest within the sample and are the most difficult from which to obtain high quality images. Higher quality images allow for more in-depth analysis

due to the increased level of information present with the image compared to lower resolution scans.

5.3.2.1 Exposure Time

The exposure time is the amount of time the sample is exposed to x-rays. It was found that an increase in time and more than one exposure per bone created a sharper image. The optimal value for the fetal individual was found to be 2 exposures at 40 seconds each, exposing each bone to x-rays for a total of 80 seconds. For consistency, all bones were scanned with this exposure time.

5.3.2.2 Binning

Binning is the process of joining adjacent pixels within an image in to enhance the final image. It was considered detrimental to join adjacent pixels as it lowered the resolution of the image. Therefore, binning was kept at 0 by 0 pixels.

5.3.2.3 KVP

KVP relates to the power of the machine. Full power, 35kvp, was chosen for scanning as lower powers resulted in lower quality images.

5.3.2.4 X-Ray Filter

A selection of copper filters were available for use. These filters, when placed over the x-ray source, absorb differing amounts of x-ray energy. When placed over the x-ray source, the 0.8mm copper filter removed any blur or lack of focus from the radiographic image, as perceived by the observer, and was therefore chosen.

5.3.2.5 F-Stop

The F-Stop controls the amount of light allowed into the camera. The more closed the F-Stop, the darker the image becomes. Therefore, the F-Stop was chosen to be fully open at 2.5mm.

5.3.2.6 Field of View

The Field of View (FOV) is the size of the area that is included in the scan. This is the only parameter that is dependent on the individual, as bones are of varying size. For the fetal individual scanned during the parameter testing phase, a FOV of 29.81mm was found to be optimal. All scans had a FOV of between 29.81mm and 90mm and were dependent on the size of the bone. The FOVs used were roughly 10mm apart and were chosen as the optimal FOV for each

bone scanned. The FOV could not be set separately for each bone due to the addition of a set reference scan (see section 5.3.2.8).

5.3.2.7 Focal Plane

This denotes the focus of the x-ray source. The focal plane can be controlled through a sliding mechanism and this was moved to the point in which the bone was in focus and not blurred, as perceived by the observer. The final value for the focal plane was 13.5mm.

5.3.2.8 Reference Scan

The reference scan function allowed the addition of a reference scan to correct for the background of the radiograph taken. To add a reference scan to the radiograph of the scanned bone, a blank scan matching the parameters of the radiograph were captured prior to taking the radiograph of the bone. This scan was saved and could be added as a correction for the background to reduce any noise or disruptions in the radiograph. The reference scan could only be added if the parameters matched those of the scan to be taken. For example, if the reference scan was at a FOV of 40mm, but the bone was to be scanned at 50mm, the reference scan would not be compatible.

It was found that, without a reference scan, the image produced was particularly bright and the background was not consistent. Without a background scan, the image had to be inverted, as the original scan depicted the background as white and bone as black. Without a reference scan, it was also observed that the background varied throughout the image, being lighter in the centre and darker around the edges. With the addition of a reference scan, the image was automatically inverted to show bone as white and any background as black. The background colour was also found to be more consistent within each image. Further preliminary testing was needed to identify the optimal preference for this parameter.

5.3.2.9 Screen Protection

To protect the radiographic screen from tears caused by placing bones in direct association with it, an acetate sheet was cut down to size and used to cover the screen at all times. Up to the age of neurocentral fusion (around 3 years in most cases), bones were placed directly onto the covered screen in the anatomical position. However, once fusion had begun to occur, there was

difficulty in placing bones in the anatomical position as the vertebral body had to be elevated for the scan to be taken.

5.3.2.10 Preliminary Investigation for Inclusion of Reference Scan

To assess whether the addition of a reference scan increased the resolution of the radiograph produced, the mechanism by which fused vertebrae could be placed in the anatomical position needed to be decided. Two options were available. The first option involved embedding individual vertebrae in anhydrous Oasis ‘wet’ florist foam. This method was considered due to its ability to deform when a bone is pressed into the medium. In this option, it would be necessary to use ParaFilm biofilm as a barrier between the bone and the anhydrous foam to stop the foam from damaging the bone. Secondly, an anhydrous foam block could be used to elevate the vertebral body to the required height to achieve the anatomical position.

To identify the optimal outcome of both the use of anhydrous foam and the addition of a background scan, a preliminary study was undertaken. Overall, it was decided that 8 different conditions would be tested, assessing both the method of recreating the anatomical position, and the inclusion of a background scan. Individual SC-010 L1 (4 years of age) was utilised for this preliminary study. All other parameters were set as described above, with the FOV set at 60mm for this individual. The 8 conditions, the outcomes and the resulting images can be seen in Table 5.2 and Figure 5.2.

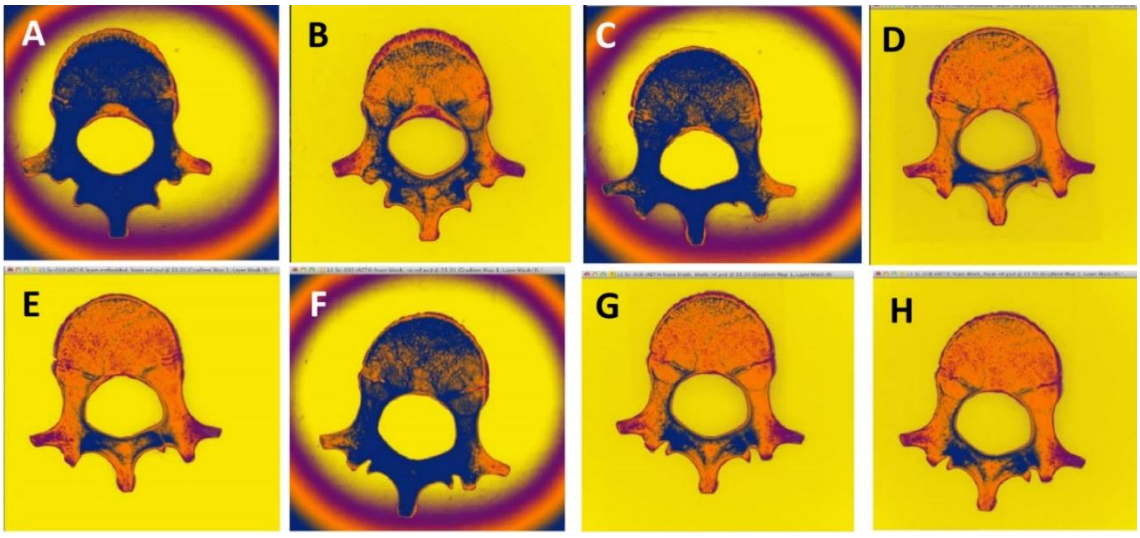

Figure 5.2: The images produced of the 4th lumbar vertebra of SC-010 (AET4) as a result of the 8 different conditions with regards to the reference scan and sample preparation.

Table 5.2: Conditions, their description and the outcome of potential mechanisms for scanning.

Condition	Description	Outcome
1. No foam, no reference scan	No foam was used, and no reference scan was added.	Fig 5.2A: With no reference scan, the background varied in colour and caused the centre of the scan to be more radiographically intense.
2. No foam, reference scan	No foam was used, but a reference scan was added to correct for the background.	Fig 5.2B: With a reference scan added, the background was more consistent. However, the purple rim was an artefact due to the tilting body of the vertebra as it is not in the anatomical position.
3. Foam embedded, no reference scan	The vertebra was embedded in florists' foam (along with a layer of protective biofilm between the foam and the bone). No reference scan was added.	Fig 5.2C: Once again, no reference scan caused the centre of the vertebra to appear more radiographically intense.
4. Foam embedded, blank reference scan	The vertebra was embedded in foam and a blank background scan was added.	Fig 5.2D: The scan was of acceptable quality due to the addition of a reference scan, however, the foam block was evident, having not been corrected for.
5. Foam embedded, foam reference scan	For the background, the vertebra was removed from the foam, which was then included in the reference scan to correct for the background.	Fig 5.2E: The scan was relatively clear however, removing and replacing the embedded vertebra without moving the foam between the reference scan and main scan was difficult. Also, the biofilm used to protect the vertebra could be seen in the final scan.
6. Foam block, no reference scan	The vertebral body was propped up using a block of foam. No protective parafilm was needed. No reference scan was added.	Fig 5.2F: A lack of reference scan meant that the background varied in consistency in the final image.
7. Foam block, blank reference scan	The vertebral body was propped up by a foam block, a blank reference scan was added.	Fig 5.2G: The scan was of acceptable quality and the issues regarding the protective biofilm were no longer applicable. However, the floral foam block could be seen as it had not been corrected for.
8. Foam block, foam reference scan	The vertebral body was propped up by a block of foam. The reference scan added included the foam block.	Fig 5.2H: This condition was considered to be the most acceptable, with the vertebral body in the anatomical position and the foam block successfully corrected by the background scan.

This preliminary study identified that the most appropriate method of recreating the anatomical position was by allowing the vertebral body to sit on a foam block of appropriate size. Furthermore, inclusion of a reference scan was important in regulating the consistency of the background once gradient mapping of the radiograph had occurred. Finally, the inclusion of the foam block in the reference scan was important as it removed noise created by the foam block included in the radiograph, hence meaning condition 8 (Figure 5.2H) was optimal.

5.3.3 *Bone Preparation and Scanning Protocol*

After identifying that the use of an anhydrous foam block to place the vertebra in the anatomical position was optimal for scanning, six foam blocks of varying height (4mm, 6mm, 8mm, 10mm,12mm and 14mm) were created. Blocks were fixed to acetate sheets with clear tape to reduce any movement of the foam block between the reference scan and radiograph. Reference scans were created for each acetate sheet and fixed block at set FOVs at 10mm intervals, from 30mm to 90mm.

For the scan, fused vertebrae were positioned with the spinous process in contact with the acetate sheet and the vertebral body placed on the anhydrous foam block, elevating it into the anatomical position. The most appropriately sized block was used based on each bone. Each scan was taken at the lowest FOV available (to the nearest 10mm) for the bone and included the associated reference scan to reduce noise.

5.3.4 *Image Post-Processing*

Once all radiographs had been collected, a number of post-processing steps were completed. Firstly, each scan was converted from a .bip file format to a useable image format. The ImageJ plug-in ‘Bioformats’ was used to convert scans to .tiff. To facilitate data interpretation from greyscale values in Adobe Photoshop CS5, files were further converted to .bmp file format.

5.3.5 *Gradient Map Application*

Adobe Photoshop CS5 was used to analyse the .bmp scan images. Scans were first converted to RGB colour and the gradient mapping tool was used to convert the 256 grey levels within the image into four gradients: yellow, purple, orange and blue (Table 5.3).

Table 5.3: The four colours comprising the gradient mapping system utilised.

Gradient	Description
Yellow	This was restricted to the background colour and denoted area of the lowest radiographic intensity, from 0% to 30%.
Purple	This colour indicated areas of low radiographic intensity within the bone from 31% to 53%.
Orange	This colour presented areas of intermediate radiographic intensity within the bone from 54% to 77%.
Blue	Blue denoted areas of the highest radiographic intensity within the bone, from 78% to 100%.

Each scan was gradient mapped manually. The first marker to be placed was yellow, which corresponded to the background. This was placed at the point in which the background became one solid colour. The three other colours were assigned equally over the remaining grey levels based on the level of the background. For example, in a case where the background is placed at 8%, the intervals of the remaining colours would be 23% apart. This was computed by subtracting the 8% from 100, then dividing by 4 (Figure 5.3). This method has been utilised previously by Cunningham and Black (2009b), O'Malley (2013), Yusof (2013) and Maclean *et al* (2014). Figure 5.4 shows the original digital radiograph and the gradient mapped image. Once gradient mapped, files were converted from .psd files to .jpeg file format. Each scan was printed onto A4 paper for ease of analysis.

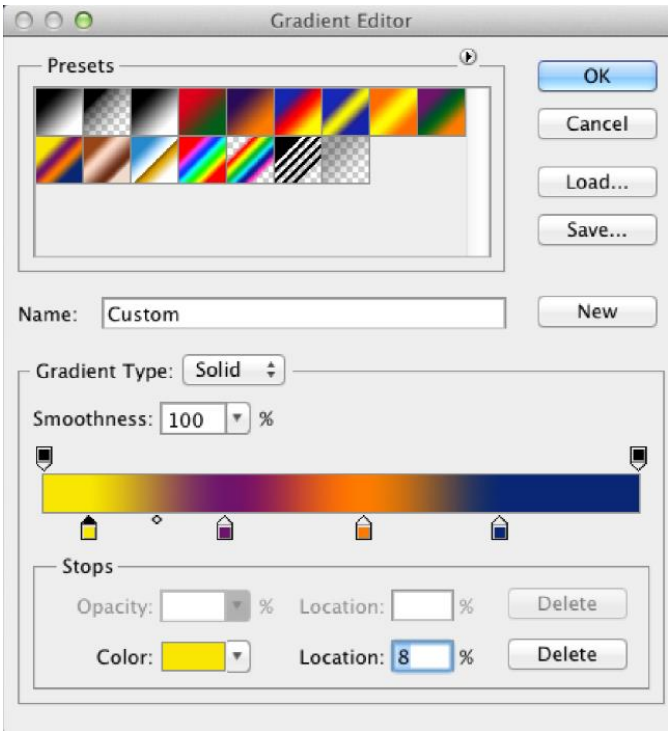

Figure 5.3: The dialog box for the selection of colours in the gradient mapping process.

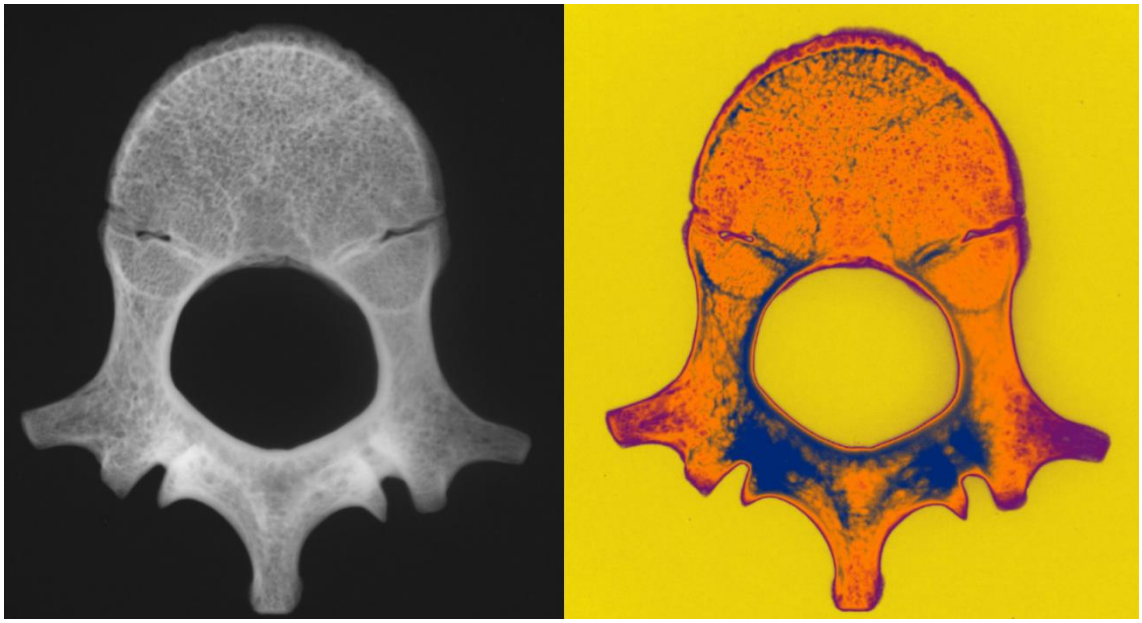

Figure 5.4: Left: Original digital radiograph of the 1st lumbar vertebra of individual SC-010, 4 years of age. Right: SC-010 L1 with gradient map.

5.3.6 *Analysis Protocol*

During analysis, information pertaining to individuals was unavailable to the observer, only the unique reference number and level of the vertebral column was available alongside the scan. This removed any potential age-related bias. The qualitative analysis was separated into two stages. The first documented the changes in radiographic intensity with development while the second was to identify whether different vertebral levels displayed different patterns of radiographic intensity within individuals.

The first aspect of the analysis began with the radiographic images being placed in order of least developed to most developed. In order to achieve this, the size and morphology of the developing vertebra was considered. This was later checked with the actual ages of the individuals and the order was found to follow a general age-related pattern. The changes in radiographic intensity throughout development for both the centra and neural hemiarches were documented. For this analysis, each vertebral level was analysed separately

Once this had been completed, the radiographs of the most developed vertebrae were pooled per individual and any information regarding the vertebral level was removed. An attempt was then made to identify any differences in the pattern of radiographic intensity between the five lumbar vertebral levels per individual.

5.4 Results

5.4.1 *Age Group Analyses*

5.4.1.1 Fetal Age Cohort (n=14)

The fetal age cohort comprised 14 vertebrae from 3 individuals. Variability in the morphology of the centrum was observed, most notably at the posterior margin of the vertebral centra, which was flattened or billowed in appearance (Figure 5.5A, B, white dashed line). A majority of the centra within this age cohort exhibited a central area of high radiographic intensity, denoted by areas of blue, Figure 5.5A, B, labelled C). This central area of radiopacity exhibited a number of posteriorly radiating 'projections' along the anteroposterior axis.

The neural hemiarches most commonly exhibited areas of high radiopacity in the developing laminae (Figure 5.5A, B, labelled La). In some cases, this extended into the pedicular bouton of the neural hemiarch (Figure 5.5A, B, labelled Pd).

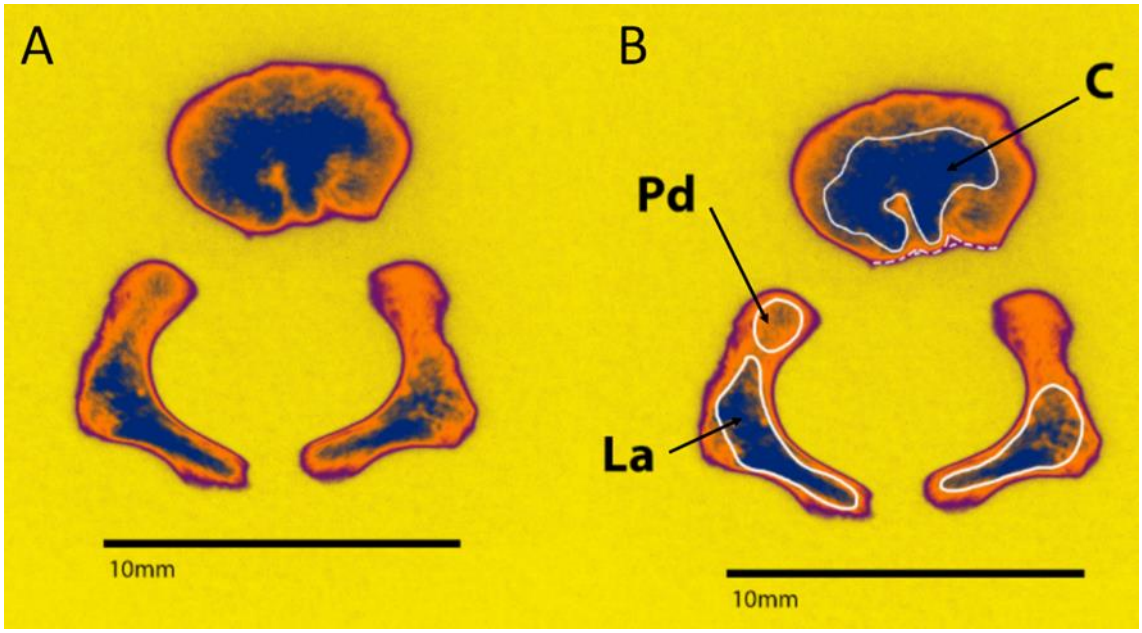

Figure 5.5: A. Original gradient mapped image of the 4th lumbar vertebra of SC-093, 28 weeks in utero. B. An overlay has been added to scan A, indicating areas of interest where C= centrum, Pd= pedicular bouton and La= future lamina.

5.4.1.2 Perinatal Age Cohort (n=64)

The perinatal age cohort comprised 64 vertebrae from 14 individuals. Similar to the fetal age cohort, the morphology of the centrum continued to exhibit variation at the posterior margin. Overall, radiopacity within the perinatal age cohort was found to have increased compared to the fetal age cohort.

Variation in the posterior margin was observed, with some individuals presenting billowing at the posterior aspect of the centrum. The amount of billowing observed was variable between individuals. Areas of billowing were observed to correlate to vascular foramina, with inward billowing indicating areas of vascular foramina, and areas of outward billowing correlating with a lack of vascular foramina (Figure 5.6A, B, white dashed line).

The perinatal age cohort displayed a clear, organised, symmetrical radiopacity system within the centrum. In the majority of cases, this system was more defined than in the fetal age cohort. Multiple posterior ‘projections’ were once again observed radiating from the centre mass of radiopacity. These ‘projections’ mirrored the pattern of vascular foramina observed at the posterior margin of the centrum on the dry bone, following the outward billowing.

Radiopacity of the neural hemiarches was observed to be restricted to either the external (lateral) aspect of the lamina, or both the internal (medial) and external aspects of the lamina. The pedicular boutons of the neural hemiarches also exhibited an increase in radiographic intensity when compared to the fetal age cohort.

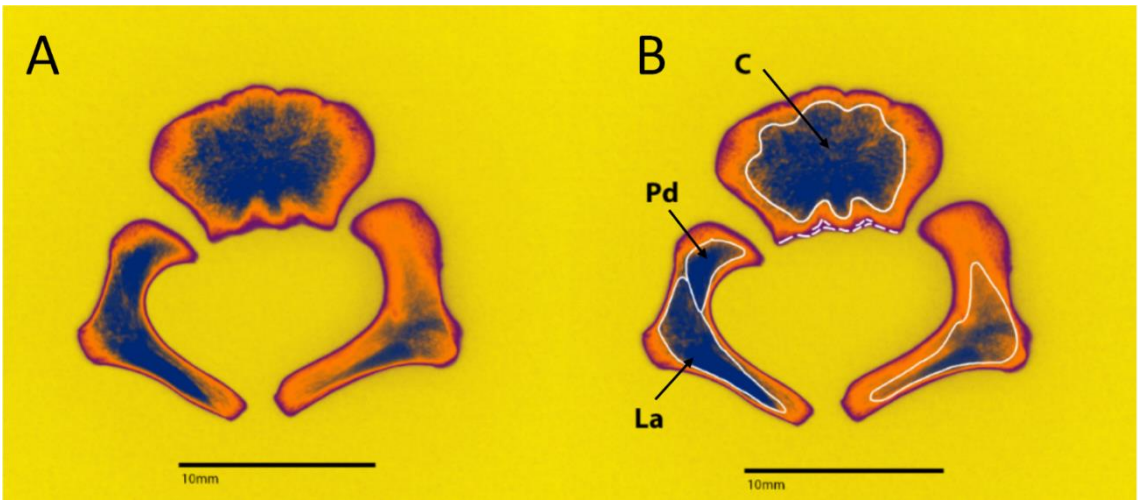

Figure 5.6: A. Original gradient mapped image of the 5th lumbar vertebra of perinatal individual SC-088. B. An overlay has been added to highlight areas of interest, where C= centrum, Pd= pedicular bouton and La= future lamina.

5.4.1.3 4 weeks-2y Age Cohort (n=47)

This developmental cohort comprised 47 vertebrae from 14 individuals and was characterised by an extensive loss of radiopacity within all areas of the vertebra.

Almost all evidence of the ‘projections’ seen within the fetal and perinatal age cohorts was absent, with the majority of vertebral centra exhibiting a more speckled appearance comprising of medium (orange) and low (purple) radiopacity (figure 5.7A, B).

Developmental changes could be observed within this age cohort. Fusion of the posterior synchondrosis could be observed within higher levels of the vertebral column, with this fusion event leading to the formation of a more prominent spinous process (figure 5.7A, B, labelled Sp). Bony outgrowths in the areas of the transverse processes could also be observed, although these areas remained of relatively low radiopacity (figure 5.7A, B, labelled Tr). Radiographic intensity persisted in the laminae, with radiopacity extending laterally into the area of the future mamillary processes (figure 5.7A, B, labelled La). A triangular shaped area of particularly low radiopacity could be observed at the posterior aspect of the centrum in some individuals (figure 5.7A, B, labelled *).

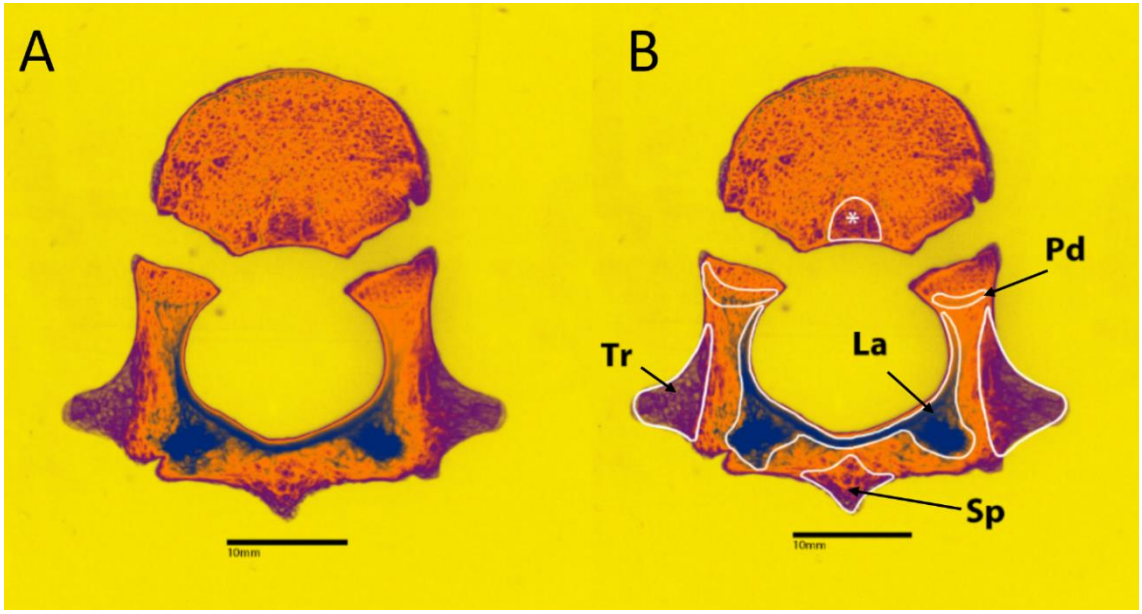

*Figure 5.7: A. Gradient mapped image of SC-024 L3, 2 years of age. B. Addition of an overlay where La= lamina, Pd= pedicular bouton, Tr= transverse process, Sp= spinous process and *= area of low radiopacity.*

5.4.1.4 3-5y Age Cohort (n=43)

The 3-5 years of age cohort comprised 43 vertebrae from 11 individuals. Several more extensive developmental changes could be observed within this age cohort.

Neurocentral fusion was observed to occur within this age cohort, along with increased radiopacity in the pedicles (figure 5.8A, B, labelled Pd). Further to this, an area of increasing radiopacity was seen developing around the anterior aspect of the vertebral body, corresponding with the formation of the annular ring on the dry bone (figure 5.8A, B, labelled An).

The area of decreased radiographic intensity previously seen at the posterior aspect of the vertebral body in the 0-2y age cohort continued to be present. In this case, lines of increased radiopacity originating from the pedicles flanked the area (figure 5.8A, B, labelled *).

Further development of the neural arches were observed, with increasing radiographic intensity at the junction between the pedicles and the laminae, at the site of the future mamillary processes (figure 5.8A, B, labelled Pd, La). An increase in radiopacity was also seen extending into the spinous process from the highly dense area of the lamina (figure 5.8A, B, labelled La, posterior projections towards Sp).

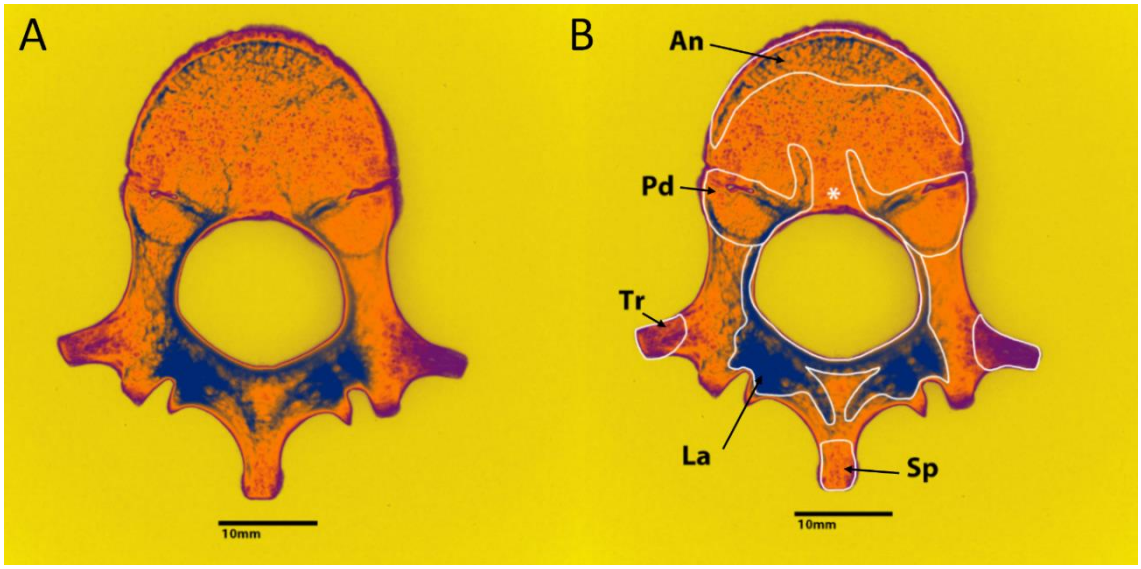

*Figure 5.8: A. Gradient mapped radiograph of SC-010 L1, 4 years of age. B. Addition of an overlay to image A, with An= developing annular ring, Pd= pedicle, Tr= transverse process, La= lamina, Sp=spinous process and *= area of low radiopacity.*

5.4.1.5 6y+ Age Cohort (n=123)

The 6+ age cohort comprised 4 separate age cohorts (6-8y, 9-12y, 13-16y, 17y+) that were combined, resulting in 123 vertebrae from 27 individuals. After the documentation of changes in radiographic intensity with development, it was noted that while the developmental pattern that existed generally correlated with age, there was considerable variation and overlap between individuals aged 6 and over. This made it difficult to identify specific developmental differences between these age groups. For example, some individuals within the 6-8 years of age cohort were found to display increased radiographic intensity compared to individuals within the 9-12y cohort and no differences could be identified between any individuals 13 years onwards. Therefore, it was decided to pool the four age cohorts.

A general increase in radiopacity over the entirety of the vertebra was observed within these age cohorts (figure 5.9A, C). After neurocentral fusion, the area pertaining to the pedicles continued to increase in radiopacity, connecting with the radiopacity observed around the anterior aspect of the vertebral body and also of the lamina (figure 5.9A, B, C, D, labelled Pd). The regions of the laminae, developing mamillary processes and superior and inferior articular facets also continued to increase in radiopacity (figure 5.9A, B, C, D, labelled La).

While the spinous process was observed to increase in radiographic intensity along with other areas of the vertebra, the radiopacity at the transverse processes remained low (figure 5.9A, B, C, D, labelled Sp, Tr). The area void of radiographic intensity at the posterior aspect of the vertebral body, seen in previous age cohorts, adopted a triangular shape bordered by radiations of dense radiopacity originating from the pedicles (figure 5.9A, B, C, D, labelled *).

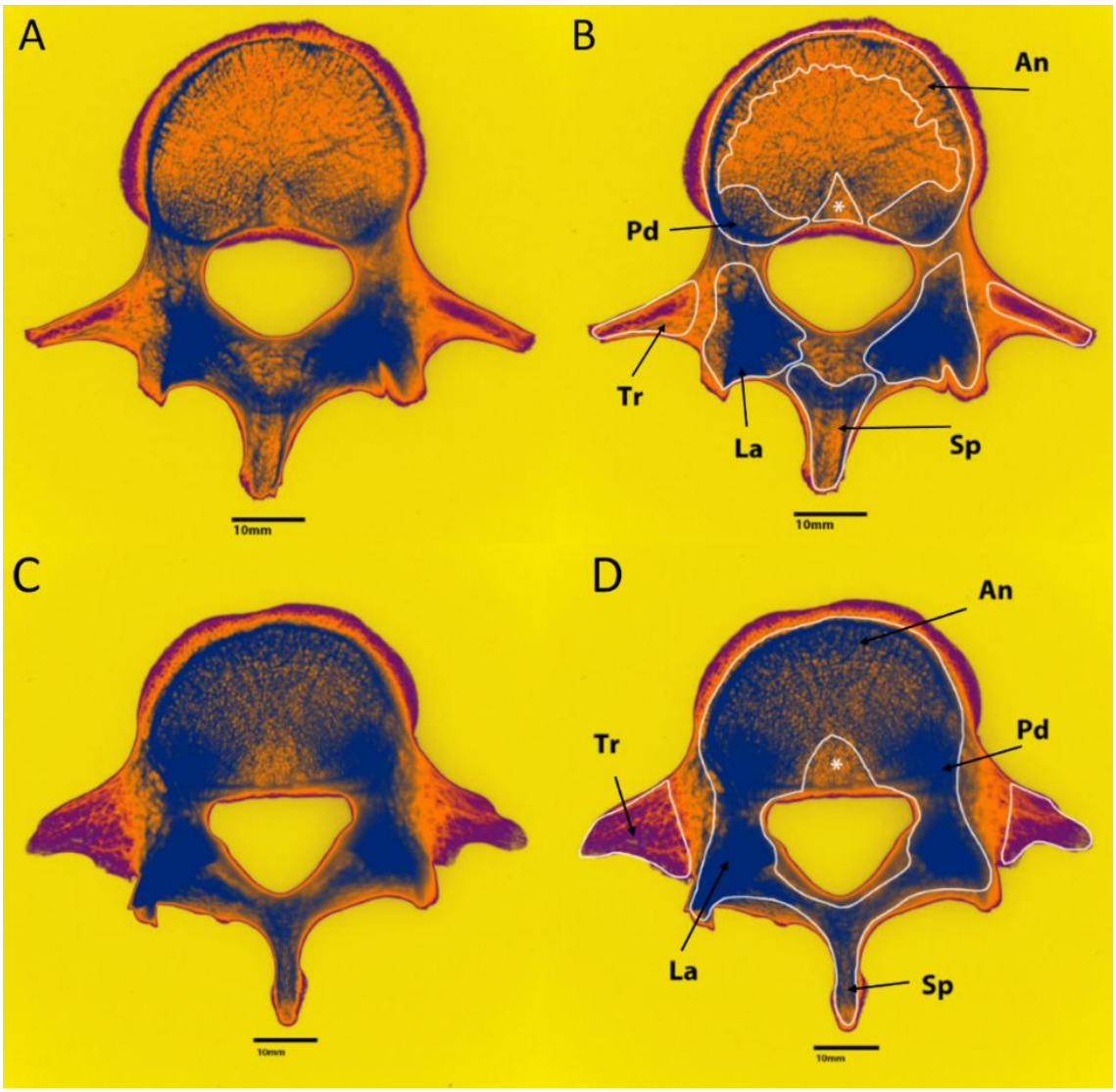

*Figure 5.9: A and C. Gradient mapped radiographs of SC-171 L3 (aged 9-12 years) and SC-035 L5 (aged 19 years) respectively. B and D. Areas of interest labelled, where An= Annular ring, Pd= pedicle, Tr= transvers process, La= lamina, Sp= spinous process and *= area of low radiopacity.*

5.4.2 *Analysis of each level of the lumbar vertebral column*

It was not possible to identify different levels of the vertebral column from the pattern of radiographic intensity alone. While it was generally possible to identify the age cohort in which the vertebra belonged, identifying whether this was L1 or L5 was not possible. This only became possible in individuals older than around 2-4 years and was not due to the pattern of radiopacity, but rather the ability of the investigator to identify the level of the vertebral column from the morphology of the vertebra, or from developmental events such as fusion of the posterior synchondrosis or neurocentral fusion.

5.5 Discussion

This qualitative analysis observed that, while no qualitative differences between vertebral levels could be identified, differences between developmental cohorts were present. A pattern of increased radiographic intensity was present within the fetal and perinatal periods. This pattern of radiographic intensity was obliterated in the early postnatal period before beginning to increase in intensity in particular areas of the developing lumbar vertebra in childhood and adolescence. The early pattern of radiographic intensity in the fetal and perinatal periods is likely due to the pattern of ossification of the lumbar vertebrae, alongside the presence of vasculature. The later changes observed postnatally have been attributed to a period of bone loss followed by remodelling.

5.5.1 *Differentiation Between Levels of the Lumbar Vertebral Column*

It was expected that prior to any load-bearing requirements, the lumbar vertebrae would not be distinguishable by their vertebral level via radiography. This was anticipated due to the lack of expected differences in the internal architecture of the lumbar vertebrae at this age, as any developmental changes would be expected to occur post load-bearing. However, once the lumbar vertebral column becomes load bearing, there is the potential for vertebral trabecular structure to differ at each level due to potential differences in biomechanical demands. It was expected that L5 would exhibit thicker trabeculae and therefore may have appeared more radiographically intense than higher levels of the lumbar vertebral column, as it is the lowest of the lumbar vertebrae and bears the greatest load transfer of all lumbar vertebrae. However, this was not the case in this qualitative study. It may be that there are no significant differences in the trabecular structure between L5 and other levels of the lumbar vertebral column. Conversely, it may be that the imaging modality utilised for this section of the project may have led to this result. Radiography is a two-dimensional representation of a three-dimensional structure, causing superimposition that may have led to inaccurate assessment of the gradient mapped images produced. Equally, it may have been that the resolution at which the scans were acquired was not high enough to detect these changes. Further limitations of the methodology are discussed in section 5.5.4. The presence of differences in the internal architecture of different levels of the lumbar vertebral column will be addressed later in the quantitative aspect of this project.

5.5.2 *Patterns of Radiographic Intensity in the Fetal and Perinatal Period*

Gradient map analysis of digital radiographs has shown that the lumbar vertebrae present an organised system of radiographically intense ‘projections’ radiating from the centre of the centrum, within the fetal and perinatal age cohorts.

5.5.2.1 Pattern of ossification

Ossification of the lumbar centra commences around 8 weeks *in utero* and is endochondral in nature. Each centrum arises from either one or two primary centres of ossification, dorsal to the regressing notochord (O’Rahilly *et al.*, 1990; Szpinda *et al.*, 2013) which has been found to have an inducive role in the initiation of ossification (Fleming *et al.*, 2001). In all individuals, the area pertaining to the primary centre(s) of the lumbar centrum was found to be radiographically intense, with the radiopaque ‘projections’ radiating towards the periphery from the centre of the centrum, the site of the primary ossification centre. Conversely, the peripheral regions of the centrum were less radiographically intense. This pattern of radiographic intensity has been observed previously by Nuzzo *et al.* (2003) who described ossification of the developing fetal lumbar vertebrae as ‘an expansion from a central nucleus by the formation of shells of new mineralised structure’. As the ossification centre originates at the centre of the cartilaginous centrum, bone found in this area is the oldest and consequently has undergone more extensive bone remodelling compared to younger bone laid down at the periphery. Therefore, bone closer to the primary ossification centre may be of a higher radiographic intensity due to its increased maturity.

5.5.2.2 The role of vasculature

The morphology of the posterior margin of the centrum was observed to be related to the posteriorly radiating ‘projections’ seen extending from the central radiopaque area of the centrum. This pattern of radiopacity was observed to mirror the billowing seen at the posterior border of the centrum, which was further observed to be related to vascular foramina within the posterior aspect of the dry bone.

The posterior aspect of the lumbar vertebral centra are drained by the basivertebral veins, while segmental arteries, arising from the abdominal aorta, perforate the centrum anteriorly, laterally and posteriorly (Ratcliffe, 1980; 1981;

Ebraheim *et al.*, 2004). In cases where the posterior margin of the centrum was billowed, multiple vascular foramina were observed in the dry bone. In cases where billowing was not present, only one large vascular opening, with its associated posterior radiopaque ‘projections’ was present. Variability within the vascularisation of the vertebral centra has been observed previously, with studies observing between 1 and 4 nutrient arteries entering the centrum from the posterior aspect. Two nutrient arteries were found most commonly (Skawina *et al.*, 1997). Furthermore, venous drainage has also been found to be variable, leading to the discrepancies in number of vascular foramina and the pattern of billowing observed posteriorly.

The vertebral centra develop via endochondral ossification, with the primary ossification centre(s) developing in the area of the regressing notochord (O’Rahilly *et al.*, 1990). It is thought that, at first, remnants of the notochord release an angiogenic-inhibiting factor that prevents vascular penetration of the region for a short time (Skawina *et al.*, 1997). After regression of the notochord, the cartilaginous anlage converts to hypertrophic cartilage and begins to release angiogenic stimulators (Alini *et al.*, 1996). This leads to vascular penetration of the cartilaginous anlage from a posterior aspect, in the form of nutrient arteries arising from the anterior vertebral canal branch of the lumbar artery of the descending aorta. Venous drainage also develops in the form of the posteriorly located basivertebral veins, draining into venous plexuses within the vertebral canal (Ratcliffe, 1980; 1981; 1982; Crock, 1996; Skawina *et al.*, 1997; Ebraheim *et al.*, 2004; Moore *et al.*, 2019). Vascularisation of the area initiates ossification at the site of the primary ossification centre by transporting cell types involved in osteogenesis (Colnot *et al*., 2004; Ortega *et al.*, 2004; Mackie *et al.*, 2008; Maes *et al.*, 2010). From here, ossification occurs in an outward manner, from the centre of the centrum. As the vasculature is already present within the cartilaginous anlage when ossification begins, bone surrounds the vessels but cannot invade them. It is thought that the areas of higher radiopacity observed more centrally within the centrum, in the region of the primary ossification centre, are indicative of areas lacking vascularisation. Meanwhile, areas of lower radiopacity around the periphery, where periosteal vessels are present, and at the posterior aspect of the centrum, where the nutrient arteries and basivertebral veins are present, equate more with more highly vascularised areas.

This observation has also been made in the developing human ilium, where areas of high vascularity equated with areas of low radiopacity (Cunningham and Black, 2010). These regions of low radiopacity persist throughout development, with a characteristic area of low radiopacity seen at the posterior aspect of the vertebral body in the majority of lumbar vertebrae, even around late adolescence, supporting the concept that areas of low radiopacity coincide with areas that have a pre-existing space occupation.

An area void of radiographic intensity can be seen in a number of vertebral bodies in the 6y+ age cohort. This area, posteriorly in the central region of the bone, can be linked back to the fetal and perinatal age cohorts, where the cartilaginous centrum undergoes vascularisation from the nutrient arteries at the posterior aspect (Skawina *et al.*, 1997). This vasculature continues to be present in the adult, and its presence leads to a lack of bone in the region and hence a lack of radiopacity.

5.5.2.3 Proximity of the Neural Hemiarches

The pattern of radiopacity observed within the lumbar centra may also be affected by the proximity of the neural hemiarches. In early development, the lumbar vertebrae are present as a cartilaginous anlage (Maat *et al*., 1996; Cunningham *et al.*, 2016). Therefore, until fusion, the developing neural hemiarches are connected to the centrum via a cartilaginous connection in the form of a cartilaginous growth plate (Maat *et al.*, 1996).

Radiopacity was observed to increase in the region of the pedicular boutons of the developing neural hemiarches between the fetal and perinatal age cohorts. Simultaneously, the more lateral of the posterior radiopaque ‘projections’ increased in radiopacity into the perinatal age cohort. The proximity of the pedicular boutons to the neural hemiarches through this cartilaginous connection, or *vice versa*, may play a role in the induction of ossification in the region through mechanical stimulation. There is evidence that mechanical stimuli play a vital role in the initiation of ossification. Numerous research into animal models have illustrated that reduced muscle mass or immobility during the embryonic and fetal period leads to reduced development of the cortical and trabecular architecture in load bearing bones (Rodriguez *et al.*, 1988; Nowlan *et al.*, 2008; Nowlan *et al.*, 2010; Nowlan *et al.*, 2012; Shea *et al.*, 2015; Verbruggen *et al.*, 2016).

Consequently, it is entirely possible that, through *in utero* limb movements and stimulation of musculature and associated ligamentous structures within the area of the developing lumbar vertebral column, ossification is initiated in both the pedicular bouton of the neural hemiarches and the lateral areas of the centrum. Bagnall *et al.* (1977a; b) discussed the role *of in utero* movements in relation to the development of the vertebral column, with particular reference to the early gasp reflex and respiratory movements for the development of the secondary cervical curvature, and the role of *in utero* lower limb movements for the initiation of ossification of the lower thoracic and lumbar centra. These movements have been observed to occur as early as 6-7 weeks *in utero*, just prior to the commencement of ossification in the upper lumbar region. Therefore, these movements may play a role in the induction of ossification, potentially through the initiation of cartilaginous hypertrophy and the coinciding vascularisation of the cartilaginous anlage. A number of mechanosensitive genes have been identified as responsible for the production of important factors such as Indian Hedgehog (IHH), fibroblast growth factor 3 (FGFr3), parathyroid hormone-related protein (PTHrP) and runt-related transcription factor 2 (Runx2) (Nowlan *et al.*, 2008; Nowlan *et al.*, 2012) which play a role in the initiation of cartilage hypertrophy and osteogenesis (Mackie *et al.*, 2008; Schipani *et al.*, 2009; Dirckx *et al.*, 2013; Maes, 2013).

The pattern of radiographic intensity in the developing laminae of the neural hemiarches reflects the pattern of intramembranous ossification observed by Chandraraj and Briggs (1991) and Maat *et al.* (1996). Ossification commences on the internal aspect of the developing lamina as a perichondral lamella. Osteogenesis then occurs with ossification extending into the cartilaginous anlage of the neural hemiarches. As development continues, three growth zones have been identified within the developing hemiarch. These are at the site of the future pedicle, lamina and transverse process. From this point, ossification progresses centripetally (Cunningham *et al.*, 2016). The area of the developing lamina is also the site for the development of the future mamillary processes, secondary centres that appear and fuse at around puberty. The mamillary processes are a key site of muscular and ligamentous attachment. Therefore, this pattern may also be linked to nearby developing muscular and ligamentous attachments. It has recently been discovered that large muscle groups have

already formed and are of adult morphology at 8 weeks *in utero*. While the mamillary process has yet to ossify and fuse at this age (Cardoso and Ríos, 2011), the transversospinales muscle group, of which multifidus and rotatores have attachments to the mamillary and spinous processes of the adult lumbar vertebrae, are identifiable as a muscular mass adjacent to the vertebral column (Warmbrunn *et al.*, 2018). The proximity of these muscles may drive ossification in the region, leading to this pattern of radiopacity.

The vascular supply of the neural hemiarches arises predominantly from branches of the lumbar artery of the descending aorta. The posterior vertebral canal branch of the spinal branch of the lumbar artery supplies the internal aspect of the neural arches, while the posterior branch of the lumbar artery gives nutrient and periosteal vessels to the laminae and spinous process from the external aspect. Meanwhile, the neural arches are drained by the internal and external venous plexuses (Ebraheim *et al.*, 2004; Moore *et al.*, 2019). As with the radiopacity seen in the centrum, the pattern of radiopacity within the neural hemiarches may be due to the pattern of vasculature. The periphery of the neural hemiarches is lower in radiopacity than the central portion of the neural hemiarches, where vascular supply is less dominant, while the periphery houses a number of vessels and therefore has a pre-existing space occupation.

5.5.3 *Loss of Radiographic Intensity Postnatally*

5.5.3.1 A Period of Constructive Regression

After the perinatal period, a loss of radiographic intensity was observed. In the 0-2y age cohort, radiopacity decreased compared to earlier age cohorts. These findings have been noted previously. A number of researchers have remarked on a decrease in either radiopacity or bone density in this age cohort in a number of skeletal elements including the scapula (O'Malley, 2013), the vertebral column (Nuzzo *et al.*, 2003; Acquaah *et al.*, 2015), the ischium (Maclean *et al.*, 2014), the sacrum (Yusof, 2013), the femur (Ryan and Krovitz, 2006) and the tibia (Gosman and Ketcham, 2009).

Acquaah *et al.* (2015) defined the stage at which a loss of density was observed as 'constructive regression', one of three stages in the development of trabecular architecture: overproduction, constructive regression, refinement. The first stage, overproduction, was found to occur in the fetal and perinatal periods,

where surplus bone is laid down to create a mineral reservoir during periods of excess mineral availability in preparation for post-natal bone growth. During constructive regression, the resorption of bone releases these stored nutrients for use. Furthermore, with excess bone resorbed, there is the potential for the now reduced microarchitecture to undergo remodelling, which occurs in the refinement stage. Highly radiopaque regions within the fetal and perinatal centra may be an example of the overproduction phase of microarchitectural development. Post-birth, the lumbar vertebral column has little biomechanical significance and therefore can afford to undergo constructive regression (Rauch and Schoenau, 2002; Acquaah *et al.*, 2015). However, it is surprising that lack of radiopacity is present throughout the entirety of the 0-2y age cohort, as a number of key developmental milestones occur during this time including the infant sitting upright unsupported, crawling and walking unaided (Keen, 1993; WMGRSG, 2006). Thus, it would be expected that remodelling would begin to occur and radiopacity would begin to increase once again.

5.5.3.2 The Potential for Refinement

After the period of constructive regression, refinement commences and radiographic intensity within the centrum begins to increase once again. This has been observed to occur first and foremost at the pedicles, an area known for its importance in weight bearing within the adult vertebral column (Pal and Routal, 1987). The pedicles have also been observed as highly radiopaque by Maat *et al.* (1996), who described the region as a ‘trabecula-packed area’. While the direct cause of the radiopacity seen in the pedicles in this study cannot be ascertained, it may imply the presence of a previously observed dense trabecular network, indicating the importance of the pedicles as load-bearing areas within the neural arch.

The radiopacity seen extending into the laminae, transverse processes, mamillary processes and spinous process from the pedicles may also reflect strengthening muscular and ligamentous attachments in the region.

The ossification and fusion of the superior and inferior annular rings may explain the radiopaque extensions seen from the pedicle and circling the outer rim of the vertebral body. These ring shaped, posteriorly deficient secondary centres appear and fuse at around the ages of 14-23 years of age (Albert *et al*.,

2010; Cardoso and Ríos, 2011), although they can appear as early as 2-6 years of age (Hindman and Poole, 1970). This wide age range for fusion, along with variability, could be used to explain the variability within the 6y+ age cohort and why younger individuals presented these radiopaque extensions, while some older individuals do not. Furthermore, in this investigation, individuals were not separated by sex, in part due to the lack of documentation for some individuals and the issues surrounding juvenile sex estimation. However, it is known that male and female individuals mature at different rates, and hence pubertal timing is variable between the sexes. Moreover, there is variation within the sexes due to differing rates of growth and maturation in each individual (Cunningham *et al.*, 2016). This may also describe the variability observed after the age of 6 years.

5.5.4 *Limitations of the Methodology*

5.5.4.1 Limitations of radiography as an imaging modality

Perhaps the most prominent issue with radiography as an imaging modality in general is the superimposition of the object that occurs. More specifically, the lumbar vertebrae have been found to differ in the superior, inferior and central regions in terms of trabecular structure. This information is lost when a radiograph is taken from the superior aspect of the bone.

It is arguable that the pattern of radiographic intensity observed within this preliminary investigation cannot be related directly to bone density. It is important to note that actual density values cannot be determined through the methodology utilised. However, the observations of this study, in particular within the fetal period, imply that in this case, intensity and density are closely related. Nuzzo *et al.* (2003) assessed density within developing fetal lumbar vertebral and found that the centra were particularly dense within the central region compared to the periphery. The observations of this investigation mirror this finding.

Furthermore, the aim of this study was to identify areas of further interest for an in-depth quantitative analysis and all analyses within this investigation were of a qualitative nature. As all radiographs were taken with the same machine, all imaging parameters kept constant and all gradient mapping following a set protocol, it is possible to compare the images produced to gain insight into developmental patterns throughout ageing, and to identify areas for further quantitative analysis.

5.5.4.2 Gradient Map Analysis

One aspect of this investigation open to human error is the placing of the gradient map onto the radiographed vertebra. The first step comprises setting the background colour by sliding a marker to the point at which the background is a solid colour. The definition of a ‘solid colour’ is potentially different to different researchers. However, in this investigation, all radiographs were gradient mapped by the same researcher and the same computer and setting was used in each case, to improve the reliability of setting the same background colour each time. Furthermore, scans could be compared against one another and any scans with backgrounds differing from the majority were adjusted.

5.5.4.3 Scheuer Collection

While the Scheuer collection is invaluable in allowing the non-invasive assessment of developing trabecular architecture, it is not without its limitations. The collection comprises skeletal material from forensic, anatomical, archaeological and historical sources meaning not all skeletal elements are considered modern. Moreover, there is a paucity of information regarding a majority of the sample including social status, nutritional availability and their cause of death.

At the start of this study, it was decided that individuals presenting more than 30% damage to the cortical or trabecular bone were to be excluded. In some cases, there appeared to be slight damage to some lumbar vertebra, however, as this was deemed to be below the somewhat arbitrary 30% threshold, these individuals were included in the study. This may have had some effect on the radiopacity seen in these cases, although this is perceived to be a negligible difference.

It is important to note that the age of a number of individuals included in this sample is an estimation and given as a range. This is part could be a factor in the variation seen in individuals above the age of 6 years. The age ranges given tend to increase in size as individuals age, due to the decreasing accuracy of the methods from which age can be established. Furthermore, overlap of age ranges could also explain some of the overlap seen in the 6 years of age + cohort.

5.5.5 *Future Avenues*

This investigation is one of number completed on different developing skeletal elements. As this investigation focuses solely on the lumbar vertebral column, a potential future avenue would be to explore patterns of radiographic intensity in other unstudied regions of the human vertebral column, such as the cervical or thoracic columns.

Furthermore, the sample utilised was relatively small and only included individuals aged up to late adolescence. The sample size could be increased, and older individuals could be included to study senescence and the radiographic profile of healthy aging bone versus osteoporotic bone.

6 A Quantitative Analysis of the Developing Human Lumbar Vertebrae

6.1 Aims

This section of the project utilised micro Computed Tomography (μCT) and histomorphometric analysis software (CTAnalyser) to quantify the trabecular structure within the centra of the 1st, 3rd and 5th lumbar vertebrae from the fetal period through to 8 years of age. The aim was to gain an understanding of the developmental pattern of the trabecular bone architecture in an attempt to link age-related trabecular signatures to potential developmental milestones. To accomplish this aim, it was necessary to undertake a preliminary study to identify an optimal methodology for the scanning and analysis of the trabecular architecture within the lumbar vertebral centra, which can be found in Appendix 6.1.

6.2 Materials and Methods

6.2.1 *Sample Collection*

Vertebrae at the levels of L1, L3 and L5 were chosen for analysis, as together these three levels represent the superior, central and inferior portions of the lumbar vertebral column and enable the analysis of any potential differences in trabecular structure relating to the lumbar lordosis and differential loading of the column at the lumbar level. Secondly, only individuals up to the age of 8 years were chosen for analysis. This was due to neurocentral fusion nearing completion in the lumbar vertebrae around this age. Individuals within the 6-8 years of age cohort were assessed individually to identify whether it was possible to differentiate between the centrum and pedicular bouton of the fusing neural arches. If this was not possible due to near complete or completed fusion, the vertebra was excluded from this part of the study. Below is a table of the final sample utilised in this section of the project (Table 6.1). More information about this sample can be found in Appendix 6.2.

Table 6.1: Sample demographic for quantitative analysis

Age Cohort	L1	L3	L5	Total
Fetal	2	3	2	7
Perinatal	14	13	11	38
4 weeks to 2 years	10	11	5	26
3-5 years	7	5	4	16
6-8 years	1	1	0	2
Total	34	33	22	89

6.2.2 *Scanning and Reconstruction*

6.2.2.1 Nikon X-Tek XT H 225 ST and Inspect X

The micro computed tomography apparatus used to scan the chosen sample was a Nikon X-Tek XT H 225 ST housed within the Fulton Building, School of Science and Engineering at the University of Dundee, where all scanning occurred. This machine was controlled through Inspect X dual screen computer software.

The vertebra to be scanned was placed on a foam block on a circular metal table within the cabinet of the µCT machine (Figure 6.1). The placement on foam was necessary as the metal table was visible on the scan when the bones were placed on it directly and due to the proximity of the bone to the table, there was difficultly in removing this digitally from the scan at the post-processing stage. The foam, which was less dense and therefore easier to remove during post-processing, elevated the bone, removing the metal table from scan view. An effort was made to place the bone within the centre of the foam block, as close to the centre of rotation of the metal table as possible. This was necessary as any deviation from the centre of the table caused the vertebra to extend more laterally when rotated, increasing the size of the Field of View (FOV) needed, and hence decreasing the resolution of the scan. Vertebrae between the fetal period and 3 years of age were also embedded in floral foam with a protective plastic covering (Figure 6.2). The floral foam acted to stabilise smaller unfused elements during scanning, while the protective plastic covering prevented the incursion of the floral foam into the trabecular spaces which could cause irreparable damage to the fragile bone. Stability of the vertebral elements was important as any movement

of individual elements during the scanning process could potentially increase the noise of the scan, for example a motion artefact (Boas and Fleischmann, 2012). There was no requirement to place the older vertebrae, where neurocentral fusion had occurred, in the anatomical position as the scan could be manipulated during post-processing to achieve this. However, the vertebrae embedded in floral foam were already in the anatomical position as a result of the previous qualitative study and this was not altered.

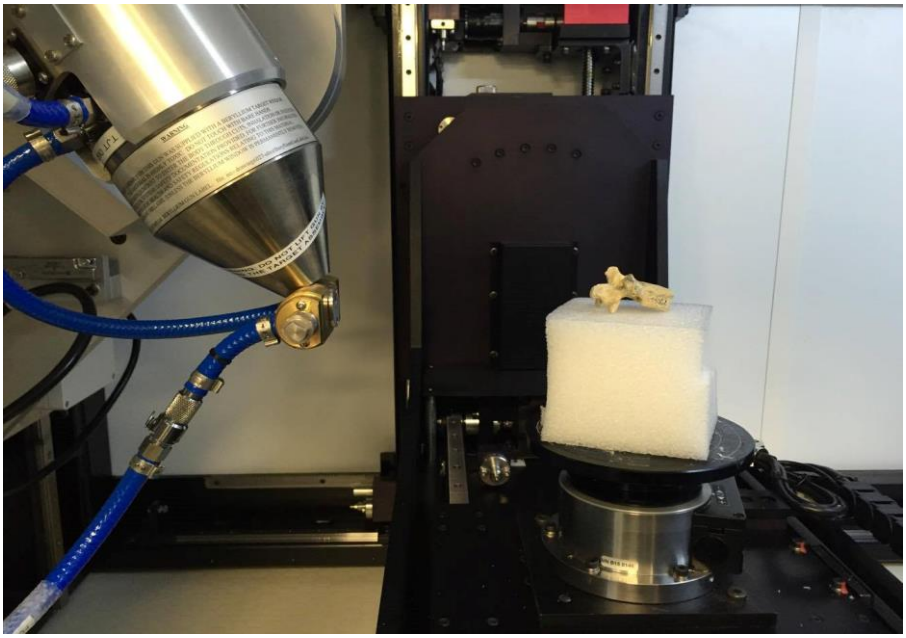

Figure 6.1: A lumbar vertebra placed on a foam block on the metal table within the animal cabinet of the Nikon X-Tek XT H 225 ST machine. In the left aspect of the image, the X-ray source is present. The X-ray detector is on the right-hand side but is out of view.

Figure 6.2: The fifth lumbar vertebra of a perinatal individual, embedded in floral foam with a parafilm covering for protection.

Once the vertebra had been placed within the μCT cabinet, Inspect X software was used to create the scan. The scanning process involved positioning the vertebra and setting scan parameters: the beam energy (kV), beam current (uA) and machine power (W), both of which were individual dependent. The values for these parameters can be found in Appendix 6.3. A background scan was created, to similar effect of the background scan in the radiographic study. Finally, the conditions of the scan were set. It was possible to set both the number of projections and number of frames per projection of the scan. The number of projections is the number of smaller rotations made by the metal table within the cabinet, to total 360°. An increased number of projections would lead to smaller degree increments and therefore more rotations to reach 360°. The number of frames per projection is the number of x-ray images taken at each projection, an average of these images gives the final image for that projection. A preliminary study was completed to identify the optimal scan parameters for the sample (Appendix 6.1). Individuals were scanned at 1,682 projections with 2 frames per projection. The duration of each scan was 28 minutes and 26 seconds. Further details of the scanning process can be found in Appendix 6.4.

After acquisition, each scan was reconstructed manually using CTPro3D. Manual reconstruction of the data allowed increased control over the post-processing of the scans. Scans were inverted, meaning bone became ‘white’ and the background dark. At the second tab, the centre of rotation was identified to minimise any ring artefacts. Ring artefacts are rings around the centre of rotation on a scan, most often caused by machine calibration issues (Boas and Fleischmann, 2012). The options for this were set at ‘Automatic’, High Quality’ and ‘Dual’. These options indicate that the identification of the centre of rotation was completed automatically by the computer and that the computation was completed at a high quality. The latter required the placing of two horizontal, linear red lines onto the thumbnail of the bone in the top left corner to aid in the computation of the centre of rotation. It was important that these red lines were in contact with the superior and inferior aspect of the vertebra for the centre of rotation to be computed. Setup allowed the option to add filters to the scan to reduce any potential noise. The filters available can be seen in Table 6.2.

Table 6.2: Filter options in CT Pro 3D.

Filter	Description	Options	Outcome
Beam Hardening Correction	When x-rays pass through the object, the lower energy x-rays are weakened, while the higher energy x-rays are not. These high energy x-rays can cause artefacts such as dark streaks, especially at higher kV values, leading to 'Beam Hardening' (Boas and Fleischmann, 2012). This filter aims to correct this.	Scale of 1-6 (where 1=none applied).	The addition of a beam hardening correction was not found to greatly increase the quality of the scan at BH2 and BH3, although there was an improvement in the reduction of beam hardening artefacts in the form of streaks. However, at BH4 onwards, streak artefacts seemed to increase and cause the scan to become blurry. Beam hardening correction was kept at 1 (none) as no significant improvement could be identified by adding a correction (Figure 6.3).
Noise Reduction	Noise is caused by a low x-ray flux over a large number of pixels. The number of x-rays in a given pixel varies slightly, especially with lower x-ray dosage. Noise can be reduced by increasing x-ray dosage or through post-processing (Ramsay, 2009).	Scale of 1-6 (where 1=none applied).	The addition of a noise reduction filter did not seem to reduce noise, but instead increased the brightness of the image, which in turn increased the streak artefacts present. Therefore, it was decided to keep noise reduction at 1 (Figure 6.4).
Median Filter	Applied to reduce noise, each pixel is replaced by the median of neighbouring pixel values (Ferreira and Rasband, 2012).	0x0 (none), 3x3, 5x5	While the addition of a median increased the brightness of the scan, once again, this caused streak artefacts to appear more clearly. Therefore, none were applied (Figure 6.5).
Image Processing	A generic filter based on decreasing differentiation between the object and background in order to remove any image imperfections.	None, Mild, Moderate, Severe	The addition of image processing greatly reduced the differentiation between the object and the background and therefore, this was kept at none (Figure 6.6).

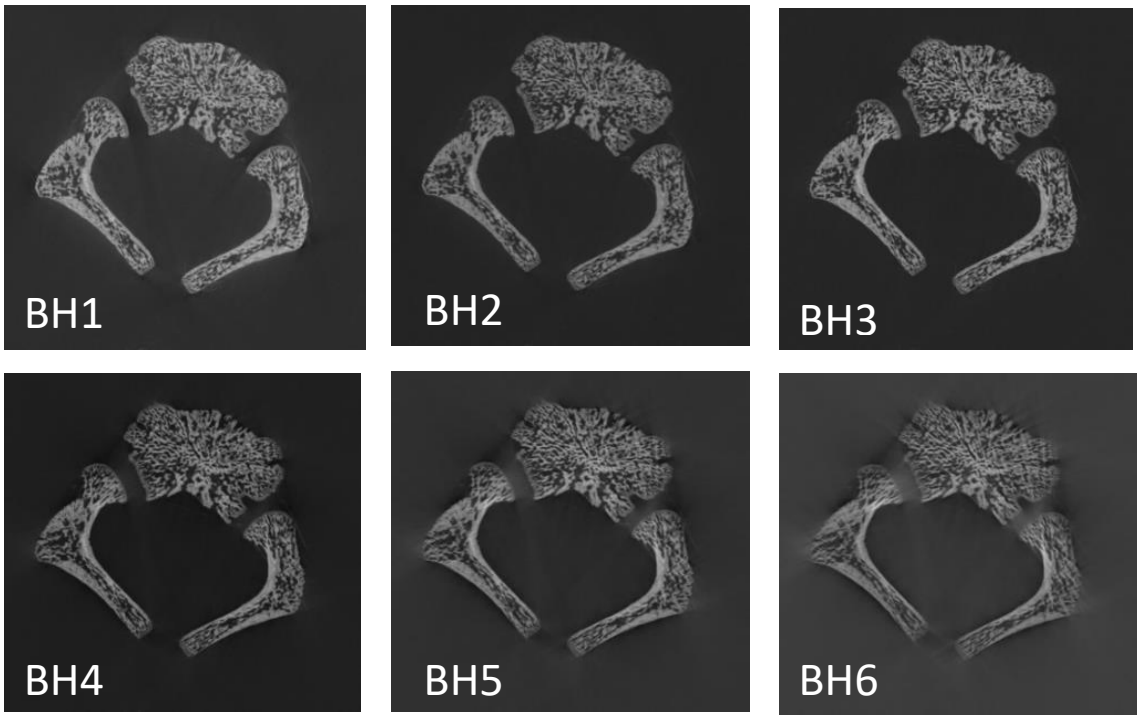

Figure 6.3: Outcomes of the application of the beam hardening correction where BH1= No beam hardening correction applied and BH6= the highest beam hardening correction applied. Up to BH3, beam hardening can be seen to decrease, however, between BH4 and BH6, streak artefacts can be seen to increase along with blurriness of the edges of the vertebra.

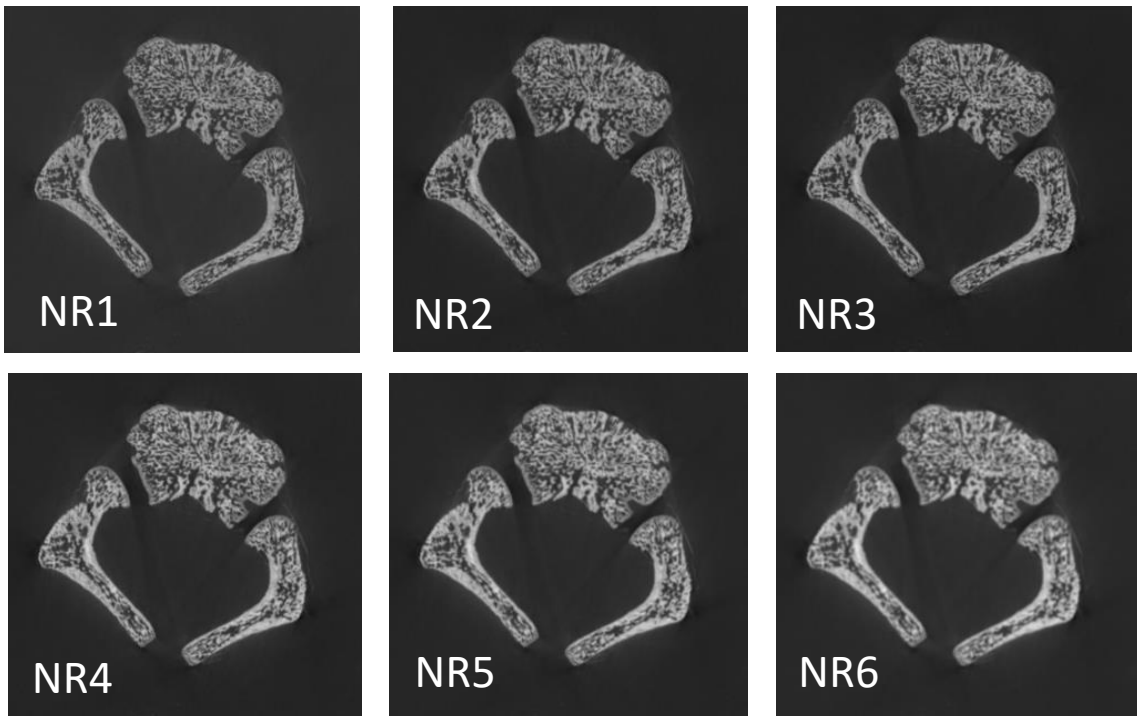

Figure 6.4: Outcomes of the application of noise reduction. NR1 (no filter)-NR6 (greatest filter). NR2/ 3 display a darker background which increases the visualisation of streak artefacts. Nr4-6 also display this, alongside less distinctive trabecular architecture.

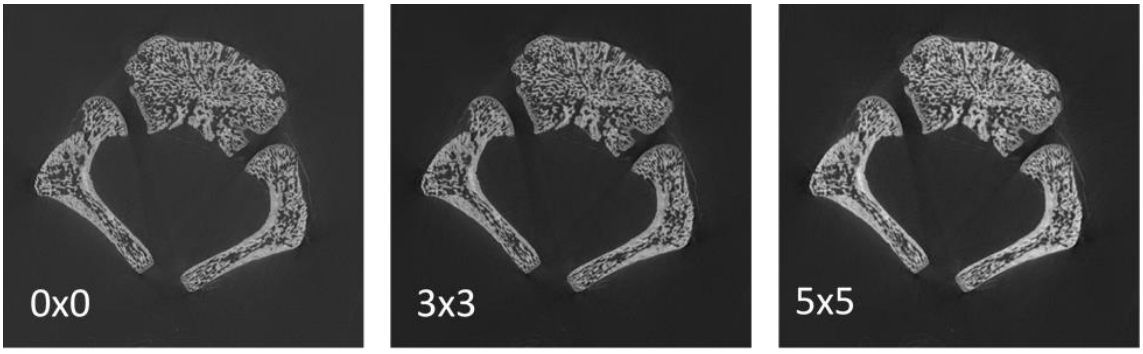

Figure 6.5: Outcomes of the application of the median filter, where 0x0 shows the original scan with no filter applied, and 5x5 the greatest median filter available. At 3x3, the background is darker, causing the vertebra to seem clearer. At 5x5, the background becomes darker again. However, these filter options cause the streak artefacts of the original scan to appear more obvious.

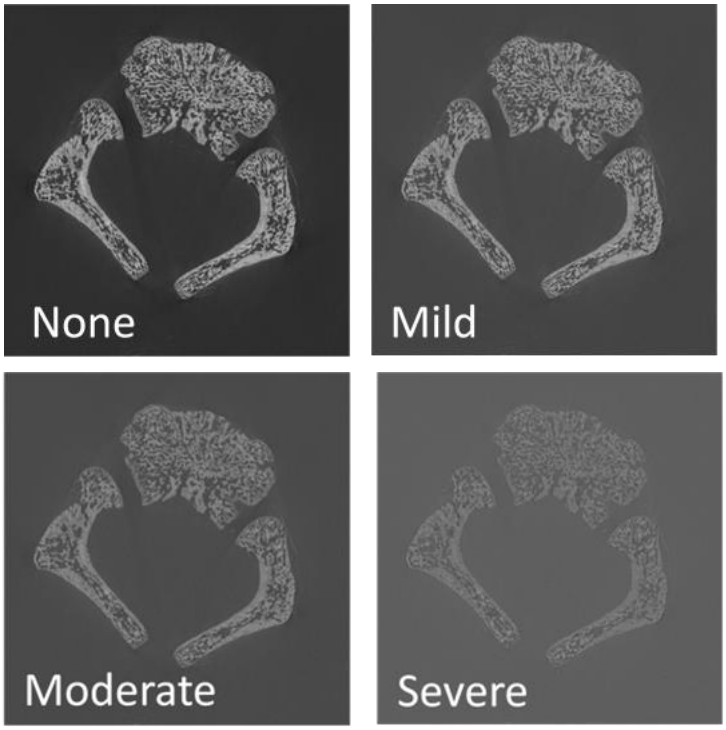

Figure 6.6: Outcomes of the application of Image Processing. The application of this filter causes the background to lighten and, as a result, the vertebra becomes less distinct.

The testing of these filters was on a preliminary basis, as a later step in the data collection process involved the binarisation of the scan. As the noise within the original scan was found to be minimal, due to the high quality of the original scan, it was deemed there was no need for filters to reduce noise.

Therefore, the low level of noise present, could be reduced through binarisation alone.

Finally, the scan was cropped to include only the volume of interest (VOI), in this case the entire vertebra with minimal background. This was to minimise the overall size of the scan. The scan was then exported as floating-point data.

After manual reconstruction, the scan was modified in VG Studio Max. The .vgl volume was imported as an unsigned 16-bit .tiff file. At this point, it was possible to remove a section of the histogram thumbnail by cropping away the area of the histogram where no peaks were present. This involved changing the size of a highlighted area by moving the boundaries of the area. This was done if the peaks of the histogram were contained in a reduced portion of the thumbnail and equates to ‘zooming in’ on the required area. This meant that once the scan had loaded, it was easier to view the section of the histogram pertaining to the bone.

Several tasks were required prior to the scan being acceptable for histomorphometric analysis and these were completed in VG Studio Max. The first task was the removal of the foam block, as well as floral foam and plastic covering in the case of vertebrae from individuals younger than three years of age. Both tasks were achieved by eliminating the peaks on the histogram relating to these structures by moving the red line of the histogram past the peaks pertaining to the foam block, floral foam and plastic covering, while being careful not to remove any of the cortical surface of the vertebra (Figure 6.7).

Secondly, each vertebra was registered using the simple registration tool, which enabled the manual identification of the correct anteroposterior plane of the bone (Figure 6.8). Superior, posterior, lateral and 3D views were used to register the vertebra. Once the scan had been registered, it was then exported as a superior-inferior stack of .tiff files by selecting the ‘Top (x-y plane)’ option in the dialog box.

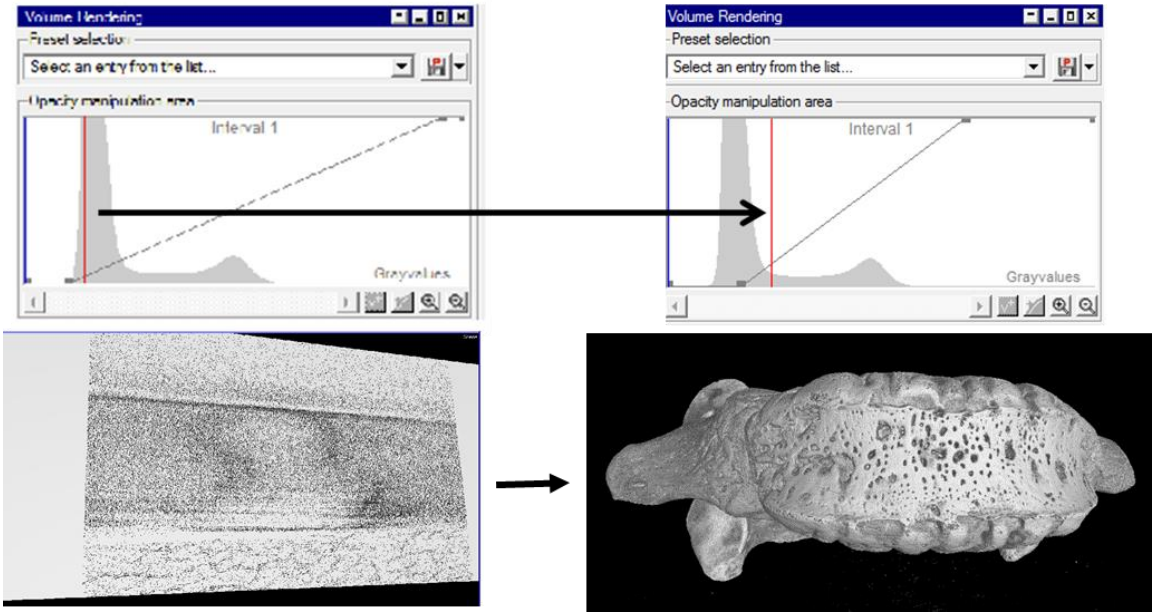

Figure 6.7: Left: Histogram and corresponding VG Studio Max visual output prior to removal of foam block and floral foam via the histogram. Right: Histogram and corresponding VG Studio Max visual output after elimination of histogram peaks relating to the foam block and floral foam.

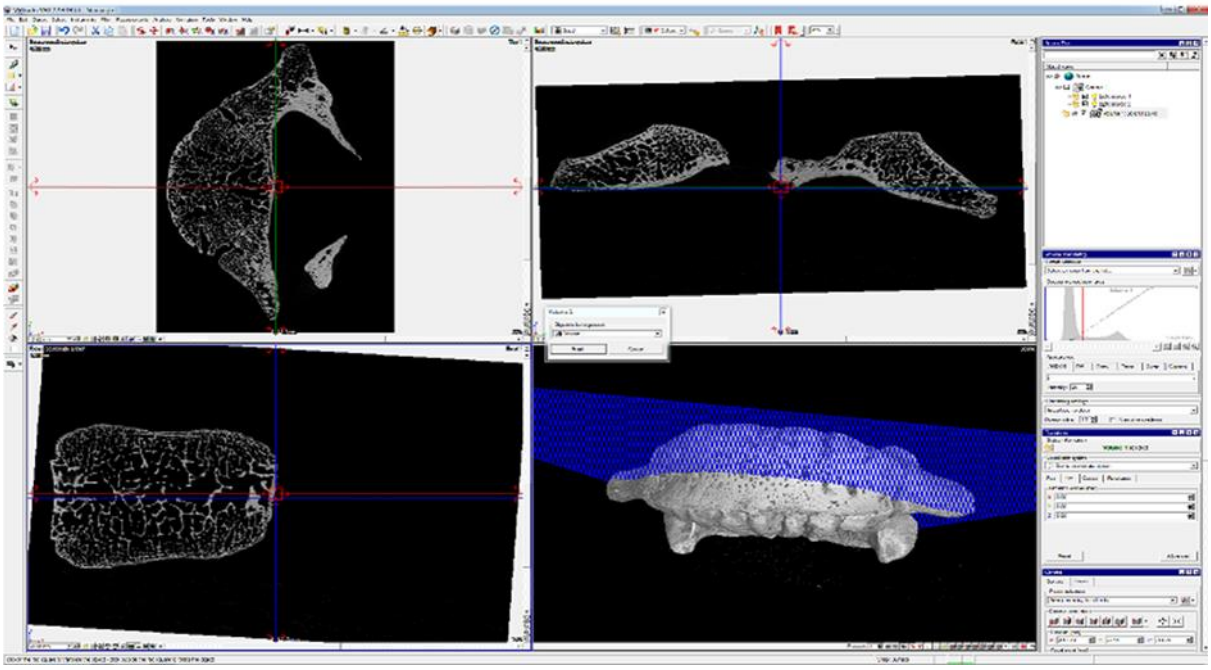

Figure 6.8: Registration of a lumbar vertebra. Top left: superior view; Top right: Posterior view; Bottom left: lateral view (L-R); Bottom right: 3D render (anterior view).

6.2.3 *Histomorphometric data collection*

6.2.3.1 Grid system creation

To optimally assess the trabecular architecture of the lumbar vertebral centra, a grid system was utilised (Figure 6.9) which separated each centrum into

27 VOIs. A 3 x 3 grid comprising nine regions in total was superimposed onto the superior aspect of each centrum (Figure 6.9, left image). The centrum was then separated into three equal layers, from inferior to superior (Figure 6.9, right image). To place the grid accurately for each centrum, 5 anatomical landmarks were utilised: the most anterior point of the vertebral centrum (Figure 6.9, red dot), the two most lateral points (Figure 6.9, blue dots), and the two most posterior points (Figure 6.9, green dots). It was only possible to place this grid on centra that had yet to fully undergo neurocentral fusion. Once neurocentral fusion had been completed, it became difficult to accurately assess the two posterior landmarks. Hence, older individuals that had begun to undergo neurocentral fusion were individually assessed based on the ability to identify these two posterior points. While this grid resulted in a large number of VOIs, it was the most applicable grid as it encompassed not only the differentiation between anterior, posterior, lateral and central areas of the centrum, but also accounted for the depth of the bone, which differed in superior, inferior and central layers (Banse *et al.*, 2001; Gong *et al.*, 2005). VOIs were numbered according to their location within the grid, and their level through a letter system: S (superior), C (central) and I (inferior). For example, the most central region would be in the 5th region, and the central layer, and would therefore be referred to as 5C.

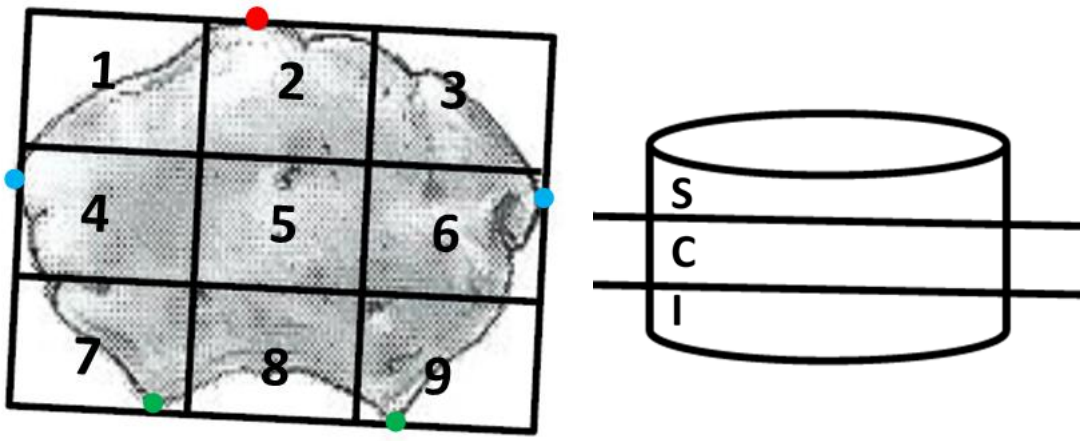

Figure 6.9: Left: Superimposable 3 x 3 grid differentiating between anterior, posterior, central and lateral areas of the centrum. Coloured dots represent the anatomical landmarks used to place the grid. Right: Diagram from the anterior aspect denoting the three layers each centrum will be divided into, Superior (S), Central (C) and Inferior (I).

6.2.3.2 Programme selection for histomorphometric analysis

Two programmes were considered for the histomorphometric analysis: ImageJ with the BoneJ plug-in, and Skyscan CTAnalyser. ImageJ was considered due to the programme being open source and easily accessible. While ImageJ was utilised successfully during the preliminary study for the identification of scan parameters (see Appendix 6.1), it presented several drawbacks when being considered as a viable method for the collection of histomorphometric data as a whole. ImageJ utilises the 'fit sphere' method for the placing of VOIs. In this method, six points are used to create a spherical VOI. These points are: one inferior and one superior point to denote the outer points of the sphere, and four central points placed on the same slice (Figure 6.10, red stars). Once set, the programme produces a sphere based on the location of the points placed, and several options are made available for analysis: the sphere itself (Figure 6.10, blue circle), the outer cube (Figure 6.10, yellow square) and the inner cube (Figure 6.10, green square). The light blue square denotes the original square ROI placed on the central slice of the VOI and is not available for 3D analysis. For the preliminary study, the outer cube was used for analysis as it was inferred that no information was lost by using this option.

By using the inner cube or sphere, areas within the original cuboidal VOI would not be included and therefore information would be lost. While this was suitable for testing the aims of the preliminary study, this method has several drawbacks. The use of the fit sphere method only allows the placing of 6 points and therefore makes it difficult to place VOIs that are not cuboidal in shape. Only one VOI out of the 27 proposed in the grid method described above could be considered cuboidal, VOI 5C. While 5C is a basic cuboidal shape, all other VOIs are not, and placing them as basic cuboids would result in the inclusion of cortical bone information and/ or scan area external to the centrum. By including these areas, the histomorphometric data for the trabecular architecture would not be accurate. One option would have been to analyse only the inner cube for all irregular VOIs, however, this method was deemed undesirable due to the loss of trabecular data.

Therefore, it was decided that Skyscan CTAnalyser would be used for the analysis of histomorphometric data. This programme has been utilised in similar studies with success (Cunningham, 2009; O'Malley, 2013; Yusof, 2013;

Maclean, 2017) and allowed irregular VOIs to be placed more easily and without loss of data.

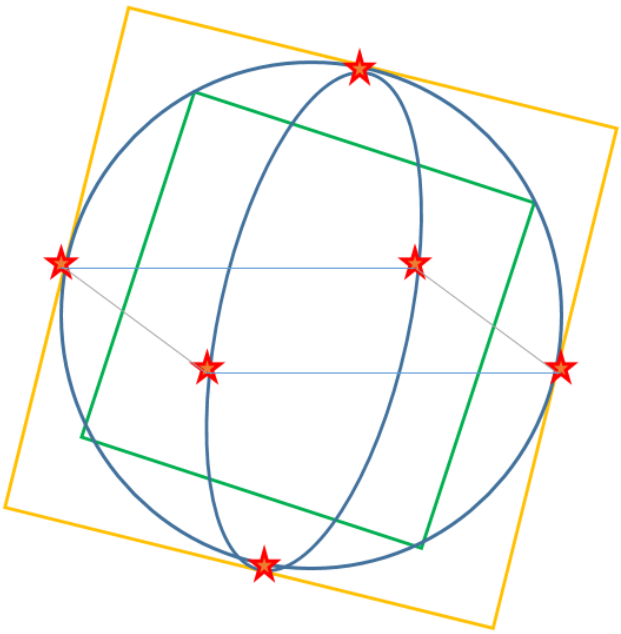

Figure 6.10: Diagram explaining the 'Fit Sphere' method utilised for VOI placement in BoneJ. The light blue square indicates the ROI formed by 4 points placed on a single slice. The yellow square denotes the outer cube, the darker blue circle denotes the sphere and the green square denotes the inner cube. The red stars show the six mandatory points that must be placed for the VOI to be computed. Please note that this diagram is a 2D representation of a 3D structure.

6.2.3.3 Histomorphometric parameters

While Skyscan CTAnalyser tests many histomorphometric parameters, six common parameters were considered for this quantitative project. A description of each of these parameters can be seen below, as described in the 'Bruker microCT: Morphometric parameters measured by Skyscan CT-Analyser software' User Guide which can be found in Appendix 6.5.

6.2.3.3.1 BV/TV

This parameter calculates the proportion of the VOI that is occupied by binarised solid objects (in this case: bone). Bone Volume Fraction (BV/TV) is calculated by first calculating the total volume and the bone volume of the VOI considered, then dividing the Bone Volume by the Total Volume. This parameter

is presented as a percentage (%). Both the BV value and TV value are computed using the marching cubes volume model (Lorensen and Cline, 1987).

6.2.3.3.2 SMI

Structural Model Index (SMI) is a numerical value that indicates the shape of the trabecular architecture within the VOI considered. SMI is output as a value between 0 and 4, where 0 indicates plate-like trabeculae within the volume, 3 indicates rod-like trabeculae and 4 indicates spherical trabeculae. SMI is calculated by dilation of the 3D voxel model, where one voxel thickness is added to each binarised object surface (Hildebrand and Rüegsegger, 1997a). SMI is calculated using the following equation:

$$SMI = 6 \times \left\{ \frac{S' \times V}{S^2} \right\}$$

where *S* is the object surface area before voxel dilation, *S'* is the change in surface area caused by the voxel dilation and V is the initial undilated object volume. An important point to consider when calculating SMI is that it is affected by the volume of bone within the VOI considered. Concave surfaces are represented by a negative *S'* value, leading to an overall negative SMI value, indicating the presence of cylindrical and spherical cavities (values of -3 and -4 respectively).

6.2.3.3.3 Tb.Th

Trabecular thickness (Tb.Th) is a numerical value assessing the thickness of trabeculae within a given VOI. A model-independent method formulated by Hildebrand and Rüegsegger (1997b) is utilised to assess this parameter. This method involves placing spheres within the trabeculae in the VOI to measure their thickness. This parameter is measured in µm.

6.2.3.3.4 Tb.N

Trabecular number (Tb.N), also known as structure linear density, calculates the number of trabeculae within a given VOI by registering the number of times trabecular structures pass through a random linear path within the VOI. Tb.N can be calculated by the equation below:

$$Tb.N = \frac{1}{(Tb.Th + Tb.Sp)}$$

Where *Tb.Th* is the calculated value for trabecular thickness and *Tb.Sp* is the calculated value for trabecular separation. Tb.N is measured in μm^{-1}.

6.2.3.3.5 Tb.Sp

Trabecular separation (Tb.Sp) is a measure of the space between the trabeculae within the given volume and is calculated in a similar fashion to Tb.Th. For Tb.Sp, spheres are placed between trabeculae to measure the width of the space between them, giving a value for their separation, which is recorded in µm.

6.2.3.3.6 DA

This parameter measures the 3D symmetry of the trabeculae within the VOI, assessing whether the trabeculae present are in alignment along an axis. Degree of anisotropy (DA) is an important parameter in assessing the mechanical strength of a structure (Odgaard, 1997). DA is calculated using Mean Intercept Length (MIL) and eigenvalues. It is output as a value between 0 and 1, where 0= total isotropy (organisation) and 1= total anisotropy (disorganisation).

6.2.3.4 Grid placement

A Microsoft computer with Windows 7 Enterprise and 8GB RAM was used. BMP image stacks were opened in Skyscan CTAnalyser and, once opened, the resolution of the image stack was set through the ‘Properties’ tab. The resolution information could be found in the XTEKCT notepad file within the associated folder for each vertebra scan data. This value was converted from mm to µm (x1000).

Due to the inability to differentiate between superior and inferior surfaces of vertebral centra prior to neurocentral fusion, it was assumed for these centra that inferior was at the beginning of the image stack and superior was the end of the stack. In some cases, cartilaginous tissue was present and the neural hemiarches were attached in the centrum in the anatomical position meaning that superior and inferior was identifiable. In individuals that had commenced neurocentral fusion, the process of identifying superior and inferior was simpler. It is important to note that, while in the majority of cases, inferior was at the lower end of the stack and superior at the top of the image stack, there were a small number of image stacks where this was not the case. This most likely occurred during the exportation of registered .tiff stacks. In cases where neurocentral fusion had occurred, it was possible to identify what was superior and inferior. In

all cases, the next step was to identify the most inferior and superior slices that contained trabeculae.

Once the most inferior and superior images had been identified, the central slice was calculated using the equation below:

[(Superior slice- inferior slice)/2] +Inferior slice= central slice

For example, if the most inferior trabeculae were seen in slice 83, while the most superior were seen in 625, the calculation would be as follows:

[(625-83)/2] +83=

Once the central slice had been identified, a clear plastic sheet was fixed onto the computer screen with either clear tape or BlueTac™, and the central slice was outlined onto the plastic using a black Sharpie™ permanent marker. Using a ruler and set square, a line was drawn firstly between the two most posterior points of the vertebral centrum, followed by lateral lines and finally by a line running anteriorly, creating a rectangular box around the centrum. The antero-posterior and transverse lines were measured and divided by three to identify the correct placement of the 3x3 grid. For example, if from the most anterior to the most posterior point of the centrum was measured as 99mm, the lateral lines of the grid would be placed 33mm (99mm/3) apart.

Once the grid had been placed successfully, a number of steps were completed to identify the stack size for each VOI. These steps can be seen in Table 6.3. For each individual assessed, a table was produced with the stack size and slice values of each VOI noted (see Table 6.4 as an example for individual SC-063 L1).

Table 6.3: The steps taken to calculate the stack information for VOI analysis ion Skyscan CTAnalyser, with their objective, method and an example calculation.

Step	Objective	Method	Example
1	Identification of superior-most and inferior-most slices	These slices were identified by viewing all slices within the scan and selecting the lower-most and upper-most slices with trabeculae present.	Inferior-most slice with trabeculae present: 83 Superior-most slice with trabeculae present: 625
2	The total number of slices with trabeculae present is calculated	*Superior slice-inferior slice*	*625-83=542 slices*
3	Slice size of each layer calculated	*Total no. of slices/3*	*542/3=180.ȯ*
3A	Calculation of inferior layer	*Inferior-most slice + layer size (rounded up/down as appropriate) = Uppermost inferior layer slice to give range*	*83+180=263* *Range=83 to 263*
3B	Calculation of central layer	*Top of inferior range slice + 1= Lower central slice* *Lower central slice + layer size= Upper central slice to give range*	*263+1=264* *264+180=444* *Range=264 to 444*
3C	Calculation of superior layer	*Top of central range slice + 1= Lower superior slice* *Lower superior slice + layer size= Upper superior slice (should equate to most superior slice with trabeculae present) to give range*	*444+1=445* *445+180=625* *Range= 445 to 625*
4	True calculation of inferior and superior layers for each VOI	As not all VOIs had trabeculae present within the VOI at the most inferior or most superior slices, the inferior-most and superior-most slices for each were identified.	Eg. VOI 2I: Trabeculae not present until slice 95, so new range for VOI= 95 to 263 VOI 2S: Trabeculae present until slice 560, so new range for VOI= 445 to 560

Table 6.4: Stack and slice information for the VOIs of individual SC-063 L1.

VOI	Inferior	Central	Superior
1	83→263	264→444	445→545
2	95→263	264→444	445→560
3	91→263	264→444	445→555
4	93→263	264→444	445→596
5	109→263	264→444	445→617
6	105→263	264→444	445→615
7	144→263	264→444	445→615
8	148→263	264→444	445→625
9	155→263	264→444	445→625

6.2.3.5 VOI placement

Once the grid had been placed correctly over the computer screen and the properties of the scan had been updated, the identification of each VOI could begin.

The first step in VOI identification was to set the selection of slices within the volume to be analysed. The ‘Region of Interest’ (ROI) tab was opened in CTAnalyser and the superior and inferior slices of the VOI were set as the ‘Top and Bottom Selection’. For example, in individual SC-065 L1 for VOI 7I (Inferior) the most inferior slice was slice 189 (figure 6.11), and the most superior was 288 (figure 6.12).

Once the superior and inferior slices of the VOI had been set, the Polygonal ROI tool was selected. This tool allowed the placing of a polygonal shape that could be adjusted to accurately describe the shape of the trabecular region present within the slice. The polygonal ROI tool enabled the placing of points that were joined by a linear line. It was possible to add as many points as needed in order to produce the most accurate shape. Once placed, these points surrounded and formed the region of interest (ROI) and were highlighted in red/ blue (figures 6.11-6.13).

An ROI was always placed on both the most inferior (Figure 6.11) and the most superior slice (Figure 6.12) within the VOI stack. From there, the Polygonal ROI tool interpolated the shape of the VOI between these slices. However, this was not always accurate as the shape of the ROI at each slice within the VOI differed. In order to reproduce the VOI, further ROIs were placed within the image stack to create the most accurate depiction of the VOI being assessed. This was more commonly needed for irregular VOIs (those that were not cuboidal in nature).

For example, VOI 7I is irregular and often needed single or multiple further ROIs placed in more centrally located slices within the VOI. An example of this can be seen in figure 6.11 to 6.13. At 6.11 and 6.12, ROIs have been placed on the most inferior and most superior slices respectively. However, these ROIs are significantly different in their shape and size. Often, Skyscan could not accurately interpolate the shape of the VOI between these slices and hence, a further ROI needed to be placed in another slice in order to produce this. This can be seen in figure 6.13, where an ROI has also been placed between slices 189 and 288, at slice 265. There was no limit to the number of further ROIs that could be added. In some cases, such as for most 5C VOIs, only two ROIs were needed. This VOI is more regular in shape due to the fact that the trabecular region throughout the VOI was rectangular and matched for all slices throughout the volume. In these cases, Skyscan was capable of accurately interpolating the shape of the VOI between the inferior and superior slices.

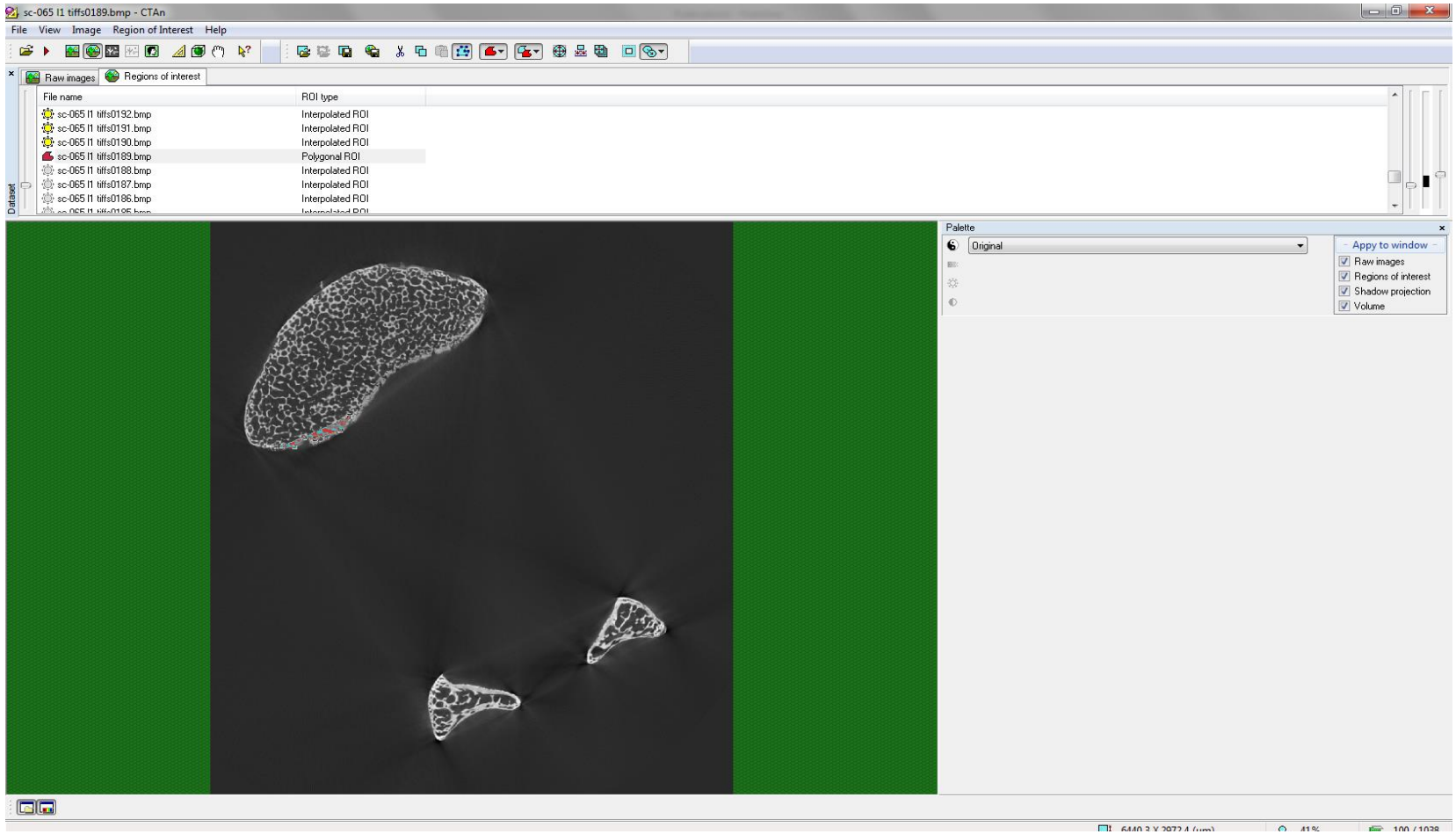

Figure 6.11: Placement of the inferior-most ROI for VOI 7I in individual SC-065 L1 (4 years of age). Bone within the ROI is shown in blue, while the 'space' is shown in red.

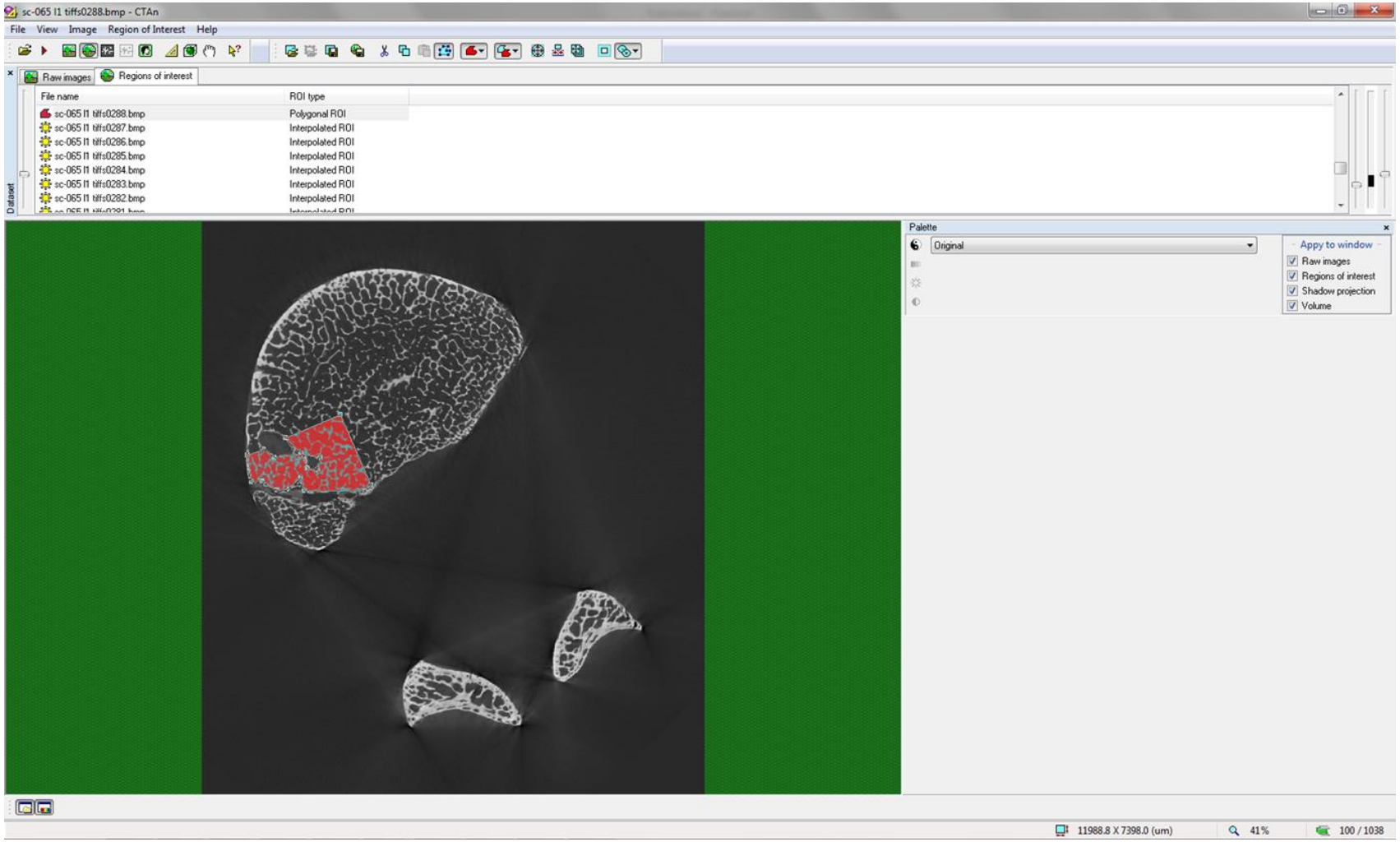

Figure 6.12: Placement of the superior-most ROI for VOI 7I in individual SC-065 L1 (4 years of age). Bone within the ROI is shown in blue, while the 'space' is shown in red.

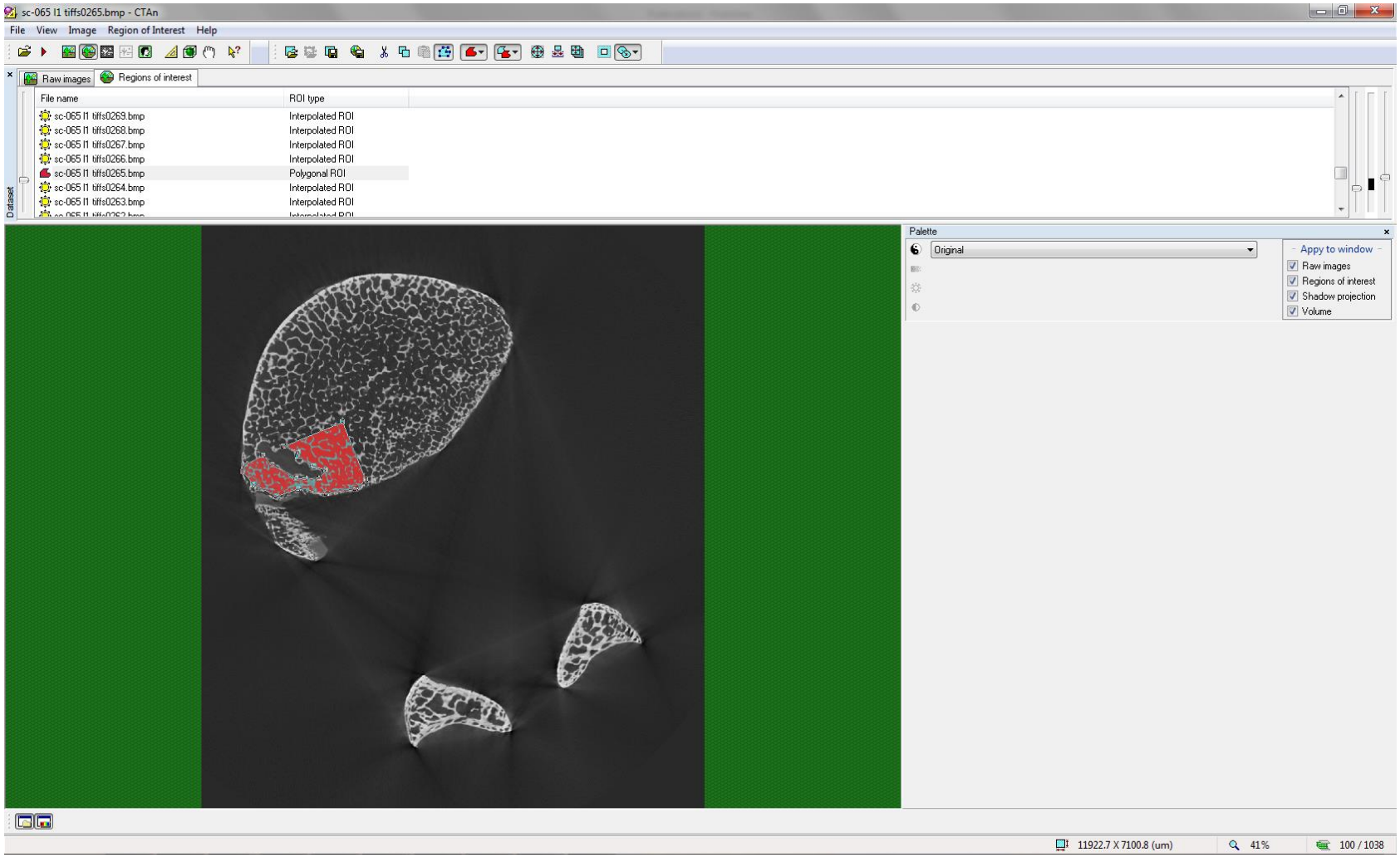

Figure 6.13: Placement of a further ROI on a slice between the superior and inferior-most slices to aid in the setting of VOI 7I in individual SC-065 L1 (years of age). Bone within the ROI is shown in blue, while the 'space' is shown in red.

Once all ROIs had been placed successfully, with the VOI depicted accurately through the interpolation of the ROIs placed, the next step was binarization of the VOI. Binarisation, or thresholding, converts the scan into a black and white image (rather than greyscale) where the bone is depicted as white and the background black. This is a requirement for the analysis of histomorphometric parameters in Skyscan CTAnalyser. Binarisation was achieved by clicking the 'Binarisation' tab and using the interactive histogram to set the threshold level. To set the threshold level accurately, several areas within the set VOI were used as focus points. These points were most commonly well connected or irregularly shaped trabeculae that could be compared easily between the original and binarised slice. Figure 6.14 is an example of an original slice, compared to a binarised slice. All VOIs were manually binarised individually, a process known as local thresholding.

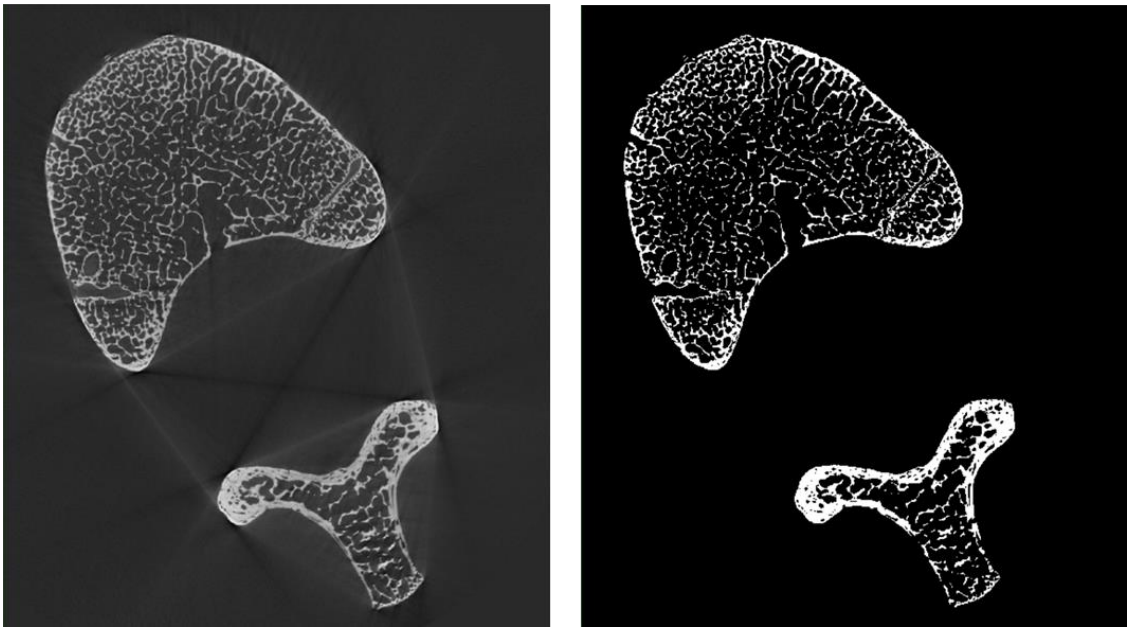

Figure 6.14: : Left: Original slice of SC-065 L1. Right: Binarised slice of SC-065 L1, set at a threshold of 130.

Once binarised, the histomorphometric data pertaining to the VOI could be collected. This was completed by selecting the 'Processed Images' tab and choosing '3D Analysis'. This gave a dialog box, where all basic and additional values were selected. The time taken for the computation of the histomorphometric parameters varied between both VOIs and individuals, with computation times ranging from around 1 minute, to around 10 minutes for larger vertebrae. Once completed, data was saved as a notepad file and transferred to an excel file for statistical analysis.

6.2.4 *Analysis of histomorphometric data*

6.2.4.1 Analyses

Three separate analyses were undertaken on the histomorphometric data. Analysis 1 focused on differences between individuals and between age cohorts. Analysis 1A focused specifically on differences between individuals of the same age cohort to assess developmental changes within each cohort and to quantify variation between individuals of similar ages. This was achieved by assessing the significant differences between individuals at each vertebral level studied (L1, L3 and L5) and per histomorphometric parameter. Comparable values were at the whole bone level. Analysis 1B focused on quantifying differences between age cohorts and was also from a whole bone perspective, focusing on each histomorphometric parameter and vertebral level separately. Analysis 2 focused on differences between levels of the vertebral column. This was assessed within each age cohort studied. The three vertebral levels: L1, L3 and L5; were compared per pooled individuals values for each VOI. Analysis 3 assessed differences between VOIs. This analysis was conducted within age cohorts and assessed each vertebral level and histomorphometric parameter separately, comparing pooled values from each individual within the cohort for each VOI.

6.2.4.2 Statistical analyses

All statistical tests were carried out with the SigmaPlot statistical programme. The first step for the analysis of all data was to identify whether the data was parametric or non-parametric. This was achieved by testing data sets for normality using the Shapiro-Wilk test. Data was normally distributed if it passed the test ($p>0.050$). For normally distributed data, the next step was to test for equal variance using the Brown-Forsythe test. A p value of greater than 0.05 indicated that the data had passed the equal variance test and was considered parametric. An analysis of variance (ANOVA) was then utilised to identify whether differences between conditions existed. In situations where differences were present, a multiple pairwise comparison procedure (MCP) was used to identify the location and significance of these differences. A flow diagram of these statistical tests utilised can be seen in figure 6.15.

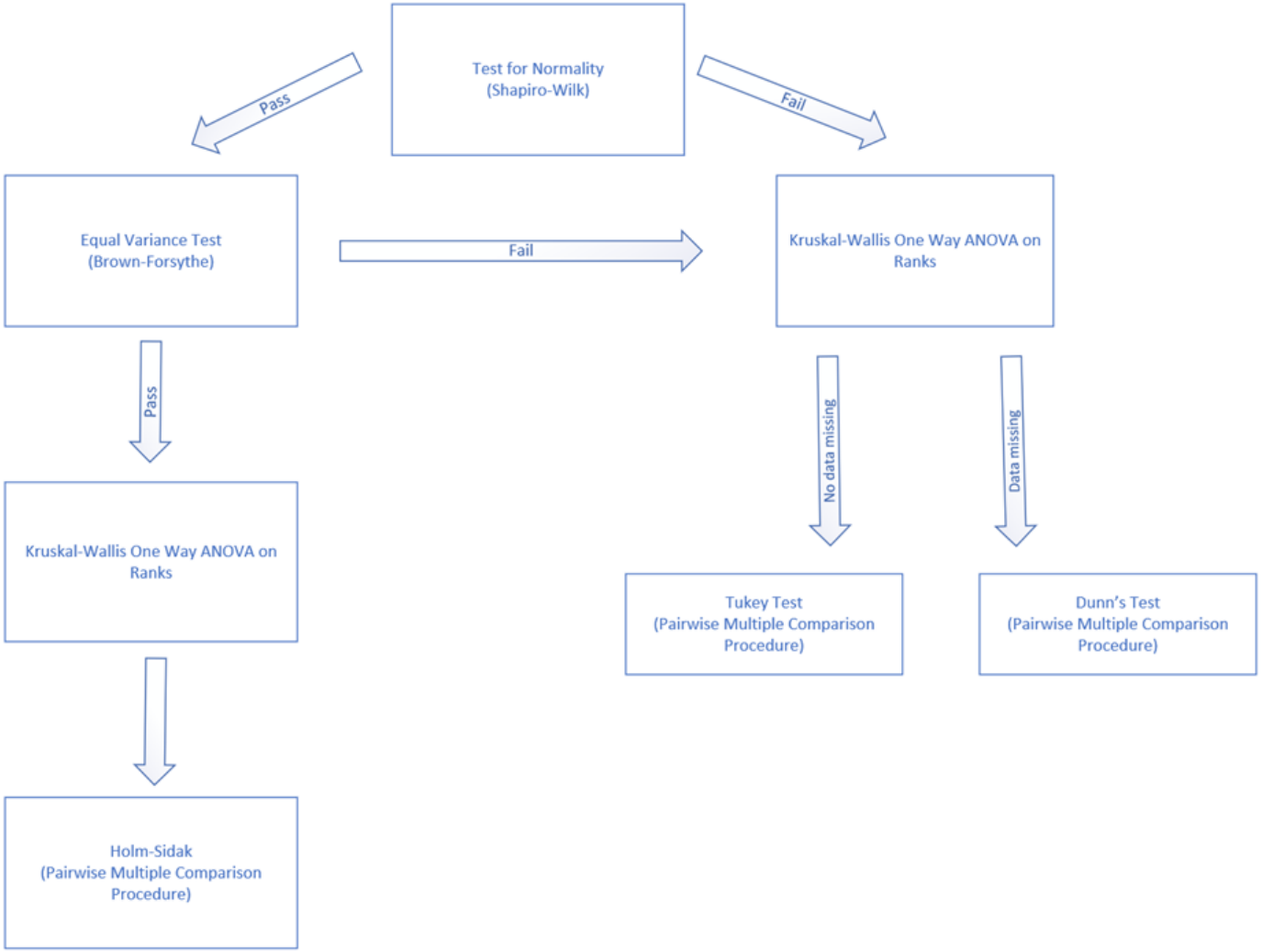

Figure 6.15: A flow diagram displaying the statistical tests utilised to assess the quantitative data.

For parametric data, a one-way ANOVA was utilised to identify differences between conditions. The descriptive statistics produced by this test included the data source/ group, the number of values per group (N), the number of values missing for each group and the mean values, standard deviations and standard error of the mean for each group. The source of variation was also calculated, giving values for the degrees of freedom of the dataset, the sum and mean of squares, an F value and a P value. The latter two values give an indication as to the presence of differences between the data sources tested. In cases where the F value is low, for example, close to 1, it indicates that no significant differences are present between data sources. In cases where the F value is much larger, it indicates significant differences are present. The P value is also important in understanding differences between data sources. A small P value implies there is a lower chance of the differences indicated by the F value being false. In cases of high F values, the Holm-Sidak method was utilised to identify the significance of the differences. The Holm-Sidak method calculates a t value and p value for each comparison, based on the difference of means. A larger t value indicated that the difference between the two means compared was significant. In all cases, a difference was considered to be significant at the level of $p \leq 0.01$. This p value was chosen due to the relatively small sample sizes for some cohorts, in order to assure that the significant differences were not incorrectly identified.

In cases where data was non-parametric, a Kruskal Wallis one-way ANOVA on Ranks was utilised to assess whether the data presented any statistically significant differences. The descriptive statistics produced by this test included the data source/ group, the number of values per group (N), the number of values missing for each group, and the median value and 25^{th} and 75^{th} percentiles for each group. Similar to the F value in parametric data, an H value is computed. A lower H value also indicates than no differences between groups are present, while a larger H value indicates significant differences are present within the dataset. The corresponding P value, like with the parametric datasets, indicates the accuracy of the H value, with lower P values indicating that the H value is less likely to be false. In cases where significant differences were found, two multiple pairwise comparison procedures (MCP) were considered. The Tukey test was utilised in cases where no data was missing. In cases of missing data, the MCP used was Dunn’s test. Both tests are based on the principle of

comparison of ranks between data groups, producing a q (Tukey test) or Q (Dunn's test) value and associated p value. The larger the Q/q value, the larger the difference between the two groups studied, and subsequently, the lower the p value. As with parametric data, differences were considered significant where the p value was equal to, or less than, 0.01.

6.3 Intra-Observer Error Study

6.3.1 *Aims*

The aim of the intra-observer error study was to assess the accuracy and repeatability of the methodology concerning the use of Skyscan CTAnalyser. In particular, this study focused on the placing and binarisation of VOIs, which was completed manually by the author and is potentially subject to error.

6.3.2 *Methodology*

One vertebra was chosen for the intra-observer error study, SC-065 L1 (4 years of age). This individual was selected to achieve two goals. The first goal was to achieve the aim stated above. The second goal was to analyse the ability of the observer to place VOIs repeatedly. Individual SC-065 L1 was suitable for to assess this second aim as, due to its age, it had begun to undergo neurocentral fusion. Therefore, it allowed a comparison between the placing of posterior VOIs which were less defined once neurocentral fusion had begun and hence attested to the authors ability to accurately place these posterior VOIs consistently.

The methodology was followed as stated in section 6.2.3 and repeated three times during the period of histomorphometric data collection. A number of other individuals were analysed between each repeat to decrease the likelihood of the observer recalling any information pertaining to the collection of data for SC-065 L1. The shortest period between repeats was 11 days .

Once collected, data was analysed following the statistical protocol described in section 6.2.4. Each histomorphometric parameter was analysed separately. Data was also analysed by VOI. The threshold values collected during binarisation of each VOI was also collected and analysed.

6.3.3 *Results*

Initial steps within the methodology, such as identification of the most superior and inferior slices containing trabecular information, were generally

consistent over each repeat. The computation of the superior, central and inferior layers was also consistent, with no upper or lower limit differing by more than 6 slices when compared to other repeats. No significant differences were found between threshold values between repeats of the same VOI. This information can be seen in Table 6.5.

Table 6.5: Raw data collected from each repeat of the histomorphometric analysis of individual SC-065 L1 including the upper and lower slice limits of each VOI from 1I to 9S, and threshold values for each VOI. Values in bold show the lowest and highest slice numbers for the image stack.

Repeat 1									
	I Lower	I Upper	Threshold	C Lower	C Upper	Threshold	S Lower	S Upper	Threshold
1	**117**	287	145	288	458	140	459	544	135
2	**117**	287	138	288	458	138	459	566	131
3	146	287	145	288	458	145	459	573	139
4	124	287	137	288	458	137	459	588	133
5	136	287	133	288	458	133	459	603	128
6	163	287	132	288	458	136	459	608	132
7	192	287	129	288	458	129	459	619	126
8	204	287	133	288	458	129	459	**629**	124
9	224	287	129	288	458	129	459	**629**	129
Repeat 2									
	I Lower	I Upper	Threshold	C Lower	C Upper	Threshold	S Lower	S Upper	Threshold
1	**117**	288	138	289	460	141	461	543	140
2	**117**	288	138	289	460	142	461	565	138
3	151	288	143	289	460	145	461	572	145
4	122	288	136	289	460	136	461	586	129
5	134	288	133	289	460	127	461	609	127
6	163	288	131	289	460	131	461	607	126
7	189	288	137	289	460	132	461	617	131
8	205	288	126	289	460	126	461	**632**	126
9	226	288	134	289	460	134	461	626	130
Repeat 3									
	I Lower	I Upper	Threshold	C Lower	C Upper	Threshold	S Lower	S Upper	Threshold
1	**116**	288	145	289	460	145	461	547	136
2	**116**	288	145	289	460	148	461	566	141
3	148	288	152	289	460	152	461	572	145
4	122	288	139	289	460	136	461	586	130
5	136	288	130	289	460	130	461	607	130
6	162	288	135	289	460	140	461	606	130
7	191	288	133	289	460	130	461	618	130
8	209	288	129	289	460	129	461	**632**	125
9	223	288	133	289	460	133	461	627	132

No significant differences were found for any of the histomorphometric parameters. Furthermore, no significant differences were found at each VOI. All raw data and results of these statistical analyses can be found in Appendix 6.6.

6.3.4 *Discussion*

The methodology utilised in any study should be such that the results produced aid in answering the research questions set. The methodology selected in this case demonstrates several areas in which error can affect the quantitative data produced. While error can sometimes be unavoidable, it is important to reduce any sources of error where possible. In these cases, there were several areas within the methodology potentially subject to human error and it was important to identify whether human error existed in these cases and hence would have any effect on the results collected.

Local thresholding was chosen for the binarisation of VOIs. While this is considered more accurate than global thresholding, which involves picking one threshold value for the entire bone in question, local thresholding may also lead to increased error which can affect the histomorphometric data collected (Ding *et al*., 1999; Hara *et al.*, 2002; Hangartner, 2007). For local thresholding, each VOI is binarised independently based upon the trabecular structure within the associated VOI (Burghardt *et al.*, 2007). While it is not possible in this case to ascertain that the thresholding level was ‘correct’ in defining the accurate size and shape of the trabecular architecture within the volume, it is important to assess the ability of the author to consistently decide upon the same threshold levels for VOIs. Even in cases where the threshold may not accurately present the trabecular information displayed, it can be said with certainty that the author has binarised each VOI consistently and all data would continue to follow the same pattern and is therefore still appropriate for comparison.

This study also aimed to determine whether it was possible to identify the posterior borders of the centrum consistently through the use of non-invasive imaging techniques, in bones that were showing active neurocentral fusion. This step is important as inclusion of data from the fused neural arches may not be comparable to younger individuals in which fusion has not commenced. The VOIs in question, 7 and 9, were characterised by semi-obliterated posterior borders after around 6 years of age, which increased the difficultly of identifying the

centrum from the fusing neural arch. The results indicated that it was possible to continuously place these VOIs in the same location. However, it cannot be said with certainty that the trabecular architecture contained within these VOIs did not also contain trabecular information pertaining to the fusing neural arch. Even so, as it has been found that the author was capable of consistently placing the VOI, this implies that visual cues were available that aided in the delineation of the centrum and neural arch borders.

6.3.5 *Conclusions*

Overall, no significant differences were found within any area of the methodology tested and exhibited that the author was capable of consistently placing and binarising VOIs, as well as being competent in consistently placing VOIs 7 and 9 in an individual undergoing neurocentral fusion.

7 Analysis of Quantitative Data: Analyses 1a and 1b

7.1 Introduction

The first analysis of the quantitative data aimed to quantify: a. the variation between individuals of the same age cohort, and b. the variation between age cohorts. The first section of the analysis, 1a (between individuals), focused on quantifying any differences in the six parameters studied between individuals of the same developmental age cohort, within a single vertebral level. The second analysis, 1b (between age cohorts) also separated individuals by vertebral level for each of the six parameters. Due to the sample sizes within the age cohorts and the resulting power of the data analysed, any differences were only considered as significant at the level of $p \leq 0.01$. All raw data and results of these statistical analyses can be found in Appendix 7.

7.2 Results of Analysis 1a

7.2.1 *Fetal Age Cohort*

7.2.1.1 BV/TV

Of the three vertebral levels, only L3 presented any significant differences between individuals for bone volume fraction (BV/TV). The descriptive statistics for the three datasets can be viewed in Table 7.1. Median values for BV/TV ranged between 23.81%, which was displayed by the oldest individual at 32 weeks *iu*, and 27.47%. These results can be visualised in Figure 7.1 (BV/TV).

Table 7.1: Descriptive statistics for BV/TV (%) within the fetal age cohort at the levels of L1, L3 and L5. P= parametric, NP= non-parametric. DF= degrees of freedom. Y= significant differences (red), N= no significant differences (green).

	L1	L3	L5
Parametric?	P	NP	P
F/H Value	3.368	9.382	0.0354
DF	1	2	1
P Value	0.072	0.009	0.852
p≤0.01?	N	Y	N
Mean/Median	Mean	Median	Mean
SC-089	N/A	25.49	N/A
SC-093	35.60	27.47	34.45
SC-096	33.72	23.87	34.22

7.2.1.2 SMI

For structural model index (SMI), significant differences between individuals were found at the level of L3 only. The descriptive statistics for these datasets can be found in Table 7.2. Values for SMI ranged between 0.99 and 1.80. The Tukey Test found that the oldest individual within the cohort displayed a significantly higher value for SMI. For SMI, a value of 0 indicates the structure comprises entirely of plates, a value of 3 indicates rods, and a value of 4, spheres. For all individuals within this cohort, the value for SMI indicated a mixture of both plate-like and rod-like trabeculae, while the oldest individual tended more towards plate-like trabeculae. These results can be visualised in Figure 7.1 (SMI).

Table 7.2: Descriptive statistics for SMI within the fetal age cohort at the levels of L1, L3 and L5. For SMI, 0= plates, 3=rods and 4=spheres.

	L1	**L3**	**L5**
Parametric?	NP	NP	NP
F/H Value	0.377	20.304	1.488
DF	1	2	1
P Value	0.539	<0.001	0.223
p≤0.01?	N	Y	N
Mean/Median	Median	Median	Median
SC-089	N/A	1.15	N/A
SC-093	0.99	1.58	1.02
SC-096	1.04	1.80	1.11

7.2.1.3 Tb.Th

For trabecular thickness (Tb.Th), significant differences between individuals were also found at the third lumbar vertebral level. The descriptive statistics for these datasets can be seen in Table 7.3. Mean/ median values ranged between 57.90µm and 88.81µm. The oldest individual displayed a significantly higher trabecular thickness. These results can be visualised in Figure 7.1 (Tb.Th).

Table 7.3: Descriptive statistics for Tb.Th (µm) within the fetal age cohort at the levels of L1, L3 and L5.

	L1	L3	L5
Parametric?	P	NP	NP
F/H Value	6.155	17.037	6.336
DF	1	2	1
P Value	0.016	<0.001	0.012
p≤0.01?	N	Y	N
Mean/Median	Mean	Median	Median
SC-089	N/A	61.99	N/A
SC-093	76.47	57.90	68.66
SC-096	88.81	75.21	81.38

7.2.1.4 Tb.N

For the histomorphometric parameter trabecular number (Tb.N), all three vertebral levels displayed significant differences between individuals. The descriptive statistics for these datasets can be found in Table 7.4. Values for Tb.N ranged between 0.00328µm^{-1} and 0.00483 µm^{-1}.

At all vertebral levels, the oldest individual displayed significantly lower trabecular number. No differences were found between the younger individuals at 28 weeks *iu*. The results for the level of L3 can be visualised in Figure 7.1 (Tb.N).

Table 7.4: Descriptive statistics for Tb.N (µm^{-1}) within the fetal age cohort at the levels of L1, L3 and L5.

	L1	L3	L5
Parametric?	P	P	P
F/H Value	10.89	24.095	11.885
DF	1	2	1
P Value	0.002	<0.001	0.001
p≤0.01?	Y	Y	Y
Mean/Median	Mean	Mean	Mean
SC-089	N/A	0.0044	N/A
SC-093	0.00483	0.00455	0.00449
SC-096	0.00397	0.00328	0.00412

7.2.1.5 Tb.Sp

As with Tb.N, all three vertebral levels presented significant differences between individuals for trabecular separation (Tb.Sp). Descriptive statistics for these three analyses can be found in Table 7.5. Median values for Tb.Sp ranged between 136.44µm and 192.57µm.

As with other parameters, the oldest individual was once again found to differ significantly from the younger individuals with in the cohort, displaying a significantly higher value for trabecular separation. The results for the level of L3 can be visualised in Figure 7.1 (Tb.Sp).

Table 7.5: Descriptive statistics for Tb.Sp (µm) within the fetal age cohort at the levels of L1, L3 and L5.

	L1	**L3**	**L5**
Parametric?	NP	NP	NP
F/H Value	16.178	25.132	15.764
DF	1	2	1
P Value	<0.001	<0.001	<0.001
p≤0.01?	Y	Y	Y
Mean/Median	Median	Median	Median
SC-089	N/A	159.03	N/A
SC-093	139.27	139.00	136.44
SC-096	179.66	192.57	182.25

7.2.1.6 DA

For degree of anisotropy (DA), no significant differences were found between individuals within the fetal age cohort for any vertebral level. Average values for DA ranged between 0.357 and 0.458. A value of 0 indicates an isotropic (more organised structure), while a value of 1 indicates a more anisotropic structure (less organised). These values indicate a more isotropic structure present within the fetal vertebral centra. Descriptive statistics for these analyses can be found in Table 7.6.

Table 7.6: Descriptive statistics for DA within the fetal age cohort at the levels of L1, L3 and L5. A value of 0= total isotropy while 1= total anisotropy.

	L1	L3	L5
Parametric?	P	NP	P
F/H Value	1.831	4.189	4.4
DF	1	2	1
P Value	0.182	0.123	0.041
p≤0.01?	N	N	N
Mean/Median	Mean	Median	Mean
SC-089	N/A	0.384	N/A
SC-093	0.425	0.425	0.398
SC-096	0.390	0.407	0.347

7.2.1.7 Summary

The oldest individual within the cohort at 32 weeks *in utero,* displayed higher BV/TV, higher SMI, and a lower number of more separated, thicker trabeculae.

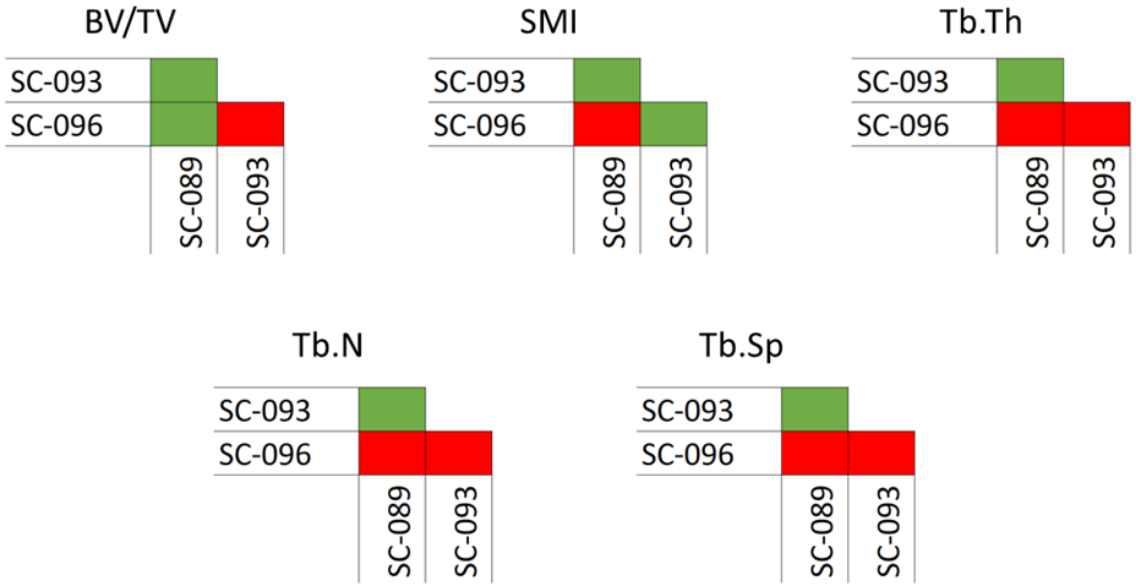

Figure 7.1: The significant differences between individuals of the fetal age cohort at the vertebrla level L3. Differences are considered significant at p≤0.01 and are displayed as red squares. Green squares indicate no significant difference between individuals for a histomorphometric parameter.

7.2.2 *Perinatal Age Cohort*

7.2.2.1 BV/TV

The descriptive statistics for bone volume fraction (BV/TV) at the levels of L1, L3 and L5 within the perinatal age cohort can be seen in Table 7.7.

Significant variation in BV/TV between individuals was observed at all three vertebral levels. The individuals differing from each other can be visualised in Figure 7.2, where the red squares indicate significance.

At the level of L1, median values for BV/TV ranged between 10.19% to 43.84%. At L3, median values ranged between 6.20% to 33.96%. Finally, at the level of L5, between 24.48% to 47.31%. In all cases, individual SC-084 displayed the highest values, while individual SC-040, which was present at L1 and L3 displayed the lowest. At all vertebral levels, individuals SC-084, SC-086 and SC-088, who are of the same origin, presented significantly higher values for BV/TV compared to all other perinatal individuals. Meanwhile, individuals SC-040, SC-041 and SC-043, the three oldest individuals at 2 weeks and 3 weeks of age, displayed significantly lower values for BV/TV compared to other perinates.

Table 7.7: Descriptive statistics for BV/TV (%) within the perinatal age cohort at the levels of L1, L3 and L5.

	L1	L3	L5
Parametric?	NP	NP	NP
F/H Value	268.283	249.238	182.842
DF	13	12	10
P Value	<0.001	<0.001	<0.001
p≤0.01?	Y	Y	Y
Mean/Median	Median	Median	Median
SC-020	29.03	24.61	31.92
SC-084	43.84	33.96	47.31
SC-086	32.65	30.74	43.70
SC-087	33.54	28.32	34.69
SC-088	32.82	32.21	45.92
SC-092	30.26	24.20	35.31
SC-097	22.35	21.65	27.48
SC-154	24.47	21.59	29.32
SC-155	20.21	N/A	24.48
SC-158	23.81	25.72	27.53
SC-161	28.03	22.59	32.03
SC-040	10.19	6.20	N/A
SC-041	14.73	12.87	N/A
SC-043	20.35	17.77	N/A

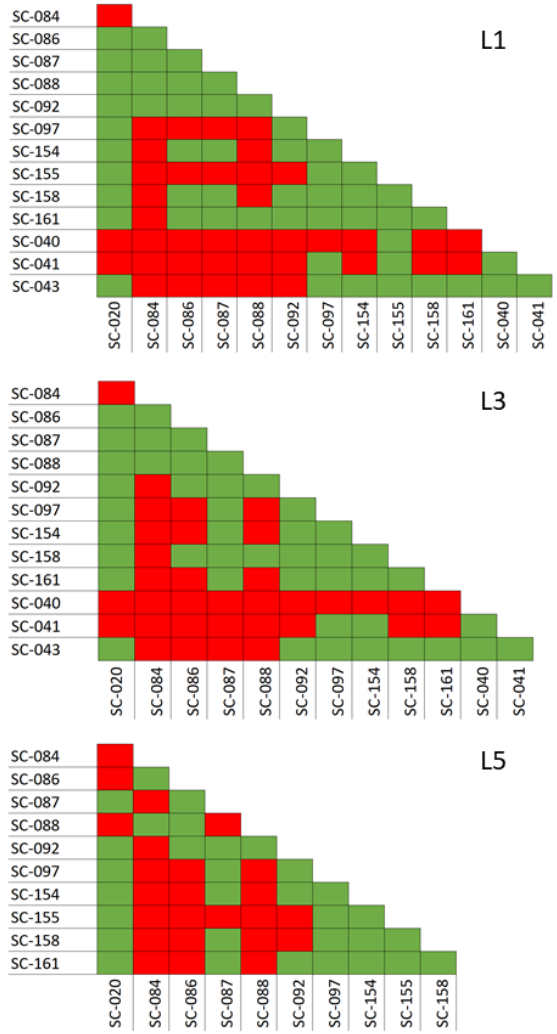

Figure 7.2: Data visualisation for BV/TV in the perinatal age cohort at the levels of L1, L3 and L5. Red squares denote significant differences.

7.2.2.2 SMI

The descriptive statistics for structural model index at the levels of L1, L3 and L5 within the perinatal age cohort can be seen in Table 7.8.

Significant differences for SMI between individuals were found at all three vertebral levels. The significant differences observed can be found in Figure 7.3.

The median values for SMI within the L1 perinatal age cohort ranged from 0.252 to 2.099. At the level of L3, values ranged from 0.725 to 2.303. L5 median values ranged from 0.079 to 1.449.

Overall, all values for SMI indicated the presence of predominantly plate-like trabeculae, with a smaller number of rod-like trabeculae. Once again, the oldest individuals within the cohort were significantly different from other perinates. They displayed a significantly higher SMI indicating the increased presence of rod-like trabeculae within the centrum. Individuals SC-084, SC-086 and SC-088 presented the lowest values for SMI indicating a trabecular structure comprised principally of plates.

Table 7.8: Descriptive statistics for SMI within the perinatal age cohort at the levels of L1, L3 and L5. 0= plates, 3= rods and 4=spheres.

	L1	L3	L5
Parametric?	NP	NP	NP
F/H Value	196.684	186.503	173.771
DF	13	12	10
P Value	<0.001	<0.001	<0.001
p≤0.01?	Y	Y	Y
Mean/Median	Median	Median	Median
SC-020	1.262	1.412	1.007
SC-084	0.252	0.725	0.079
SC-086	1.182	1.079	0.305
SC-087	1.357	1.687	1.363
SC-088	1.138	0.903	0.116
SC-092	1.110	1.426	0.667
SC-097	1.533	1.591	1.437
SC-154	1.518	1.720	1.278
SC-155	1.755	N/A	1.449
SC-158	1.441	1.431	1.342
SC-161	1.249	1.489	1.020
SC-040	2.099	2.303	N/A
SC-041	1.773	1.853	N/A
SC-043	1.571	1.672	N/A

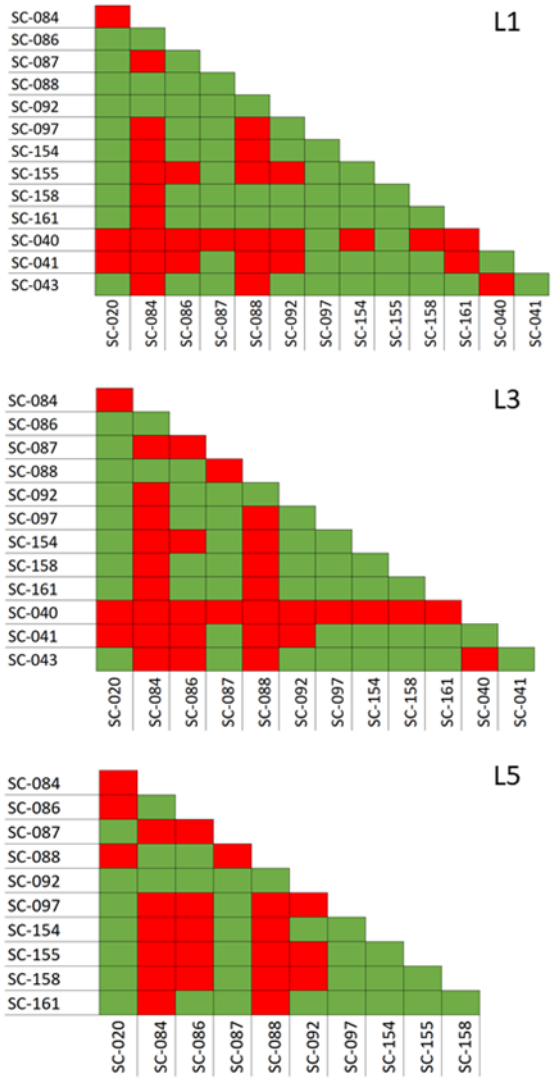

Figure 7.3: Data visualisation for SMI in the perinatal age cohort at the levels of L1, L3 and L5, where red squares denote significant differences between individuals.

7.2.2.3 Tb.Th

The descriptive statistics for trabecular thickness within the perinatal age cohort can be viewed in Table 7.9.

Trabecular thickness also varied significantly between individuals at the three vertebral levels studied. These significant differences can be visualised in Figure 7.4.

The median values for trabecular thickness for the vertebral level L1 ranged between 73.34µm to 123.54µm. The range of median values at the level of L3 were between 62.78µm and 123.95µm. At the level of L5, Tb.Th ranged between 109.13µm and 149.05µm. For Tb.Th within the perinatal age cohort, individuals SC-084, SC-087 and SC-088 consistently displayed the highest values for Tb.Th at all vertebral levels, while individuals SC-040 and SC-041, the oldest within the perinatal age cohort, consistently displayed the lowest values.

.

Table 7.9: Descriptive statistics for Tb.Th (µm) within the perinatal age cohort at the levels of L1, L3 and L5.

	L1	L3	L5
Parametric?	NP	NP	NP
F/H Value	127.812	119.508	70.793
DF	13	12	10
P Value	<0.001	<0.001	<0.001
p≤0.01?	Y	Y	Y
Mean/Median	Median	Median	Median
SC-020	99.74	93.97	122.97
SC-084	108.64	94.15	131.44
SC-086	100.37	91.40	123.89
SC-087	123.54	123.95	149.05
SC-088	112.60	90.34	132.40
SC-092	100.94	90.07	118.07
SC-097	84.58	87.78	109.13
SC-154	91.32	83.06	120.47
SC-155	85.76	N/A	110.22
SC-158	103.08	97.37	118.73
SC-161	97.32	91.57	123.27
SC-040	73.34	62.78	N/A
SC-041	98.03	89.99	N/A
SC-043	84.45	76.52	N/A

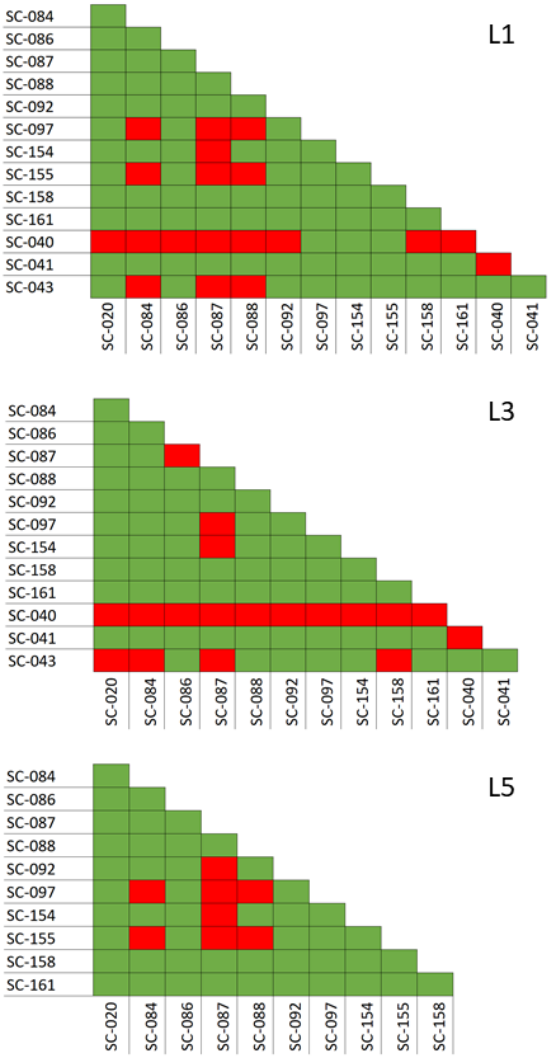

Figure 7.4: Data visualisation for Tb.Th in the perinatal age cohort at the levels of L1, L3 and L5. Red squares denote significant differences between individuals.

7.2.2.4 Tb.N

The descriptive statistics for trabecular number within the perinatal age cohort can be viewed in Table 7.10.

As with previous parameters, all three vertebral levels displayed significant variations in trabecular number between individuals. Specific significant differences between individuals for Tb.N within the perinatal age cohort can be viewed in Figure 7.5.

Tb.N at the level of L1 ranged between 0.00128μm^{-1} and 0.00401μm^{-1}. At the level of L3, median values ranged between 0.00101μm^{-1} and 0.00369μm^{-1}. Average values at the level of L5 ranged from 0.00231μm^{-1} to 0.00372μm^{-1}. Once again, the oldest individuals within the cohort, in particular SC-040, displayed significantly lower values for Tb.N at L1 and L3. Individuals SC-084, SC-086 and SC-088 all displayed the lowest values for Tb.N at all vertebral levels.

Table 7.10: Descriptive statistics for Tb.N (µm^{-1}) within the perinatal age cohort at the levels of L1, L3 and L5.

	L1	L3	L5
Parametric?	NP	NP	NP
F/H Value	213.910	236.151	149.586
DF	13	12	10
P Value	<0.001	<0.001	<0.001
p≤0.01?	Y	Y	Y
Mean/Median	Median	Median	Median
SC-020	0.00293	0.00273	0.00272
SC-084	0.00401	0.00369	0.00372
SC-086	0.00324	0.00340	0.00352
SC-087	0.00262	0.00239	0.00236
SC-088	0.00316	0.00348	0.00361
SC-092	0.00331	0.00278	0.00307
SC-097	0.00269	0.00271	0.00264
SC-154	0.00259	0.00242	0.00263
SC-155	0.00230	N/A	0.00239
SC-158	0.00259	0.00266	0.00231
SC-161	0.00286	0.00246	0.00268
SC-040	0.00128	0.00101	N/A
SC-041	0.00147	0.00145	N/A
SC-043	0.00233	0.00225	N/A

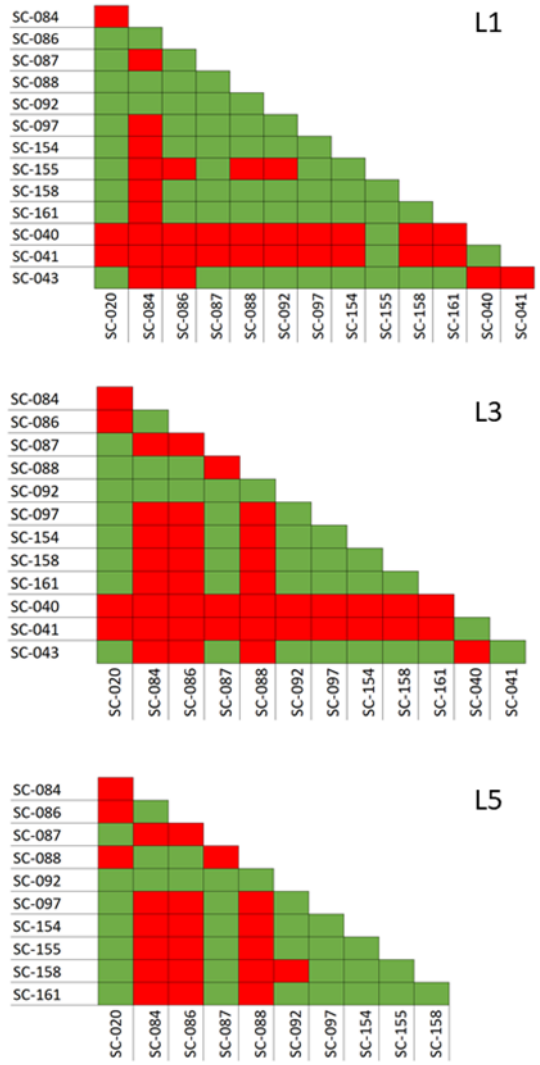

Figure 7.5: Data visualisation for Tb.N in the perinatal age cohort at the levels of L1, L3 and L5. Red squares denote significant differences between individuals.

7.2.2.5 Tb.Sp

The descriptive statistics for trabecular separation within the perinatal age cohort can be viewed in Table 7.11.

Vertebral levels L1, L3 and L5 displayed significant differences for trabecular separation. Figure 7.6 displayed the significant differences between individuals for each vertebral level.

The median values for Tb.Sp at L1 ranged between 170.64µm and 424.19µm. At the level of L3, values ranged from 191.91µm to 485.50µm. At L5, median values ranged between 169.53µm and 264.49µm. Two of the three oldest individuals, at 2 and 3 weeks of age, displayed the highest values for Tb.Sp at the vertebral levels L1 and L3. These individuals were not present in the L5 sample. As with other parameters within this age cohort, a collection of individuals of the same archaeological origin, the Roman era (SC-084, SC-086, SC-088), also differed significantly to the majority of other perinates. These individuals displayed significantly lower Tb.Sp at all vertebral levels.

Table 7.11: Descriptive statistics for Tb.Sp (µm) within the perinatal age cohort at the levels of L1, L3 and L5.

	L1	L3	L5
Parametric?	NP	NP	NP
F/H Value	176.981	175.403	100.885
DF	13	12	10
P Value	<0.001	<0.001	<0.001
p≤0.01?	Y	Y	Y
Mean/Median	Median	Median	Median
SC-020	227.28	224.93	228.47
SC-084	170.64	191.91	169.53
SC-086	200.01	202.03	179.44
SC-087	222.55	233.91	226.12
SC-088	206.74	204.771	181.28
SC-092	207.01	240.25	211.50
SC-097	240.03	250.00	226.40
SC-154	238.50	246.93	230.83
SC-155	245.79	N/A	222.30
SC-158	257.99	250.38	264.49
SC-161	226.67	262.45	231.01
SC-040	423.05	485.50	N/A
SC-041	424.19	443.31	N/A
SC-043	255.56	262.34	N/A

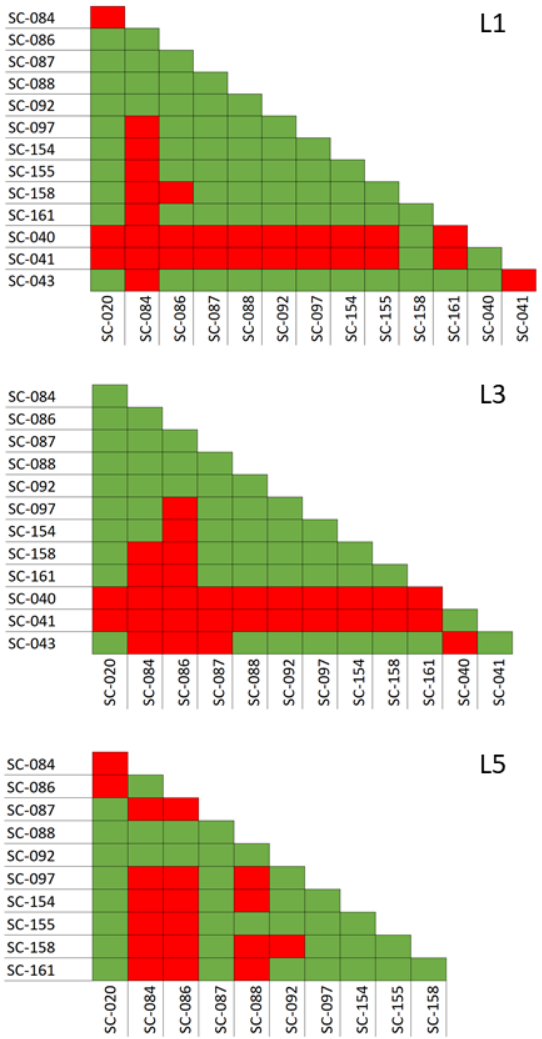

Figure 7.6: Data visualisation for Tb.Sp in the perinatal age cohort at the levels of L1, L3 and L5. Red squares denote significant differences between individuals.

7.2.2.6 DA

The descriptive statistics for degree of anisotropy within the perinatal age cohort can be viewed in Table 7.12.

All three vertebral levels displayed significant variation between individuals for DA. These differences can be visualised in Figure 7.7.

At the level of L1, median values ranged between 0.270 and 0.428. Values ranged from 0.278 to 0.457 at the level of L3. At L5, median values ranged between 0.344 and 0.548. Overall, individuals were generally found to have DA values indicating more isotropic structures (<0.5). Individual SC-040, 2 weeks of age, consistently displayed the lowest values, while the individuals presenting the higher values were more variable.

Table 7.12: Descriptive statistics for DA within the perinatal age cohort at the levels of L1, L3 and L5.

	L1	L3	L5
Parametric?	NP	NP	NP
F/H Value	55.194	76.845	81.819
DF	13	12	10
P Value	<0.001	<0.001	<0.050
p≤0.01?	Y	Y	Y
Mean/Median	Median	Median	Median
SC-020	0.379	0.453	0.548
SC-084	0.351	0.363	0.344
SC-086	0.401	0.374	0.424
SC-087	0.352	0.342	0.377
SC-088	0.401	0.347	0.521
SC-092	0.431	0.457	0.476
SC-097	0.436	0.414	0.464
SC-154	0.395	0.408	0.465
SC-155	0.428	N/A	0.410
SC-158	0.375	0.331	0.548
SC-161	0.418	0.428	0.412
SC-040	0.270	0.278	N/A
SC-041	0.319	0.344	N/A
SC-043	0.396	0.399	N/A

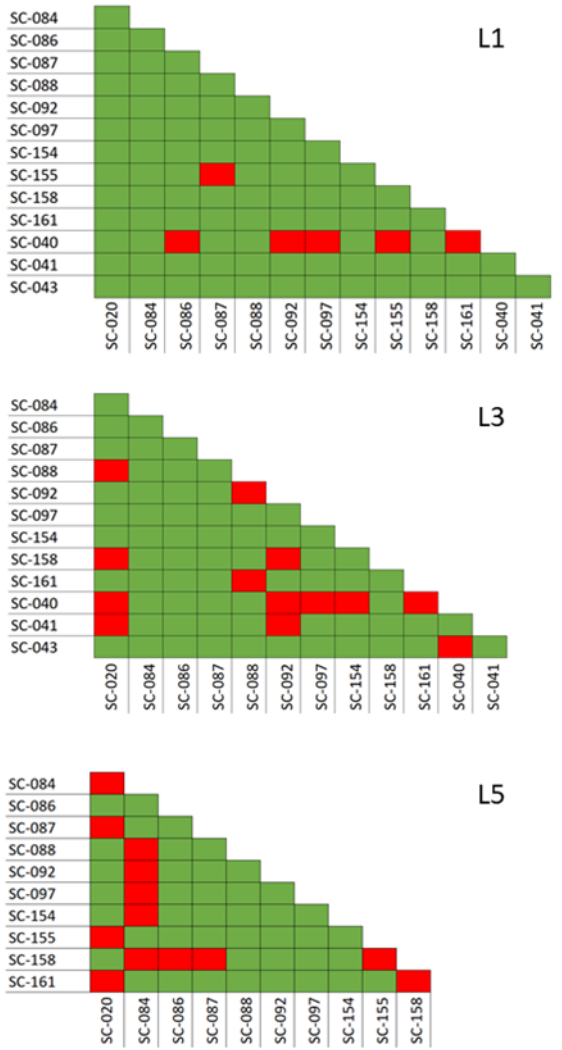

Figure 7.7: Data visualisation for DA in the perinatal age cohort at the levels of L1, L3 and L5. Red squares denote significant differences between individuals.

7.2.3 *4 weeks to 2 years of age cohort*

7.2.3.1 BV/TV

The descriptive statistics for bone volume fraction within the 4 weeks to 2 years of age cohort can be viewed in Table 7.13.

All three vertebral levels displayed significant variation between individuals for BV/TV within the 4 weeks to 2 years of age cohort. These significant differences can be visualised in Figure 7.8.

At the level of L1, values for BV/TV ranged between 11.09% and 20.29%. At the level of L3, these values ranged from 10.07% to 19.90%. Finally, at L5, average values per individual ranged between 13.93% and 19.90%. Individual SC-046, the youngest individual at 7 weeks of age, consistently displayed the highest median values for BV/TV at all vertebral levels with the age cohort. A variety of individuals displayed the lowest values for BV/TV and was not observed to be related to an increase in age.

Table 7.13: Descriptive statistics for BV/TV (%) within the 4wks-2y cohort at the levels of L1, L3 and L5.

	L1	L3	L5
Parametric?	NP	NP	NP
F/H Value	130.1	150.508	59.514
DF	9	10	4
P Value	<0.001	<0.001	<0.001
p≤0.01?	Y	Y	Y
Mean/Median	Median	Median	Median
SC-046	20.29	18.97	19.90
SC-047	16.46	15.26	N/A
SC-050	11.09	10.07	N/A
SC-021	11.67	11.23	13.93
SC-054	16.75	15.47	N/A
SC-070	N/A	N/A	18.25
SC-056	16.60	14.46	N/A
SC-057	16.28	13.75	N/A
SC-060	11.72	10.36	N/A
SC-071	N/A	N/A	14.45
SC-061	14.44	11.37	N/A
SC-024	N/A	12.11	15.67
SC-062	13.13	10.27	N/A

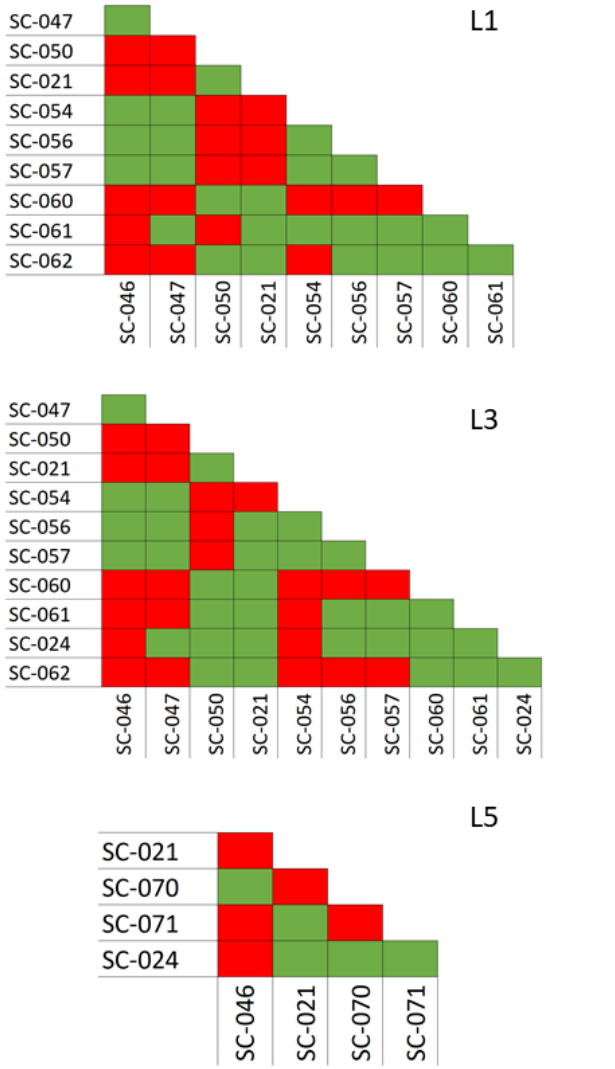

Figure 7.8: Data visualisation for BV/TV in the 4wks-2y cohort at the levels of L1, L3 and L5. Red squares denote significant differences between individuals.

7.2.3.2 SMI

The descriptive statistics for structural model index within the 4 weeks to 2 years of age cohort can be viewed in Table 7.14.

All vertebral levels displayed significant variation in SMI within the 4 weeks to 2 years of age cohort. The significant differences between individuals can be visualised in Figure 7.9.

Average values for SMI at the level of L1 ranged between 1.169 and 1.775. Values at the level of L3 ranged from 1.276 to 1.851. Median values at the level of L5 ranged from 1.230 to 1.715. All values within each vertebral level indicated that the internal trabecular architecture presented a mixture of rod-like and plate-like trabeculae. The youngest individual (SC-046) presented significantly lower SMI values, indicating more plate-like trabeculae, compared to most individuals within the cohort.

Table 7.14: Descriptive statistics for SMI within the 4wks-2y cohort at the levels of L1, L3 and L5.

	L1	L3	L5
Parametric?	NP	NP	NP
F/H Value	126.708	118.017	87.404
DF	9	10	4
P Value	<0.001	<0.001	<0.001
p≤0.01?	Y	Y	Y
Mean/Median	Median	Median	Median
SC-046	1.169	1.276	1.233
SC-047	1.775	1.812	N/A
SC-050	1.725	1.751	N/A
SC-021	1.771	1.666	1.544
SC-054	1.403	1.526	N/A
SC-070	N/A	N/A	1.230
SC-056	1.422	1.569	N/A
SC-057	1.511	1.595	N/A
SC-060	1.570	1.627	N/A
SC-071	N/A	N/A	1.715
SC-061	1.573	1.685	N/A
SC-024	N/A	1.570	1.408
SC-062	1.678	1.851	N/A

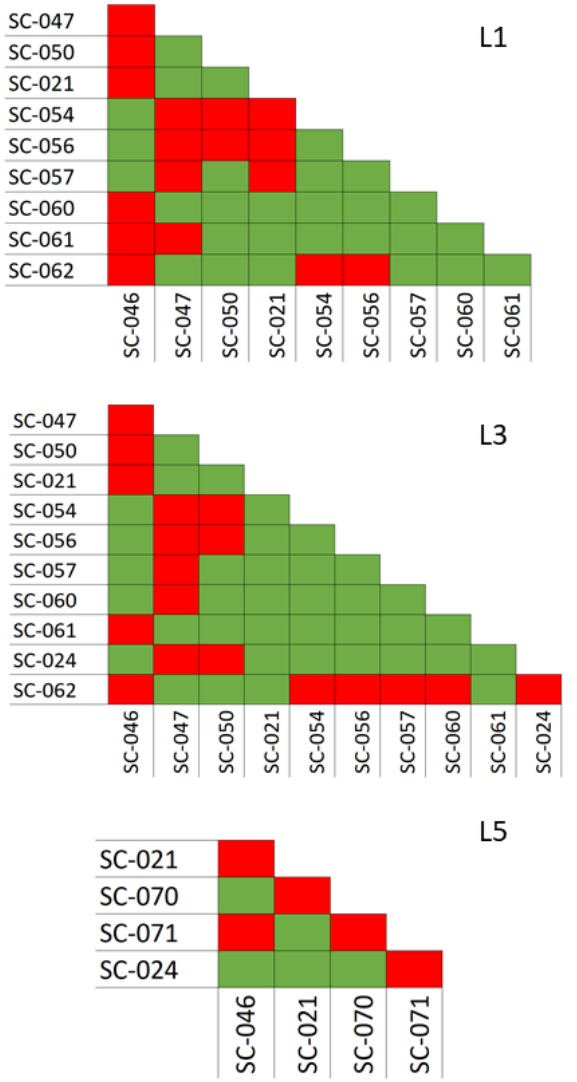

Figure 7.9: Data visualisation for SMI in the 4wks-2y cohort at the levels of L1, L3 and L5. Red squares denote significant differences between individuals.

7.2.3.3 Tb.Th

The descriptive statistics for trabecular thickness within the 4 weeks to 2 years of age cohort can be viewed in Table 7.15.

The vertebral levels L1, L3 and L5 all displayed significant differences in Tb.Th between individuals. These differences can be visualised in Figure 7.10.

Average values for Tb.Th ranged from 75.34µm to 124.97µm at the level of L1. At the level of L3, values ranged between 76.47µm and 122.25µm. At L5, median values ranged from 86.42µm and 130.34µm. Individual SC-046 once again differed from a number of individuals over all vertebral levels, presenting a significantly lower trabecular thickness. Older individuals in the cohort, for example SC-057 (17 months of age) and SC-061 (2 years of age) displayed the highest Tb.Th values.

Table 7.15: Descriptive statistics for Tb.Th (µm) within the 4wks-2y cohort at the levels of L1, L3 and L5.

	L1	L3	L5
Parametric?	NP	NP	NP
F/H Value	144.696	141.059	71.247
DF	9	10	4
P Value	<0.001	<0.001	<0.001
p≤0.01?	Y	Y	Y
Mean/Median	Median	Median	Median
SC-046	77.04	80.26	86.42
SC-047	99.05	97.07	N/A
SC-050	75.34	76.47	N/A
SC-021	99.39	96.26	104.73
SC-054	109.11	103.99	N/A
SC-070	N/A	N/A	130.34
SC-056	112.08	104.78	N/A
SC-057	122.44	122.25	N/A
SC-060	97.42	93.20	N/A
SC-071	N/A	N/A	108.76
SC-061	124.97	114.28	N/A
SC-024	N/A	102.45	115.88
SC-062	99.15	98.96	N/A

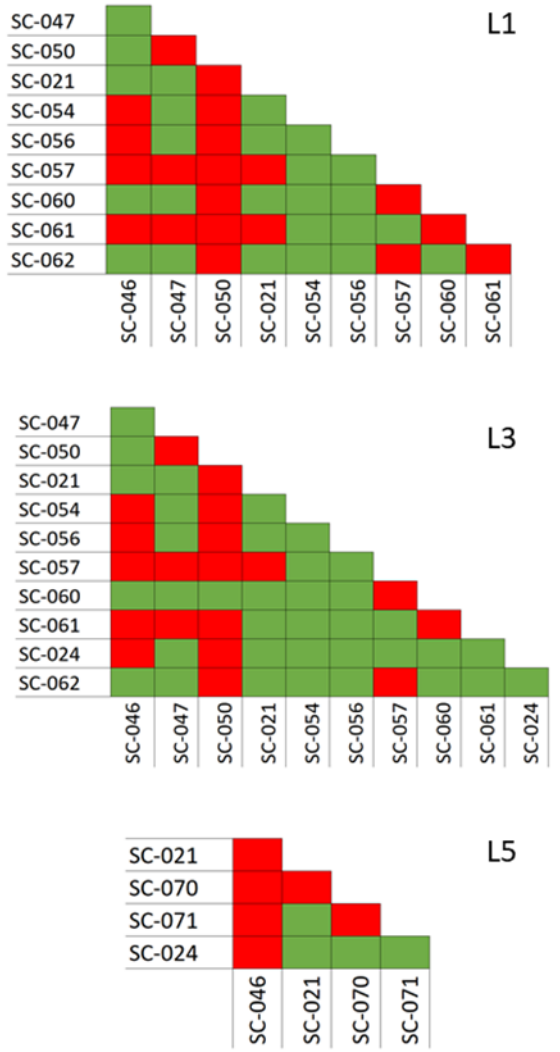

Figure 7.10: Data visualisation for Tb.Th in the 4wks-2y cohort at the levels of L1, L3 and L5. Red squares denote significant differences between individuals.

7.2.3.4 Tb.N

The descriptive statistics for trabecular number within the 4 weeks to 2 years of age cohort can be viewed in Table 7.16.

All three vertebral levels studied displayed significant differences between individuals for Tb.N. These can be visualised in Figure 7.11.

The median number of trabeculae present within the 4 weeks – 2 years of age cohort ranged from 0.00111μm^{-1} to 0.00266μm^{-1} at the level of L1. The vertebral level L3 displayed median values ranging between 0.00097μm^{-1} and 0.0023μm^{-1}, while at the level of L5 these values ranged between 0.0024μm^{-1} and 0.00137μm^{-1}. As with other parameters within the age cohort, individual SC-046, the youngest individual within the cohort at 7 weeks of age, consistently displayed significantly higher values for Tb.N. Older individuals such as SC-061 (2 years of age) and SC-062 (aged 2 years and 7 months) consistently displayed the lowest Tb.N values at each vertebral level. Individual variation unrelated to age was also present within the sample.

Table 7.16: Descriptive statistics for Tb.N (μm^{-1}) within the 4wks-2y cohort at the levels of L1, L3 and L5.

	L1	L3	L5
Parametric?	NP	NP	NP
F/H Value	131.687	163.177	59.611
DF	9	10	4
P Value	<0.001	<0.001	<0.001
p≤0.01?	Y	Y	Y
Mean/Median	Median	Median	Median
SC-046	0.00266	0.00230	0.00232
SC-047	0.00170	0.00160	N/A
SC-050	0.00147	0.00135	N/A
SC-021	0.00112	0.00116	0.00130
SC-054	0.00155	0.00149	N/A
SC-070	N/A	N/A	0.00137
SC-056	0.00139	0.00130	N/A
SC-057	0.00133	0.00120	N/A
SC-060	0.00121	0.00109	N/A
SC-071	N/A	N/A	0.00124
SC-061	0.00111	0.00097	N/A
SC-024	N/A	0.00116	0.00132
SC-062	0.00128	0.00105	N/A

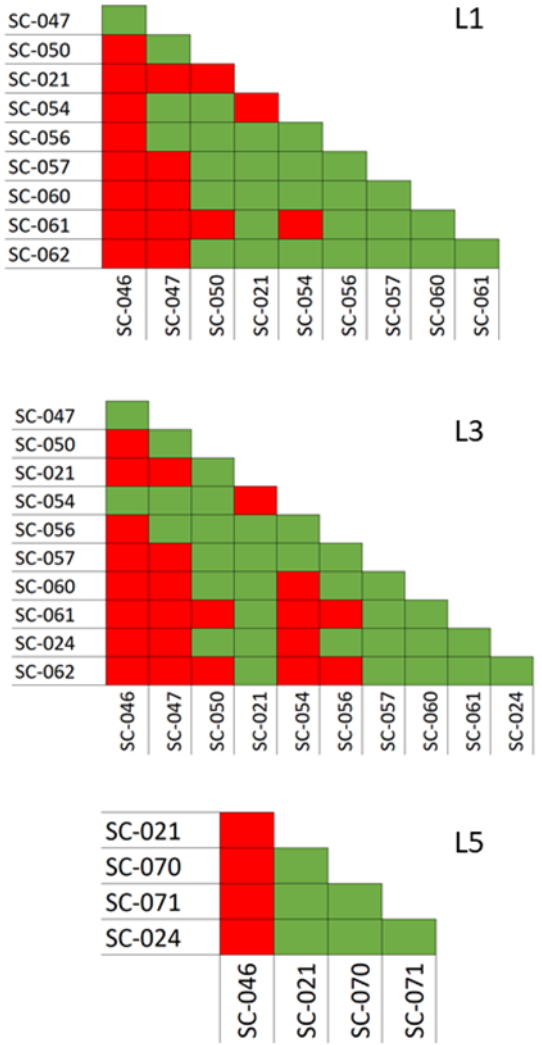

Figure 7.11: Data visualisation for Tb.N in the 4wks-2y cohort at the levels of L1, L3 and L5. Red squares denote significant differences between individuals.

7.2.3.5 Tb.Sp

The descriptive statistics for trabecular separation within the 4 weeks to 2 years of age cohort can be viewed in Table 7.17.

All three vertebral levels studied displayed significant differences between individuals for Tb.Sp within the 4 weeks to 2 years of age cohort. The individuals differing significantly from each other can be viewed in Figure 7.12.

Values for Tb.Sp, at the level of L1, ranged between 293.84µm and 623.91µm. At the level of L3, median values ranged between 316.36µm and 642.28µm. At L5, Tb.Sp ranged from 329.31µm to 586.84µm. Younger individuals within the age cohort generally displayed lower values for Tb.Sp. for example, individual SC-046, the youngest at 7 weeks of age, consistently displayed the lowest values over all vertebral levels. Older individuals, like SC-061 (2 years of age), displayed the highest values for Tb.Sp.

Table 7.17: Descriptive statistics for Tb.Sp (µm) within the 4wks-2y cohort at the levels of L1, L3 and L5.

	L1	L3	L5
Parametric?	NP	NP	NP
F/H Value	139.319	174.547	64.922
DF	9	10	4
P Value	<0.001	<0.001	<0.001
p≤0.01?	Y	Y	Y
Mean/Median	Median	Median	Median
SC-046	293.84	316.46	329.31
SC-047	362.05	373.95	N/A
SC-050	420.38	434.44	N/A
SC-021	572.69	579.28	542.58
SC-054	438.45	458.38	N/A
SC-070	N/A	N/A	596.84
SC-056	510.03	507.86	N/A
SC-057	517.81	564.36	N/A
SC-060	543.39	555.49	N/A
SC-071	N/A	N/A	492.34
SC-061	623.91	642.28	N/A
SC-024	N/A	556.27	546.03
SC-062	492.47	527.76	N/A

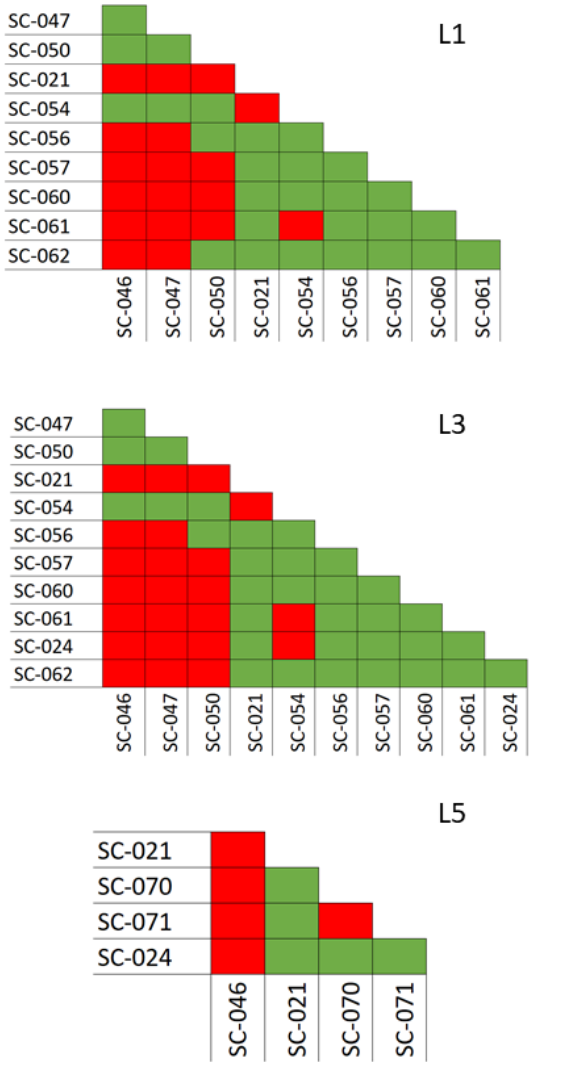

Figure 7.12: Data visualisation for Tb.Sp in the 4wks-2y cohort at the levels of L1, L3 and L5. Red squares denote significant differences between individuals.

7.2.3.6 DA

The descriptive statistics for degree of anisotropy within the 4 weeks to 2 years of age cohort can be viewed in Table 7.18.

Only the vertebral levels L1 and L3 displayed significant variation between individuals for DA. These differences between individuals can be viewed in Figure 7.13.

At the level of L1, values for DA ranged from 0.249 to 0.396. At the level of L3, values for DA ranged between 0.281 and 0.455. At L5, the range of the dataset was from 0.268 to 0.378. DA presented the lowest number of significant differences of all parameters within the 4 weeks to 2 years of age cohort. All values indicated that the internal trabecular architecture was more isotropic than anisotropic. However, individual SC-061, 2 years of age, displayed the lowest average value for DA at L1 and L3.

Table 7.18: Descriptive statistics for DA within the 4wks-2y cohort at the levels of L1, L3 and L5.

	L1	L3	L5
Parametric?	NP	NP	NP
F/H Value	19.564	27.826	8.341
DF	9	10	4
P Value	0.021	0.002	0.080
p≤0.01?	Y	Y	N
Mean/Median	Median	Median	Median
SC-046	0.320	0.371	0.350
SC-047	0.396	0.364	N/A
SC-050	0.370	0.396	N/A
SC-021	0.356	0.359	0.343
SC-054	0.314	0.390	N/A
SC-070	N/A	N/A	0.268
SC-056	0.336	0.377	N/A
SC-057	0.321	0.344	N/A
SC-060	0.392	0.455	N/A
SC-071	N/A	N/A	0.354
SC-061	0.249	0.281	N/A
SC-024	N/A	0.306	0.378
SC-062	0.340	0.358	N/A

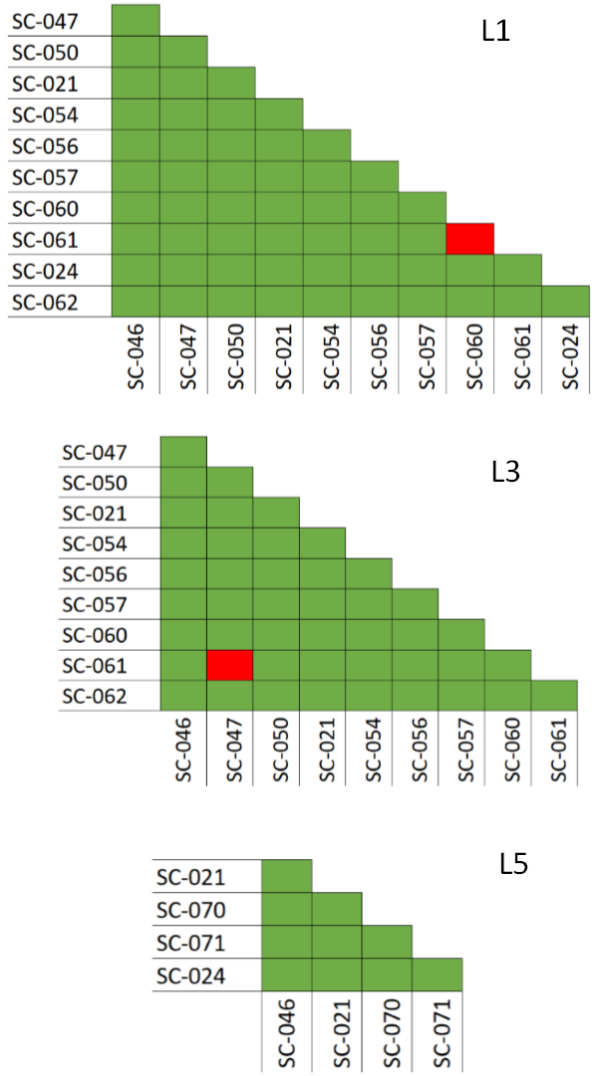

Figure 7.13: Data visualisation for DA in the 4wks-2y cohort at the levels of L1, L3 and L5. Red squares denote significant differences between individuals.

7.2.4 *3 to 8 years age cohort*

Due to the majority of individuals over the age of 6 years displaying near complete neurocentral fusion, only one individual (SC-229, aged 6-8 years) was analysed for the quantitative study. As this individual was the only one within the 6-8 year cohort, histomorphometric data for this individual was included with data from the 3-5 year cohort. Due to the addition of this individual within the 3-5 years of age cohort, this cohort was renamed 3 to 8 years of age to accommodate individual SC-229.

7.2.4.1 BV/TV

The descriptive statistics for bone volume fraction within the 3-8 years of age cohort can be viewed in Table 7.19.

Significant variation between the values for BV/TV of individuals within the 3-8 years of age cohort were present at the vertebral levels L3 and L5. These differences can be visualised in Figure 7.14.

Values for BV/TV at the level of L1 ranged between 12.52% and 14.72%. At the level of L3, median values ranged from 9.83% to 13.84%. At L5, values ranged between 15.23% and 20.22%. Individual SC-025 (3 years of age) consistently displayed higher values for BV/TV within the 3-8 year cohort. No other individual differences were present.

Table 7.19: Descriptive statistics for BV/TV (%) within the 3-8y cohort at the levels of L1, L3 and L5.

	L1	L3	L5
Parametric?	NP	NP	NP
F/H Value	19.656	37.279	42.070
DF	7	5	3
P Value	0.006	<0.001	<0.001
p≤0.01?	N	Y	Y
Mean/Median	Median	Median	Median
SC-063	13.43	N/A	N/A
SC-064	N/A	13.05	N/A
SC-002	14.20	12.28	18.13
SC-025	14.72	9.83	15.23
SC-065	14.27	N/A	N/A
SC-066	12.52	N/A	N/A
SC-010	14.71	13.84	19.17
SC-026	12.99	11.85	20.22
SC-229	13.10	10.80	N/A

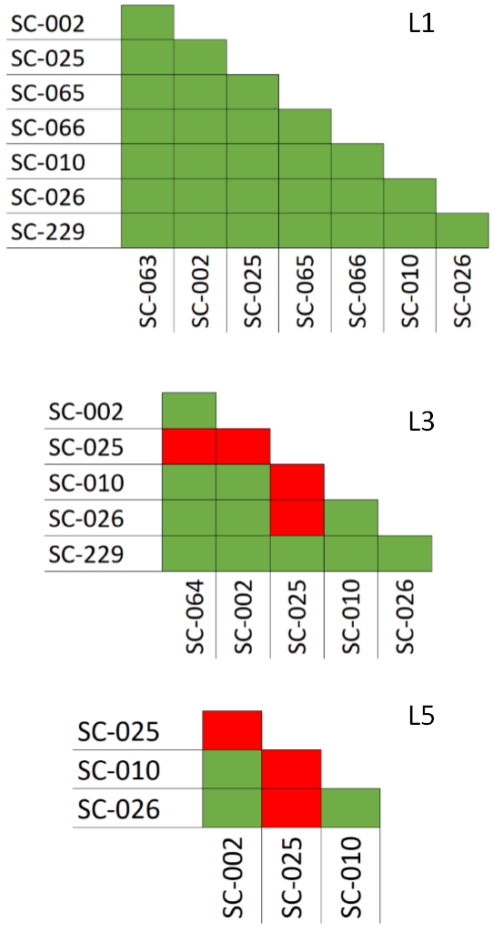

Figure 7.14: Data visualisation for BV/TV in the 3-8y cohort at the levels of L1, L3 and L5. Red squares denote significant differences between individuals.

7.2.4.2 SMI

The descriptive statistics for structural model index within the 3-8 years of age cohort can be viewed in Table 7.20.

All three vertebral levels displayed significant differences between individuals for SMI. These differences can be visualised in Figure 7.15.

SMI at the level of L1 ranged between 1.365 and 1.838. At the level of L3, average values ranged from 1.513 to 1.904. At L5, SMI ranged between 1.227 and 1.558. Individual SC-229, the oldest within the cohort (6-8 years of age) consistently displayed the highest value for SMI. However, all values indicated a trabecular architecture comprised of both plate-like and rod-like trabeculae.

Table 7.20: Descriptive statistics for SMI within the 3-8y cohort at the levels of L1, L3 and L5.

	L1	L3	L5
Parametric?	NP	NP	NP
F/H Value	29.447	33.391	12.495
DF	7	5	3
P Value	<0.001	<0.001	0.006
p≤0.01?	Y	Y	Y
Mean/Median	Median	Median	Median
SC-063	1.508	N/A	N/A
SC-064	N/A	1.520	N/A
SC-002	1.724	1.726	1.558
SC-025	1.365	1.513	1.277
SC-065	1.568	N/A	N/A
SC-066	1.618	N/A	N/A
SC-010	1.600	1.649	1.326
SC-026	1.599	1.689	1.364
SC-229	1.838	1.904	N/A

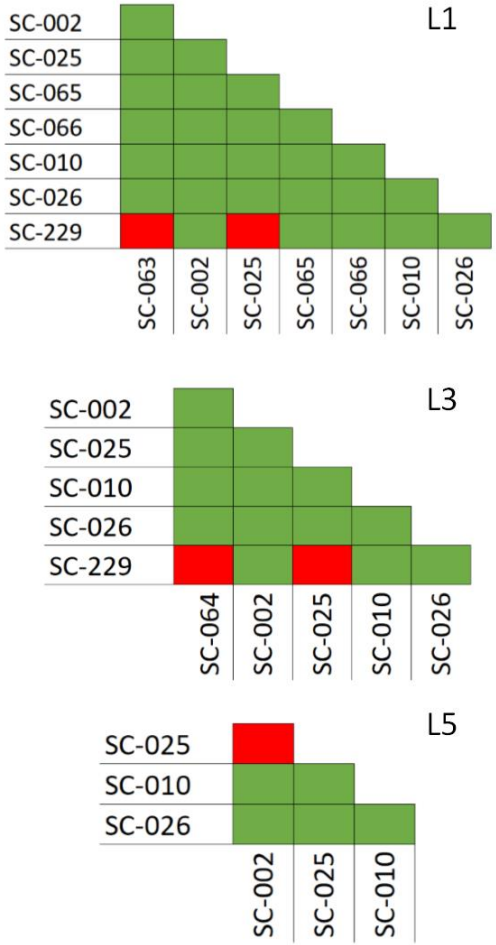

Figure 7.15: Data visualisation for SMI in the 3-8y cohort at the levels of L1, L3 and L5. Red squares denote significant differences between individuals.

7.2.4.3 Tb.Th

The descriptive statistics for trabecular thickness within the 3-8 years of age cohort can be viewed in Table 7.21.

Significant variation in Tb.Th between individuals was observed at all three vertebral levels. The individuals differing from each other can be visualised in Figure 7.16.

Trabecular thickness ranged from 99.20µm to 134.37µm at the level of L1. At L3, median values ranged between 87.39µm and 112.87µm. At the level of L5, average values for Tb.Th ranged from 106.423µm to 142.63µm. Overall, individual SC-025 (3 years of age) consistently displayed lower values for Tb.Th compared to other individuals at each vertebral level. Individuals displaying the highest values included SC-010, SC-026 and SC-065 (all aged 4 years).

Table 7.21: Descriptive statistics for Tb.Th (µm) within the 3-8y cohort at the levels of L1, L3 and L5.

	L1	L3	L5
Parametric?	NP	NP	NP
F/H Value	60.139	47.512	48.452
DF	7	5	3
P Value	<0.001	<0.001	<0.001
p≤0.01?	Y	Y	Y
Mean/Median	Median	Median	Median
SC-063	113.085	N/A	N/A
SC-064	N/A	108.09	N/A
SC-002	99.20	98.83	124.13
SC-025	105.15	87.39	106.42
SC-065	134.37	N/A	N/A
SC-066	122.98	N/A	N/A
SC-010	117.23	112.87	142.63
SC-026	111.58	112.14	142.61
SC-229	107.06	99.76	N/A

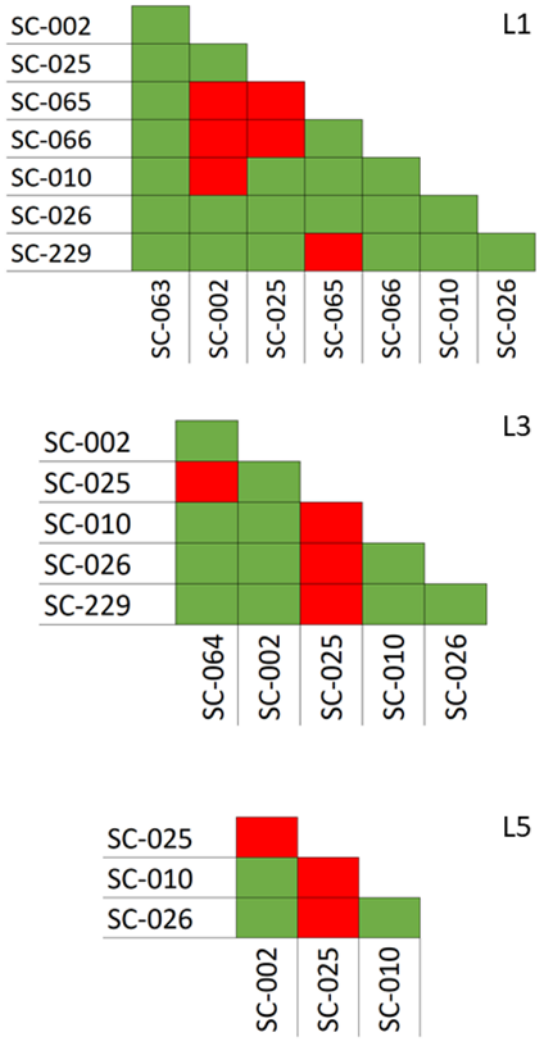

Figure 7.16: Data visualisation for Tb.Th in the 3-8y cohort at the levels of L1, L3 and L5. Red squares denote significant differences between individuals.

7.2.4.4 Tb.N

The descriptive statistics for trabecular number within the 3 to 8 years of age cohort can be viewed in Table 7.22.

Only the vertebral level L1 displayed any significant variation in Tb.N between individuals for Tb.N in the 3-8 years of age cohort. Significant differences can be visualised in Figure 7.17.

Average values at the level of L1 ranged between 0.00100μm^{-1} and 0.00144μm^{-1}. At the level of L3, median values ranged from 0.00108μm^{-1} to 0.00124μm^{-1}. At the level of L5, mean values for Tb.N ranged between 0.00136μm^{-1} and 0.00142μm^{-1}. At L1, younger individuals such as SC-002 and SC-025 (3 years of age) displayed higher values for Tb.N compared to older individuals such as SC-002, SC-065 and SC-066 (4 years of age).

Table 7.22: Descriptive statistics for Tb.N (µm^{-1}) within the 3-8y cohort at the levels of L1, L3 and L5.

	L1	L3	L5
Parametric?	NP	NP	Y
F/H Value	65.063	10.061	0.313
DF	7	5	3
P Value	<0.001	0.074	0.816
p≤0.01?	Y	N	N
Mean/Median	Median	Median	Mean
SC-063	0.00113	N/A	N/A
SC-064	N/A	0.00121	N/A
SC-002	0.00144	0.00124	0.00142
SC-025	0.00141	0.00114	0.00136
SC-065	0.00106	N/A	N/A
SC-066	0.00100	N/A	N/A
SC-010	0.00125	0.00114	0.00136
SC-026	0.00118	0.00108	0.00139
SC-229	0.00120	0.00110	N/A

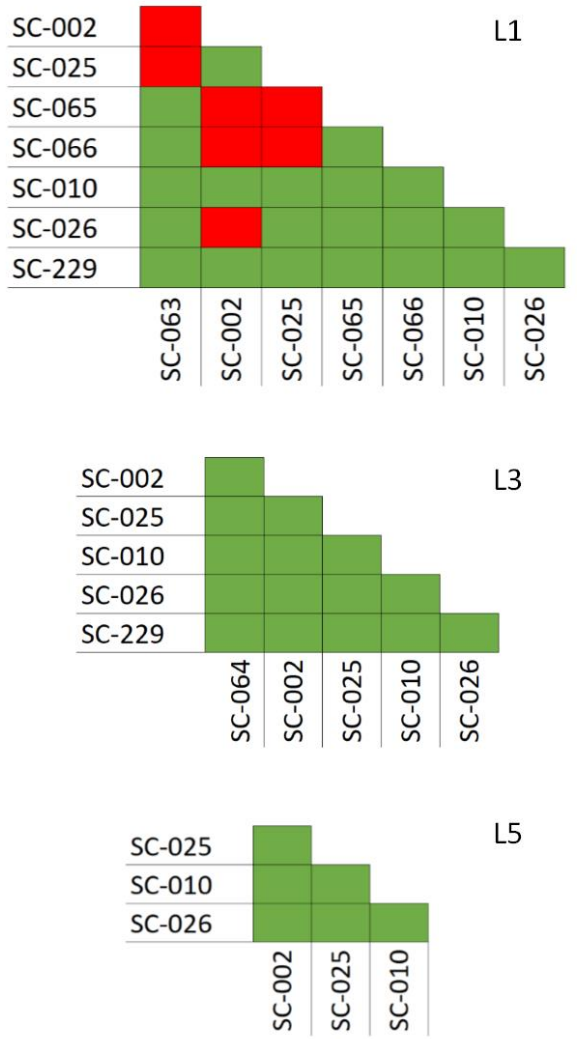

Figure 7.17: Data visualisation for Tb.N in the 3-8y cohort at the levels of L1, L3 and L5. Red squares denote significant differences between individuals.

7.2.4.5 Tb.Sp

The descriptive statistics for trabecular separation within the 3 to 8 years of age cohort can be viewed in Table 7.23.

As with Tb.N, only the vertebral level L1 displayed any significant differences between individuals. These differences can be found in Figure 7.18.

The median values for Tb.Sp at the level of L1 ranged between 449.29µm and 652.42µm. At the level of L3, trabecular separation ranged from 488.68µm to 616.02µm. At L5, median values ranged between 504.82µm and 548.09µm. Individuals SC-063, SC-065 and SC-066 displayed the highest values while individual SC-002 displayed the lowest.

Table 7.23: Descriptive statistics for Tb.Sp (µm) within the 3-8y cohort at the levels of L1, L3 and L5.

	L1	L3	L5
Parametric?	NP	NP	NP
F/H Value	55.192	15.433	2.033
DF	7	5	3
P Value	<0.001	0.009	0.566
p≤0.01?	Y	N	N
Mean/Median	Median	Median	Median
SC-063	606.91	N/A	N/A
SC-064	N/A	616.02	N/A
SC-002	449.29	488.68	504.82
SC-025	513.61	575.60	548.09
SC-065	652.42	N/A	N/A
SC-066	631.12	N/A	N/A
SC-010	552.54	574.10	514.58
SC-026	566.87	576.39	521.10
SC-229	465.82	509.33	N/A

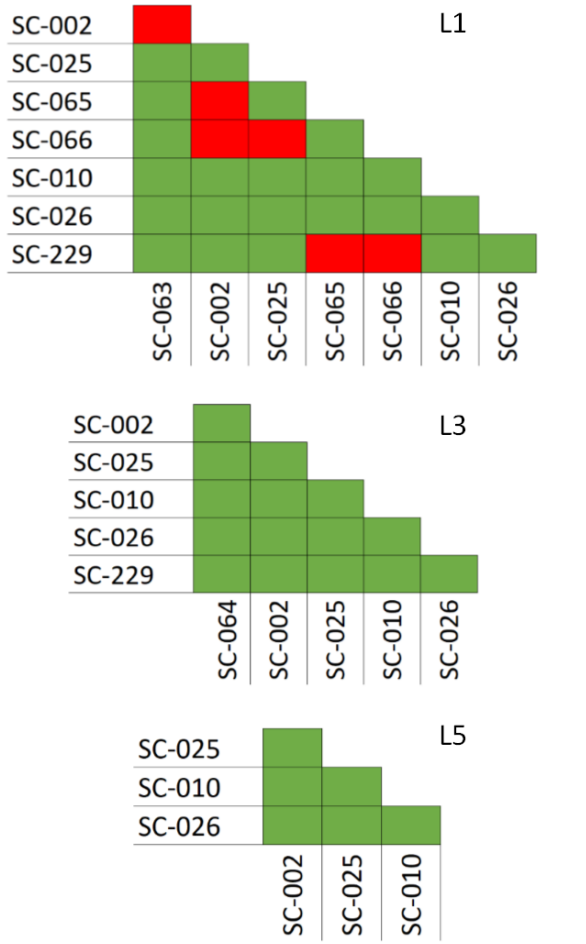

Figure 7.18: Data visualisation for Tb.Sp in the 3-8y cohort at the levels of L1, L3 and L5. Red squares denote significant differences between individuals.

7.2.4.6 DA

The descriptive statistics for degree of anisotropy within the 3 to 8 years of age cohort can be viewed in Table 7.24.

The vertebral levels L3 and L5 displayed significant variation between individuals for DA. These differences can be found in Figure 7.19.

Values for DA at the level of L1 ranged from 0.296 to 0.406. At the level of L3, median values ranged between 0.284 and 0.452. At L5, average values for DA ranged from 0.262 to 0.391.

Individual SC-002 (3 years) displayed the highest values for DA at all vertebral levels, while SC-010 (4 years) and SC-229 (6-8 years) displayed the lowest. However, all values indicated more isotropic, rather than anisotropic structures.

Table 7.24: Descriptive statistics for DA within the 3-8y cohort at the levels of L1, L3 and L5.

	L1	L3	L5
Parametric?	NP	NP	NP
F/H Value	14.752	20.620	14.104
DF	7	5	3
P Value	0.039	<0.001	0.003
p≤0.01?	N	Y	Y
Mean/Median	Median	Median	Median
SC-063	0.306	N/A	N/A
SC-064	N/A	0.342	N/A
SC-002	0.406	0.452	0.391
SC-025	0.340	0.332	0.345
SC-065	0.296	N/A	N/A
SC-066	0.386	N/A	N/A
SC-010	0.317	0.284	0.262
SC-026	0.308	0.304	0.306
SC-229	0.384	0.313	N/A

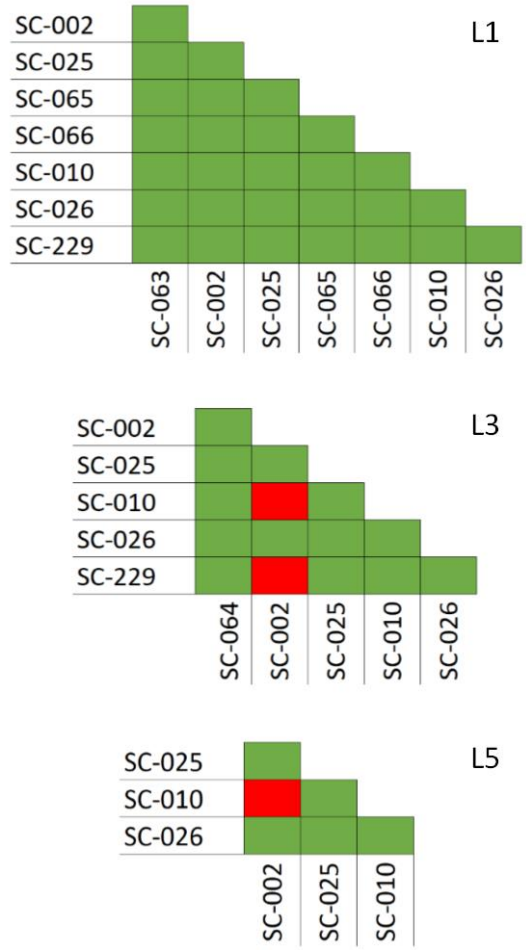

Figure 7.19: Data visualisation for DA in the 3-8y cohort at the levels of L1, L3 and L5. Red squares denote significant differences between individuals.

7.3 Results for Analysis 1b

7.3.1 *L1*

The descriptive statistics for the six histomorphometric parameters, at the level of L1, can be viewed in Table 7.25.

7.3.1.1 BV/TV

Values for bone volume fraction (BV/TV) at the level of L1 ranged from 14.13 % to 34.34%. The fetal age cohort displayed the highest median value for BV/TV, which was observed to decrease with age. The fetal age cohort was significantly different to the 4 weeks to 2 years of age cohort and the 3-8 years of age cohort, however, was not significantly different to the perinatal age cohort at the level of $p \leq 0.01$. The perinatal age cohort also displayed a significantly higher average BV/TV compared to the two later age cohorts. No significant difference was found between the 4 weeks to 2 years of age cohort and the 3-8 years cohort, with both cohorts displaying lower median BV/TV values (Figure 7.20).

7.3.1.2 SMI

Average values for structural model index (SMI) ranged from 1.050 to 1.609. SMI was found to increase with age at the level of L1. The 3-8 years of age cohort displayed the highest median value for SMI and was found to be significantly different to both the fetal and perinatal age cohorts. The fetal age cohort displayed the lowest median SMI value, differing from all other age cohorts. The perinatal age cohort was not found to differ significantly to the 4 weeks to 2 years of age cohort at the level of $p \leq 0.010$. Overall, values for SMI indicated a trabecular architecture formed of both plate-like and rod-like trabeculae (Figure 7.20).

7.3.1.3 Tb.Th

As with SMI, trabecular thickness exhibited an increase with age. Average values ranged from 81.84µm to 113.52µm. The 3-8 years age cohort differed significantly to the fetal and perinatal age cohorts, displaying significantly higher trabecular thickness. The fetal age cohort displayed the lowest average values and differed significantly from the 4 weeks to 2 years cohort also. No differences were found between the two younger age cohorts, or between the two older age

cohorts. There were also no differences found between the perinatal and the 4 weeks to 2 years of age cohort (Figure 7.20).

7.3.1.4 Tb.N

Trabecular number was observed to decrease with age, with values ranging from 0.00110μm^{-1} to 0.00436μm^{-1}. While the fetal and perinatal age cohorts did not differ significantly from each other, they were found to displayed significantly higher Tb.N values compared to the 4 weeks to 2 years and 3-8 years age cohorts. Furthermore, the two older age cohorts did not differ significantly from each other, but displayed significantly lower values when compared to the fetal and perinatal age cohorts (Figure 7.20).

7.3.1.5 Tb.Sp

Trabecular separation increased with age. Average values ranged between 161.84μm and 542.60μm. Once again, the fetal and perinatal age cohorts did not differ from each other though did display significantly lower Tb.Sp compared to the two older age cohorts. The 4 weeks to 2 years, and 3-8 years cohorts were not significantly different to each other in terms of Tb.Sp (Figure 7.20).

7.3.1.6 DA

Degree of anisotropy was the only parameter not to display any significant differences at $p \leq 0.010$ between age cohorts at the level of L1. However, while not significant, DA displayed a slight decrease with age. Values ranged from 0.299 to 0.398 indicating a more isotropic structure present within all centra (Figure 7.20).

Table 7.25: Statistical protocol and descriptive statistics for each histomorphometric parameter between age cohorts at the level of L1.

	Statistical Protocol						Age Cohort			
Parameter	Parametric?	H/F Value	DF	P Value	p≤0.01?	Mean/ Median	Fetal	Perinatal	4wks-2y	3-8y
BV/TV (%)	NP	90.028	3	<0.001	Y	Median	34.34	25.67	15.08	14.13
SMI	NP	60.025	3	<0.001	Y	Median	1.050	1.312	1.556	1.609
Tb.Th (μm)	NP	46.069	3	<0.001	Y	Median	81.84	96.34	103.00	113.52
Tb.N (μm^{-1})	NP	92.113	3	<0.001	Y	Median	0.00436	0.00227	0.00150	0.00110
Tb.Sp (μm)	NP	87.733	3	<0.001	Y	Median	161.84	250.05	465.61	542.60
DA	NP	11.866	3	0.008	N	Median	0.398	0.386	0.339	0.299

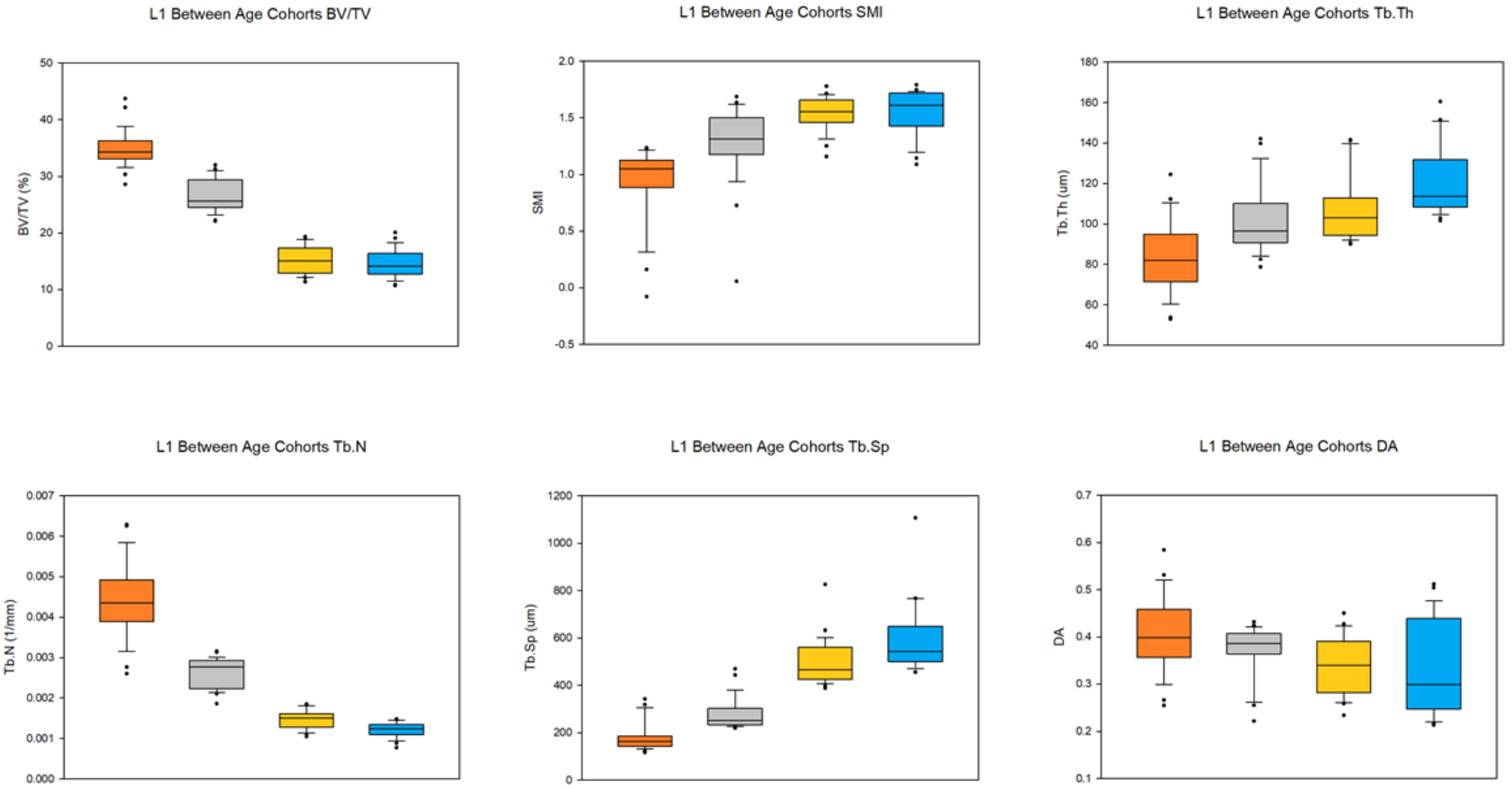

Figure 7.20: Box plots displaying the spread of data for the fetal (orange), perinatal (grey), 4wks -2y (yellow) and 3-8y (blue) age cohorts per histomorphometric parameter, at the level of the 1st lumbar vertebra.

7.3.2 *L3*

The descriptive statistics for the six histomorphometric parameters at the level of L3 can be viewed in Table 7.26.

7.3.2.1 BV/TV

Bone volume fraction was observed to decrease with age at the level of L3. Values ranged between 11.70% to 25.89%. The fetal and perinatal age cohorts presented significantly higher BV/TV compared to individuals aged 4 weeks and above. The 4 weeks to 2 years and 3 to 8 years cohorts did not differ significantly from each other for this parameter (Figure 7.21).

7.3.2.2 SMI

Structural model index values increased with age at the level of L3 although no significant differences were found between age cohorts at the level of $p \leq 0.010$. Median values ranged between 1.472 to 1.706, indicating trabeculae were both plate-like and rod-like in morphology (Figure 7.21).

7.3.2.3 Tb.Th

Trabecular thickness was observed to increase with age. Average values ranged between 64.04µm and 103.97µm. The fetal age cohort was found to differ significantly to all other cohorts. No significant differences were found between the perinatal and 4 weeks to 2 years of age individuals, and the 4 weeks to 2 years of age and the 3 to 8 years of age individuals. The perinatal cohort displayed significantly lower trabecular thickness compared to the oldest individuals within the 3-8y cohort (Figure 7.21).

7.3.2.4 Tb.N

Trabecular number decreased with age, with average values ranging from $0.00115\mu m^{-1}$ to $0.00419\mu m^{-1}$. The fetal and perinatal age cohorts were found to differ to individuals above the age of 4 weeks, though did not differ from each other. The 4 weeks to 2 years of age and 3 to 8 years of age cohorts were also not significantly different (Figure 7.21).

7.3.2.5 Tb.Sp

At L3, trabecular thickness increased with age, with values ranging from 163.44µm to 546.34µm. The fetal and perinatal age cohorts did not differ from

each other but were found to display significantly lower trabecular separation. The 4 weeks to 2 years and 3 to 8 years of age cohorts did not differ significantly from each other but did differ from the two youngest cohorts (Figure 7.21).

7.3.2.6 DA

As at the level of the first lumbar vertebra, no significant differences were found between age cohorts for degree of anisotropy. Values ranged from 0.298 to 0.393 and decreased slightly with age. All values indicated more isotropic structures (Figure 7.21).

Table 7.26: Statistical protocol and descriptive statistics for each histomorphometric parameter between age cohorts at the level of L3.

	Statistical Protocol						Age Cohort			
Parameter	Parametric?	H/F Value	DF	P Value	p≤0.01?	Mean/ Median	Fetal	Perinatal	4wks-2y	3-8y
BV/TV (%)	NP	82.867	3	<0.001	Y	Median	25.89	23.83	13.11	11.70
SMI	NP	12.235	3	0.007	N	Median	1.472	1.486	1.643	1.706
Tb.Th (μm)	NP	65.703	3	<0.001	Y	Median	64.06	89.44	98.44	103.97
Tb.N (μm^{-1})	NP	92.038	3	<0.001	Y	Median	0.00419	0.00267	0.00135	0.00115
Tb.Sp (μm)	NP	85.790	3	<0.001	Y	Median	163.44	268.05	495.37	546.34
DA	NP	3.883	3	0.274	N	Median	0.393	0.376	0.355	0.298

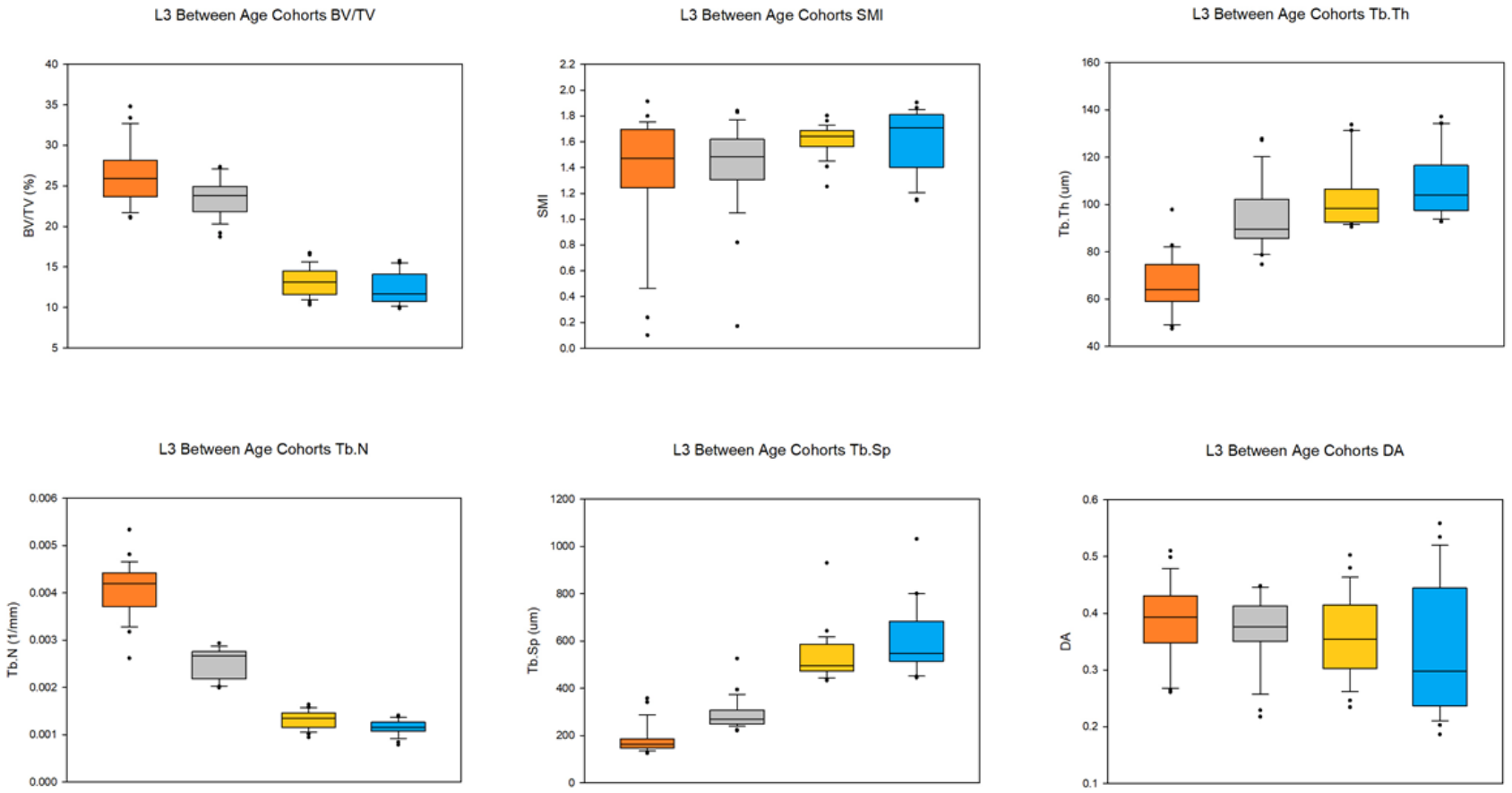

Figure 7.21: Box plots displaying the spread of data for the fetal (orange), perinatal (grey), 4wks -2y (yellow) and 3-8y (blue) age cohorts per histomorphometric parameter, at the level of the 3rd lumbar vertebra.

7.3.3 *L5*

The descriptive statistics for the six histomorphometric parameters, at the level of L5, can be viewed in Table 7.27.

7.3.3.1 BV/TV

Values for bone volume fraction at the vertebral level L5 ranged from 16.52% to 36.03%. The fetal and perinatal age cohorts were found to display significantly higher BV/TV values compared to the 4 weeks to 2 years and 3 to 8 years cohorts. No differences were found between the fetal and perinatal cohorts, or the 4 weeks to 2 years and 3 to 8 years cohorts (Figure 7.22).

7.3.3.2 SMI

For structural model index, the fetal and perinatal age cohorts displayed statistically similar median values for SMI which were found to be significantly lower compared to the two older age cohorts. No differences were found between the 4 weeks to 2 years, and 3 to 8 years of age individuals. Average values for SMI ranged from 0.858 to 1.421 with all values indicating a trabecular architecture of rod-like and plate-like trabeculae (Figure 7.22).

7.3.3.3 Tb.Th

The average values for trabecular thickness at L5 ranged between 75.03µm to 131.77µm. While the fetal age cohort displayed the lowest median values for trabecular thickness, and the 3-8 years of age cohort displayed the highest, a consistent increase between age cohorts was not observed. Both the fetal and 4 weeks to 2 years age cohorts displayed significantly lower Tb.Th values compared to the 3-8y cohort. The perinatal age cohort and the 4 weeks to 2 years of age cohort also displayed significantly higher values compared to the fetal cohort (Figure 7.22).

7.3.3.4 Tb.N

Trabecular number was observed to decrease with age at the level of L5, from an average value of 0.00447µm^{-1} within the fetal age cohort, to 0.0141µm^{-1} within the 3-8 years of age cohort. As with a number of other parameters, the fetal and perinatal cohorts were statistically similar, as were the 4 weeks to 2 years of age and 3 to 8 years of age cohorts. However, the fetal/perinatal and 4 weeks of age + individuals differed significantly from each other (Figure 7.22).

7.3.3.5 Tb.Sp

Trabecular separation increased with age, although this increase was not significant between the fetal and perinatal periods, and the 4 weeks to 2 years and 3 to 8 years of age cohorts. Average values ranged from 156.80µm to 506.60µm (Figure 7.22).

7.3.3.6 DA

Unlike the first and third lumbar vertebral centra, L5 displayed significant differences between individuals for degree of anisotropy. The perinatal age cohort displayed the highest median value for DA and was found to be significantly different from all other cohorts. No other significant differences were present. Median values for DA ranged between 0.333 to 0.468 and indicated that volumes were more isotropic in nature (Figure 7.22).

Table 7.27: Statistical protocol and descriptive statistics for each histomorphometric parameter between age cohorts at the level of L5.

	Statistical Protocol						Age Cohort			
Parameter	Parametric?	H/F Value	DF	P Value	p≤0.01?	Mean/ Median	Fetal	Perinatal	4wks-2y	3-8y
BV/TV (%)	NP	82.586	3	<0.001	Y	Median	34.35	36.03	16.52	18.64
SMI	NP	65.649	3	<0.001	Y	Median	1.121	0.858	1.421	1.405
Tb.Th (μm)	NP	68.428	3	<0.001	Y	Median	75.03	123.15	109.30	131.77
Tb.N (μm^{-1})	NP	89.695	3	<0.001	Y	Median	0.00447	0.00297	0.00155	0.00141
Tb.Sp (μm)	NP	86.046	3	<0.001	Y	Median	156.80	207.42	503.31	506.56
DA	P	18.288	3	<0.001	Y	Mean	0.372	0.468	0.333	0.336

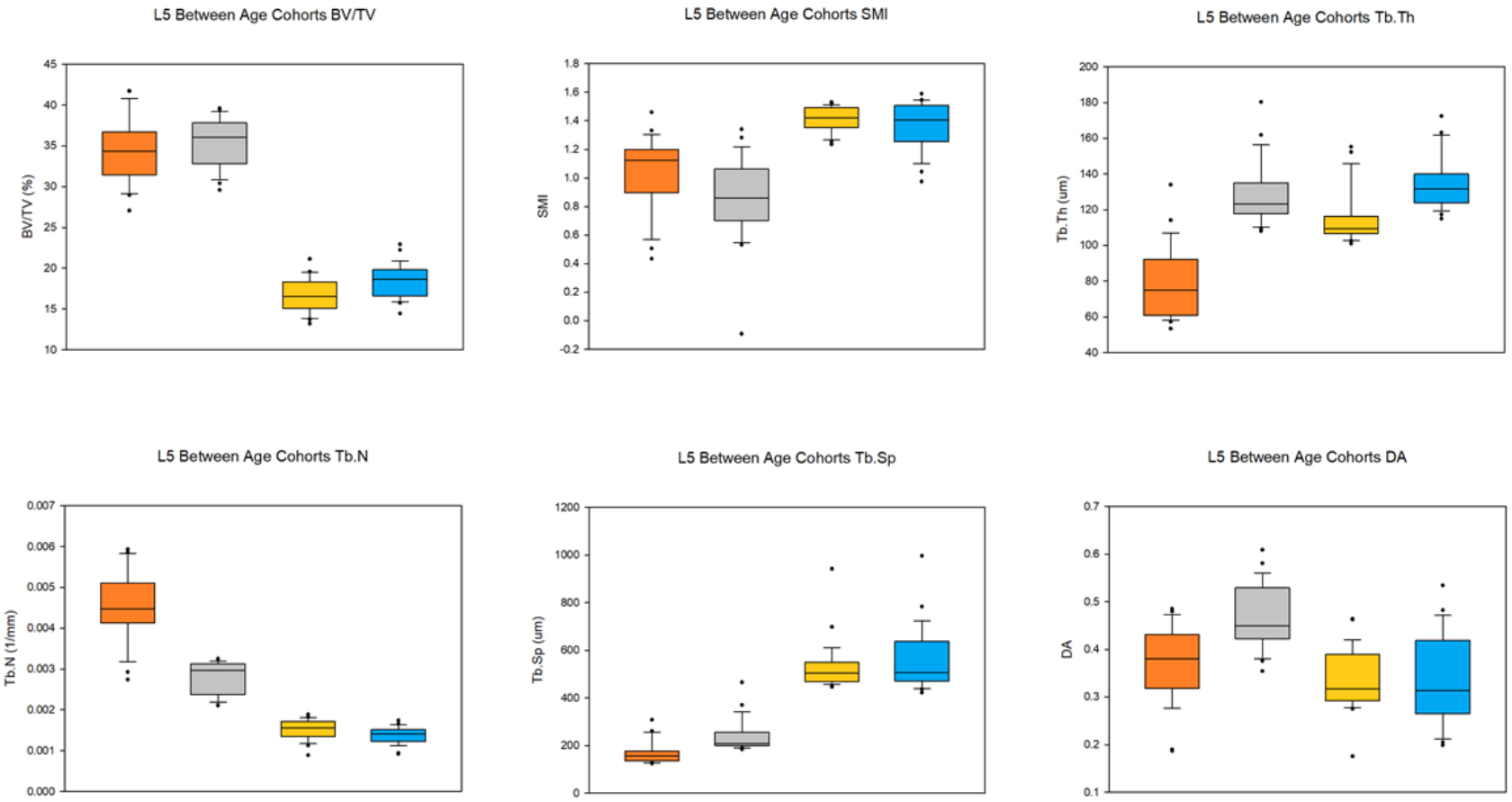

Figure 7.22: Box plots displaying the spread of data for the fetal (orange), perinatal (grey), 4wks -2y (yellow) and 3-8y (blue) age cohorts per histomorphometric parameter, at the level of the 5th lumbar vertebra.

8 Analysis of Quantitative Data: Analysis 2

8.1 Introduction

The second analysis of the quantitative data aimed to quantify any differences in the histomorphometric parameters between the three lumbar vertebral levels studied: L1, L3 and L5. For this analysis, each age cohort and parameter were considered per volume of interest (VOI). Once again, due to the sample sizes of some age cohorts and the resulting power of some datasets, differences between individuals were deemed significant at the level of $p \leq 0.01$. All raw data and results of these statistical analyses can be found in Appendix 8. Figure 8.1 displays the location of VOIs within the lumbar vertebral centrum.

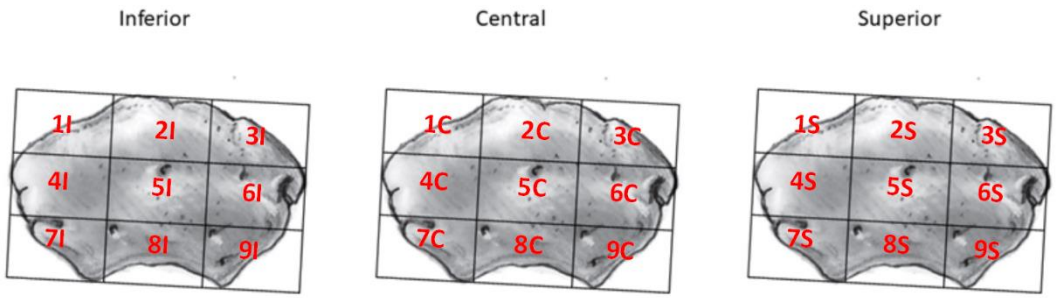

Figure 8.1: Visual representation of the 27 VOIs within the lumbar centrum, separated into inferior, central and superior layers. I=Inferior, C=Central and S=Superior.

8.2 Results

8.2.1 *Fetal Age Cohort*

8.2.1.1 BV/TV

For bone volume fraction, no significant differences were found between the three vertebral levels for each VOI. Descriptive statistics can be found in Table 8.1.

Table 8.1: Descriptive statistics for BV/TV (%) in the fetal age cohort. P/NP indicates whether the data is parametric (P) or non-parametric (NP).

VOI	P/NP	F/H	P Value	P≤0.01	Mean/ Median	L1	L3	L5
1I	P	7.501	0.044	N	Mean	32.48	27.40	36.16
1C	NP	4.714	0.048	N	Median	32.14	22.21	30.29
1S	NP	5.357	0.029	N	Median	33.43	22.59	33.01
2I	NP	4.500	0.067	N	Median	30.34	24.25	31.42
2C	P	2.967	0.162	N	Mean	28.58	21.20	28.98
2S	P	10.905	0.024	N	Mean	33.20	24.62	32.00
3I	P	21.172	0.007	N	Mean	33.06	21.06	32.43
3C	P	8.762	0.035	N	Mean	32.05	21.81	29.62
3S	NP	4.714	0.048	N	Median	33.87	22.48	30.70
4I	P	12.554	0.019	N	Mean	37.99	28.23	36.63
4C	P	4.440	0.096	N	Mean	34.80	27.25	34.11
4S	P	20.483	0.008	N	Mean	35.65	25.57	37.00
5I	P	5.729	0.067	N	Mean	42.17	34.81	41.70
5C	NP	4.714	0.048	N	Median	34.24	30.54	36.59
5S	P	18.989	0.009	N	Mean	43.74	33.40	40.57
6I	P	16.879	0.011	N	Mean	36.79	26.21	37.80
6C	P	7.665	0.043	N	Mean	36.85	25.89	34.35
6S	NP	4.714	0.048	N	Median	36.23	24.76	35.28
7I	NP	1.607	0.524	N	Median	35.36	29.09	31.50
7C	P	10.241	0.027	N	Mean	34.34	23.77	32.53
7S	NP	5.357	0.029	N	Median	34.47	26.63	35.40
8I	P	1.835	0.272	N	Mean	31.91	32.51	41.75
8C	NP	5.357	0.029	N	Median	33.20	27.30	36.71
8S	NP	1.607	0.524	N	Median	34.67	28.77	39.45
9I	P	5.995	0.063	N	Mean	36.33	24.00	34.88
9C	P	15.274	0.013	N	Mean	33.17	25.97	27.07
9S	P	10.928	0.024	N	Mean	34.88	23.70	29.16

8.2.1.2 SMI

Once again, no differences were found between L1, L3 and L5 at the level of p≤0.01 for structural model index. All vales indicated a mix of rod-like and plate-like trabeculae. Descriptive statistics can be viewed in Table 8.2.

Table 8.2: Descriptive statistics for SMI in the fetal age cohort. 0= Plates, 3= Rods and 4=Spheres.

VOI	P/NP	F/H	P Value	P≤0.01	Mean/ Median	L1	L3	L5
1I	NP	5.357	0.029	N	Median	1.236	1.641	0.833
1C	P	5.110	0.079	N	Mean	1.065	1.694	1.207
1S	NP	4.500	0.067	N	Median	1.098	1.734	1.122
2I	P	20.300	0.008	N	Mean	1.201	1.705	1.066
2C	P	0.0317	0.969	N	Mean	1.231	1.246	1.173
2S	P	0.557	0.612	N	Mean	1.208	1.472	1.207
3I	NP	4.500	0.067	N	Median	1.056	1.938	1.112
3C	P	9.179	0.032	N	Mean	1.033	1.697	1.159
3S	P	11.479	0.022	N	Mean	0.886	1.704	1.265
4I	P	0.864	0.488	N	Mean	0.960	1.464	1.104
4C	P	0.622	0.582	N	Mean	1.002	1.259	1.045
4S	NP	4.500	0.067	N	Median	1.050	1.406	0.993
5I	P	0.0834	0.922	N	Mean	0.399	0.603	0.582
5C	P	0.302	0.755	N	Mean	0.160	0.239	0.434
5S	P	0.436	0.674	N	Mean	0.354	0.520	0.780
6I	NP	4.500	0.067	N	Median	1.008	1.494	0.996
6C	NP	3.929	0.181	N	Median	0.852	1.390	1.127
6S	P	4.738	0.088	N	Mean	0.939	1.571	1.121
7I	NP	2.429	0.381	N	Median	1.091	1.461	1.460
7C	NP	4.500	0.067	N	Median	1.123	1.709	1.148
7S	NP	1.357	0.619	N	Median	1.126	1.478	1.332
8I	NP	0.607	0.800	N	Median	1.172	0.822	0.896
8C	NP	2.750	0.324	N	Median	-0.079	0.083	0.506
8S	P	0.303	0.754	N	Mean	0.649	0.932	0.719
9I	P	11.055	0.023	N	Mean	0.894	1.800	1.153
9C	NP	3.179	0.267	N	Median	1.105	1.495	1.200
9S	NP	5.357	0.029	N	Median	1.183	1.677	1.298

8.2.1.3 Tb.Th

No differences were found between the three vertebral levels studied for trabecular thickness. Descriptive statistics can be seen in Table 8.3.

Table 8.3: Descriptive statistics for Tb.Th (µm) in the fetal age cohort.

VOI	P/NP	F/H	P Value	P≤0.01	Mean/ Median	L1	L3	L5
1I	P	1.871	0.267	N	Mean	71.41	53.69	60.93
1C	NP	4.714	0.048	N	Median	78.61	63.52	74.08
1S	P	2.714	0.180	N	Mean	61.88	49.18	58.22
2I	P	1.634	0.303	N	Mean	81.84	62.71	74.42
2C	P	3.409	0.137	N	Mean	110.06	81.99	100.17
2S	NP	1.607	0.524	N	Median	76.12	66.30	72.66
3I	P	0.836	0.497	N	Mean	52.93	48.56	57.26
3C	P	0.377	0.708	N	Mean	72.21	64.06	69.01
3S	P	1.742	0.286	N	Mean	53.76	47.47	60.15
4I	P	1.661	0.298	N	Mean	88.35	68.91	82.67
4C	P	1.646	0.301	N	Mean	94.91	76.22	92.07
4S	P	1.304	0.366	N	Mean	83.36	64.58	76.43
5I	P	2.704	0.181	N	Mean	112.30	82.74	101.27
5C	P	2.554	0.193	N	Mean	124.47	97.88	134.04
5S	NP	3.179	0.267	N	Median	106.67	78.00	104.96
6I	NP	2.857	0.286	N	Median	89.16	66.52	76.24
6C	P	2.875	0.168	N	Mean	95.76	71.89	90.36
6S	P	2.172	0.230	N	Mean	81.88	61.67	80.78
7I	P	0.764	0.524	N	Mean	72.76	62.25	62.52
7C	NP	4.714	0.048	N	Median	78.97	61.99	75.03
7S	P	0.802	0.509	N	Mean	69.87	59.05	70.66
8I	P	1.133	0.407	N	Mean	82.16	74.64	86.51
8C	P	2.724	0.179	N	Mean	103.02	81.52	114.18
8S	P	3.366	0.139	N	Mean	82.03	69.12	94.09
9I	NP	1.357	0.619	N	Median	64.20	56.98	59.61
9C	P	1.869	0.267	N	Mean	71.74	61.43	53.43
9S	P	0.758	0.526	N	Mean	70.92	56.97	58.88

8.2.1.4 Tb.N

No significant differences were found between L1, L3 and L5 in the fetal age cohort for trabecular number. Descriptive statistics can be found in Table 8.4.

Table 8.4: Descriptive statistics for Tb.N (μm^{-1}) in the fetal age cohort.

VOI	P/NP	F/H	P Value	P≤0.01	Mean/ Median	L1	L3	L5
1I	NP	1.929	0.467	N	Median	0.00455	0.00550	0.00594
1C	P	0.334	0.734	N	Mean	0.00416	0.00360	0.00413
1S	P	2.474	0.200	N	Mean	0.00545	0.00445	0.00570
2I	P	0.281	0.768	N	Mean	0.00371	0.00401	0.00435
2C	P	0.220	0.812	N	Mean	0.00260	0.00262	0.00292
2S	P	0.732	0.536	N	Mean	0.00443	0.00383	0.00442
3I	NP	3.179	0.267	N	Median	0.00626	0.00446	0.00583
3C	P	2.591	0.324	N	Median	0.00443	0.00342	0.00447
3S	P	4.453	0.096	N	Mean	0.00629	0.00481	0.00519
4I	P	0.0392	0.962	N	Mean	0.00432	0.00426	0.00451
4C	P	0.00669	0.993	N	Mean	0.00377	0.00367	0.00371
4S	P	0.563	0.609	N	Mean	0.00435	0.00408	0.00485
5I	P	0.229	0.805	N	Mean	0.00376	0.00441	0.00415
5C	P	0.763	0.524	N	Mean	0.00277	0.00318	0.00274
5S	NP	0.607	0.800	N	Median	0.00415	0.00418	0.00388
6I	P	0.939	0.463	N	Mean	0.00417	0.00400	0.00508
6C	NP	0.500	0.857	N	Median	0.00389	0.00424	0.00386
6S	P	0.181	0.841	N	Mean	0.00451	0.00405	0.00439
7I	P	0.0949	0.911	N	Mean	0.00491	0.00462	0.00496
7C	NP	2.000	0.438	N	Median	0.00437	0.00394	0.00435
7S	P	0.175	0.846	N	Mean	0.00499	0.00456	0.00511
8I	P	0.395	0.697	N	Mean	0.00392	0.00442	0.00485
8C	P	0.0202	0.980	N	Mean	0.00326	0.00331	0.00325
8S	P	0.00102	0.999	N	Mean	0.00426	0.00431	0.00431
9I	NP	4.500	0.067	N	Median	0.00574	0.00409	0.00586
9C	P	0.909	0.473	N	Mean	0.00473	0.00425	0.00514
9S	P	0.808	0.507	N	Mean	0.00505	0.00422	0.00503

8.2.1.5 Tb.Sp

For trabecular separation, no VOIs presented significant differences between vertebral levels. Descriptive statistics can be found in Table 8.5.

Table 8.5: Descriptive statistics for Tb.Sp (µm) in the fetal age cohort.

VOI	P/NP	F/H	P Value	P≤0.01	Mean/ Median	L1	L3	L5
1I	NP	1.464	0.562	N	Median	153.34	121.69	126.37
1C	NP	0.607	0.800	N	Median	177.62	188.16	170.77
1S	P	0.409	0.689	N	Mean	132.37	147.78	124.23
2I	P	0.428	0.679	N	Mean	196.27	165.96	171.23
2C	P	0.477	0.652	N	Mean	302.94	341.29	253.92
2S	P	0.174	0.846	N	Mean	161.84	176.11	159.90
3I	NP	0.500	0.857	N	Median	116.47	134.82	130.19
3C	P	0.383	0.704	N	Mean	162.70	193.86	164.55
3S	P	0.501	0.639	N	Mean	122.44	125.20	143.13
4I	P	0.0118	0.988	N	Mean	157.70	154.84	153.14
4C	P	0.00513	0.995	N	Mean	184.76	180.50	183.29
4S	P	0.140	0.874	N	Mean	156.24	161.78	147.19
5I	P	0.129	0.883	N	Mean	186.08	173.12	175.88
5C	P	0.597	0.593	N	Mean	318.32	273.74	307.84
5S	P	0.344	0.728	N	Mean	164.58	184.86	179.86
6I	P	0.590	0.596	N	Mean	166.65	157.48	135.91
6C	NP	0.500	0.857	N	Median	173.92	160.76	172.92
6S	P	0.0534	0.949	N	Mean	150.77	159.64	152.31
7I	P	0.0130	0.987	N	Mean	142.11	140.75	137.77
7C	P	0.128	0.884	N	Mean	153.34	168.14	168.08
7S	P	0.105	0.902	N	Mean	132.96	147.45	134.94
8I	NP	1.464	0.562	N	Median	216.30	172.25	136.37
8C	P	1.116	0.412	N	Mean	342.41	357.52	260.94
8S	P	0.00242	0.998	N	Mean	188.74	190.94	186.03
9I	NP	0.714	0.743	N	Median	136.11	137.67	127.70
9C	P	0.0341	0.967	N	Mean	148.14	149.46	156.80
9S	P	0.354	0.722	N	Mean	133.31	152.88	153.00

8.2.1.6 DA

As with the other histomorphometric parameters studies, no significant differences were found between the three vertebral levels studied for degree of anisotropy. Descriptive statistics can be found in Table 8.6.

Table 8.6: Descriptive statistics for DA in the fetal age cohort.

VOI	P/NP	F/H	P Value	P≤0.01	Mean/ Median	L1	L3	L5
1I	P	0.310	0.749	N	Mean	0.357	0.297	0.335
1C	NP	2.000	0.438	N	Median	0.368	0.283	0.397
1S	NP	0.000	1.000	N	Median	0.372	0.388	0.394
2I	P	1.915	0.261	N	Mean	0.254	0.351	0.379
2C	P	4.574	0.093	N	Mean	0.326	0.261	0.318
2S	P	0.251	0.789	N	Mean	0.310	0.365	0.298
3I	P	3.394	0.137	N	Mean	0.434	0.348	0.381
3C	P	0.759	0.525	N	Mean	0.432	0.375	0.472
3S	NP	0.179	0.971	N	Median	0.393	0.410	0.396
4I	NP	0.500	0.857	N	Median	0.379	0.416	0.365
4C	NP	3.750	0.219	N	Median	0.584	0.479	0.480
4S	P	3.881	0.116	N	Mean	0.489	0.428	0.431
5I	P	0.832	0.499	N	Mean	0.266	0.391	0.315
5C	NP	4.464	0.105	N	Median	0.337	0.270	0.187
5S	NP	3.929	0.181	N	Median	0.398	0.382	0.190
6I	P	4.887	0.084	N	Mean	0.394	0.435	0.358
6C	P	0.460	0.661	N	Mean	0.515	0.499	0.452
6S	P	0.840	0.496	N	Mean	0.446	0.344	0.408
7I	NP	3.750	0.219	N	Median	0.460	0.445	0.368
7C	P	2.385	0.208	N	Mean	0.531	0.510	0.392
7S	P	2.279	0.218	N	Mean	0.517	0.465	0.466
8I	P	0.470	0.656	N	Mean	0.364	0.410	0.341
8C	P	0.0240	0.976	N	Mean	0.308	0.324	0.304
8S	P	10.913	0.024	N	Mean	0.459	0.393	0.313
9I	NP	0.000	1.000	N	Median	0.409	0.407	0.447
9C	P	1.176	0.397	N	Mean	0.454	0.397	0.380
9S	P	4.499	0.095	N	Mean	0.450	0.355	0.485

8.2.1.7 Summary of results

No significant differences were found between vertebral levels for any of the histomorphometric parameters studied within the fetal age cohort.

8.2.2 *Perinatal Age Cohort*

8.2.2.1 BV/TV

Values for bone volume fraction within the perinatal age cohort displayed significant differences between vertebral levels for some VOIs. Vertebral level L5 differed significantly from vertebral level L3 at VOIs 1I, 1S, 2I, 3S, 4I, 4S, 6S, 7I, 7C, 7S, 8S, 9C and 9S. In all cases, the values for BV/TV at L5 were significantly higher than that at L3. L5 was also found to differ significantly to L1 at the VOIs 3S, 4S, 6S, 7S, 8S and 9S. Once again, L5 presented significantly higher BV/TV values. No significant differences were found between vertebral levels L1 and L3. Descriptive statistics can be viewed in Table 8.7. Figure 8.2 depicts the significant differences found within the perinatal age cohort.

Table 8.7: Descriptive statistics for BV/TV (%) in the perinatal age cohort.

VOI	P/NP	F/H	P Value	P≤0.01	Mean/ Median	L1	L3	L5
1I	P	7.265	0.002	Y	Mean	26.61	21.45	34.80
1C	P	4.249	0.022	N	Mean	25.21	20.99	31.70
1S	P	8.498	<0.001	Y	Mean	24.54	20.54	34.80
2I	P	7.605	0.002	Y	Mean	27.11	23.35	36.98
2C	P	2.961	0.065	N	Mean	24.33	24.37	32.79
2S	P	4.660	0.016	N	Mean	26.10	23.59	34.49
3I	P	5.247	0.010	N	Mean	24.91	22.94	34.32
3C	P	2.970	0.064	N	Mean	23.74	22.35	31.30
3S	P	6.832	0.003	Y	Mean	23.41	23.62	34.14
4I	P	6.107	0.005	Y	Mean	29.39	24.90	37.01
4C	P	4.492	0.018	N	Mean	24.75	21.01	30.99
4S	P	10.526	<0.001	Y	Mean	25.38	23.83	37.80
5I	P	3.936	0.029	N	Mean	32.02	27.24	39.62
5C	P	1.448	0.249	N	Mean	30.59	27.36	35.56
5S	P	4.997	0.012	N	Mean	28.42	27.06	39.18
6I	P	4.165	0.024	N	Mean	28.64	25.17	36.03
6C	P	3.914	0.029	N	Mean	24.16	21.81	31.69
6S	P	9.474	<0.001	Y	Mean	25.54	24.46	37.42
7I	P	5.434	0.009	Y	Mean	31.27	24.71	38.03
7C	P	5.084	0.012	Y	Mean	22.24	18.70	29.60
7S	P	8.174	0.001	Y	Mean	25.67	23.59	38.48
8I	P	3.831	0.031	N	Mean	30.23	25.92	37.44
8C	P	2.865	0.070	N	Mean	30.92	27.02	36.51
8S	P	8.407	0.001	Y	Mean	27.10	24.78	39.50
9I	P	4.783	0.015	N	Mean	29.92	24.95	37.19
9C	P	5.436	0.009	Y	Mean	22.10	19.19	30.41
9S	P	8.617	<0.001	Y	Mean	25.25	24.39	38.71

8.2.2.2 SMI

For structural model index, differences were found between L5 and the two other vertebral levels studied for some VOIs. L5 displayed significantly lower SMI values compared to L1 at VOIs 3S, 4S, 6S and 7S. When compared to L3, L5 differed at VOIs 1I, 1S, 2I, 3S, 4I, 4S, 6S, 7I and 7S. All values over each vertebral level generally indicated a transition between plate-like and rod-like trabecular morphology. No significant differences were found between vertebral levels L1 and L3. Descriptive statistics for this dataset can be viewed in Table 8.8 and a visualisation of the significant differences can be viewed in Figure 8.2.

Table 8.8: Descriptive statistics for SMI in the perinatal age cohort.

VOI	P/NP	F/H	P Value	P≤0.01	Mean/ Median	L1	L3	L5
1I	P	5.210	0.010	Y	Mean	1.502	1.705	1.036
1C	NP	5.388	0.068	N	Median	1.366	1.620	1.265
1S	P	11.862	0.003	Y	Mean	1.636	1.831	1.342
2I	P	5.961	0.006	Y	Mean	1.312	1.449	0.732
2C	P	2.003	0.150	N	Mean	1.125	1.106	0.594
2S	NP	5.642	0.060	N	Median	1.361	1.572	1.033
3I	P	3.867	0.030	N	Mean	1.540	1.639	1.109
3C	NP	2.868	0.238	N	Median	1.592	1.647	1.278
3S	P	6.524	0.004	Y	Mean	1.614	1.614	1.044
4I	P	5.053	0.012	Y	Mean	1.166	1.395	0.778
4C	NP	5.480	0.065	N	Median	1.591	1.758	1.357
4S	P	8.458	0.001	Y	Mean	1.404	1.425	0.743
5I	P	2.772	0.076	N	Mean	0.990	1.170	0.551
5C	P	0.449	0.642	N	Mean	0.727	0.820	0.532
5S	P	3.233	0.051	N	Mean	1.176	1.209	0.635
6I	P	2.841	0.072	N	Mean	1.208	1.337	0.858
6C	NP	6.502	0.039	N	Median	1.457	1.686	1.328
6S	P	9.388	<0.001	Y	Mean	1.365	1.394	0.722
7I	P	5.253	0.010	Y	Mean	1.227	1.539	0.819
7C	P	3.720	0.034	N	Mean	1.687	1.841	1.282
7S	P	6.648	0.004	Y	Mean	1.459	1.552	0.801
8I	P	3.188	0.053	N	Mean	1.107	1.305	0.622
8C	P	0.226	0.799	N	Mean	0.0561	0.172	-0.0915
8S	P	3.123	0.057	N	Mean	1.225	1.293	0.703
9I	P	4.055	0.026	N	Mean	1.304	1.486	0.868
9C	P	2.297	0.317	N	Mean	1.633	1.841	1.483
9S	NP	9.213	0.010	N	Median	1.663	1.460	1.094

8.2.2.3 Tb.Th

As with previous parameters, significant differences between L5 and the two other vertebral levels studied were found within the perinatal cohort for trabecular thickness. L5 exhibited significantly higher trabecular thickness compared to L3 at all VOIs, and compared to L1 at all VOIs excluding 3C, 4C, 5C, 6C, 7I, 8I and 8C. No significant differences were found between vertebral levels L1 and L3. Descriptive statistics can be viewed in Table 8.9 and significant differences can be viewed in Figure 8.2.

Table 8.9: Descriptive statistics for Tb.Th (µm) in the perinatal age cohort.

VOI	P/NP	F/H	P Value	P≤0.01	Mean/ Median	L1	L3	L5
1I	NP	22.619	<0.001	Y	Median	92.19	80.65	111.24
1C	P	12.960	<0.001	Y	Mean	114.35	91.54	128.58
1S	P	34.630	<0.001	Y	Mean	82.51	74.67	110.48
2I	P	17.923	<0.001	Y	Mean	94.96	86.81	118.39
2C	P	6.853	0.003	Y	Mean	130.60	118.43	154.85
2S	P	14.300	<0.001	Y	Mean	90.89	85.91	115.47
3I	P	20.149	<0.001	Y	Mean	84.42	81.13	108.01
3C	P	7.725	0.002	Y	Mean	106.70	99.74	128.90
3S	P	23.662	<0.001	Y	Mean	78.72	78.92	110.71
4I	P	23.240	<0.001	Y	Mean	100.00	89.99	116.33
4C	NP	16.513	<0.001	Y	Median	114.49	103.17	131.32
4S	P	45.855	<0.001	Y	Mean	90.74	87.81	121.21
5I	P	10.269	<0.001	Y	Mean	115.62	102.29	142.33
5C	NP	10.880	0.004	Y	Median	129.42	122.13	148.83
5S	NP	14.664	<0.001	Y	Median	106.81	103.49	136.30
6I	P	20.185	<0.001	Y	Mean	96.34	89.44	118.77
6C	NP	13.419	0.001	Y	Median	110.37	103.52	134.95
6S	NP	17.814	<0.001	Y	Median	90.57	87.11	123.43
7I	NP	19.634	<0.001	Y	Median	98.60	85.28	110.90
7C	NP	17.327	<0.001	Y	Median	98.74	90.86	122.24
7S	P	27.490	<0.001	Y	Mean	85.45	81.20	117.96
8I	NP	16.471	<0.001	Y	Median	105.42	93.86	124.90
8C	NP	12.663	0.002	Y	Median	129.72	115.05	169.60
8S	NP	20.898	<0.001	Y	Median	93.38	93.05	131.04
9I	P	19.237	<0.001	Y	Mean	94.01	85.78	116.42
9C	NP	16.903	<0.001	Y	Median	95.77	89.96	127.08
9S	NP	18.742	<0.001	Y	Median	83.89	84.57	119.10

8.2.2.4 Tb.N

The number of trabeculae within each VOI did not differ significantly between any of the vertebral levels studied within the perinatal age cohort. The descriptive statistics for this dataset can be found in Table 8.10.

Table 8.10: Descriptive statistics for Tb.N (μm^{-1}) in the perinatal age cohort.

VOI	P/NP	F/H	P Value	P≤0.01	Mean/ Median	L1	L3	L5
1I	P	1.101	0.344	N	Mean	0.00297	0.00268	0.00318
1C	P	0.522	0.598	N	Mean	0.00218	0.00226	0.00245
1S	P	0.863	0.431	N	Mean	0.00294	0.00270	0.00313
2I	P	1.207	0.311	N	Mean	0.00281	0.00265	0.00312
2C	P	0.480	0.623	N	Mean	0.00186	0.00204	0.00210
2S	P	0.491	0.616	N	Mean	0.00280	0.00268	0.00297
3I	P	0.511	0.604	N	Mean	0.00293	0.00279	0.00316
3C	P	0.490	0.617	N	Mean	0.00218	0.00218	0.00241
3S	P	0.106	0.900	N	Mean	0.00295	0.00293	0.00305
4I	P	0.570	0.571	N	Mean	0.00293	0.00272	0.00301
4C	P	0.595	0.557	N	Mean	0.00216	0.00202	0.00229
4S	NP	1.668	0.434	N	Median	0.00284	0.00277	0.00292
5I	P	0.271	0.765	N	Mean	0.00268	0.00259	0.00278
5C	P	0.0882	0.916	N	Mean	0.00211	0.00211	0.00221
5S	P	0.885	0.422	N	Mean	0.00249	0.00256	0.00283
6I	P	0.346	0.710	N	Mean	0.00291	0.00276	0.00302
6C	P	1.119	0.338	N	Mean	0.00215	0.00199	0.00237
6S	P	1.319	0.280	N	Mean	0.00276	0.00269	0.00309
7I	P	0.379	0.687	N	Mean	0.00313	0.00293	0.00316
7C	P	0.496	0.613	N	Mean	0.00223	0.00208	0.00234
7S	P	0.702	0.503	N	Mean	0.00294	0.00284	0.00324
8I	P	0.140	0.870	N	Mean	0.00280	0.00271	0.00287
8C	P	0.115	0.892	N	Mean	0.00226	0.00220	0.00212
8S	P	0.557	0.578	N	Mean	0.00277	0.00259	0.00295
9I	P	0.629	0.539	N	Mean	0.00316	0.00285	0.00315
9C	P	0.762	0.474	N	Mean	0.00226	0.00203	0.00233
9S	P	1.077	0.352	N	Mean	0.00290	0.00281	0.00325

8.2.2.5 Tb.Sp

As with Tb.N, no differences were found between vertebral levels for trabecular separation within the perinatal age cohort. The descriptive statistics for Tb.Sp within the perinatal cohort can be viewed in Table 8.11.

Table 8.11: Descriptive statistics for Tb.Sp (µm) in the perinatal age cohort.

VOI	P/NP	F/H	P Value	P≤0.01	Mean/ Median	L1	L3	L5
1I	NP	6.576	0.037	N	Median	211.82	223.12	189.58
1C	NP	4.747	0.093	N	Median	301.06	273.98	269.46
1S	NP	3.302	0.192	N	Median	199.28	222.02	194.10
2I	NP	5.830	0.054	N	Median	214.15	231.99	191.98
2C	P	1.232	0.304	N	Mean	443.17	394.11	369.95
2S	NP	5.602	0.061	N	Median	235.89	234.11	203.07
3I	NP	2.592	0.274	N	Median	202.42	205.35	189.20
3C	NP	3.226	0.199	N	Median	284.16	289.88	254.06
3S	NP	2.301	0.317	N	Median	209.97	216.96	194.52
4I	NP	3.807	0.149	N	Median	232.89	233.91	209.82
4C	NP	4.441	0.109	N	Median	288.03	292.91	255.28
4S	NP	4.441	0.109	N	Median	218.39	228.03	192.96
5I	NP	1.396	0.498	N	Median	233.09	242.18	229.46
5C	P	0.536	0.590	N	Mean	362.86	368.11	333.80
5S	NP	5.152	0.076	N	Median	256.66	246.07	222.58
6I	NP	2.831	0.243	N	Median	208.80	232.18	215.88
6C	NP	5.909	0.052	N	Median	279.91	286.83	234.67
6S	NP	7.761	0.021	N	Median	234.75	242.10	196.03
7I	NP	1.429	0.489	N	Median	203.46	212.37	210.11
7C	NP	1.238	0.538	N	Median	265.99	260.68	247.96
7S	NP	2.651	0.266	N	Median	214.04	206.72	197.19
8I	NP	2.591	0.274	N	Median	228.85	260.33	217.24
8C	NP	0.572	0.751	N	Median	417.83	517.96	430.11
8S	NP	5.950	0.051	N	Median	234.97	282.34	209.88
9I	NP	1.799	0.407	N	Median	194.62	219.06	204.11
9C	NP	3.523	0.172	N	Median	253.79	281.05	241.66
9S	NP	5.615	0.060	N	Median	217.81	206.49	180.88

8.2.2.6 DA

For degree of anisotropy, the vertebral level L5 displayed significantly higher values compared to L1 and L3 at several VOIs. When compared to L1, L5 displayed significantly higher DA at VOIs 1S, 2C and 2S. When compared to L3, L5 differed at VOIs 1I, 1C, 2C, 2S and 8S. No differences were found between vertebral levels L1 and L3. All values for DA at each vertebral level generally indicated a more isotropic structure. Descriptive statistics can be viewed in Table 8.12. A summary of the significant differences found within the perinatal cohort can be viewed in Figure 8.2.

Table 8.12: Descriptive statistics for DA in the perinatal age cohort.

VOI	P/NP	F/H	P Value	P≤0.01	Mean/ Median	L1	L3	L5
1I	NP	11.794	0.003	Y	Median	0.427	0.363	0.505
1C	NP	9.174	0.010	Y	Median	0.370	0.303	0.468
1S	NP	10.473	0.005	Y	Median	0.375	0.384	0.500
2I	NP	8.490	0.014	N	Median	0.381	0.401	0.498
2C	P	8.093	0.001	Y	Mean	0.263	0.264	0.430
2S	P	15.927	<0.001	Y	Mean	0.346	0.334	0.534
3I	NP	1.726	0.422	N	Median	0.376	0.390	0.431
3C	P	0.466	0.632	N	Mean	0.372	0.342	0.382
3S	NP	3.481	0.175	N	Median	0.407	0.382	0.511
4I	P	0.432	0.652	N	Mean	0.407	0.413	0.441
4C	NP	0.259	0.879	N	Median	0.392	0.364	0.384
4S	P	0.962	0.392	N	Mean	0.408	0.446	0.423
5I	P	3.243	0.051	N	Mean	0.350	0.359	0.446
5C	NP	1.618	0.445	N	Median	0.216	0.239	0.263
5S	NP	3.208	0.201	N	Median	0.338	0.382	0.407
6I	P	1.696	0.198	N	Mean	0.400	0.447	0.419
6C	P	1.834	0.175	N	Mean	0.395	0.351	0.386
6S	P	1.150	0.328	N	Mean	0.416	0.405	0.446
7I	P	2.539	0.093	N	Mean	0.405	0.418	0.474
7C	P	1.226	0.306	N	Mean	0.394	0.425	0.445
7S	P	1.079	0.351	N	Mean	0.416	0.448	0.414
8I	NP	9.886	0.007	N	Median	0.380	0.377	0.548
8C	NP	5.282	0.071	N	Median	0.259	0.186	0.705
8S	NP	11.590	0.003	N	Median	0.386	0.351	0.571
9I	P	0.767	0.472	N	Mean	0.398	0.418	0.447
9C	P	2.573	0.091	N	Mean	0.424	0.396	0.477
9S	NP	3.560	0.169	N	Median	0.432	0.388	0.470

8.2.2.7 Summary of results

Overall, in the perinates, vertebral L5 was found to differ significantly to vertebral levels L1 and L3, displaying a significantly higher bone volume fraction, lower structural model index, higher trabecular thickness and higher degree of anisotropy. These differences occurred more commonly at superior and inferior VOIs. These significant differences can be visualised in Figure 8.2.

	L1 VS L3			L1 VS L5			L3 VS L5		
1I	BV/TV	SMI	Tb.Th	BV/TV	SMI	Tb.Th	BV/TV	SMI	Tb.Th
	Tb.N	Tb.Sp	DA	Tb.N	Tb.Sp	DA	Tb.N	Tb.Sp	DA
1C	BV/TV	SMI	Tb.Th	BV/TV	SMI	Tb.Th	BV/TV	SMI	Tb.Th
	Tb.N	Tb.Sp	DA	Tb.N	Tb.Sp	DA	Tb.N	Tb.Sp	DA
1S	BV/TV	SMI	Tb.Th	BV/TV	SMI	Tb.Th	BV/TV	SMI	Tb.Th
	Tb.N	Tb.Sp	DA	Tb.N	Tb.Sp	DA	Tb.N	Tb.Sp	DA
2I	BV/TV	SMI	Tb.Th	BV/TV	SMI	Tb.Th	BV/TV	SMI	Tb.Th
	Tb.N	Tb.Sp	DA	Tb.N	Tb.Sp	DA	Tb.N	Tb.Sp	DA
2C	BV/TV	SMI	Tb.Th	BV/TV	SMI	Tb.Th	BV/TV	SMI	Tb.Th
	Tb.N	Tb.Sp	DA	Tb.N	Tb.Sp	DA	Tb.N	Tb.Sp	DA
2S	BV/TV	SMI	Tb.Th	BV/TV	SMI	Tb.Th	BV/TV	SMI	Tb.Th
	Tb.N	Tb.Sp	DA	Tb.N	Tb.Sp	DA	Tb.N	Tb.Sp	DA
3I	BV/TV	SMI	Tb.Th	BV/TV	SMI	Tb.Th	BV/TV	SMI	Tb.Th
	Tb.N	Tb.Sp	DA	Tb.N	Tb.Sp	DA	Tb.N	Tb.Sp	DA
3C	BV/TV	SMI	Tb.Th	BV/TV	SMI	Tb.Th	BV/TV	SMI	Tb.Th
	Tb.N	Tb.Sp	DA	Tb.N	Tb.Sp	DA	Tb.N	Tb.Sp	DA
3S	BV/TV	SMI	Tb.Th	BV/TV	SMI	Tb.Th	BV/TV	SMI	Tb.Th
	Tb.N	Tb.Sp	DA	Tb.N	Tb.Sp	DA	Tb.N	Tb.Sp	DA
4I	BV/TV	SMI	Tb.Th	BV/TV	SMI	Tb.Th	BV/TV	SMI	Tb.Th
	Tb.N	Tb.Sp	DA	Tb.N	Tb.Sp	DA	Tb.N	Tb.Sp	DA
4C	BV/TV	SMI	Tb.Th	BV/TV	SMI	Tb.Th	BV/TV	SMI	Tb.Th
	Tb.N	Tb.Sp	DA	Tb.N	Tb.Sp	DA	Tb.N	Tb.Sp	DA
4S	BV/TV	SMI	Tb.Th	BV/TV	SMI	Tb.Th	BV/TV	SMI	Tb.Th
	Tb.N	Tb.Sp	DA	Tb.N	Tb.Sp	DA	Tb.N	Tb.Sp	DA
5I	BV/TV	SMI	Tb.Th	BV/TV	SMI	Tb.Th	BV/TV	SMI	Tb.Th
	Tb.N	Tb.Sp	DA	Tb.N	Tb.Sp	DA	Tb.N	Tb.Sp	DA
5C	BV/TV	SMI	Tb.Th	BV/TV	SMI	Tb.Th	BV/TV	SMI	Tb.Th
	Tb.N	Tb.Sp	DA	Tb.N	Tb.Sp	DA	Tb.N	Tb.Sp	DA
5S	BV/TV	SMI	Tb.Th	BV/TV	SMI	Tb.Th	BV/TV	SMI	Tb.Th
	Tb.N	Tb.Sp	DA	Tb.N	Tb.Sp	DA	Tb.N	Tb.Sp	DA
6I	BV/TV	SMI	Tb.Th	BV/TV	SMI	Tb.Th	BV/TV	SMI	Tb.Th
	Tb.N	Tb.Sp	DA	Tb.N	Tb.Sp	DA	Tb.N	Tb.Sp	DA
6C	BV/TV	SMI	Tb.Th	BV/TV	SMI	Tb.Th	BV/TV	SMI	Tb.Th
	Tb.N	Tb.Sp	DA	Tb.N	Tb.Sp	DA	Tb.N	Tb.Sp	DA
6S	BV/TV	SMI	Tb.Th	BV/TV	SMI	Tb.Th	BV/TV	SMI	Tb.Th
	Tb.N	Tb.Sp	DA	Tb.N	Tb.Sp	DA	Tb.N	Tb.Sp	DA
7I	BV/TV	SMI	Tb.Th	BV/TV	SMI	Tb.Th	BV/TV	SMI	Tb.Th
	Tb.N	Tb.Sp	DA	Tb.N	Tb.Sp	DA	Tb.N	Tb.Sp	DA
7C	BV/TV	SMI	Tb.Th	BV/TV	SMI	Tb.Th	BV/TV	SMI	Tb.Th
	Tb.N	Tb.Sp	DA	Tb.N	Tb.Sp	DA	Tb.N	Tb.Sp	DA
7S	BV/TV	SMI	Tb.Th	BV/TV	SMI	Tb.Th	BV/TV	SMI	Tb.Th
	Tb.N	Tb.Sp	DA	Tb.N	Tb.Sp	DA	Tb.N	Tb.Sp	DA
8I	BV/TV	SMI	Tb.Th	BV/TV	SMI	Tb.Th	BV/TV	SMI	Tb.Th
	Tb.N	Tb.Sp	DA	Tb.N	Tb.Sp	DA	Tb.N	Tb.Sp	DA
8C	BV/TV	SMI	Tb.Th	BV/TV	SMI	Tb.Th	BV/TV	SMI	Tb.Th
	Tb.N	Tb.Sp	DA	Tb.N	Tb.Sp	DA	Tb.N	Tb.Sp	DA
8S	BV/TV	SMI	Tb.Th	BV/TV	SMI	Tb.Th	BV/TV	SMI	Tb.Th
	Tb.N	Tb.Sp	DA	Tb.N	Tb.Sp	DA	Tb.N	Tb.Sp	DA
9I	BV/TV	SMI	Tb.Th	BV/TV	SMI	Tb.Th	BV/TV	SMI	Tb.Th
	Tb.N	Tb.Sp	DA	Tb.N	Tb.Sp	DA	Tb.N	Tb.Sp	DA
9C	BV/TV	SMI	Tb.Th	BV/TV	SMI	Tb.Th	BV/TV	SMI	Tb.Th
	Tb.N	Tb.Sp	DA	Tb.N	Tb.Sp	DA	Tb.N	Tb.Sp	DA
9S	BV/TV	SMI	Tb.Th	BV/TV	SMI	Tb.Th	BV/TV	SMI	Tb.Th
	Tb.N	Tb.Sp	DA	Tb.N	Tb.Sp	DA	Tb.N	Tb.Sp	DA

Figure 8.2: Data visualisation of the significant differences between vertebral levels L1, L3 and L5 for all parameters within the perinatal age cohort. A red square indicates a significant difference ($p \leq 0.01$) while a green square indicates no significant difference.

8.2.3 *4 weeks to 2 years of age cohort*

8.2.3.1 BV/TV

Values for bone volume fraction within the 4 weeks to 2 years of age cohort displayed significant differences between vertebral levels. L5 differed significantly from vertebral level L3 at VOIs 4C, 4S, 5C, 5S and 6C. In all cases, the values for BV/TV at L5 were significantly higher than those at L3. L5 was also found to differ significantly to L1 at VOI 4C. Once again, L5 presented significantly higher BV/TV values. L1 and L3 were also found to differ significantly from each other at VOI 4C, with the BV/TV value for L1 being significantly higher than that of L3. Descriptive statistics can be viewed in Table 8.13. Figure 8.3 depicts the significant differences found within the 4 weeks to 2 years of age cohort.

Table 8.13: Descriptive statistics for BV/TV (%) in the 4wks-2y age cohort.

VOI	P/NP	F/H	P Value	P≤0.01	Mean/ Median	L1	L3	L5
1I	P	1.177	0.326	N	Mean	18.53	15.05	18.02
1C	P	2.585	0.097	N	Mean	18.75	14.51	17.56
1S	NP	2.164	0.339	N	Median	14.35	13.32	17.90
2I	NP	1.936	0.380	N	Median	17.69	15.15	16.57
2C	NP	3.935	0.140	N	Median	15.51	12.95	15.87
2S	P	1.654	0.213	N	Mean	14.61	13.93	19.17
3I	P	0.691	0.511	N	Mean	19.32	16.72	19.58
3C	P	0.802	0.461	N	Mean	19.13	16.50	18.95
3S	NP	2.696	0.260	N	Median	15.47	12.94	20.59
4I	P	1.655	0.213	N	Mean	15.19	13.10	15.53
4C	P	15.638	<0.001	Y	Mean	12.17	10.65	14.27
4S	P	6.693	0.005	Y	Mean	12.10	11.48	15.64
5I	P	2.481	0.106	N	Mean	14.17	12.59	15.08
5C	P	5.530	0.011	Y	Mean	12.17	11.09	13.73
5S	P	7.108	0.004	Y	Mean	11.38	10.34	14.55
6I	P	1.732	0.199	N	Mean	15.58	13.35	15.90
6C	P	7.861	0.003	Y	Mean	12.92	10.99	13.82
6S	P	4.869	0.017	N	Mean	12.86	11.61	16.52
7I	P	1.008	0.381	N	Mean	17.46	15.41	19.20
7C	P	2.589	0.097	N	Mean	14.79	12.96	16.73
7S	P	2.689	0.089	N	Mean	14.30	12.55	16.51
8I	P	1.909	0.171	N	Mean	15.31	13.32	15.99
8C	P	0.615	0.549	N	Mean	13.32	12.01	13.20
8S	P	2.621	0.094	N	Mean	12.17	11.31	14.58
9I	NP	4.002	0.135	N	Median	17.29	13.66	16.07
9C	NP	4.867	0.088	N	Median	14.09	11.95	15.36
9S	P	2.510	0.103	N	Mean	14.65	12.71	16.76

8.2.3.2 SMI

For structural model index, only two significant differences were found within the 4 weeks to 2 years of age cohort. Vertebral level L5 was found to display a significantly lower SMI value compared to L3, at VOIs 5S and 6S. These differences can be visualised in Figure 8.3. Descriptive statistics for this dataset can be found in Table 8.14.

Table 8.14: Descriptive statistics for SMI in the 4wks-2y age cohort.

VOI	P/NP	F/H	P Value	P≤0.01	Mean/ Median	L1	L3	L5
1I	P	0.535	0.593	N	Mean	1.479	1.596	1.453
1C	P	0.626	0.544	N	Mean	1.327	1.469	1.384
1S	P	2.131	0.142	N	Mean	1.700	1.763	1.394
2I	NP	0.937	0.626	N	Median	1.420	1.554	1.377
2C	P	0.956	0.399	N	Mean	1.345	1.462	1.290
2S	P	2.693	0.089	N	Mean	1.660	1.655	1.271
3I	P	0.333	0.720	N	Mean	1.457	1.506	1.374
3C	P	0.713	0.501	N	Mean	1.252	1.408	1.339
3S	P	2.916	0.074	N	Mean	1.606	1.720	1.236
4I	P	1.683	0.208	N	Mean	1.560	1.648	1.456
4C	P	1.849	0.180	N	Mean	1.543	1.619	1.451
4S	P	3.289	0.055	N	Mean	1.715	1.719	1.493
5I	P	2.692	0.089	N	Mean	1.624	1.671	1.507
5C	P	4.509	0.022	N	Mean	1.644	1.656	1.493
5S	P	6.184	0.007	Y	Mean	1.780	1.803	1.531
6I	P	1.873	0.176	N	Mean	1.513	1.634	1.446
6C	P	3.013	0.069	N	Mean	1.533	1.623	1.431
6S	P	5.543	0.011	Y	Mean	1.656	1.708	1.393
7I	P	1.054	0.365	N	Mean	1.556	1.623	1.379
7C	P	1.841	0.181	N	Mean	1.480	1.563	1.351
7S	P	1.803	0.187	N	Mean	1.656	1.712	1.498
8I	P	2.858	0.078	N	Mean	1.589	1.646	1.421
8C	NP	0.209	0.901	N	Median	1.332	1.215	1.261
8S	P	1.476	0.249	N	Mean	1.690	1.678	1.501
9I	P	1.740	0.198	N	Mean	1.511	1.643	1.395
9C	P	1.544	0.235	N	Mean	1.455	1.569	1.437
9S	P	1.353	0.278	N	Mean	1.588	1.689	1.522

8.2.3.3 Tb.Th

No significant differences were found between L1, L3 and L5 for trabecular thickness in the 4 weeks to 2 years of age cohort. Descriptive statistics can be found in Table 8.15.

Table 8.15: Descriptive statistics for Tb.Th (μm) in the 4wks-2y age cohort.

VOI	P/NP	F/H	P Value	P≤0.01	Mean/ Median	L1	L3	L5
1I	P	0.142	0.868	N	Mean	109.71	104.43	105.56
1C	P	0.755	0.482	N	Mean	139.27	123.80	139.06
1S	NP	4.656	0.098	N	Median	84.65	89.61	98.66
2I	P	0.441	0.649	N	Mean	112.92	106.48	116.20
2C	P	1.141	0.337	N	Mean	141.64	133.78	155.24
2S	NP	3.506	0.173	N	Median	93.43	93.59	103.23
3I	P	0.129	0.880	N	Mean	114.05	108.91	111.48
3C	P	0.386	0.684	N	Mean	141.17	131.38	144.16
3S	P	2.547	0.100	N	Mean	92.20	91.64	114.20
4I	P	0.213	0.810	N	Mean	99.69	96.26	101.09
4C	P	0.573	0.571	N	Mean	108.93	101.72	110.14
4S	P	2.386	0.114	N	Mean	92.67	92.45	107.48
5I	P	0.415	0.665	N	Mean	101.45	98.98	106.69
5C	P	0.407	0.670	N	Mean	113.54	110.20	116.50
5S	NP	2.340	0.310	N	Median	93.41	93.71	103.65
6I	P	0.279	0.759	N	Mean	100.97	97.42	102.54
6C	P	0.679	0.517	N	Mean	112.14	102.69	108.25
6S	P	2.588	0.097	N	Mean	92.83	91.61	108.00
7I	P	1.315	0.288	N	Mean	99.34	96.15	109.21
7C	P	1.334	0.283	N	Mean	103.29	98.44	111.06
7S	P	0.693	0.510	N	Mean	96.01	92.09	102.56
8I	P	1.002	0.383	N	Mean	99.90	95.94	109.30
8C	NP	3.684	0.159	N	Median	134.88	136.82	162.58
8S	P	0.136	0.873	N	Mean	108.80	104.45	106.86
9I	P	0.589	0.563	N	Mean	103.24	97.86	106.56
9C	P	1.581	0.227	N	Mean	103.00	99.17	114.42
9S	P	1.904	0.172	N	Mean	94.33	92.29	107.83

8.2.3.4 Tb.N

As with Tb.Th, no significant differences were present between the three vertebral levels studied for trabecular number in the 4 weeks to 2 years of age cohort. The descriptive statistics for Tb.N can be found in Table 8.16.

Table 8.16: Descriptive statistics for Tb.N (μm^{-1}) in the 4wks-2y age cohort.

VOI	P/NP	F/H	P Value	P≤0.01	Mean/ Median	L1	L3	L5
1I	NP	3.897	0.142	N	Median	0.00158	0.00130	0.00141
1C	P	2.189	0.135	N	Mean	0.00135	0.00116	0.00131
1S	NP	1.635	0.442	N	Median	0.00147	0.00135	0.00151
2I	NP	1.250	0.535	N	Median	0.00143	0.00137	0.00139
2C	NP	4.481	0.106	N	Median	0.00114	0.00099	0.00105
2S	NP	0.389	0.823	N	Median	0.00146	0.00137	0.00144
3I	NP	1.637	0.441	N	Median	0.00161	0.00147	0.00147
3C	NP	2.126	0.345	N	Median	0.00129	0.00121	0.00122
3S	NP	2.039	0.361	N	Median	0.00157	0.00138	0.00166
4I	NP	1.785	0.410	N	Median	0.00147	0.00131	0.00139
4C	NP	5.191	0.075	N	Median	0.00103	0.00105	0.00120
4S	NP	2.613	0.271	N	Median	0.00127	0.00119	0.00142
5I	NP	1.491	0.475	N	Median	0.00132	0.00121	0.00135
5C	NP	5.165	0.076	N	Median	0.00103	0.00098	0.00114
5S	NP	3.149	0.207	N	Median	0.00109	0.00117	0.00132
6I	NP	3.424	0.181	N	Median	0.00143	0.00130	0.00139
6C	NP	5.255	0.072	N	Median	0.00113	0.00103	0.00121
6S	NP	2.395	0.302	N	Median	0.00124	0.00111	0.00149
7I	NP	0.922	0.631	N	Median	0.00172	0.00144	0.00145
7C	NP	1.737	0.420	N	Median	0.00136	0.00116	0.00137
7S	NP	2.217	0.330	N	Median	0.00143	0.00126	0.00150
8I	NP	1.273	0.529	N	Median	0.00151	0.00129	0.00129
8C	NP	1.753	0.416	N	Median	0.00094	0.00083	0.00083
8S	NP	2.979	0.225	N	Median	0.00101	0.00102	0.00132
9I	NP	2.464	0.292	N	Median	0.00177	0.00137	0.00148
9C	NP	3.070	0.216	N	Median	0.00134	0.00121	0.00128
9S	NP	1.368	0.505	N	Median	0.00147	0.00130	0.00151

8.2.3.5 Tb.Sp

Trabecular separation exhibited no significant differences between vertebral levels within the 4 weeks to 2 years of age cohort. Descriptive statistics can be viewed in Table 8.17.

Table 8.17: Descriptive statistics for Tb.Sp (µm) in the 4wks-2y age cohort.

VOI	P/NP	F/H	P Value	P≤0.01	Mean/ Median	L1	L3	L5
1I	NP	2.215	0.330	N	Median	439.88	488.48	507.60
1C	P	0.694	0.510	N	Mean	536.75	586.51	588.96
1S	NP	4.398	0.111	N	Median	418.43	438.41	486.21
2I	NP	0.922	0.631	N	Median	481.72	507.86	529.76
2C	P	0.578	0.569	N	Mean	632.52	643.51	698.66
2S	NP	2.121	0.346	N	Median	447.91	464.90	507.74
3I	NP	3.041	0.219	N	Median	428.77	487.39	474.57
3C	P	0.0272	0.973	N	Mean	561.29	566.93	575.71
3S	NP	2.415	0.299	N	Median	423.32	448.79	488.72
4I	P	0.329	0.723	N	Mean	465.61	491.32	506.69
4C	NP	1.152	0.562	N	Median	659.25	648.35	574.53
4S	P	0.176	0.840	N	Mean	491.34	517.58	506.72
5I	P	0.516	0.604	N	Mean	464.07	494.50	509.70
5C	NP	0.468	0.791	N	Median	607.12	640.87	625.97
5S	NP	0.971	0.615	N	Median	507.64	540.00	504.46
6I	P	0.314	0.734	N	Mean	462.63	495.37	496.67
6C	NP	1.094	0.579	N	Median	627.36	630.65	623.28
6S	P	0.104	0.901	N	Mean	488.20	509.01	501.75
7I	P	0.257	0.776	N	Mean	416.63	432.83	457.15
7C	P	0.0481	0.953	N	Mean	493.98	507.80	503.31
7S	P	0.0879	0.916	N	Mean	462.64	478.22	459.78
8I	P	0.438	0.650	N	Mean	452.04	479.51	508.13
8C	NP	1.268	0.530	N	Median	813.30	964.74	960.44
8S	P	0.940	0.405	N	Mean	594.03	610.39	525.87
9I	P	0.514	0.605	N	Mean	410.32	444.02	458.38
9C	P	0.605	0.555	N	Mean	486.75	514.17	549.11
9S	P	0.154	0.858	N	Mean	454.49	479.02	469.50

8.2.3.6 DA

As with several of the previous parameters, there were no significant differences in the values for degree of anisotropy between vertebral levels L1, L3 and L5 within the 4 weeks to 2 years of age cohort. The descriptive statistics for this dataset can be viewed in Table 8.18.

Table 8.18: Descriptive statistics for DA in the 4wks-2y age cohort.

VOI	P/NP	F/H	P Value	P≤0.01	Mean/ Median	L1	L3	L5
1I	P	2.360	0.117	N	Mean	0.451	0.451	0.369
1C	P	2.318	0.121	N	Mean	0.422	0.503	0.464
1S	P	0.489	0.620	N	Mean	0.384	0.415	0.404
2I	P	1.219	0.314	N	Mean	0.367	0.374	0.305
2C	P	0.916	0.414	N	Mean	0.306	0.352	0.282
2S	P	0.896	0.422	N	Mean	0.347	0.356	0.392
3I	P	3.140	0.062	N	Mean	0.396	0.459	0.352
3C	P	1.136	0.338	N	Mean	0.428	0.480	0.463
3S	P	0.0149	0.985	N	Mean	0.404	0.402	0.410
4I	NP	0.138	0.933	N	Median	0.249	0.253	0.268
4C	NP	9.959	0.007	N	Median	0.414	0.457	0.399
4S	P	1.235	0.310	N	Mean	0.391	0.365	0.311
5I	NP	8.415	0.015	N	Median	0.276	0.306	0.178
5C	P	1.762	0.194	N	Mean	0.352	0.392	0.361
5S	P	0.300	0.743	N	Mean	0.266	0.246	0.287
6I	P	0.109	0.897	N	Mean	0.265	0.282	0.293
6C	NP	0.690	0.512	N	Median	0.390	0.417	0.395
6S	P	1.382	0.271	N	Mean	0.382	0.356	0.317
7I	P	0.124	0.884	N	Mean	0.286	0.303	0.292
7C	P	0.153	0.859	N	Mean	0.319	0.338	0.319
7S	P	0.610	0.552	N	Mean	0.281	0.325	0.288
8I	P	3.936	0.034	N	Mean	0.339	0.234	0.278
8C	P	2.239	0.129	N	Mean	0.261	0.326	0.324
8S	P	1.162	0.330	N	Mean	0.234	0.271	0.303
9I	P	0.391	0.681	N	Mean	0.289	0.266	0.309
9C	P	0.456	0.640	N	Mean	0.326	0.355	0.333
9S	P	0.492	0.617	N	Mean	0.296	0.336	0.307

8.2.3.7 Summary

For the 4 weeks to 2 years of age cohort, the only parameters that displayed significant differences were bone volume fraction (BV/TV) and structural model index (SMI). Where L5 differed from L1 and L3, L5 displayed significantly higher BV/TV and lower SMI. L1 also displayed higher BV/TV compared to L3. These differences were restricted to VOIs 4, 5 and 6. These findings can be visualised in Figure 8.3.

	L1 VS L3			L1 VS L5			L3 VS L5		
1I	BV/TV	SMI	Tb.Th	BV/TV	SMI	Tb.Th	BV/TV	SMI	Tb.Th
	Tb.N	Tb.Sp	DA	Tb.N	Tb.Sp	DA	Tb.N	Tb.Sp	DA
1C	BV/TV	SMI	Tb.Th	BV/TV	SMI	Tb.Th	BV/TV	SMI	Tb.Th
	Tb.N	Tb.Sp	DA	Tb.N	Tb.Sp	DA	Tb.N	Tb.Sp	DA
1S	BV/TV	SMI	Tb.Th	BV/TV	SMI	Tb.Th	BV/TV	SMI	Tb.Th
	Tb.N	Tb.Sp	DA	Tb.N	Tb.Sp	DA	Tb.N	Tb.Sp	DA
2I	BV/TV	SMI	Tb.Th	BV/TV	SMI	Tb.Th	BV/TV	SMI	Tb.Th
	Tb.N	Tb.Sp	DA	Tb.N	Tb.Sp	DA	Tb.N	Tb.Sp	DA
2C	BV/TV	SMI	Tb.Th	BV/TV	SMI	Tb.Th	BV/TV	SMI	Tb.Th
	Tb.N	Tb.Sp	DA	Tb.N	Tb.Sp	DA	Tb.N	Tb.Sp	DA
2S	BV/TV	SMI	Tb.Th	BV/TV	SMI	Tb.Th	BV/TV	SMI	Tb.Th
	Tb.N	Tb.Sp	DA	Tb.N	Tb.Sp	DA	Tb.N	Tb.Sp	DA
3I	BV/TV	SMI	Tb.Th	BV/TV	SMI	Tb.Th	BV/TV	SMI	Tb.Th
	Tb.N	Tb.Sp	DA	Tb.N	Tb.Sp	DA	Tb.N	Tb.Sp	DA
3C	BV/TV	SMI	Tb.Th	BV/TV	SMI	Tb.Th	BV/TV	SMI	Tb.Th
	Tb.N	Tb.Sp	DA	Tb.N	Tb.Sp	DA	Tb.N	Tb.Sp	DA
3S	BV/TV	SMI	Tb.Th	BV/TV	SMI	Tb.Th	BV/TV	SMI	Tb.Th
	Tb.N	Tb.Sp	DA	Tb.N	Tb.Sp	DA	Tb.N	Tb.Sp	DA
4I	BV/TV	SMI	Tb.Th	BV/TV	SMI	Tb.Th	BV/TV	SMI	Tb.Th
	Tb.N	Tb.Sp	DA	Tb.N	Tb.Sp	DA	Tb.N	Tb.Sp	DA
4C	BV/TV	SMI	Tb.Th	BV/TV	SMI	Tb.Th	BV/TV	SMI	Tb.Th
	Tb.N	Tb.Sp	DA	Tb.N	Tb.Sp	DA	Tb.N	Tb.Sp	DA
4S	BV/TV	SMI	Tb.Th	BV/TV	SMI	Tb.Th	BV/TV	SMI	Tb.Th
	Tb.N	Tb.Sp	DA	Tb.N	Tb.Sp	DA	Tb.N	Tb.Sp	DA
5I	BV/TV	SMI	Tb.Th	BV/TV	SMI	Tb.Th	BV/TV	SMI	Tb.Th
	Tb.N	Tb.Sp	DA	Tb.N	Tb.Sp	DA	Tb.N	Tb.Sp	DA
5C	BV/TV	SMI	Tb.Th	BV/TV	SMI	Tb.Th	BV/TV	SMI	Tb.Th
	Tb.N	Tb.Sp	DA	Tb.N	Tb.Sp	DA	Tb.N	Tb.Sp	DA
5S	BV/TV	SMI	Tb.Th	BV/TV	SMI	Tb.Th	BV/TV	SMI	Tb.Th
	Tb.N	Tb.Sp	DA	Tb.N	Tb.Sp	DA	Tb.N	Tb.Sp	DA
6I	BV/TV	SMI	Tb.Th	BV/TV	SMI	Tb.Th	BV/TV	SMI	Tb.Th
	Tb.N	Tb.Sp	DA	Tb.N	Tb.Sp	DA	Tb.N	Tb.Sp	DA
6C	BV/TV	SMI	Tb.Th	BV/TV	SMI	Tb.Th	BV/TV	SMI	Tb.Th
	Tb.N	Tb.Sp	DA	Tb.N	Tb.Sp	DA	Tb.N	Tb.Sp	DA
6S	BV/TV	SMI	Tb.Th	BV/TV	SMI	Tb.Th	BV/TV	SMI	Tb.Th
	Tb.N	Tb.Sp	DA	Tb.N	Tb.Sp	DA	Tb.N	Tb.Sp	DA
7I	BV/TV	SMI	Tb.Th	BV/TV	SMI	Tb.Th	BV/TV	SMI	Tb.Th
	Tb.N	Tb.Sp	DA	Tb.N	Tb.Sp	DA	Tb.N	Tb.Sp	DA
7C	BV/TV	SMI	Tb.Th	BV/TV	SMI	Tb.Th	BV/TV	SMI	Tb.Th
	Tb.N	Tb.Sp	DA	Tb.N	Tb.Sp	DA	Tb.N	Tb.Sp	DA
7S	BV/TV	SMI	Tb.Th	BV/TV	SMI	Tb.Th	BV/TV	SMI	Tb.Th
	Tb.N	Tb.Sp	DA	Tb.N	Tb.Sp	DA	Tb.N	Tb.Sp	DA
8I	BV/TV	SMI	Tb.Th	BV/TV	SMI	Tb.Th	BV/TV	SMI	Tb.Th
	Tb.N	Tb.Sp	DA	Tb.N	Tb.Sp	DA	Tb.N	Tb.Sp	DA
8C	BV/TV	SMI	Tb.Th	BV/TV	SMI	Tb.Th	BV/TV	SMI	Tb.Th
	Tb.N	Tb.Sp	DA	Tb.N	Tb.Sp	DA	Tb.N	Tb.Sp	DA
8S	BV/TV	SMI	Tb.Th	BV/TV	SMI	Tb.Th	BV/TV	SMI	Tb.Th
	Tb.N	Tb.Sp	DA	Tb.N	Tb.Sp	DA	Tb.N	Tb.Sp	DA
9I	BV/TV	SMI	Tb.Th	BV/TV	SMI	Tb.Th	BV/TV	SMI	Tb.Th
	Tb.N	Tb.Sp	DA	Tb.N	Tb.Sp	DA	Tb.N	Tb.Sp	DA
9C	BV/TV	SMI	Tb.Th	BV/TV	SMI	Tb.Th	BV/TV	SMI	Tb.Th
	Tb.N	Tb.Sp	DA	Tb.N	Tb.Sp	DA	Tb.N	Tb.Sp	DA
9S	BV/TV	SMI	Tb.Th	BV/TV	SMI	Tb.Th	BV/TV	SMI	Tb.Th
	Tb.N	Tb.Sp	DA	Tb.N	Tb.Sp	DA	Tb.N	Tb.Sp	DA

Figure 8.3: Data visualisation of the significant differences between vertebral levels L1, L3 and L5 for all parameters within the 4 weeks to 2 years of age cohort. A red square indicates a significant difference ($p \leq 0.01$) while a green square indicates no significant difference.

8.2.4 *3-8 years of age cohort*

8.2.4.1 BV/TV

For bone volume fraction within the 3-8 years of age cohort, significant differences were found between the three vertebral levels L1, L3 and L5 for some VOIs. Firstly, L1 differed significantly from L3 at VOI 6S, with L1 exhibiting a significantly higher BV/TV. Differences were also found between L5 and the other vertebral levels. As with other age cohorts, L5 displayed a significantly higher BV/TV. When compared to L1, this occurred at VOIs 4I, 4C, 4S, 5S, 6S, 7C, 7S, 8C and 9S. When compared to L3, this was at VOIs 2S, 3S, 4I, 4C, 4S, 5S, 6C, 6S, 7C, 7S, 8C, 9C and 9S. Descriptive statistics for this dataset can be viewed in Table 8.19. The significant differences can be visualised in Figure 8.4.

Table 8.19: Descriptive statistics for BV/TV (%) in the 3-8y age cohort.

VOI	P/NP	F/H	P Value	P≤0.01	Mean/ Median	L1	L3	L5
1I	P	3.127	0.073	N	Mean	16.79	15.49	20.53
1C	P	2.745	0.096	N	Mean	18.04	15.49	20.22
1S	NP	7.901	0.019	N	Median	13.06	12.22	17.85
2I	P	3.986	0.041	N	Mean	17.01	14.69	19.87
2C	P	4.174	0.036	N	Mean	17.00	14.65	18.83
2S	NP	10.474	0.005	N	Median	13.45	11.64	16.96
3I	P	3.528	0.055	N	Mean	19.09	14.85	18.77
3C	P	3.571	0.054	N	Mean	20.07	15.76	19.34
3S	NP	11.447	0.003	Y	Median	14.68	11.70	16.94
4I	P	11.008	0.001	Y	Mean	13.58	12.48	19.90
4C	P	12.759	<0.001	Y	Mean	12.32	10.99	16.22
4S	P	22.202	<0.001	Y	Mean	11.63	10.39	16.64
5I	NP	3.655	0.161	N	Median	12.16	12.21	20.09
5C	P	4.823	0.024	N	Mean	10.70	10.15	14.45
5S	P	20.620	<0.001	Y	Mean	10.86	9.87	15.74
6I	NP	6.256	0.044	N	Median	15.23	13.10	20.71
6C	P	10.281	0.002	Y	Mean	13.68	10.72	15.93
6S	P	23.045	<0.001	Y	Mean	12.76	10.07	16.46
7I	P	5.974	0.012	N	Mean	15.92	14.12	22.25
7C	P	17.224	<0.001	Y	Mean	13.46	11.43	18.51
7S	P	44.243	<0.001	Y	Mean	12.76	10.60	18.93
8I	NP	7.651	0.022	N	Median	13.66	12.00	20.51
8C	P	8.069	0.004	Y	Mean	11.61	10.87	15.92
8S	NP	7.462	0.024	N	Median	12.44	10.52	15.31
9I	NP	4.396	0.111	N	Median	15.98	13.84	23.76
9C	NP	12.598	0.002	Y	Median	14.10	11.50	18.30
9S	P	11.589	<0.001	Y	Mean	12.92	10.62	19.51

8.2.4.2 SMI

For structural model index, significant differences were found between the vertebral levels L3 and L5 within the 3-8 years of age cohort. These differences were found at VOIs 4I, 6I, 7I, 7S, 9C and 9S. In all cases, L5 displayed significantly lower values for SMI, mirroring findings at other ages. However, all values indicated a transitional morphology with both plate-like and rod-like trabeculae present within the internal architecture. The descriptive statistics for SMI within the 3-8 years of age cohort can be viewed in Table 8.20. Significant differences for this cohort can be found in Figure 8.4.

Table 8.20: Descriptive statistics for SMI in the 3-8y age cohort.

VOI	P/NP	F/H	P Value	P≤0.01	Mean/ Median	L1	L3	L5
1I	P	0.901	0.427	N	Mean	1.544	1.536	1.367
1C	P	1.829	0.195	N	Mean	1.210	1.155	1.043
1S	NP	6.211	0.045	N	Median	1.805	1.850	1.519
2I	NP	6.045	0.049	N	Median	1.388	1.463	1.291
2C	P	1.451	0.265	N	Mean	1.144	1.146	0.975
2S	NP	5.475	0.065	N	Median	1.762	1.884	1.570
3I	P	0.318	0.732	N	Mean	1.486	1.561	1.464
3C	P	0.821	0.459	N	Mean	1.089	1.220	1.114
3S	NP	8.013	0.018	N	Median	1.765	1.956	1.583
4I	P	8.667	0.003	Y	Mean	1.623	1.714	1.389
4C	P	0.744	0.492	N	Mean	1.326	1.366	1.253
4S	P	4.118	0.038	N	Mean	1.749	1.797	1.508
5I	P	1.802	0.199	N	Mean	1.695	1.706	1.543
5C	P	0.299	0.746	N	Mean	1.428	1.392	1.322
5S	P	3.839	0.045	N	Mean	1.791	1.811	1.532
6I	P	6.405	0.010	Y	Mean	1.591	1.706	1.405
6C	P	1.715	0.213	N	Mean	1.275	1.403	1.274
6S	P	4.322	0.033	N	Mean	1.692	1.845	1.500
7I	P	6.743	0.008	Y	Mean	1.630	1.693	1.406
7C	NP	8.934	0.011	N	Median	1.497	1.540	1.249
7S	P	6.995	0.007	Y	Mean	1.730	1.836	1.483
8I	P	2.951	0.083	N	Mean	1.680	1.728	1.546
8C	P	0.893	0.430	N	Mean	1.245	1.249	1.117
8S	NP	3.273	0.195	N	Median	1.616	1.668	1.525
9I	NP	3.940	0.139	N	Median	1.595	1.723	1.294
9C	P	8.464	0.003	Y	Mean	1.483	1.641	1.173
9S	P	6.187	0.011	Y	Mean	1.717	1.864	1.426

8.2.4.3 Tb.Th

Trabecular thickness differed significantly between vertebral levels within the 3-8 years of age cohort. The vertebral level L5 displayed significantly higher values for trabecular thickness compared to L1 (VOI 4S) and L3 (VOIs 2S, 4S, 6S and 8I). No significant differences were found between the 1st and 3rd lumbar vertebral levels. Descriptive statistics for this dataset can be found in Table 8.21. The significant differences between vertebral levels can be visualised in Figure 8.4.

Table 8.21: Descriptive statistics for Tb.Th (µm) in the 3-8y age cohort.

VOI	P/NP	F/H	P Value	P≤0.01	Mean/ Median	L1	L3	L5
1I	P	0.288	0.754	N	Mean	123.16	114.54	126.34
1C	P	1.178	0.335	N	Mean	148.41	134.39	161.59
1S	NP	7.276	0.026	N	Median	102.42	94.97	119.20
2I	P	0.901	0.427	N	Mean	127.69	114.82	134.15
2C	P	4.609	0.028	N	Mean	150.65	129.41	163.20
2S	P	7.681	0.005	Y	Mean	108.21	92.87	121.87
3I	P	1.016	0.386	N	Mean	132.75	112.58	120.46
3C	P	2.100	0.157	N	Mean	160.53	134.30	158.07
3S	P	4.076	0.039	N	Mean	109.12	92.71	115.01
4I	P	5.205	0.019	N	Mean	109.09	100.15	130.33
4C	P	1.783	0.202	N	Mean	131.73	116.61	134.48
4S	P	9.570	0.002	Y	Mean	101.61	96.06	119.99
5I	P	4.576	0.028	N	Mean	108.41	110.12	145.40
5C	P	5.088	0.021	N	Mean	121.12	119.63	155.52
5S	P	6.108	0.011	N	Mean	106.45	102.08	131.77
6I	P	2.750	0.096	N	Mean	113.52	102.06	121.48
6C	NP	6.352	0.042	N	Median	143.35	117.79	135.67
6S	P	8.891	0.003	Y	Mean	105.90	93.92	117.44
7I	P	4.333	0.033	N	Mean	110.17	99.88	125.81
7C	NP	4.396	0.111	N	Median	114.47	100.04	139.13
7S	NP	5.787	0.055	N	Median	104.10	91.61	125.84
8I	P	14.876	<0.001	Y	Mean	112.40	98.83	127.60
8C	P	4.583	0.028	N	Mean	151.47	137.16	172.43
8S	P	0.580	0.572	N	Mean	126.85	120.95	139.06
9I	NP	5.787	0.055	N	Median	108.95	97.94	131.50
9C	P	4.209	0.035	N	Mean	122.67	104.18	140.02
9S	P	2.916	0.085	N	Mean	109.43	97.42	132.03

8.2.4.4 Tb.N

As with the previous histomorphometric parameters within the 3-8 years of age cohort, significant differences between vertebral levels were present for trabecular number. The fifth lumbar vertebral level was found to display significantly higher trabecular number compared to the 1st and 3rd lumbar vertebrae. L5 was found to differ from L1 at VOI 9C, and from L3 at VOIs 6I, 9C and 9S. The descriptive statistics for Tb.N within the 3-8 years of age cohort can be viewed in Table 8.22. Differences between vertebral levels can be viewed in Figure 8.4.

Table 8.22: Descriptive statistics for Tb.N (μm^{-1}) in the 3-8y age cohort.

VOI	P/NP	F/H	P Value	P≤0.01	Mean/ Median	L1	L3	L5
1I	NP	4.609	0.100	N	Median	0.00128	0.00131	0.00163
1C	NP	1.778	0.411	N	Median	0.00116	0.00109	0.00124
1S	P	0.708	0.509	N	Mean	0.00141	0.00132	0.00152
2I	NP	3.708	0.157	N	Median	0.00126	0.00130	0.00147
2C	NP	0.817	0.665	N	Median	0.00111	0.00103	0.00116
2S	NP	2.924	0.232	Y	Median	0.00126	0.00120	0.00139
3I	NP	3.452	0.178	N	Median	0.00137	0.00127	0.00152
3C	NP	0.871	0.647	N	Median	0.00119	0.00108	0.00123
3S	P	1.396	0.278	N	Mean	0.00141	0.00126	0.00149
4I	P	5.377	0.017	N	Mean	0.00126	0.00124	0.00151
4C	P	6.912	0.007	N	Mean	0.00095	0.00094	0.00121
4S	P	4.067	0.039	N	Mean	0.00115	0.00108	0.00139
5I	NP	2.031	0.362	N	Median	0.00112	0.00110	0.00124
5C	P	0.646	0.538	N	Mean	0.00088	0.00085	0.00094
5S	NP	6.138	0.046	N	Median	0.00101	0.00098	0.00119
6I	P	7.112	0.007	Y	Mean	0.00132	0.00124	0.00156
6C	NP	6.958	0.031	N	Median	0.00096	0.00090	0.00121
6S	P	4.938	0.023	N	Mean	0.00121	0.00107	0.00141
7I	P	2.782	0.094	N	Mean	0.00145	0.00141	0.00174
7C	P	3.911	0.043	N	Mean	0.00117	0.00110	0.00136
7S	P	4.448	0.030	N	Mean	0.00123	0.00111	0.00153
8I	P	1.988	0.172	N	Mean	0.00127	0.00121	0.00146
8C	P	2.912	0.085	N	Mean	0.00077	0.00079	0.00092
8S	NP	5.907	0.052	N	Median	0.00097	0.00091	0.00117
9I	P	2.331	0.131	N	Mean	0.00148	0.00138	0.00166
9C	P	10.747	0.001	Y	Mean	0.00117	0.00110	0.00141
9S	P	6.839	0.008	Y	Mean	0.00120	0.00109	0.00149

8.2.4.5 Tb.Sp

Unlike the previous parameters, no significant differences were found for trabecular separation between vertebral levels within the 3-8 years of age cohort. The descriptive statistics for this dataset can be found in Table 8.23.

Table 8.23: Descriptive statistics for Tb.Sp (µm) in the 3-8y age cohort.

VOI	P/NP	F/H	P Value	P≤0.01	Mean/ Median	L1	L3	L5
1I	P	0.622	0.550	N	Mean	499.26	505.97	439.93
1C	P	0.125	0.883	N	Mean	648.65	684.04	653.74
1S	P	0.0674	0.935	N	Mean	455.30	445.04	461.54
2I	P	0.147	0.864	N	Mean	523.86	537.43	505.31
2C	P	0.146	0.866	N	Mean	676.28	694.15	709.39
2S	P	0.301	0.745	N	Mean	481.03	458.58	483.91
3I	P	0.556	0.585	N	Mean	484.98	523.89	454.00
3C	P	0.0920	0.913	N	Mean	637.06	657.15	665.07
3S	P	0.147	0.865	N	Mean	455.64	449.71	474.60
4I	P	0.701	0.512	N	Mean	535.06	515.58	487.62
4C	P	5.669	0.015	N	Mean	767.56	800.80	657.91
4S	P	0.618	0.552	N	Mean	549.75	559.05	515.24
5I	P	0.991	0.394	N	Mean	570.41	588.24	548.33
5C	P	0.341	0.716	N	Mean	763.83	799.63	783.76
5S	P	0.632	0.545	N	Mean	582.85	608.59	571.48
6I	P	1.783	0.202	N	Mean	523.29	514.27	468.31
6C	P	6.229	0.011	N	Mean	765.51	765.23	637.20
6S	P	0.460	0.640	N	Mean	542.60	546.34	506.56
7I	P	0.924	0.418	N	Mean	478.83	453.13	421.68
7C	P	1.117	0.353	N	Mean	598.08	591.92	550.88
7S	P	0.810	0.464	N	Mean	531.94	516.85	470.68
8I	P	0.297	0.747	N	Mean	522.80	516.77	482.18
8C	P	0.789	0.472	N	Mean	1107.37	1031.47	996.51
8S	P	1.403	0.276	N	Mean	686.84	691.53	568.66
9I	P	0.439	0.653	N	Mean	474.65	451.66	436.22
9C	P	3.473	0.058	N	Mean	592.63	580.25	528.79
9S	P	1.093	0.360	N	Mean	541.22	516.94	481.64

8.2.4.6 DA

As with Tb.Sp, no differences were present for degree of anisotropy between vertebral levels within the 3-8 years of age cohort. The descriptive statistics can be seen in Table 8.24.

Table 8.24: Descriptive statistics for DA in the 3-8y age cohort.

VOI	P/NP	F/H	P Value	P≤0.01	Mean/ Median	L1	L3	L5
1I	P	0.676	0.524	N	Mean	0.469	0.506	0.463
1C	P	0.757	0.486	N	Mean	0.504	0.558	0.534
1S	P	0.456	0.642	N	Mean	0.439	0.473	0.482
2I	P	0.969	0.402	N	Mean	0.440	0.445	0.382
2C	P	2.003	0.169	N	Mean	0.446	0.516	0.387
2S	P	0.331	0.723	N	Mean	0.391	0.373	0.419
3I	P	2.139	0.152	N	Mean	0.454	0.515	0.456
3C	P	1.416	0.273	N	Mean	0.512	0.535	0.469
3S	NP	0.408	0.816	N	Median	0.440	0.427	0.442
4I	P	0.803	0.466	N	Mean	0.299	0.217	0.240
4C	P	0.738	0.495	N	Mean	0.430	0.423	0.372
4S	P	0.116	0.891	N	Mean	0.316	0.338	0.310
5I	P	0.794	0.470	N	Mean	0.280	0.221	0.238
5C	NP	2.221	0.329	N	Median	0.379	0.356	0.327
5S	P	0.129	0.880	N	Mean	0.252	0.232	0.213
6I	P	0.177	0.840	N	Mean	0.282	0.256	0.241
6C	P	0.429	0.659	N	Mean	0.410	0.425	0.387
6S	P	0.0134	0.987	N	Mean	0.284	0.294	0.291
7I	P	0.761	0.484	N	Mean	0.239	0.212	0.279
7C	P	1.335	0.293	N	Mean	0.251	0.295	0.284
7S	P	1.364	0.286	N	Mean	0.241	0.238	0.314
8I	P	0.0809	0.923	N	Mean	0.216	0.203	0.199
8C	P	2.001	0.170	N	Mean	0.213	0.298	0.205
8S	P	2.378	0.127	N	Mean	0.221	0.186	0.265
9I	P	0.974	0.400	N	Mean	0.243	0.237	0.319
9C	P	0.897	0.429	N	Mean	0.247	0.251	0.292
9S	NP	0.808	0.667	N	Median	0.258	0.247	0.229

8.2.4.7 Summary of results

As with other age cohorts, the majority of differences between vertebral levels within the 3-8 years of age cohort were between L5 and the two other vertebral levels, where L5 displayed significantly higher values for BV/TV, Tb.Th and Tb.N, and significantly lower values for SMI when compared to vertebral levels L1 and L3. These differences generally occurred at superior and inferior VOIs. One significant difference was found between L1 and L3, for BV/TV, where L1 displayed a significantly higher value.

	L1 VS L3			L1 VS L5			L3 VS L5		
1I	BV/TV	SMI	Tb.Th	BV/TV	SMI	Tb.Th	BV/TV	SMI	Tb.Th
	Tb.N	Tb.Sp	DA	Tb.N	Tb.Sp	DA	Tb.N	Tb.Sp	DA
1C	BV/TV	SMI	Tb.Th	BV/TV	SMI	Tb.Th	BV/TV	SMI	Tb.Th
	Tb.N	Tb.Sp	DA	Tb.N	Tb.Sp	DA	Tb.N	Tb.Sp	DA
1S	BV/TV	SMI	Tb.Th	BV/TV	SMI	Tb.Th	BV/TV	SMI	Tb.Th
	Tb.N	Tb.Sp	DA	Tb.N	Tb.Sp	DA	Tb.N	Tb.Sp	DA
2I	BV/TV	SMI	Tb.Th	BV/TV	SMI	Tb.Th	BV/TV	SMI	Tb.Th
	Tb.N	Tb.Sp	DA	Tb.N	Tb.Sp	DA	Tb.N	Tb.Sp	DA
2C	BV/TV	SMI	Tb.Th	BV/TV	SMI	Tb.Th	BV/TV	SMI	Tb.Th
	Tb.N	Tb.Sp	DA	Tb.N	Tb.Sp	DA	Tb.N	Tb.Sp	DA
2S	BV/TV	SMI	Tb.Th	BV/TV	SMI	Tb.Th	BV/TV	SMI	Tb.Th
	Tb.N	Tb.Sp	DA	Tb.N	Tb.Sp	DA	Tb.N	Tb.Sp	DA
3I	BV/TV	SMI	Tb.Th	BV/TV	SMI	Tb.Th	BV/TV	SMI	Tb.Th
	Tb.N	Tb.Sp	DA	Tb.N	Tb.Sp	DA	Tb.N	Tb.Sp	DA
3C	BV/TV	SMI	Tb.Th	BV/TV	SMI	Tb.Th	BV/TV	SMI	Tb.Th
	Tb.N	Tb.Sp	DA	Tb.N	Tb.Sp	DA	Tb.N	Tb.Sp	DA
3S	BV/TV	SMI	Tb.Th	BV/TV	SMI	Tb.Th	BV/TV	SMI	Tb.Th
	Tb.N	Tb.Sp	DA	Tb.N	Tb.Sp	DA	Tb.N	Tb.Sp	DA
4I	BV/TV	SMI	Tb.Th	BV/TV	SMI	Tb.Th	BV/TV	SMI	Tb.Th
	Tb.N	Tb.Sp	DA	Tb.N	Tb.Sp	DA	Tb.N	Tb.Sp	DA
4C	BV/TV	SMI	Tb.Th	BV/TV	SMI	Tb.Th	BV/TV	SMI	Tb.Th
	Tb.N	Tb.Sp	DA	Tb.N	Tb.Sp	DA	Tb.N	Tb.Sp	DA
4S	BV/TV	SMI	Tb.Th	BV/TV	SMI	Tb.Th	BV/TV	SMI	Tb.Th
	Tb.N	Tb.Sp	DA	Tb.N	Tb.Sp	DA	Tb.N	Tb.Sp	DA
5I	BV/TV	SMI	Tb.Th	BV/TV	SMI	Tb.Th	BV/TV	SMI	Tb.Th
	Tb.N	Tb.Sp	DA	Tb.N	Tb.Sp	DA	Tb.N	Tb.Sp	DA
5C	BV/TV	SMI	Tb.Th	BV/TV	SMI	Tb.Th	BV/TV	SMI	Tb.Th
	Tb.N	Tb.Sp	DA	Tb.N	Tb.Sp	DA	Tb.N	Tb.Sp	DA
5S	BV/TV	SMI	Tb.Th	BV/TV	SMI	Tb.Th	BV/TV	SMI	Tb.Th
	Tb.N	Tb.Sp	DA	Tb.N	Tb.Sp	DA	Tb.N	Tb.Sp	DA
6I	BV/TV	SMI	Tb.Th	BV/TV	SMI	Tb.Th	BV/TV	SMI	Tb.Th
	Tb.N	Tb.Sp	DA	Tb.N	Tb.Sp	DA	Tb.N	Tb.Sp	DA
6C	BV/TV	SMI	Tb.Th	BV/TV	SMI	Tb.Th	BV/TV	SMI	Tb.Th
	Tb.N	Tb.Sp	DA	Tb.N	Tb.Sp	DA	Tb.N	Tb.Sp	DA
6S	BV/TV	SMI	Tb.Th	BV/TV	SMI	Tb.Th	BV/TV	SMI	Tb.Th
	Tb.N	Tb.Sp	DA	Tb.N	Tb.Sp	DA	Tb.N	Tb.Sp	DA
7I	BV/TV	SMI	Tb.Th	BV/TV	SMI	Tb.Th	BV/TV	SMI	Tb.Th
	Tb.N	Tb.Sp	DA	Tb.N	Tb.Sp	DA	Tb.N	Tb.Sp	DA
7C	BV/TV	SMI	Tb.Th	BV/TV	SMI	Tb.Th	BV/TV	SMI	Tb.Th
	Tb.N	Tb.Sp	DA	Tb.N	Tb.Sp	DA	Tb.N	Tb.Sp	DA
7S	BV/TV	SMI	Tb.Th	BV/TV	SMI	Tb.Th	BV/TV	SMI	Tb.Th
	Tb.N	Tb.Sp	DA	Tb.N	Tb.Sp	DA	Tb.N	Tb.Sp	DA
8I	BV/TV	SMI	Tb.Th	BV/TV	SMI	Tb.Th	BV/TV	SMI	Tb.Th
	Tb.N	Tb.Sp	DA	Tb.N	Tb.Sp	DA	Tb.N	Tb.Sp	DA
8C	BV/TV	SMI	Tb.Th	BV/TV	SMI	Tb.Th	BV/TV	SMI	Tb.Th
	Tb.N	Tb.Sp	DA	Tb.N	Tb.Sp	DA	Tb.N	Tb.Sp	DA
8S	BV/TV	SMI	Tb.Th	BV/TV	SMI	Tb.Th	BV/TV	SMI	Tb.Th
	Tb.N	Tb.Sp	DA	Tb.N	Tb.Sp	DA	Tb.N	Tb.Sp	DA
9I	BV/TV	SMI	Tb.Th	BV/TV	SMI	Tb.Th	BV/TV	SMI	Tb.Th
	Tb.N	Tb.Sp	DA	Tb.N	Tb.Sp	DA	Tb.N	Tb.Sp	DA
9C	BV/TV	SMI	Tb.Th	BV/TV	SMI	Tb.Th	BV/TV	SMI	Tb.Th
	Tb.N	Tb.Sp	DA	Tb.N	Tb.Sp	DA	Tb.N	Tb.Sp	DA
9S	BV/TV	SMI	Tb.Th	BV/TV	SMI	Tb.Th	BV/TV	SMI	Tb.Th
	Tb.N	Tb.Sp	DA	Tb.N	Tb.Sp	DA	Tb.N	Tb.Sp	DA

Figure 8.4: Data visualisation of the significant differences between vertebral levels L1, L3 and L5 for all parameters within the 3-8 years age cohort. A red square indicates a significant difference ($p \leq 0.01$) while a green square indicates no significant difference.

9 Analysis of Quantitative Data: Analysis 3

9.1 Introduction

The third analysis of the quantitative data addressed the trabecular architecture of the developing first, third and fifth lumbar vertebrae. The trabecular architecture of twenty-seven volumes of interest (VOIs) are described in relation to the six histomorphometric parameters studied. Furthermore, this third analysis aimed to assess any significant differences in trabecular architecture between VOIs. For this analysis, VOIs of each age cohort and vertebral level were considered per histomorphometric parameter. As with previous analyses, a difference was considered significant at the level of $p \leq 0.01$. All raw data and results of these statistical analyses can be viewed in Appendix 9.1.

For this analysis, visualisation of the data displays the differentiation between high, intermediate and low average values of VOIs. High values are denoted by red, intermediate by yellow, and low values by green. The differentiation of high, medium and low values was achieved by identifying the range of each dataset and calculating which values lay within the lower third, the middle third and upper third of the dataset. These colours have been superimposed upon three images of lumbar vertebral centra correlating to the inferior, central and superior layers studied and have been overlaid by the 3 x 3 grid as described in section 6.2.3.1 and Figure 6.9. The average value of the histomorphometric parameter for each VOI can be found in the accompanying tables. Appendix 9.2 contains bar graphs which are also colour coded based upon the red/ yellow/ green system. While tables are included for all datasets, colour-coded VOI figures are only included where significant differences are present. A figure visualising significant differences between VOIs, where red squares denote a significant difference between two VOIs and a green square indicate no significant difference, is also included per dataset with significant differences.

9.2 Results

9.2.1 *Fetal age cohort*

9.2.1.1 BV/TV

For bone volume fraction within the fetal period, significant differences between VOIs were present at the vertebral level L3 only. Descriptive statistics for L1, L3 and L5 can be found in Table 9.1.

Table 9.1: Descriptive statistics for BV/TV (%) at L1, L3 and L5 in the fetal period.

	L1	L3	L5
Parametric?	NP	P	NP
F/H Value	28.675	3.264	40.158
DF	26	26	26
P Value	0.326	<0.001	0.038
p≤0.01?	N	Y	N
Mean/Median	Median	Mean	Median
1I	32.48	27.40	36.16
1C	32.14	22.48	30.29
1S	33.43	21.89	33.01
2I	30.34	24.49	31.42
2C	28.58	21.20	28.98
2S	33.20	24.62	32.00
3I	33.06	21.06	32.43
3C	32.05	21.81	29.62
3S	33.87	22.70	30.70
4I	37.99	28.23	36.63
4C	34.80	27.25	34.11
4S	35.65	25.57	37.00
5I	42.17	34.81	41.70
5C	34.24	30.23	36.59
5S	43.74	33.40	40.57
6I	36.79	26.21	37.80
6C	36.85	25.89	34.35
6S	36.23	24.13	35.28
7I	35.36	28.18	31.50
7C	34.34	23.77	32.53
7S	34.47	26.16	35.40
8I	31.91	32.51	41.75
8C	33.20	26.85	36.71
8S	34.67	29.34	39.45
9I	36.33	24.00	34.88
9C	33.17	25.97	27.07
9S	34.88	23.70	29.16

At the level of L1, values for BV/TV ranged from 28.58% (2C) to 43.74% (5S). At the level of L3, values ranged between 21.06% (3I) and 34.81% (5I). VOI 5I was found to display significantly higher BV/TV compared to VOIs 1S, 2C, 3I and 3C. The high, intermediate and low VOIs for BV/TV at the level of L3 can be found in figure 9.1. Significant differences can be visualised in figure 9.2. At the level of L5, values ranged between 27.07% (9C) and 41.75% (8I).

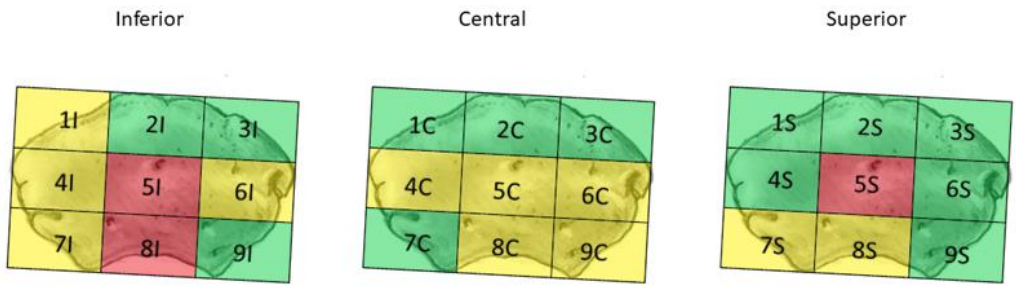

Figure 9.1: The high (red), intermediate (yellow) and low (green) mean values for BV/TV (%) at L3 within the fetal age cohort.

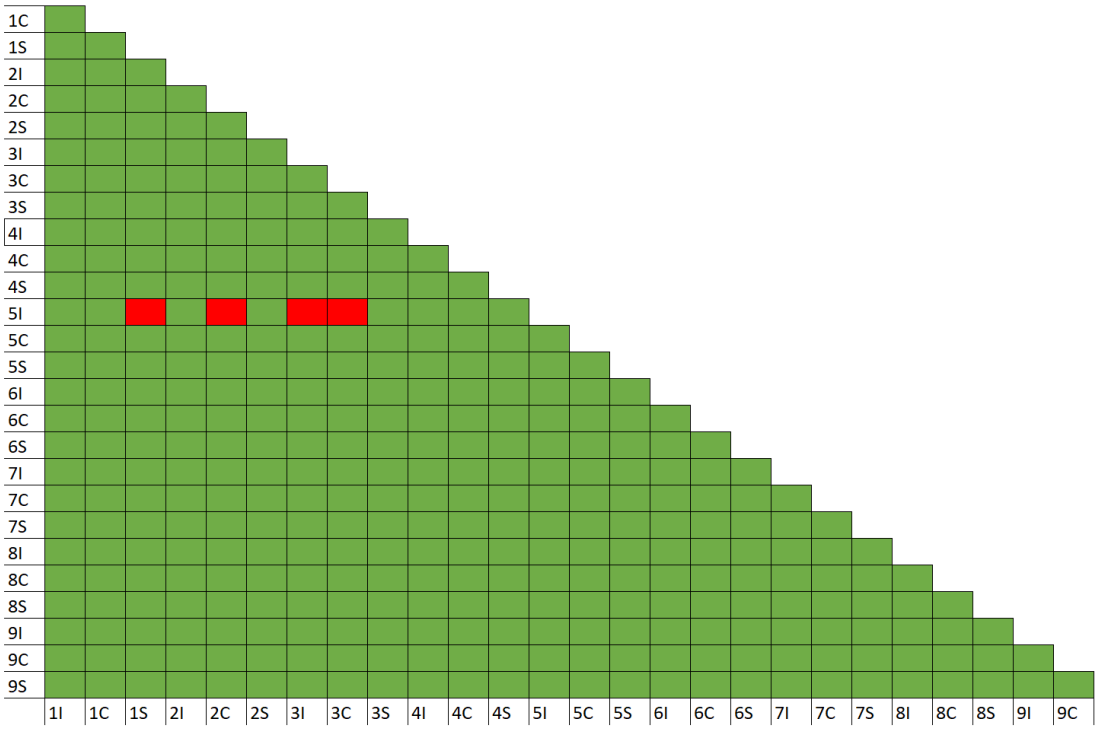

Figure 9.2: The significant differences present between VOIs for BV/TV at L3 within the fetal age cohort. Significant differences are denoted by red squares.

Overall, VOIs 5I and 5S continuously displayed higher values for BV/TV, although this was only significant at the level of L3. Generally, higher values were found within superior and inferior VOIs as opposed to central VOIs.

9.2.1.2 SMI

For structural model index within the fetal period, significant differences between VOIs were only present at the vertebral level L3. Descriptive statistics for L1, L3 and L5 can be found in Table 9.2.

Table 9.2: Descriptive statistics for SMI at L1, L3 and L5 in the fetal period.

	L1	L3	L5
Parametric?	NP	P	NP
F/H Value	37.846	4.235	35.438
DF	26	26	26
P Value	0.063	<0.001	0.102
p≤0.01?	N	Y	N
Mean/Median	Median	Mean	Median
1I	1.236	1.636	0.833
1C	1.065	1.694	1.207
1S	1.098	1.745	1.122
2I	1.201	1.705	1.066
2C	1.231	1.246	1.173
2S	1.208	1.472	1.207
3I	1.056	1.914	1.112
3C	1.033	1.697	1.159
3S	0.886	1.704	1.265
4I	0.960	1.464	1.104
4C	1.002	1.259	1.045
4S	1.050	1.431	0.993
5I	0.399	0.603	0.582
5C	0.160	0.239	0.434
5S	0.354	0.520	0.780
6I	1.008	1.496	0.996
6C	0.852	1.385	1.127
6S	0.939	1.571	1.121
7I	1.091	1.459	1.460
7C	1.123	1.720	1.148
7S	1.126	1.467	1.332
8I	1.172	0.814	0.896
8C	-0.079	0.101	0.506
8S	0.649	0.932	0.719
9I	0.894	1.800	1.153
9C	1.105	1.497	1.200
9S	1.183	1.670	1.298

At L1, median values ranged between -0.079 (8C) and 1.236 (1I). At the level of L3, mean values ranged between 0.101 (8C) and 1.914 (3I). At L3, VOI 8C displayed significantly lower values for SMI compared to VOIs 1I, 1C, 1S, 2I, 3I, 3C, 3S, 7C, 9I and 9S. VOI 5C also displayed a significantly lower value for SMI, differing from 1S, 3I and 9I. The high, intermediate and low values per VOI for SMI can be viewed in figure 9.3. The significant differences between VOIs can be found in Figure 9.4. At the level of L5, average values ranged between 0.434 (5C) and 1.460 (7I).

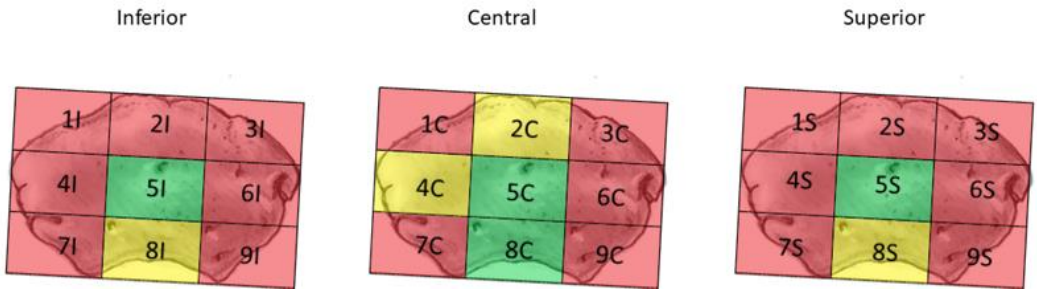

Figure 9.3: The high (red), intermediate (yellow) and low (green) mean values for SMI at L3 within the fetal age cohort.

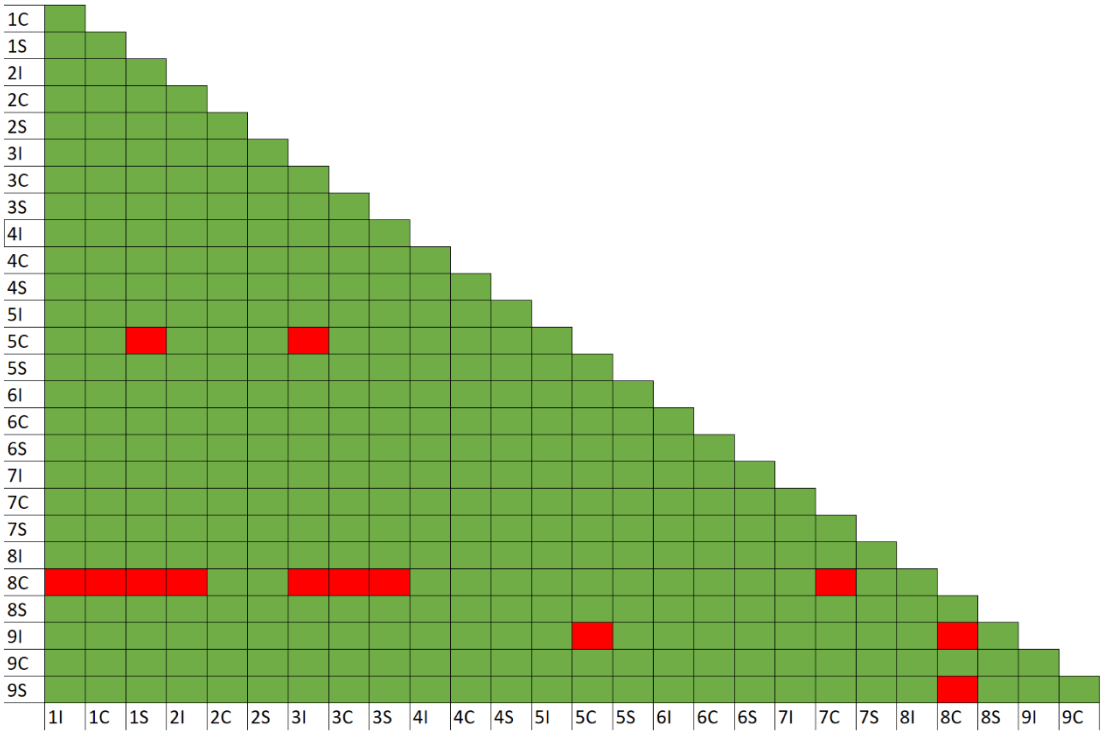

Figure 9.4: The significant differences present between VOIs for SMI at L3 within the fetal age cohort. Significant differences are denoted by red squares.

In summary, VOIs 5 and 8 (I, C and S) consistently displayed low values for SMI over the three vertebral levels, although not all were significantly different to other VOIs. Peripheral VOIs (1, 2, 3, 4, 6, 7 and 9) generally displayed higher values. While significant differences were present, all values for SMI indicate the trabecular architecture contains a mixture of plate-like and rod-like trabeculae, although it is possible those with higher values contain more rod-like trabeculae compared to plate-like.

9.2.1.3 Tb.Th

For trabecular thickness in the fetal period, the vertebral level L3 displayed significant differences between VOIs, while level L1 and L5 did not. The descriptive statistics for L1, L3 and L5 can be viewed in Table 9.3.

Table 9.3: Descriptive statistics for Tb.Th (μm) at L1, L3 and L5 in the fetal period.

	L1	L3	L5
Parametric?	NP	P	NP
F/H Value	43.370	3.104	43.628
DF	26	26	26
P Value	0.018	<0.001	0.017
p≤0.01?	N	Y	N
Mean/Median	Median	Mean	Median
1I	71.41	53.69	60.93
1C	78.61	62.81	74.08
1S	61.88	49.18	58.22
2I	81.84	62.71	74.42
2C	110.06	81.99	100.17
2S	76.12	65.37	72.66
3I	52.93	48.56	57.26
3C	72.21	64.06	69.01
3S	53.76	47.47	60.15
4I	88.35	68.91	82.67
4C	94.91	76.22	92.07
4S	83.36	64.58	76.43
5I	112.30	82.74	101.27
5C	124.47	97.88	134.04
5S	106.67	79.48	104.96
6I	89.16	66.44	76.24
6C	95.76	71.89	90.36
6S	81.88	61.67	80.78
7I	72.76	62.25	62.52
7C	78.97	61.90	75.03
7S	69.87	59.05	70.66
8I	82.16	74.64	86.51
8C	103.02	81.52	114.18
8S	82.03	69.12	94.09
9I	64.20	57.16	59.61
9C	71.74	61.43	53.43
9S	70.92	56.97	58.88

At the level of L1, average values ranged from 52.93µm (3I) to 124.47µm (5C). At L3, mean values ranged from 47.47µm (3S) to 97.88µm (5C). VOI 5C displayed the highest trabecular thickness and differed significantly from VOIs 1I, 1S, 3I and 3S. The high, intermediate and low values for Tb.Th can be viewed in figure 9.5, while significant differences between VOIs can be found in figure 9.6. Average values for L5 ranged from 53.43µm (9C) to 134.04µm (5C).

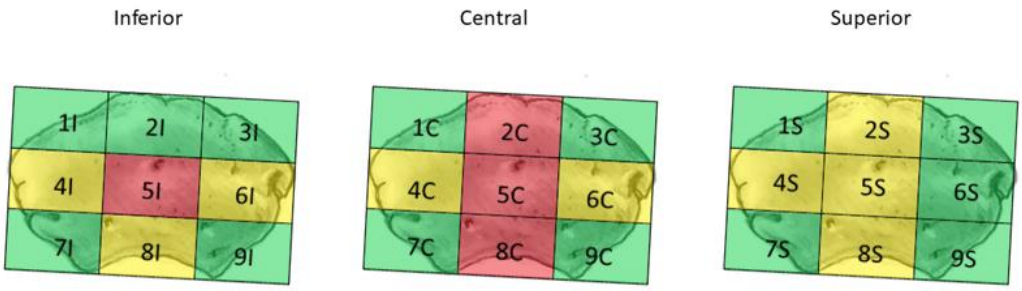

Figure 9.5: The high (red), intermediate (yellow) and low (green) median values for Tb.Th (µm) at L3 within the fetal age cohort.

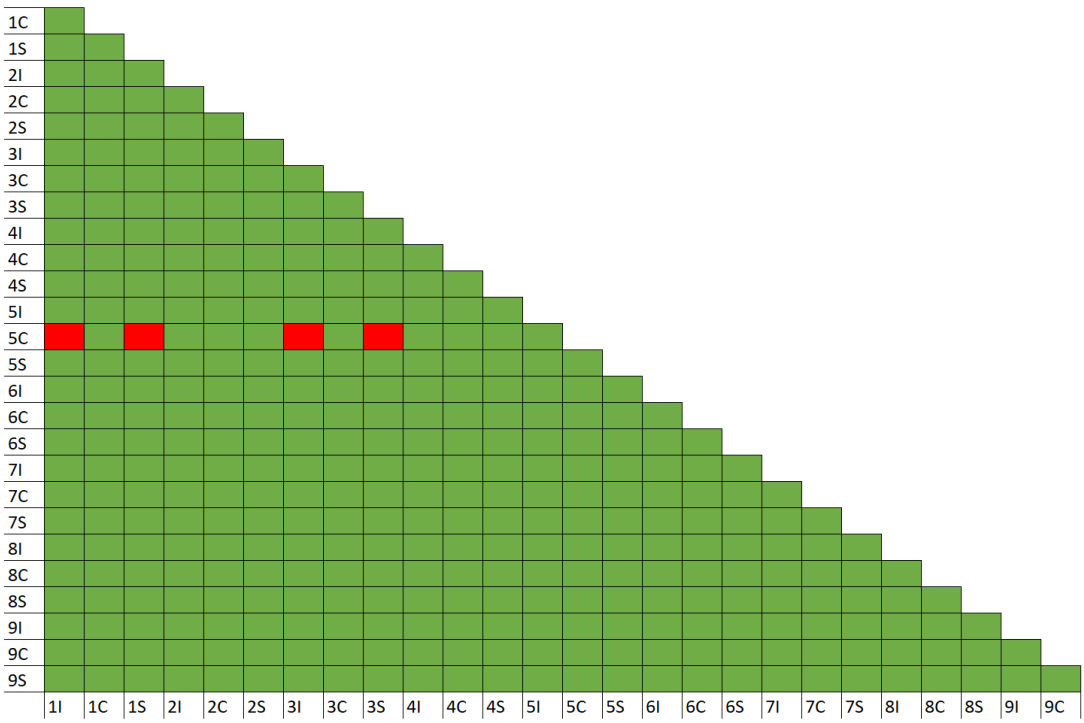

Figure 9.6: The significant differences present between VOIs for Tb.Th at L3 within the fetal age cohort. Significant differences are denoted by red squares.

While only the 3rd lumbar vertebral level displayed significant differences between VOIs, a common pattern over the vertebral levels was present. Generally, central VOIs 2C, 5C and 8C displayed higher values for trabecular thickness, while peripheral VOIs within the superior and inferior layers, and lateral VOIs in the central layer displayed lower values.

9.2.1.4 Tb.N

For trabecular number in the fetal period, no significant differences between VOIs were present for any vertebral level studied. Descriptive statistics for L1, L3 and L5 can be found in Table 9.4.

Table 9.4: Descriptive statistics for Tb.N (μm^{-1}) at L1, L3 and L5 in the fetal period.

	L1	L3	L5
Parametric?	NP	P	NP
F/H Value	33.717	1.103	34.789
DF	26	26	26
P Value	0.142	0.371	0.116
p≤0.01?	N	N	N
Mean/Median	Median	Mean	
1I	0.00455	0.00534	0.00594
1C	0.00416	0.00360	0.00413
1S	0.00545	0.00445	0.00570
2I	0.00371	0.00401	0.00435
2C	0.00260	0.00262	0.00292
2S	0.00443	0.00383	0.00442
3I	0.00626	0.00442	0.00583
3C	0.00443	0.00347	0.00447
3S	0.00629	0.00481	0.00519
4I	0.00432	0.00426	0.00451
4C	0.00377	0.00367	0.00371
4S	0.00435	0.00408	0.00485
5I	0.00376	0.00441	0.00415
5C	0.00277	0.00318	0.00274
5S	0.00415	0.00432	0.00388
6I	0.00417	0.00400	0.00508
6C	0.00389	0.00371	0.00386
6S	0.00451	0.00405	0.00439
7I	0.00491	0.00462	0.00496
7C	0.00437	0.00387	0.00435
7S	0.00499	0.00456	0.00511
8I	0.00392	0.00442	0.00485
8C	0.00326	0.00331	0.00325
8S	0.00426	0.00431	0.00431
9I	0.00574	0.00419	0.00586
9C	0.00473	0.00425	0.00514
9S	0.00505	0.00422	0.00503

At the level of the 1st lumbar vertebra, values ranged between 0.00277μm^{-1} (5C) and 0.00626μm^{-1} (3I). At L3, values ranged between 0.00262μm^{-1} (2C) and 0.00534μm^{-1} (1I). Values for L5 ranged between 0.00274μm^{-1} (5C) and 0.00594μm^{-1} (1I).

9.2.1.5 Tb.Sp

For trabecular separation in the fetal period, no significant differences were found between VOIs at any vertebral level within the fetal age cohort. Descriptive statistics can be found in Table 9.5.

Table 9.5: Descriptive statistics for Tb.Sp (µm) at L1, L3 and L5 in the fetal period.

	L1	L3	L5
Parametric?	NP	NP	NP
F/H Value	30.590	37.320	25.968
DF	26	26	26
P Value	0.244	0.070	0.465
p≤0.01?	N	N	N
Mean/Median	Median	Median	Median
1I	153.34	121.69	126.37
1C	177.62	188.16	170.77
1S	132.37	163.82	124.23
2I	196.27	154.94	171.23
2C	302.94	367.23	253.91
2S	161.84	188.36	159.90
3I	116.47	134.82	130.19
3C	162.70	188.71	164.55
3S	122.44	109.52	143.13
4I	157.70	136.38	153.14
4C	184.76	164.41	183.29
4S	156.24	159.03	147.19
5I	186.08	187.29	175.88
5C	318.32	264.40	307.84
5S	164.58	167.83	179.86
6I	166.65	149.21	135.91
6C	173.92	160.76	172.92
6S	150.77	152.30	152.31
7I	142.11	130.36	137.77
7C	153.34	174.24	168.08
7S	132.96	140.32	134.94
8I	216.30	172.25	136.37
8C	342.41	338.47	260.94
8S	188.74	143.90	186.03
9I	136.11	137.67	127.70
9C	148.14	155.22	156.80
9S	133.31	158.07	153.00

Values for L1 ranged between 116.47µm (3I) and 342.41µm (8C). At L3, median values ranged between 109.52µm (3S) and 367.23µm (2C). At L5, median values ranged between 124.229µm (1S) and 307.835µm (5C). However, central VOIs 2C, 5C and 8C generally displayed higher trabecular separation than VOIs within the superior and inferior layers.

9.2.1.6 DA

For degree of anisotropy in the fetal period, no significant differences were present between VOIs for any vertebral level studied. The descriptive statistics can be found in Table 9.6.

Table 9.6: Descriptive statistics for DA at L1, L3 and L5 in the fetal period.

	L1	L3	L5
Parametric?	NP	P	NP
F/H Value	38.279	2.158	35.883
DF	26	26	26
P Value	0.057	0.009	0.094
p≤0.01?	N	N	N
Mean/Median	Median	Mean	Median
1I	0.357	0.297	0.335
1C	0.368	0.264	0.397
1S	0.372	0.396	0.394
2I	0.254	0.351	0.379
2C	0.326	0.261	0.318
2S	0.31	0.365	0.298
3I	0.434	0.348	0.381
3C	0.432	0.375	0.472
3S	0.393	0.425	0.396
4I	0.379	0.431	0.365
4C	0.584	0.474	0.480
4S	0.489	0.428	0.431
5I	0.266	0.391	0.315
5C	0.337	0.269	0.187
5S	0.398	0.371	0.190
6I	0.394	0.435	0.358
6C	0.515	0.499	0.452
6S	0.446	0.344	0.408
7I	0.46	0.452	0.368
7C	0.531	0.510	0.392
7S	0.517	0.465	0.466
8I	0.364	0.410	0.341
8C	0.308	0.324	0.304
8S	0.459	0.393	0.313
9I	0.409	0.411	0.447
9C	0.454	0.397	0.380
9S	0.45	0.355	0.485

At L1, median values ranged between 0.254 (2I) and 0.584 (4C). Values at the level of L3 ranged between 0.261 (2C) and 0.510 (7C). At L5, values ranged between 0.187 (5C) and 0.485 (9S).

9.2.2 *Perinatal Age Cohort*

9.2.2.1 BV/TV

For bone volume fraction in the perinatal period, no significant differences were present at any vertebral level studied. Descriptive statistics can be viewed in Table 9.7.

Table 9.7: Descriptive statistics for BV/TV (%) at L1, L3 and L5 in the perinatal period.

	L1	L3	L5
Parametric?	P	NP	NP
F/H Value	1.194	26.450	32.981
DF	26	26	26
P Value	0.238	0.439	0.163
p≤0.01?	N	N	N
Mean/Median	Mean	Median	Median
1I	26.61	20.20	33.93
1C	25.21	20.44	27.51
1S	24.54	20.73	32.36
2I	27.11	24.28	39.96
2C	24.33	27.16	32.36
2S	26.10	24.39	31.92
3I	24.91	23.71	32.03
3C	23.74	21.70	27.43
3S	23.41	24.14	31.07
4I	29.39	25.04	35.12
4C	24.75	20.69	27.05
4S	25.38	25.24	35.25
5I	32.02	28.94	37.68
5C	30.59	25.22	35.31
5S	28.42	30.75	37.61
6I	28.64	25.67	32.56
6C	24.16	20.11	29.55
6S	25.54	24.90	37.07
7I	31.27	25.45	34.78
7C	22.24	20.30	27.35
7S	25.67	25.97	38.10
8I	30.23	28.14	32.71
8C	30.92	27.90	32.71
8S	27.10	23.66	36.48
9I	29.92	22.90	30.26
9C	22.10	17.42	27.01
9S	25.25	26.49	35.54

At the level of L1, values ranged from 22.10% (9C) to 32.02% (5I). At L3, BV/TV ranged between 17.42% (9C) to 30.75% (5S). L5 values ranged between 27.01% (9C) to 39.96% (2I). While no significant differences between VOIs were present for BV/TV in the perinatal age cohort, VOIs within the superior and inferior layers generally displayed higher BV/TV. Central VOIs 1,3,4,6,7 and 9 generally displayed lower BV/TV.

9.2.2.2 SMI

For structural model index in the perinatal period, vertebral levels L1 and L3 displayed significant differences between VOIs. Descriptive statistics can be found in Table 9.8.

Table 9.8: Descriptive statistics for SMI at L1, L3 and L5 in the perinatal period.

	L1	L3	L5
Parametric?	NP	NP	NP
F/H Value	69.817	77.477	48.323
DF	26	26	26
P Value	<0.001	<0.001	0.005
p≤0.01?	Y	Y	N
Mean/Median	Median	Median	Median
1I	1.612	1.813	1.178
1C	1.366	1.620	1.265
1S	1.636	1.831	1.342
2I	1.351	1.593	0.620
2C	1.294	1.111	0.617
2S	1.361	1.572	1.033
3I	1.399	1.717	1.345
3C	1.592	1.647	1.278
3S	1.613	1.688	1.308
4I	1.224	1.417	0.969
4C	1.591	1.758	1.357
4S	1.407	1.539	0.841
5I	1.080	1.212	0.780
5C	0.894	0.718	0.667
5S	1.392	1.219	0.759
6I	1.160	1.367	1.081
6C	1.457	1.686	1.328
6S	1.470	1.439	0.809
7I	1.246	1.449	1.165
7C	1.869	1.750	1.301
7S	1.705	1.474	0.886
8I	1.194	1.251	0.929
8C	-0.039	0.213	0.122
8S	1.369	1.327	0.679
9I	1.302	1.601	1.249
9C	1.633	1.841	1.483
9S	1.663	1.460	1.094

For L1, values ranged between -0.0390 (8C) and 1.869 (7C). VOI 8C displayed the lowest median value for SMI and differed significantly from VOIs 1S, 3S, 7C and 9C. The high, intermediate and low median values can be viewed in figure 9.7. Significant differences can be visualised in figure 9.8.

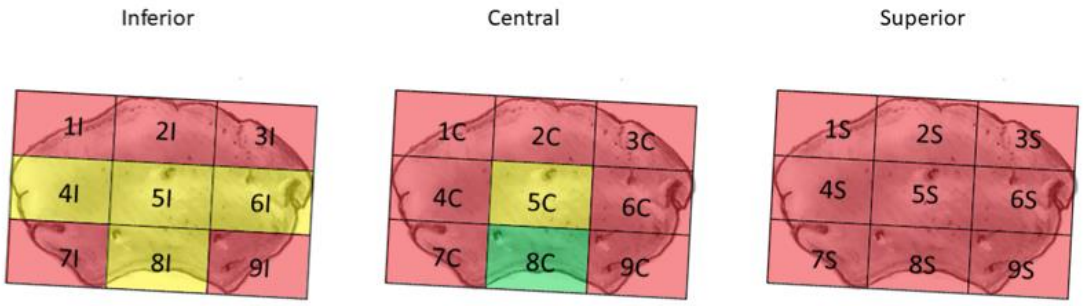

Figure 9.7: The high (red), intermediate (yellow) and low (green) median values for SMI at L1 within the perinatal age cohort.

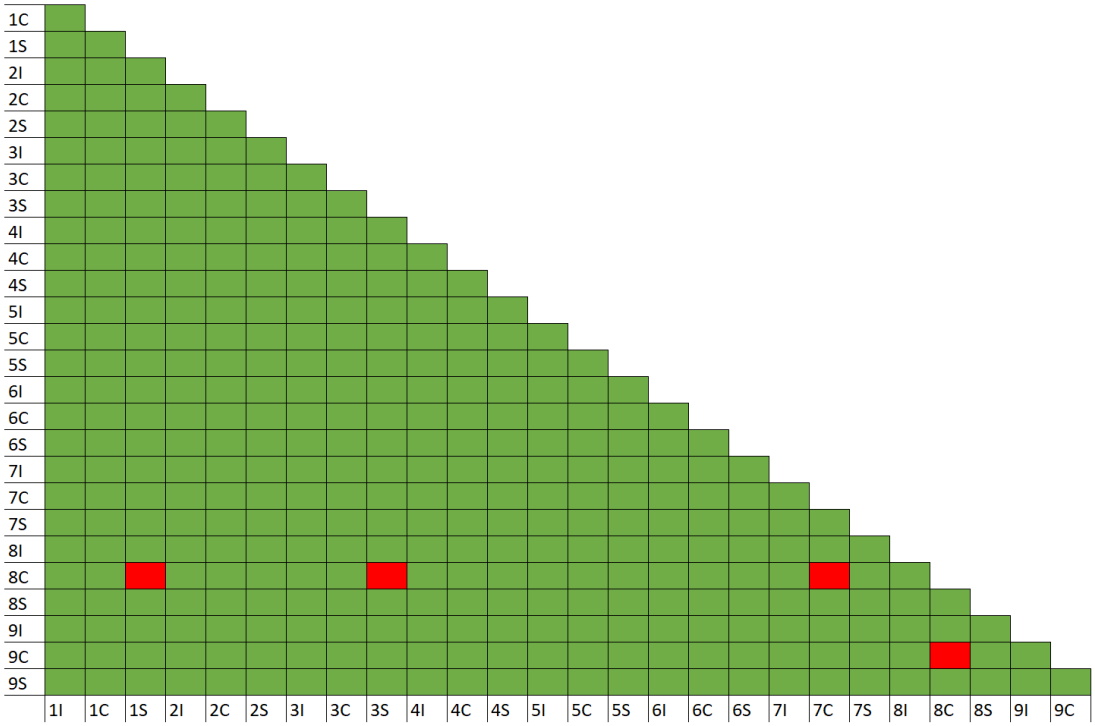

Figure 9.8: The significant differences present between VOIs for SMI at L1 within the perinatal age cohort. Significant differences are denoted by red squares.

At L3, values ranged from 0.213 (8C) to 1.841 (9C). As with L1, VOI 8C displayed the lowest SMI. This VOI differed significantly from VOIs 1I, 1S, 3I, 4C, 6C, 7C and 9C. No other significant differences were present. The high,

intermediate and low median values for this dataset per VOI can be found in figure 9.9. Significant differences can be visualised in figure 9.10.

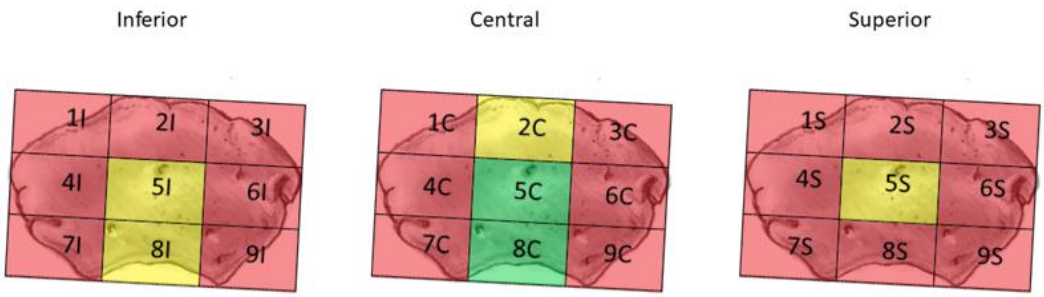

Figure 9.9: The high (red), intermediate (yellow) and low (green) median values for SMI at L3 within the perinatal age cohort.

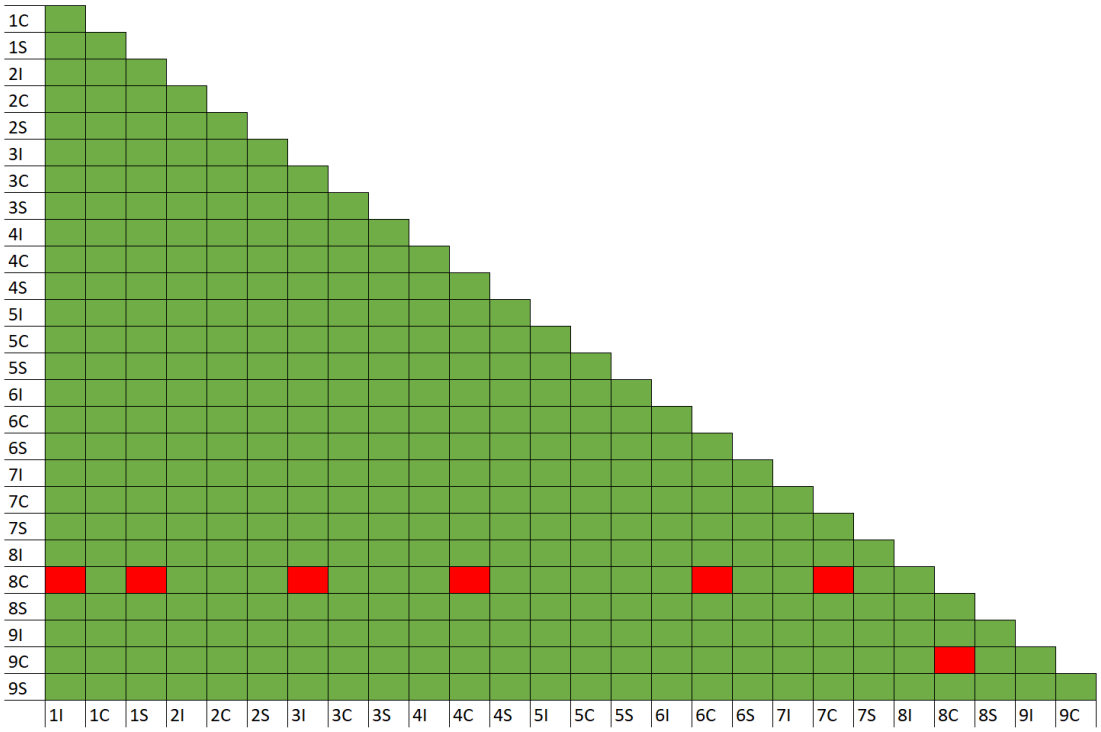

Figure 9.10: The significant differences present between VOIs for SMI at L3 within the perinatal age cohort. Significant differences are denoted by red squares.

At L5, Values for SMI ranged from 0.122 (8C) to 1.483 (9C). For SMI within the perinatal age cohort, peripheral VOIs within the inferior, central and superior layers generally displayed higher SMI values, while central VOIs, in particular 8C, displayed lower SMI values. VOI 8C displayed predominantly plate-like trabeculae, while SMI values for other VOIs displayed transitional architecture with plate-like and rod-like trabeculae.

9.2.2.3 Tb.Th

For trabecular thickness in the perinatal period, all three vertebral levels displayed differences between VOIs. The descriptive statistics for L1, L3 and L5 can be viewed in Table 9.9.

Table 9.9: Descriptive statistics for Tb.Th (μm) at L1, L3 and L5 in the perinatal period.

	L1	L3	L5
Parametric?	NP	NP	NP
F/H Value	159.453	138.077	147.111
DF	26	26	26
P Value	<0.001	<0.001	<0.001
p≤0.01?	Y	Y	Y
Mean/Median	Median	Median	Median
1I	92.19	80.65	111.24
1C	114.84	90.98	130.35
1S	82.58	77.75	110.54
2I	98.05	86.93	117.54
2C	128.29	110.48	159.70
2S	93.95	90.30	118.73
3I	84.35	80.35	110.85
3C	106.16	99.45	131.14
3S	81.85	79.13	110.78
4I	100.00	89.99	116.33
4C	114.49	103.17	131.32
4S	91.84	90.24	122.56
5I	113.01	103.10	143.81
5C	129.42	122.13	148.83
5S	106.81	103.49	136.30
6I	96.84	90.02	116.74
6C	110.37	103.52	134.95
6S	90.57	87.11	123.43
7I	98.60	85.28	110.90
7C	98.74	90.86	122.24
7S	84.22	79.73	114.97
8I	105.42	93.86	124.90
8C	129.72	115.05	169.60
8S	93.38	93.05	131.04
9I	92.80	84.80	115.43
9C	95.77	89.96	127.08
9S	83.89	84.57	119.10

At L1, median values for Tb.Th ranged between 81.85µm (3S) and 129.72µm. (5C). Central VOIs 1C, 2C, 4C, 5C, 6C and 8C displayed significantly higher Tb.Th. VOI 5C displayed the highest value of all VOIs and differed significantly to 1I, 1S, 2S, 3I, 3S, 4S, 6S, 7S and 9S. VOI 8C differed from those stated above excluding 2S. VOI 2C differed from 1I, 1S, 3I, 3S, 7S and 9S. VOI 4C differed from 1S and 3S, while 1C and 6C differed from 3S only. The high, intermediate and low median values for Tb.Th can be viewed in figure 9.11. The significant differences between VOIs for this dataset can be visualised in figure 9.12.

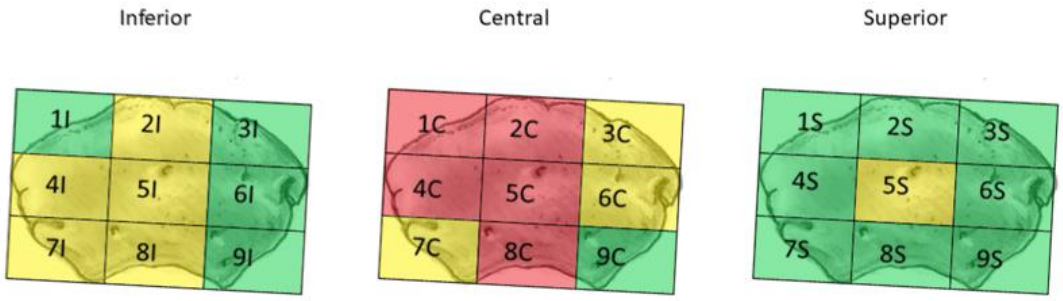

Figure 9.11: The high (red), intermediate (yellow) and low (green) median values for Tb.Th (µm) at L1 within the perinatal age cohort.

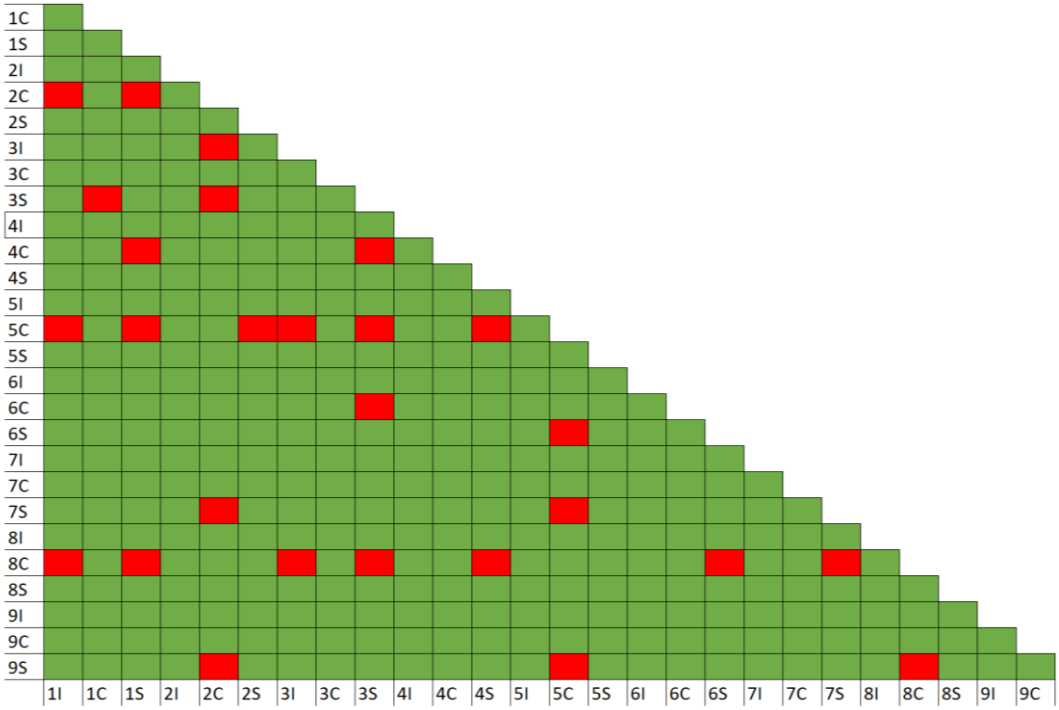

Figure 9.12: The significant differences present between VOIs for Tb.Th at L1 within the perinatal age cohort. Significant differences are denoted by red squares.

At the level of L3, values ranged between 77.75µm (1S) and 122.13µm (5C).Central VOIs once again displayed the highest values for Tb.Th, with VOI 5C displaying the highest value and differing from VOIs 1I, 1S, 3I, 3S, 7I, 7S and 9S. VOI 8C differed from the same individuals as 5C excluding 9S. VOI 2C differed from the superior and inferior layers of VOIs 1 and 3, while 4C, 5I and 6C differed from 1S. The high, intermediate and low median values can be viewed in figure 9.13, while the significant differences between VOIs can be visualised in figure 9.14.

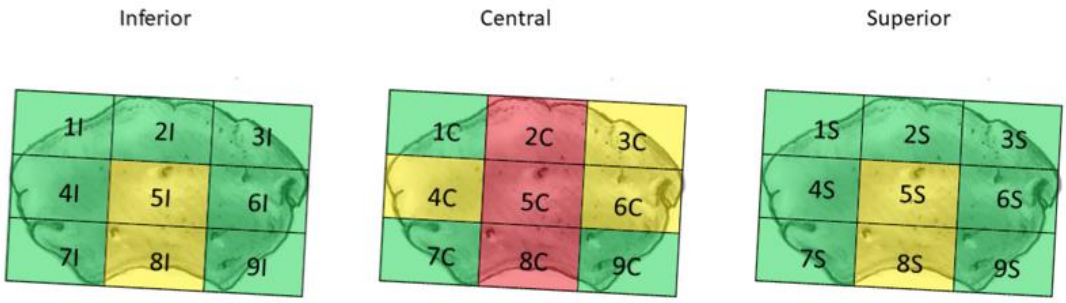

Figure 9.13: The high (red), intermediate (yellow) and low (green) median values for Tb.Th (µm) at L3 within the perinatal age cohort.

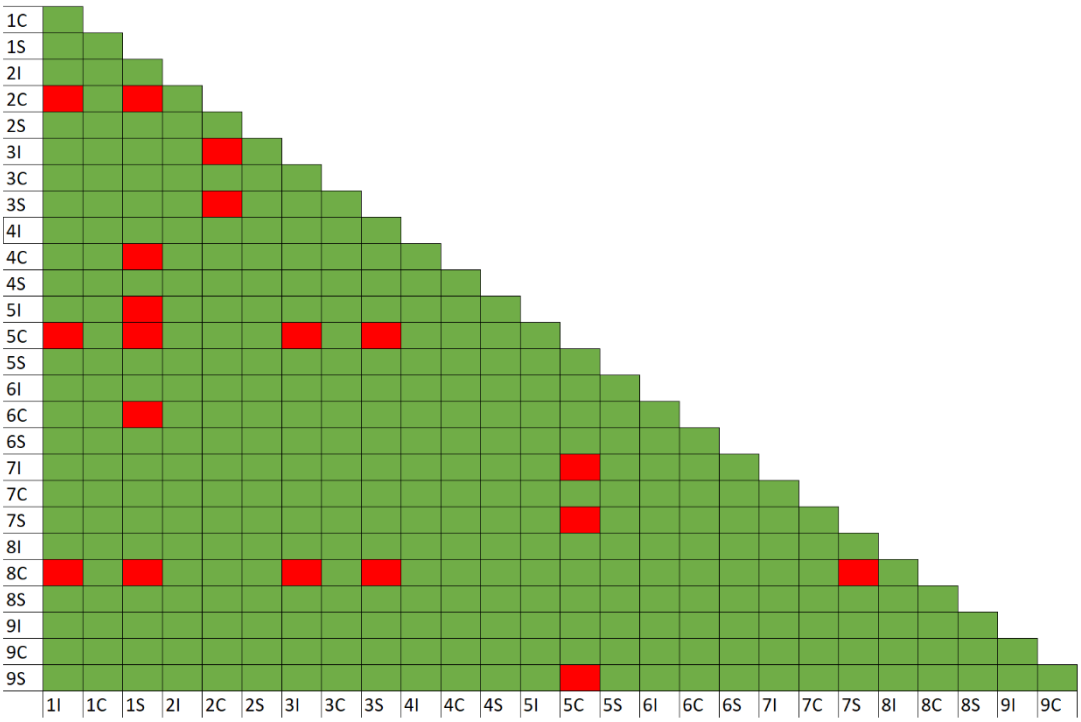

Figure 9.14: The significant differences present between VOIs for Tb.Th at L3 within the perinatal age cohort. Significant differences are denoted by red squares.

At L5, values ranged from 110.54µm (1S) to 169.60µm (8C). Central VOI 8C displayed the highest trabecular thickness within this dataset, and differed significantly from VOIs 1I, 1S, 2I, 2S, 3I, 3S, 6I, 7I, 7S, 9I and 9S. VOIs 2C and 5C exhibited significantly higher Tb.Th compared to 1I, 1S, 3I and 3S, while 5I displayed significantly higher Tb.Th to 1I and 3I. The high, intermediate and low median values for Tb.Th per VOI can be viewed in figure 9.15, while significant differences between VOIs can be visualised in figure 9.16.

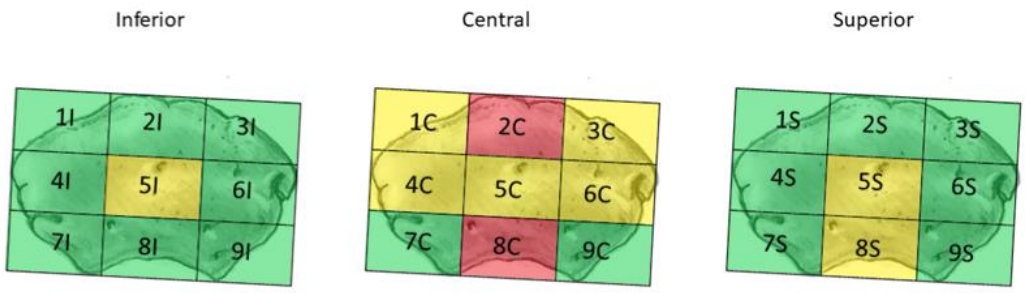

Figure 9.15: The high (red), intermediate (yellow) and low (green) median values for Tb.Th (µm) at L5 within the perinatal age cohort.

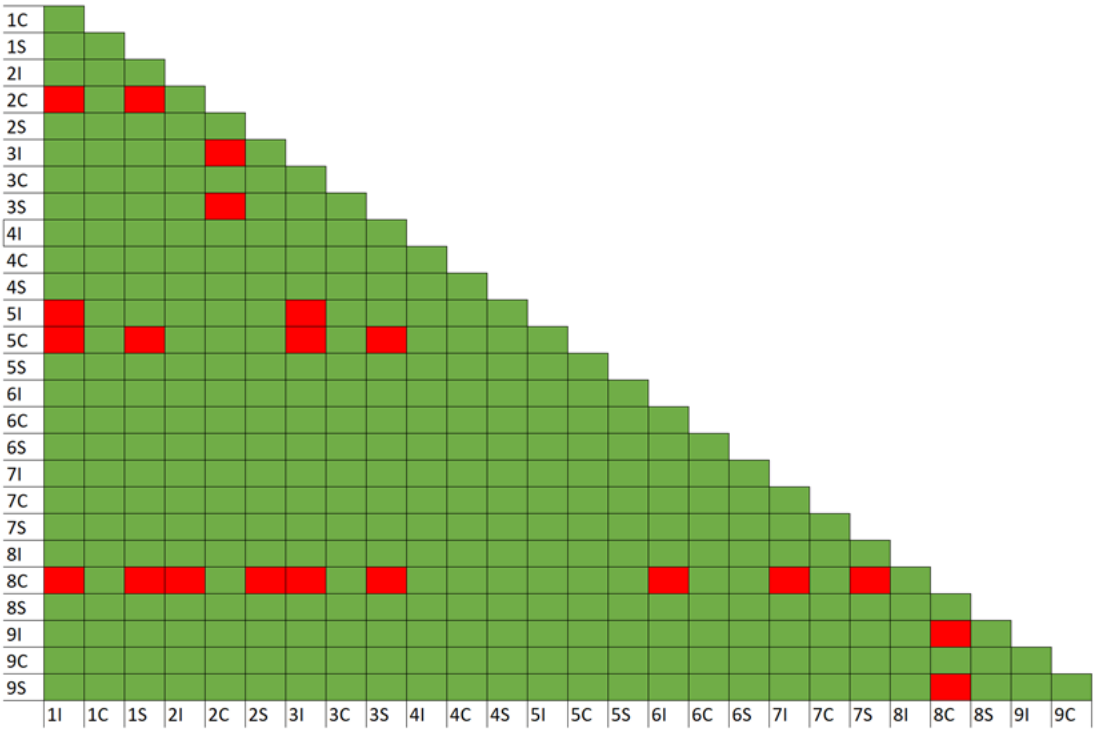

Figure 9.16: The significant differences present between VOIs for Tb.Th at L5 within the perinatal age cohort. Significant differences are denoted by red squares.

For trabecular thickness, central VOIs 2C, 5C and 8C consistently displayed higher values compared to other VOIs over all three vertebral levels studied. In many cases, these values were significantly different. Generally, VOIs within the superior and inferior layers, and at the periphery (1, 2, 3, 4, 6, 7 and 9) displayed lower values for trabecular thickness.

9.2.2.4 Tb.N

For trabecular number within the perinatal period, no significant differences were found between VOIs for any vertebral level studied. The descriptive statistics for the datasets of L1, L3 and L5 can be found in Table 9.10.

Table 9.10: Descriptive statistics for Tb.N (μm^{-1}) at L1, L3 and L5 in the perinatal period.

	L1	L3	L5
Parametric?	NP	NP	NP
F/H Value	84.272	53.999	93.463
DF	26	26	26
P Value	<0.001	0.001	<0.001
p≤0.01?	N	N	N
Mean/Median	Median	Median	Median
1I	0.00309	0.00254	0.00302
1C	0.00213	0.00213	0.00218
1S	0.00306	0.00260	0.00268
2I	0.00290	0.00275	0.00324
2C	0.00195	0.00202	0.00199
2S	0.00272	0.00262	0.00285
3I	0.00322	0.00291	0.00294
3C	0.00221	0.00204	0.00218
3S	0.00290	0.00295	0.00291
4I	0.00299	0.00285	0.00290
4C	0.00204	0.00192	0.00214
4S	0.00284	0.00277	0.00292
5I	0.00279	0.00267	0.00276
5C	0.00219	0.00194	0.00210
5S	0.00255	0.00277	0.00267
6I	0.00322	0.00278	0.00282
6C	0.00221	0.00190	0.00225
6S	0.00266	0.00271	0.00314
7I	0.00324	0.00306	0.00283
7C	0.00212	0.00215	0.00224
7S	0.00284	0.00297	0.00332
8I	0.00310	0.00274	0.00279
8C	0.00202	0.00213	0.00202
8S	0.00286	0.00249	0.00282
9I	0.00332	0.00272	0.00274
9C	0.00226	0.00190	0.00221
9S	0.00279	0.00298	0.00335

At the level of L1, median values ranged from 0.00195μm^{-1} (2C) to 0.00332μm^{-1} (9I). At L3, values for Tb.N ranged between 0.00190μm^{-1} (9C) and 0.00306μm^{-1} (7I). At L5, the median values ranged from 0.00199μm^{-1} (2C) to 0.00335μm^{-1} (9S). While no significant differences were present between VOIs within the perinatal cohort for Tb.N, the central layer of VOIs display lower values compared to the superior and inferior layers. Within the superior and inferior layers, VOI 5 consistently displayed an intermediate number of trabeculae.

9.2.2.5 Tb.Sp

For trabecular separation within the perinatal period, all three vertebral levels studied displayed significant differences. Descriptive statistics can be viewed in Table 9.11.

Table 9.11: Descriptive statistics for Tb.Sp (μm) at L1, L3 and L5 in the perinatal period.

	L1	L3	L5
Parametric?	NP	NP	NP
F/H Value	133.449	105.198	138.759
DF	26	26	26
P Value	<0.001	<0.001	<0.001
p≤0.01?	Y	Y	Y
Mean/Median	Median	Median	Median
1I	211.82	223.12	189.58
1C	301.06	273.98	269.46
1S	199.28	222.02	194.10
2I	214.15	231.99	191.98
2C	402.32	355.25	327.42
2S	235.89	234.11	203.07
3I	202.42	205.35	189.20
3C	284.16	289.88	254.06
3S	209.97	216.96	194.52
4I	232.89	233.91	209.82
4C	288.03	292.91	255.28
4S	218.39	228.03	192.96
5I	233.09	242.18	229.46
5C	346.42	366.34	350.63
5S	256.66	246.07	222.58
6I	208.80	232.18	215.88
6C	279.91	286.83	234.67
6S	234.75	242.10	196.03
7I	203.46	212.37	210.11
7C	265.99	260.68	247.96
7S	214.04	206.72	197.19
8I	228.85	260.33	217.24
8C	417.83	517.96	430.11
8S	234.97	282.34	209.88
9I	194.62	219.06	204.11
9C	253.79	281.05	241.66
9S	217.81	206.49	180.88

At the level of L1, median values for Tb.Sp ranged between 194.624µm (9I) and 417.833µm (8C). 194.624µm and 417.833µm. Central VOIs 8C, 2C and 5C displayed the highest Tb.Sp values respectively. VOI 8C differed from 1I, 1S, 2I, 3I, 3S, 6I, 7I, 7S, 9I and 9S. VOI 2C differed from the same VOIs excluding 2I. VOI 5C displayed significantly higher Tb.Sp compared to VOIs 7I and 9I. The high, intermediate and low median values can be viewed in figure 9.17. Significant differences between VOIs can be visualised in figure 9.18.

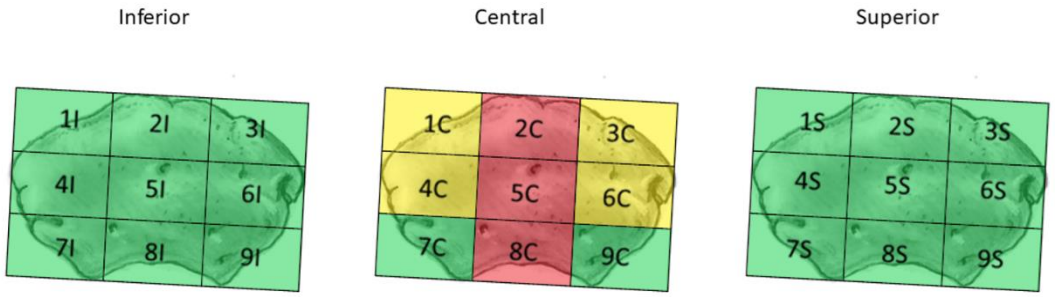

Figure 9.18: The high (red), intermediate (yellow) and low (green) median values for Tb.Sp (µm) at L1 within the perinatal age cohort.

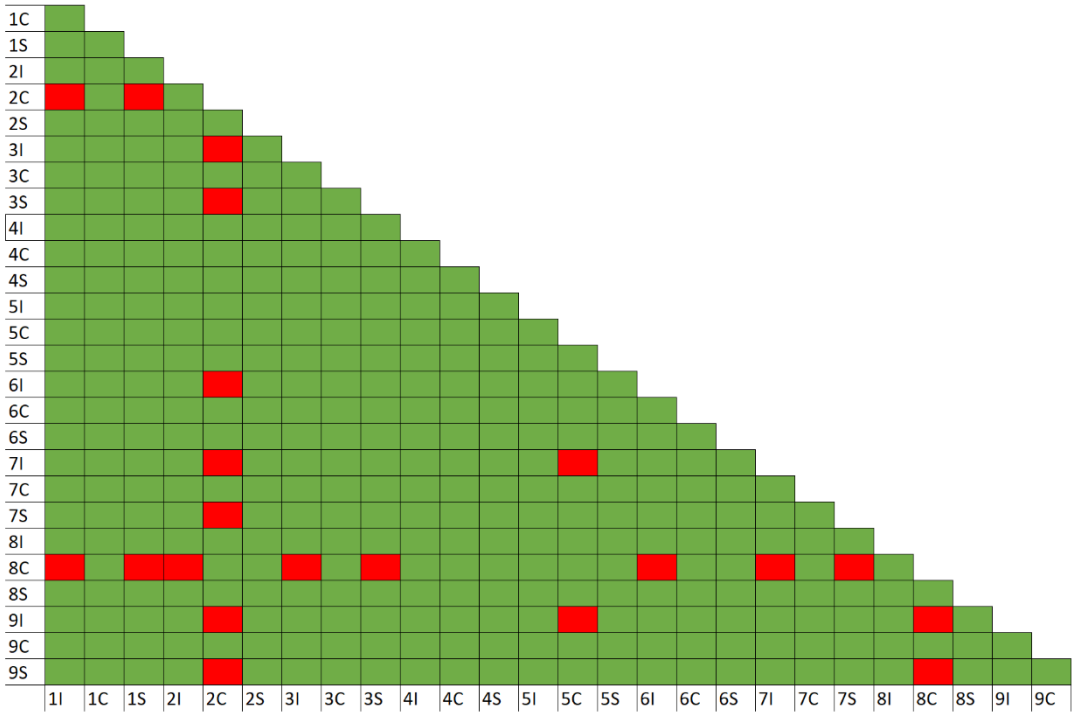

Figure 9.17: The significant differences present between VOIs for Tb.Sp at L1 within the perinatal age cohort. Significant differences are denoted by red squares.

At the level of L3, median values ranged from 205.349µm (3I) to 517.962µm (8C). Central VOIs 8C and 2C respectively displayed the highest values for trabecular separation. VOI 8C differed significantly from VOIs 1S, 3I, 3S, 7I, 7S and 9S while VOI 2C differed from 3S, 7I and 9S. The high, intermediate and low median values per VOI can be viewed in figure 9.19. Significant differences can be visualised in figure 9.20.

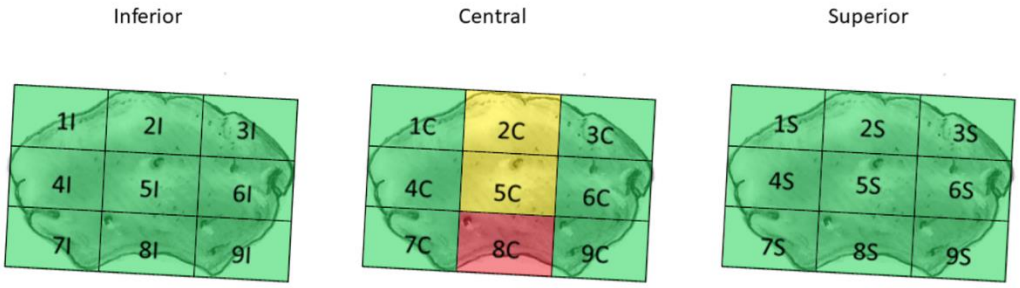

Figure 9.19: The high (red), intermediate (yellow) and low (green) median values for Tb.Sp (µm) at L3 within the perinatal age cohort.

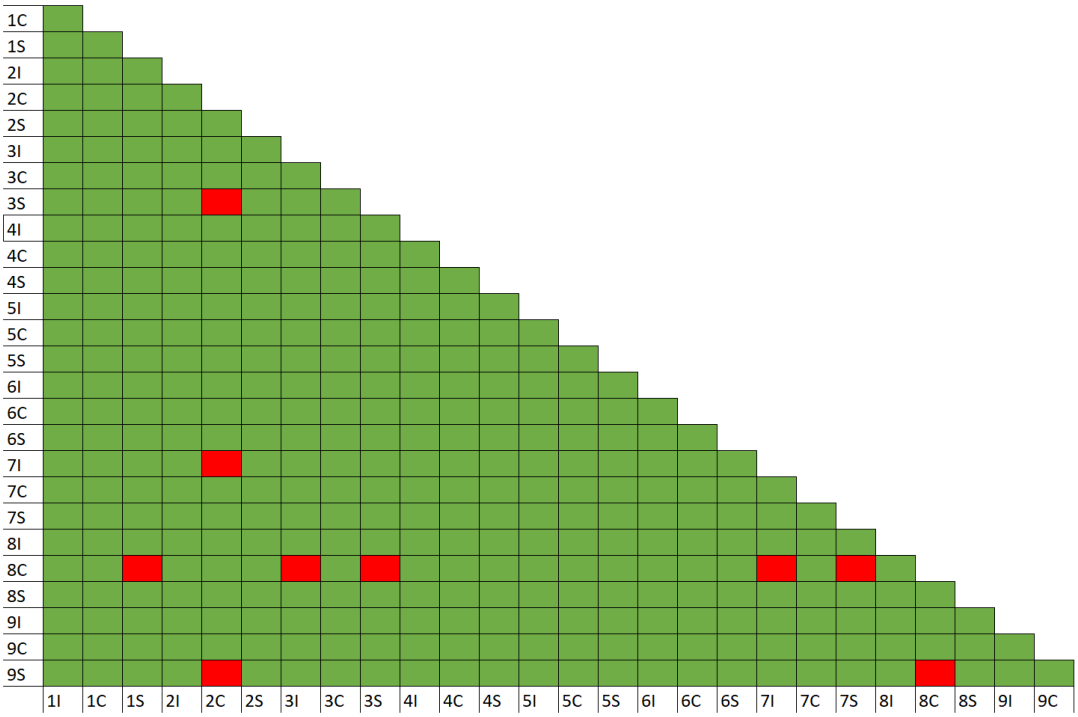

Figure 9.20: The significant differences present between VOIs for Tb.Sp at L3 within the perinatal age cohort. Significant differences are denoted by red squares.

The median values for Tb.Sp at L5 ranged between 180.878µm (9S) and 430.114µm (8C). As with previous vertebral levels, central VOIs 8C, 2C and 5C

displayed the highest values for Tb.Sp respectively. VOI 8C differed significantly from 1I, 1S, 2I, 2S, 3I, 3S, 4S, 6I, 6S, 7I, 7S, 9I and 9S, while 2C and 5C differed from 1I, 1S, 3I, 3S, 7S and 9S. The high, intermediate and low median values per VOI can be viewed in figure 9.21. Significant differences between VOIs can be visualised in figure 9.22.

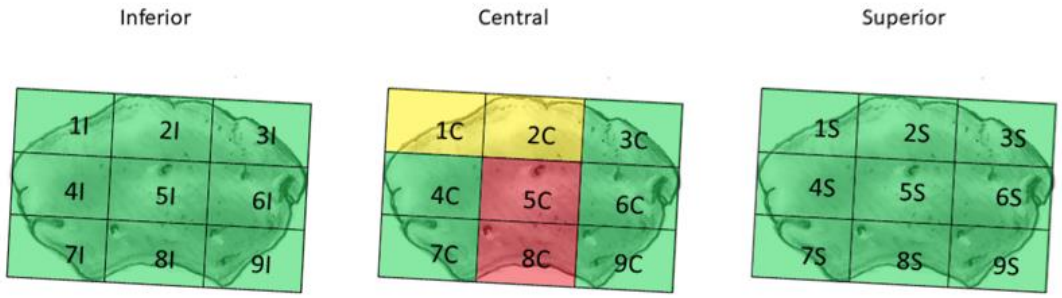

Figure 9.21: The high (red), intermediate (yellow) and low (green) median values for Tb.Sp (µm) at L5 within the perinatal age cohort.

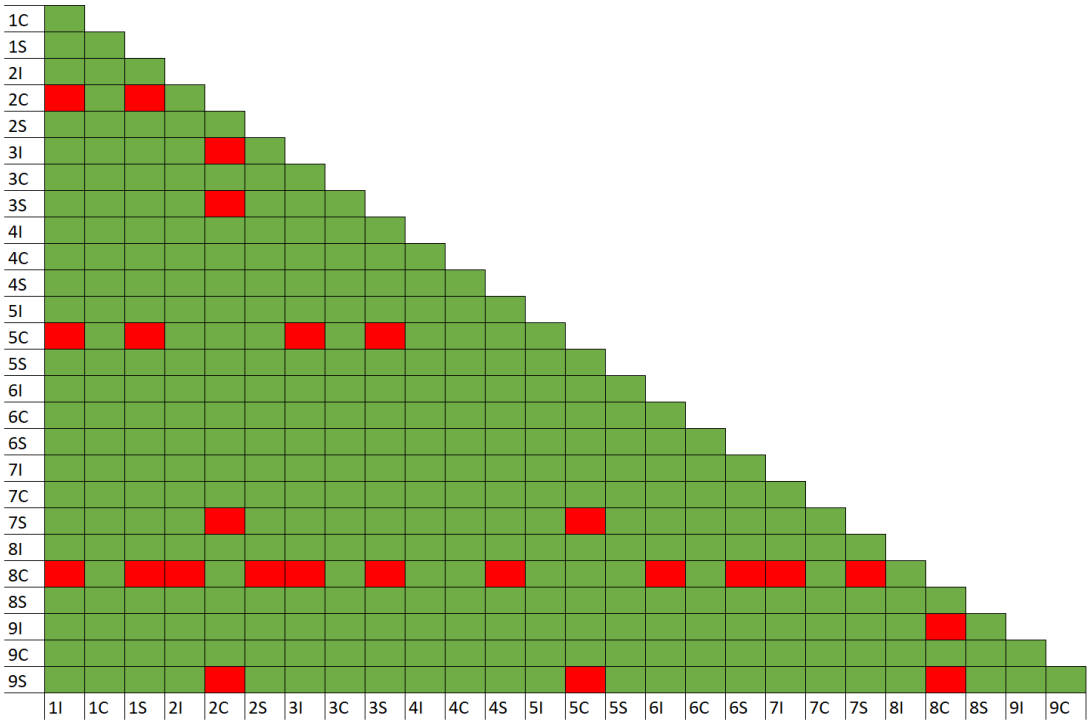

Figure 9.22: The significant differences present between VOIs for Tb.Sp at L5 within the perinatal age cohort. Significant differences are denoted by red squares.

Central VOIs 2C, 5C and 8C consistently display significantly higher trabecular separation compared to other VOIs over L1, L3 and L5. VOIs within the inferior and superior layers consistently displayed low trabecular separation.

9.2.2.6 DA

For degree of anisotropy within the perinatal period, the vertebral levels L1 and L3 displays significant differences between VOIs. The descriptive statistics for L1, L3 and L5 can be found in Table 9.12.

Table 9.12: Descriptive statistics for DA at L1, L3 and L5 in the perinatal period.

	L1	L3	L5
Parametric?	NP	P	NP
F/H Value	99.550	7.090	41.727
DF	26	26	26
P Value	<0.001	<0.001	0.026
p≤0.01?	Y	Y	N
Mean/Median	Median	Mean	Median
1I	0.427	0.350	0.505
1C	0.370	0.308	0.468
1S	0.375	0.379	0.500
2I	0.381	0.376	0.498
2C	0.25	0.264	0.476
2S	0.343	0.334	0.559
3I	0.376	0.406	0.431
3C	0.359	0.342	0.323
3S	0.407	0.386	0.511
4I	0.411	0.413	0.456
4C	0.392	0.368	0.384
4S	0.408	0.446	0.442
5I	0.351	0.359	0.395
5C	0.216	0.229	0.263
5S	0.338	0.356	0.407
6I	0.432	0.447	0.412
6C	0.406	0.351	0.378
6S	0.431	0.405	0.451
7I	0.412	0.418	0.480
7C	0.391	0.425	0.459
7S	0.422	0.448	0.435
8I	0.380	0.364	0.548
8C	0.259	0.218	0.705
8S	0.386	0.373	0.571
9I	0.443	0.418	0.401
9C	0.455	0.396	0.458
9S	0.432	0.409	0.470

Values for DA at the level of L1 ranged between 0.216 (5C) and 0.455 (9C). Central VOIs 5C, 8C and 2C displayed significantly lower values for degree of anisotropy respectively, with 5C differing from VOIs 1I, 4I, 4S, 6I, 6S, 7I, 7S, 9I, 9C and 9S. VOI 8C differed from 6S, 9C and 9S and 2C from 9C and 9S. The high, intermediate and low median values per VOI can be viewed in figure 9.23. Significant differences between VOIs can be visualised in figure 9.24.

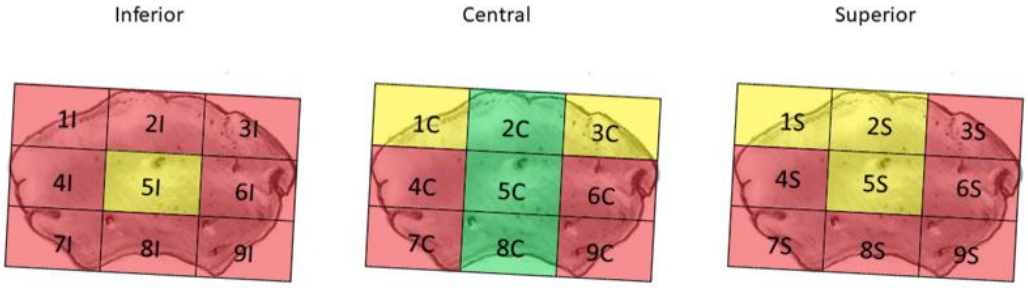

Figure 9.23: The high (red), intermediate (yellow) and low (green) median values for DA at L1 within the perinatal age cohort.

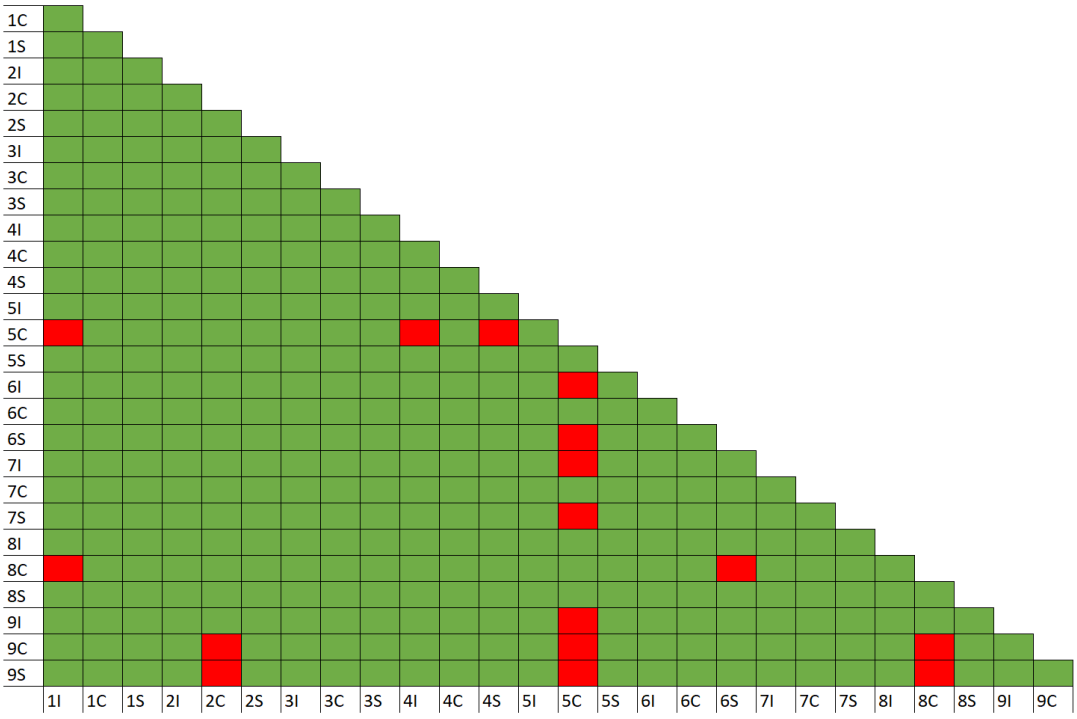

Figure 9.24: The significant differences present between VOIs for DA at L1 within the perinatal age cohort. Significant differences are denoted by red squares.

At L3, mean values ranged between 0.218 (8C) and 0.448 (7S). Central VOIs 8C, 5C and 2C displayed the lowest values respectively. VOI 8C differed from VOIs 1S, 2I, 3I, 3S, 4I, 4C, 4S, 4S, 5I, 5S, 6I, 6S, 7I, 7C, 8I, 8S, 9I, 9C and 9S. VOI 5C differed from 1S, 2I, 3I, 3S, 4I, 4C, 4S, 6I, 6S, 7I, 7C, 7S, 8I, 8S, 9I, 9C and 9S. VOI 2C differed from 3I, 4I, 4S, 6I, 6S, 7I, 7C, 7S, 9I and 9S. VOI 1C also displayed a relatively low value for DA and differed from VOIs 4S, 6I and 7S, all of whom displayed the highest DA values. VOI 7S, which displayed the highest value, also differed from 8I. The high, intermediate and low mean values per VOI can be viewed in figure 9.25. Significant differences between VOIs can be visualised in figure 9.26.

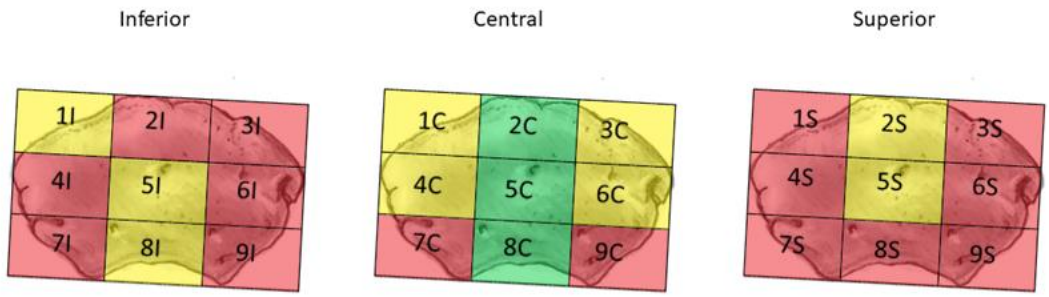

Figure 9.25: The high (red), intermediate (yellow) and low (green) mean values for DA at L3 within the perinatal age cohort.

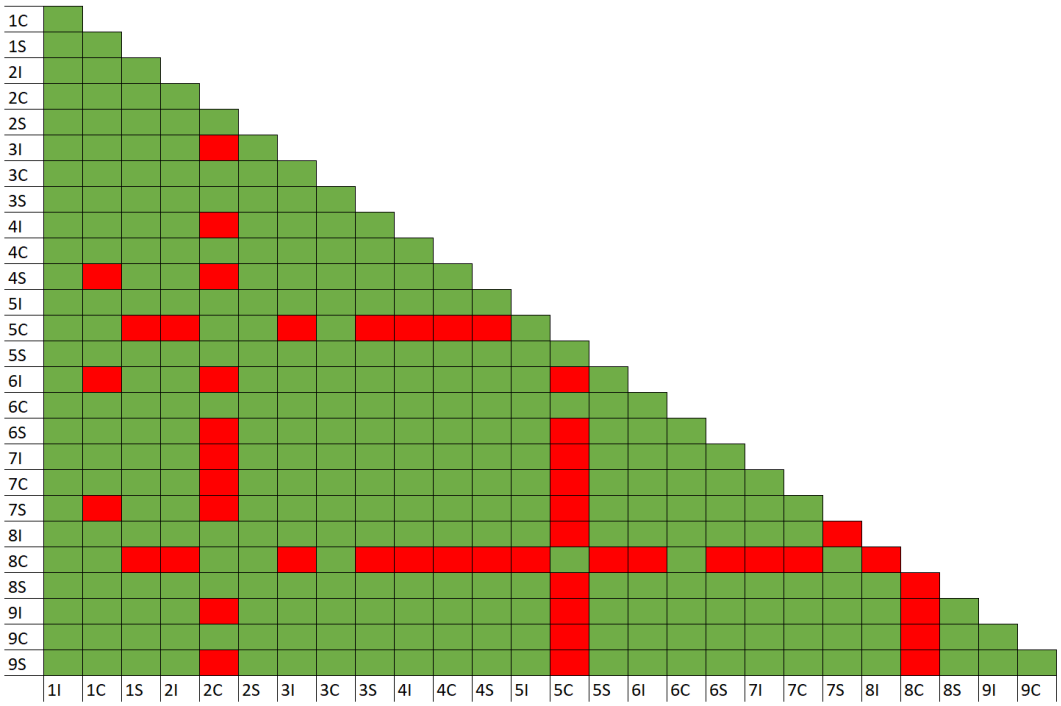

Figure 9.26: The significant differences present between VOIs for DA at L3 within the perinatal age cohort. Significant differences are denoted by red squares.

At the level of L5, values ranged between 0.263 (5C) and 0.705 (8C). In summary, central VOIs 2C, 5C and 8C displayed significantly lower values for DA compared to VOIs within the superior and inferior layers. This pattern was also present at the level of L5. Overall, values for DA indicated an isotropic structure within more central VOIs while some VOIs within the superior and inferior layers of the L5 vertebral centra displayed a more anisotropic structure.

9.2.3 *4 weeks to 2 years of age cohort*

9.2.3.1 BV/TV

For bone volume fraction within the 4wks-2y cohort, no significant differences were observed for any vertebral level studied Descriptive statistics can be viewed in Table 9.13.

Table 9.13: Descriptive statistics for BV/TV (%) at L1, L3 and L5 in the 4wks-2y cohort.

	L1	L3	L5
Parametric?	NP	NP	NP
F/H Value	72.982	59.601	23.611
DF	26	26	26
P Value	<0.001	<0.001	0.598
p≤0.01?	N	N	N
Mean/Median	Median	Median	Median
1I	18.39	13.95	15.67
1C	18.24	12.52	18.30
1S	14.35	13.32	17.90
2I	17.69	15.15	16.57
2C	15.51	12.95	15.87
2S	14.19	12.62	16.83
3I	18.89	16.16	19.14
3C	19.81	16.04	20.15
3S	15.47	12.94	20.59
4I	15.80	12.65	14.90
4C	12.25	10.54	14.11
4S	11.68	11.59	15.31
5I	14.62	12.11	14.94
5C	11.79	10.21	14.19
5S	10.58	10.24	15.12
6I	15.93	12.20	14.95
6C	12.77	11.30	13.41
6S	12.08	10.86	18.81
7I	17.51	13.96	15.99
7C	14.76	11.85	15.87
7S	13.54	11.76	15.45
8I	15.35	12.18	15.32
8C	12.62	11.68	12.58
8S	12.08	11.08	14.57
9I	17.29	13.66	16.07
9C	14.09	11.95	15.36
9S	14.41	12.14	17.70

At L1, values ranged between 10.58% (5S) and 19.81% (3C). At L3, median values for BV/TV ranged from 10.21% (5C) to 16.16% (3I). At L5, values ranged between 12.58% (8C) and 20.59% (3S). Overall, VOIs displaying higher BV/TV were limited to peripheral VOIs (1I, 1C, 2I, 3I, 3C, 3S, 6S, 7I and 9I). Furthermore, the anterior aspect of the inferior and superior central layers displayed higher BV/TV values when compared to the posterior. Meanwhile, VOIs 5 and 8 generally displayed lower values for BV/TV overall.

9.2.3.2 SMI

For structural model index in the 4wks-2y cohort, the vertebral levels L1 and L3 displayed significant differences between VOIs. The descriptive statistics can be found in Table 9.14.

Table 9.14: Descriptive statistics for SMI at L1, L3 and L5 in the 4wks-2y cohort.

	L1	L3	L5
Parametric?	NP	NP	P
F/H Value	71.102	67.115	0.384
DF	26	26	26
P Value	<0.001	<0.001	0.997
p≤0.01?	Y	Y	N
Mean/Median	Median	Median	Mean
1I	1.500	1.596	1.453
1C	1.295	1.513	1.384
1S	1.808	1.796	1.394
2I	1.420	1.554	1.256
2C	1.357	1.404	1.290
2S	1.751	1.636	1.271
3I	1.382	1.498	1.374
3C	1.205	1.306	1.339
3S	1.631	1.689	1.236
4I	1.582	1.686	1.456
4C	1.496	1.624	1.451
4S	1.724	1.688	1.493
5I	1.608	1.659	1.507
5C	1.614	1.661	1.493
5S	1.829	1.821	1.531
6I	1.514	1.653	1.446
6C	1.490	1.603	1.431
6S	1.645	1.750	1.393
7I	1.626	1.663	1.379
7C	1.494	1.571	1.351
7S	1.718	1.745	1.498
8I	1.593	1.640	1.421
8C	1.332	1.215	1.309
8S	1.678	1.606	1.501
9I	1.584	1.630	1.395
9C	1.433	1.569	1.437
9S	1.605	1.725	1.522

At L1, average values for SMI ranged between 1.205 (3C) and 1.829 (5S). VOI 8C displayed significantly lower SMI compared to 5S. The high, intermediate and low median values per VOI can be viewed in figure 9.27. Significant differences can be viewed in figure 9.28.

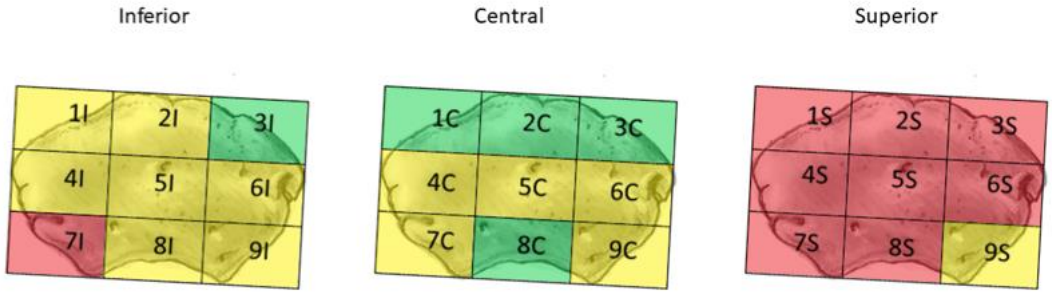

Figure 9.27: The high (red), intermediate (yellow) and low (green) median values for SMI at L1 within the 4 weeks to 2 years of age cohort.

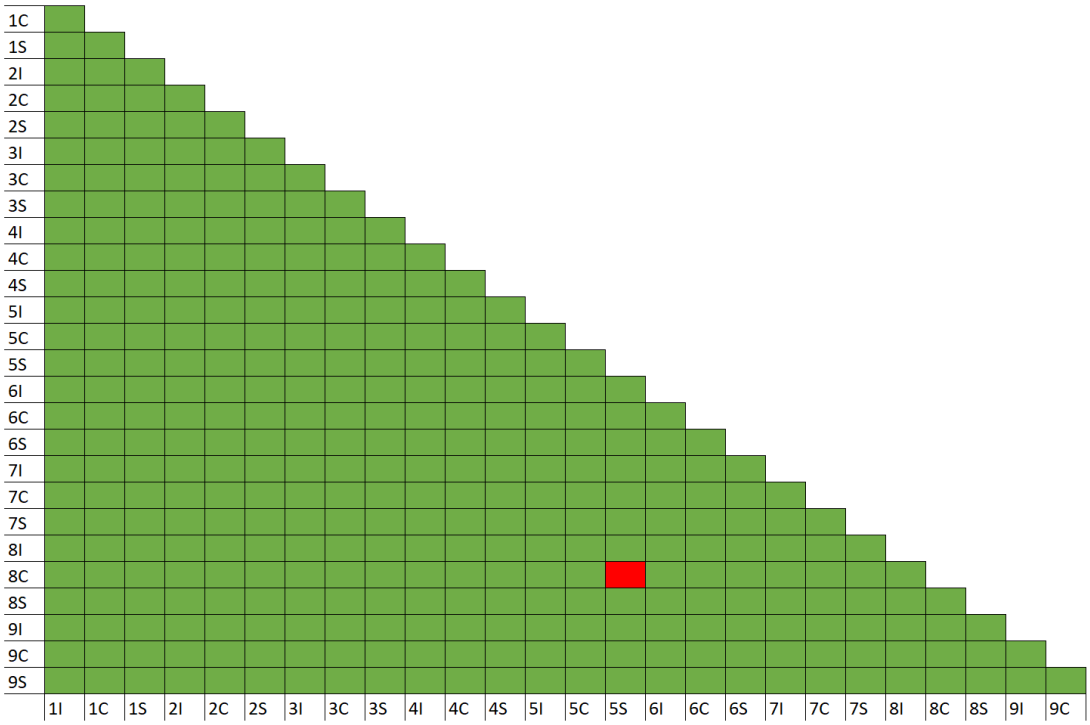

Figure 9.28: The significant differences present between VOIs for SMI at L1 within the 4wks-2y age cohort. Significant differences are denoted by red squares.

Median values for L3 ranged from 1.215 (8C) to 1.821 (5S). VOI 8C displayed a significantly lower median value for SMI compared to 1S and 5S. The high, intermediate and low median values per VOI can be viewed in figure 9.29. Significant differences can be found in figure 9.30.

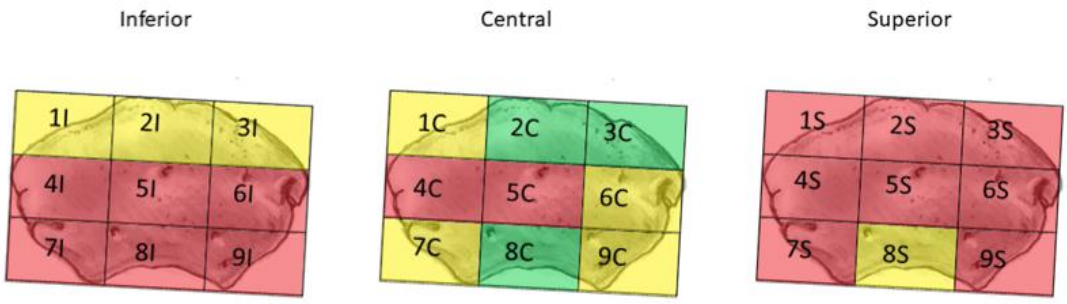

Figure 9.29: The high (red), intermediate (yellow) and low (green) median values for SMI at L3 within the 4 weeks to 2 years of age cohort.

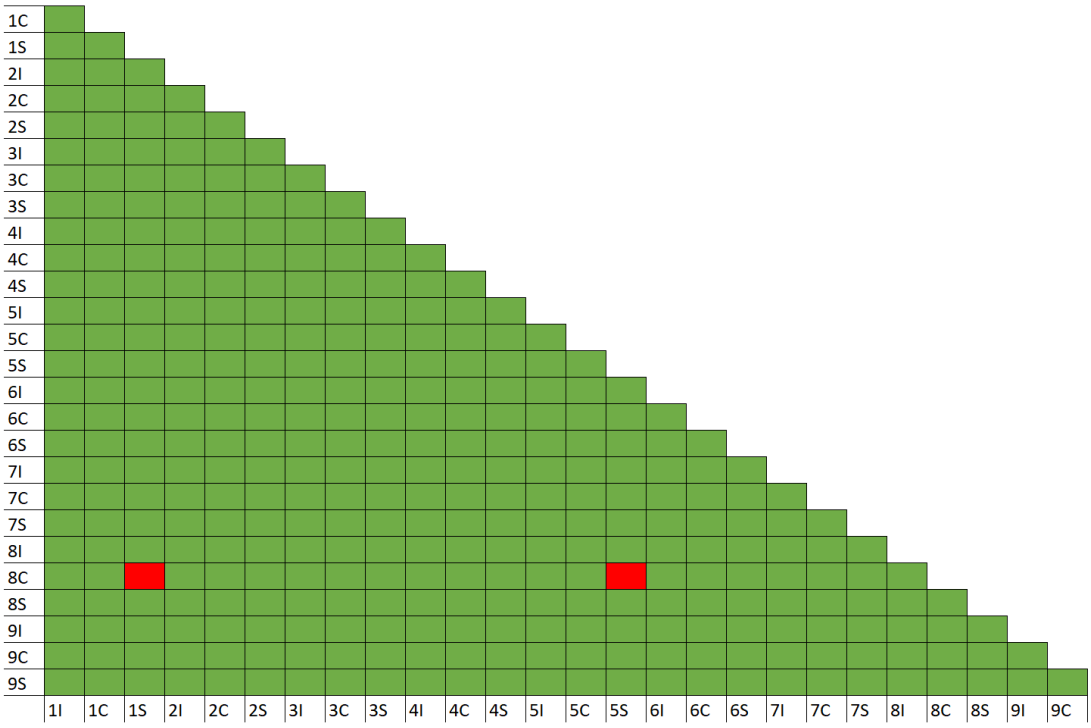

Figure 9.30: The significant differences present between VOIs for SMI at L3 within the 4 weeks to 2 years of age cohort.

Values for L5 ranged between 1.236 (3S) and 1.531 (5S). Over the three vertebral levels studied, VOI 8C displayed significantly lower values for SMI at L1 and L3. While not significant, VOI 2C also displayed lower SMI values. The highest SMI values were found within the inferior and superior layers of. The average values for each vertebral level all indicated a mixture of both plate-like and rod-like trabeculae.

9.2.3.3 Tb.Th

For trabecular thickness within the 4wks-2y cohort, only the vertebral level L3 displayed any significant differences between VOIs. Descriptive statistics for L1, L3 and L5 can be found in Table 9.15.

Table 9.15: Descriptive statistics for Tb.Th (μm) at L1, L3 and L5 in the 4wks-2y cohort.

	L1	L3	L5
Parametric?	NP	P	P
F/H Value	79.696	6.269	2.524
DF	26	26	26
P Value	<0.001	<0.001	<0.001
p≤0.01?	N	Y	N
Mean/Median	Median	Mean	Mean
1I	104.48	104.43	105.56
1C	131.16	123.80	139.06
1S	84.65	93.77	111.31
2I	106.26	106.48	116.20
2C	135.78	133.78	155.24
2S	93.43	92.04	116.75
3I	109.16	108.91	111.48
3C	142.77	131.38	144.16
3S	91.09	91.64	114.20
4I	99.11	96.26	101.09
4C	104.07	101.72	110.14
4S	92.91	92.45	107.48
5I	97.39	98.98	106.69
5C	117.13	110.20	116.50
5S	93.41	90.47	106.77
6I	99.19	97.42	102.54
6C	105.06	102.69	108.25
6S	93.61	91.61	108.00
7I	101.42	96.15	109.21
7C	104.88	98.44	111.06
7S	99.38	92.09	102.56
8I	103.07	95.94	109.30
8C	134.88	131.21	152.35
8S	104.82	104.45	106.86
9I	102.35	97.86	106.56
9C	104.63	99.17	114.42
9S	98.23	92.29	107.83

At the level of L1, median values for Tb.Th ranged between 84.65µm (1S) and 142.77µm (3C). At L3, average values ranged from 90.47µm (5S) to 133.78µm (2C). VOI 2C displayed the highest and differed significantly to VOIs 1S, 2S, 3S, 4I, 4C, 4S, 5I, 5S, 6I, 6C, 6S, 7I, 7C, 7S, 8I, 9I, 9C and 9S. VOIs 3C and 8C differed from those above excluding 4C and 6C. VOI 1C also displayed a higher trabecular thickness and differed from VOIs 2S, 3S, 4S, 5S, 6S, 7S and 9S. The high, intermediate and low mean values per VOI can be viewed in figure 9.31. Significant differences between VOIs can be visualised in figure 9.32. At L5, values for Tb.Th ranged between 102.54µm (6I) and 155.24µm (2C).

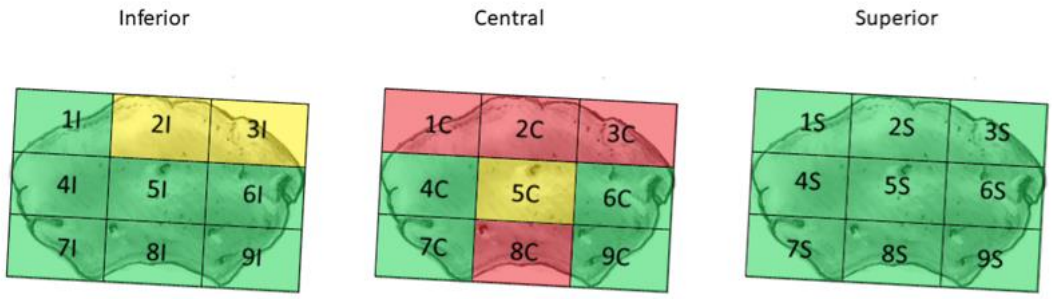

Figure 9.31: The high (red), intermediate (yellow) and low (green) mean values for Tb.Th (µm) at L3 within the 4 weeks to 2 years of age cohort.

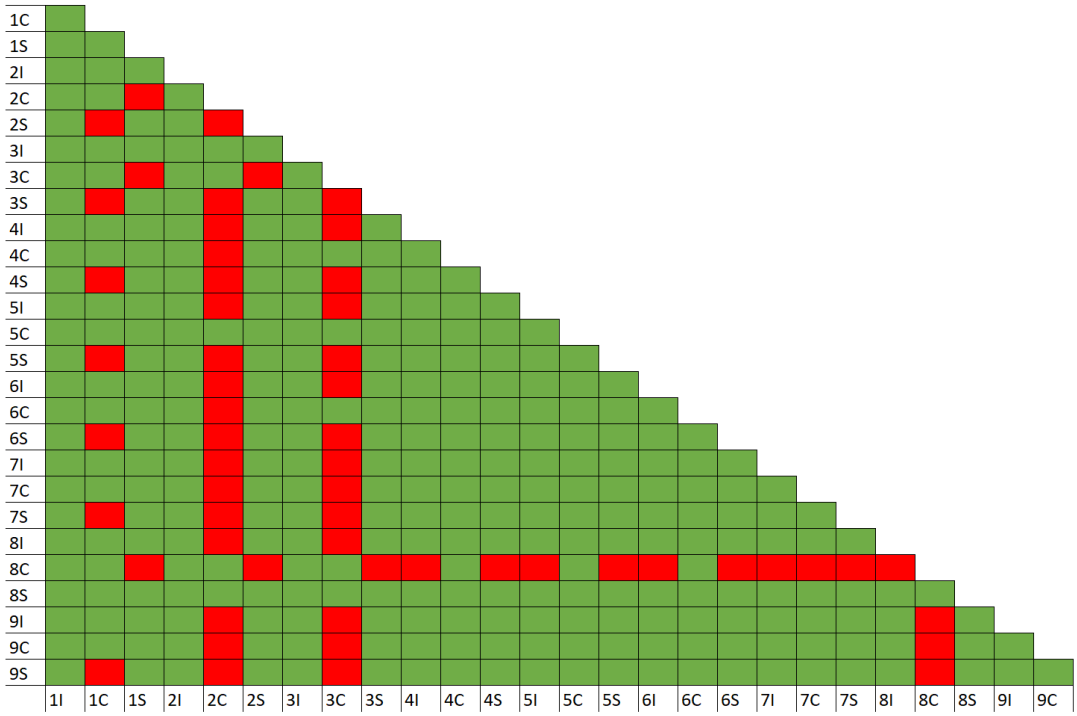

Figure 9.32: The significant differences present between VOIs for Tb.Th at L3 within the 4 weeks to 2 years of age cohort. Significant differences are denoted by red squares.

While significant differences were not present in the L1 or L5 datasets, all three vertebral levels displayed higher trabecular thickness within the anterior portion of the central layer (VOIs 1C, 2C and 3C). VOI 8C also displayed higher trabecular thickness, which was significant at the vertebral level L3.

9.2.3.4 Tb.N

For trabecular number in the 4wks-2y cohort, vertebral levels L1 and L3 displayed significant differences between VOIs. The descriptive statistics for the L1, L3 and L5 datasets can be found in Table 9.16.

Table 9.16: Descriptive statistics for Tb.N (μm^{-1}) at L1, L3 and L5 in the 4wks-2y cohort.

	L1	L3	L5
Parametric?	NP	NP	NP
F/H Value	93.672	85.144	40.414
DF	26	26	26
P Value	<0.001	<0.001	0.036
p≤0.01?	Y	Y	N
Mean/Median	Median	Median	Median
1I	0.00158	0.00130	0.00141
1C	0.00136	0.00110	0.00122
1S	0.00147	0.00135	0.00151
2I	0.00143	0.00137	0.00139
2C	0.00114	0.00099	0.00105
2S	0.00146	0.00137	0.00144
3I	0.00161	0.00147	0.00147
3C	0.00129	0.00121	0.00122
3S	0.00157	0.00138	0.00166
4I	0.00147	0.00131	0.00139
4C	0.00103	0.00105	0.00120
4S	0.00127	0.00119	0.00142
5I	0.00132	0.00121	0.00135
5C	0.00103	0.00098	0.00114
5S	0.00109	0.00117	0.00132
6I	0.00143	0.00130	0.00139
6C	0.00113	0.00103	0.00121
6S	0.00124	0.00111	0.00149
7I	0.00172	0.00144	0.00145
7C	0.00136	0.00116	0.00137
7S	0.00143	0.00126	0.00150
8I	0.00151	0.00129	0.00129
8C	0.00094	0.00083	0.00083
8S	0.00101	0.00102	0.00132
9I	0.00177	0.00137	0.00148
9C	0.00134	0.00121	0.00128
9S	0.00147	0.00130	0.00151

At the level of L1, median values for Tb.N ranged between 0.00094µm^{-1} (8C) and 0.00177µm^{-1} (9I). VOI 9I displayed the highest trabecular number of all VOIs and differed from 8C and 5C, who displayed the lowest values respectively. The high, intermediate and low median values per VOI can be viewed in figure 9.33. Significant differences can be visualised in figure 9.34.

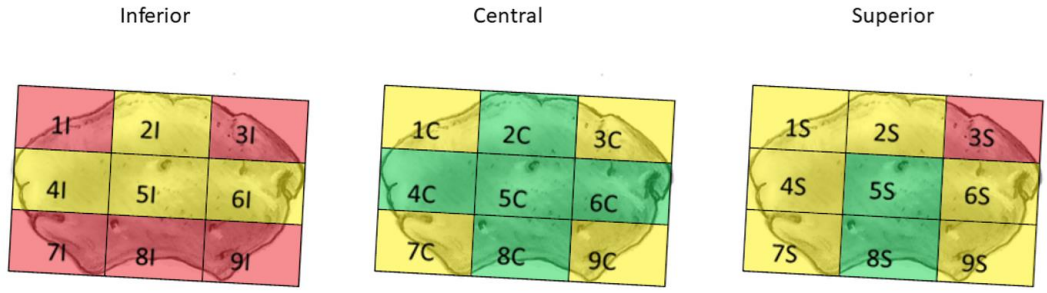

Figure 9.33: The high (red), intermediate (yellow) and low (green) median values for Tb.N (µm^{-1}) at L1 within the 4 weeks to 2 years of age cohort.

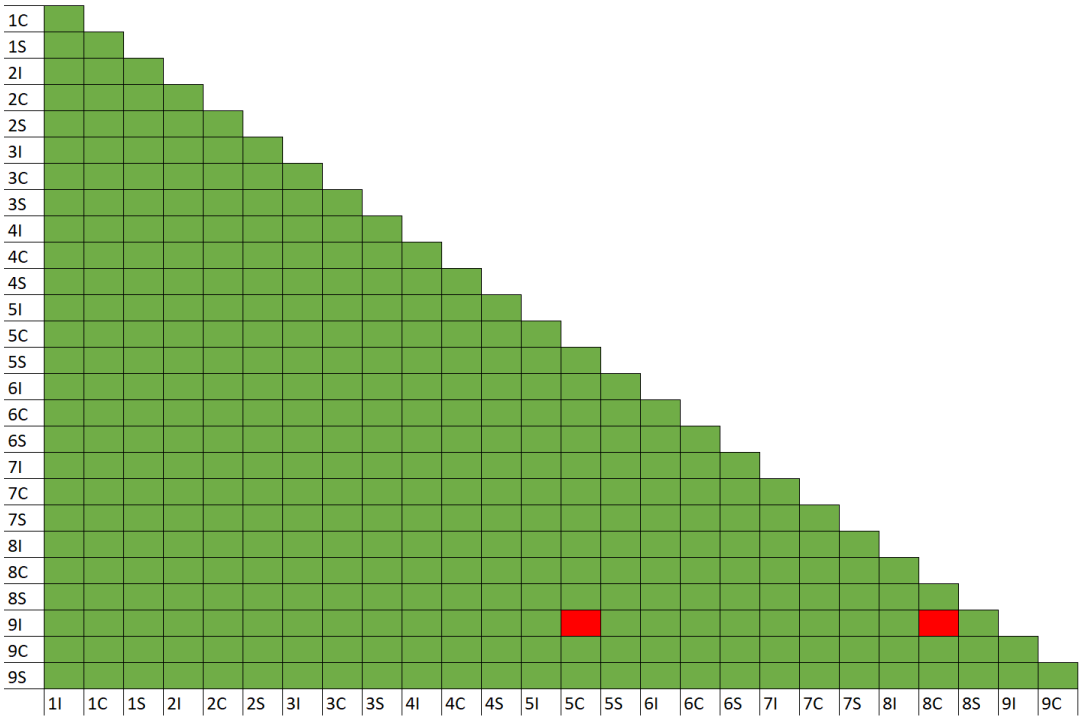

Figure 9.34: The significant differences present between VOIs for Tb.N at L1 within the 4 weeks to 2 years of age cohort. Significant differences are denoted by red squares.

At L3, values ranged between 0.00083µm^{-1} (8C) and 0.00147µm^{-1} (3I). VOI 8C displaying significantly lower trabecular number than 7I. The high, intermediate and low median values per VOI can be viewed in figure 9.35. Significant differences can be found in figure 9.36. At L5, values ranged from 0.00083µm^{-1} (8C) to 0.00166µm^{-1} (3S).

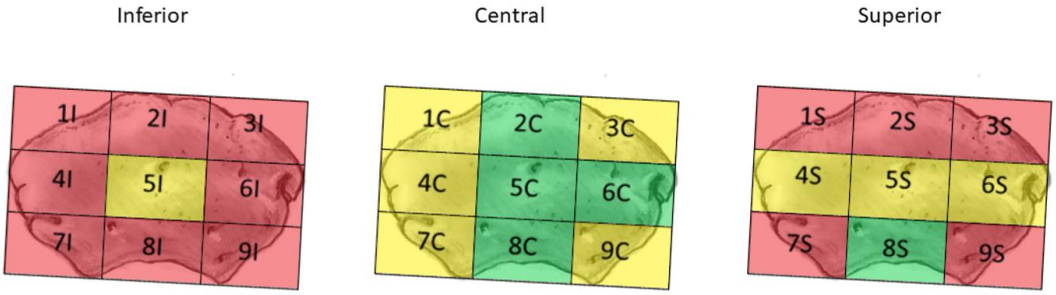

Figure 9.35: The high (red), intermediate (yellow) and low (green) median values for Tb.N (µm^{-1}) at L3 within the 4 weeks to 2 years of age cohort.

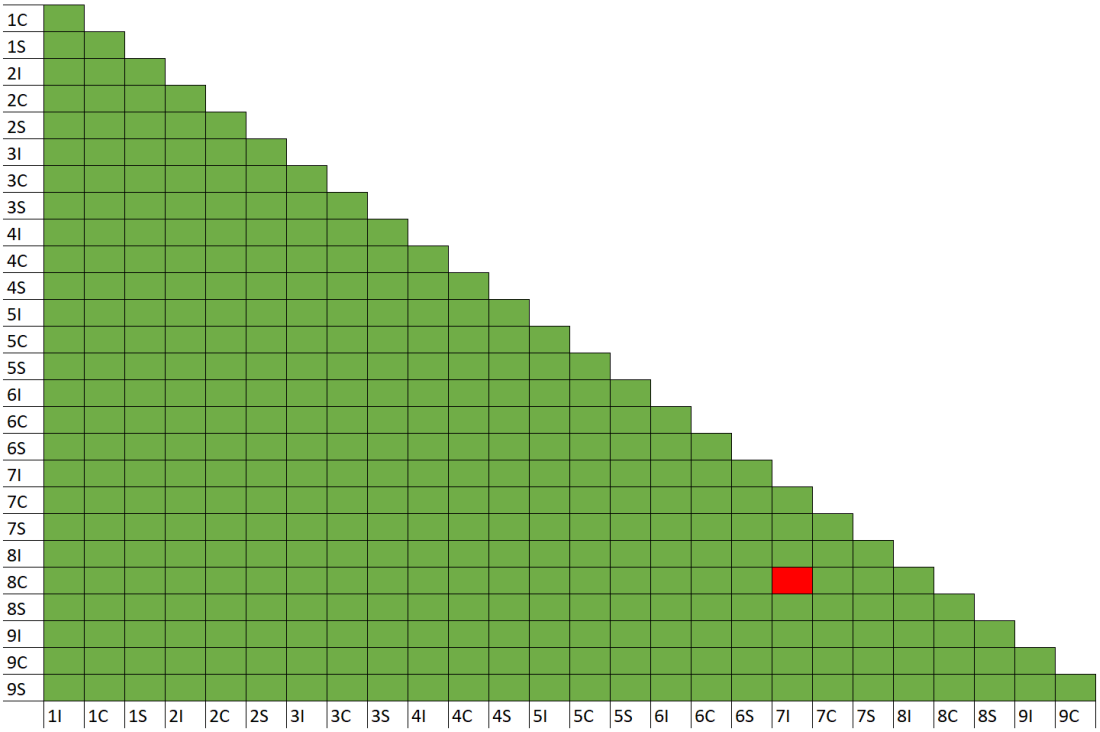

Figure 9.36: The significant differences present between VOIs for Tb.N at L3 within the 4 weeks to 2 years of age cohort. Significant differences are denoted by red squares.

The central layer of the developing centrum consistently displayed a lower number of trabeculae at all vertebral levels, although this was only significant at L1 and L3 with VOI 8C and L1 with VOI 5C. Peripheral VOIs within the superior and inferior layers of the centrum generally contained a higher number of trabeculae.

9.2.3.5 Tb.Sp

For trabecular separation in the 4wks-2y cohort, vertebral levels L1 and L3 displayed significant differences between VOIs. The descriptive statistics can be found in Table 9.17.

Table 9.17: Descriptive statistics for Tb.Sp (µm) at L1, L3 and L5 in the 4wks-2y cohort.

	L1	L3	L5
Parametric?	NP	NP	NP
F/H Value	102.192	93.904	43.176
DF	26	26	26
P Value	<0.001	<0.001	0.019
p≤0.01?	Y	Y	N
Mean/Median	Median	Median	Median
1I	439.88	488.48	507.60
1C	546.31	623.00	649.01
1S	418.43	438.41	486.21
2I	481.72	507.86	529.76
2C	623.35	659.90	654.28
2S	447.91	464.90	507.74
3I	428.77	487.39	474.57
3C	543.86	598.40	610.15
3S	423.32	448.79	488.72
4I	492.28	512.85	535.58
4C	659.25	648.35	574.53
4S	507.59	551.46	512.72
5I	482.34	511.68	551.22
5C	607.12	640.87	625.97
5S	507.64	540.00	504.46
6I	473.15	511.70	519.84
6C	627.36	630.65	623.28
6S	513.71	532.65	508.03
7I	422.73	437.55	525.56
7C	513.36	533.72	547.49
7S	472.94	476.74	482.61
8I	443.03	460.97	533.87
8C	813.30	964.74	960.44
8S	609.81	588.27	530.60
9I	408.67	457.66	497.60
9C	512.26	520.95	600.18
9S	471.17	490.45	513.27

At L1, values ranged between 408.67µm (9I) and 813.30µm (8C). VOI 8C displayed the highest median value for trabecular separation and differed significantly from VOIs 1I, 1S, 2S, 3I, 3S, 7I and 9I. VOI 2C also displayed a significantly higher Tb.Sp and differed from VOIs 1S and 3I. The high, intermediate and low median values per VOI can be viewed in figure 9.37. Significant differences can be viewed in figure 9.38

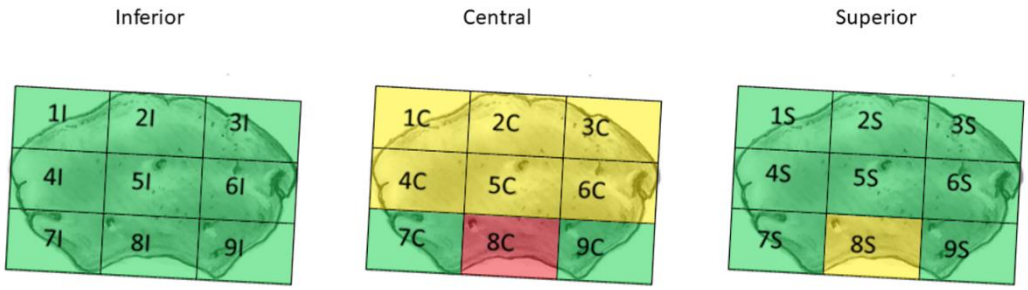

Figure 9.37: The high (red), intermediate (yellow) and low (green) median values for Tb.Sp (µm) at L1 within the 4 weeks to 2 years of age cohort.

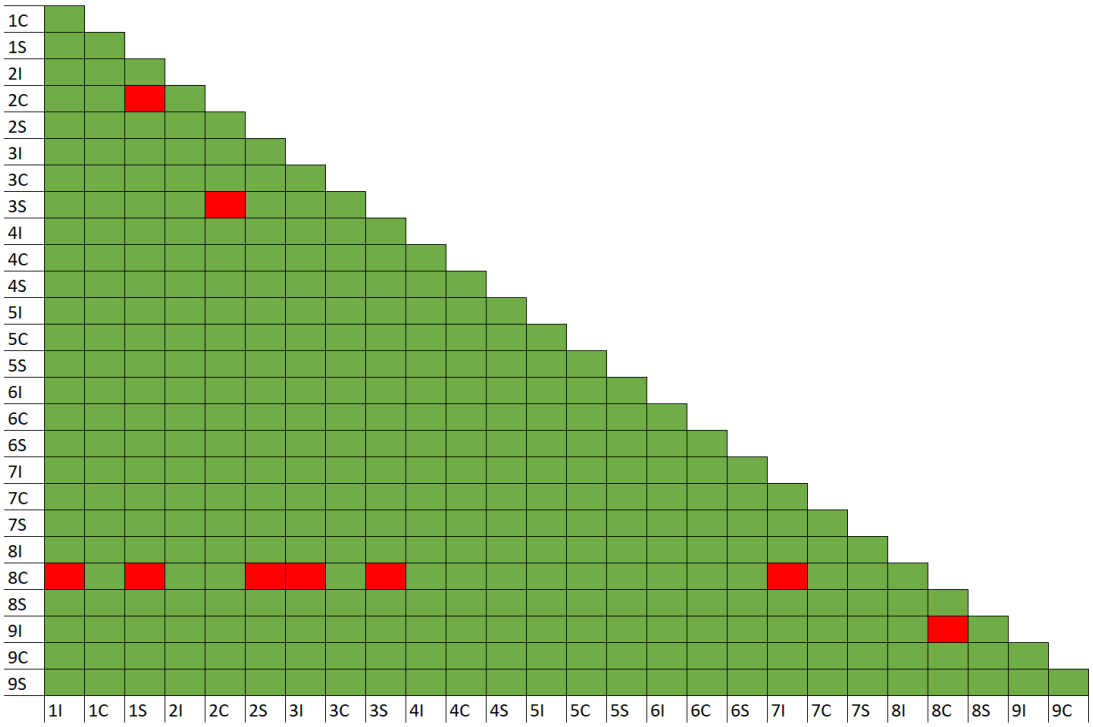

Figure 9.38: The significant differences present between VOIs for Tb.Sp at L1 within the 4 weeks to 2 years of age cohort. Significant differences are denoted by red squares.

For L3, values ranged between 437.55µm (7I) and 964.74µm (8C). VOI 8C once again displayed a significantly higher trabecular separation and differed significantly from VOIs 1S, 2S, 3S, 7I and 9I. The high, intermediate and low median values per VOI can be viewed in figure 9.39. Significant differences can be viewed in figure 9.40. At L5, values ranged from 474.57µm (3I) to 960.44µm (8C).

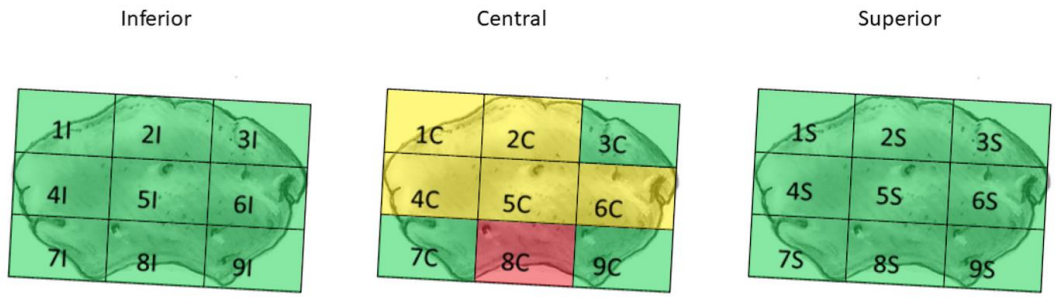

Figure 9.39: The high (red), intermediate (yellow) and low (green) median values for Tb.Sp (µm) at L3 within the 4 weeks to 2 years of age cohort.

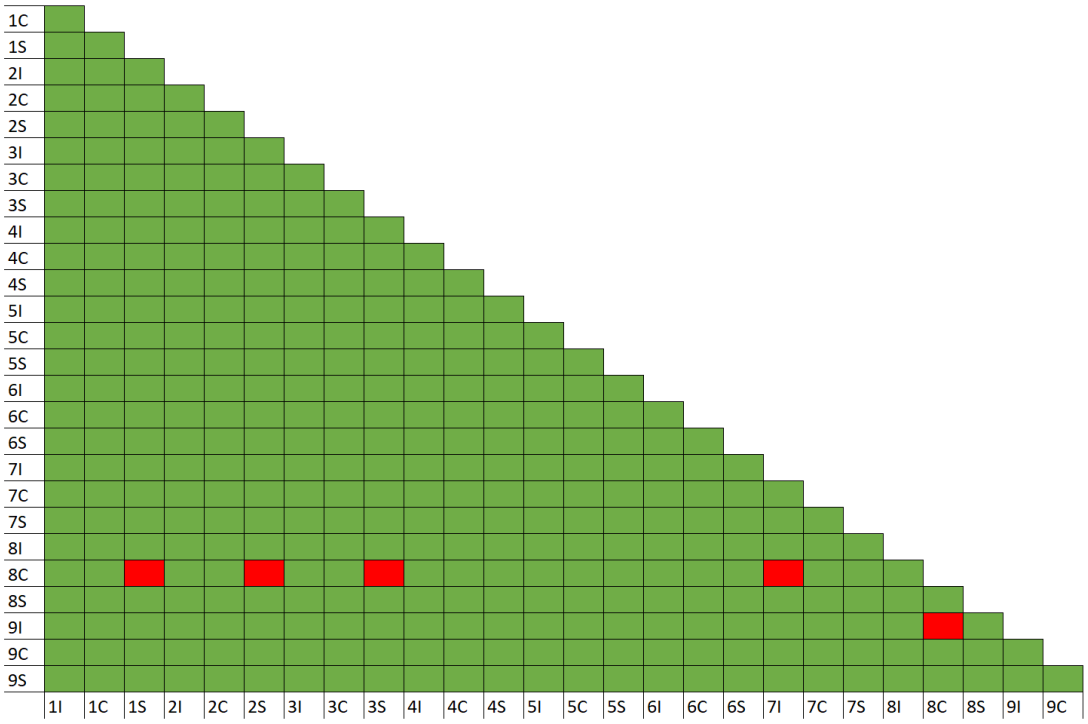

Figure 9.40: The significant differences present between VOIs for Tb.Sp at L3 within the 4 weeks to 2 years of age cohort. Significant differences are denoted by red squares.

Central VOI 8C consistently displayed the highest trabecular separation of all VOIs at the three vertebral levels studied. The inferior and superior layers of the developing centrum displayed lower trabecular separation, while the rest of the central layer generally displayed intermediate values.

9.2.3.6 DA

For degree of anisotropy in the 4wks-2y cohort, all three vertebral levels displayed significant differences between VOIs. Descriptive statistics can be found in Table 9.18.

Table 9.18: Descriptive statistics for DA at L1, L3 and L5 in the 4wks-2y cohort.

	L1	L3	L5
Parametric?	NP	P	P
F/H Value	94.640	7.914	3.507
DF	26	26	26
P Value	<0.001	<0.001	<0.001
p≤0.01?	Y	Y	Y
Mean/Median	Median	Mean	Mean
1I	0.444	0.451	0.369
1C	0.428	0.503	0.464
1S	0.370	0.415	0.404
2I	0.374	0.374	0.305
2C	0.311	0.352	0.282
2S	0.364	0.356	0.392
3I	0.411	0.459	0.352
3C	0.447	0.480	0.463
3S	0.410	0.402	0.410
4I	0.249	0.284	0.275
4C	0.414	0.448	0.390
4S	0.408	0.365	0.311
5I	0.276	0.303	0.176
5C	0.361	0.392	0.361
5S	0.293	0.246	0.287
6I	0.279	0.282	0.293
6C	0.403	0.417	0.395
6S	0.402	0.356	0.317
7I	0.268	0.303	0.292
7C	0.314	0.338	0.319
7S	0.258	0.325	0.288
8I	0.357	0.234	0.278
8C	0.244	0.326	0.324
8S	0.232	0.271	0.303
9I	0.269	0.266	0.309
9C	0.302	0.355	0.333
9S	0.274	0.336	0.307

At L1, values ranged between 0.232 (8S) and 0.447 (3C). Only two significant differences were present: VOI 1I, which exhibited a significantly higher degree of anisotropy, differed from VOIs 8C and 8S. The high, intermediate and low median values per VOI can be viewed in figure 9.41. Significant differences can be visualised in figure 9.42.

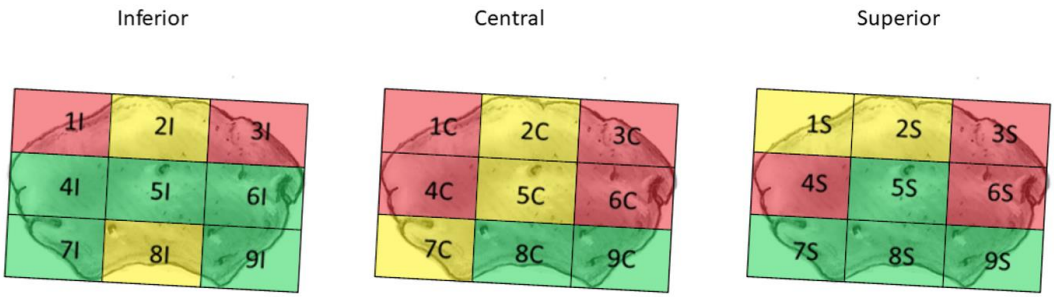

Figure 9.41: The high (red), intermediate (yellow) and low (green) median values for DA at L1 within the 4 weeks to 2 years of age cohort.

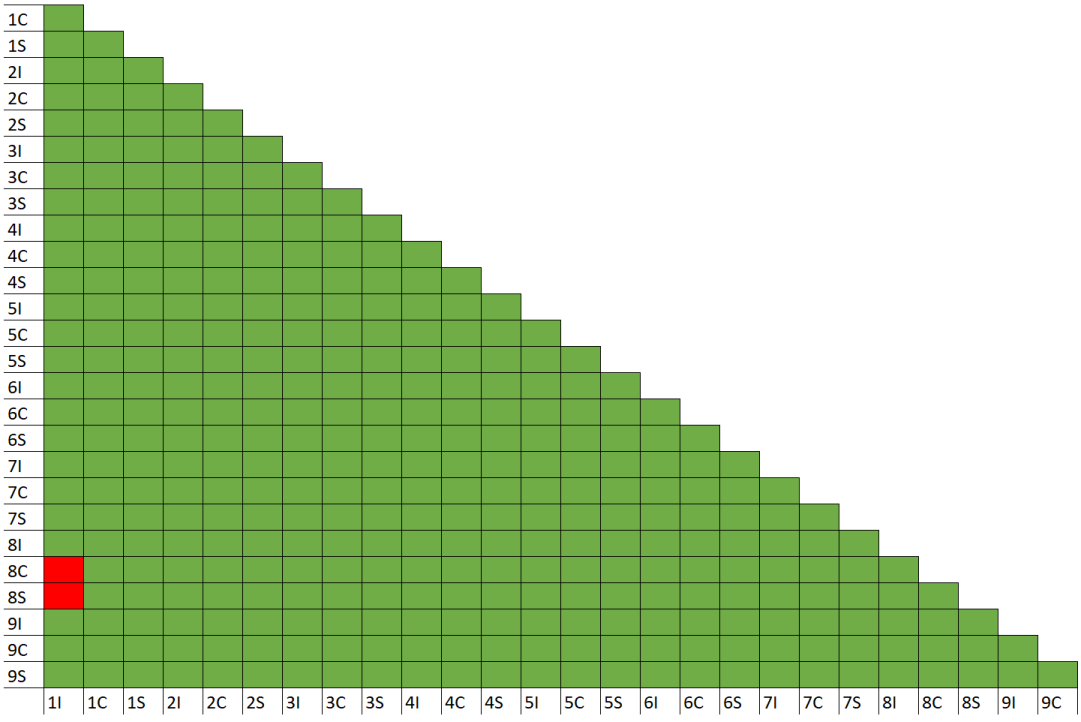

Figure 9.42: The significant differences present between VOIs for DA at L1 within the 4 weeks to 2 years of age cohort. Significant differences are denoted by red squares.

At L3, values for DA ranged from 0.234 (8I) to 0.503 (1C). VOIs 1I, 1C, 3I, 3C and 4C displayed significantly higher values for DA compared to other VOIs.

All differed significantly from VOIs 4I, 5S, 6I, 8I, 8S and 9I. VOIs 1C, 3I and 3C also differed from 5I and 7I while 1C and 3C differed from 7S and 8C. Finally, 1C further differed from 7C and 9S. VOIs 5S and 8I displayed significantly lower DA values, differing from VOIs as stated above, as well as VOIs 1S, 3S and 6C. VOI 8I also differed from 5C. The high, intermediate and low mean values per VOI can be found in figure 9.43. Significant differences between VOIs can be visualised in figure 9.44.

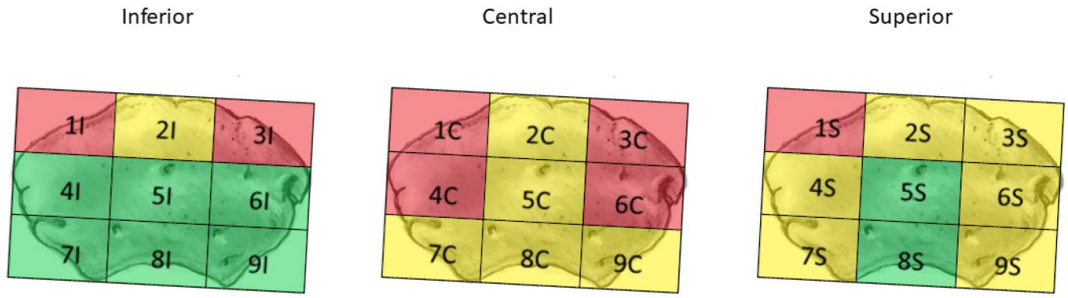

Figure 9.43: The high (red), intermediate (yellow) and low (green) mean values for DA at L3 within the 4 weeks to 2 years of age cohort.

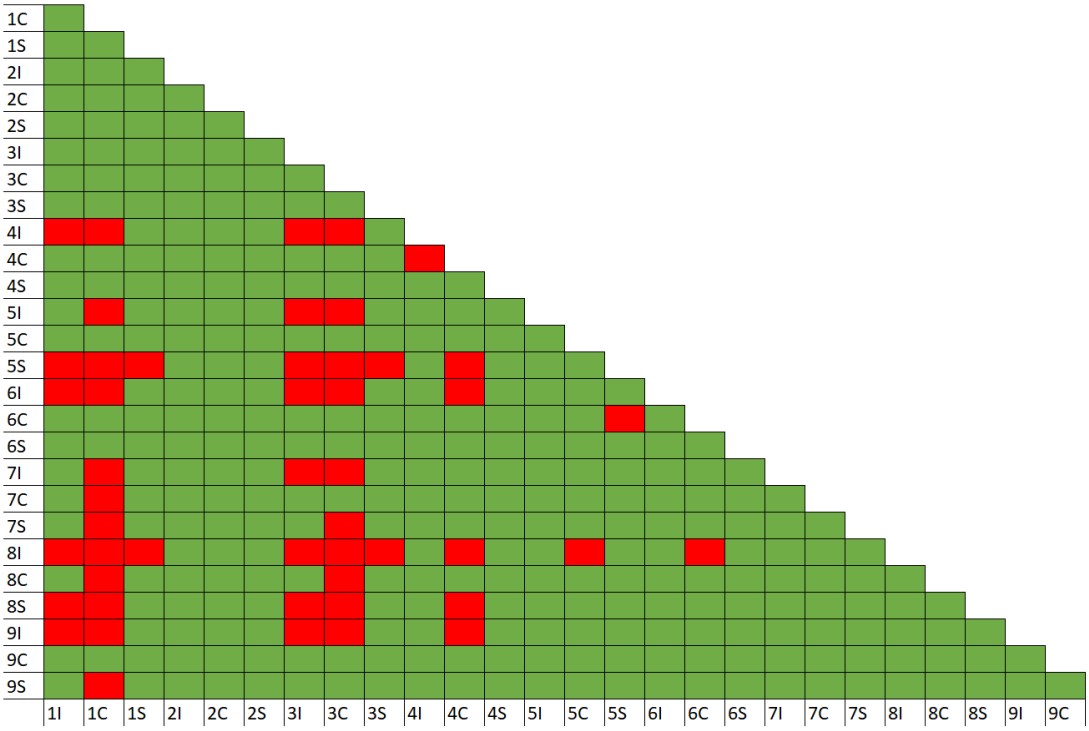

Figure 9.44: The significant differences present between VOIs for DA at L3 within the 4 weeks to 2 years of age cohort. Significant differences are denoted by red squares.

L5, average values ranged between 0.176 (5I) and 0.464 (1C). VOI 5I displayed the lowest mean value for DA and differed significantly from VOI 1C,

which displayed the highest average value. The high, intermediate and low mean values per VOI can be found in figure 9.45. Significant differences can be visualised in figure 9.46.

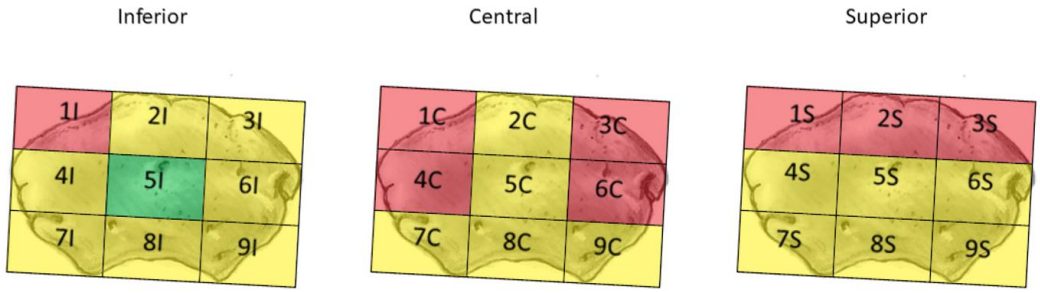

Figure 9.45: The high (red), intermediate (yellow) and low (green) mean values for DA at L5 within the 4 weeks to 2 years of age cohort.

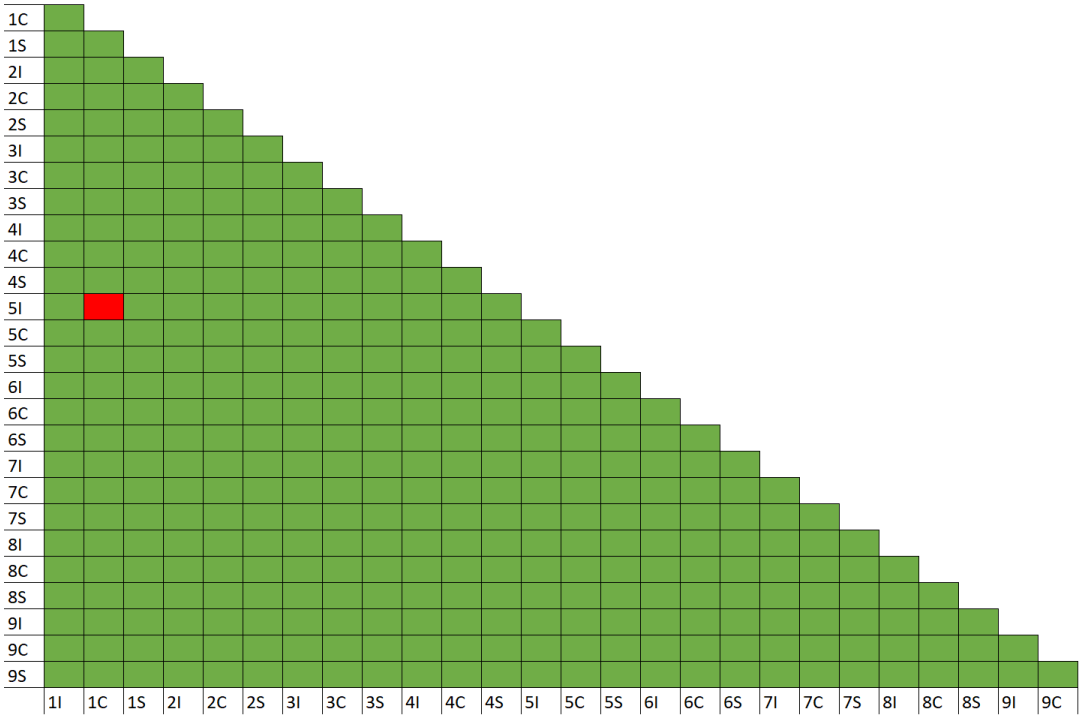

Figure 9.46: The significant differences present between VOIs for DA at L5 within the 4 weeks to 2 years of age cohort. Significant differences are denoted by red squares.

Anterior and lateral VOIs tended to display higher values for degree of anisotropy while central and posterior VOIs displayed lower values for DA. Overall, values from DA indicated all VOIs were more isotropic than anisotropic.

9.2.4 *3 to 8 years of age cohort*

9.2.4.1 BV/TV

For bone volume fraction in the 3-8y cohort, vertebral levels L1 and L3 displayed significant differences between VOIs. Descriptive statistics can be found in Table 9.19.

Table 9.19: Descriptive statistics for BV/TV (%) at L1, L3 and L5 in the 3-8y cohort.

	L1	L3	L5
Parametric?	NP	P	NP
F/H Value	128.057	4.394	30.455
DF	26	26	26
P Value	<0.001	<0.001	0.249
p≤0.01?	Y	Y	N
Mean/Median	Median	Mean	Median
1I	15.99	15.49	20.37
1C	19.01	15.49	20.52
1S	13.06	12.44	17.85
2I	16.82	14.69	20.70
2C	16.21	14.65	18.83
2S	13.45	11.70	16.96
3I	18.65	14.85	18.97
3C	21.09	15.76	19.12
3S	14.68	11.59	16.94
4I	13.02	12.48	21.25
4C	12.36	10.99	16.73
4S	11.14	10.39	17.28
5I	12.16	11.87	20.09
5C	10.66	10.15	14.87
5S	10.92	9.87	15.89
6I	15.23	12.72	20.71
6C	13.27	10.72	16.41
6S	12.11	10.07	16.58
7I	15.22	14.12	23.79
7C	13.46	11.43	18.44
7S	12.18	10.60	18.80
8I	13.66	11.96	20.51
8C	11.56	10.87	15.90
8S	12.44	11.46	15.31
9I	15.98	13.65	23.76
9C	14.10	11.45	18.30
9S	12.97	10.62	17.77

At L1, the median values for BV/TV ranged from 10.66% (5C) to 21.09% (3C). VOI 3C displayed the highest average value for BV/TV and differed significantly from VOIs 4S, 5I, 5C, 5S and 8C. VOI 3I also displayed a high value for BV/TV differed from 4S, 5C, 5S and 8C. VOI 1C displayed a significantly higher BV/TV to VOIs 5C and 5S, while VOI 2C had a higher BV/TV compared to 5C only, which displayed the lowest average value for BV/TV. Figure 9.47 displays the high, intermediate and low median values for BV/TV within the 3-8y age cohort at L1 while significant differences between VOIs can be visualised in figure 9.48.

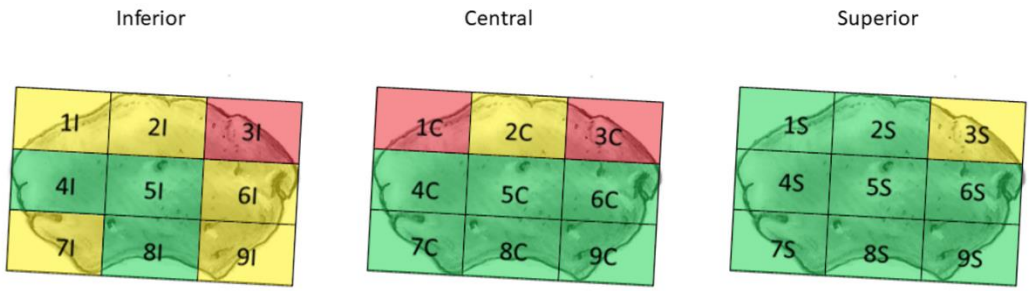

Figure 9.47: The high (red), intermediate (yellow) and low (green) median values for BV/TV (%) at L1 within the 3-8 years age cohort.

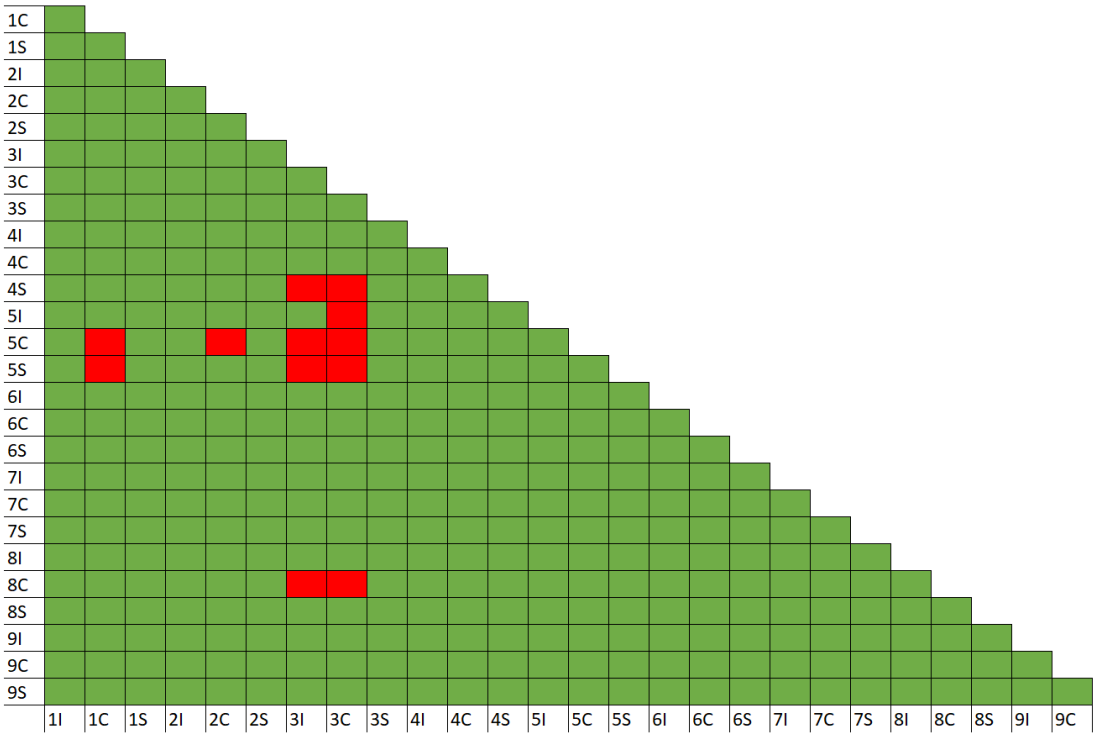

Figure 9.48: The significant differences present between VOIs for BV/TV at L1 within the 3-8 years of age cohort. Significant differences are denoted by red squares.

At L3, mean values ranged from 9.87% (5S) to 15.76% (3C). VOI 3C once again displayed the highest BV/TV and differed significantly from VOIs 5C, 5S and 6S. VOIs 1I and 1C also exhibited significantly higher BV/TV values and differed from 5S and 6S, who present the lowest values respectively. The high, intermediate and low mean values for the dataset can be found in figure 9.49. Significant differences can be viewed in figure 9.50. For L5, values ranged between 14.87% (5C) and 23.79% (7I).

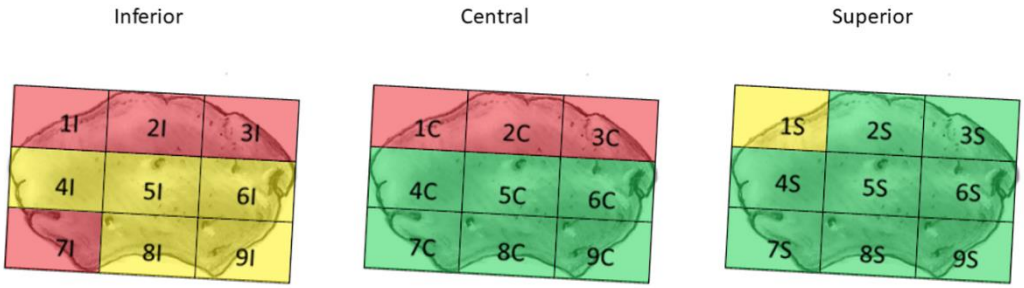

Figure 9.49: The high (red), intermediate (yellow) and low (green) mean values for BV/TV (%) at L3 within the 3-8 years age cohort.

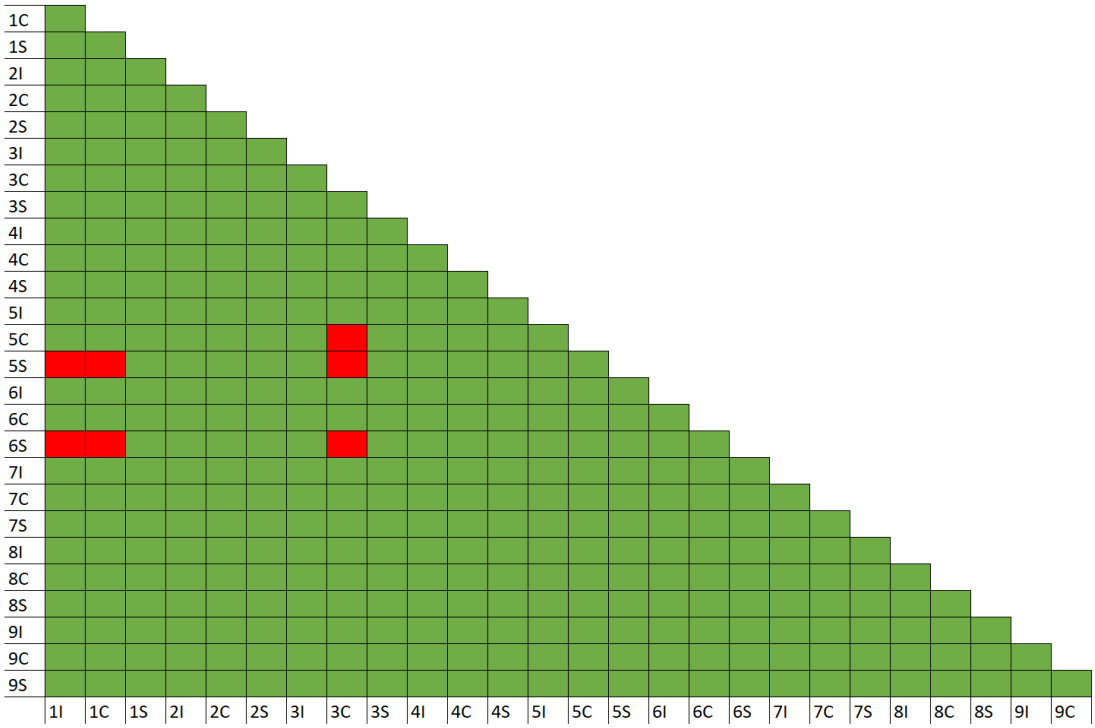

Figure 9.50: The significant differences present between VOIs for BV/TV at L3 within the 3-8 years of age cohort. Significant differences are denoted by red squares.

VOI 3C displayed the highest average value for BV/TV at the vertebral levels L1 and L3. At the level of L3, BV/TV is higher at anterior VOIs. At all levels, central VOIs 5C and 8C displayed lower BV/TV.

9.2.4.2 SMI

For structural model index within the 3-8y cohort, all three vertebral levels displayed significant differences between VOIs. The descriptive statistics can be found in Table 9.20.

Table 9.20: Descriptive statistics for SMI at L1, L3 and L5 in the 3-8y cohort.

	L1	L3	L5
Parametric?	NP	P	P
F/H Value	126.863	8.599	3.908
DF	26	26	26
P Value	<0.001	<0.001	<0.001
p≤0.01?	Y	Y	Y
Mean/Median	Median	Mean	Mean
1I	1.477	1.536	1.367
1C	1.238	1.155	1.043
1S	1.805	1.823	1.485
2I	1.388	1.500	1.285
2C	1.163	1.146	0.975
2S	1.762	1.837	1.511
3I	1.477	1.561	1.464
3C	1.091	1.220	1.114
3S	1.765	1.904	1.522
4I	1.599	1.714	1.389
4C	1.275	1.366	1.253
4S	1.757	1.797	1.508
5I	1.691	1.706	1.543
5C	1.472	1.392	1.322
5S	1.848	1.811	1.532
6I	1.592	1.706	1.405
6C	1.210	1.403	1.274
6S	1.694	1.845	1.500
7I	1.625	1.693	1.406
7C	1.497	1.580	1.247
7S	1.760	1.836	1.483
8I	1.671	1.728	1.546
8C	1.251	1.249	1.117
8S	1.616	1.742	1.589
9I	1.595	1.735	1.343
9C	1.461	1.641	1.173
9S	1.697	1.864	1.426

At L1, average values ranged between 1.091 (3C) and 1.848 (5S). VOIs 2C and 3C exhibited significantly lower SMI values compared to VOIs 1S, 2S, 3S, 4S, 5S and 7S. VOI 1C also displayed a lower SMI value but only differed significantly from 5S, which presented the highest median value for SMI within this dataset. The high, intermediate and low median values per VOI can be viewed in figure 9.51. Significant differences can be viewed in figure 9.52.

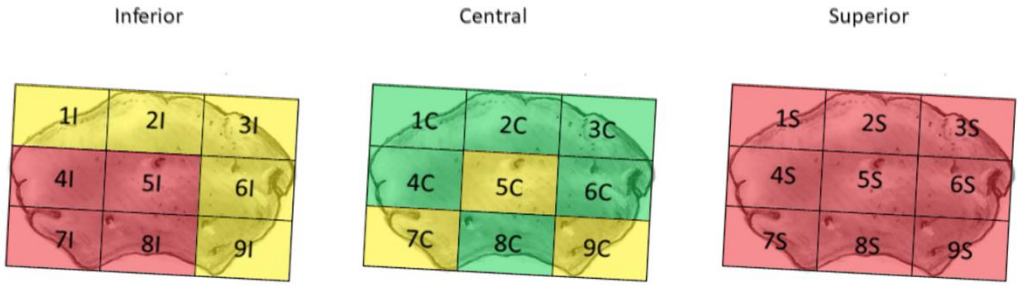

Figure 9.51: The high (red), intermediate (yellow) and low (green) median values for SMI at L1 within the 3-8 years age cohort.

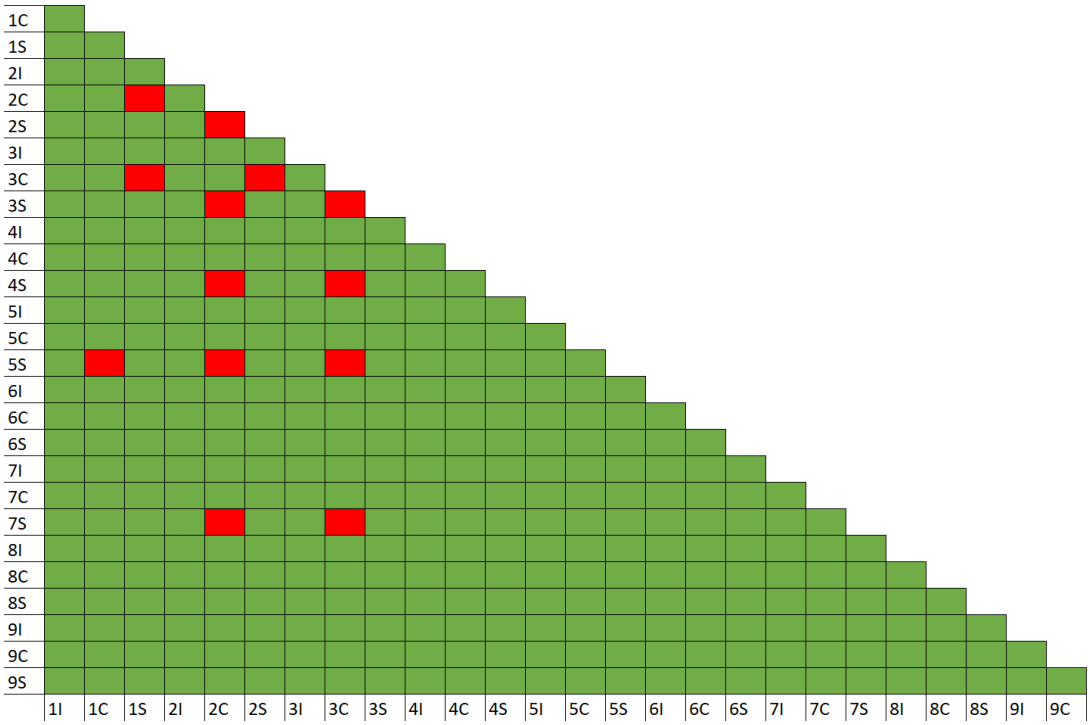

Figure 9.52: The significant differences present between VOIs for SMI at L1 within the 3-8 years of age cohort. Significant differences are denoted by red squares.

At L3, mean values for SMI ranged between 1.146 (2C) and 1.904 (3S). VOIs 1C and 2C displayed a significantly lower SMI compared to 1S, 2S, 3S, 4I, 4S,

5I, 5S, 6I, 6S, 7I, 7S, 8I, 8S, 9I, 9C and 9S, while VOI 3C displayed a lower SMI compared to those above excluding 7I and 9C. VOI 8C also displayed a lower SMI and differed from VOIs 1S, 2S, 3S, 4S, 5S, 6S, 7S, 8I, 8S, 9I and 9S. VOI 3S displayed the highest value and was also significantly different to 4C, 5C and 6C. VOIs 6S and 9S also displayed higher average values for SM and differed from VOI 4C as well as those stated above. The high, intermediate and low values can be viewed in figure 9.53 while significant differences between VOIs can be visualised in figure 9.54.

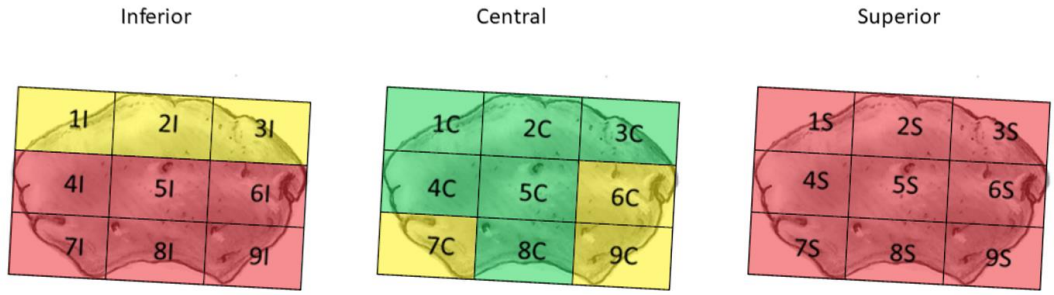

Figure 9.53: The high (red), intermediate (yellow) and low (green) mean values for SMI at L3 within the 3-8 years age cohort.

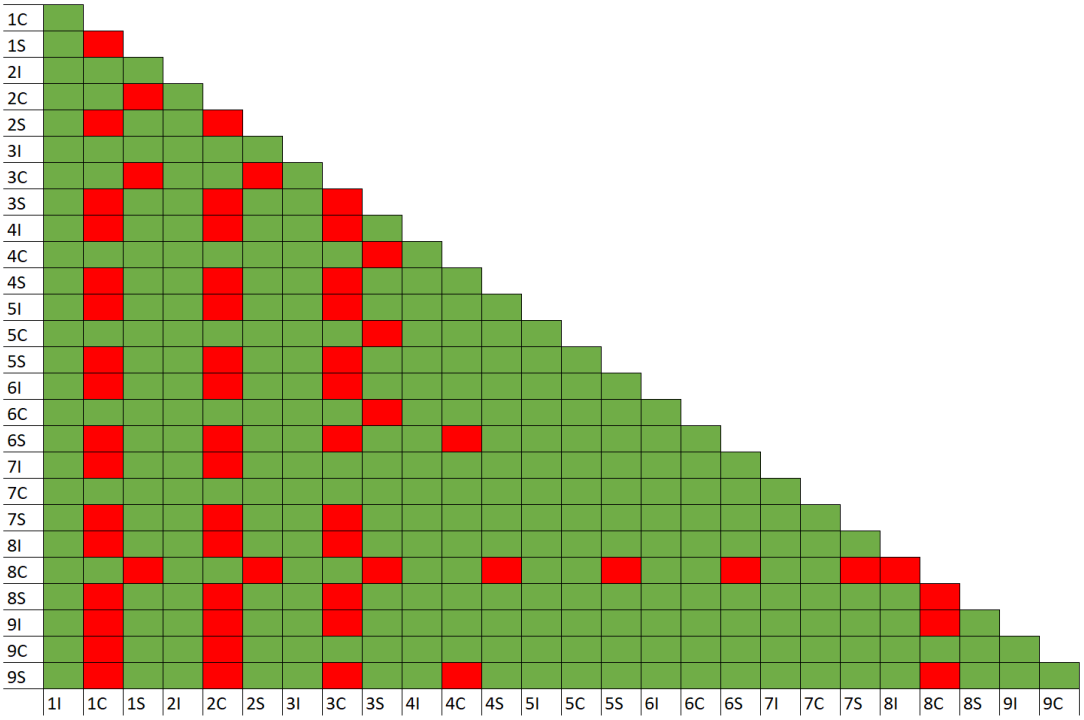

Figure 9.54: The significant differences present between VOIs for SMI at L3 within the 3-8 years of age cohort. Significant differences are denoted by red squares.

At L5, average values per VOI ranged from 0.975 (2C) to 1.589 (8S). VOI 2C displayed the lowest value for SMI and differed significantly from VOIs 2S, 3S, 4S, 5I, 5Sm 6S, 8I and 8S. VOI 8S displayed the highest average value and also differed significantly from VOI 1C. The high, intermediate and low average SMI values per VOI can be viewed in figure 9.55. Significant differences can be viewed in figure 9.56.

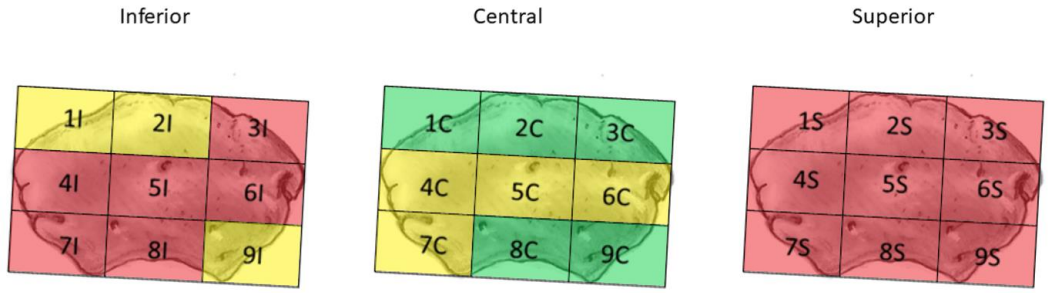

Figure 9.55: The high (red), intermediate (yellow) and low (green) mean values for SMI at L5 within the 3-8 years age cohort.

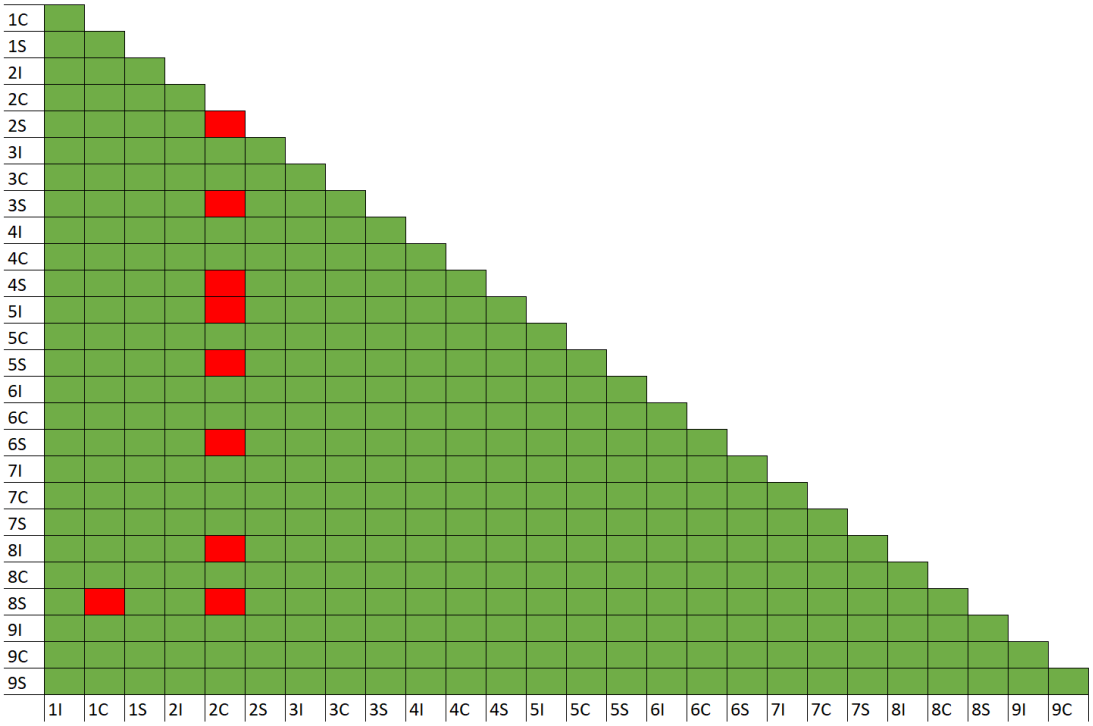

Figure 9.56: The significant differences present between VOIs for SMI at L5 within the 3-8 years of age cohort. Significant differences are denoted by red squares.

For SMI, higher values were present within the superior and inferior layers, while the central layer displayed significantly lower values for SMI. Overall, all values indicated a trabecular morphology formed of plate-like and rod-like trabecular struts.

9.2.4.3 Tb.Th

For trabecular thickness in the 3-8y cohort, only L1 displayed significant differences between VOIs. The descriptive statistics can be viewed in Table 9.21.

Table 9.21: Descriptive statistics for Tb.Th (µm) at L1, L3 and L5 in the 3-8y cohort.

	L1	L3	L5
Parametric?	NP	NP	P
F/H Value	95.841	70.840	1.608
DF	26	26	26
P Value	<0.001	<0.001	0.056
p≤0.01?	Y	N	N
Mean/Median	Median	Median	Mean
1I	124.18	119.67	126.34
1C	141.67	127.22	161.59
1S	102.42	94.97	123.76
2I	121.08	124.02	134.15
2C	149.01	133.37	163.20
2S	106.92	92.41	121.87
3I	128.96	120.19	120.46
3C	158.06	134.98	158.07
3S	107.19	95.17	115.01
4I	108.49	102.42	130.33
4C	129.62	120.64	134.48
4S	97.47	97.60	119.99
5I	108.47	110.76	145.40
5C	117.09	122.33	155.52
5S	104.18	102.94	131.77
6I	112.65	106.00	121.48
6C	143.35	117.79	129.37
6S	103.88	94.47	117.44
7I	108.66	97.35	125.81
7C	114.47	100.04	137.16
7S	104.10	91.61	127.12
8I	109.15	98.62	127.60
8C	143.01	136.16	172.43
8S	123.23	121.10	139.06
9I	108.95	97.94	135.62
9C	125.16	100.31	140.02
9S	110.30	90.90	132.03

At L1, average values ranged between 97.47µm (4S) and 158.06µm (3C). VOI 4S displayed the lowest trabecular thickness of all VOIs and differed significantly to VOIs 2C, 3C and 8C. No other differences were present at p≤0.01. The high, intermediate and low values can be found in figure 9.57. Significant differences between VOIs can be found in figure 9.58.

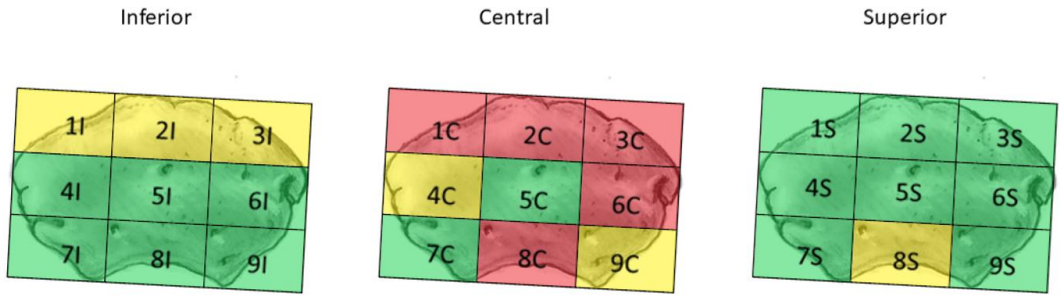

Figure 9.57: The high (red), intermediate (yellow) and low (green) median values for Tb.Th (µm) at L1 within the 3-8 years of age cohort.

..

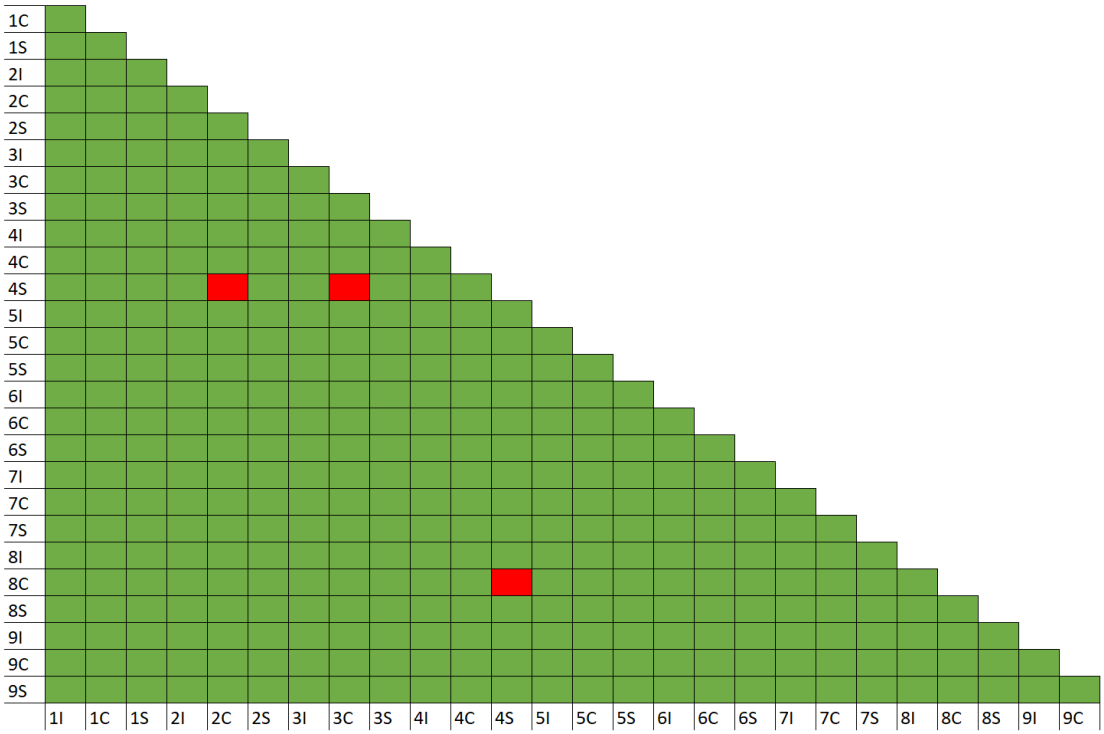

Figure 9.58: The significant differences present between VOIs for Tb.Th at L1 within the 3-8 years of age cohort. Significant differences are denoted by red squares.

Median values ranged between 90.90µm (9S) and 136.16µm (8C). Average values ranged between 115.01µm (3S) and 172.43µm (8C). Central VOIs generally displayed higher trabecular thickness compared to VOIs within the superior and inferior layers. In particular, VOIs 2C, 5C, 8C and 8S generally displayed high or intermediate values. Anterior VOIs also tended to display either high or intermediate values within the central and sometimes inferior layers.

9.2.4.4 Tb.N

For trabecular number within the 3-8y cohort, all three vertebral levels studied displayed significant differences between VOIs. The descriptive statistics for L1, L3 and L5 can be found in Table 9.22.

Table 9.22: Descriptive statistics for Tb.N (μm^{-1}) at L1, L3 and L5 in the 3-8y cohort.

	L1	L3	L5
Parametric?	NP	NP	P
F/H Value	108.250	106.112	5.362
DF	26	26	26
P Value	<0.001	<0.001	<0.001
p≤0.01?	Y	Y	Y
Mean/Median	Median	Median	Mean
1I	0.00128	0.00131	0.00163
1C	0.00116	0.00109	0.00126
1S	0.00130	0.00133	0.00152
2I	0.00126	0.00130	0.00149
2C	0.00111	0.00103	0.00117
2S	0.00126	0.00120	0.00143
3I	0.00137	0.00127	0.00158
3C	0.00119	0.00108	0.00123
3S	0.00133	0.00125	0.00149
4I	0.00126	0.00125	0.00151
4C	0.00095	0.00093	0.00121
4S	0.00110	0.00105	0.00139
5I	0.00112	0.00110	0.00126
5C	0.00091	0.00081	0.00094
5S	0.00101	0.00098	0.00121
6I	0.00134	0.00124	0.00156
6C	0.00096	0.00090	0.00123
6S	0.00114	0.00107	0.00141
7I	0.00142	0.00140	0.00174
7C	0.00110	0.00112	0.00136
7S	0.00116	0.00112	0.00153
8I	0.00125	0.00123	0.00146
8C	0.00082	0.00080	0.00092
8S	0.00097	0.00091	0.00121
9I	0.00147	0.00133	0.00166
9C	0.00116	0.00109	0.00141
9S	0.00116	0.00110	0.00149

For L1, average values ranged from 0.00082µm^{-1} (8C) to 0.00147µm^{-1} (9I). VOI 8C displayed the lowest trabecular number and differed significantly from VOIs 1I, 1S, 3I, 3S, 6I, 7I and 9I. VOI 5C also displayed a lower trabeculae number, differing from VOIs 3I, 7I and 9I. The high, intermediate and low median values per VOI can be viewed in figure 9.59. Significant differences between VOIs can be visualised in figure 9.60.

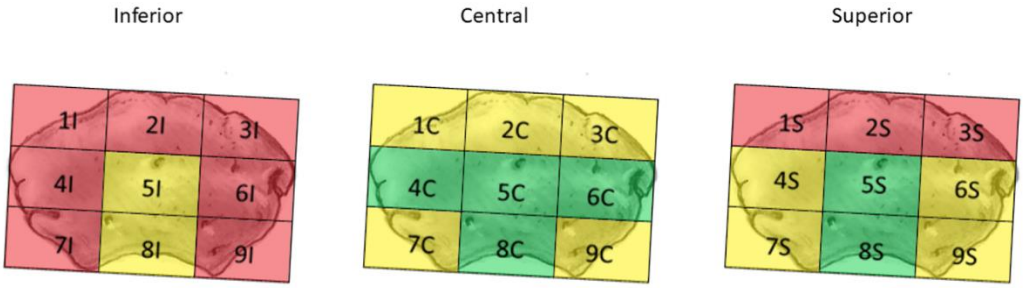

Figure 9.59: The high (red), intermediate (yellow) and low (green) median values for Tb.N (µm^{-1}) at L1 within the 3-8 years of age cohort.

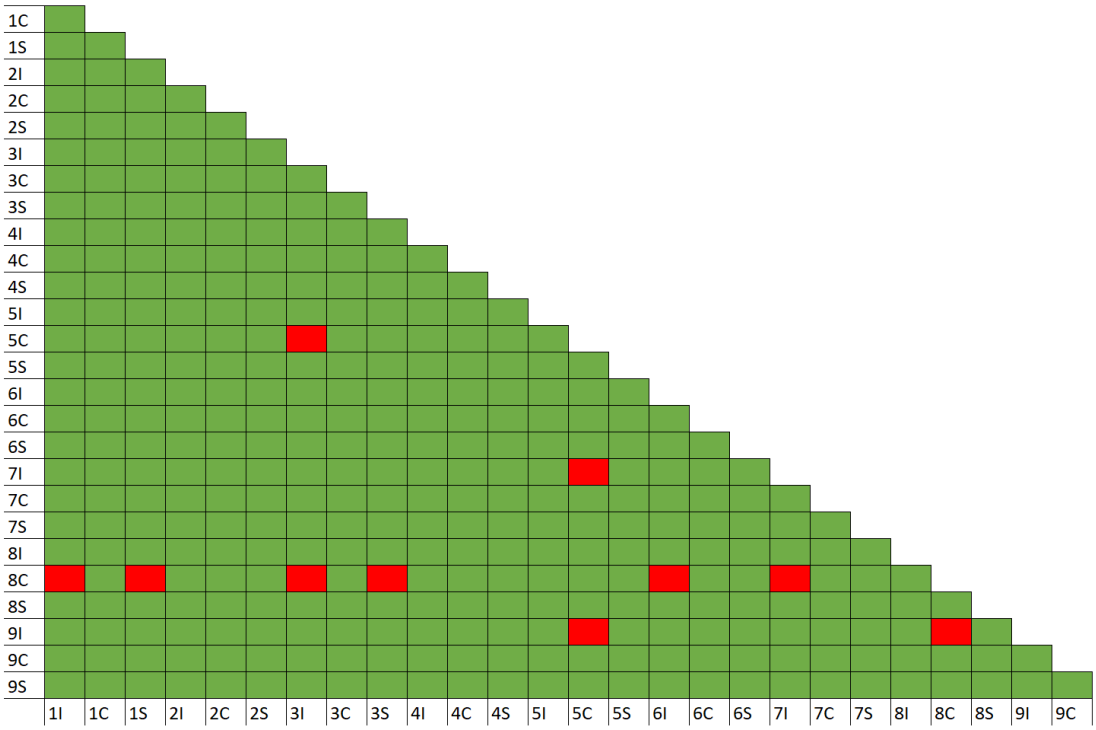

Figure 9.60: The significant differences present between VOIs for Tb.N at L1 within the 3-8 years of age cohort. Significant differences are denoted by red squares.

At L3, trabecular number ranged between 0.00080µm^{-1} (8C) to 0.00140µm^{-1} (7I). VOI 8C once again displayed the lowest average Tb.N and

differed from 1I, 7I and 9I. VOI 5C also displayed significantly lower Tb.N and differed from 7I and 9I. The high, intermediate and low values can be found in figure 9.61. Significant differences between VOIs can be visualised in figure 9.62.

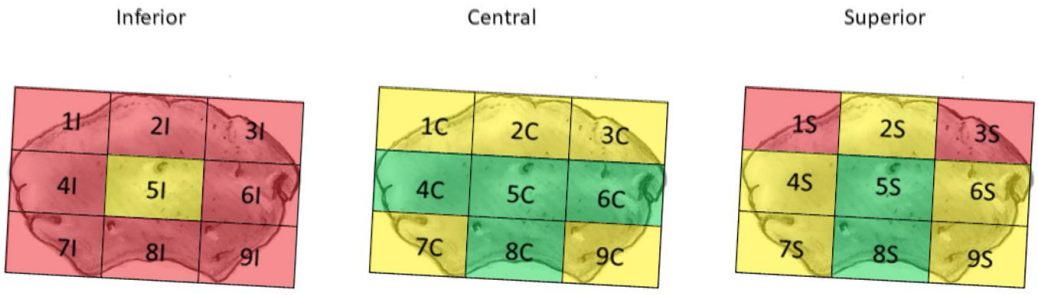

Figure 9.61: The high (red), intermediate (yellow) and low (green) median values for Tb.N (μm^{-1}) at L3 within the 3-8 years age cohort.

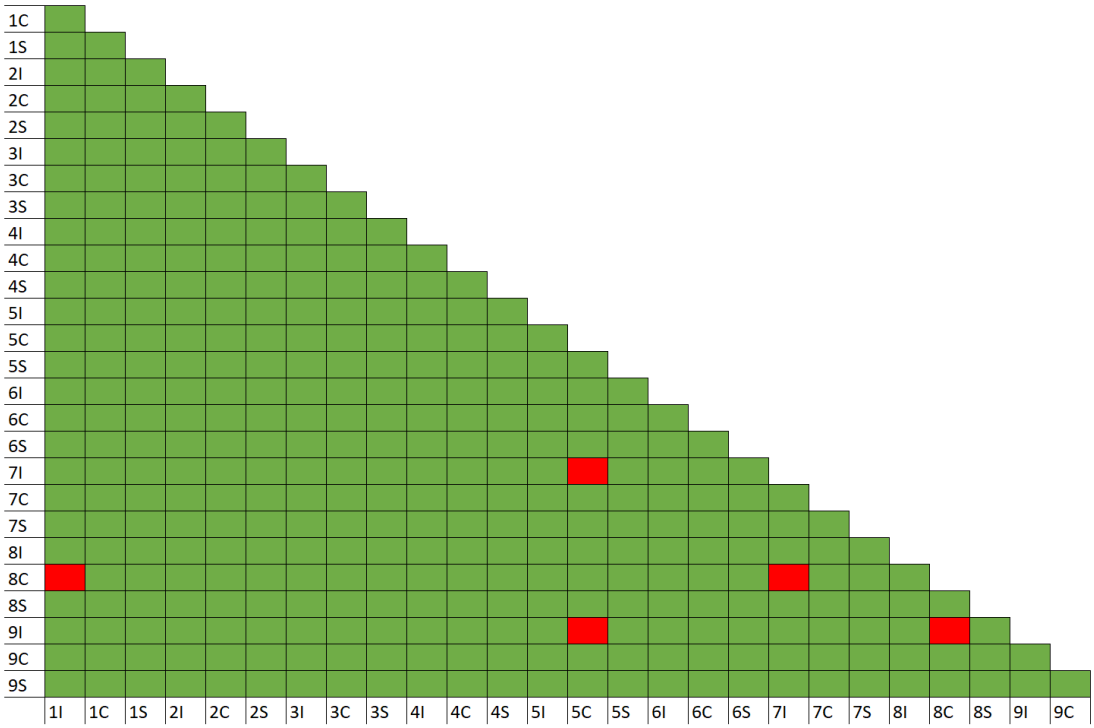

Figure 9.62: The significant differences present between VOIs for Tb.N at L3 within the 3-8 years of age cohort. Significant differences are denoted by red squares.

Average values for Tb.N at the level of L5 ranged from 0.00092μm^{-1} (8C) to 0.00174μm^{-1} (7I). As with the previous vertebral levels, VOI 8C once again displayed the lowest average value. VOIs 5C and 8C both differed significantly to VOIs 1I, 1S, 2I, 3I, 3S, 4I, 6I, 7I 7S, 9I and 9S, with *C also differing to 8I. VOI 2C also displayed a lower Tb.N and differed significantly to VOI 7I, which displayed

the highest average value. The high, intermediate and low values can be found in figure 9.63, significant differences between VOI can be visualised in figure 9.64.

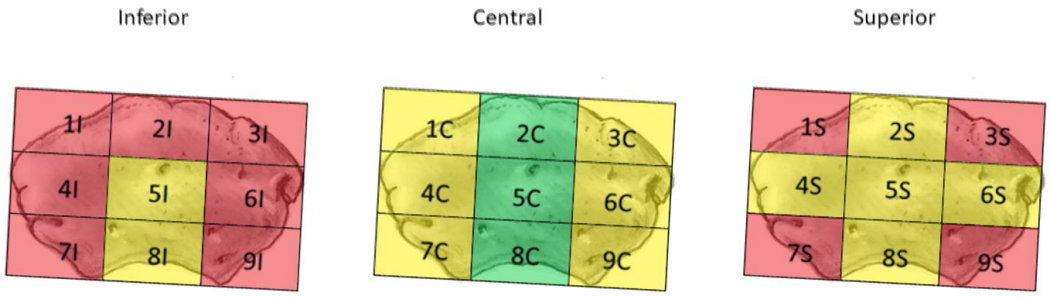

Figure 9.63: The high (red), intermediate (yellow) and low (green) mean values for Tb.N (μm^{-1}) at L5 within the 3-8 years age cohort.

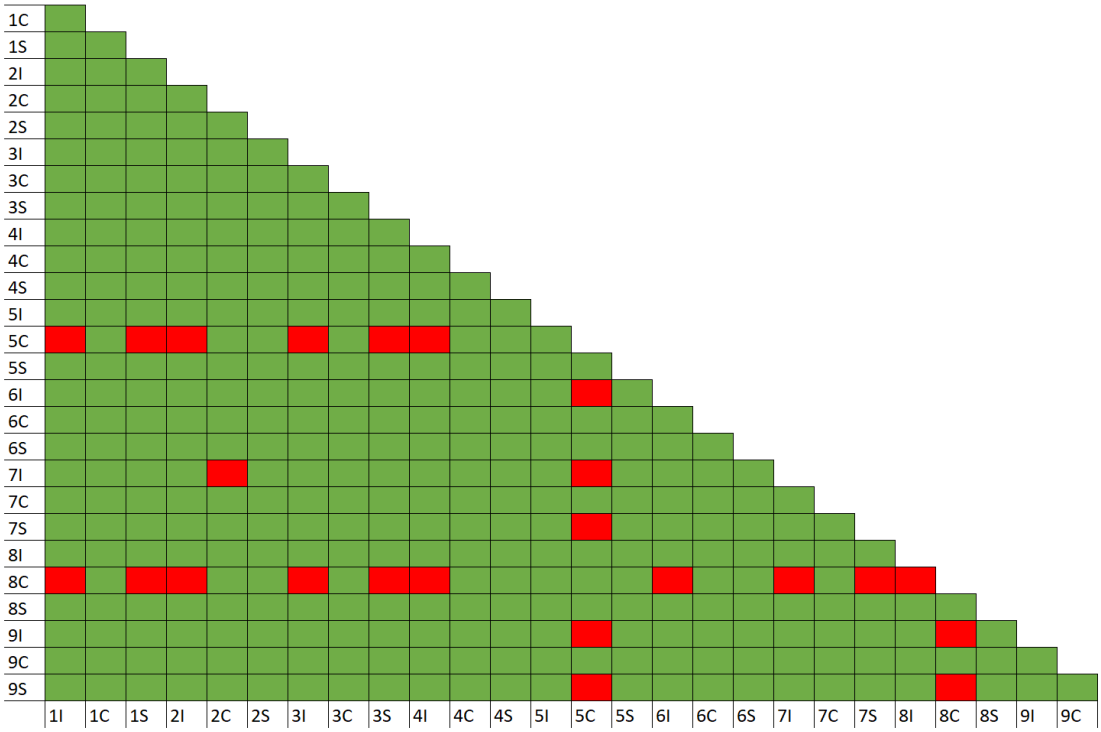

Figure 9.64: The significant differences present between VOIs for Tb.N at L5 within the 3-8 years of age cohort. Significant differences are denoted by red squares.

Central VOIs 5C and 8C consistently displayed a lower number of trabeculae compared to other VOIs while peripheral VOIs within the superior and inferior layers contained more trabeculae over all three vertebral levels studied.

9.2.4.5 Tb.Sp

For trabecular separation within the 3-8y cohort, vertebral levels L1 and L3 displayed significant differences between VOIs. Descriptive statistics for L1, L3 and L5 can be viewed in Table 9.23.

Table 9.23: Descriptive statistics for Tb.Sp (µm) at L1, L3 and L5 in the 3-8y cohort.

	L1	L3	L5
Parametric?	NP	NP	NP
F/H Value	118.33	113.504	76.410
DF	26	26	26
P Value	<0.001	<0.001	<0.001
p≤0.01?	Y	Y	N
Mean/Median	Median	Median	Median
1I	505.59	529.16	435.25
1C	639.38	691.92	669.90
1S	450.37	463.28	481.00
2I	551.32	551.46	506.80
2C	669.20	702.81	682.93
2S	477.53	469.66	479.94
3I	526.46	532.20	477.55
3C	676.61	664.51	682.27
3S	462.35	471.19	478.52
4I	536.95	512.70	477.94
4C	775.10	785.72	644.20
4S	563.31	560.96	527.06
5I	566.75	588.66	556.65
5C	778.00	789.13	776.72
5S	590.79	616.14	576.33
6I	527.03	516.36	458.93
6C	789.72	770.05	636.30
6S	549.14	545.73	494.33
7I	498.24	458.00	386.83
7C	599.19	581.07	537.94
7S	508.94	527.44	468.61
8I	528.09	489.25	438.69
8C	1049.91	1014.13	1001.26
8S	703.02	687.29	573.80
9I	466.91	441.30	416.66
9C	580.82	574.54	524.20
9S	548.53	519.82	482.09

At L1, average values ranged between 450.37µm (1S) to 1049.91µm (8C). VOI 8C exhibited the highest average value and differed significantly from VOIs 1I, 1S, 2S, 3I, 3S, 7I and 9I. Central VOIs 4C, 5C and 6C also displayed higher Tb.Sp values and differed from VOIs 1S and 3S, which displayed the lowest trabecular separation. Figure 9.65 displays the high, intermediate and low values associated with the dataset, while figure 9.66 displays the significant differences between VOIs.

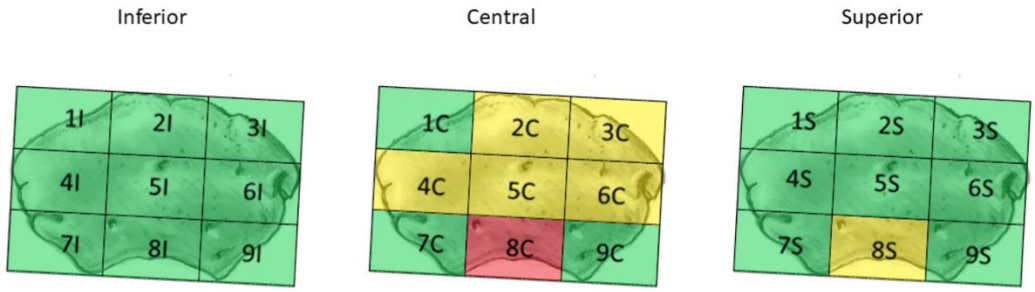

Figure 9.65: The high (red), intermediate (yellow) and low (green) median values for Tb.Sp (µm) at L1 within the 3-8 years of age cohort.

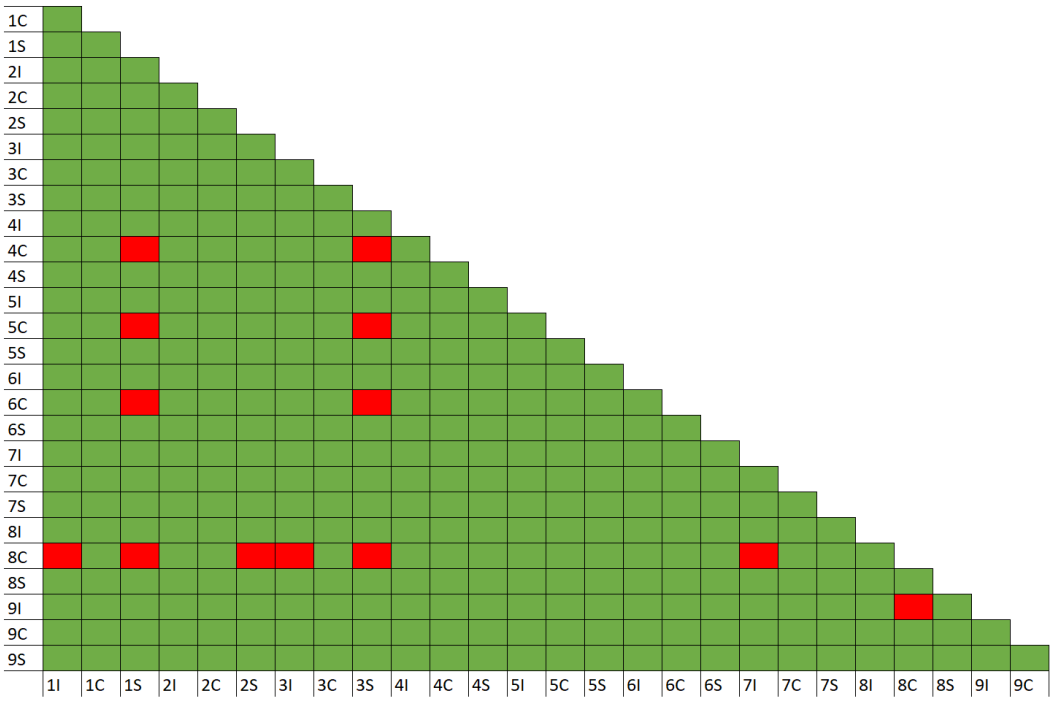

Figure 9.66: The significant differences present between VOIs for Tb.Sp at L1 within the 3-8 years of age cohort. Significant differences are denoted by red squares.

At L3, average values ranged from 441.30µm (9I) to 1014.13µm (8C). VOI 8C once again displayed the highest average value for trabecular separation, and

differed from VOIs 1S, 2S, 3S, 7I and 9I. VOI 9I displayed the lowest trabecular separation and also differed from VOI 4C and 5C. Finally, VOI 1S also displayed lower Tb.Sp and also differed from 4C. The high, intermediate and low values for Tb.Sp per VOI can be viewed in figure 9.67. Significant differences can be found in figure 9.68.

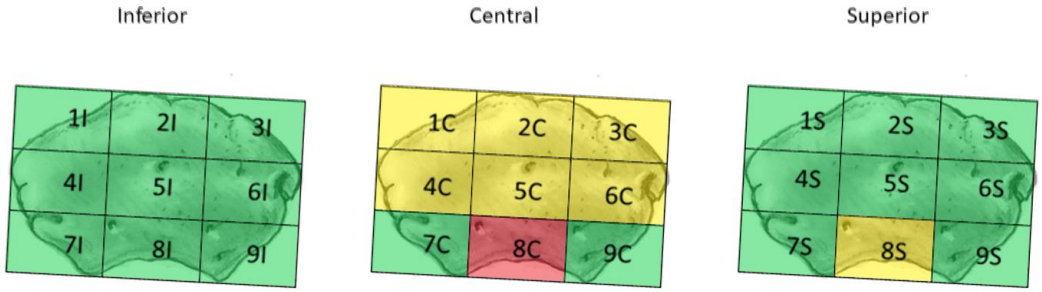

Figure 9.67: The high (red), intermediate (yellow) and low (green) median values for Tb.Sp (μm) at L3 within the 3-8 years of age cohort.

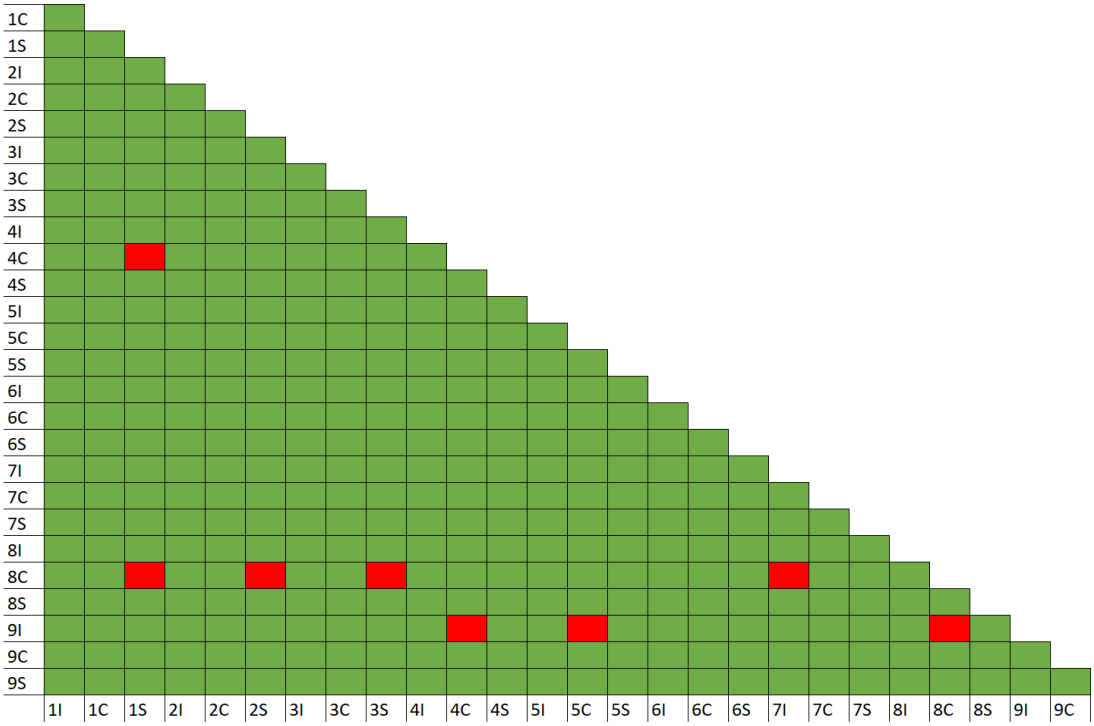

Figure 9.68: The significant differences present between VOIs for Tb.Sp at L3 within the 3-8 years of age cohort. Significant differences are denoted by red squares.

At L5, values for Tb.Sp ranged from 386.83μm (7I) to 1001.26μm (8C). Over all lumbar vertebral levels studied, VOI 8C displayed the highest trabecular separation of all VOIs. VOIs within the central layer generally displayed intermediate values for Tb.Sp while VOIs within the superior and inferior layers displayed lower trabecular separation.

9.2.4.6 DA

For degree of anisotropy, the vertebral levels L1 and L3 displayed significant differences between VOIs. The descriptive statistics can be found in Table 9.24.

Table 9.24: Descriptive statistics for DA at L1, L3 and L5 in the 3-8y cohort.

	L1	L3	L5
Parametric?	NP	NP	NP
F/H Value	136.558	113.483	56.401
DF	26	26	26
P Value	<0.001	<0.001	<0.001
p≤0.01?	Y	Y	N
Mean/Median	Median	Median	Median
1I	0.461	0.513	0.491
1C	0.498	0.570	0.539
1S	0.434	0.483	0.469
2I	0.459	0.446	0.374
2C	0.479	0.512	0.405
2S	0.418	0.315	0.414
3I	0.450	0.525	0.457
3C	0.512	0.539	0.467
3S	0.440	0.427	0.442
4I	0.316	0.185	0.210
4C	0.440	0.415	0.351
4S	0.319	0.319	0.265
5I	0.281	0.212	0.199
5C	0.379	0.356	0.327
5S	0.239	0.218	0.174
6I	0.295	0.248	0.261
6C	0.420	0.398	0.385
6S	0.308	0.270	0.243
7I	0.238	0.178	0.260
7C	0.231	0.314	0.290
7S	0.243	0.217	0.321
8I	0.210	0.200	0.202
8C	0.220	0.314	0.228
8S	0.230	0.175	0.260
9I	0.240	0.206	0.296
9C	0.252	0.240	0.279
9S	0.258	0.247	0.229

At L1, values ranged from 0.210 (8I) to 0.512 (3C). VOI 3C exhibited the highest median value for DA and differed from VOIs 7I, 7C, 7S, 8I, 8C, 8S, 9I and 9C. VOI 1C also differed from VOIs 8I, 8C and 8S, displaying significantly higher degree of anisotropy. The high, intermediate and low values can be viewed in figure 9.69. Significant differences can be viewed in figure 9.70.

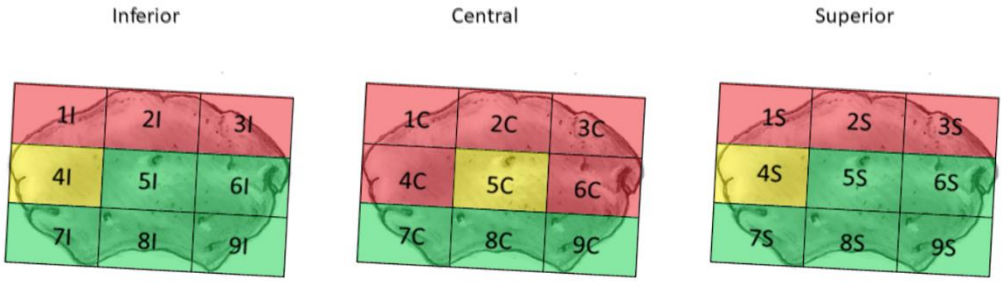

Figure 9.69: The high (red), intermediate (yellow) and low (green) median values for DA at L1 within the 3-8 years of age cohort.

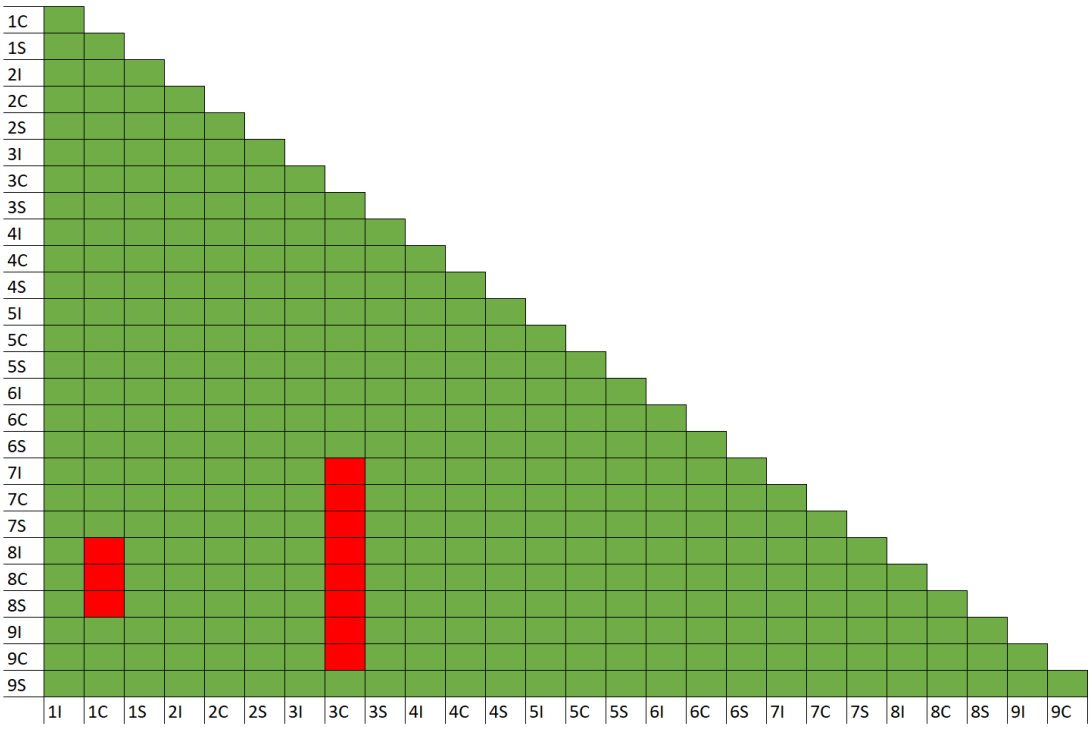

Figure 9.70: The significant differences present between VOIs for DA at L1 within the 3-8 years of age cohort. Significant differences are denoted by red squares.

At L3, average values for DA ranged between 0.175 (8S) and 0.570 (1C). At p≤0.01, VOI 1C differed from 8S, with 1C displaying the highest median value for DA and 8S the lowest. The high, intermediate and low median values can be viewed in figure 9.71. Significant differences can be found in figure 9.72.

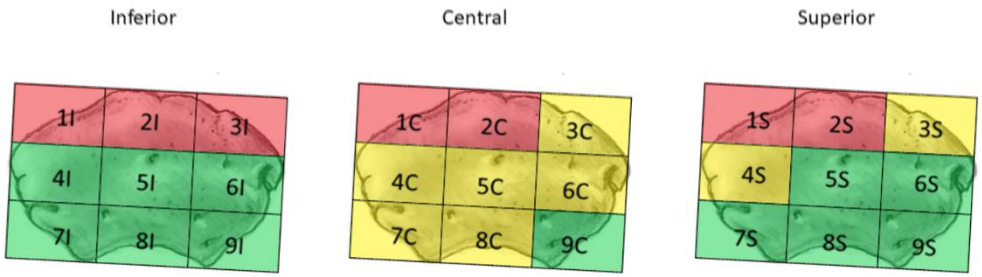

Figure 9.71: The high (red), intermediate (yellow) and low (green) median values for DA at L3 within the 3-8 years of age cohort.

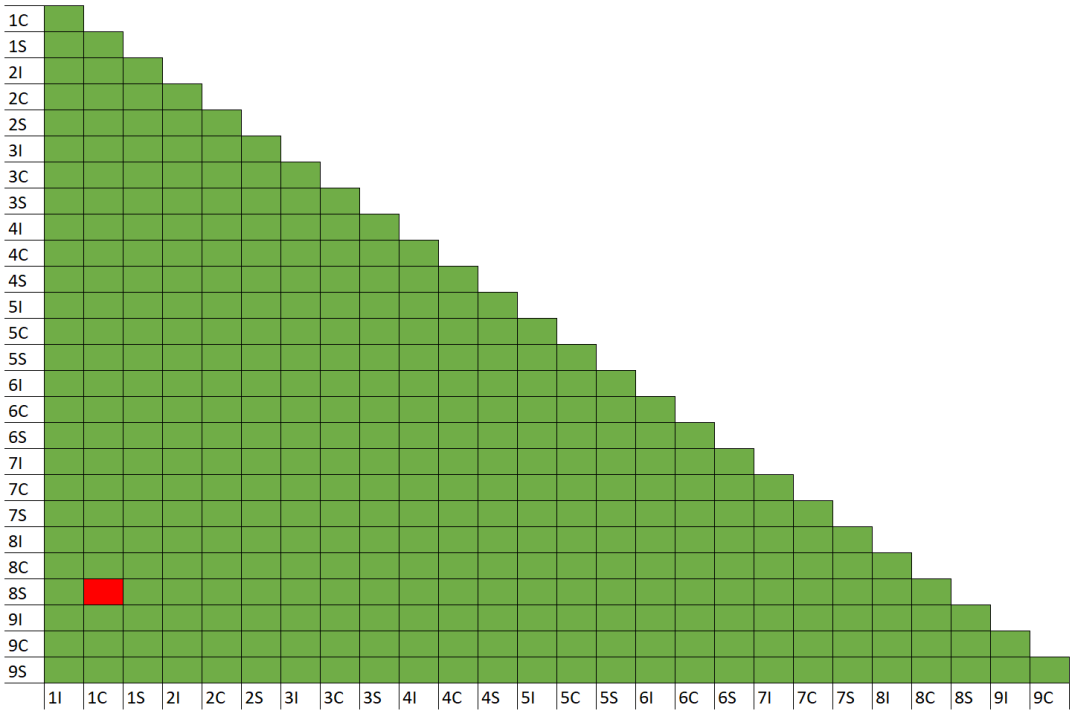

Figure 9.72: The significant differences present between VOIs for DA at L3 within the 3-8 years of age cohort. Significant differences are denoted by red squares.

For L5, the average values ranged between 0.174 (5S) to 0.539 (1C). For DA, anterior VOIs were more likely to display higher anisotropy/ organisation. Central VOI also tended to display more intermediate values, however, this was not significant.

9.3 Summary of Results

A summary of the internal trabecular architecture within the lumbar vertebral centra per VOI can be found in Table 9.25 for the fetal age cohort, Table 9.26 for the perinatal age cohort, 9.27 for the 4 weeks to 2 years of age cohort and Table 9.28 for the 3-8 years of age cohort.

Table 9.25: Table summarising the findings for the fetal age cohort for each parameter per VOI. High, intermediate and low relates to the figures in section 9.2.1.

VOI	BV/TV	SMI	Tb.Th	Tb.N	Tb.Sp	DA
1I	Low to intermediate	High	Low	Intermediate to high	Low	Low to intermediate
1C	Low	High	Low to intermediate	Intermediate	Low	Intermediate
1S	Low to intermediate	High	Low	High	Low	Intermediate to high
2I	Low	Intermediate to high	Low to intermediate	Low to intermediate	Low to intermediate	Low to intermediate
2C	Low	Intermediate to high	Intermediate to high	Low	High	Low to intermediate
2S	Low to intermediate	High	Low to intermediate	Intermediate	Low	Low to intermediate
3I	Low to intermediate	Intermediate to high	Low	High	Low	Intermediate
3C	Low	High	Low to intermediate	Low to intermediate	Low	Intermediate to high
3S	Low to intermediate	High	Low	High	Low	Intermediate to high
4I	Intermediate	Intermediate to high	Intermediate	Intermediate	Low	Intermediate to high
4C	Intermediate	Intermediate to high	Intermediate	Low to intermediate	Low	High
4S	Low to high	Intermediate to high	Low to intermediate	Intermediate	Low	High
5I	High	Low to intermediate	Intermediate to high	Low to high	Low	Low to intermediate
5C	Intermediate	Low to intermediate	High	Low	Intermediate to high	Low
5S	High	Low to intermediate	Intermediate to high	Intermediate	Low	Low to intermediate
6I	Intermediate to high	Intermediate to high	Low to intermediate	Intermediate to high	Low	Intermediate to high
6C	Intermediate	High	Intermediate	Intermediate	Low	High
6S	Low to intermediate	High	Low to intermediate	Intermediate	Low	Low to high
7I	Low to intermediate	High	Low	Intermediate to high	Low	Intermediate to high
7C	Low to intermediate	High	Low to intermediate	Intermediate	Low	High
7S	Intermediate	High	Low	Intermediate to high	Low	High
8I	Generally high	Intermediate to high	Intermediate	Intermediate to high	Low to intermediate	Low to intermediate
8C	Low to intermediate	Low	High	Low	High	Low to intermediate
8S	Intermediate to high	Low to intermediate	Intermediate	Intermediate	Low to intermediate	Intermediate
9I	Low to intermediate	High	Low	Intermediate to high	Low	Intermediate to high
9C	Low to intermediate	High	Low	Intermediate to high	Low	Intermediate
9S	Low to intermediate	High	Low	Intermediate to high	Low	Intermediate to high

Table 9.26: Table summarising the findings for the perinatal age cohort for each parameter per VOI. High, intermediate and low relates to the figures in section 9.2.2.

VOI	BV/TV	SMI	Tb.Th	Tb.N	Tb.Sp	DA
1I	Low to intermediate	High	Low	Intermediate to high	Low	Intermediate to high
1C	Low	High	Low to high	Low	Low to intermediate	Intermediate
1S	Low to intermediate	High	Low	Intermediate to high	Low	Intermediate to high
2I	Intermediate to high	Intermediate to high	Low to intermediate	High	Low	Intermediate to high
2C	Low to high	Intermediate to high	High	Low	Intermediate to high	Low to intermediate
2S	Intermediate	High	Low	Intermediate	Low	Intermediate to high
3I	Low to intermediate	High	Low	High	Low	Intermediate to high
3C	Low	High	Intermediate	Low	Low to intermediate	Low to intermediate
3S	Low to intermediate	High	Low	High	Low	Intermediate to high
4I	Intermediate to high	Intermediate to high	Low to intermediate	High	Low	Intermediate to high
4C	Low	High	Intermediate to high	Low	Low to intermediate	Intermediate to high
4S	Low to intermediate	Intermediate to high	Low	Intermediate to high	Low	Intermediate to high
5I	High	Intermediate	Intermediate	Intermediate	Low	Low to intermediate
5C	Intermediate to high	Low to intermediate	Intermediate to high	Low	Intermediate to high	Low
5S	Intermediate to high	Intermediate to high	Intermediate	Intermediate to high	Low	Low to intermediate
6I	Intermediate	Intermediate to high	Low	Intermediate to high	Low	Intermediate to high
6C	Low	High	Intermediate	Low	Low to intermediate	Low to high
6S	Intermediate to high	Intermediate to high	Low	Intermediate to high	Low	Intermediate to high
7I	Intermediate to high	High	Low to intermediate	Intermediate to high	Low	Intermediate to high
7C	Low	High	Low to intermediate	Low	Low	Intermediate to high
7S	Intermediate to high	Intermediate to high	Low	Intermediate to high	Low	Intermediate to high
8I	Intermediate to high	Intermediate	Low to intermediate	Intermediate to high	Low	Intermediate to high
8C	Intermediate to high	Low to intermediate	High	Low	High	Mostly low
8S	Intermediate to high	Intermediate to high	Low to intermediate	Intermediate	Low	High
9I	Low to high	High	Low	Intermediate to high	Low	Mostly high
9C	Low	High	Low	Low	Low	Intermediate to high
9S	Low to high	High	Low	Intermediate to high	Low	Intermediate to high

Table 9.27: Table summarising the findings for the 4 weeks to 2 years of age cohort for each parameter per VOI. High, intermediate and low relates to the figures in section 9.2.3.

VOI	BV/TV	SMI	Tb.Th	Tb.N	Tb.Sp	DA
1I	Intermediate to high	Intermediate to high	Low to intermediate	High	Low	High
1C	Intermediate to high	Low to intermediate	High	Intermediate	Intermediate	High
1S	Intermediate	Low to intermediate	Low	Intermediate to high	Low	Intermediate to high
2I	Intermediate to high	Low to intermediate	Low to intermediate	Intermediate to high	Low	Intermediate
2C	Intermediate	Low	High	Low	Intermediate	Intermediate
2S	Intermediate	Mostly high	Low	Intermediate to high	Low	Intermediate to high
3I	High	Low to intermediate	Low to intermediate	High	Low	Intermediate to high
3C	High	Low to intermediate	High	Intermediate	Low to intermediate	High
3S	Intermediate to high	Mostly high	Low	High	Low	Intermediate to high
4I	Low to intermediate	Intermediate to high	Low	Intermediate to high	Low	Low to intermediate
4C	Low	Intermediate to high	Low to intermediate	Low to intermediate	Low to intermediate	High
4S	Low to intermediate	High	Low	Intermediate to high	Low	Intermediate to high
5I	Low to intermediate	Intermediate to high	Low	Intermediate	Low	Low
5C	Low	Intermediate to high	Low to intermediate	Low to intermediate	Low to intermediate	Intermediate
5S	Low	High	Low	Low to intermediate	Low	Low to intermediate
6I	Low to intermediate	Intermediate to high	Low	Intermediate to high	Low	Low to intermediate
6C	Low	Intermediate	Low to intermediate	Low to intermediate	Low to intermediate	High
6S	Mostly low	Intermediate to high	Low	Intermediate to high	Low	Intermediate to high
7I	Intermediate to high	Intermediate to high	Low	High	Low	Low to intermediate
7C	Low to intermediate	Intermediate	Low to intermediate	Intermediate	Low	Intermediate
7S	Low to intermediate	High	Low	Intermediate to high	Low	Low to intermediate
8I	Low to intermediate	Intermediate to high	Low	Intermediate to high	Low	Low to intermediate
8C	Low	Low	High	Low	High	Low to intermediate
8S	Low	Intermediate to high	Low to intermediate	Low to intermediate	Low to intermediate	Low to intermediate
9I	Intermediate to high	Intermediate to high	Low	High	Low	Low to intermediate
9C	Low to intermediate	Intermediate to high	Low to intermediate	Low	Low	Low to intermediate
9S	Low to intermediate	Intermediate to high	Low	Intermediate to high	Low	Low to intermediate

Table 9.28: Table summarising the findings for the 3-8 years of age cohort for each parameter per VOI. High, intermediate and low relates to the figures in section 9.2.4.

VOI	BV/TV	SMI	Tb.Th	Tb.N	Tb.Sp	DA
1I	Intermediate to high	Intermediate	Low to intermediate	High	Low	High
1C	Intermediate to high	Low	High	Intermediate	Low to intermediate	High
1S	Low to intermediate	High	Low	Intermediate to high	Low	High
2I	Intermediate to high	Intermediate	Low to high	High	Low	Intermediate to high
2C	Low to high	Low	High	Low to intermediate	Intermediate	Intermediate to high
2S	Low	High	Low	Intermediate to high	Low	Intermediate to high
3I	Intermediate to high	Intermediate to high	Low to intermediate	High	Low	High
3C	Intermediate to high	Low	High	Intermediate	Intermediate	Intermediate to high
3S	Low to intermediate	High	Low	High	Low	Intermediate to high
4I	Low to high	High	Low	High	Low	Low to intermediate
4C	Low	Low to intermediate	Intermediate	Low to intermediate	Intermediate	Intermediate to high
4S	Low	High	Low	Intermediate	Low	Low to intermediate
5I	Low to intermediate	High	Low to intermediate	Intermediate	Low	Low
5C	Low	Low to intermediate	Mostly high	Low	Intermediate	Intermediate
5S	Low	High	Low	Low to intermediate	Low	Low
6I	Intermediate	Intermediate to high	Low to intermediate	High	Low	Low
6C	Low	Low to intermediate	Low to high	Low to intermediate	Intermediate	Intermediate to high
6S	Low	High	Low	Intermediate	Low	Low
7I	Intermediate to high	High	Low	High	Low	Low
7C	Low to intermediate	Intermediate	Low to intermediate	Intermediate	Low	Low to intermediate
7S	Low to intermediate	High	Low	Intermediate to high	Low	Low to intermediate
8I	Low to intermediate	High	Low	Intermediate to high	Low	Low
8C	Low	Low	High	Low	High	Low to intermediate
8S	Low	High	Intermediate to high	Low to intermediate	Low to intermediate	Low
9I	Intermediate to high	Intermediate to high	Low to intermediate	High	Low	Low to intermediate
9C	Low to intermediate	Low to intermediate	Low to intermediate	Intermediate	Low	Low
9S	Low	High	Low	Intermediate to high	Low	Low to intermediate

10 Discussion

10.1 The structure of the lumbar vertebral trabecular architecture

The adult architecture of the lumbar vertebrae has been studied extensively, perhaps in part due to its implication in osteoporosis among the aging population. The fetal, perinatal and early postnatal architecture of the lumbar vertebrae has been observed to differ to the adult structure. However, few studies have focused on understanding the implications of the fetal and perinatal trabecular architecture in the lumbar vertebral column or its change with age or locomotor demands (Kneissel *et al*., 1997; Roschger *et al*., 2001; Nuzzo *et al*., 2003; Acquaah *et al*., 2015) and hence, the architecture has not been well considered.

The developing lumbar centrum was divided into 27 VOIs that enabled the separation of central region (VOIs 2C, 5C, 8C) from peripheral regions (VOIs 1, 3, 4, 6, 7, 9), superior regions (VOIs 1S-9S) from inferior regions (VOIs 1I-9I), and anterior regions (VOIs 1, 2, 3) from posterior regions (VOIs 7, 8, 9).

10.1.1 *The structure and function of central VOIs*

Throughout all age cohorts, the trabecular architecture of the central region was characterised by a lower number of thick, well-spaced trabeculae predominantly plate-like in origin. While the general trabecular morphology of the central region does not seem to display any significant changes with age, there is the potential that the development of the architecture observed prenatally and postnatally are driven by different factors.

10.1.1.1 Fetal and perinatal architecture

The ossification of the lumbar vertebral centrum has been identified as a significant factor influencing the microarchitecture of the vertebral centrum during the early stages of skeletal development (Roschger *et al*., 2001; Nuzzo *et al*., 2003). The lumbar vertebral centrum develops from a central primary ossification centre that appears around the 2nd month *in utero*. The central region of the developing centrum is in proximity to the centre of ossification. The lumbar vertebral centra undergo endochondral ossification. The conversion of the cartilaginous anlage to bone is driven by proliferation, hypertrophy and apoptosis of chondrocytes which occurs at the growth plate, driving bone growth (Byers *et al.*, 2000; Abad *et al.*, 2002; Burdan *et al.*, 2009). The trabecular architecture in

the central region is most likely affected by its proximity to the ossification centre, characterised by significantly thicker trabeculae (Nuzzo *et al*., 2003). The trabecular thickness observed at this stage of development is most likely due to the increased maturity afforded by proximity to the ossification centre. This observation has also been made in the fetal femur (Salle *et al*., 2002; Reissis and Abel, 2012) and humerus (Reissis and Abel, 2012). Salle *et al*. (2002) observed that trabeculae located closer to the centre of ossification were 41µm thicker than those closest to the growth plate. In the current study, trabecular thickness in the central regions differed from the growth plate by as much as 80µm in some cases during the fetal period. This change in thickness was linked to the age of the trabeculae in the fetal femur, with the central trabeculae in the femur being around 14 days older than its peripheral counterpart and was attributed to bone modelling, rather than remodelling due to the rate of bone deposition needed to produce such thickening within the relatively short time period (Salle *et al*., 2002). While bone remodelling is a coupled process involving both bone resorption and bone formation, it was unlikely that it could produce the thickening seen, however bone modelling is characterised by bone formation that is not coupled with bone resorption (Salle *et al*., 2002; Roberts *et al.*, 2004; Clarke, 2008; Brandi, 2009). As the central region of the fetal lumbar vertebral centra display a similar, if not more pronounced thickening than in the fetal femur, it is reasonable to assume that this trabecular thickening is also a result of increased bone modelling having occurred at central sites compared to more immature bone found at the peripheral growth plates.

The initiation of ossification in all skeletal elements that undergo endochondral ossification relies on vascularisation of the cartilaginous anlage. Without vascularisation, ossification cannot be initiated as the invading arterial supply delivers cells such as osteoprogenitor cells, osteoclasts, osteoblasts and haematopoietic cells to the area to initiate the conversion of cartilage to bone (Alini *et al.*, 1996; Olsen *et al.*, 2000; Petersen *et al*., 2002; Colnot *et al.*, 2004; Maes, 2013; Jiang *et al.*, 2017). Vascularisation of the central region of the vertebral centra is via at least four nutrient arteries. Posteriorly, one or two nutrient arteries enter the cartilaginous anlage (Ratcliffe, 1981), while multiple branches from segmental arteries enter the central portion of the centrum anterolaterally (Guida *et al.*, 1969; Skawina *et al.*, 1997; Demed *et al.*, 2013).

These vessels are present prior to the formation of the lumbar vertebral trabecular architecture and thus occupy space within the developing centrum around which bone must be laid down. Trabeculae can only extend into free space and form between vascular channels, which has a significant holistic effect on their architecture. This central region of trabeculae displays a decrease in BV/TV compared to other areas of the centrum, as more of the volume is likely comprised of vascular tissue. Central VOIs within the fetal period also display relatively lower values for SMI, indicating more plate-like trabeculae are present centrally. The morphology of trabeculae, as described by SMI, can give an indication of the mechanical strength of the structure in question (Ding *et al*., 2002; Liu *et al*., 2008). Plate-like trabeculae are considered to be mechanically strong and correlated positively with bone elasticity. Meanwhile, rod-like trabeculae are considered a product of increased remodelling and are less mechanically strong (Hildebrand and Rüegsegger, 1997a; Liu *et al*., 2006; Liu *et al.,* 2008). As a decrease in BV/TV leads to a less mechanically strong structure, a plate-like morphology likely acts to reinforce the trabecular structure.

The lumbar vertebral centra are not the only skeletal structure to display an early trabecular architecture related to vasculature. The developing scapula was also identified to display a relatively low BV/TV and high SMI in areas in close proximity to the ossification centre, with voids within the structure attributed to vasculature (O'Malley, 2013). The ischium has also displayed a similar structure, where more plate-like trabeculae were also attributed to reinforcing a region of low BV/TV and hence a region of potential failure (Maclean, 2017). In the fetal ilium, initial modelling of the trabecular structure was observed to be largely dictated by vascular invasion of the cartilaginous ilium. The pattern of vascularisation within the developing ilium was also proposed to have a bearing on the trabecular orientation within the early stages of development. As vascularisation increases along with the size of the ilium, it continues to occupy increased space and may fundamentally dictate the pattern of growth of the trabeculae within the highly vascularised region (Cunningham and Black, 2010). Furthermore, in the fetal tibia, trabeculae were oriented in vertical columns due to the pattern of ossification and anatomy of the growth plate, with vasculature extending superiorly from the ossification centre and inferiorly from the metaphyseal surface (Gosman and Ketcham, 2009). As the degree of anisotropy

of the lumbar vertebral centra does not seem to change over the developmental cohorts studied, it may be that the presence of vascular space occupying structures within the region are responsible for the predominantly vertical trabecular struts seen in the adult.

Ossification is a closely controlled and coordinated process and one such factor implicated in the initiation and control of ossification is mechanical stimulation (LeVeau and Bernhardt, 1984; Dirckx *et al*., 2013). Initiation of ossification within the lumbar vertebrae occurs around 8 weeks *in utero*, while fetal movements occur from 7 weeks *in utero* and begins with sideways bending (Nowlan, 2015). Sideways bending involves the trunk and coincides with the initiation of ossification in the vertebral column, while the musculature of the trunk is also identifiable around this time (Warmbrunn *et al*., 2018). It is possible that this early fetal movement stimulates osteogenesis in the lumbar vertebral column. Furthermore, *in utero* limb movements have been found to coincide with osteogenesis within the limbs (Nowlan, 2015), hence it is possible that the same is true for the lumbar vertebral centra. Fetal movement is not only implicated in osteogenesis, but also continued bone development in the fetal period (Miller, 2005; Nowlan, 2015; Shea *et al.*, 2015; Verbruggen *et al.*, 2016). Reduced fetal movement has been found to result in weaker, hypomineralised bones, which indicates that fetal movement most likely plays a vital role in normal ossification (Shea *et al*., 2015; Verbruggen *et al*., 2016). In cases where fetal movement is reduced, decreased fetal loading leads to decreased bone strength (Miller, 2005). This is due to the mechanostat theory of bone remodelling, where decreased loading leads to stimulation of osteoclasts rather than osteoblasts and the resulting bone produced is of less than optimal strength.

10.1.1.2 Postnatal architecture

In the adult, the central region of the lumbar vertebral body is characterised by a low number of thick, plate-like trabeculae that are well separated and predominantly vertically oriented (Amstutz and Sissons, 1969; Whitehouse *et al.*, 1971; Kneissel *et al.*, 1997; Thomsen *et al.*, 2002a). It is well established that the trabecular architecture within the adult lumbar vertebral body is heavily influenced by its functions (Smit, 1996; Briggs *et al*., 2004; Liu *et al*., 2009). Trabecular orientation has long been observed to mirror the predominant loads placed upon it (Wolff, 1870; Huiskes, 2000; Hammer, 2010). The proximal femur has been

extensively studied in this regard, with two trabecular trajectories present equating to the compressive and tensile forces placed upon it (Hammer, 2010; 2015).Therefore, the predominantly vertically oriented trabeculae within the central region of the lumbar vertebral bodies can be explained in terms of the axial compressive load that is placed upon them most notably during upright posture in sitting and standing (Adams and Hutton, 1980).

In a study of trabecular architecture of the lumbar vertebral body and its relation to principal stresses placed upon it, Smit *et al*. (1997) identified that the trabecular struts within the central region were loaded significantly under axial compression and extension, which helped to explain their predominantly vertical orientation. Furthermore, in studies of vertebral compressive strength, the central portion of the vertebral body can withstand axial compressive load (Ochia *et al*., 2003; Eswaran *et al.*, 2006; Gong *et al*., 2005; 2007). However, in the same vertebral compressive studies, when compared to the vertebral endplates, the central region of the vertebral body is significantly weaker and reinforced by the vertebral endplates under all stresses. This implies that the central region, while displaying a trabecular architecture adapted to withstand compressive loading, performs other functions that may also influence its trabecular architecture. Other than load-bearing, the primary function of the central portion of the lumbar vertebral body is haematopoiesis (Palastanga *et al.*, 2002; Moore *et al.*, 2019).

Haematopoiesis is the process by which mature blood and immune cells are formed (Cool and Forsberg, 2019). The primary site for haematopoiesis is bone marrow, which occupies the space between trabeculae within cancellous bone (Lowe, 2015). Bone marrow is dependent on both arterial supply and venous drainage to perform its function, with the nutrient artery supplying the bone marrow while venous drainage acts as a passage for the newly formed blood cells to enter the blood stream. Due to haematopoiesis, vascularisation of the postnatal lumbar centrum continues to play a pivotal role in the architecture of the central region. Kneissel *et al*. (1997) attributed the large spaces between the trabeculae within the centrum in the first decade of life to space occupying vascular structures, particularly from the posterior aspect of the centrum. The basivertebral vein is the primary vessel for venous drainage from the lumbar centrum (Crock and Yoshizawa, 1976), and likely contributes significantly to the large spaces observed by Kneissel *et al*. (1997), the area of low radiographic

intensity observed posteriorly in all ages in the qualitative aspect of this project and the low BV/TV found in the posterior aspect of the developing central region quantitatively.

The developing trabecular architecture has been observed to display its characteristic adult pattern early within the postnatal period (Roschger *et al.,* 2001). Although this study did not identify any apparent significant changes in trabecular orientation in the central region between the prenatal and postnatal periods, a transition from the radial orientation seen in the central portion in the fetal and perinatal period to the characteristic vertically and horizontally oriented trabecular architecture characteristic in the adult vertebral body was observed early within the postnatal period in other studies (Kneissel *et al*., 1997; Roschger *et al*., 2001). In the literature, this transition is considered to be in response to increased biomechanical demand (Roschger *et al*., 2001). However, the early postnatal period is considered a period of relatively decreased biomechanical demand compared to the fetal period, with the *in utero* environment providing increased resistance for *in utero* movements that is removed at birth. This implies that other factors may be at work for this trabecular transition to occur.

A predetermined trabecular architecture prior to the onset of habitual load-bearing has been observed previously in the ilium (Cunningham and Black, 2009a; 2010; Abel and Macho, 2011). The lack of significant changes in organisation in this study over all cohorts may imply that this may also be the case of the lumbar vertebrae, with the architecture of the central region predominantly due to the pattern of ossification and the presence of vasculature.

10.1.2 *The structure and function of superior and inferior VOIs*

The superior and inferior regions of the developing centrum generally displayed a less organised trabecular architecture with a lower bone volume fraction that increased with age and a larger number of thinner, more rod-like trabeculae that were more densely packed compared to the central region. However, the central areas of the superior and inferior regions tended to display an architecture similar to that of the developing central region.

10.1.2.1 Fetal and perinatal architecture

As with the central region, the trabecular architecture of the fetal and perinatal centrum peripherally is thought to be influenced by the pattern of ossification.

As the lumbar vertebral centra follow the pattern of endochondral ossification, while central trabeculae are thicker due to increased remodelling, trabeculae within the superior and inferior regions are more immature and as a result have undergone less modelling. Therefore, they are significantly thinner and more rod-like in morphology. In the developing bone, the superior and inferior regions equate to the growth plate region of a growing bone. Other studies into fetal and perinatal vertebral architecture have identified that these areas of bone growth are characterised by radially oriented, thinner, more rod like trabeculae (Roschger *et al*., 2001; Nuzzo *et al*., 2003). It has been observed that trabecular thickness and trabecular separation are around 10 times lower in the external portion of the developing fetal lumbar vertebral centrum compared to the internal (Nuzzo *et al*., 2003). Furthermore, these observations are not limited to the developing vertebral centrum. Trabecular architecture at the location of the growth plate in the fetal proximal tibia has been observed to be significantly more dense compared to bone closer to the ossification centre, as well as displaying thinner, more immature trabeculae (Gosman and Ketcham, 2009). In a histological study of the proximal femoral metaphysis in the fetal period, trabeculae were observed to thicken with gestational age, hence the youngest trabeculae at the growth plate were considerably thinner to trabeculae that had formed 14 days prior. The rapid rate of bone formation at the metaphysis was attributed to the increased number of trabeculae present within the region (Salle *et al*., 2002).

The central parts of the superior and inferior regions displayed a higher bone volume fraction when compared to peripheral superior and inferior regions and displayed the highest BV/TV of all VOIs studied in the fetal period. These areas are situated directly superior and inferior to the ossification centre and accommodate vascular branches directly from the central nutrient arteries that branch superiorly and inferiorly to supply the IV discs and metaphyseal plates. However, these branches are smaller and thinner, branch less and thus occupy less space compared to the nutrient artery of the ossification centre in the fetal

period (Ratcliffe, 1981). The proximity of these trabeculae to the ossification centre likely leads to increased maturity and thickness of the trabecular struts compared to those in peripheral superior and inferior volumes, while increased space to occupy leads to increased Tb.N and, as a result, BV/TV. The peripheral areas of the superior and inferior regions of the developing centrum also contain space occupying vascular structures including metaphyseal and equatorial branches in the form of centripetally directed arcades formed from the perichondral vessels (Demed *et al*., 2013). As with the central superior and inferior regions, these vessels are relatively simple in the fetus and occupy less space within the peripheral regions (Ratcliffe, 1981), allowing more space for bone tissue, leading to the increased in trabecular number and bone volume fraction observed.

10.1.2.2 Postnatal architecture

In the adult, the superior and inferior areas of the vertebral body are characterised by a dense network of horizontally and vertically oriented, thinner, more rod-like trabeculae (Amstutz and Sissons, 1969; Whitehouse *et al.*, 1971; Kneissel *et al.*, 1997; Thomsen *et al.*, 2002a).

The end plates of the vertebral body have long been considered to play an important role in vertebral strength under compression (Grant *et al*., 2001; Ferguson and Steffen, 2003; Ochia *et al*., 2003; Eswaran *et al*., 2006; Hou *et al.*, 2013). This has been identified in studies of vertebral compressive strength, where removal of the superior and inferior endplate regions of the vertebral body leads to a decrease in the compressive load needed to fracture the vertebral body (Grant *et al*., 2001; Ochia *et al*., 2003; Eswaran *et al*., 2006; Hou *et al*., 2013).

Some, but not all, studies into adult vertebral trabecular architecture have observed significant differences in trabecular architecture between the superior and inferior regions of the vertebral body (Banse *et al*., 2002; Gong *et al*., 2005). The inferior endplate has been observed to be significantly denser in some studies (Banse *et al*., 2001; Gong *et al*., 2005) which has been linked to a mechanically stronger inferior end plate in vertebral compressive studies (Grant *et al*., 2001). While the superior and inferior regions did not always display a similar architecture across VOIs and cohorts, no consistent differences between the regions could be established in this study. However, it is important to note

that some individuals studied, including all fetal and perinatal individuals, had yet to undergo neurocentral fusion and it was not possible to differentiate accurately between the superior and inferior regions of the centrum in these cases. Due to this, differences between the regions may have been concealed. However, there were also no apparent differences in older cohorts that had commenced neurocentral fusion implying that the development of these differences occurs after the age of 6-8 years.

As with the central region, the trabecular architecture of the superior and inferior regions has been observed to transition into its adult architecture early in the postnatal period with the superior and inferior regions displaying a high number of thin trabeculae of both horizontal and vertical orientation (Roschger *et al.,* 2001). This orientation has been observed to reinforce the vertical trabeculae of the central region (Smit *et al*., 1997). As mentioned previously, early postnatal biomechanical demand is generally lower than in the fetal period, however, this transition is still observed. In the adult, the superior and inferior regions play a major role in the conversion of torsional, sheer and tensile forces into axial compression, which the adult lumbar vertebral architecture is optimal to withstand (Smit *et al*., 1997; Boszczyk *et al*., 2002). These torsional, shear and tensile forces are also present in the early pre- and post-natal periods, more so than axial compression, as the individual has not yet begun to sit and stand. Movements such as side bending and general contraction of the musculature attached to developing neural hemiarches leads to these forces being placed upon the developing lumbar column (LeVeau and Bernhardt, 1984). Hence, a potential explanation for the early orientational transition consistently observed in this period may be due to these forces being translated in axial compressive force, while axial compression itself has yet to become a major load acting on the vertebral column.

10.1.3 *The structure and function of peripheral VOIs*

The peripheral regions of the developing centrum displayed a similar architecture to the superior and inferior regions, with lower bone volume fraction and a higher number of thinner trabeculae when compared to the central region.

10.1.3.1 Fetal and perinatal architecture

Growth does not only occur longitudinally, but also radially at the periosteum. As with the superior and inferior regions of the developing centrum, the peripheral areas of the centrum are also predominantly formed of immature bone laid down, though this bone is now laid down through periosteal apposition (Prentice, 2001).

Furthermore, a second pair of growth plates are present posterolaterally, extending towards the pedicular boutons of the developing neural hemiarches (Maat *et al.*, 1996; Zhou *et al.*, 2014). There is evidence of the presence of these growth plates within the fetal and perinatal period, with these areas formed of radiographically intense projections caused by increased Tb.N and BV/TV. The initiation of these posterolateral growth plates may be different to the superior and inferior metaphyseal growth plates. It has been suggested that axial rotation of the trunk in the fetal period stimulates the development of the facet joints as it plays a role in change in orientation of the facet joints postnatally (Boszczyk *et al*., 2002). As with all synovial joints, the superior and inferior facet joints are bony surfaces covered by articular cartilage and are formed during the chondrification process (Decker *et al.*, 2014). Joint formation is initiated with the formation of an interzone between cartilaginous elements. The interzone is formed of dense mesenchymal cells (Pacifici *et al.*, 2006). Unlike the cells around it, the interzone does not become chondrogenic and cells undergo apoptosis, initiating cavitation of the joint (Archer *et al.*, 2003). Outer cells do not undergo apoptosis and instead differentiate into the layered articular cartilage surrounding the articular surfaces of the joint (Decker, 2017). Mechanical stimulation has been implicated in the early stages of the development of the facet joints. Early synovial joint formation has been observed to fail when *in utero* movement is absent or reduced in chick models (Shea *et al*., 2015).

The pattern of ossification in the developing ilium could be considered similar to the ossification of the lumbar centrum. Both skeletal elements display evidence of multiple growth plates, with growth of the ilium occurring at metaphyseal growth fronts at the iliac crest and acetabular region (Cunningham and Black, 2010). It was speculated that modelling of the early trabecular architecture was partially controlled by metaphyseal drivers which caused the radiating pattern of trabeculae from the location of the ossification centre towards

the growth plates observed. Alongside the growth plates, areas of restricted growth sections were also observed. These were in the location of the anterior inferior iliac spine, the greater sciatic notch and the caudal auricular region (Cunningham and Black, 2010). In the lumbar vertebrae, four growth plates have been observed: the superior growth plate, the inferior growth plate and the left and right posterolateral growth plates. No growth plate has been observed regarding growth of the anterior, or lateral regions. However, while there is a lack of metaphyseal growth plates in these regions, rather than them being regions of growth, it is likely that growth anteriorly and laterally is primarily achieved through periosteal apposition. This is corroborated by radial distribution of trabeculae within the developing lumbar vertebral centrum, extending outwards from the ossification centre (Roschger *et al*., 2002; Nuzzo *et al*., 2003)

10.1.3.2 Postnatal architecture

In the adult literature, the anterior third of the vertebral body has been found to display lower values for BVTV, characterised by fewer trabecular with greater spacing when compared to the posterior two thirds of the vertebral body (Chen *et al*., 2008). Meanwhile, the posterolateral aspect of the vertebral endplate regions has been found to display a denser architecture and greater strength (Ferguson and Steffen, 2003; Thomsen *et al*., 2002a). This posterolateral region is in close approximation to the pedicles in the adult, and the site of neurocentral fusion in the juvenile. In the adult, the pedicles are closely associated with the facet joints, which act to transmit both axial compressive force in standing, and shear force in lateral bending and rotation movements through the intervertebral disc (Adams and Hutton, 1980; Smit *et al*., 1997). The increased strength in the posterolateral region of the adult endplate is therefore likely related to the shear force dissipated towards the posterolateral intervertebral discs and hence, the posterolateral region of the vertebral body.

In early infancy, the facet joints have yet to adopt their characteristic vertical positioning seen in the adult and this has also been related to the shear and torsional forces placed upon the vertebral column (O'Rahilly *et al.*, 1990; Boszczyk *et al.*, 2002). Their morphology is based upon two principles: support and mobility; and it is the latter that has a large involvement in the postnatal morphological change seen at the facet joint. Torsional forces placed upon the spine cause the lateral aspects of the joint to become more sagittally oriented

(Boszczyk *et al.*, 2002). The characteristic vertical position seen in the adult is not attained until the 1st year of life (Cunningham *et al.*, 2016) however the formation of the joint occurs simultaneously with the ossification of the vertebral centra in the fetal period.

In this study, the most posterolateral regions do not display a trabecular architecture that implied increased strength compared to other regions. No consistent, significant increase in SMI, BV/TV or Tb.Th was observed. This may be due to the mechanism of fusion at the neurocentral junction. Even after fusion has occurred, a bony plate has been found to remain between the posterolateral centrum and pedicular bouton. Hence, it is likely that it is instead the architecture within the pedicular bouton that is more accommodated to accept these shear forces (Maat *et al.*, 1996).

However, this study found that the anterior region of the vertebral centrum tended to present slightly higher values for BV/TV and Tb.N postnatally, as well as being more structurally organised than the posterior region. The reasons for the posterior region to display a structure considered to be more mechanically strong have been considered above. However, this study indicates a potentially more mechanically strong anterior region hence there must be a reason for this finding. Perhaps a major initiator of this anterior trabecular architecture is the anterior longitudinal ligament. Of all the ligamentous structures, it is the largest and strongest (Ebraheim *et al*., 2004; Drake *et al*., 2010; Moore *et al*., 2019) and attaches along the length of the column, wrapping around the entirety of the anterior surface of the vertebral bodies. It is also the only ligament that acts to limit extension of the vertebral body. Hence, its attachment to the anterior vertebral body may play a role in stimulating the trabecular architecture to develop more robustly than the posterior. Perhaps this is only present in infancy and early childhood, prior to neurocentral fusion, and perhaps, once neurocentral fusion has occurred and formed the mature vertebra, the posterior region begins to develop more mechanically strong trabeculae in relation to the extensive musculature and ligamentous structures associated with the neural arch. It is less likely for the posterior longitudinal ligament (PLL) to have an effect on the posterior vertebral architecture due to its lack of attachment to the posterior aspect of the vertebral body. As it only attaches to the IV discs, and is considerably thinner and weaker than the ALL, it may explain why the posterior

region is less organised and mechanically strong. It is also important to note that a number of studies focus only on quantifying the trabecular architecture of frontal vertebral sections (Thomsen *et al*., 2000). While a difference between anterior and posterior regions may have been present it was not possible within these studies to compare the anterior and posterior regions and identify these differences.

10.2 Ontogenetic changes in lumbar vertebral trabecular architecture

Ontogenetic changes in the juvenile skeleton are characterised by an increase in size and change in shape (Bachrach, 2001; Acquaah *et al.*, 2015). Changes in juvenile trabecular architecture are achieved through bone modelling and remodelling, driven by the process of bone formation and resorption. It has been contemplated that the early development of trabecular bone plays a significant role in adult trabecular architecture and bone health (Bailey *et al*., 1999; Bachrach, 2001; Javaid and Cooper, 2002; Cooper *et al*., 2005; Goldberg, 2006; Ay *et al*., 2011; Acquaah *et al.*, 2015). As vertebral bone is a predominant site for osteoporotic fracture in later life (Cooper *et al*., 2005), this finding may have major implications for early vertebral development.

Radiographically, the lumbar vertebral centra displayed a decrease in radiographic intensity in the early postnatal period. Quantitative analysis of the developing trabecular architecture has identified that this loss of intensity can be, in part, attributed to significant changes in the trabecular architecture with age.

Studies into the ontogenetic pattern of the human vertebral column, and other skeletal areas, have identified three distinct phases in vertebral development. Acquaah *et al*. (2015) termed these phases overproduction, constructive regression and refinement. A three-phase system has also been observed in other skeletal elements such as the ischium (Maclean, 2017) and in the scapula (O'Malley, 2013), the latter of which predated the research conducted by Acquaah *et al*. (2015) and described these phases as pre-reboot, reboot and post-reboot. However, these phases in the scapula were initially considered to be of an evolutionary nature and a transition from our ancient quadrupedal roots to the prehensile upper limb of the modern human (O'Malley, 2013). It was postulated that an increase in bone formation within the perinatal period was an anticipatory mechanism of load-bearing which did not occur, and the subsequent

excess bone was resorbed to allow for remodelling. However, both the ischium and the vertebral column are predominantly load-bearing structures and also undergo this process of excessive bone formation, followed by bone resorption at a time in which load-bearing is beginning to occur. It has been hypothesised that the period of constructive regression is in response to a period of nutritional change and as a preparatory mechanism for rapid growth in the early postnatal period (Acquaah *et al*., 2015*;* Maclean, 2017).

10.2.1 *Bone mineral accrual in the prenatal and perinatal periods*

Both the qualitative and quantitative aspects of this project display evidence of a period of bone mineral accrual in the fetal and perinatal periods of the developing lumbar vertebrae. This is characterised by increased bone volume fraction and trabecular number, which peaks in the fetal period and remains significantly higher within the perinatal period when compared to infancy and early childhood. These parameters, along with a lower trabecular separation, are likely the cause of the high radiographic intensity observed qualitatively. This period has been previously observed in the scapula and was termed pre-reboot (O'Malley, 2017), while Acquaah *et al*. (2015) also observed this in the developing vertebral column, terming it 'overproduction' and attributing it to a likely surplus in mineralised bone tissue when considering the biomechanical demands of the skeletal element at that developmental stage.

Interestingly, this study observed that, while a significant loss of bone occurred in the early postnatal period, a loss of bone volume fraction was also observed within the perinatal period and potentially as early as 32 weeks *in utero*. This indicates that it is within the fetal period that the developing vertebral bone reaches peak bone volume fraction before beginning to decrease, rather than peaking in the fetal period and remaining constant at birth (Acquaah *et al.*, 2015). This is corroborated by the finding that the number of trabeculae also decrease, and bony struts begin to transition from plate-like to more rod-like in the late fetal period and into the perinatal period. These findings corroborate Reissis and Abel (2012), who quantified trabecular architecture in the developing fetal femur, also finding a decrease in trabecular number. However, this loss in trabeculae has been challenged and considered as potentially due to less than adequate resolution which may not have identified thinner trabeculae (Reissis and Abel,

2012; Maclean, 2017). The resolution of fetal scans within this study averaged around 14µm, as opposed to 60 µm. Therefore, it is considerably less likely that the decrease in trabecular number observed in the late fetal period in this study was due to resolution. Acquaah *et al*. (2015) characterised overproduction as an increase in bone volume fraction, trabecular number and more plate-like trabeculae, which seems to occur up to 32 weeks *in utero* in this study. There are several potential reasons for the discrepancy between this and the current study. Perhaps most likely is a consideration of the sample sizes within each study. For this study, only three individuals were included in the fetal cohort, with only one individual aged 32 weeks *in utero*. However, a larger number of individuals comprised the perinatal cohort indicating that it is likely this period of bone mineral accrual occurs predominantly within the fetal period. In comparison, a total of 120 vertebrae from complete vertebral columns were utilised in the study by Acquaah *et al.* (2015) which equates to 5 individuals aged 6 months and 7 months gestation, term, 1.5 years and 2.5 years of age, meaning only one individual represented the perinatal period in the latter study.

The rapid increase in bone volume fraction characteristic of this period of bone mineral accrual has been attributed to an increase in trabecular number in this study. This is due to the fact that as BV/TV begins to decrease in the late fetal period, trabecular number also declines. However, it has been speculated that the speed at which this bone deposition occurs may not allow for the complete mineralisation of the bone tissue deposited (Hadjidakis and Androulakis, 2006; Maclean, 2017). As this period is considered as a preparatory mechanism for the nutritional stress and increased growth expected postnatally, it is vital that bone mineral accrual occurs.

Other load-bearing and non-load bearing skeletal elements have displayed evidence of a period of fetal and perinatal bone mineral accrual (Salle *et al*., 2002; Gosman and Ketcham, 2009; O'Malley, 2013; Maclean, 2017). As with the developing lumbar vertebrae, an increase in bone volume fraction in the ischium was characterised by an increase in trabecular number (Maclean, 2017). However, increased bone volume fraction in the femur was instead attributed to an increase in trabecular thickness within the fetal period (Salle *et al*., 2002). Acquaah *et al*. (2015) found that while trabecular number increased in the vertebral centra in the latter part of gestation (between 7 and 9 months), an

increase in BV/TV was attributed to trabecular thickness between 6-7 months *in utero*. Hence, while it may seem that the increase in BV/TV is driven by differing parameters in different skeletal elements, it may in fact be driven by different periods within gestation. As this study did not analyse any individuals under 28 weeks *in* utero, this more intense increase in trabecular thickness was not observed. A potential reason for trabecular thickness to increase more intensely in the earlier period of gestation and contribute more to the BV/TV increase observed may be due to the need for the initially formed centrally located trabecular struts to be strengthened in relation to increasing biomechanical demand, facilitated by intensifying *in utero* movements. However, due to decreased space *in utero* later in gestation, these movements decrease. Yet, the skeletal elements continue to increase in size, which in this period is facilitated more by an increase in the number of trabeculae peripherally, rather than the thickening of trabecular struts already present. Gosman and Ketcham (2009) found that the number of trabeculae in the proximal tibia peaked in the fetal period, a finding corroborated by a number of other studies in other skeletal elements (Roschger *et al*., 2001; Nuzzo *et al*., 2003; Reissis and Abel, 2012; Acquaah *et al*., 2015; Maclean, 2017), including this study. It has been considered that the number of trabeculae increased in the fetal period due to the ossification of the dense cartilaginous anlage during endochondral ossification. These abundant trabeculae may then be lost due to their redundancy in the late fetal and early perinatal period, prior to habitual load bearing (Gosman and Ketcham, 2009).

It is well accepted that maternal factors play a role in fetal bone health and early bone mineral accrual (Javaid and Cooper, 2002). In particular, maternal nutritional status influences bone mineral accrual in the fetus (Specker, 2004; Cooper *et al*., 2005), and has also been found to play a role in BMD in childhood (Cooper *et al.*, 1997; McDevitt and Ahmed, 2014). Hence, malnutrition in the fetal period and early life can have significant effects on bone mineral accrual and bone mineral density into adulthood (Cooper *et al*., 1997). The importance of vitamin D and calcium in bone growth and maintenance has been discussed previously. The last trimester of pregnancy has been identified as vitally important as it is the period in which the majority of transference of calcium from the mother to the fetus occurs. Increased levels of maternal serum vitamin D have also been

identified in this period (Cooper *et al*., 2005). Hence, maternal malnutrition can lead to decreased fetal bone mineral accrual, lower birth weight and increased risk of fracture both in early infancy and later life (Javaid and Cooper, 2002).

Genetic factors have also been implicated in early bone mineral accrual. It is well understood that around 60-80% of BMD is hereditary (Bachrach, 2001; Prentice, 2001). The role of genetic determinance has been identified through the study of BMD between relatives. Javaid and Cooper (2002) observed that daughters with osteoporotic mothers displayed lower BMD, indicating a genetic link. Furthermore, BMD has been found to differ between populations, with Caucasian individuals generally more likely to develop osteoporosis, while Nigerian children are more likely to display a vitamin D receptor polymorphism that leads to increased susceptibility to rickets (McDevitt and Ahmed, 2014). While it is difficult to say whether these observed differences within families and populations occur during the fetal period, it has been well established that genetic influences play a much more significant role in bone health earlier in life and that 'programming' in intrauterine life may lead to disease and skeletal pathology in later life (Javaid and Cooper, 2002).

Mechanical stimulation may also play a minor role in bone mineral accrual in this period (Acquaah *et al*., 2015). While the fetus is not weight bearing at this time, *in utero* limb movements act as a form of resistance training and stimulate the development of the musculoskeletal system affecting bone growth and likely also affecting bone mineral accrual (Land and Schoenau, 2008).

This early period of bone formation is most likely a developmentally pre-programmed response to cache minerals such as calcium, establishing a mineral store and preventing deficiencies in the later phases of development (Cooper *et al*., 1997; Acquaah *et al*., 2015). Maternal factors and mechanical stimuli likely also play a role in the extent of bone mineral accrual in the fetal and early post-natal life (Cooper *et al*., 1997; Javaid and Cooper, 2002; Cooper *et al*., 2005; McDevitt and Ahmed, 2014; Acquaah *et al.*, 2015).

10.2.2 *Loss of bone in early infancy*

The period of early infancy represented by intense bone resorption and rapid bone growth has been termed reboot (O'Malley, 2013) and constructive regression (Acquaah *et al*., 2015). Due to the lack of significant differences

between the two postnatal cohorts in this study, it is not possible to identify the exact age at which this bone loss occurs and the following phase of increased remodelling commences. However, it is obvious that this loss of bone occurs predominantly within the 4 weeks to 2 years of age cohort in this study and is characterised by a decrease in bone volume fraction driven by a decrease in trabecular number and increase in trabecular separation. Furthermore, this loss of bone may begin to occur as early as the perinatal period. While BV/TV remains relatively consistent between the fetal and perinatal cohorts, trabecular number decreases considerably, while trabecular thickness increases, leading to the consistency in bone volume. This initial loss in the number of trabeculae may indicate the initiation of constructive regression in the perinatal period.

A period of bone loss in early infancy has been observed in the vertebral column and other skeletal elements. Acquaah *et al*. (2015) observed a decrease in BV/TV and Tb.N after term. In the proximal tibia, BV/TV was found to decrease by 40%, due to trabecular thinning and increased trabecular separation (Gosman and Ketcham, 2009). Meanwhile in the developing proximal femur, the trabecular architecture between 6 and 12 months of age displayed a decrease in BV/TV and Tb.N (Ryan and Krovitz, 2006). Maclean (2017) also found evidence of this period in the developing ischium.

As with the previous phases of development, there is a lack of understanding regarding the driving force for this period of bone resorption, although a number of potential factors have been considered. These include a potential period of nutritional stress, the early load-bearing of the column and movements of the limbs, and the rapid allometric growth of the lumbar vertebrae during the period of infancy.

A potential driving force for bone resorption in this period may be due to increased nutritional stress placed upon the infant postnatally. Vitamin and mineral deficiencies in the early postnatal period may lead to the resorption of bone in order to release these into the bloodstream (Power *et al*., 1999). Differing methods of infant feeding have been related to bone mineral accrual. In particular, there is a large debate on the effects of breast-feeding as opposed to bottle feeding and the relation to bone mineral accrual. Breastfeeding for a significant period has been observed to have a protective, rather than deleterious role regarding bone mass in infancy, with an increase in BMD in the lumbar spine

observed when compared to bottle-fed infants (Jones *et al*., 2000). However, other studies have identified that breast milk contains lower amounts of vitamin D and has been linked to decreased accrual rates in early infancy when compared to formula-fed infants (Specker, 2004; Holick, 2007; McDevitt and Ahmed, 2014). It is likely that these mixed results are due to maternal nutritional status and that overall, the importance of maintaining the bone mineral accrued in the fetal period and the additional accrual of bone mineral in early infancy is related to nutritional availability, whether maternal or external. Perhaps most importantly, both mechanisms of feeding seem to lead to reduced intake of vital nutrients when compared to the fetal period hence leading to the period of bone loss observed.

This period may also, in part, be due to the altered environment postnatally, particularly in relation to mechanical stimulation. While *in utero* limb movements are considered a form of resistance training, movements post birth have less resistance and hence smaller loads may be placed upon skeletal elements in the early postnatal period (Land and Schoenau, 2008). This may also begin to explain the loss of bone observed in the early postnatal period.

Worryingly, this period of bone resorption occurs either just prior or during a time in which an infant is beginning to achieve important early developmental milestones and the trabecular architecture present within the weight-bearing skeleton may not be of sufficient biomechanical competence to achieve these. However, it has been hypothesised that this bone loss plays a vital role in the development of a highly orientated architecture vital in the fulfilment of the biomechanical role of load-bearing skeletal elements by forming a ‘blank slate’ by which trabeculae can be remodelled (O’Malley, 2013; Acquaah *et al*., 2015; Maclean, 2017), and that extensive resorption of trabecular architecture may not affect the basic arrangement of trabeculae, instead only affecting parameters such as trabecular thickness, spacing and anisotropy (Abel and Macho, 2011). Even so, a decrease in the number of trabeculae has been found to be detrimental for bone strength, even more so than a decrease in trabecular thickness (Guo and Kim, 2002) and there is evidence that the period leads to increased fracture risk in infancy. Osteoporosis in childhood is relatively uncommon and likely caused by a variety of pre-existing health conditions. However, in cases of idiopathic juvenile osteoporosis, normal bone loss has been

observed to occur in early infancy, however bone turnover is significantly lower than in healthy children meaning bone loss in this period cannot be recovered in childhood (Rauch *et al*., 2000).

Loss of bone mass in the early postnatal period has also been linked to increasing bone marrow mass, with the rate of bone marrow increase more rapid than bone growth. This has been termed as ‘physiological osteoporosis of infancy’ (Land and Schoenau, 2008). This has been observed in the long bones, however, as haematopoiesis is a significant role of the lumbar vertebral centrum it is acceptable to assume that an increase in bone marrow mass is a potential mechanism for the bone loss observed in the early postnatal period.

It is important to note that this period of early infancy is characterised by rapid growth, known as the infant growth spurt (Ay *et al*., 2011). Due to the increase in size that also occurs in this period, bone resorption may not occur as extensively as it may seem. Rather, a lack of bone formation and increase in volume may lead to the reduction in BV/TV observed. However, the transition from plate-like to more rod-like trabeculae, and the significant loss in trabecular number indicates that bone resorption does occur in this period.

While Acquaah *et al*. (2015) found some differences in bone loss at different vertebral levels, no focus was placed upon whether sites within the centrum were affected differentially. In the adult, age related degeneration has been found to be site specific (Thomsen *et al*., 2002a; 2002b) while other skeletal elements such as the ilium were found to display site specific trabecular resorption that did not affect the trabecular bundles present prior to the onset of loading (Abel and Macho, 2011). It is possible that this period of bone resorption is site specific within the lumbar vertebral centrum. Furthermore, as bone loss in the lumbar centra is likely driven in majority by a loss of trabeculae, it would be expected that the superior and inferior regions, as well as peripheral regions, which were observed to have a higher number of trabeculae, may be more affected during this period. As the vertebral centra were analysed on a whole bone level, it is not possible to ascertain whether site-specific bone resorption occurs. This is an area for future research.

10.2.3 *A period of growth and remodelling*

This period has been observed to occur in early childhood and is characterised by the remodelling of the trabecular architecture, most likely in relation to functional interactions that occur in this period (Acquaah *et al*., 2015). O'Malley (2013) termed this period 'recovery', stating that it was in this period that the juvenile scapula recovered from the bone loss that had occurred in early infancy. Acquaah *et al*. (2015) observed that, in the vertebral column, this period, which they termed 'refinement', had begun to occur in early childhood and was evident in the 2.5 year old individual studied. Hence, it is likely that both the 4 weeks to 2 years of age, and 3 to 8 years of age cohorts contain individuals in this phase.

While there is significant emphasis placed upon the fetal period and early infancy in the determination of bone health in later life, childhood still plays a major role in bone development and adult trabecular architecture is largely determined in childhood (Mitchell *et al*., 2018). The periods of early bone mineral accrual and reduction in bone volume are likely driven by the need to store essential nutrients for later use. The period of later remodelling, while involving bone mineral accrual, is likely driven more by mechanical stimulation and the increasing biomechanical demands placed upon the structure.

Mechanical stimulation has been identified as vitally important in the development of bone in the postnatal period and the attainment of peak bone mineral density (Bailey *et al*., 1999) and the stress on bone exerted by muscle is vital for bone formation and bone growth, with exercise in children found to have a positive effect on bone mass (McDevitt and Ahmed, 2014).

In this study, trabecular architecture after the period of bone resorption did not display any significant changes in any histomorphometric parameters. The number of trabeculae remained relatively constant postnatally, as did structural model index, even though these parameters are important in the strength of the trabecular architecture (Guo and Kim, 2002). Furthermore, Kneissel *et al*. (1997) found that the period of early childhood was characterised by more plate-like trabeculae in a vertebral sample, while this study found a mixture of both plate-like and rod-like trabeculae. It would make sense that the period of remodelling is defined by sculpting of trabeculae into a more plate-like morphology, which are

more mechanically strong than rods, as this period is characterised by sculpting the internal architecture of a skeletal element to fulfil its biomechanical role. A potential reason for the discrepancy between this study and that of Kneissel *et al*. (1997) is the separation of the age cohorts studied, with the latter study pooling individuals between the ages of 0-9 years to achieve this result, likely skewed by the predominantly plate-like trabeculae found in younger individuals. Furthermore, it would be expected that even remodelled vertebral architecture displays a mixture of both rods and plates, as plate-like trabeculae are predominantly found centrally, while an increased number of more rod-like trabeculae are found in the superior, inferior and peripheral regions (Amstutz and Sissons, 1969; Whitehouse *et al.*, 1971; Kneissel *et al.*, 1997; Thomsen *et al.*, 2002a).

The maturation of other skeletal elements has been directly related to the achievement of biomechanical milestones, particularly in load-bearing elements such as the femur (Ryan and Krovitz, 2006) and tibia (Gosman and Ketcham, 2009).

In both the proximal femur and proximal tibia, an alteration in trabecular architecture, characterised by increased anisotropy, decreased trabecular number and increased trabecular thickness, could be observed after around 1.5 to 2 years of age. Trabecular structure mirrored that of the adult by the ages of 10 years in both skeletal elements (Ryan and Krovitz, 2006; Gosman and Ketcham, 2009). Both authors attributed the significant change in the developing trabecular architecture to the onset of bipedality, with these alterations transpiring contemporaneously with the onset of the attainment of developmental milestones associated with early load-bearing and bipedalism (Keen, 1993; Garrett *et al*., 2002; WMGRSG, 2006; Sheldrick and Perrin, 2013; Hadders-Algra, 2018). The alignment of trabecular architecture within the proximal femur occurred contemporaneously with the maturation of the bicondylar angle as a result of bipedal gait (Ryan and Krovitz, 2006). It has been considered that the early, immature gait adopted in infancy prior to gait maturation in childhood is mechanically inefficient and increases the biomechanical demand on these structures more so than mature gait. Hence, both the proximal femur and proximal tibia may be more susceptible to changes in early infancy due to this (Gosman and Ketcham, 2009). Stability of the trabecular structure in both

elements was observed by the ages of 8-10 years, which also corresponds to the developmental milestone of mature gait attainment (Keen, 1993; Ryan and Krovitz, 2006; Lacquaniti *et al*., 2012).

In the vertebral column, Acquaah *et al*. (2015) observed that selective deposition and resorption of tissue at different sites did occur in childhood and that increased organisation of the trabecular architecture occurred with age. This was attributed to the mechanical stimulation of the vertebral column through a number of mechanisms (Acquaah *et al*., 2015). Firstly, the attainment of postural milestones such as sitting and standing unassisted increases the compressive load placed upon the vertebral column as the weight of the head and trunk is now bore through the vertebral bodies (Ferguson and Steffen, 2003; Briggs *et al*., 2004). Secondly, reactive compressive forces travel upwards through the vertebral column from the onset of bipedal gait (Acquaah *et al*., 2015). Furthermore, bipedal locomotion causes rotational movements of the lumbar spine, which are translated into shear forces by the facet joints and stimulate reinforcement of the superior and inferior regions of the vertebral body and in turn the central regions (Smit *et al*., 1997). Muscular contraction also plays a role in the mechanical stimulation of the trabecular architecture of the lumbar vertebral centrum in the period of refinement. Generally, muscular contraction enables movements of the vertebral column as a whole such as flexion, extension and side bending (LeVeau and Bernhardt, 1984; Drake *et al*., 2010; Moore *et al*., 2019), but muscular forces also act to stabilise the lumbar vertebral column during these movements (Smit *et al*., 1997). This act of stabilisation results in additional forces placed upon the lumbar vertebrae such as increased axial compression, alongside shear and torsional forces. The effects of these forces on the lumbar vertebral body has been discussed previously, with the latter forces converted via the dense superior and inferior regions into compressive load which then reinforces the central, vertically oriented, trabeculae (Smit *et al*., 1997).

It is important to note that, while studies on juvenile trabecular architecture are of vital importance in understanding the factors that affect the developing trabecular bone, these studies do not form a large part of the greater literature and all suffer from similar limitations. The sample sizes of juvenile trabecular studies tend to be low, with Acquaah *et al*. (2015) studying only 5 individuals and only one individual of each age. Not only are the samples small, they also usually

suffer from a lack of demographic information with age at death estimated and cause of death commonly unknown (Kneissel *et al*., 1997). While the majority of juvenile studies are non-destructive in nature, there are still differences between methodologies, with some studies focusing on quantifying trabecular architecture from 2D histological images, and others 3D radiographic images. However, the data collected from 2D and 3D methods has been observed to be comparable (Fajardo *et al*., 2002). Finally, it is important to consider that while these studies often attempt to quantify 'normal' bone growth and development, the individuals being assessed are deceased and hence their bone development may not be comparable to healthy, living children.

Human locomotor behaviour undergoes major modifications that begin in infancy and continue into adulthood (Abel and Macho, 2011). The age ranges for attainment of these developmental milestones are related to a number of factors, with different children and different populations attaining developmental milestones at different times (WMGRSG, 2006; Hadders-Algra, 2018) while attainment is also affected by early fetal and postnatal growth (Cheung *et al*., 2001). Furthermore, another potential reason for variations in attainment may be the given definitions for each milestone and contradictory author interpretation. Multiple studies use 'walking unaided' as a key developmental milestone, although it is not clear whether this relates to a single unaided step, more than one step or multiple confident steps (Malina, 2004). Hence, it is difficult to relate specific attained movements, such as walking unaided, to the refinement of trabecular architecture within the lumbar vertebral centra, due to the variable nature of attainment between individuals and populations. That being said, the attainment of these developmental milestones within early infancy likely do contribute to changes in trabecular architecture, particularly in terms of the increasing thickness and separation of trabeculae. These two parameters in particular have been observed to be more responsive to an altered loading environment (Abel and Macho, 2011).

While other skeletal elements have been observed to display a trabecular architecture that becomes more anisotropic during the refinement period (Ryan and Krovitz, 2006; Gosman and Ketcham, 2009), which has also been identified in the lumbar vertebrae (Kneissel *et al*., 1997; Acquaah *et al*., 2015), it is difficult to say with certainty that these findings are corroborated by this study due to the

lack of significant differences in DA between the four age cohorts studied. The lumbar vertebral centra within this study generally display relatively isotropic, randomly arranged architecture throughout development. That being said, there is some evidence of site specific differences in DA within the lumbar centra that may be masked by the pooling of data from all VOIs within the first analysis. Peripheral areas of the central layer of the vertebral centrum begin to display higher values for DA in the 4 weeks to 2 years of age cohort. This is reinforced in the 3 years and older age cohort, with an emphasis on the anterior region of the central layer displaying higher DA. In an earlier section, this discrepancy has been explained in terms of the association of the anterior aspect of the vertebral body with the anterior longitudinal ligament, which acts to limit extension. However, this finding may also be due to the computation of DA. Anterior VOIs are irregular in nature, and the irregularity of VOI shape has been linked to increased inaccuracy in DA calculation.

Overall, it appears that the degree of anisotropy does not change markedly over the period of development of the lumbar vertebral centra. Increases in trabecular thickness and trabecular separation can be linked to a general increase in size in the lumbar centra, as these parameters have been linked to increasing body mass (Gosman and Ketcham, 2009). This, of course, presents a paradox. If trabecular organisation does not obviously occur throughout development in the lumbar centra, yet the majority of evidence suggests that the trabecular architecture of the lumbar centra display trabeculae oriented to withstand compressive loading (Briggs *et al*., 2004), when does this architecture develop? There is the potential that the trabecular architecture is predetermined within the fetal period, an observation that has previously been made in the ilium (Cunningham *et al*., 2009a; b). More site-specific comparative data is needed to identify whether trabecular organisation may occur at selective sites within the centrum. Furthermore, to reduce the likely inaccuracy of the computation of degree of anisotropy that occurred in this study, modifications to the grid method utilised may need to be considered, with an emphasis on a number of equally sized, regularly shaped VOIs studied.

10.2.4 *Attainment of adult trabecular architecture*

Skeletal elements continue to undergo bone modelling and remodelling throughout life and the lumbar vertebrae are no exception to this rule. The

attainment of developmental milestones continues into late childhood, with some studies claiming that mature gait is not achieved until between 7-9 years of age (Keen, 1993; Hadders-Algra, 2018) although this has been contested (Chester *et al*., 2006). From a biomechanical perspective, the attainment of a mature gait should result in a trabecular architecture that is characteristic of the adult. However, changes in trabecular architecture of load-bearing skeletal elements have continued to be observed in late childhood and adolescence. These changes contribute to bone strength, for example, an increase in plate-like and decrease in rod-like trabeculae has been observed in the tibia and distal radius between 9 and 18 years of age (Mitchell *et al*., 2018), while ischio-iliac trabecular bundles within the ilium have been observed to align in late adolescence indicating that there is still the potential for remodelling in later life (Abel and Macho, 2011). SMI has also been closely linked to microarchitectural damage in the lumbar vertebrae in older individuals (Arlot *et al*., 2008).

Hence, the age at which the trabecular architecture of the lumbar centra attains its stable adult structure is unclear. Table 10.1 displays the average values for histomorphometric parameters in the adult literature, and within the 3-8y cohort for this project. Through this numerical comparison, it seems that the internal trabecular architecture within the 3 to 8 years age cohort, while following the same patterns as the adult structure, has not achieved the numerical values observed in the adult.

Table 10.1: A collection of studies with comparable results within the literature, including the sample demographic, methodology and 5 of the 6 parameters studied. DA is not included due to paucity of comparable values within the literature.

Author	Sample	Vertebral level	Methodology	BV/TV (%)	SMI	Tb.Th (μm)	Tb.N (mm^{-1})	Tb.Sp (μm)
Sato (1967)	3-10th decade of life	L4/5	Quantitative microradiography, 80μm slices	N/A	N/A	100-130	N/A	N/A
Kneissel *et al*. (1997)	1 (0-9y) 2(10-19y) 3(20-29y)	L4	BSE-SEM	(1) 10-16 (2) 10-20 (3)10-16	N/A	(1) 75-100 (2) 90-130 (3) 90-120	(1) 1.2-1.8 (2) 1.15-1.65 (3) 1.1-1.4	(1) 450-750 (2) 450-800 (3) 600-900
Hildebrand *et al*. (1999)	52 cadavers between 24 and 92 years of age	L2 and L4	Micro CT	(L2) 8 (L4) 8	(L2) 2.13 (L4) 2.12	(L2)122 (L4) 139	(L2)1.28 (L4)1.39	(L2) 792 (L4) 854
Thomsen *et al*. (2002d)	19-96	L2	Quantitative histomorphometry	7-15	N/A	87-100	N/A	400-1000
Agarwal *et al*. (2004)	54 adults, archaeological	L4	Quantitative microradiography	26-38	N/A	170-198	1.5-2	327-515
Gong *et al*. (2005)	6 Chinese male cadavers, 62-69 years of age	L4	Micro CT	6.93-7.96	N/A	106.10-116.67	1.03-1.17	N/A
Rapillard *et al*. (2006)	29 individuals, 29-86y	Lumbar vertebral bodies	Micro CT	3-21	0.26-2.10	N/A	N/A	N/A
Sutton-Smith *et al*. (2006)	15 individuals, 17-79 years	L1	SEM	N/A	N/A	119	N/A	N/A
Hulme *et al*. (2007)	Osteoporotic functional spine units (mean age 74 years)	T9-L5 pooled	Micro CT	12.5	2.42	215	0.896	1110
Parkinson *et al*. (2012)	12 individuals, 53-83 years	L1, L4, L5 (SI and AP)	Micro CT	10.7/10.8 (SI/AP)	1.83/1.85	183/187	0.58/0.59	1003/1020
Perilli *et al*. (2012)	Cadavers of mean age 77.5	L2 and L3	Micro CT	6	N/A	N/A	N/A	N/A
This study	3-8 years	L1, L3, L5	Micro CT	(L1) 14 (L3) 12 (L5) 18	(L1) 1.54 (L3) 1.61 (L5) 1.37	(L1) 121 (L3) 108 (L5) 135	(L1) 1.19 (L3) 1.12 (L5) 1.37	(L1) 592 (L3) 593 (L5) 554

It is clear that the quantitative data collected in this study differs when compared to quantitative data within the adult literature. Generally, the trabecular architecture of childhood, as quantified in this study, described a lumbar vertebral centrum that was considerably more mechanically strong when compared to the adult architecture. Individuals within the 3-8 years age cohort in this study generally displayed higher values for BV/TV and SMI, both of which are important parameters in quantifying bone strength (Ding and Hvid, 2000; Ding *et al*., 2002; Liu *et al*., 2008; Maquer *et al*., 2015).

Altering functions of the lumbar vertebrae may play a role in the attainment of adult architecture, and hence the discrepancies seen within this study and studies of adult architecture. An important function of the developing lumbar vertebral centrum is its role in haematopoiesis. However, in the adult this role is diminished with the amount of bone marrow present within the cavitity decreasing with age. Bone marrow within the developing ilium has been observed to affect internal trabecular architecture. Parfitt *et al*. (2000) found that enlargement of the marrow cavity caused by lateral cortical drift in the normal developmental process led to the formation of trabeculae within this space borne out of cortical cancellisation. As the need for bone marrow tissue decreases throughout development, it no longer occupies new space produced by bone growth. Hence, newly formed trabeculae are able to occupy this space instead. This may explain why some studies have found higher trabecular number when compared to this study (Kneissel *et al*., 1997; Hildebrand *et al*., 1999; Agarwal *et al*., 2004). The decrease in trabecular number with age is seen in other studies (Gong *et al*., 2005; Hulme *et al.,* 2007; Parkinson *et al*., 2012) could also be related to the diminishing role of haematopoiesis in the adult. Marrow adiposity has been observed to increase with age, leading to increased marrow fat in the central region of the lumbar vertebral body. This has been correlated with decreased bone density in older individuals (Schwartz, 2015).

Overall, the BV/TV values collected in this study are almost double that of those found in the adult literature, which seem to be in agreement with each other. BV/TV is positively correlated with mechanical strength (Hildebrand *et al*., 1999; Ding *et al*., 2002; MacNeil and Boyd, 2007; Perilli *et al*., 2008; Maquer *et al*., 2015) and this result may imply that peak vertebral strength occurs prior to adulthood. This is corroborated by the fact that SMI values within this study

display more plate-like trabeculae, another predictor of vertebral strength. Conversely, rod-like trabecular architecture is an indication of more extensive remodelling and increased rod-like trabeculae in a structure is also an indicator of osteoporotic bone (Thomsen *et al*., 2002b; Liu *et al*., 2006*).* Generally, values for SMI stay constant in adulthood but its decrease can indicate increased likelihood of vertebral fracture (Ding and Hvid, 2000; Stauber and Müller, 2006; Arlot *et al*., 2008; Melton *et al*., 2010; Parkinson and Fazzalari, 2013).

The finding that relative bone strength may peak prior to adulthood, or in the early stages of adulthood, may be relevant to understanding the potential for an individual to develop osteoporosis in later life. Trabecular number is an example of this, with many studies observing that Tb.N peaks in the fetal period and then decreases in the early postnatal period, with adult Tb.N never recovering to fetal levels (Ryan and Krovitz, 2006; Gosman and Ketcham, 2009; Acquaah *et al*., 2015). While this study has identified that parameters related to vertebral strength are higher in early life, this does not mean that these values do not continue to increase prior to the decrease observed in adulthood, with the exception of trabecular number. Bone mineral accrual continues into early adulthood, with the pubertal growth spurt identified as a vitally important period of bone mineral accrual, particularly in the lumbar spine (Baroncelli and Saggese, 2000; Bachrach, 2001; Javaid and Cooper, 2002). It is thought that up to 25% of peak bone mass is acquired in this period (McDevitt and Ahmed, 2014). The increased rate of bone mineral accrual in this period is likely the reason for the increased trabecular thickness seen in some studies (Agarwal *et al*., 2004; Hulme *et al*., 2007; Parkinson *et al*., 2012). Furthermore, general size increases seen in the pubertal period likely lead to the increased trabecular separation seen in adulthood. Peak bone mass in the lumbar vertebrae is thought to occur during the second decade of life (Kneissel *et al*., 1997), so studies quantifying early adult architecture may display more numerical similarities to this study. Furthermore, the most substantial muscle mass increase occurs after the pubertal growth spurt (Abel and Macho, 2011) due to increase in growth hormones and has been linked to the later development of the acetabular buttress. This implies that morphological shape changes observed during late adolescence are primarily due to the development of internal structures (Abel and Macho, 2011).

Osteoporotic vertebral bone is characterised by a decrease in bone volume fraction, caused by a decrease in trabecular number as well as, in some cases, trabecular thickness. An increase in trabecular separation also contributes to the decrease in bone volume fraction. Furthermore, the characteristic plate-like trabeculae found principally within the central region shifts to become significantly more rod-like. These architectural changes all contribute to the degeneration of the vertebral trabecular architecture that leads to a fragile structure at risk of fracture (Agarwal *et al.,* 2004; Hulme *et al*., 2007; Parkinson *et al*., 2012). As the prevalence of osteoporosis is increasing, the majority of studies quantifying the adult trabecular architecture of the lumbar vertebrae are in relation to age-related changes and senescence, in order to understand the structural deterioration in trabecular architecture that leads to vertebral osteoporosis and increased fracture risk (Agarwal *et al*., 2004; Hulme *et al*., 2007; Parkinson *et al*., 2012). Therefore, the findings of these studies may not accurately represent the architecture of a healthy adult.

Of course, it is possible that the differences seen between the current study and those in the literature is instead related to methodological differences, which make direct numerical comparisons between studies difficult. Hildebrand *et al*. (1999) has identified that the comparison between two dimensional and three dimensional parameters is poor, with parameters like Tb.Th found to differ significantly when assessed using the two dimensional plate-model assumption, compared to the three dimensional model independent method. Tb.Th values were found to be significantly higher when computed by the model-independent method as opposed to the plate-model assumption. The lumbar spine was observed to be particularly affected by this, due to the higher presence of rod-like trabeculae compared to other skeletal sites with Tb.Th and was sometimes underestimated by 30%.

Furthermore, the majority of studies analyse only one vertebral level (Kneissel *et al*., 1997; Thomsen *et al*., 2002a; Agarwal *et al*., 2004; Gong *et al*., 2005; Sutton-Smith *et al*., 2006), or in cases of studying multiple vertebral levels, pool these results together (Sato, 1967; Rapillard *et al*., 2006; Hulme *et al*., 2007; Parkinson *et al*., 2012; Perilli *et al*., 2012). This study identified differences between vertebral levels in the 3 years and older age cohort. Therefore, numerical differences may be due to the differences in vertebral levels studied.

Differences between vertebral levels have been found in the adult literature, particularly in relation to BV/TV and Tb.N, which have been observed to decrease from L1 to L5 (Banse *et al*., 2001; Buck *et al*., 2002). Therefore, by studying only a single lumbar vertebra, or pooling data from multiple lumbar vertebrae, numerical discrepancies may arise.

As mentioned previously, multiple studies have focused on the aging architecture of the lumbar vertebrae due to its implications in osteoporosis (Agarwal *et al*., 2004; Hulme *et al*., 2007; Parkinson *et al*., 2012), however, the age of a sample is not the only demographic factor that may cause numerical differences in trabecular architecture between studies. Sex differences have been found in adult lumbar vertebral trabecular architecture in some studies. Banse *et al*. (2001) observed that females displayed a more rod-like trabecular architecture compared to males, along with higher trabecular separation, although other studies have found no such differences (Thomsen *et al*., 2002a). It is important to note that this study did not analyse whether differences between sexes existed. This is due to the general lack of sexual dimorphism present in juveniles prior to puberty. Different populations may also display differences in trabecular architecture, which can be related to a number of factors, the most likely being lifestyle factors coupled with genetic factors. Nutritional intake differs around the world, with calcium intake of a number of non-US populations below the required intake for optimal bone health (Power *et al*., 1999). Other lifestyle factors such as physical activity and smoking have also been implicated as factors in bone health (Javaid and Cooper, 2002).

10.3 Differences in trabecular architecture between vertebral levels

10.3.1 *The lumbar lordosis and differences between vertebral levels*

The lumbar lordosis is thought to appear in relation to the achievement of motor milestones such as sitting unaided, walking and developing a mature gait (Keen, 1993; Giglio and Volpon, 2007). While the lumbar lordosis is predominantly due to the changes in shape of the intervertebral disc (Been *et al*., 2010), its development may affect the trabecular architecture of the lumbar vertebrae. Once the lumbar lordosis has developed, the central axis traverses through the posterior aspect of the 1st and 5th lumbar vertebral bodies, and

posterior to the vertebral bodies of L2, 3 and 4 in the adult. In life, this central axis is effectively a vertical line of compressive force acting upon the vertebral column (Palastanga *et al*., 2002). It is possible that the discrepancy in force dissipation caused by the lumbar lordosis leads to significantly different trabecular morphology between vertebral levels L1, L3 and L5. In particular, it is likely that the trabecular architecture of L3 may display a more mechanically strong posterior region, potentially characterised by increased BV/TV with thicker, more plate-like trabeculae, due to the location of the central axis posteriorly. Meanwhile, as the central axis runs through the vertebral bodies of L1 and L5, the trabecular architecture at these levels would not be expected to differ between the anterior and posterior regions and display a more mechanically strong central region.

Other than the lumbar column, the only region to display a lordosis is the cervical spine. It has been observed that the cervical lordosis commences development prenatally in response to reflexive movements that occur in this period, such as head movements and the gasp reflex (Bagnall *et al*., 1977b). However, the same study did not identify any evidence of the formation of the lumbar lordosis. Hence, it is likely that early *in utero* limb movements may not be enough to stimulate lordosis formation. This is corroborated by the observation that no significant differences between the three lumbar levels were found during this study.

Instead of early *in utero* limb movements playing a role in the development of the lumbar lordosis, early postural changes have instead been implicated (Sparrey *et al*., 2014). In particular, the role of musculature during postural development has been identified as particularly important. Due to the predominantly flexed nature of the fetal vertebral column, musculature associated with the spine develops corresponding to this flexed position. Hence, as the muscles of the trunk develop, they are shortened. However, during the attainment of early postural milestones such as sitting up, rolling over and crawling, these muscles are stimulated to support the trunk and these movements. However, they cannot lengthen and instead force the lumbar column to begin to develop a lordotic curve (LeVeau and Bernhardt, 1984). There is evidence that muscular forces play a role in lordotic development, with lumbar hyperlordoses in individuals with cerebral palsy observed to be of neuromuscular origin. While this

form of hyperlordosis is rare, one potential mechanism of development was considered to be the psoas muscle acting as an extensor of the lumbar spine, rather than a flexor of the hip, implicating the psoas muscle in particular to the development of the lordosis (Vialle *et al*., 2006). Furthermore, a mechanism of loss of the lumbar lordosis with age, is postural degeneration. As the IV discs play a significant role in maintaining the structure of the lumbar lordosis (Been *et al*., 2010; Sparrey *et al*., 2014) and degeneration of the IV discs leads to a decreased lumbar lordosis and enhanced lumbar kyphosis and hence postural degeneration (Sparrey *et al*., 2014). Decreased muscular strength, potentially due to overuse or extended sedentary periods has been attributed to postural degeneration (Sparrey *et al*., 2014).

A potential reason for the fifth lumbar vertebra to display significant differences over the entirety of the centrum may be due to the potential role of the sacrum in the development of the lumbar lordosis. While it is accepted that the lumbar lordosis develops postnatally, evidence of a developing lordosis has been observed in a fetal sample. Choufani *et al.* (2009) identified a lumbosacral lordosis in the fetal period and indicated the main driving force of the lumbosacral angle created was the observed posterior tilt of the sacrum. It is possible that this prenatal transition in the positioning of the sacrum may be the initiation of the development of the lumbar lordosis. This may help to explain why in the fetal period, the vertebral level L5 is significantly different from L1 and L3.

Overall, this study seems to display a lack of evidence of a change in trabecular architecture that can be attributed to the development of the lumbar lordosis. The most likely reason for this is that the lumbar lordosis does not affect internal vertebral architecture. Studies into the strength of the vertebral endplate and IV disc have found that these structures act to dissipate loads placed upon the lumbar vertebral column over the vertebral body (Adams and Dolan, 2005). While there is evidence that this dissipation is not equal over the vertebral body itself, there is no evidence that this mechanism of dissipation differs between vertebral levels (Ferguson and Steffen, 2003). Of course, it is also possible that, as research suggests, the lumbar lordosis is not present until around 5 years of age and continues to develop throughout childhood (Giglio and Volpon, 2007), the ages analysed in this study simply have yet to develop enough of a lordosis to produce such architectural change.

10.3.2 *The pattern of ossification and differences between vertebral levels*

It has already been observed that trabeculae in closer proximity to the ossification centre are more mature, characterised by increased thickness and more plate-like morphology. Meanwhile peripheral bone at the growth plate displays a lower bone volume fraction and thinner, more rod-like trabeculae (Roschger *et al*., 2001; Salle *et al*., 2002; Nuzzo *et al*., 2003). The lumbar vertebral centra do not begin to ossify in unison: the upper lumbar vertebrae commence ossification as early as 2 months prenatally while L5 commences ossification by the 3rd month gestation (Cunningham *et al*., 2016). Salle *et al*. (2002) found differences in trabecular architecture within a bone in relation to earlier ossification and maturity, hence, it would be expected that as the ossification centre for L3 can appear potentially 1 month earlier than that of L5 (Bagnall *et al*., 1977a; Cunningham *et al*., 2016), there may be differences in the trabecular architecture at a given age. For example, increased trabecular thickness and BV/TV, plate-like morphology and increased trabecular number at the level of L3 compared to L5. Furthermore, Acquaah *et al*. (2015) found evidence of increased maturation in the developing thoracic vertebrae as opposed to the lumbar vertebrae, with the lumbar vertebrae displaying significantly lower BV/TV, Tb.Th and DA. They attributed this to the pattern of ossification, with the centra of the thoracic region appearing prior to the lumbar centra.

However, if the pattern of ossification was the underlying cause of the differences in trabecular architecture, it can be expected that significant differences between architecture would be present within the fetal period. For this study, this is not the case, with significant differences in trabecular architecture between vertebral levels not present until the perinatal period. Furthermore, it would be expected that the 5th lumbar vertebral centrum would display a generally less mature architecture characterised by thinner, more rod-like trabeculae. In contrast, L5 exhibited significantly thicker, more plate-like trabeculae compared to the centra of L1 and L3 indicative of a more mature and mechanically strong architecture.

10.3.3 *Mechanical stimulation and the differences between vertebral levels*

Significant differences in the internal trabecular structure of different lumbar vertebral levels have been observed in the adult, with upper lumbar vertebrae displaying a denser architecture with less trabecular separation when compared to lower vertebral levels such as L4 (Banse *et al*., 2001). Loss of horizontal trabeculae, leading to a reduction in trabecular number, from L1 to L5 was also observed, although these findings have been increased in older individuals and are potentially due to age-related degeneration (Buck *et al*., 2002).

From the perinatal period onwards, the trabecular architecture of the 5th lumbar vertebral centra displays a significantly more mechanically strong structure with trabeculae of increased BV/TV, increased thickness, increased number and more plate-like morphology. A potential mechanism for this is the increased compressive load placed upon L5 when compared to L1 and L3. Vertebral body surface area has been observed to increase from L1 to L5 (LeVeau and Bernhardt, 1984; Boszczyk *et al*., 2001), indicating that increased load is placed upon L5 compared to L1. The pedicles, which are an important structure in converting shear and torsional forces, have also been found to increase in diameter from L1 to L5 (Pal and Routal, 1987; Amonoo-Kuofi, 1995; Ebraheim *et al*., 2004). These increases in size indicate that load increases craniocaudally. Hence, it would be expected that the trabecular architecture also increases in size, in this case trabecular thickness.

It is possible that the sacrum and sacroiliac joints affect the trabecular architecture of L5. A study into the trabecular architecture of the developing sacrum has identified that the anteromedial portion of S1 displayed a trabecular architecture more suited to load-bearing compared to the posterior region. Due to the anterior tilting of the sacrum, this architecture in the anteromedial aspect of the S1 body may be due to loads transferred from L5. Furthermore, as S1 transfers this load through the sacroiliac joint into the pelvic complex, the loads placed on S2-S5 decrease which leads to an observable decrease in bone density and remodelled trabecular architecture (Yusof, 2013).

Interestingly, within the 4 weeks to 2 years of age cohort, the significant differences between vertebral levels reduced and were confined to the central

region. The trabecular architecture of this cohort is driven by constructive regression, characterised by a decrease in BV/TV and Tb.N, and an increase in SMI, all of which are detrimental to the mechanical strength of the structure. As the fifth lumbar vertebra seems to retain some qualities of its mechanical strength by continuing to display increased BV/TV and more plate-like trabeculae in some cases, this implies that the bone loss characteristic of phase 2 may be specific to vertebral level. As phase 2 is represented by a significant decrease in trabecular number, it would make sense that these are lost predominantly from the superior and inferior regions rather than the central region as more trabeculae are present prior to constructive regression in these regions. Meanwhile, significantly less trabeculae are present in the central region and the loss of trabeculae in an area of fewer trabeculae initially is likely to be more detrimental to load-bearing. Furthermore, the increase in significant differences between vertebral levels between the 4 weeks to 2 years and 3 years onwards cohort implies that vertebral architecture is differentially refined and likely related to load-bearing.

10.4 Factors affecting variation within age cohorts

While it is possible that differences seen within cohorts are attributed to individuals at differing developmental stages, several other factors may also have contributed to the significant variation observed in some cases.

The Scheuer collection is an active repository of juvenile skeletal remains, with individuals arising from a variety of origins. These differing origins may be an explanation as to why some individuals vary significantly. A variety of differing factors may be responsible for skeletal variation observed between individuals of different origins or time periods. These can be broadly grouped into two sets of factors.

The first collection of factors pertains to the period post the death of the individual(s) in question. Diagenesis is the term used to describe the changes that occur in bone after death and encompasses all geochemical factors that affect degradation and remineralisation (Farquharson and Brickley, 1997). It is possible that external factors such as these have caused diagenesis within the internal trabecular architecture of one or more of the skeletal sub collections studied, which has led to the significant differences found within the trabecular architecture between individuals of a similar age.

Alternatively, several factors may have affected the trabecular architecture during the lifetime of the individual. It is well accepted that certain lifestyle factors can influence bone maintenance (Sommerfeldt and Rubin, 2001; Agarwal *et al.*, 2004; Pearson and Lieberman, 2004). One factor that is important to consider in this case is nutritional availability. Archaeological and historical populations may have consumed diets lacking in essential vitamins and minerals for adequate bone maintenance and, while in the adult this may not have greatly influenced internal bone structure, developing bone is more sensitive to such nutritional deficiency (Power *et al*., 1999; Agarwal *et al*., 2004). Alternatively, it has been speculated that prior to sustained agriculture, populations may have had more nutrients such as calcium in their diets, which in turn led to increased BMD (Power *et al*., 1999). Due to the highly active metabolic nature of trabecular bone, it can be more susceptible to such lifestyle factors, and minor loss of trabecular bone can lead to substantial changes in trabecular architecture (Brickley and Howell, 1999).

Disease and disorders can also impact the internal trabecular architecture of bone. The Scheuer collection is comprised of deceased juvenile individuals. While there may be many reasons for the cause of death of a juvenile individual, diseases and other disorders most commonly play a part. Rickets and osteomalacia are examples of disorders caused by deficiency in vitamin D, either through dietary malnutrition or malabsorption (Cooper *et al.*, 2005, Holick, 2007). Schamall *et al.* (2003) observed that while rickets only affected the trabecular number within the central portion of the lumbar vertebral bodies studied, osteomalacic vertebrae displayed decreased BV/TV over the entirety of the vertebral body. While this study excluded individuals with external damage and obvious pathological conditions, it was not possible to ascertain conditions that affected the bone at the microscopic level and it is entirely possible that the differences between individuals observed may be due to these conditions.

Other factors such as physical exertion also affects the maintenance of the internal trabecular architecture from a load-bearing capacity. In adults, this factor may be important in understanding variation between populations and archaeological versus modern skeletal collections, as evidence suggests modern adult humans are more sedentary than their archaeological counterparts (Sievänen *et al.*, 2007). While this cannot explain the variation found within the

fetal and perinatal cohorts, due to the lack of load-bearing in these individuals beyond *in utero* and early limb movements, it may help to explain differences found in older cohorts.

While it is clear that some individuals within the same age cohort do differ significantly from each other in terms of internal trabecular architecture, a general pattern of changing trabecular architecture can still be identified over VOIs. Furthermore, general variation exists between and within all populations, and a range of values is expected for each histomorphometric parameter in response to this. The differing findings for these individuals gives an idea of the variation that may be present within all populations.

10.5 Strengths and Limitations

10.5.1 *Sample*

The Scheuer collection, which was utilised in this study, is a large active repository of juvenile remains. The use of this collection greatly improved the sample size and demographic of this project compared to other studies on juvenile vertebral trabecular architecture.

However, due to the availability of individuals of certain ages, some cohorts within this study were significantly smaller than others. For example, while the perinatal cohort contained a total of 38 vertebral centra, only 7 vertebral centra were within the fetal cohort. Furthermore, a lack of individuals between the ages of 4 weeks to 2 years meant that individuals of these ages were pooled together within this cohort rather than separated into smaller cohorts. A further separation would have been an improvement to the study, as this cohort represents a vital age range when considering developmental milestones attained within this time frame and the effects they may have on vertebral trabecular architecture. It was unfortunate that for some cohorts, a reduced number of individuals were suitable for this analysis. This led to the separation of ages for the cohorts studied. If more individuals were available within the 4 week to 2 year age range, further separation of this cohort would have occurred as it is an important age range in development with multiple developmental milestones occurring.

Furthermore, a number of individuals included in the sample were of estimated age. While the age ranges were generally narrow due to the availability

of multiple skeletal elements that allowed for accurate estimation of age at death, estimated ages were based on differing methodologies which may have affected ranges given.

Generally, the level of preservation of skeletal elements from the Scheuer collection is high however, a selection of individuals were found to display man-made holes within the vertebral centra that were previously created to seriate the centra on wire. As these individuals formed in majority the 4 weeks to 2 years of age cohort, they were considered too important to exclude from the study. Results from the initial qualitative study did not identify any changes to the area surrounding the holes, and during the quantitative analysis, these holes were excluded from quantitative analysis when creating the VOI in Skyscan. Therefore, this damage is not considered to have materially affected the results of this analysis.

Finally, a number of sample assumptions were relied upon for this analysis. Firstly, for Analyses 1b, 2 and 3, data from individuals of the same age cohort were pooled together. However, Analysis 1A indicated differences existed between these individuals. A number of potential factors for these differences have been discussed in section 10.4. The differences between individuals may have affected the findings of these analyses, however, it is important to note that variation between individuals is entirely normal and that Analysis 1a, while displaying numerical differences between individuals, did not display any differing trends within the data. Secondly, this is a cross-sectional study that compares the data of different age cohorts. Cross-sectional studies make the assumption that the data collected is comparable even though it is derived from different sources. In the case of this study, age cohorts were compared however there is no evidence that the findings between age cohorts could be extrapolated. On the other hand, a longitudinal study would allow analysis of the same individual over time. Unfortunately, a longitudinal study was not possible for a number of reasons, including the difficulty in collecting data regarding to trabecular architecture in living individuals and the ethical issues surrounding exposure to imaging techniques such as radiography and CT.

10.5.2 *Grid creation*

A superimposed grid system was utilised in this study to distinguish between areas of interest within the vertebral centrum. This method has been used successfully in similar studies (Cunningham, 2009; Yusof, 2013; O'Malley, 2013; Maclean, 2017).

The grid system created for this project aimed to enable the differentiation not only between central and peripheral volumes within the developing lumbar centrum, but also to differentiate between superior and inferior regions. While this was achieved successfully in older individuals that had begun to undergo neurocentral fusion, it was not possible to differentiate between superior and inferior in younger individuals. There is the potential that differences between the superior and inferior regions of the developing centrum have been overlooked due to this as data for the superior and inferior regions would be pooled together. Although a number of studies have identified differences between the superior and inferior regions of the lumbar vertebral body in adulthood, no consistent differences were observed within older cohorts for this project. Therefore, it would not be expected for younger cohorts to display differences between the superior and inferior regions and hence, the implications of this are considered not to have affected the results found.

Of the 27 volumes of interest studied in this project, only a single VOI could be considered as regular in shape: 5C, which was cuboidal. All other VOIs are considered to be irregular in shape. The irregularity of VOIs may have influenced the computation of degree of anisotropy, which is based upon placing a best-fitting sphere within a volume. Due to the irregularity of VOI shape, the spheres created in the computation of DA were likely significantly different sizes and hence led to the variability found.

Finally, the grid system utilised was a limiting factor for the age cohorts studied. As the grid considered only the developing centrum, once neurocentral fusion had occurred and the centrum could no longer be distinguished from the neural arch, that individual could not be considered. Therefore, the majority of individuals above the age of six years had to be excluded from the project. Furthermore, the grid system relied on fixed points. This was created when considering fetal and perinatal vertebral centra. However, postnatally, allometric

growth made the identification of these points more challenging. The importance of the grid system was to identify comparable volumes of interest easily within the vertebral centra over all age cohorts. With the change in size and shape that occurs the fixed grid system may not have been accurately identifying comparable VOIs.

10.5.3 *µCT as a method of bone quantification*

Before the introduction of non-invasive imaging techniques, many effective yet destructive methods were used to assess trabecular architecture. Some studies used macroscopic analysis, including histology and stereology, to qualitatively describe internal architecture (Sato *et al*., 1967; Amstutz and Sissons, 1969), while others used more complex methodologies such as scanning electron microscopy (Kneissel *et al*., 1997). With destructive methods that involve the sectioning of bone tissue, it is likely that bone loss occurs during sample preparation. More recent technological advancements, such as µCT have allowed more detailed assessment of trabecular architecture, focusing on quantitative, rather than qualitative, analysis while also utilising technology to understand the dynamic three-dimensional structure of the lumbar vertebrae and relate this to their weight bearing and locomotive functions (Ulrich *et al*., 1998). Perhaps most importantly, particularly when considering juvenile skeletal samples, µCT is a non-invasive and non-destructive technique, which is vital in the protection of irreplaceable juvenile collections.

While µCT has many strengths as a method of visualising and quantifying trabecular architecture, it is also important to consider its limitations. Notably, a limitation of µCT as an imaging technique is its accessibility to researchers, with equipment oftentimes unavailable or of prohibitively high cost (Griffith *et al.*, 2012).

10.5.4 *Histomorphometric parameter calculation and statistical analysis*

It has been observed that specific histomorphometric parameters are seemingly more likely to present significant differences in this study. In these cases, the variation within the dataset, and hence the spread of data, within these parameters is increased. The three parameters in which this is most commonly identified are BV/TV, SMI and DA. While factors such as trabecular number,

trabecular thickness and trabecular separation all focus on quantifying a physical feature of the internal trabecular architecture, values for BV/TV, SMI and DA rely on more complex calculations, often based upon assumptions about the nature of the structure. The fact that these parameters are derived from other parameters may explain the increase in variation between individuals within the same age cohort. A full definition of these parameters along with their calculation can be found in Section 6.2.3.3 of this thesis.

With any multi-step calculation, error of measurement in initial steps of the calculation can be amplified. The calculation of BV/TV is based on the values for bone volume (BV) and the total volume (TV) of the VOI. Any differences between BV and TV would be amplified by the calculation to produce BV/TV and, while BV and TV alone may not display significant differences between individuals, this amplification of differences could cause them to lead to significance for the BV/TV parameter. Trabecular number is another example of this, as it relies on the values for BV/TV and Tb.Th within its calculation.

SMI is a numerical value that aims to describe the three-dimensional morphology of trabecular struts within a given volume. Its computation relies on factors such as object volume and object surface area and involves volume dilation to compute the calculation (Hildebrand *et al.*, 1997a). The SMI value calculated may not actually imply trabecular shape. Salmon *et al.* (2015) studied the calculation of SMI in trabecular bone and noted that assumptions were made during the computation of SMI. Current SMI calculations are based on the assumption that the surface of the structure under analysis is convex. However, due to the connectivity of trabeculae, surfaces may also present as concave. In these cases, negative values are produced. Several negative SMI values were computed for the current study, implying concavity of the bone surface within VOIs. While Salmon *et al.* (2015) found that negative SMI values were more representative of the morphology of the trabecular struts than positive values, such negative values can impact the average SMI values used in the calculation of significant differences, and the majority of data collected for SMI was positive and hence potentially less accurate.

The computation of degree of anisotropy is perhaps the most complex of the parameters studied and relied upon the placing of a sphere of best fit within the volume. As previously mentioned, the irregularity of the majority of VOIs within

the lumbar vertebral centrum leads to the more difficult and potentially inaccurate calculation of the parameter.

Meanwhile, trabecular thickness and trabecular separation are not derived factors, and the noise that affects the other factors considered above does not affect them. However, in most cases, significant differences between individuals for these parameters were present. While this may be due to differences between individuals, it may also be due to the statistical test used. For Analysis 1, an ANOVA was used, which produced a median or mean value (depending on the normality of the data) which were then ranked. Single outliers for specific VOIs can easily skew results to imply there is a significant difference where no significant differences are present. Conversely, significantly higher or lower values may be masked by others by taking an average value for each VOI, and significant differences may in turn be masked.

Due to the lack of individuals within some age cohorts, some statistical analyses calculated higher P values, which may indicate that differences identified as significant may not be significant or *vice versa*. This was evident in the fetal age cohort, where the L3 cohort consistently displayed significant results due to increased sample size, while datasets at L1 and L5, while displaying a similar spread of data, were not considered significant during statistical testing.

10.6 Future research

The three phases of development identified within this study are important in understanding the early mechanisms of trabecular development (Acquaah *et al*., 2015). While this study identified successfully that the lumbar vertebrae undergo these phases of development in early infancy and childhood, this was studied at a whole bone level. Site specific changes within these periods may shed light on the potential genetic, epigenetic and evolutionary forces driving these phases and early bone development (O'Malley, 2013; Acquaah *et al*., 2015; Maclean, 2017). Furthermore, site specific changes may also aid in understanding the significant differences seen between vertebral levels and why these significant differences decreased in the early postnatal period.

This study focused on quantifying the trabecular architecture of three of the five lumbar vertebral centra. Significant differences between vertebral levels

were observed and were attributed to increased axial forces placed upon the vertebral column from L1 to L5. Quantifying the trabecular architecture within L2 and L4 would allow further insight into differences in trabecular architecture over the entire column.

Only the vertebral centrum was considered for analysis in the quantitative aspect of this study. However, within the qualitative project, the neural hemiarches displayed patterns of radiographic intensity that would be of interest to investigate further. The neural hemiarches are a vitally important structure in the conversion and transference of shear and torsional loads to the vertebral body through the facet joints and pedicles (LeVeau and Bernhardt, 1984; O'Rahilly *et al.*, 1990; Smit *et al*., 1997; Boszczyk *et al.*, 2002) and an understanding of their developing trabecular architecture may indicate the potential mechanisms by which this occurs.

A future avenue of this study would be to quantify cortical bone thickness within the lumbar vertebrae. The cortical shell of the lumbar vertebral body has been identified as important in vertebral compressive strength (Eswaran *et al*., 2006). Furthermore, increased rates of cortical bone remodelling have been observed in early development, potentially driven by mechanical stimulation, such as muscular contraction (Schoenau and Fricke, 2008). The quantification of developmental changes in cortical thickness may also help to understand the results seen in the radiographic study that in some regards do not match the findings of the trabecular study and hence may be due to the superimposition of the cortex.

The sample for this study comprised entirely of the Scheuer collection. An addition to this project would be the inclusion of other juvenile skeletal collections to increase the sample size studied and provide a wider range of juveniles from multiple origins.

Outwith the lumbar vertebral column, there are still several skeletal elements within the developing skeleton that have yet to be subject to analysis in terms of the internal trabecular architecture. Initially, it is deemed that further research into the vertebral column is needed. Neither the thoracic nor cervical vertebrae have been analysed in such depth in the juvenile. As these regions of the vertebral column differ in some aspects of their functions to the lumbar vertebrae,

for example the articulation of the ribs in the thoracic region and the decreased axial compression in the more cranial parts of the column, it would be of interest to compare the trabecular architecture within these regions to that of the lumbar vertebrae. Beyond this, there are multiple other skeletal elements, of human and non-human origin, that have yet to be studied in relation to early ontogenetic changes in bone architecture in order to understand the genetic, epigenetic and evolutionary factors that drive the development of bone.

11 Conclusions

The objectives of this project were to document the developing trabecular architecture of the lumbar vertebral centra at the vertebral levels L1, L3 and L5, to identify any regional differences in trabecular architecture throughout development, to identify any changes in architecture throughout development, and to identify whether significant differences were present between vertebral levels. These objectives were met through the use of radiography and μCT to visualise and quantify the developing internal trabecular architecture of the lumbar vertebral centrum.

The qualitative section of the project was utilised as a preliminary study to identify general trends of radiographic intensity within the lumbar vertebral centra and neural arches at all lumbar levels, from the fetal period to late adolescence. A symmetrical pattern of radiographically intense projections was observed in the fetal and perinatal cohort, which was attributed to the pattern of growth, while areas of low radiographic intensity were most likely indicative of space occupying vascular structures. These findings were corroborated by the quantitative aspect of this project, which found that one of the greatest influences on fetal and perinatal trabecular architecture was the pattern of ossification. The immature nature of the trabecular architecture within the peripheral regions of the centrum was attributed to four growth plates: the superior and inferior metaphyseal surfaces along with paired posterolateral growth plates in proximity to the developing neural hemiarches. Centrally, the increased trabecular thickness was attributed to the increased maturity of trabeculae within the region, while decreased trabecular number was associated with the presence of space occupying vascular channels. As there was no evidence that the trabecular architecture of the lumbar centrum became more anisotropic throughout development, it was considered that the trabecular architecture seen in the adult may be predetermined in the fetal and perinatal cohorts in relation to the pattern of development, alongside *in utero* limb movements.

The fetal and perinatal periods displayed a high radiographic intensity qualitatively, which was observed to decrease postnatally. This qualitative finding was corroborated by a significant loss of bone volume and trabecular number in the early postnatal period, along with the transition from more plate-like

trabeculae to rod-like trabeculae. This transition in trabecular architecture was considered to be detrimental to mechanical strength. The initial early increased bone volume within the lumbar vertebral centrum was identified as a period of increased bone mineral accrual. This was followed by a period where previously accrued mineral is resorbed, and the trabecular architecture significantly reduced, while the skeletal element increases in size. Identifying the extent of early bone mineral accrual and bone loss in the developing lumbar spine is important in understanding the potential factors driving the early development of trabecular architecture and the effects these may have on bone health in the juvenile period and in later life. For example, it highlights the importance of maternal nutrition during pregnancy and breastfeeding in bone mineral accrual in the fetal period, alongside nutrition in early life. This may be of importance in later life as the lumbar vertebral column is a risk site for compressive fracture in osteoporosis with advancing age. Finally, a third period of development was also identified in the lumbar vertebral centra, where the trabecular architecture began to display evidence of remodelling after the period of bone loss in early infancy. This period is likely driven by the attainment of developmental milestones, in particular postural milestones such as sitting unaided and standing without assistance, which greatly increase the axial compressive load placed upon the vertebral column. Hence, it highlights the importance of the attainment of developmental milestones in the normal development of the lumbar vertebral trabecular architecture in early childhood.

Overall, this study found that significant differences were present in the trabecular architecture of different lumbar vertebral levels. However, these differences could not be linked to the developing lumbar lordosis. Instead, they were discussed as a potential response to the differing mechanical demands of each vertebra level, with L5 displaying a structure more suited to withstanding increased compressive loading. The proximity and relation of L5 to the first sacral vertebra may also have played a role in the development of the trabecular architecture seen at the level of L5.

12 References

Abad, V., Meyers, J.L., Weise, M, Gafni, R.I., Barnes, K.N., Nilsson, O., Bacher, J.D. and Baron, J. (2002). The role of the resting zone in growth plate chondrogenesis. *Endocrinology,* **143(5)**: 1851-1857.

Abel, R. and Macho, G.A. (2011). Ontogenetic changes in the internal and external morphology of the ilium in modern humans. *Journal of Anatomy*, **218**: 324-335.

Acquaah, F., Robson-Brown, K.A., Ahmed, F., Jeffrey, N. and Abel, R.L. (2015). Early trabecular development in human lumbar vertebra: overproduction, constructive regression, and refinement. *Frontiers in Endocrinology*, **6**: 1-9.

Adams, M.A. and Dolan, P. (2005). Spine biomechanics. *Journal of Biomechanics*, **38**: 1972-1983.

Adams, M.A. and Hutton, W.C. (1980). The effect of posture on the role of the apophysial joints in resisting intervertebral compressive forces. *Journal of Bone and Joint Surgery*, **62B**: 358-362.

Agarwal, S.C., Dumitriu, M., Tomlinson, G.A. and Grynpas, M.D. (2004). Medieval trabecular bone architecture: the influence of age, sex, and lifestyle. *American Journal of Physical Anthropology*, **124**: 33-44.

Aguirre, J.I., Plotkin, L. I., Stewart, S.A., Weinstein, R.S., Parfitt, A.M., Manolagas, S.C. and Bellido, T. (2006). Osteocyte apoptosis is induced by weightlessness in mice and precedes osteoclast recruitment and bone loss. *Journal of Bone and Mineral Research,* **21**: 605-615.

Ahn, D.K., Lee, S., Moon, S.H., Boo, K.H., Chang, B.K. and Lee, J.I. (2014). Ossification of the ligamentum flavum. *Asian Spine Journal*, **8**: 89-96.

Ajubi, N.E., Alblas, M.J., Nijweide, P.J., Burger, E.H. and Klein-Nulend, J. (1999). Signal transduction pathways involved in fluid flow-induced PGE 2 production by cultured osteocytes. *American Journal of Physiology-Endocrinology and Metabolism,* **276**: E171-E178.

Albert, A. and Maples, W. (1995). Stages of epiphyseal union for thoracic and lumbar vertebral centra as a method of age determination for teenage and young adult skeletons. *Journal of Forensic Sciences,* **40(4)**: 623-633.

Albert, M., Mulhern, D., Torpey, A. A. and Boone, E. (2010). Age estimation using thoracic and first two lumbar vertebral ring epiphyseal union. *Journal of Forensic Sciences*, **55(2)**: 287-294.

Alini, M., Marriot, A., Chen, T., Abe, S. and Poole, A. R. (1996). A novel angiogenic molecule produced at the time of chondrocyte hypertrophy during endochondral bone formation. *Developmental Biology,* **176**: 124-132.

Amonoo-Kuofi, H.S. (1995). Age-related variations in the horizontal and vertical diameters of the pedicles of the lumbar spine. *Journal of Anatomy*, **186**: 321-328.

Amstutz, H.C. and Sissons, H.A. (1969). The structure of the vertebral spongiosa. *Journal of Bone and Joint Surgery*, **51(B)**: 540-550.

Andersen, T.L., Abdelgawad, M.E., Kristensen, H.B., Hauge, E.M., Rolighed, L., Bollerslev, J., Kjaersgaard-Andersen, P. and Delaisse, J-M. (2013). Understanding coupling between bone resorption and formation. *American Journal of Pathology,* **183**: 235-246.

Aoyama, H. and Asamoto, K. (2000). The developmental fate of the rostral/ caudal half of a somite for vertebra and rib formation: experimental confirmation of the resegmentation theory using chick-quail chimeras. *Mechanisms of Development*, **99**: 71-82.

Archer, C.W., Dowthwaite, G.P. and Francis-West, P. (2003). Development of synovial joints. *Birth Defects Research (Part C),* **69**: 144-155.

Arlot, M.E., Burt-Pichat, B., Roux, J.P., Vashishth, D., Bouxsein, M.L. and Delmas, P.D. (2008). Microarchitecture influences microdamage accumulation in human vertebral trabecular bone. *Journal of Bone and Mineral Research*, **23(10)**: 1613-1618.

Aubin, J.E. and Bonnelye, E. (2000). Osteoprotegerin and its ligand: a new paradigm for regulation of osteoclastogenesis and bone resorption. *Osteoporosis International*, **11**: 905-913.

Ay, L., Jaddoe, V.W.V., Hofman, A., Moll, H.A., Raat, H., Steegers, E.A.P. and Hokken-Koelega, A.C.S. (2011). Foetal and postnatal growth and bone mass at 6 months: the Generation R study. *Clinical Endocrinology*, **74**: 181-190.

Bachrach, L.K. (2001). Acquisition of optimal bone mass in childhood and adolescence. *Trends in Endocrinology and Metabolism*, **12(1)**: 22-28.

Bagnall, K.M., Harris, P.F. and Jones, P.R.M. (1977a). A radiographic study of the human fetal spine. 2. The sequence of development of ossification centres in the vertebral column. *Journal of Anatomy*, **124**: 791-802.

Bagnall, K.M., Harris, P.F. and Jones, P.R.M. (1977b). A radiographic study of the human fetal spine. 1. The development of the secondary cervical curvature. *Journal of Anatomy*, **123**: 777-782.

Bagnall, K.M., Higgins, S.J. and Sanders, E.J. (1988). The contribution made by a single somite to the vertebral column: experimental evidence in support of resegmentation using the chick-quail chimera model. *Development*, **103**: 69-85.

Bailey, D.A., McKay, H.A., Mirwald, R.L., Crocker, P.R.E. and Faulkner, R.A. (1999). A six year longitudinal study of the relationship of physical activity to bone mineral accrual in growing children: The University of Saskatchewan bone mineral accrual study. *Journal of Bone and Mineral Research*, **14(10)**: 1672-1679.

Baldock, P.A., Thomas, G.P., Hodge, J.M., Baker, S.U.K., Dressel, U., O'Loughlin, P.D., Nicholdson, G.C., Briffa, K.H., Eisman, J.A. and Gardiner, E.M. (2006). Vitamin D action and regulation of bone remodelling: suppression of osteoclastogenesis by the mature osteoblast. *Journal of Bone and Mineral Research*, **21 (10)**: 1618 – 1626.

Banse, X., Devogelaer, J.P. and Grynpas, M. (2002). Patient-specific microarchitecture of vertebral cancellous bone: A peripheral quantitative computed tomographic and histological study. *Bone*, **30**: 829-835.

Banse, X., Devogelaer, J.P., Munting, E., Delloye, C., Cornu, O. and Grynpas, M. (2001). Inhomogeneity of human vertebral cancellous bone: systematic density and structure patterns inside the vertebral body. *Bone*, **28**: 563-571.

Bardeen, C.R. (1905). Studies of the development of the human skeleton. *American Journal of Anatomy,* **4**: 265-302.

Baroncelli, G.I. and Saggese, G. (2000). Critical Ages and Stages of Puberty in the Accumulation of Spinal and Femoral Bone Mass: The Validity of Bone Mass Measurements. *Hormone Research in Paediatrics,* **54(S1)**: 2-8.

Barrey, C., Roussouly, P., Le Huec, J.C., D'Acunzi, G., Perrin, G. (2013). Compensatory mechanisms contributing to keep the sagittal balance of the spine. *European Spine Journal,* **22(Suppl.6)**: S834-S841.

Bassett, J.H. and Williams, G.R. (2008). Critical role of the hypothalamic-pituitary-thyroid axis in bone. *Bone*, **43**: 418-426.

Basso, N. and Heersche, J.N. (2006). Effects of hind limb unloading and reloading on nitric oxide synthase expression and apoptosis of osteocytes and chondrocytes. *Bone*, **39(4)**: 807-814.

Bassuk, A.G. and Kibar, Z. (2009). Genetic basis of neural tube defects. *Seminars in Pediatric Neurology*, **16**: 101-110.

Bauer, J.S. and Link, T.M. (2009). Advances in osteoporosis imaging. *European Journal of Radiology*, **71**: 440-449.

Been, E., Barash, A., Marom, A. and Kramer, P.A. (2010). Vertebral bodies or discs: Which contributes more to human-like lumbar lordosis? *Clinical Orthopaedics and Related Research*, **468**: 1822-1829.

Blair, H.C., Zaidi, M. and Schlesinger, P.H. (2002). Mechanisms balancing skeletal matrix synthesis and degradation. *Biomechemical Journal,* **364(pt 2)**: 329-341.

Boas, F.E. and Fleischmann, D. (2012). CT artifacts: causes and reduction techniques. *Imaging in Medicine,* **4(2)**: 229-240.

Bogduk, N. (1980). A reappraisal of the anatomy of the human lumbar erector spinae. *Journal of Anatomy*, **131**: 525-540.

Bonewald, L.F. (2007). Osteocytes as dynamic multifunctional cells. *Annals of the New York Academy of Sciences*, **1116**: 281-290.

Boszczyk, A.A., Boszczyk, B.M. and Putz, R.V. (2002). Prenatal rotation of the lumbar spine and its relevance for the development of the zygapophyseal joints. *Spine*, **27(10)**: 1094-1101.

Boszczyk, B.M., Boszczyk, A.A. and Putz, R.V. (2001). Comparative and functional anatomy of the mammalian lumbar spine. *The Anatomical Record*, **264**: 157-168.

Boyle, C. and Kim, I.Y. (2011). Three-dimensional micro-level computation study of Wolff's law via trabecular bone remodelling in the human proximal femur using design space topology optimization. *Journal of Biomechanics*, **44**: 935-942.

Brandi, M.L. (2009). Microarchitecture, the key to bone quality. *Rheumatology*, **48**: iv3-iv8.

Brickley, M. and Howell, P.G.T. (1999). Measurement of changes in trabecular bone structure with age in an archaeological population. *Journal of Archaeological Science*, **26**: 151-157.

Briggs, A.M., Greig, A.M., Wark, J.D., Fazzalari, N.L. and Bennel, K.L. (2004). A review of anatomical and mechanical factors affecting vertebral body integrity. *International Journal of Medical Sciences*, **1**: 170-180.

Buck, A.M., Price, R.I., Sweetman, I. M. and Oxnard, C.E. (2002). An investigation of thoracic and lumbar cancellous vertebral architecture using power-spectral analysis of plain radiographs. *Journal of Anatomy*, **200**: 445-456.

Buckley, J.M., Loo, K. and Motherway, J. (2007). Comparison of quantitative computed tomography-based measures in predicting vertebral compressive strength. *Bone*, **40**: 767-774.

Burdan, F., Szumilo, J., Korobowicz, A., Farooquee, R., Patel, S., Patel, A., Dave, A., Szumilo, M., Solecki, M., Klepacz, R. and Dudka, J. (2009). Morphology and physiology of the epiphyseal growth plate. *Folia Histochemica et Cytobiologica,* **47(1)**: 5-16.

Burger, E.H. and Klein-Nulend, J. (1999). Mechanotransduction in bone – role of the lacuno-canalicular network. *The FASEB Journal*, **S13**: S101-S112.

Burghardt, A.J., Kazakia, G.J. and Majumdar, S. (2007). A local adaptive threshold strategy for high resolution peripheral quantitative computed tomography of trabecular bone. *Annals of Biomedical Engineering*, **35(10)**: 1678 – 1686.

Burr, D.B. and Guillot, G.M. (2012). Almost invisible, often ignored: periosteum, the living lace of bone. *Medicographia*, **34(2)**: 221-227.

Burra, S., Nicolella, D.P., Francis, W.L., Freitas, C.J., Mueschke, N.J., Poole, K and Jiang, J.X. (2010). Dendritic processes of osteocytes are mechanotransducers that induce the opening of hemichannels. *Proceedings of the National Academy of Sciences*, **107(31)**: 13648-13653.

Bustami, F. (1986). A new description of the lumbar erector spinae muscle in man. *Journal of Anatomy*, **144**: 81-91.

Byers, S., Moore, A.J., Byard, R.W. and Fazzalari, N.L. (2000). Quantitative histomorphometric analysis of the human growth plate from birth to adolescence. *Bone,* **27(4)**: 495-501.

Cardoso, H.V.F. and Ríos, L. (2011). Age estimation from stages of epiphyseal union in the presacral vertebrae. *American Journal of Physical Anthropology*, **144**: 238-247.

Carlier, E.W. (1890). The fate of the notochord and development of the intervertebral disc in the sheep, with observations on the structure of the adult disc in these animals. *Journal of Anatomy and Physiology,* **24(4)**: 573-584.

Carter, P.H. and Schipani, E. (2006). The roles of parathyroid hormone and calcitonin in bone remodelling: prospects for novel therapeutics. *Endocrine, Metabolic & Immune Disorders - Drug Targets*, **6**: 59-76.

Chandraraj, S. and Briggs, C.A. (1991). Multiple growth cartilages in the neural arch. *Anatomical Record*, **230**: 114-120.

Chen, H., Shoumura, S., Emura, S. and Bunai, Y. (2008). Regional variations of vertebral trabecular bone microstructure with age and gender. *Osteoporosis International*, **19**: 1473-1483.

Chen, J., Liu, C., You, L. and Simmons, C.A. (2010). Boning up on Wolff's Law: Mechnaical regulation of the cells that make and maintain bone. *Journal of Biomechanics*, **43**: 108-118.

Chester, V.L., Tingley, M. and Biden, E.N. (2006). A comparison of kinetic gait parameters for 3-13 year olds. *Clinical Biomechanics*, **21**: 726-732.

Cheung, Y.B., Yip, P.S.F. and Karlberg, J.P.E. (2001). Fetal growth, early postnatal growth and motor development in Pakistani infants. *International Journal of Epidemiology*, **30**: 66-74.

Choufani, E., Jouve, J.L., Pomero, V., Adalian, P., Chaumoitre, K. and Panuel, M. (2009). Lumbosacral lordosis in fetal spine: genetic or mechanic parameter. *European Spine Journal*, **18**: 1342-1348.

Clarke, B. (2008). Normal bone anatomy and physiology. *Clinical Journal of the American Society of Nephorology*, **3**: S131-S139.

Colloca, C. J. and Hinrichs, R. N. (2005). The biomechanical and clinical significance of the lumbar erector spinae flexion-relaxation phenomenon: A review of literature. *Journal of Manipulative and Physiological Therapeutics*, **28**: 623-631.

Colnot, C., Lu, C., Hu, D. and Helms, J.A. (2004). Distinguishing the contributions of the perichondrium, cartilage, and vascular endothelium to skeletal development. *Developmental Biology*, **269**: 55-69.

Cool, T. and Forsberg, E.C. (2019). Chapter One – Chasing Mavericks: The quest for defining developmental waves of haematopoiesis. *Current Topics in Developmental Biology*, **132**: 1-29.

Cooper, C., Fall, C., Egger, P., Hobbs, R., Eastell, R. and Barker, D. (1997). Growth in infancy and bone mass in later life. *Annals of the Rheumatic Diseases*, **56(1)**: 17-21.

Cooper, C., Javaid, K., Westlake, S., Harvey, N. and Dennison, E. (2005). Developmental origins of osteoporotic fracture: the role of maternal vitamin D insufficiency. *The Journal of Nutrition*, **135**: 2726S-2734S.

Cristofolini, L., Brandolini, N., Danesi, V., Juszczyk, M. M., Erani, P. and Viceconti, M. (2013). Strain distribution in the lumbar vertebrae under different loading configurations. *The Spine Journal*, **13**: 1281-1292.

Crock, H.V. (1996). An Atlas of Vascular Anatomy of the Skeleton and Spinal Cord, London: Martin Dunitz.

Crock, H.V. and Yoshizawa, H. (1976). The blood supply of the lumbar vertebral column. *Clinical Orthopaedics and Related Research,* **115**: 6-21.

Cuijpers, A.G.F.M. (2006). Histological identification of bone fragments in archaeology: Telling humans apart from horses and cattle. *International Journal of Osteoarchaeology*, **16**: 465-480.

Cunningham, C.A. (2009). A qualitative and quantitative investigation of structural morphology in the neonatal ilium. PhD in Anatomy and Forensic Anthropology, University of Dundee, Dundee.

Cunningham, C.A. and Black, S.M. (2009a). Anticipating bipedalism: Trabecular architecture in the newborn ilium. *Journal of Anatomy*, **214**: 817-829.

Cunningham, C.A. and Black, S.M. (2009b). Development of the fetal ilium—challenging concepts of bipedality. *Journal of Anatomy*, **214**: 91-99.

Cunningham, C.A. and Black, S.M. (2010). The neonatal ilium- metaphyseal drivers and vascular passengers. *The Anatomical Record*, **293**: 1297-1309.

Cunningham, C.A., Scheuer, L. and Black, S.M. (2016). Developmental Juvenile Osteology, 2nd Ed. London: Elsevier Academic Press.

Currey, J.D. (2003a). Role of collagen and other organics in the mechanical properties of bone. *Osteoporosis International*, **14**: 29-36.

Currey, J.D. (2003b). The many adaptations of bone. *Journal of Biomechanics*, **36**: 1487-1495.

Daggfelt, K. and Thorstensson, A. (2003). The mechanics of back-extensor torque production about the lumbar spine. *Journal of Biomechanics*, **36**: 815-825.

Dalstra, M. and Huiskes, R. (1995). Load transfer across the pelvic bone. *Journal of Biomechanics*, **28(6)**: 715-724.

Davis, P. (1959). Posture of the trunk during the lifting of weights. *British Medical Journal*, **1(5114):** 87-89.

Decker, R.S. (2017). Articular cartilage and joint development from embryogenesis to adulthood. *Seminars in Cell and Developmental Biology,* **62**: 50-56.

Decker, R.S., Koyama, E. and Pacifici, M. (2014). Genesis and morphogenesis of limb synovial joints and articular cartilage. *Matrix Biology,* **October; 0**: 5-10.

del Rio, L., Carrascosa, A., Pons, F., Gusinye, M., Yeste, D. and Domenech, F.M. (1994). Bone mineral density of the lumbar spine in white Mediterranean Spanish children and adolescents: Changes related to age, sex, and puberty. *Pediatric Research*, **35:** 362-366.

Delaisse, J. (2014). The reversal phase of the bone-remodelling cycle: cellular prerequisites for coupling resorption and formation. *BoneKEy Reports*, **3(561)**: 1-8.

Demed, O., Damdinjav, Y., Amgalanbaatar, A., Sundui, E. and Dorjkhuu, A. (2013). The structure of internal blood vessels in Mongolian fetal vertebral bodies. *Open Journal of Applied Sciences*, **3**: 62-66.

Detrait, E.R., George, T.M., Etchevers, H.C., Gilbert, J.R., Vekemans, M. and Speer, M.C. (2005). Human neural tube defects: Developmental biology, epidemiology, and genetics. *Neurotoxicology and Teratology*, **27**: 515-524.

Ding, M. and Hvid, I. (2000). Quantification of age-related changes in the structure model type and trabecular thickness of human tibial cancellous bone. *Bone*, **26**: 291-295.

Ding, M., Odgaard, A. and Hvid, I. (1999). Accuracy of cancellous bone volume fraction measured by micro-CT scanning. *Journal of Biomechanics*, **32(3)**: 323 – 326.

Ding, M., Odgaard, A., Danielsen, C.C. and Hvid, I. (2002). Mutual associations among microstructural properties of human cancellous bone. *Journal of Bone and Joint Surgery* **84B(6)**: 900-907.

Dion, N. and Ste-Marie, L.G. (2012). The fragile beauty of bone architecture. *Medicographia,* **34 (2)**: 163-169.

Dirckx, N., Hul., M. and Maes, C. (2013). Osteoblast recruitment to sites of bone formation in skeletal development, homeostasis and regeneration. *Birth Defects Research Part C*, **99**: 170-191.

Doube, M., Klosowski, M.M., Arganda-Carreras, I., Cordelières, F.P., Dougherty, R.P., Jackson, J.S., Schmid, B., Hutchinson, J.R. and Shefelbine, S.J. (2010). BoneJ: Free and extensible bone image analysis in ImageJ. *Bone*, **47**: 1076-1079.

Drake, R.L., Vogl, A.W. and Mitchell, A.W.M. (2010). Grey's Anatomy for Students. Philadelphia, Churchill Livingstone Elsevier.

Dwek, J.R. (2010). The periosteum: what is it, where is it, and what mimics it in its absence? *Skeletal Radiography*, **39**: 319-323.

Ebraheim, N.A., Hassan, A., Lee, M. and Xu, R. (2004) Functional anatomy of the lumbar spine. *Seminars in Pain Medicine*, **2**: 131-137.

Eisman, J.A. and Bouillon, R. (2014). Vitamin D: direct effects of vitamin D metabolites on bone: lessons from genetically modified mice. *BoneKEy Reports,* **3 (499)**: 1 -6.

Eswaran, S., Gupta, A., Adams, M. and Keaveny, T.M. (2006). Cortical and trabecular load sharing in the human vertebral body. *Journal of Bone and Mineral Research*, **21**: 307-314.

Fajardo, R.J., Ryan, T.M. and Kappelman, J. (2002). Assessing the accuracy of high resolution x-ray computed tomography of primate trabecular bone by comparisons with histological sections. *American Journal of Physical Anthropology*, **118(1)**: 1-10.

Farquharson, M.J. and Brickley, M. (1997). Determination of mineral composition of archaeological bone using energy dispersive low-angle X-ray scattering. *International Journal of Osteolarchaeology*, **7**: 95-99.

Fazekas, I.G. and Kósa, F. (1978). Forensic Fetal Osteology, Budapest: Akadémiai Kiadó.

Ferguson, S.J. and Steffen, T. (2003). Biomechanics of the aging spine. *European Spine Journal*, **12(S2)**: S97-S103.

Ferreira, T. and Rasband, W. (2012). ImageJ User Guide – IJ 1.46. Accessed at https://imagej.nih.gov/ij/docs/guide/index.html.

Fields, A.J., Eswaran, S.K., Jekir, M.G. and Keaveny, T.M. (2009). Role of trabecular microarchitecture in whole-vertebral body biomechanical behaviour. *Journal of Bone and Mineral Research*, **24(9)**: 1523-1530.

Fleming, A., Keynes, R.J. and Tannahill, D. (2001). The role of the notochord in vertebral column formation. *Journal of Anatomy*, **199**: 177-180.

Fleming, A., Keynes, R.J. and Tannahill, D. (2004). A central role for the notochord in vertebral patterning. *Development,* **131(4)**: 873-880.

Fonseca, J.E. (2012). Bone biology: from macrostructure to gene expression. *Medicographia,* **34 (2)**: 142-148.

Forero, L. L., Narayanan, R., Huitema, L.F.A., Vanbergen, M., Apschner, A., Peterson-Maduro, J., Logister, I., Valentin, G., Morelli, L.G. and Oates, A.C. (2018). Segmentation of the zebrafish axial skeleton relies on notochord sheath cells and not on the segmentation clock. *eLife,* **7(e33843)**: 1-28.

Frost, H.M. (1996). Perspectives: A proposed general model of the 'mechanostat' (suggestions from a new skeletal-biologic paradigm). *The Anatomical Record*, **244**: 139-147.

Frost, H.M. (2004). Update of bone physiology and Wolff's law for clinicians. *Angle Orthodontist*, **74**: 3-15.

Gajewska, E., Sobieska, M. and Moczko, J. (2018). Position of the pelvis in the 3rd month of life predicts further motor development. *Human Movement Science,* **59**: 37-45.

Garrett, M., McElroy, A.M. and Staines, A. (2002). Locomotor milestones and babywalkers: cross sectional study. *British Medical Journal*, **324**: 1494.

Gayon, J. (2000). History of the concept of allometry. *American Zoologist,* **40**: 748-758.

Gelineau-van Waes, J. and Finnell, R.H. (2001). Genetics of neural tube defects. *Seminars in Pediatric Neurology,* **8(3)**: 160-164.

Giambini, H., Roghani, R.S., Thoreson, A. R., Melton III, L.J., An, K.N. and Gay, R. E. (2014). Lumbar trabecular bone mineral density distribution in patients with and without vertebral fractures: a case – control study. *European Spine Journal,* **23**: 1346-1353.

Gibb, S., Maroto, M. and Dale, J.K. (2010). The segmentation clock mechanism moves up a notch. *Trends in Cell Biology*, **20**: 593-600.

Giglio, C.A. and Volpon, J.B. (2007). Development and evaluation of thoracic kyphosis and lumbar lordosis during growth. *Journal of Child Orthopaedics*, **1**: 187-193.

Gocmen-Mas, N., Karabekir, H., Ertekin, T., Edizer, M., Canan, Y. and Duyar, I. (2010). Evaluation of lumbar vertebral body and disc: A stereological morphometric study. *International Journal of Morphology*, **28**: 841-847.

Goldberg, G. (2006). Nutrition and bone. *Women's Health Medicine*, **3(4)**: 157-159.

Goldman, H.M., McFarlin, S.C., Cooper, D.M.L, Thomas, C.D.L. and Clement, J.G. (2009). Ontogenetic patterning of cortical bone microstructure and geometry at the human mid-shaft femur. *The Anatomical Record*, **292(1)**: 48-64.

Goldstein, S.A. (1987). The mechanical properties of trabecular bone: Dependence on anatomic location and function. *Journal of Biomechanics*, **20**: 1055-1061.

Gong, H., Zhang, M., Qin, L. and Hou, Y. (2007). Regional variations in the apparent and tissue-level mechanical parameters of vertebral trabecular bone with aging using micro-finite element analysis. *Annals of Biomedical Engineering*, **35**: 1622-1631.

Gong, H., Zhang, M., Yeung, H.Y. and Qin, L. (2005). Regional variations in microstructural properties of vertebral trabeculae with aging. *Journal of Bone and Mineral Metabolism*, **23**: 174-80.

Gosman, J.H. and Ketcham, R.A. (2009). Patterns in ontogeny of human trabecular bone from SunWatch Village in the Prehistoric Ohio Valley: general features of microarchitectural change. *American Journal of Physical Anthropology*, **138**: 318-332.

Grant, J.P., Oxland, T.R. and Dvorak, M.F. (2001). Mapping the structural properties of the lumbosacral vertebral endplates. *Spine*, **26**: 889-896.

Greer, F.R. and Krebs, N.F. (2006). Optimising bone health and calcium intakes of infants, children and adolescents. *Paediatrics*, **117(2)**: 578-585.

Griffith, J.F., Link, T.M. and Genant, H.K. (2012). Bone imaging – the closest thing to art in medicine. *Medicographia*, **34(2)**: 170-177.

Guida, G., Cigala, F. and Riccio, V. (1969). The vascularization of the vertebral body in the human fetus at term. *Clinical Orthopaedics and Related Research*, **65**: 229-234.

Guldberg, R.E., Lin, A.S.P., Coleman, R., Robertson, G. and Duvall, C. (2004). Microcomputed tomography imaging of skeletal development and growth. *Birth Defects Research Part C - Embryo Today: Reviews*, **72**: 250-259.

Guo, X.E. and Kim, C.H. (2002). Mechanical consequence of trabecular bone loss and its treatment: A three-dimensional model simulation. *Bone*, **30**: 404-411.

Hadders-Algra, M. (2018). Early human motor development: From variation to the ability to vary and adapt. *Neuroscience and Biobehavioural Reviews*, **90**: 411-427.

Hadders-Algra, M. (2018). Early human motor development: From variation to the ability to vary and adapt. *Neuroscience and Biobehavioral Reviews,* **90**: 411-427.

Hadjidakis, D.J. and Androulakis, I.I. (2006). Bone remodelling. *Annals of the New York Academy of Sciences*, **1092**: 385-396.

Haidekker, M.A., Andresen, R. and Werner, H.J. (1999). Relationship between structural parameters, bone mineral density and fracture load in lumbar vertebrae, based on high-resolution computed tomography, quantitative computed tomography and compression tests. *Osteoporosis International*, **9**: 433-440.

Hall, B. (2015). Dedifferentiation of chondrocytes and endochondral ossification. In Hall, B. (2015) Bones and Cartilage, 2nd Ed. London: Elsevier Academic Press.

Hammer, A. (2010). The structure of the femoral neck: A physical dissection with the emphasis on the internal trabecular system. *Annals of Anatomy*, **192**: 168-177.

Hammer, A. (2015). The paradox of Wolff's theories. *Irish Journal of Medical Science*, **184**: 13-22.

Hangartner, T.N. (2007). Thresholding technique for accurate analysis of density and geometry in QCT, PQCT and μCT images. *Journal of Musculoskeletal and Neuronal Interactions*, **7(1)**: 9-16.

Hara, T., Tanck, E., Homminga, J. and Huiskes, R. (2002). The influence of microcomputed tomography threshold variations on the assessment of structural and mechanical trabecular bone properties. *Bone*, **31(1)**: 107-109.

Harada, S. and Rodan, G.A. (2003). Control of osteoblast function and regulation of bone mass. *Nature*, **423**: 349-355.

Heino, T.J., Hentunen, T.A. and Väänänen, H.K. (2002). Osteocytes inhibit osteoclastic bone resorption through transforming Growth Factor-β: enhancement by estrogen. *Journal of Cellular Biochemistry*, **85**: 185-197.

Hildebrand, T. and Rüegsegger, P. (1997a). Quantification of bone microarchitecture with the structural model index. *Computer Methods in Biomechanics and Biomedical Engineering*, **1(1)**: 15-23.

Hildebrand, T. and Rüegsegger, P. (1997b). A new method for the model-independent assessment of thickness in three-dimensional images. *Journal of Microscopy*, **185(1)**: 67-75.

Hildebrand, T., Laib, A., Müller, R., Dequeker, J. and Rüegsegger, P. (1999). Direct three-dimensional morphometric analysis of human cancellous bone: Microstructural data from spine, femur, iliac crest and calcaneus. *Journal of Bone and Mineral Research*, **14(7)**: 1167-1174.

Hindman, B.W., and Poole, C.A. (1970). Early appearance of the secondary vertebral ossification centres. *Radiology*, **95**: 359–361.

Hofbauer, L.C., Khosla, S., Dunstan, C.R., Lacey, D.L., Boyle, W.J. & Riggs, B.L. (2000). The role of osteoprogeterin and osteoprogeterin ligand in the paracrine regulation of bone resorption. *Journal of Bone and Mineral Research*, **15**: 2-12.

Holick, M.F. (2007). Vitamin D deficiency. *New England Journal of Medicine,* **357 (3)**: 266-281.

Hou, Y., Wen, Y., Kang, J. and Yang, L. (2013). Influences of endplate removal and bone mineral density on the biomechanical properties of lumbar spine. *Plos One*, **8(e76843)**: 1-8.

Hughes, J. and Petit, M. (2010). Biological underpinnings of Frost's mechanostat thresholds: the important role of osteocytes. Journal of Musculoskeletal and Neuronal Interactions, **10**: 128-135.

Huiskes, R. (2000). If bone is the answer, then what is the question? *Journal of Anatomy*, **197**: 145-156.

Hulme, P.A., Boyd, S.K. and Ferguson, S.J. (2007). Regional variation in vertebral morphology and its contribution to vertebral fracture strength. *Bone*, **41**: 946-957.

Jacobson, A.G. and Sater, A.K. (1988). Features of embryonic induction. *Development*, **104**: 341-359.

Jang, I.G. and Kim, I.Y. (2008). Computational study of Wolff's law with trabecular architecture in the human proximal femur using topology optimization. *Journal of Biomechanics*, **41**: 2353-2361.

Jang, I.G. and Kim, I.Y. (2010a). Computational study on the effect of loading alteration caused by disc degeneration on the trabecular architecture in human lumbar spine. *Journal of Biomechanics*, **43**: 492-499.

Jang, I.G. and Kim, I.Y. (2010b). Computational simulation of simultaneous cortical and trabecular bone change in human proximal femur during bone remodelling. *Journal of Biomechanics*, **43**: 294-301.

Javaid, M.K. and Cooper, C. (2002). Prenatal and childhood influences on osteoporosis. *Best Practice and Research Clinical Endocrinology and Metabolism*, **16(2)**: 349-367.

Jemmett, R.S., MacDonald, D.A. and Agur, A.M.R. (2004). Anatomical relationships between selected segmental muscles of the lumbar spine in the context of multi-planar segmental motion: a preliminary investigation. *Manual Therapy*, **9**: 203-210.

Ji, B. and Gao, H. (2004). Mechanical properties of nanostructure of biological materials. *Journal of the Mechanics and Physics of Solids,* **52**: 1963-1990.

Jiang, L., Xie, Y., Wei, L., Zhou, Q., Shen, X., Jiang, X. and Gao, Y. (2017). Identification of the vascular endothelial growth factor signalling pathway by quantitative proteomic analysis of rat condylar cartilage. *FEBS Open Bio*, **7**: 44-53.

Jones, G., Riley, M. and Dwyer, T. (2000). Breastfeeding in early life and bone mass in prepubertal children: a longitudinal study. *Osteoporosis International*, **11(2)**: 146-152.

Kaplan, K.M., Spivak, J.M. and Bendo, J.A. (2005). Embryology of the spine and associated congenital abnormalities. *The Spine Journal*, **5**: 564-576.

Karsenty, G. (2001). Chondrogenesis just ain’t what it used to be. *Journal of Clinical Investigations*, **107(4)**: 405-407.

Keen, M. (1993). Early development and attainment of normal mature gait. *Journal of Prosthetics and Orthotics*, **5**: 23-26.

Kerr, J.B. (2010). Functional Histology, 2nd ed. London: Mosby.

Kneissel, M., Roschger, P., Steiner, W., Schamall, D., Kalchhauser, G., Boyde, A. and Teschler-Nicola, M. (1997). Cancellous bone structure in the growing and aging

lumbar spine in a historic Nubian population. *Calcified Tissue International*, **61**: 95-100.

Lacquaniti, F., Ivaneko, Y.P. and Zago, M. (2012). Development of human locomotion. *Current Opinion in Neurobiology*, **22(5)**: 822-828.

Land, C. and Schoenau, E. (2008). Fetal and postnatal bone development: reviewing the role of mechanical stimuli and nutrition. *Best Practice and Research in Clinical Endocrinology and Metabolism,* **22**: 107-118.

Lanyon, L. (1974). Experimental support for the trajectorial theory of bone structure. *Journal of Bone and Joint Surgery*, **56(B)**: 160-166.

LeVeau, B.F. and Bernhardt, D.B. (1974). Effect of force on growth, development and maintenance of the human body. *Physical Therapy*, **64**: 1874-1882.

Liu, X. S., Sajda, P., Saha, P.K., Wehrli, F.W., Bevill, G., Keaveny, T.M. and Guo, X.E. (2008). Complete volumetric decomposition of individual trabecular plates and rods and its morphological correlations with anisotropic elastic moduli in human trabecular bone. *Journal of Bone and Mineral Research,* **23(2)**: 223-235.

Liu, X.S., Sajda, P., Saha, P.K., Wehrli, F.W. and Guo, X.E. (2006). Quantification of the roles of trabecular microarchitecture and trabecular type in determining the elastic modulus of human trabecular bone. *Journal of Bone and Mineral Research,* **21(10)**: 1608-1617.

Liu, X.S., Zhang, X.H. and Guo, X.E. (2009). Contributions of trabecular rods of various orientations in determining the elastic properties of human vertebral trabecular bone. *Bone*, **45**: 158-163.

Lorensen, W. and Cline, H. (1987). Marching cubes: A high resolution 3D surface construction algorithm. *Computer Graphics*, **21**: 163-169.

Lovejoy, C. (2005). The natural history of human gait and posture. Part 1. Spine and pelvis. *Gait and Posture,* **21**: 95-112.

Lowe, J.S. (2015). Stevens and Lowe's Human Histology. 4th Ed. Elsevier.

Maat, G.J.R, Matricali, B. and Van Persijn van Meerten, E.L. (1996). Postnatal development and structure of the neurocentral junction. *Spine*, **21**: 661-666.

MacDonald, D.A., Lorimer Moseley, G. and Hodges, P.W. (2006). The lumbar multifidus: Does the evidence support clinical beliefs? *Manual Therapy*, **11**: 254-263.

Mackie, E.J., Ahmed, Y.A., Tatarczuch, L., Chen, K.S and Mirams, M. (2008). Endochondral ossification: how cartilage is converted into bone in the developing skeleton. *The International Journal of Biochemistry and Cell Biology,* **40(1)**: 46-62.

Maclean, S.J, Black, S.M. and Cunningham, C.A. (2014). The developing juvenile ischium: Macro-radiographic insights. *Clinical Anatomy*, **27**: 906-914.

Maclean, S.J. (2017). A qualitative and quantitative analysis of the juvenile ischium. PhD in Anatomy and Human Identification, University of Dundee, Dundee.

MacNeil, J.A. and Boyd, S.K. (2007). Load distribution and the predictive power of morphological indices in the distal radius and tibia by high resolution peripheral quantitative computed tomography. *Bone*, **41(1)**: 129-137.

Maes, C. (2013). Role and regulation of vascularization processes in endochondral bones role and regulation of vascularization processes in endochondral bones. *Calcified Tissue International,* **93**: 307-323.

Maes, C. and Kronenberg, H. (2016). Chapter 60: Bone Development and Remodelling. In: Jameson, J.L., De Groot, L.J., de Kretser, D.M, Guidice, L.C., Grossman, A.B., Potts Jr, J.T. and Weir, G.C. (2016) Endocrinology: Adult and Pediatric, 7th Ed. Philadelphia: Saunder's Elsevier.

Maes, C., Kobayashi, T., Selig, M.K., Torrekens, S., Roth, S.I., Mackem, S., Carmeliet, G. and Kronenberg, H. M. (2010). Osteoblast precursors, but not mature osteoblasts, move into developing and fractured bones along with invading blood vessels. *Developmental Cell*, **19(2)**: 329-344.

Malina, R. (2004). Motor development during infancy and early childhood: Overview and suggested directions for research. *International Journal of Sport and Health Science,* **2**: 50-66.

Malina, R.M. (2004). Motor development during infancy and early childhood: Overview and suggested directions for research. *International Journal of Sport and Health Science*, **2**: 50-66.

Manolagas, S.C. (2000). Birth and death of bone cells: Basic regulatory mechanisms and implications for the pathogenesis and treatment of osteoporosis. *Endocrine Reviews*, **21:** 115-137.

Maquer, G., Musy, S.N., Wandel, J., Gross, T. and Zysset, P.K. (2015). Bone volume fraction and fabric anisotropy are better determinants of trabecular bone stiffness than other morphological variables. *Journal of Bone and Mineral Research*, **30(6)**: 1000-1008.

Marie, P.J. (2012). Bone remodelling: a social network of cells. *Medicographia*, **34(2)**: 149-154.

Martin, T.J. and Sims, N.A. (2005). Osteoclast-derived activity in the coupling of bone formation to resorption. *Trends in Molecular Medicine*, **11(2)**: 76-81.

Martinón-Torres, M. (2003). Quantifying trabecular orientation in the pelvic cancellous bone of modern humans, chimpanzees, and the Kebara 2 Neanderthal. *American Journal of Human Biology*, **15**: 647-661.

McDevitt, H. and Ahmed, S. (2014). Establishing good bone health in children. *Paediatrics and Child Health,* **20(2)**: 83-87.

Melton III, L.J., Christen, D., Riggs, B.L., Achenbach, S.J., Müller, R., van Lenthe, G.H., Amin, S., Atkinson, E.J. and Khosla, S. (2010). Assessing forearm fracture risk in postmenopausal women. *Osteoporosis International*, **21(7)**: 1161-1169.

Miller, M. (2005). Hypothesis: Fetal movement influences fetal and infant bone strength. *Medical Hypotheses*, **65(5)**: 880-886.

Mitchell, D.M., Caksa, S., Yuan, A., Bouxsein, M.L., Misra, M. and Burnett-Bowie, S.A. (2018). Trabecular bone morphology correlates with skeletal maturity and body composition in healthy adolescent girls. *Journal of Endocrinology and Metabolism,* **103**: 336-345.

Moore, K.L., Dalley, A.F. and Agur, A.M.R. (2019). Clinically Oriented Anatomy. Philadelphia: Lippincott Williams and Wilkins.

Mulder, L. Koolstra, J. H., den Toonder, J.M.J. and van Eijden, T.M.G.J. (2008). Relationship between tissue stiffness and degree of mineralization of developing trabecular bone. *Journal of Biomedical Materials Research Part A,* **84(2)**: 508-515.

Mulder, L., van Ruijven, L.J., Koolstra, J.H. and van Eijden, T.M.G.J. (2007). Biomechanical consequences of developmental changes in trabecular architecture and mineralization of the pig mandibular condyle. *Journal of Biomechanics,* **40**: 1575-1582.

Müller, F. and O'Rahilly, R. (1994). Occipitocervical segmentation in staged human embryos. *Journal of Anatomy*, **185**: 251-258.

Müller, F., O'Rahilly, R. and Benson, D.R. (1986). The early origin of vertebral anomalies, as illustrated by a 'butterfly vertebra'. *Journal of Anatomy*, **149**: 157-169.

Mundlos, S. and Olsen, B. (1997). Heritable diseases of the skeleton. Part I: Molecular insights into skeletal development-transcription factors and signaling pathways. *FASEB Journal,* **11**: 125-132.

Musgrove, J. (1891). Persistence of the notochord in the human subject. *Journal of Anatomy and Physiology*, **25**: 386-389.

Nathan, H., Weizenbluth, M. and Halperin, N. (1982). The lumbosacral ligament (LSL), with special emphasis on the 'lumbosacral tunnel' and the entrapment of the 5th lumbar nerve. *International Orthopaedics*, **6**: 197-202.

Nazarian, A., von Stechow, D., Zurakowski, D., Müller, R. and Snyder, B.D. (2008). Bone volume fraction explains the variation in strength and stiffness of cancellous bone affected by metastatic cancer and osteoporosis. *Calcified Tissue International*, **83(6)**: 368 – 379.

Nishimura, R., Hata, K., Ono, K., Takashima, R., Yoshida, M. and Yoneda, T. (2012). Regulation of endochondral ossification by transcription factors. *Journal of Oral Biosciences*, **54(4)**: 180-183.

Northrup, H. and Volcik, K.A. (2000). Spina bifida and other neural tube defects. *Current Problems in Pediatrics*, **November/ December 2000**: 317-332.

Nowlan, N.C. (2015). Biomechanics of foetal movement. *European Cells and Materials,* **29**: 1-21.

Nowlan, N.C., Bourdon, C., Dumas, G., Tajbaksh, S., Prendergast, P.J. and Murphy, P. (2010). Developing bones are differentially affected by compromised skeletal muscle formation. *Bone*, **46**: 1275-1285.

Nowlan, N.C., Dumas, G., Tajbanksh, S., Prendergast, P.J. and Murphy, P. (2012) Biophysical stimuli induced by passive movements compensate for lack of skeletal muscle during embryonic skeletogenesis. *Biomechanics and Modelling in Mechanobiology*, **11**: 207-219.

Nowlan, N.C., Prendergast, P.J. and Murphy, P. (2008). Identification of mechanosensitive genes during embryonic bone formation. *PLoS Computational Biology*, **4**: e1000250.

Nuzzo, S., Meneghini, C., Braillon, P., Bouvier, R., Mobilio, S. and Peyrin, F. (2003). Microarchitectural and physical changes during fetal growth in human vertebral bone. *Journal of Bone and Mineral Research*, **18**: 760-768.

O'Malley, A.S. (2013) *A qualitative and quantitative investigation of the functional morphology of the juvenile scapula.* PhD, University of Dundee.

O'Rahilly, R., Müller, F. and Meyer, D.B. (1990). The human vertebral column at the end of the embryonic period proper 3. The thoracolumbar region. *Journal of Anatomy*, **168**: 81-83.

Ochia, R.S., Tencer, A.F. and Ching, R.P. (2003). Effect of loading rate on endplate and vertebral body strength in human lumbar vertebrae. *Journal of Biomechanics*, **36**: 1875-1881.

Odgaard, A. (1997). Three-dimensional methods for quantification of cancellous bone architecture. *Bone*, **20(4)**: 315-328.

Olsen, B.R., Reginato, A.M. and Wang, W. (2000). Bone development. *Annual Review of Cell and Developmental Biology*, **16**: 191-220.

Pacifici, M., Koyama, E., Shibukawa, Y., Wu, C., Tamamura, Y., Enomoto-Iwamoto, M. and Iwamoto, M. (2006). Cellular and molecular mechanisms of synovial joint and articular cartilage formation. *Annals of the New York Academy of Sciences,* **1068**: 74-86.

Pal, G.P. and Routal, R.V. (1987). Transmission of weight through the lower thoracic and lumbar regions of the vertebral column in man. *Journal of Anatomy*, **152**: 93-105.

Palastanga, N., Field, D. and Soames, R. (2002). Anatomy and Human Movement. London: Elsevier.

Parfitt, A.M., Travers, R., Rauch, F. and Glorieux, F.H. (2000). Structural and cellular changes during bone growth in healthy children. *Bone*, **27**: 487-494.

Parkinson, I.H. and Fazzalari, N.L. (2013). Characterisation of trabecular bone structure. *Studies in Mechanobiology, Tissue Engineering and Biomaterials*, **5**: 31-51.

Parkinson, I.H., Badiei, A., Stauber, M., Cordington, J., Müller, R. and Fazzalari, N.L. (2012). Vertebral body bone strength: the contribution of individual trabecular element morphology. *Osteoporosis International*, **23**: 1957-1965.

Pawlina, W. and Ross, M.H. (2019). Histology: A text and atlas: with correlated cell and molecular biology, 8th Ed. Philadelphia: Lippincott, Williams and Wilkins.

Pearson, O.M. and Lieberman, D.E. (2004). The aging of Wolff's "law": ontogeny and responses to mechanical loading in cortical bone. *American Journal of Physical Anthropology*, **S39**: 63-99.

Perilli, E., Baleani, M., Öhman, C., Fognani, R., Baruffaldi, F. and Viceconti, M. (2008). Dependence of mechanical compressive strength on local variations in microarchitecture in cancellous bone of proximal human femur. *Journal of Biomechanics,* **41**: 438-446.

Perilli, E., Briggs, A.M., Kantor, S., Codrington, J., Wark, J.D., Parkinson, I.H. and Fazzalari, N.L. (2012). Failure strength of human vertebrae: Prediction using bone mineral density measured by DXA and bone volume by micro-CT. *Bone*, **50**: 1416-1425.

Petersen, W., Tsokos, M. and Pufe, T. (2002). Expression of VEGF121 and VEGF165 in hypertrophic chondrocytes of the human growth plate and epiphyseal cartilage. *Journal of Anatomy,* **201**: 153-157.

Petronic, I., Nikolic, D., Cirovic, D., Cvjeticanin, S., Knezevic, T., Raicevic, M., Brdar, R., Dzamic, D., Janic, N. and Golubovic, Z. (2011). Distribution of affected muscles and degree of neurogenic lesion in patients with spina bifida. *Archives of Medical Science,* **7(6)**: 1049-1054.

Pourquie, O. (2001). The vertebrate segmentation clock. *Journal of Anatomy*, **199**: 169-175.

Poussa, M.S., Heliövaara, M.M., Seitsamo, J.T., Könönen, M.H., Hurmerinta, K.A. and Nissinen, M.J. (2005). Development of spinal posture in a cohort of children from the age of 11 to 22 years. *European Spine Journal*, **14**: 738-742.

Power, M.L., Heaney, R.P., Kalkwarf, H.J., Pitkin, R.M., Repke, J.T., Tsan, R.C. and Schulkin, J. (1999). The role of calcium in health and disease. *American Journal of Obstetrics and Gynecology*, **181(6)**: 1560-1569.

Prakash, Prabhu, L.V., Saralaya, V.V., Pai, M.M., Ranade, A.V., Singh, G. and Madhyastha, S. (2007). Vertebral body integrity: a review of various anatomical factors involved in the lumbar region. *Osteoporosis International*, **18**: 891-903.

Prentice, A. (2001). The relative contribution of diet and genotype to bone development. *Proceedings of the Nutrition Society*, **60(1)**: 45-52.

Prideaux, M. and Bonewald, L.F. (2012). The osteocyte: doing the hard work backstage. *Medicographia,* **34 (2)**: 228-237.

Provot, S., Schipani, J., Wu, J.Y. and Kronenberg, H. (2013). Development of the skeleton. In Marcus, R., Feldman, D., Dempster, D.W., Luckey, M. and Cauley, J.A. (2013). Osteoporosis, 4th Ed. Oxford: Elsevier Academic Press.

Raisz, L. (1999). Physiology and pathophysiology of bone remodelling. *Clinical Chemistry*, **45:8(B)**: 1353-1358.

Ramsay, A. (2009). How to get the most out of your X-Tek CT system. Tring: X-Tek Systems Ltd.

Rapillard, L., Charlebois, M. and Zysset, P.K. (2006). Compressive fatigue behavior of human vertebral trabecular bone. *Journal of Biomechanics*, **39**: 2133-2139.

Ratcliffe, J.F. (1980). The arterial anatomy of the adult human vertebral body: a microarteriographic study. *Journal of Anatomy*, **131**: 57-79.

Ratcliffe, J.F. (1981) The arterial anatomy of the developing human dorsal and lumbar vertebral body. A microarteriographic study. *Journal of Anatomy*, **133**: 625-638.

Ratcliffe, J.F. (1982). An evaluation of the intra-osseous arterial anastomoses in the human vertebral body at different ages. A microarteriographic study. *Journal of Anatomy*, **134**: 373-382.

Rauch, F. and Schoenau, E. (2002). Skeletal development in premature infants: a review of bone physiology beyond nutritional aspects. *Archives of Disease and Childhood. Fetal and Neonatal Edition,* **86**: F82-85.

Rauch, F., Travers, R., Norman, M.E., Taylor, A., Parfitt, A.M. and Glorieux, F.H. (2000). Deficient bone formation in idiopathic juvenile osteoporosis: a histomorphometric study of cancellous iliac bone. *Journal of Bone and Mineral Research*, **15(5)**: 957-963.

Reissis, D. and Abel, R.L. (2012). Development of fetal trabecular micro-architecture in the humerus and femur. *Journal of Anatomy,* **220**: 496-503.

Rissech, C. and Black, S. (2007). Scapular development from the neonatal period to skeletal maturity: a preliminary study. *International Journal of Osteoarchaeology*, **17(5)**: 451-464.

Roberts, W.E., Huja, S. and Roberts, J.A. (2004). Bone modelling: Biomechanics, biomechanics, molecular mechanisms, and clinical perspectives. *Seminars in Orthodontics,* **10**: 123-161.

Rodriguez, J.I., Palacios, J., Garcia-Alix, A., Pastor, I. and Paniaqua, R. (1988). Effects of immobilization on fetal bone development. A morphometric study in newborns with congenital neuromuscular diseases with intrauterine onset. *Calcified Tissue International*, **43**: 335-339.

Roschger, P., Grabner, B.M., Rinnerthaler, S., Tesch, W., Kneissel, M., Berzlanovich, A., Klaushofer, K. and Fratzl, P. (2001). Structural development of the mineralized tissue in the human L4 vertebral body. *Journal of Structural Biology*, **136**: 126-136.

Roschger, P., Misof, B.M. and Klaushofer, K. (2012). The complexity and heterogeneity of bone material. *Medicographia*, **34(2)**: 155-162.

Ruff, C., Holt, B. and Trinkaus, E. (2006). Who's afraid of the big bad Wolff?: "Wolff's law" and bone functional adaptation. *American Journal of Physical Anthropology*, **129**: 484-498.

Ryan, T.M. and Krovitz, G.E. (2006). Trabecular bone ontogeny in the proximal femur. *Journal of Human Evolution*, **51**: 591-602.

Sadler, T. W. 2019. Langman's Medical Embryology, 14th Ed. USA: Lippincott Williams and Wilkins.

Salle, B.L., Rauch, F., Travers, R., Bouvier, R. and Glorieux, F.H. (2002). Human fetal bone development: Histomorphometric evaluation of the proximal femoral metaphysis. *Bone*, **30(6)**: 823-828.

Salmon, P.L., Ohlsson, C., Shefelbine, S.J. and Doube, M. (2015). Structural model index does not measure rods and plates in trabecular bone. *Frontiers in Endocrinology,* **6(162)**: 1-10.

Sato, K. (1967). Quantitative microradiographic study on the mineralisation and trabecular density of human vertebral body. *Tohoku Journal of Experimental Medicine*, **92**: 161-173.

Schaffler, M.B., Cehung, W. Y., Majeska, R. and Kennedy, O. (2014). Osteocytes: Master orchestrators of bone. *Calcified Tissue International*, **94**: 5-24.

Schamall, D., Teschler-Nicola, M., Kainberger, F., Tangl, S.T., Brandstätter, F., Patzak, B., Muhsil, J. and Plenk Jr., H. (2003). Changes in trabecular bone structure in rickets and osteomalacia: the potential of a medico-historical collection. *International Journal of Osteoarchaeology*, **13**: 283-288.

Schipani, E., Maes, C., Carmeliet, G. and Semenza, G.L. (2009). Regulation of osteogenesis coupling by HIFs and VEGF. *Journal of Bone and Mineral Research,* **24**: 1347-1353.

Schoenau, E and Fricke, O. (2008). Mechanical influences on bone development in children. *European Journal of Endocrinology*, **159(S1)**: S27-S31.

Schwartz, A.V. (2015). Marrow fat and bone: review of clinical findings. *Frontiers in Endocrinology*, **6(40)**: 1-6.

Seeman, E. and Delmas, P. (2006). Bone quality – The material and structural basis of bone strength and fragility. *The New England Journal of Medicine,* **354**: 2250-2261.

Selleck, M.A.J. and Stern, C.D. (1991). Fate mapping and cell lineage analysis of Hensen's node in the chick embryo. *Development*, **112**: 615-626.

Shahi, M., Peymani, A., Sahamani, M. (2017). Regulation of bone metabolism. *Reports of Biochemistry and Molecular Biology*, **5(2):** 73-82.

Shea, C.A., Rolfe, R.A., Murphy, P. (2015). The importance of foetal movement for co-ordinated cartilage and bone development *in utero*. *Bone and Joint Research*, **4**: 105-116.

Sheldrick, R.C. and Perrin, E.C. (2013). Evidence-based milestones for surveillance of cognitive, language, and motor development. *Academic Pediatrics*, **13(6)**: 577-586.

Sievänen, H., Józsa, L., Pap, I., Järvinen, M., Järvinen, T.A., Kannus, P. and Järvinen, T.L. (2007). Fragile external phenotype of modern human proximal femur in comparison with medieval bone. *Journal of Bone and Mineral Research*, **22**: 537-543.

Skawina, A., Litwin, J.A., Gorczyca, J. and Miodoński, A.J. (1997). The architecture of internal blood vessels in human fetal vertebral bodies. *Journal of Anatomy*, **191**: 259-267.

Skedros, J.G. and Baucom, S.L. (2007). Mathematical analysis of trabecular 'trajectories' in apparent trajectorial structures: The unfortunate historical emphasis on the human proximal femur. *Journal of Theoretical Biology*, **244**: 15-45.

Smit, T. H. (1996). The mechanical significance of the trabecular bone architecture in a human vertebra. Aachen: Shaker.

Smit, T.H., Odgaard, A. and Schneider, E. (1997). Structure and function of vertebral trabecular bone. *Spine*, **22**: 2823-2833.

Sommerfeldt, D.W. and Rubin, C.T. (2001). Biology of bone and how it orchestrates the form and function of the skeleton. *European Spine Journal*, **10**: S86-S95.

Sorrell, J., Somoza, R. and Caplan, A. (2018). Human mesenchymal stem cells induced to differentiate as chondrocytes follow a biphasic pattern of extracellular matrix production. *Journal of Orthopaedic Research,* **36**: 1757-1766.

Soysa, N.S. and Alles, N. (2016). Osteoclast function and bone-resorbing activity: An overview. *Biochemical and Biophysical Research Communications,* **476**: 115-120.

Sparrey, C.J., Bailey, J.F., Safaee, M., Clark, A.J., Lafage, V., Schwab, F., Smith, J.S. and Ames, C.P. (2014). Etiology of lumbar lordosis and its pathophysiology: a review of the evolution of lumbar lordosis, and the mechanics and biology of lumbar degeneration. *Neurosurgical Focus,* **36(5)**: E1(1-16).

Specker, B. (2004). Nutrition influences bone development from infancy through toddler years. *Journal of Nutrition*, **143(3)**: 691S-695S.

Stauber, M. and Müller, R. (2006). Age-related changes in trabecular bone microstructures: global and local morphometry. *Osteoporosis International*, **17(4)**: 616-626.

Stokes, I.A.F. and Gardner-Morse, M. (1999). Quantitative anatomy of the lumbar musculature. *Journal of Biomechanics*, **32**: 311-316.

Sutton-Smith, P., Parkinson, I. H., Linn, A.M.J., Kooke, S.A. and Fazzalari, N.L. (2006). Trabecular rod buckling index in thoraco-lumbar vertebral bone. *Clinical Anatomy*, **19**: 12-18.

Szpinda, M., Baumgart, M., Szpinda, A., Woniak, A., Małkowski, B., Wiåniewski, M., Mila-Kierzenkowska, C. and Króliczewski, D. (2013a). Cross-sectional study of the ossification center of the C1-S5 vertebral bodies. *Surgical and Radiologic Anatomy,* **35**: 395-402.

Szpinda, M., Baumgart, M., Szpinda, A., Wozniak, A. and Mila-Kierzenkowska, C. (2013b). Cross-sectional study of the neural ossification centres of vertebrae C1-S5 in the human fetus. *Surgical and Radiologic Anatomy*, **35**: 701-711.

Szpinda, M., Baumgart, M., Szpinda, A., Woźniak, A. and Mila-Kierzenkowska, C. (2013c). New patterns of the growing L3 vertebra and its 3 ossification centers in

human fetuses – a CT, digital, and statistical study. *Medical Science Monitor Basic Research*, **19**: 169-180.

Thelen, E. and Fisher, D.M. (1984). Newborn stepping: an explanation for a disappearing reflex. *Developmental Psychology*, **18(5)**: 760-775.

Thomsen, J.S., Ebbensen, E.N. and Mosekilde, L. (2000). A new method of comprehensive static histomorphometry applied on human lumbar vertebral cancellous bone. *Bone*, **27**: 129-138.

Thomsen, J.S., Ebbensen, E.N. and Mosekilde, L. (2002a). Zone-dependent changes in human vertebral trabecular bone: Clinical implications. *Bone*, **30**: 664-669.

Thomsen, J.S., Ebbensen, E.N. and Mosekilde, L. (2002b). Age-related differences between thinning of horizontal and vertical trabeculae in human lumbar bone as assessed by a new computerized method. *Bone*, **31**: 136-142.

Thomsen, J.S., Ebbensen, E.N. and Mosekilde, L. (2002c). Predicting human vertebral bone strength by vertebral static histomorphometry. *Bone*, **30**: 502-508.

Thomsen, J.S., Ebbensen, E.N. and Mosekilde, L. (2002d). Static histomorphometry of human iliac crest and vertebral trabecular bone: A comparative study. *Bone*, **30**: 267-274.

Thomsen, J.S., Niklassen, A.S., Ebbesen, E.N. and Brüel, A. (2013). Age-related changes of vertical and horizontal lumbar vertebral trabecular 3D bone microstructure is different in women and men. *Bone*, **57**: 47-55.

Tian, X.Y., Zhang, Q., Zhao, R., Setterberg, R.B., Zeng, Q.Q., Iturria, S.J., Ma, Y.F. and Jee, W.S. (2008). Continuous PGE2 leads to net bone loss while intermettent PGE2 leads to net bone gain in lumbar vertebral bodies of adult female rats. *Bone*, **42(5)**: 914-920.

Trueta, J. (1963). The role of the vessels in osteogenesis. *The Journal of Bone and Joint Surgery*, **45-B(2)**: 402-418.

Tzaphlidou, M. (2005). The role of collagen in bone structure: An image processing approach. *Micron*, **36**: 593-601.

Ulrich, D., van Reitbergen, B., Weinans, H. and Rüegsegger, P. (1998). Finite element analysis of trabecular bone structure: a comparison of image-based meshing techniques. *Journal of Biomechanics*, **31**: 1187-1192.

Van Oers, R.F.M., Ruimerman, R., Tanck, E., Hilbers, P.A.J. and Huiskes, R. (2008). A unified theory for osteonal and hemi-osteonal remodelling. *Bone*, **42**: 250-259.

Vaz, G., Roussouly, P., Berthonnaud, E. and Dimnet, J. (2002). Sagittal morphology and equilibrium of pelvis and spine. *European Spine Journal*, **11**: 80-87.

Verbruggen, S.W., Loo, J.H.W., Hayat, T.T.A., Hajnal, J.V., Rutherford, M.A., Phillips, A.T.M. and Nowlan, N.C. (2016) Modelling the biomechanics of fetal movements. *Biomechanics and Modelling in Mechanobiology,* **15**: 995-1004.

Vezeridis, P.S., Semeins, C.M., Chen, Q. and Klein-Nulend, J. (2006). Osteocytes subjected to pulsating fluid flow regulate osteoblast proliferation and differentiation. *Biochemical and Biophysical Research Communications*, **348(3)**: 1082-1088.

Vialle, R., Khouri, N. and Guillaumat, M. (2006). Lumbar hyperlordosis in cerebral palsy: anatomic analysis and surgical strategy for correction. *Child's Nervous System*, **22**: 704-709.

Viguet-Carrin, S., Garnero, P. and Delmas, P.D. (2006). The role of collagen in bone strength. *Osteoporosis International*, **17**: 319-336.

von Meyer, G.H. (1867). Die architektur der spongiosa. Archiv für Anatomie, Physiologie und Wissenschaftliche Medicin 34: 615 – 628. Translated by: Amundson, P.K., Skedros, J. and Brand, R. (2011). The classic: the architecture of the trabecular bone. *Clinical Orthopaedics and Related Research,* **469(11)**: 3079 – 3084.

Wang, J., Zhou, B., Liu, X.S., Fields, A.J., Sanyal, A., Shi, X., Adams, M., Keaveny, T.M. and Guo, X.E. (2015). Trabecular plates and rods determine elastic modulus and yield strength of human trabecular bone. *Bone,* **71**: 71-80.

Wang, X. and Puram, S. (2004). The toughness of cortical bone and its relationship with age. *Annals of Biomedical Engineering*, **32**: 123-135.

Warmbrunn, M.V., Bakker, B.S., Hagoort, J., Alefs-de Bakker, P.B. and Oostra, R. (2018). Hitherto unknown detailed muscle anatomy in an 8-week-old embryo. *Journal of Anatomy,* **233(2)**: 243-254.

Waung, J.A., Bassett, J.H. and Williams, G.R. (2012). Thyroid hormone metabolism in skeletal development and adult bone maintenance. *Trends in Endocrinology and Metabolism*, **23**: 155-62.

Weiner, S., Traub, W. and Wagner, H.D. (1999). Lamellar bone: Structure-function relations*. Journal of Structural Biology*, **126**: 241-255.

Whitcome, K., Shapiro, L. and Lieberman, D. (2007). Fetal load and the evolution of lumbar lordosis in bipedal hominids. *Nature,* **450**: 1075-1078.

White, T.D., Black, M.T. and Folkens, P.A. (2012). Human Osteology. Oxford: Academic Press.

Whitehouse, W.J., Dyson, E.D. and Jackson, C.K. (1971). The scanning electron microscope in studies of trabecular bone from a human vertebral body. *Journal of Anatomy*, **108**: 481-496.

Wolff, J. (1870). Ueber die innere architectur der knochen und ihre bedeutung für die frage vom knochenwachsthum. *Virchows Archiv fur Pathologische, Anatomie und Physiologe* 50: 389 – 450. Translated by: Heller, M.O., Taylor, W.R., Aslanisis, N and Duda, G.N. (2010). The classic: on the inner architecture of bones and its importance for growth. *Clinical Orthopaedics and Related Research* **468 (4)**: 1056 – 1065.

Wolff, J. (1892). Das Gesetz der Transformation der Knochen. Verlag von August Hirschwald: Berlin. Translated by Maquet, P. and Furlong, R. (1986). The Law of Bone Remodelling. Springer-Verlag, Berlin Heidelberg.

World Health Organisation Multicentre Growth Reference Study Group (WMGRSG). (2006). WHO Motor Development Study: Windows of achievement for six gross motor development milestones. *Acta Pediatrica*, **S450**: 86-95.

Wyburn, G. M. (1944). Observations on the development of the human vertebral column. *Journal of Anatomy*, **78**: 94-102.

Yusof, N. (2013). *The development and anatomy of the sacrum in relation to the ilium and the sacroiliac joint.* PhD, University of Dundee.

Zelazo, P.R., Zelazo, N.A. and Kolb, S. (1972). “Walking” in the newborn. *Science* **176(4032)**: 314-315.

Zhou, X., Zhang, H., Sucato, D.J. and Johnston, C.E. (2014). Effect of dual screws across the vertebral neurocentral synchondrosis on spinal canal development in an immature spine. *The Journal of Bone and Joint Surgery*, **96(17)**: e146.1-e146.6.